VERIFICATION OF MECHANISTIC PREDICTION MODELS FOR PERMANENT DEFORMATION IN ASPHALT MIXES USING ACCELERATED PAVEMENT TESTING

by

MBAKISYA A. ONYANGO

M.S., University of Birmingham, UK, 1995

AN ABSTRACT OF A DISSERTATION

submitted in partial fulfillment of the requirements for the degree

DOCTOR OF PHILOSOPHY

DEPARTMENT OF CIVIL ENGINEERING
COLLEGE OF ENGINEERING

KANSAS STATE UNIVERSITY
Manhattan, Kansas

2009

Abstract

Permanent deformation (rutting) is the most critical load-associated distress that develops on asphalt pavements significantly affecting their performance. Past research work focused on estimating permanent deformation of asphalt mixes using empirical prediction models or prediction models based on linear elastic material models. In recent years, mechanistic and mechanistic-empirical prediction models have been developed to take into account the behavior of asphalt material (viscoelastic, viscoplastic or elasto-visco-plastic). This research project aims to evaluate existing mechanistic models that predict permanent deformation (rutting) in asphalt mixes by comparing computed permanent deformation to that measured in a full-scale accelerated pavement test. Six pavement sections were constructed in the Civil Infrastructure Systems Laboratory (CISL) of Kansas State University with six different asphalt mixes. The sections were loaded with up to 700,000 load repetitions of a 22,000lb single axle. The transverse profiles at the pavement surface were measured periodically. For material characterization, asphalt mix samples fabricated in the laboratory, were subjected to dynamic modulus ($|E^*|$), static creep - flow time (F_t), dynamic creep - flow number (F_n), triaxial and uniaxial strength tests, repetitive shear at constant height (RSCH) and frequency sweep at constant height (FSCH). The finite element software, Abaqus, was used to simulate and evaluate four permanent deformation prediction models, which are: creep model, elasto-visco-plastic model, viscoelastic model and Drucker-Prager model. The predicted permanent deformation was then compared to permanent deformation measured in CISL for the six of asphalt pavement sections. It was found that, with some improvements, creep and elasto-visco-plastic models could be used to predict permanent deformation in asphalt mixes. The viscoelastic model greatly under-predict permanent deformation, and the Drucker-Prager model with hardening criteria over predicts permanent deformation as compared to values measured in CISL.

VERIFICATION OF MECHANISTIC PREDICTION MODELS FOR PERMANENT DEFORMATION IN ASPHALT MIXES USING ACCELERATED PAVEMENT TESTING

by

MBAKISYA A. ONYANGO

M.S., University of Birmingham, UK, 1995

A DISSERTATION

submitted in partial fulfillment of the requirements for the degree

DOCTOR OF PHILOSOPHY

DEPARTMENT OF CIVIL ENGINEERING
COLLEGE OF ENGINEERING

KANSAS STATE UNIVERSITY
Manhattan, Kansas

2009

Approved by:

Major Professor
Dr. Stefan Romanoschi

Copyright

MBAKISYA A. ONYANGO

2009

Abstract

Permanent deformation (rutting) is the most critical load-associated distress that develops on asphalt pavements significantly affecting their performance. Past research work focused on estimating permanent deformation of asphalt mixes using empirical prediction models or prediction models based on linear elastic material models. In recent years, mechanistic and mechanistic-empirical prediction models have been developed to take into account the behavior of asphalt material (viscoelastic, viscoplastic or elasto-visco-plastic). This research project aims to evaluate existing mechanistic models that predict permanent deformation (rutting) in asphalt mixes by comparing computed permanent deformation to that measured in a full-scale accelerated pavement test. Six pavement sections were constructed in the Civil Infrastructure Systems Laboratory (CISL) of Kansas State University with six different asphalt mixes. The sections were loaded with up to 700,000 load repetitions of a 22,000lb single axle. The transverse profiles at the pavement surface were measured periodically. For material characterization, asphalt mix samples fabricated in the laboratory, were subjected to dynamic modulus ($|E*|$), static creep - flow time (F_t), dynamic creep - flow number (F_n), triaxial and uniaxial strength tests, repetitive shear at constant height (RSCH) and frequency sweep at constant height (FSCH). The finite element software, Abaqus, was used to simulate and evaluate four permanent deformation prediction models, which are: creep model, elasto-visco-plastic model, viscoelastic model and Drucker-Prager model. The predicted permanent deformation was then compared to permanent deformation measured in CISL for the six of asphalt pavement sections. It was found that, with some improvements, creep and elasto-visco-plastic models could be used to predict permanent deformation in asphalt mixes. The viscoelastic model greatly under-predict permanent deformation, and the Drucker-Prager model with hardening criteria over predicts permanent deformation as compared to values measured in CISL.

Table of Contents

List of Figures

List of Tables

Abbreviations

AASHTO	American Association of State Highway and Transportation Officials
AC	Asphalt Concrete
ARHM	Gap graded asphalt mix modified with asphalt rubber
APA	Asphalt Pavement Analyzer
APT	Accelerated Pavement Testing
CALTRANS	California Department of Transportation
CISL	Civil Infrastructure System Laboratory
CTRE	Center for Transportation Research and Education at Iowa State University
DGAC	Dense Graded Asphalt Concrete
DOT	Department of Transportation
FE	Finite Element
FEM	Finite Element Method
FHWA	Federal Highway Administration
FS/APT	Full scale accelerated pavement testing
FSCH	Frequency sweep at constant height
HMA	Hot mix Asphalt
HRB	Highway Research Board
HVS	Heavy vehicle simulator
JHPC	Japan Highway Public Cooperation
KSU	Kansas State University
LTPP	Long Term Pavement Performance
MEPDG	Mechanistic-Empirical Pavement Design Guide
NCAT-PTT	National Center for Asphalt Technology – Pavement Test Track
NCHRP	National Cooperative Highway Research Program
NMAS	Nominal maximum aggregate size
ORITE	Ohio Research Institute Transportation and Environment
PAV	Pressure aging vehicle
RSCH	Repetitive shear at constant height
SHRP	Strategic Highway Research Program

UCB	University of California Berkeley
USA	United States of America
VFA	Voids filled with asphalt
VMA	Voids in Mineral Aggregates
WASHO	Western Association of State Highway Officials

Acknowledgements

I wish to express my sincere appreciation to Dr. Stefan Romanoschi for giving me the opportunity to conduct this research. I am deeply appreciative for your guidance, encouragement and steady support during my time at Kansas State University.

I appreciate Dr. Najjar, Dr. Peric and Dr. Dissanayake for your encouragement, support when I needed it most, and believing in me. You made it easy for me to keep working hard especially at the time when my advisor was not at Kansas State University. Thank you for being in my committee. Dr. Xin, external committee member and Dr. Maginnis, external chair, your inputs and support are deeply appreciated.

I would like to express my sincere thanks to Paul Lewis for the accelerated pavement testing in CISL and helping me tirelessly with the Universal Testing Machine. Thank you Paul for the triaxial cell, you made it possible for me to finish my testing and be able to obtain parameters needed for one of my model. I also thank Phil Blackenship for running some of the laboratory tests at Asphalt Institute in Kentucky. You made it possible for me to run my model using parameters obtained from these tests.

My fellow graduate and undergraduate students, thank you for helping me with testing whenever I needed such help. Special thanks to Tito Nyamuhokya for helping me with a big part of laboratory sample fabrication. Ali Sydney, thank you for your moral support and helping me with testing, even at very odd hours. Your listening ear made it easy for me to empty my frustrations at times. Special thanks to all my dearest friends who helped me with my children, fixing them meals, taking them to and from school, and sometimes sleeping with them when I had to work late in the laboratory or I had to travel for conferences. You did this without charging me anything, all in the name of friendship. I value your friendship so much and I sincerely thank you for your moral support and encouragement. My church family at Manhattan SDA church, you made my stay in America a lot easy, I have brothers and sisters in you who are always there for me. Your prayers are so much appreciated.

Special thanks to my children Jason and Joshua for putting up with me and my crazy schedule as a PhD student. I know time lost will never be recovered but I deeply appreciate your understanding and support, and I want you to know that I love you both so much.

Last but not least are my parents, Mr. and Mrs. Mwambogela for encouraging me to try, supporting me all the way, and continually praying for me. I am so blessed to have you as my parents and I am indebted for your love and understanding. My siblings thank you for your moral support, understanding, prayers, encouragement to follow my dream and taking pride in my success. I love you all.

Dedication

To my sons Joshua and Jason

CHAPTER 1 - INTRODUCTION

Pavement structures are primarily classified into flexible and rigid pavement. Flexible pavements (also called asphalt pavements) are constructed from bituminous and granular materials, while rigid pavements are constructed from Portland cement concrete. Asphalt surfaced roads comprise of about 94% of paved roads in USA [FHWA, 2006]. The first asphalt roadway in USA was constructed in 1870 in Newark, New Jersey. The first hot mix asphalt pavement, which was a mixture of asphalt cement with clean, angular graded sand and mineral filler was laid in 1879 on Pennsylvania Avenue in Washington, D.C.; the asphalt binder was imported from Trinidad Lake [Huang, 2004].

The design methods of flexible pavement have gradually evolved from empirical to science based [Huang, 2004]. Prior to 1920s, the pavement thickness was selected based purely on experience. Same thickness was used regardless of material characteristics and local environmental conditions. As experience was gained throughout the years, various methods were developed by different agencies for determining the required pavement thickness. Design methods may be classified into six categories which are (1) Empirical Methods: These are methods based solely on the results of experiments or experience. Correlation between layer thickness and performance under traffic are established based on observations. These methods can be applied to only a given set of environmental conditions, materials and loading conditions. However, they are widely used because of their simplicity. (2) Limiting Shear Failure Methods: These methods were used to determine pavement thickness so that shear failures will not occur. The major inputs include cohesion and internal angle of friction. This method proved not to be very effective in growing traffic loads and speed. (3) Limiting Deflection Methods: In these methods the pavement thickness is designed so that the vertical deflection will not exceed the allowable limit. The use of deflection methods had an advantage that it can be measured easily in the field, but the disadvantage is that pavement failures and distresses are not always correlated to the deflection at the pavement surface. These first three methods were developed prior to 1960s and all of them had limitations, which led to development of more robust design methods [Huang, 2004].

Other design methods include (4) Regression Methods Based on Pavement Performance or Road Tests [Huang, 2004], (5) Mechanistic Empirical Methods, and (6) Mechanistic methods [Huang, 2004, SHRP-A-699, 1994]. Regression methods are based on regression equations developed from results of a road test such as the AASHTO road test, which took place between 1958 and 1961. They can also be developed from performance data of existing pavement such as those used in pavement evaluation systems, COPES [Huang, 2004; and Darter, et. al.,1985] and EXPEAR [Huang, 2004; and Hall et. al., 1989], which are representative examples. Based on the results of the AASHTO road test, the 1972, 1983 and 1993 editions of the AASHTO Guide for the Design of Pavements Structures were developed. They became the primary documents used by state highway agencies to design new and rehabilitated roads. All the three design guide versions employ empirical performance equations developed from the results of the AASHTO road test. The 1983 and 1993 guides contained some state-of-practice refinements in materials input parameters and design procedures for rehabilitation design [Romanoschi, 2004]. Due to limitations observed from these methods, such as type of materials, local environmental conditions, construction methods and equipments, and change in traffic load spectra since 1960's, a mechanistic-empirical design method, which relates mechanics of materials and traffic load as input and pavement response (strain, stress, deflection) as an output was needed.

A mechanistic-empirical method comprise of two parts: (1) the mechanistic part or model, which calculates pavement response (stress, strain and deflection) of each of the pavement layers using mechanics methods, such as the theory of elasticity, and/or viscoelasticity to calculate the response of pavement structure with known material characteristics under given traffic loading, and environmental conditions. (2) The empirical part, which predicts the future structural condition of the pavement. It is normally done by empirical relationships between the response and the rate of deterioration [Ullidtz, 1987; CTRE, 2005].

A mechanistic approach is based entirely on principles of mechanics and strength of materials (elasticity, plasticity and/or viscoelasticity/viscoplasticity). This approach is purely scientific, since it relies on the mechanistic of structural behavior to loading. It has the advantage that it can be successfully applied to different types of materials with known fundamental

engineering properties, different traffic volumes and different environmental conditions. It is therefore more appealing to civil engineers [Ali et al. 1998]. For this approach, fundamental material properties must be known as well as the geometry of the pavement structure [Ullidz, 1987]. In mechanistic approach, a key element is accurate prediction of the response of the pavement materials, and hence of the pavement itself [Carvalho and Schwartz, 2006]. The Mechanistic design approach has not been widely used because of difficulty in obtaining and simulating elasto-plastic or visco-plastic properties of various paving materials. [Ali et al. 1998].

In this dissertation, mechanistic permanent deformation prediction models have been evaluated using the Abaqus/CAE commercial software and results from the accelerated pavement testing ant the Civil and Infrastructure Systems Laboratory at Kansas State University. The evaluation considered six asphalt mixes from three States, Kansas Missouri and Iowa.

1.1 Problem Statement

According to Federal Highway Administration [FHWA 2006], as of 2006 there were about 2.57 million miles of paved roads in USA of which 94% were asphalt surfaced. Asphalt concrete is a construction material with complex mechanical behavior. It exhibits temperature susceptibility, time dependence and aging [Asphalt Institute, 2001]. At cold temperatures asphalt concrete is elastic, stiffer and brittle, while at higher temperature it is softer and viscous. At intermediate temperature, asphalt concrete is a visco-elastic material having both viscous and elastic properties. The response of asphalt concrete is also affected by time loading, that is, asphalt concrete is stiffer under shorter loading time [Asphalt Institute, 2001]. Under repeated loading asphalt concrete is damaged and deforms attaining plastic (permanent) deformation. Other properties of asphalt concrete are pressure dependency, dilation under shear loading and anisotropy due to microstructure distribution [Tashman, 2003]. The complexity of the behavior of asphalt concrete materials has made it very challenging to develop a model that will accurately predict its performance over a design/analysis period.

Numerous pavement performance prediction models have been developed by researchers in an effort to improve performance of asphalt pavements. The developed models predict distresses such as permanent deformation, fatigue cracking and thermal cracking potential of

asphalt mixtures. Due to the complexity of asphalt concrete material, researchers have developed models that encompass some of the asphalt concrete characteristics, linear viscoelastic, viscoplastic, elasto-viscoplastic, viscoplastic continuum etc. Most of the developed models have some limitations in their applications [SHRP, 1994a; Long, 2001; Huang, 2000; Daniel, 2001; Kim et. al. 1997].

According to Kim et al. (1997), a valid and fundamental constitutive model should serve two important purposes. First, it should provide accurate information on the performance of the AC under realistic conditions, leading to better prediction of the life span of a newly constructed pavement or the remaining life of an existing pavement. Second, the model parameters should be linked to mix design properties, so that the selection of materials could be related to improve mix performance [Kim et al, 1997; and Tashman, 2003].

At the moment, there is no mechanistic permanent deformation prediction model that has been universally accepted as the best prediction model for asphalt concrete pavements. Researchers are still working on refining and validating existing prediction models and developing new performance prediction models.

This research effort is aimed at verifying some of the existing mechanistic permanent deformation prediction models for asphalt mixtures, using data collected at the current Accelerated Pavement Testing (APT) experiment at the Civil and Infrastructure Systems Laboratory (CISL), Kansas State University. The verification comprises of six asphalt mixtures from three Midwestern States, Kansas, Missouri and Iowa. Four prediction models are verified using Abaqus/CAE Finite Element software. The models include:

- Creep;
- Viscoelastic;
- Drucker-Prager; and
- Elasto-Visco-Plastic.

The mechanistic prediction models use constitutive equations to predict performance. These equations require fundamental material properties, which must be obtained using laboratory testing on asphalt mixtures [SHRP, 1993; SHRP, 1994a; Kim et al, 1998; Long, 2000, Daniel, 2001; Brown et al, 2001; NCHRP-465, 2002]. For this research project, the prediction models are verified at one test temperature, $35^\circ C$, which is the temperature utilized for the accelerated pavement testing. Same temperature is used for material testing to obtain required material parameters. The models are then implemented (simulated) using ABAQUS/CAE finite element software and results from prediction models are compared to measured values from APT facility.

1.2 Objective

The objective of this research effort is to verify four existing mechanistic permanent deformation prediction models with data collected using the current APT experiment at Civil Infrastructure Systems Laboratory (CISL), Kansas State University (KSU). The selected models are implemented using the ABAQUS finite element software and results are compared with field measured data from KSU APT facility. Fundamental engineering properties needed for model implementation are obtained through laboratory testing. To accomplish the objective of this research, six asphalt mixes from three states, Kansas, Missouri and Iowa. For each mix:

- Laboratory tests were performed to characterize permanent deformation of asphalt mixtures and obtain fundamental engineering properties required for predicting rutting potential,
- ABAQUS/CAE finite element software is used to simulate selected models, and
- Results from APT, CISL 14 project, are used to verify the prediction models.

CHAPTER 2 - LITERATURE REVIEW

2.1   Permanent Deformation

Permanent deformation (or rutting) is one of the most critical distresses that affect the condition of flexible pavements. Others are fatigue cracking and thermal cracking. Permanent deformation occurs typically in the first years after construction. It is manifested as depressions along the wheel paths of the pavement surface, which develops gradually as the number of traffic load repetitions accumulates. It is a load-associated distress, which usually occurs in hot climates and/or under slow moving heavy trucks. [Huang, 2004; Park, 2004; Long, 2001; Huang, 2000; NCHRP-37A, 2004b; Deacon et al, 2002; and Rosenberger 1999]. The rut depression is sometimes accompanied with small upheavals to the sides of the rut, resulting from plastic/shear flow of bituminous materials. The width and depth of the rutting profile, depends highly on the pavement structure (layer thickness and quality), traffic volume and composition as well as on the environment [NCHRP, 2004b]. Ruts are very noticeable after a rainfall when paths are filled with water. They are, therefore, undesirable because when the rut reaches a depth of about 5mm (0.2in) it traps water, and it creates conditions for aquaplaning of vehicles, leading to unsafe traffic conditions (Figure 2.1). As the rut deepens, steering becomes increasingly difficult thus the comfort and safety of the users are compromised [NCHRP 2004, Rosenberger 1999 and SHRP 1994b].

Permanent deformation and rutting are sometimes used interchangeably, because they are both depressions that occur on a wheel path after traffic loading, the difference is accounted by the measurement method. Permanent deformation is measured as the depth of depression with reference to the original profile, while rutting is measured using a four feet straight bar, as the depth between the highest and deepest points on a profile (Figure 2.2). For this dissertation, permanent deformation measurement method is referred.

Figure 2.1 Rutting in flexible pavement

Figure 2.2 Measurement of permanent deformation and rut depth
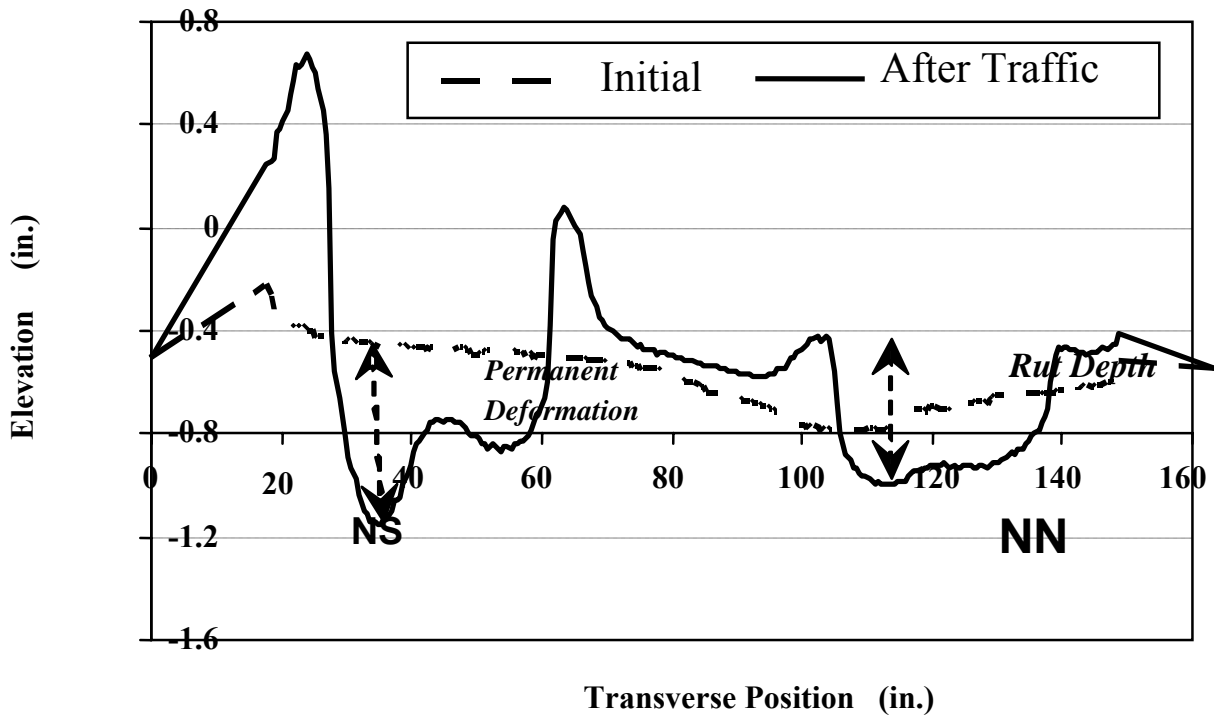
Permanent deformation/rutting represents a calibration of four phenomenon namely consolidation/densification of pavement material, surface wear, plastic/shear flow and mechanical deformation, each related to a different cause [Rosenberger 1999].

Consolidation/densification involves volumetric change in hot mix asphalt (HMA), resulting from tighter packing of material particles [Huang 2004]. It is a further compaction of HMA pavement by traffic after construction. With consolidation, the depression occurs in the wheel path, and no humps develop on either sides of the depression (Figure 2.3), [Rosenberger 1999, Asphalt Institute 2001]. Surface-wear results from the surface abrasion of chains and studded tire use in the winter. The subsequent depression on the surface is similar to that caused by consolidation but with the appearance of abrasion (Figure 2.3) [Rosenberger 1999].

Figure 2.3 Permanent deformation from consolidation/densification or surface wear [Rosenberger 1999, Asphalt Institute 2001]
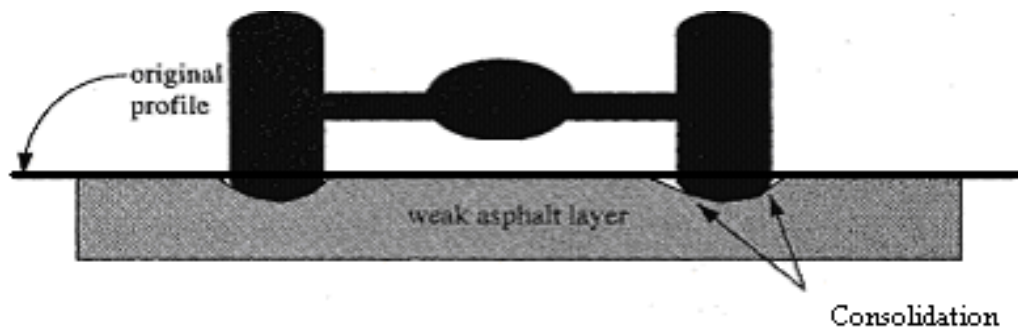
Shear or lateral plastic flow, occurs when there is insufficient stability in the hot mix asphalt (HMA). This type of rutting is common in slow moving lanes and intersections due to slow moving and stationary traffic [Rosenberger, 1999]. The use of excess asphalt cement in the mix causes reduction of internal friction between aggregate particles and results in the loads being carried by asphalt cement rather than the aggregate structure, resulting into shear flow. Hot weather or inadequate compaction during construction, contributes to plastic/shear flow [Robert et. al., 1996, Huang 2004]. Plastic flow normally leads to longitudinal depressions along wheel paths with humps (upheavals) of materials on either side of the rut (Figure 2.4). The humps are created as the material is squeezed out from under the heavy loads [Rosenberger, 1999]. Previous

researches indicate that plastic/shear flow contributes to about 90% of rutting in asphalt concrete and consolidation/densification to about 10%.

Figure 2.4 Pavement rutting from weak mixture, induced by traffic loading [Rosenberger 1999, Asphalt Institute 2001]
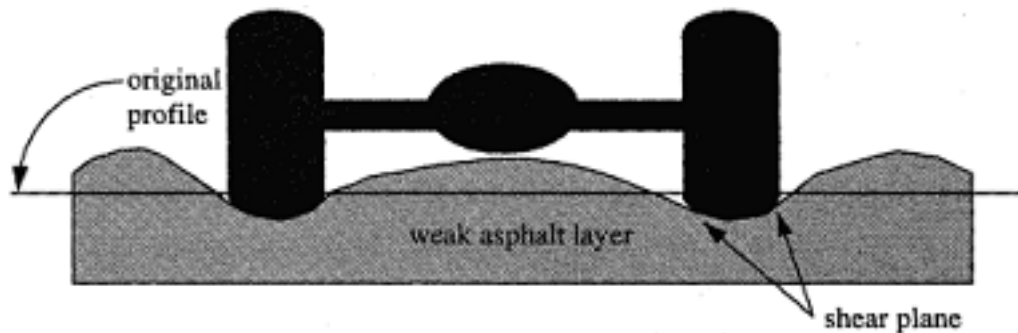
Mechanical deformation results from insufficient structural capacity of the pavement system. In this type of rutting, the strength and thickness of the pavement layers and/or subgrade provide insufficient support to the existing traffic (Figure 2.5). Usually mechanical deformation is accompanied by longitudinal and/or alligator cracking, which typically initiates at the bottom of the asphalt layer where tensile stresses are excessive [Rosenberger 1999].

Figure2.5 Pavement rutting from weak underlying layers, induced by traffic loading [Rosenberger 1999, Asphalt Institute 2001]
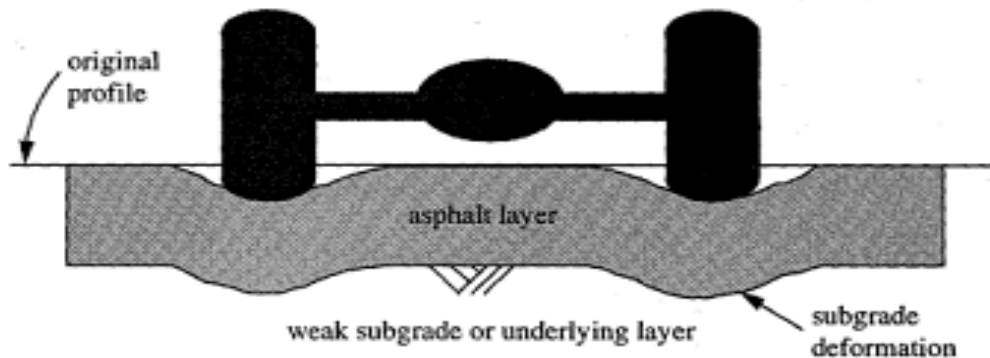
2.1.1 Factors Contributing to Permanent Deformation in Asphalt Mixes

Permanent deformation develops with the increased number of load applications in relation to HMA properties, temperature and environment. Permanent deformation is therefore a function of load magnitude and relative strength of a pavement layers [NCHRP 2002].

Asphalt mixes are complex multiphase materials consisting of a mix of aggregates, air voids and bitumen [Ullidz 1987]. In order to control permanent deformation in flexible pavements, a number of factors that contribute to rutting, need to be assessed. Some of these factors (such as materials) can be controlled or modified; while others (such as seasonal variations) are external factors and cannot be controlled. Some of the factors (such as design thickness) remain constant throughout the design period while others vary seasonally, monthly, hourly or with pavement age [NCHRP 2004]. Factors contributing to permanent deformation in asphalt mixes include asphalt, aggregates, and HMA.

2.1.1.1 Asphalt

The most important characteristics of asphalt cement are: temperature susceptibility, viscoelasticity and aging [Asphalt Institute, 2001]. The temperature susceptibility characteristic of asphalt is manifested when asphalt cement is stiffer at cold temperatures and softer at higher temperatures. This explains the importance of specifying test temperatures of asphalt materials. Asphalt cement behavior is also dependent on time of loading. It is stiffer under shorter loading time. Therefore, loading rate and temperature can be used interchangeably. That is, high temperatures can simulate a slow loading rate and low temperature simulates a fast loading rate [Asphalt Institute, 2001].

Asphalt cement is also a viscous material; it displays both viscous and elastic characteristics at the same time. At high temperatures (e.g. $>100^{\circ}$C), asphalt cement acts almost entirely as a viscous fluid and at very low temperatures (e.g. 0°C) asphalt cements acts like elastic solid, rebounding to its original shape when loaded and unloaded. At intermediate (service) temperatures asphalt cement has both characteristics of viscous fluid and elastic solid, which results in plastic deformation under repeated loading [Asphalt Institute, 2001]. Asphalt ages with time, looses its elastic properties and becomes brittle. This is manifested by fatigue

cracks at the end of design or analysis period of a pavement, which are a result of aged asphalt binder.

2.1.1.2 Aggregates

Mineral aggregates skeleton has a major contribution to the permanent deformation/rutting resistance of asphalt mixture. Superpave mix design procedure requires aggregate particles to be angular, clean (no clay content), and not flat and/or elongated. In compacted HMA, angular-shaped particles exhibit greater interlock and internal friction, and hence result in higher mechanical stability than rounded particles. Limiting flat and elongated particles ensures that the HMA will not be susceptible to aggregate breaking during handling and construction and under traffic and reduces segregation of the mixture. Limiting the amount of clay content in fine aggregates enhances the adhesive bond between asphalt and the aggregates [Roberts, et al. 1992 and Asphalt Institute 2001].

Other material properties are the source aggregates properties, which include toughness, soundness and deleterious materials. Toughness is measured by Los Angeles (LA) abrasion test, soundness is measured by the sodium or magnesium sulfate soundness test. The quantity of deleterious materials is measured by the clay lump and friable particles test [Asphalt Institute 2001].

Superpave uses the 0.45-power gradation chart to develop a design aggregate structure. This will ensure that the aggregates develop a strong aggregates skeleton to enhance resistance to permanent deformation, while allowing sufficient void space (VMA) to enhance mixture performance and to provide enough space for the binder [Asphalt Institute 2001]. Permanent deformation in HMA can be minimized by using larger size aggregates, angular and rough textured course and fine aggregates, and by providing adequate compaction at the time of construction [Robert et. al. 1996].

2.1.1.3 Hot Mix Asphalt (HMA)

Hot mix asphalt (HMA), consists of uniformly mixed aggregates coated with asphalt cement. Variation of materials characteristics in HMA (both individual materials and the mix) affects the paving mixture's resistance to rutting. The Superpave mixture design criteria for HMA include air voids, voids in mineral aggregates (VMA) and voids filled with aggregates (VFA). Voids in Mineral Aggregates (VMA) represents the total volume of voids within the mass of the compacted aggregates, expressed as a percentage. It is a function of aggregate gradation, surface texture and shape [FHWA, 2001]. There are two competing demands during mix design process: (1) sufficient inter-particle space must be available for a minimum amount of binder, but, at the same time (2) the aggregates must have a sufficiently strong skeleton to carry the traffic loads [FHWA, 2001].

VMA affects the performance of mixture because, if the VMA is too small, the mix suffers durability problems and if it is too large, the mix may show stability problems. Continuous graded aggregates are believed to have lower VMA and hence better rutting resistance [Wu, 2001]. Dense graded aggregates give more points of contact and consequently more aggregate interlock and more shear resistance. Compaction of asphalt concrete layer is required in order to acquire a stiff mix. The binder content needs to be optimal because, too little binder content results in high VMA and too much binder fills all the voids hindering proper compaction and hence results in shear flow of materials and rutting of pavements [NCHRP 2004b]. Table 2.1 summarizes the aggregates and binder properties required for production of HMA that can resist rutting.

1.1.1.4 Temperature and environmental conditions

Asphalt stiffness and dynamic modulus of asphalt concrete mixes are highly affected by temperature. Since the modulus of the asphalt layers within the pavement structure affect the overall pavement response, it is important to properly account for the temperature as function of time and depth [NCHRP 2004b].

Table 2.1:   Factors affecting rutting of asphalt concrete mixes [SHRP-A-415]

	Factor	Change in Factor	Effect of a factor on Rutting Resistance
Aggregate	Surface Texture	Smooth to rough	Increase
	Gradation	Gap to continuous	Increase
	Shape	Rounded to angular	Increase
	Size	Increase in max. size	Increase
Binder	Stiffness[1]	Increase	Increase
Mix	Binder content	Increase	Decrease
	Air voids[2]	Increase	Decrease
	VMA[3]	Increase	Decrease
	Method of compaction	[4]	[4]
Test or Field Condition	Temperature	Increase	Decrease
	State of stress/strain	Increase in tire contact	Decrease
	Load repetitions	Increase	Decrease
	Water	Dry to wet	Decrease in mix is water sensitive

NOTE

[1] Refers to stiffness at temperature at which rutting propensity is being determined. Modifiers may be utilized to increase stiffness at critical temperatures, thereby reducing rutting potential.

[2] When air voids are less than about 3 %, the rutting potential of mixes increases

[3] It is argued that very low VMA (voids in mineral aggregate) (i.e. less than 10%) should be avoided.

[4] The method of compaction, whether laboratory of field, may influence the structure of the system and therefore the propensity for rutting.

2.1.1.5 Traffic

Traffic loading is the major contributor to permanent deformation of flexible pavements. The characteristics of traffic affecting the development of permanent deformation include: traffic load, tire contact area, tire pressure, traffic operating speed and lateral wonder of the vehicles. The traffic loading is reflected by the number (or percentage) of trucks using a design lane and the axle configuration; that is single, tandem, tridem or quad axles. Likewise, traffic confined to a fixed path results in load concentration at a certain location, which leads to higher rutting. Wide lanes provide wheel wander, which reduces the load concentration, and hence reduces rutting in the asphalt layer [Huang 2004, NCHRP 2004].

2.2   Mechanistic Permanent Deformation Prediction Models

Permanent deformation reduces road serviceability and causes serious traffic safety problems. With increase in axle loading and repetitions, the permanent deformation problem becomes more serious. In an effort to control permanent deformation in flexible pavements, researchers have developed permanent deformation prediction models, which predict the mixture resistance to permanent deformation. This research evaluates some of the developed models for suitability in the prediction of rutting potential of asphalt mixes.

Mechanistic prediction models are based entirely on principles of mechanics and strength of materials. They rely on mechanics of materials and structural behavior to loading. These models use constitutive equations to model the material characteristic and utilize fundamental engineering properties of material as input in the models. Mechanistic models, therefore, can be successfully applied to different types of materials with known fundamental engineering properties, different traffic volumes and different environmental conditions. This is why they are more appealing to civil engineers [Ali et al. 1998]. The Mechanistic models have not been widely used because of difficulty in obtaining the fundamental engineering properties of materials required such as elasto-plastic or visco-plastic properties of various paving materials. The use of mechanistic prediction models is necessitated by the need of improved pavement performance and reduced maintenance cost.

An ideal material characterization model is expected to predict response of asphalt concrete over the full range of temperature, strain rates and stress states of interest in pavement systems [Zhao, 2002]. However, the behavior of asphalt concrete varies from elastic / linear viscoelastic at low temperature and/or fast loading rates, to nonlinear viscoelastic and viscoplastic/plastic at high temperature and/or slow loading rates. In general asphalt concrete is comprised of elastic, viscoelastic, viscoplastic and plastic components of strains. Figure 2.6 shows these strain components after Uzan (1966). The strain components, obtained after loading and unloading asphalt material, are explained below [Zhao, 2002].

Figure 2.6 Strain components in repetitive loading [Zhao, 2002]
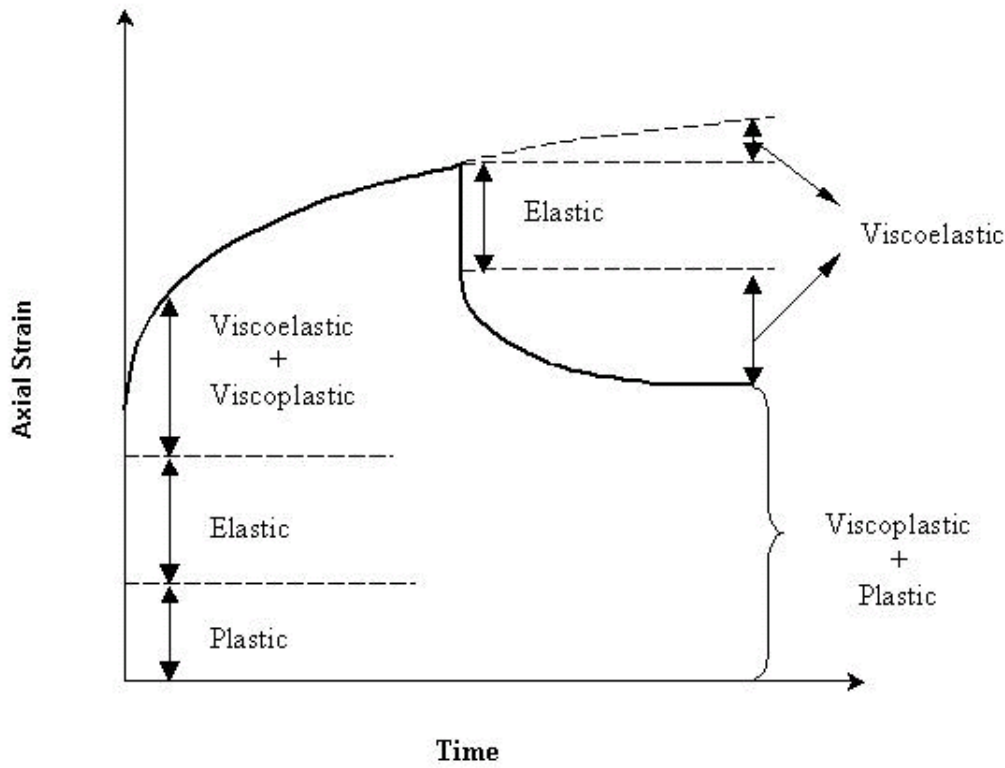
Elastic Strain is governed by Hooke's law which states that strain (ε) is proportional to stress (σ) with Young's modulus (E) being the constant of proportionality. Young modulus E is material characteristic, that is $\varepsilon = \sigma/E$.

Viscoelastic strain is derived from Newton's law, which states that, for purely viscous fluids, shear stress (τ) is directly proportional to the rate of strain ($\dot{y}$), that is $\tau = \eta \dot{y}$, where η is the constant of proportionality called viscosity. Viscoelastic strain is dependent on rate of loading and temperature; its deformation is completely recoverable with time.

Viscoplastic strain is time-dependent but its deformation is not entirely recoverable.

Plastic strain is time-independent, resulting from the mechanics of slip of dislocations at the atomic level. Such deformations occur at stress intensities above a certain threshold value known as the elastic limit or yield stress. The term "plastic flow" is used to designate an ongoing plastic deformation.

15

In order to improve the performance of asphalt mixes, researchers have developed various prediction models. However, due to difficulty in obtaining elasto-plastic or visco-plastic characterization of paving materials, and due to the lack of standardized test methods for obtaining the required material parameters, specific test protocols have been used to obtain material properties employed in the constitutive equations used in these models. Explained below are some of the mechanistic permanent deformation prediction models available in the literature.

2.2.1 *The Elasto-visco-plastic Permanent deformation Model*

The Strategic Highway Research Program developed an elasto-visco-plastic permanent deformation prediction model based on the quasi-static loading (elastic approximation) with nonlinear material properties [SHRP-A-699, 1994]. The model is broken down into four basic components of deformation strains:

- Elastic deformation which is recoverable and time independent (ε^e)
- Plastic deformation which is non-recoverable and time independent (ε^{ve})
- Visco-elastic deformation which is recoverable and time dependent (ε^{vp})
- Visco-plastic deformation which is non-recoverable and time dependent (ε^p)

Creep/recovery test characterizes the four types of asphalt concrete strains listed above. The model utilizes constitutive equations to model elastic, visco-elasto-plastic and plastic deformations.

Asphalt mixes are very complex materials. Hence they are not easily characterized to obtain fundamental engineering properties. Numerous factors affect the performance of asphalt mixes. Therefore, simplifying assumptions are normally employed in the formulation of constitutive equations by including a limited number of behavior characteristics that are relevant or critical to a problem in question. The SHRP model was therefore developed to address the elastic, elasto-visco-plastic and plastic deformations.

For the formulation of elastic deformation constitutive model, the modulus of elasticity or resilient modulus is used. Resilient modulus is defined as the ratio of repeated deviatoric stress to

the recoverable part of the axial strain [SHRP-A-699]. Equation (2.1) was used to define resilient modulus or modulus of elasticity assuming isotropic material.

$$E_R = k_1 P_a \left(\frac{\theta + k_6}{P_a} \right)^{k_2} \left(\frac{\tau_{oct}}{P_a} \right)^{k_3} \tag{2.1}$$

Where:

k_1, k_2, k_3, and k_6 are material constants determined from regression analysis from results of the triaxial laboratory test.

$\theta = I_1 =$ first stress invariant ($\sigma_1 + \sigma_2 + \sigma_3$)

$\tau =$ octahedral stress

$P_a =$ atmospheric pressure

In the resilient model (eq. 2.2), the state stress should be effective stress given by

$$\sigma_{ij} = \sigma_{ij}^t - u\delta_{ij} \tag{2.2}$$

$\sigma_{ij}^t =$ total stress

$\sigma_{ij} =$ effective stress

$\delta_{ij} =$ Kroneker delta

$u =$ suction (k_6 in equation (2.1) is the suction term $u\delta_{ij}$)

The Poisson's ratio, is obtained using volumetric tests.

Asphalt material is a time-dependent elasto-visco-plastic material. It behaves as non-linear elastic material or viscoelastic material at lower temperatures, and are non-linear elasto-visco-plastic at higher temperature [SHRP-A-699]. SHRP used the power law below, to model the visco-elasto-plastic behavior of asphalt material.

$$\varepsilon(t) = \left[\frac{d_o + d_1 a t^m}{1 + a t^m} \right] \sigma_o \tag{2.3}$$

Which was simplified to:

$$\varepsilon(t) = \left(d_o + d_1 t^m \right) \sigma_o \tag{2.4}$$

Where: $\varepsilon(t) =$ strain function describing the response of the material to a step function loading

$\sigma_o =$ amplitude of applied stress

$t =$ time

$d_o, d_1, a, m =$ material properties obtained from frequency sweep test results

Using power law for describing viscoelastic and viscoplastic components, creep compliance can be described as $D(t) = D_e + D_p + D_{ve}t^m + D_{vp}t^n$. Under repeated loads, the damage or irrecoverable strain component is expressed as [SHRP-A-699, 1994]:

$$\varepsilon_p(N) = D_p\sigma_oN^\mu \tag{2.5}$$

$$\varepsilon_{vp}(N) = D_{vp}(t)^n\sigma_oN^\nu \tag{2.6}$$

Where μ, ν and n are material constants

The complete SHRP viscoplastic model characterization requires 4 components of strains (D_e, D_p, D_{ve}, D_{vp}) and six constants (m, n, v, b, p, μ and $\varepsilon_{vp}{}^c$). It was not possible to utilise all these relations directly in pavement response models, therefore the model used an elasto-plastic formulation of the material response model based on the quasi-linear elasticity, and using the resilient model (equation 2.1). The plasticity part was considered using Vermeer's model. Therefore, SHRP model used viscoelastic and viscoplastic parts of response components at specific time intervals, unfortunately, the time intervals were not specified [SHRP-A-699, 1995].

The modified Vermeer model was used as SHRP visco-plastic permanent deformation prediction model, and has the following general expression:

$$\varepsilon = \varepsilon^e + \varepsilon^{ps} + \varepsilon^{pc} \tag{2.7}$$

Where: ε = total strain

             ε^e = elastic strain

             ε^{ps} = plastic strain due to shear

             ε^{pc} = plastic strain due to isotropic consolidation

The elastic behavior is non-linear, with Poisson's ratio equal to zero [SHRP-A-699].

The plastic volumetric strain due to consolidation is calculated as

$$\varepsilon^{pc} = \sum_{i=1}^{incr} d\varepsilon_i^{pc} \tag{2.8}$$

incr = number of load increments

The plastic shear strain is calculated from

$$\gamma^p = \gamma - \gamma^e = \frac{p_o}{2G_o}\left(\frac{p}{p_o}\right)^\beta \frac{\eta^2}{c-\eta} \tag{2.9}$$

$$\eta = \frac{q}{p} \tag{2.10}$$

$$\gamma^e = \frac{\frac{q}{2}}{G} \quad = \text{ elastic shear strain} \tag{2.11}$$

$$\gamma = B\frac{c\eta}{c-\eta} \quad = \text{ total shear strain where} \tag{2.12}$$

$$B = \frac{p_o}{2G_o}^{\beta} \left(\frac{p}{p_o}\right)^{\beta} \tag{2.13}$$

The material parameters describing the reciprocal of the initial modulus in the η - γ curve are:

$$p = -\tfrac{1}{3}(\sigma_1 + \sigma_2 + \sigma_3) \quad = \quad 1\tfrac{1}{3}(\sigma_r + \sigma_z + \sigma_\theta) \tag{2.14}$$

$$q = 1/\sqrt{2}[(\sigma_r - \sigma_\theta)^2 + (\sigma_\theta - \sigma_z)^2 + (\sigma_z - \sigma_r)^2 + 6\tau_{rx}^2]^{1/2} \tag{2.15}$$

G_o = shear modulus in simple shear test at isotropic stress on p_o.

P_o = pressure of reference for expressing laws in non-dimensional form

γ^p = plastic shear strain

2.2.1.1 Permanent deformation characterization

The SHRP permanent deformation prediction model is characterized into two basic parts: (1) the permanent deformation at the end of the first loading cycle, which is described using elasto-plastic models, and (2) The slope of the permanent deformation accumulation as measured from laboratory tests. The model chosen for pavement materials characterization is taken from Vermeer's work which uses a more general failure law than the Mohr-Coulomb one [SHRP-A-699, 1994a]. The resilient properties are obtained from a compression test simulated test with 0.1 sec loading and 0.9 sec unloading. The permanent deformation is characterized by:

$$\log \varepsilon^P(N) = \log \varepsilon^P(N=1) + S \log N \tag{2.16}$$

Where: $\varepsilon^P(N)$ = accumulated strain at N load repetitions;

$\varepsilon^P(N= 1)$ = Strains at the end of the first loading cycle;

N = Number of load repetitions

S = Slope of the $\log \varepsilon^P(N)$ versus log N curve.

The Vermeer model is used as a framework to represent $\varepsilon^P(N=1)$ as function of the state of stress in proportional loading;

The model uses (1) the stresses computed under one wheel of the dual wheel, along a vertical line, at the center of the elements; (2) the Vermeer model to compute the permanent strain in the first load application, $\varepsilon^P(N=1)$; and (3) the parameter S to compute the permanent strain at any number of load repetition (N) using the equation above.

The rut depth in the pavement is accumulated by summing the products of the plastic strain over the corresponding sub layer thickness during the analysis period for all seasons in the sequence. It can be expressed as:

$$RD_j = \sum_{i=1}^{j} \Delta RD_i = \sum_{i=1}^{j} \sum_{k=1}^{n} \varepsilon_{ik}^p h_k \qquad (2.17)$$

where: ΔRD_i = rut depth in season i

RD_j = rut depth accumulated up to season j

ε_{ik}^P = permanent strain during season i in element k

h_k = thickness of element k

This equation adds all permanent deformation along the vertical line under one wheel of the dual wheel. For each season i, ε_i^P is computed from:

$$\varepsilon_i^P = \varepsilon_i^P(atN=1)\left[\left(N_{eqi} + n_i\right)^s - N_{eq}^s\right] \qquad (2.18)$$

where: ε_i^P (at N = 1) = permanent strain for i at first load repetition computed using Vermeer model

n_i = number of load repetitions during season i

N_{eqi} = equivalent total number of load repetitions at beginning of season i

S = slope of log ε^P - log N curve derived from test results

The equivalent total number of load repetitions at the beginning of the ith season is obtained by using the total plastic strain at the end of the i - 1 season, the plastic strain at the first cycle of loading for the ith season, and slope of log ε^P versus log N curve for the ith season. It can be expressed by the following equation:

$$N_{ik} = \left(\frac{\varepsilon^P_{i-1,k}}{(\varepsilon^P_O)_{i,k}} \right)^{\frac{1}{S_{i,k}}} \tag{2.19}$$

Both of the above material properties (ε^P and S) are determined using the repeated-load simple shear laboratory test at constant height where the slope, S, and the intercept, ε_o^P are obtained by fitting a straight line through the data of log ε^P versus log N.

2.2.1.2 Laboratory Tests

The following laboratory tests were conducted to characterize materials for this model, results were analyzed using Superpave mix design software.

(i)   Frequency sweep at constant height (FSCH) (AASHTO TP 7 or SHRP-A-397) test at eleven frequencies and two temperatures to measure dynamic shear modulus (G_o) (storage and loss modulus), phase angle and parameters of the power law (σ_o, t, ε_t).

(ii)   Repetitive simple shear at constant height (RSCH) (AASHTO TP 7 or SHRP-A-397) test with haversine loading and 1.0 sec loading, 0.6 sec unloading to obtain creep compliances D(t) (D_e, D_{ve}, D_{vp}, D_p) and the parameters to be used in the power law of the creep compliance equation, d_o, d_i m and mix plastic properties (α, φ_p, x, φ_{cv}). The test was conducted at 4°, 20°, and 40°C.

(iii)   Uniaxial strength test (SHRP-A-397) to obtain initial Elastic modulus and plastic strains. Tested at 25° and 40°C.

(iv)   Triaxial compressive test (SHRP-A-397) to obtain resilient modulus E_R and k_1 to k_6 and u and Drucker-Prager parameter α, φ_p, φ_{cv}. Tested at 25° and 40°C.

(v)   Volumetric test (SHRP-A-379) at 4°, 25° and 40°C to measure the deformation characteristics on both sides of the sample and the Poisons ratio, ν.

2.2.1.3 Advantages and limitations of the model

This model uses power law and Vermeer theory to predict permanent deformation of asphalt pavements. Material properties measured using the above mentioned laboratory tests include elastic, viscoplastic and plastic. The model has the following limitations [SHRP-A-699, 1994, SHRP-A-357; 1993]: At a large angle of friction ($\varphi > 50$°C) the model does not predict well because it is numerically unstable. The peak friction angle, φ_p, obtained from the model is larger than expected from the static tests. Due to computation complications, the viscoelastic and

viscoplastic component was not used directly in the model. Instead, a Quasi-linear elastic model (Resilient model) was used with plastic model using Vermeer Model. The model uses 2-D FE axisymmetric method, moving wheel, Dynamic effects are not simulated, and dual wheel is not represented. The developed computer software for performance prediction model computes only those stresses and strains that are due to static loads applied to nonlinear quasy-elastic materials. Furthermore the software is not available at the moment. There is no evidence of model update. If updated, it could incorporate moving wheel, dynamic effects and use a 3-D simulation, which is possible with today's technology.

2.2.2 *Viscoplastic Permanent deformation Prediction Model*

Huang B. (2000) developed a 3-D dynamic finite element simulation model, which incorporated elasto-plastic and visco-plastic material properties. The model was developed as a tool for comparing the permanent deformation potential of large stone asphalt mixtures (LSAM) and that of conventional asphalt mixtures. The ABAQUS finite element commercial software was used to simulate the model. The rate-dependent viscoplastic model, which divides the total (deviatoric) strain into elastic and inelastic (visco-plastic) components, was used:

$$\dot{e}_{ij} = \dot{e}_{ij}{}^{e} + \dot{e}_{ij}{}^{vp} \qquad (2.20)$$

The superscripts, e and vp stand for elastic and viscoplastic respectively and the dot indicates the first derivative with respect to time. Huang used the isotropic elastic theory to obtain the elastic strain rate using the equations:

$$\dot{e}_{ij}^{e} = \left(\frac{1}{2}G\right) * \dot{S}_{ij} \qquad \text{and} \qquad \dot{e}_{kk}^{e} = \left(\frac{1}{3}K\right) * \dot{\sigma}_{kk} \qquad (2.21)$$

Where G = shear modulus

K = bulk modulus

e = deviatoric strain

S_{ij} = deviatoric stress.

Since plastic strain is active when the applied stress exceeds yield stress, Huang applied Perzyna's (1966) theory of viscoplasticity to account for applied total strain through the following equation:

$$\dot{e} = \frac{\dot{\sigma}}{E} + \dot{\gamma} < \Phi\left[\frac{\sigma}{\Phi(e^p)} - 1\right] >$$ (2.22)

$$\sigma = \Phi(e^p)\left\{1 + \Phi^{-1}\left(\frac{\dot{e}^{vp}}{\dot{\gamma}}\right)\right\}$$ (2.23)

Where: $\sigma = \Phi(e^p)$ = static stress-strain relations

Φ is obtained from experimental data (dynamic loading test).

Huang (2000) extended the Melvern's (1951) relation to more general constitutive relations for isotropic work hardening and strain rate sensitive materials. He also used the linear Drucker-Prager model (as elasto plastic model) to define the yield criteria of granular paving materials in study. The linear Drucker-Prager model is expressed as:

$$F = t - p\tan\beta - d(w_p) = 0$$ (2.24)

$$t = \frac{q}{2}\left(1 + \frac{1}{k}\right) - \left\{\left(1 - \frac{1}{k}\right) * \left(\frac{r}{q}\right)^3\right\}$$ (2.25)

Where: p   = equivalent pressure stress

d(w_p)   = material parameter that includes plastic work hardening

q   = the Misses equivalent deviatoric stress

r   = third invariant of deviatoric stress

k   = yield stress ratio in triaxial tension to triaxial compression.

Huang employed a uniaxial compressive strength test at different strain levels to obtain the elastic properties of materials and the triaxial test with confining stress close to in-situ stresses to obtain the Drucker Prager parameters.

This model was validated using accelerated testing pavement sections constructed at the Louisiana accelerated loading facility (ALF). The sections had test lanes with 60m long by 3.6m wide with a 12m loading length. The wheel in ALF traveled in one direction at 16km/hr (10mph). The applied load was 44.5kN for the first 400,000 cycles, and then was increased to 45.7 kN after the 400,000[th] cycle, 65.0kN after the 500,000[th] cycle, and 75.0 kN after the 650,000[th] cycle and the loading history was obtained. Permanent deformation on the pavement was measured and compared to pavement sections simulated using ABAQUS software.

Huang (2001) performed 4 types of analysis using the ABAQUS finite element analysis. 2-D static analysis; and 3-D dynamic analysis using linear elastic material model; 3-D dynamic analysis using viscoplastic and elasto-plastic material model; and 3-D permanent deformation analysis using creep model. In order to simulate a moving load in a 3-D dynamic finite element analysis, a trapezoidal shaped load amplitude function was applied to each element (Figure 2.7). Segment AB approaching wheel, BC full wheel and CD representing departure. Each of segments AB and CD occupied ¼ of the total loading time. A step load was applied on the pavement surface over the equivalent amount of time to the number of passes of ALF loads.

From the analysis Huang (2000) concluded that a 2-D static analysis was not able to simulate dynamic nature of traffic loading and the corresponding responses. The 3-D dynamic analysis was able to predict strain responses that were close to field measurements. The rate dependent viscoplastic model incorporated into the 3-D dynamic analysis was able to predict the viscous and permanent strain characteristics of the asphalt concrete materials under the traffic loading. Huang (2000) suggested that, permanent deformation could be predicted through the application of a creep model and a load function that incorporated distributions of the actual wheel wander into the 3-D dynamic finite element procedure.

Figure 2.7 Load amplitude function

24
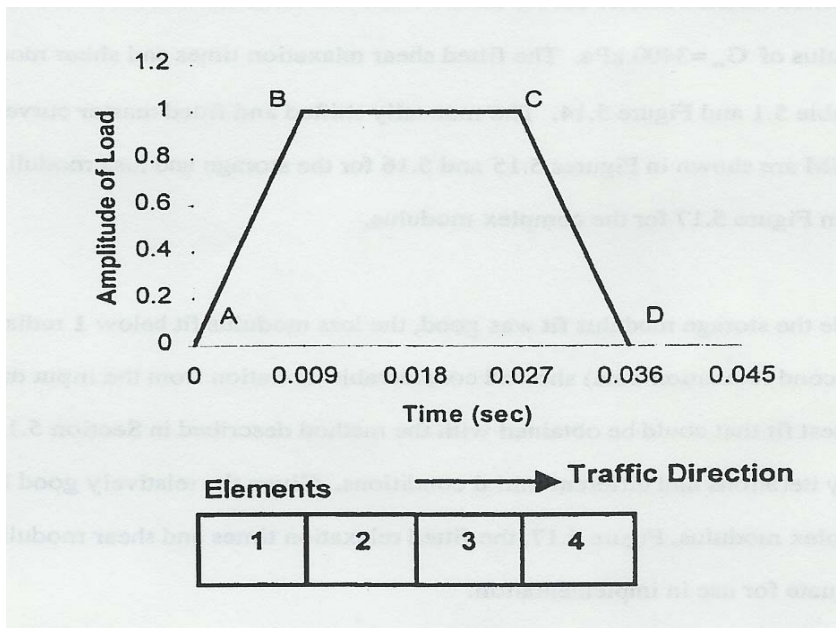
2.2.2.1 Laboratory Tests

      To characterize materials for this model the following laboratory tests were conducted:

(i)   Indirect Tensile Resilient Modulus (M_R) at 4ºC, 25ºC and 40ºC according to ASTM D4123, to measure elastic properties, (Resilient Modulus) (M_R) and Poisson's ratio.

(ii)   Uniaxial Compressive strength at different strain rates to obtain dynamic modulus and rate dependent (viscoplastic) parameters.

(iii)   Axial creep test in accordance to test method Tex-231-F (Texas DOT, 1993) to measure permanent deformation characteristics, creep compliance and power law parameters. The test was conducted at 40°C.

(iv)   Superpave Frequency Sweep at Constant Height (FSCH) test, according to AASHTO TP 7 in shear mode (strain controlled). A sinusoidal shear strain with peak amplitude of approximately 0.05μm/mm at 10 frequencies and 60°C was applied to obtain the complex shear modulus, G*, at a given frequency and the phase angle, δ.

(v)   Superpave Repetitive Shear at Constant Height (RSCH) was conducted as an optional test to estimate relative rut depth. The test was carried out to a duration of up to 5000 load cycles or until permanent strain of 5% is reached.

(vi)   Triaxial tension and triaxial compression to obtain the linear Drucker-Prager model parameters.

2.2.2.2 Advantages and limitations of the model

      According to Huang (2000), the developed model predicted dynamic strain and stress responses close to measured values. The model was also able to simulate the viscous and permanent strain characteristics of asphalt under traffic loading using 3-D finite element analysis. The model had the following limitations: The FE model did not show any significant difference on resistance to permanent deformation between large stone asphalt mixtures (LSAM) and conventional asphalt mix, while the laboratory experiments indicated that LSAM provides better resistance to permanent deformation compared to conventional asphalt mix. Permanent deformation prediction was not reported with respect to measured values. The comparisons made were mostly between LSAM and conventional DGAM using ABAQUS simulations rather than comparisons between predicted and measured values of each type of pavement analyzed. The model was not compared to field performance. No sensitivity analysis was carried out.

2.2.3 The non-linear viscoelastic constitutive model

Fenela Long (2001) developed a non-linear viscoelastic constitutive model that could be used in permanent deformation resistant mix design and analyses. The model uses shear deformation of material to model non-linear viscoelastic property of asphalt mix. The nonlinear viscoelastic constitutive equations consist of bulk (volumetric) component and shear component. Long (2001) used finite element analysis program (FEAP) to model the viscoelastic property of asphalt concrete using Maxwell elements with springs and dashpots connected in series. Any number of Maxwell elements can be combined in parallel, with a free spring to form a viscoelastic model (Figure 2.8). The model comprises of volumetric (bulk) and deviatoric (shear) components of non-linear viscoelastic strains. Long developed volumetric and deviatoric algorithms that can be used to obtain the non linear viscoelastic properties of materials.

Figure 2.8 One-dimensional representation of linear viscoelastic material
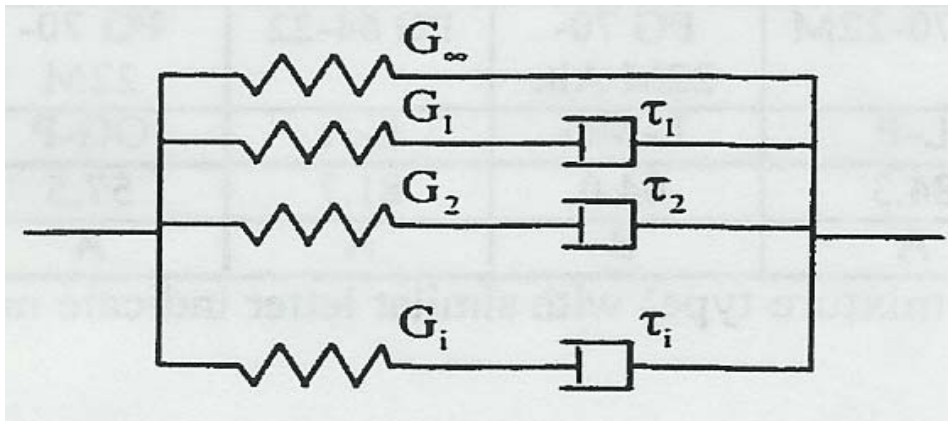
2.2.3.1 Algorithm for Volumetric (Bulk) Component

The algorithm for the bulk component of the non linear viscoelastic model was determined from the time continuous constitution equations and the bulk stress is given as [Long 2001]:

$$p(t_{n+1}) = K_\infty \theta(t_{n+1}) + \sum_{i=1}^{n} K_i q(t_{n+1})_i \qquad (2.26)$$

26

$$q(t_{n+1}) = e^{\frac{\Delta X}{\lambda_i}} g(t_n)_i + \Delta\theta \left(\frac{\lambda_i}{\Delta X}\right)\left(1 - e^{\frac{\Delta X}{\lambda_i}}\right)$$ (2.27)

Where: $p(t_{n+1})$ = Bulk stress

K_∞ and K_i = Bulk moduli of free spring and ith Maxwell element

$\theta(t_{n+1})$ = trace of strain tr($\varepsilon(t_{n+1})$)

n = number of Maxwell elements

$q(t_{n+1})$ = history term of Maxwell ith element evaluated at time t_{n+1}

$q(t_n)$ = history evaluated at the beginning of the time step for the ith Maxwell element

λ_i = corresponding relaxation time

$\Delta\theta$ = change in the bulk step in the time step and

ΔX = change in the reduced time.

$$\Delta X = \frac{\Delta t}{2}\left[\frac{1}{a_T(T(t_{n+1}))} + \frac{1}{a_T(T(t_n))}\right]$$ (2.28)

$$a_T = 10^{\left[\frac{C_{T1}(T-T_{ref})}{C_{T2}+T+T_{ref}}\right]}$$ (2.29)

Δt = change in time

a_T = temperature shift factor calculated at the beginning and end of the time step

C_{T1} and C_{T2} = are constants

T = Temperature at applicable time, and

T_{ref} = reference temperature.

2.2.3.2 Algorithm for Deviatoric (Shear) Component

Long (2001) developed the algorithm for the deviatoric component in the same manner as the bulk component, with additional inclusion of the vertical shift factor and modified horizontal shift factors. The deviatoric (shear) stress at the end of the time step, $s(_{n+1})$ is computed from equation (2.30) below:

$$s(t_{n+1}) = h(t_{n+1})_\infty + \sum_{i=1}^{m} h(t_{n+1})_i$$ (2.30)

In this equation, $h(t_{n+1})_i$ and $h(t_{n+1})_\infty$ are the tensorial history terms for the free spring and the ith Maxwell elements respectively. These history terms are calculated with equations (3.30) and (3.31).

27

$$h(t_{n+1})_\infty = e^{\frac{\Delta\xi}{\tau_i}} h(t_n)_\infty + 2G_\infty \left(\frac{e(t_{n+1})}{a_v(t_n)} - \frac{e_n(t_n)}{a_v(t_{n-1})} \right) \tag{2.31}$$

$$h(t_{n+1})_i = e^{\frac{\Delta\xi}{\tau_i}} h(t_n)_i + 2G_i \left(\frac{e(t_{n+1})}{a_v(t_n)} - \frac{e_n(t_n)}{a_v(t_{n-1})} \right) \left(\frac{\tau_i}{\Delta\xi} \right) \left(1 - e^{\frac{\Delta\xi}{\tau_i}} \right) \tag{2.32}$$

Where:

$h(t_n)_\infty$ and $h(t_n)_i$ = history terms at the beginning of the time step

τ_i = relaxation times

e_n and e_{n+1} = deviatoric strain at the beginning and end of the time step

$a_v(t_n)$ and $a_v(t_{n-1})$ = vertical shift factors evaluated at time t_n and t_{n-1} respectively

G_∞ and G_i = Shear relaxation modulus of free and i^{th} Maxwell element springs

The history term $h(t_n)_i$ was assumed to be equal to zero in the first time step. The change in the time step $\Delta\xi$ is defined in equation (2.33)

$$\Delta\xi = \Delta t \left(\frac{1}{a_H(t_n)} + \frac{1}{a_H(t_{n-1})} \right) \tag{2.33}$$

Δt = t_{n+1} - t_n

$a_H(t_n)$ = horizontal shift factor at the beginning of the time step, and

$a_H(t_{n-1})$ = horizontal shift factor at the beginning of the previous time step, and

The horizontal and vertical shift factors are as given in equations (2.34) and (2.35)

$$a_H = 10^{C_{H1}+C_{H2}(T-T_{ref})+C_{H3}\left(\log\frac{10^{-6}+\alpha}{10^{-6}+\|e_{ref}\|}\right)+C_{H4}(T-T_{ref})\left(\log\frac{10^{-6}+\alpha}{10^{-6}+\|e_{ref}\|}\right)} \tag{2.34}$$

$$a_V = 10^{C_{V1}+C_{V2}\left(\log\frac{10^{-6}+\alpha}{10^{-6}+\|e_{ref}\|}\right)+C_{V3}(T-T_{ref})\left(\log\frac{10^{-6}+\alpha}{10^{-6}+\|e_{ref}\|}\right)} \tag{2.35}$$

Where:

C_{H1} to C_{H4} and C_{V1} to C_{V3} are constants

T = temperature at time t_n

T_{ref} = reference temperature

$\|e_{ref}\|$ = reference deviatoric strain norm and

α = maximum strain at the beginning of the step as shown below

$$\alpha = \max\|e(s_n)\| \tag{2.36}$$

The temperature is typically maintained constant during simulations of pavement thus the use of the temperature at the beginning of the time step rather than the current temperature has no effect on the solution.

Using the deviatoric stress $s_{(t_{n+1})}$ and volumetric stress $p(t_{n+1})$, the stress $\sigma(t_{n+1})$ is calculated using equation (2.37).

$$\sigma(t_{n+1}) = p(t_{n+1})\mathbf{1} + s(t_{n+1}) \tag{2.37}$$

Where:

$p(t_{n+1})$ = volumetric stress (hydrostatic pressure)

$s(t_{n+1})$ = deviatoric stress and

$\mathbf{1}$ = the second rank identity.

2.2.3.3 Material Properties

Long (2001) used simple shear frequency sweep test at constant height to determine the viscoelastic shear properties of asphalt concrete. The test was conducted at five temperatures (20, 30, 40, 50, and 57°C) and seven strain levels (0.0001, 0.0005, 0.001, 0.005, 0.01, 0.015, 0.02). From the test results, the shear stress (σ^o), shear strain (γ^o), the magnitude of complex shear modulus $|G^*|$ and shear phase angle (δ) were obtained for each frequency (0.01, 0.02, 0.05, 0.1, 0.2, 0.5, 1, 2, 5, 10 Hz). ATS software, which performs Fourier series, was used to obtain the laboratory data. The values of storage (G') and loss (G") moduli were computed from the data using equations (2.38) and (2.39). It was observed that the moduli were affected by both the temperature and frequency, which is typical for viscoelastic materials.

$$G' = \frac{\sigma^o}{\varepsilon^o}\cos(\delta) \tag{2.38}$$

$$G'' = \frac{\sigma^o}{\gamma^o}\sin(\delta) \tag{2.39}$$

The curves of loss modulus against frequency and storage modulus against frequency were plotted for each temperature at all strain levels. The data obtained was reduced to a reference curve specific to each mix using vertical and horizontal shift factors. Long (2001) used a reference temperature of 40°C and reference strain of 0.1 percent. Equations (3.33) and (3.34) were used to calculate the horizontal and vertical shift factors respectively, where the constants used for DGAC are:

C_{H1}	=	0.460195		C_{V1}	=	0.085866
C_{H2}	=	-0.098896		C_{V2}	=	0.584795
C_{H3}	=	0.473146		C_{V3}	=	0.009665
C_{H4}	=	0.018655				

Long, (2000) used super-positioning of master curves technique which is widely used for many viscoelastic material [Long 2001]. Shifting a master curve by super-positioning expands the master curve to include parts of the frequency range where it is not physically possible to perform a test. Therefore, testing can be performed in a temperature range which is easy to test, then curves can be shifted to a higher or a lower temperature where testing is difficult. The time-temperature super-positioning is performed by shifting horizontally along the frequency axis (Figures 2.9) and the vertical shifting, along the modulus axis includes the dependency on strain level (Figure 2.10). The figures below show curves that were shifted horizontally and vertically respectively [Long, 2000].

Figure 2.9 Horizontal shifting for temperature at 40°C reference temperature (Long 2000)
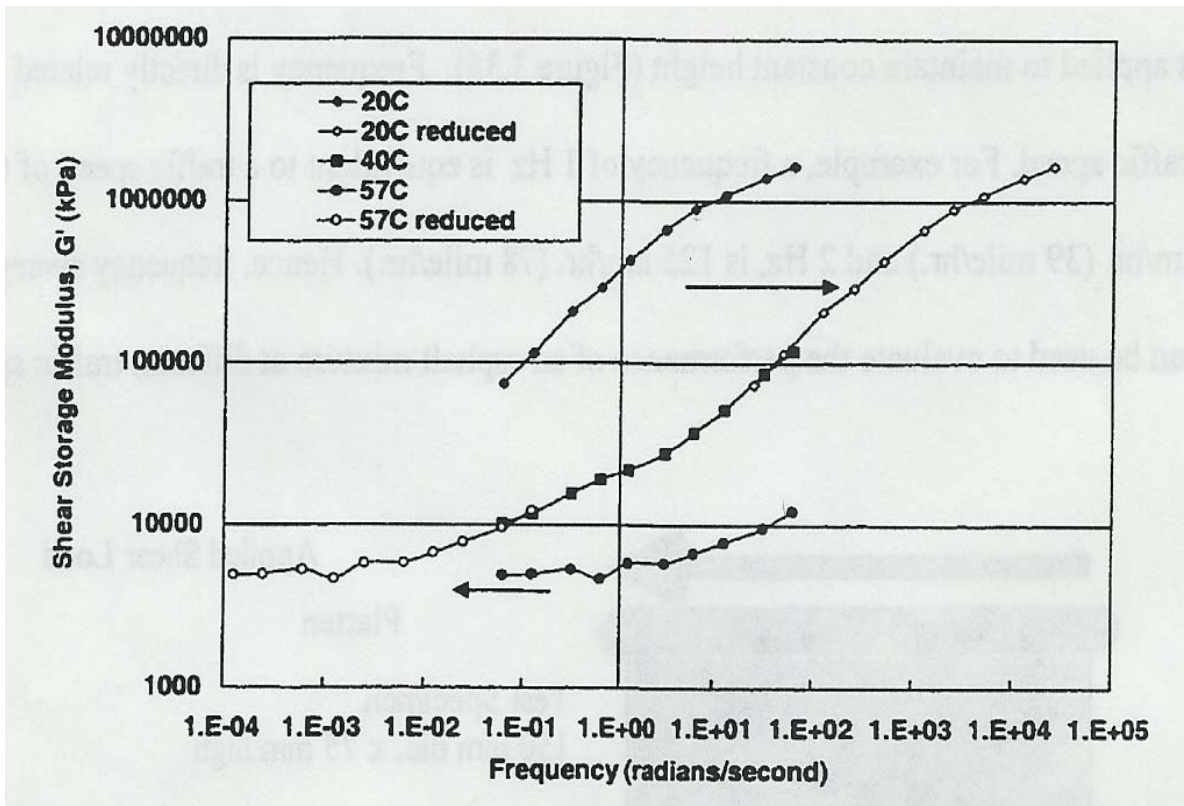
From the shifted curves, a master curves of laboratory data was obtained from which viscoelastic material properties were extracted [Long, 2001]. The relaxation modulus was then derived from the storage and loss moduli master curves. This is because it is difficult to obtain relaxation modulus from testing.

Figure 2.10 Vertical shifting for strain at 40°C and reference strain on 0.1% (Long 2000)
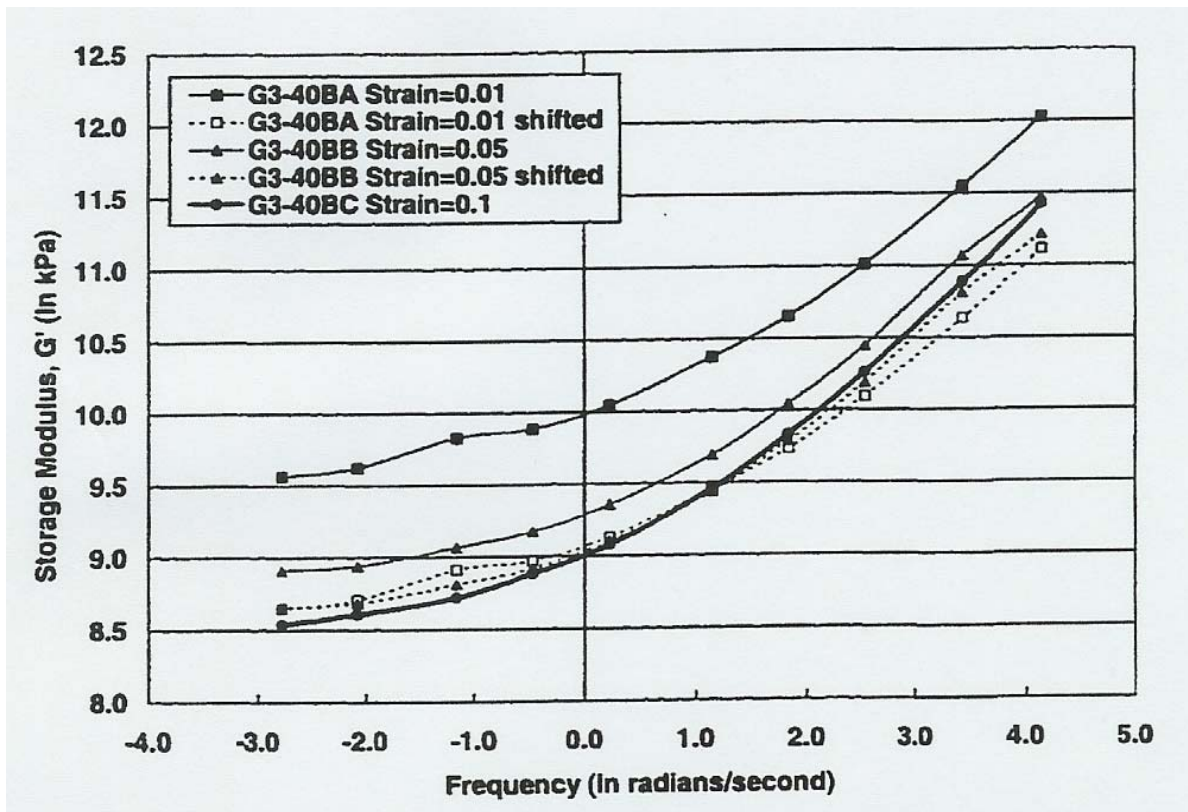
A repetitive shear test at constant height using hollow cylinders was used to obtain volumetric properties of asphalt concrete, dynamic Young's modulus ($|E^*|$), dynamic shear modulus ($|G^*|$), dynamic Poison's ration (υ). These parameters could be obtained from a different test. The laboratory results indicated that the mix behavior depends on both strain level and temperature [Long 2000].

Long (2001) used this model to compare the performance of dense graded asphalt mix (DGAC) and gap graded asphalt mix modified with asphalt rubber (ARHM). The majority of the

tests were performed in the DGAC overlay but few tests were performed on the ARHM material to evaluate the model's applicability to modified binders.

The model was validated using a repeated load simple shear test at constant height (RSCH) and heavy vehicle simulator (HVS), which were simulated using Finite Element Analysis Program (FEAP). The model showed good correlation for the RSCH simulation and laboratory test. The HVS did not correlate very well, the 2-D simulation over predicted permanent deformation while the 3-D simulation under predicted it. Finally the applied load for a 2-D simulation was reduced and used for prediction in order to get permanent deformation closer to measured values [Long, 2001].

2.2.3.4 Laboratory tests

The laboratory tests carried out for material characterization of this model include:

1. Frequency sweep at constant height FSCH (AASHOT TP 7-00) controlled strain, sine wave, 7 strain levels (0.1, 0.2, 0.5, 1.0, 2.0, 5.0), five temperatures (20, 30, 40, 50, 57°C) and 9 frequencies (5, 2, 1, 0.5, 0.2, 0.1, 0.05, 0.02, 0.01 Hz). The test was performed to measure Shear modulus parameters |G*|, G', G" and δ. The Shear Storage (G') and loss (G") moduli were used to obtain relaxation modulus and reduced time using equations:

$$G' = G_{\infty} + \sum_{i=1}^{m} G_i \frac{(w\tau_i)^2}{1+(w\tau_i)^2} \qquad (2.40)$$

$$G' = \sum_{i=1}^{m} G_i \frac{w\tau_i}{1+(w\tau_i)^2} \qquad (2.41)$$

Where: τ_i = relaxation time

w = frequency in rad/sec

G_i = relaxation modulus.

2. The repetitive shear at constant height (RSCH) test was used for model simulation.
3. Axial & shear freq. sweep using hollow cylinder frequencies with (5, 2, 1, 0.5, 0.2, 0.1, 0.05, 0.02, 0.01 Hz). The test was used to obtain dynamic modulus |E*|, dynamic shear modulus |G*|, dynamic Poisson's ratio, (ν) Bulk modulus (K) is then calculated from E, G* and ν with the formula K* = 2G*(1+ν)/(3.(1-2ν) or K* = E*/3(1-2ν).

Long (2001) observed that at high temperature, 40°C the relationships above becomes non-linear and the conventions to obtain bulk modulus becomes less valid.

2.2.3.5 Advantages and limitations of the model

This is a non-linear viscoelastic model, which predicts permanent deformation in asphalt pavements. It has an advantage that few tests are used for material characterization, but the axial and shear frequency sweep tests, on hollow cylinders is complicated and hard to perform as a daily quality control, QC, test. The model has a number of limitations:

- It cannot take into consideration densification of the mix and effect of air voids since shear strains were considered as the sole contributor to permanent deformation of asphalt mixtures [Long, 2000]. However, previous studies indicate that mix densification contribute with about 10% to the development of permanent deformation, the remaining 90% is caused by the shear movement of the material.

- Long (2001) simulated a 2-D model with reduced load values (lower values than actual values used in field) to predict permanent deformation of asphalt material using a heavy vehicle simulation (HVS). Many researchers recommend 3-D simulation for good permanent deformation prediction [SHRP, 1993; SHRP, 1994a; Huang, 2001; Wu, 2001, Park 2004].

- The asphalt rubber hot mix did not correlate at all; the predicted values were too small compared to the performance of the measured values [Long, 2004].

2.2.4   Viscoplastic Permanent Deformation Prediction Model

Zhao (2002) developed a viscoplastic model to predict the response of asphalt mixtures subjected to compression loading. The model encompasses elastic, plastic viscoelastic and viscoplastic strain components of asphalt concrete behavior and the effect of the test conditions. Each component is modeled separately, the sub-models are then integrated to obtain the final viscoelastoplastic model. The viscoelastic strain that includes elastic strain component is modeled based on Schapery's continuum damage theory and work potential theory. Uzan's strain hardening model forms the basis of the viscoplastic model that also includes the plastic strain component.

The model also uses the extended correspondence principle (Schapery, 1984), which was applied for asphalt concrete model development by Kim and Little (1990). The correspondence

principle transforms viscoelastic analysis to an elastic case by replacing physical strains with pseudostrains (Figure 3.5). The asphalt concrete damage model used a time dependent damage parameter, which is based on micro-growth parameter based on the micro crack-growth law [Zhao, 2002].

The developed model satisfactorily predicted the hysteretic behavior of sand-asphalt under cyclic loading. Zhao (2002) describes the stress strain relationship for non-aging linear viscoelastic material as follows:

$$\sigma_{ij} = \int C_{ijkl}\,(t-\tau)\,\{(d\varepsilon_{kl})/d\tau\}\,d\tau \tag{2.42}$$

$$\varepsilon_{ij} = \int S_{ijkl}\,(t-\tau)\,\{(d\sigma_{kl}/d\tau)\}\,d\tau \tag{2.43}$$

C_{ijkl} = relaxation modulus matrix   and S_{ijkl} = creep modulus matrix

C and S are mechanical properties of the viscoelastic material.

Considering the uniaxial loading test condition, the above equation can be reduced to:

$$\sigma = \int E\,(t-\tau)\,(d\varepsilon/d\tau)\,d\tau \tag{2.44}$$

$$\varepsilon = \int D\,(t-\tau)\,(d\sigma/d\tau)\,d\tau \tag{2.45}$$

$E(t)$ = relaxation modulus

$D(t)$ = Creep compliance

Zhao used a constant head rate (or constant displacement rate) compression test to validate time-temperature superposition principle for asphalt concrete with growing damage and viscoelastic plastic strain in compressive state. Zhao found out that the superposition principle is valid, thus shift factors obtained within the linear viscoelastic range (about 70 micro-strains, when the applied stress is directly proportion to pseudo strains (i.e. $\sigma = E_R * \varepsilon^R$) and there is no permanent damage to asphalt concrete), can be used for predicting material behavior at any strain level, where E_R is Young's modulus and ε^R is pseudo strains. Zhao (2002) also used a correspondence principle to mathematically transform the viscoelastic problem to elastic problem (physical strains to pseudo strains).

Figure 2.11   (a) Stress-strain behavior for mixture under LVE cyclic loading
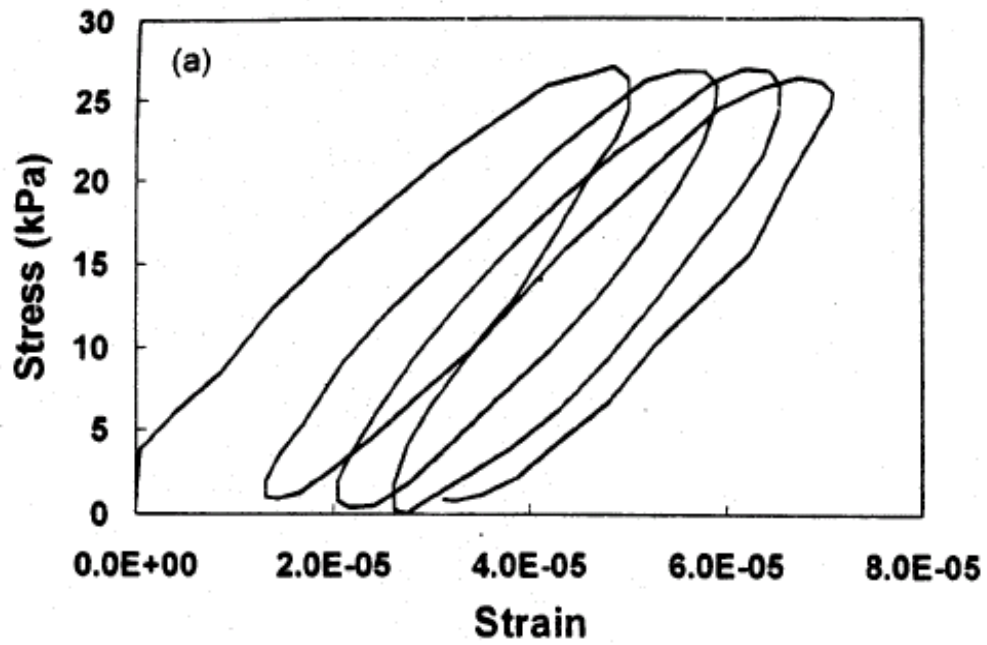
(b) Stress-pseudo strain behavior for same data
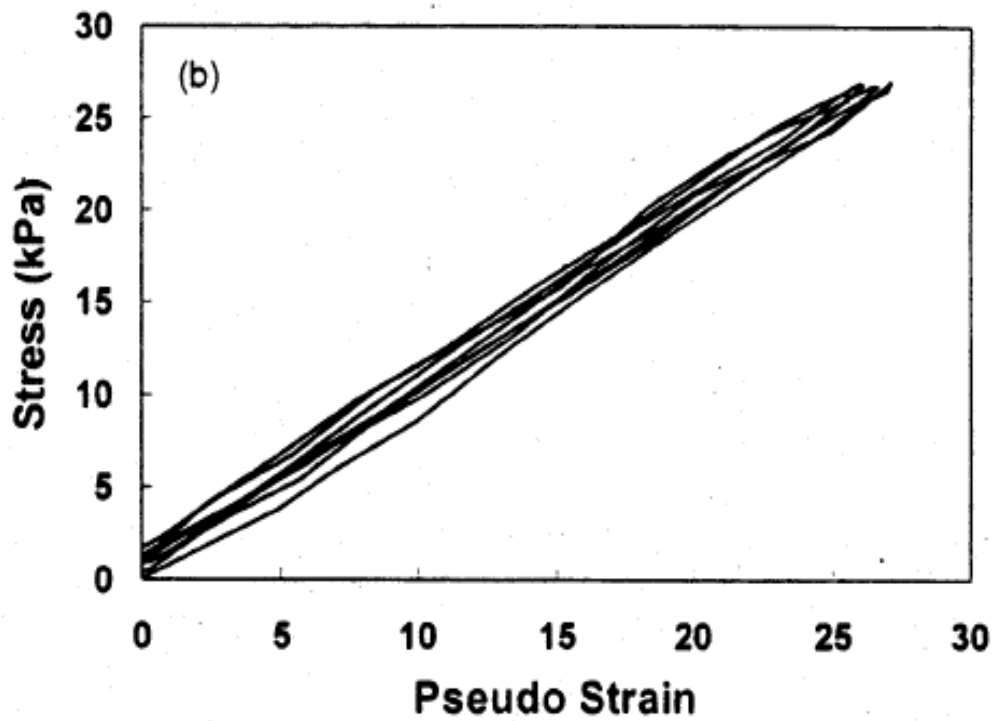
Figure 2.11 presents a typical stress strain behavior in a cyclic loading test under controlled stress mode. The pseudostrains were used to convert the problem into linear relationship Figure 2.11b. With the use of pseudostrains all the cycles collapse to a single straight line with a slope of 1.0 ($E_R = 1.0$). The pseudo strains accounts for viscoelasticity of material and makes is possible to separate the hysteretic behavior due to viscoelastic damage.

2.2.4.1 Viscoelastic Model

Zhao (2002) used Schapery's (1978) continuum damage theory, which was successfully applied by Kim (1990) to model viscoelastic strains in asphalt concrete. Kim utilized elastic - viscoelastic correspondence principle to separate time-dependent behavior from damage due to loading. The Uniaxial constitutive model developed by Kim is based on damage parameter S as given in the following constitutive equation:

$$\dot{S} = \left(\frac{\partial W^R}{\partial S} \right)^{\alpha} \qquad (2.46)$$

$$W^R = \frac{I}{2} C(S)(\varepsilon^R)^2 \qquad (2.47)$$

Where: $\dot{S}$ = damage evolution rate

W^R = Pseudostrain energy density function

C = normalized pseudostiffness = $\dfrac{S^R}{I}$

S^R = pseudostiffness = stress divided by pseudostrains = $\dfrac{\sigma}{\varepsilon^R}$

I = Initial pseudostiffness

α = material constant (Zhao used α = 1/n, where n is the slope of linear viscoelastic response function plotted as a function of time in a logarithmic scale).

Kim and Little replaced the damage parameter S with S* for a moderate extent damage. The damage parameter S* is a Lebesgue norm of the pseudostrain:

$$S* = \left(\int_0^{\xi} \left| \varepsilon^R \right|^{2\alpha} d\xi \right)^{\frac{1}{2\alpha}} \qquad (2.48)$$

Where ξ is the reduced time.

The viscoelastic strain is computed from the inverse of the convolution integral:

$$\varepsilon_{ve} = E_R \int_0^\xi D(\xi - \xi') \frac{d\left(\dfrac{\sigma}{C(S^*)}\right)}{d\xi'} d\xi' \qquad (2.49)$$

Where ε_{ve} = viscoelastic strain

ξ = reduced time

$D(\xi)$ = creep compliance

E_R = reference modulus

ξ' = integration variable.

To develop a viscoelastic prediction model, Zhao (2002) followed the procedure below:

1. Obtain the viscoelastic response functions (the complex modulus, relaxation modulus, and creep compliance) by performing small-strain triaxial complex modulus tests at several temperatures and frequencies. Construct the master curves for the response functions and determine the shift factors and n for the calculation of α.

2. Conduct constant crosshead rate (monotonic) tests at test conditions where the viscoplastic strain is minimal (when the applied stress is directly proportion to pseudo strains (i.e. $\sigma = E_{R*}\varepsilon^R$) and there is no permanent damage to asphalt concrete, about 70 micro-strains). Calculate pseudostrain, normalized pseudostiffness C, S*, and the Lebesgue norm of stress from the test results.

3. Determine the C vs. S* relationship by performing curve fitting.

4. Determine the characteristic relationship between S* and the Lebesgue norm of stress.

5. Knowing the S* vs. Lebesgue norm of stress and C vs. S* relationships, solve the viscoelastic strain using Equation (2.49) through numerical integral for the given stress and time.

The viscoelastic model was validated by predicting strains from the constant crosshead test (constant displacement rate compression test). The predicted viscoelastic strains and actual strains from the constant crosshead tests at $5^{o}C$ and $0.0001\varepsilon/sec$ had an excellent match. At $55^{o}C$ and $0.045\varepsilon/sec$ the prediction is not as close; measured viscoelastic strains are more than predicted strains because the viscoplastic strains are more significant [Zhao, 2002].

2.2.4.2 Viscoplastic model

The viscoplastic strain for uniaxial loading is assumed to follow a strain-hardening model by Uzan et.al (1985), which is of the form:

$$\dot{\varepsilon}_{vp} = \left(\frac{p+1}{D}\right)^{\frac{1}{p+1}} \left(\int_0^t \sigma^q dt\right)^{\frac{1}{p+1}} \tag{2.50}$$

was reduced to $\dot{\varepsilon}_{vp} = \left(\frac{p+1}{D}\right)^{\frac{1}{p+1}} \left(\sum \sigma_i^q \Delta t_i\right)^{\frac{1}{p+1}}$ (2.51)

Where: $\dot{\varepsilon}_{vp}$ = Viscoplastic strain rate

p, q, and D = material constants and

σ_i = strain amplitude for each cycle

Δt_i = loading time for each cycle.

Two types of repeated creep and recovery tests were performed to calibrate the viscoplastic material parameters. First type of the test (S4) applied multiple cycles of square stress pulses that varied in duration with single stress amplitude (Table 3.2). The second type of test (S5) applied multiple cycles of square pulses that varied in stress level with a constant duration (Table 3.2). These tests were conducted at t temperature of 40^oC. The model coefficients p, q, and D were determined simultaneously using nonlinear regression on test data from all S4 and S5 tests. Zhao used this method to obtain optimum parameters as p = 0.864, q = 1.974 and D = 1.42E12. When used to predict viscoplastic strains, the model performed well and the predicted viscoplastic strain were close to measured viscoplastic strains.

Table 2.1 S4 testing Parameters

Cycle	Stress (kPa)	Loading time (sec)	Recovery Time (Sec)
1	475	2	500
2	475	4	800
3	475	8	1000
4	475	16	1200
5	475	32	1400
6	475	64	1600
7	475	128	1800
8	475	256	2200
9	475	512	2600

Table 2.2 S5 testing Parameters

Cycle	Stress (kPa)	Loading time (sec)	Recovery Time (Sec)
1	42	450	1500
2	85	450	1700
3	170	450	1900
4	340	450	2100
5	510	450	2300
6	680	450	2500
7	850	450	2700
8	1020	450	2900

2.2.4.3 The Visco-elasto-plastic Model

The viscoelastic and viscoplastic models were developed separately and combined the sub models to obtain the viscoelastoplastic model as shown below:

$$\varepsilon_{vp} = E_R \int_0^\xi D(\xi - \xi') \frac{d\left(\dfrac{\sigma}{C(S^*)}\right)}{d\xi'} d\xi' + \left(\frac{p+1}{D}\right)^{\frac{1}{p+1}} \left(\int_0^\xi \sigma^q d\xi\right)^{\frac{1}{p+1}} \tag{2.52}$$

For this model, stress (σ), reduced time (ξ) and calibrated materials properties are the required inputs to obtain the Visco-elasto-plastic strains.

According to Zhao (2002), the viscoelastoplastic model predicts material responses well up to the peak (yield) stress. Predictions beyond peak stress are not accurate especially at high temperatures. Zhao attributes the inaccurate predictions to the viscoelastic model, which is based on continuum damage theory. When material fails, after peak stress, micro-cracks develop in the material. The viscoelastic model does not capture the development of micro-cracks beyond the peak stress region. This is why its predicted strains are lower that measured strains. A suitable theory may be needed to model material behavior in the post peak region. The model also used for calibration and validation a uniaxial stress state only. More research is needed to extend the model to multi axial loading conditions, including effect of confining.

2.2.4.4 Laboratory Tests

The following tests were performed to obtain material properties of asphalt concrete:

1. Frequency sweep complex modulus at 5 temp (5, 15, 25, 40, and 55°C) and 6 freq (20, 10, 3, 1, 0.3, 0.1 Hz). The test was conducted to obtain dynamic modulus |E*|, complex mod. E* with storage E' and loss E'' moduli and phase angle φ.

2. Triaxial repetitive permanent deformation characterization, to obtain flow point parameters a, b, α, and μ. Haversine load was applied with 0.1 loading and 0.9 rest periods at 55°C and 20psi confining pressure.

3. Repeated creep and recovery test constant stress loading (790kPa) and 3 temps (25, 40, 55°C) to obtain the creep compliance (D).

4. Static creep to obtain creep compliance (D).

5. Constant crosshead compression test (monotonic or constant displacement rate test) at minimum strain to obtain pseudostrain, normalized pseudostiffness C, S and the Lebesgue norm of stress S* from the test results.

2.2.4.5 Advantages and limitations of the model

This model uses a correspondence principle, continuum damage model, work potential theory, and Uzan hardening model. The model predicts strains well up to the peak values, the predicted and measured values to the peak values are close. The model has the following limitations:

- Predictions beyond peak stress are not accurate especially at high temp. The viscoelastic continuum model used is not good for prediction after peak stress.

- Model validation and calibration was conducted using uniaxial stress state only.

- Effect of confinement is not considered. Same testing protocols could be repeated at different confining pressures to study the validity of the model.

- Only one asphalt mixture was tested.

- The model was not verified with any field measurement such as accelerated testing.

2.2.5 Micro-structural Viscoplastic Continuum Model

Park (2004) developed a mechanistic elastic-viscoplastic continuum model to simulate permanent deformation of asphalt mixtures. The model uses Drucker-Prager yield function to describe the behavior of asphalt mixtures. The Drucker-Prager yield function can be looked upon as an extension of the von Misses yield function for pressure dependent materials such as soil, asphalt mixtures and concrete [Park 2004; Chen and Mizno 1990]. The Drucker-Prager yield function is in the following form $F = \sqrt{J_2} - \alpha I_1 - \kappa$. (2.53)

Where J_2 = Second invariant of the deviator stress tensor ($= {}^3\!/_2 S_{ij} S_{ij}$),

I_1 = First invariant of stress tensor ($= \sigma_{ij}/3$), and

α and κ are material constants (Figure 2.12)

Figure 2.12 shows the yield surface and flow direction for the Drucker-Prager model.

Figure 2.12 Drucker-Prager yield surface and flow direction Park 2004
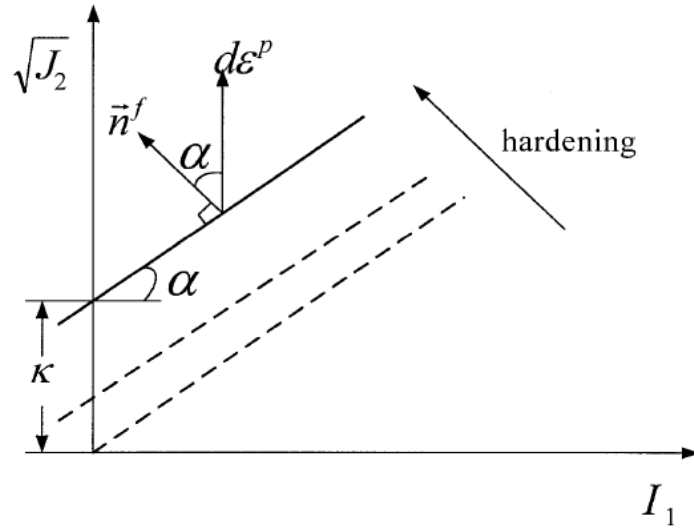
The elastic-viscoplastic formulation consists of hardening law, which determines the magnitude of viscoplastic strain rate and flow potential which gives the direction of viscoplastic strain rate vector. By the theoretical assumption of the hardening law, elastic viscoplastic theory is classified into yield surface function and overstress function [Park, 2004; Perzyna 1966]. The yield surface function employs the yield function that is dynamic loading function explicitly including the time variable that is a function of time. The overstress function is used to find the relationship between the static yield function and dynamic yield function. Park's model used the power function defined by Perzyna (1966) as follows, where n is material constant

$$\varphi(F) = F^n \tag{2.54}$$

For an elastic-visco-plastic body, a strain tensor can be represented as follows [Park, 2004]

$$\varepsilon_{ij} = \varepsilon_{ij}^e + \varepsilon_{ij}^{vp} \tag{2.55}$$

Where: ε_{ij}^e = elastic strain tensor, and

ε_{ij}^{vp} = viscoplastic tensor

Similarly, the strain rate tensor is represented in equation 3.55 where the over-dot denotes the time derivative.

$$\dot{\varepsilon}_{ij} = \dot{\varepsilon}_{ij}^e + \dot{\varepsilon}_{ij}^{vp} \tag{2.56}$$

The constitutive equation for elastic strain rate is given as

$$\dot{\varepsilon}_{ij}^{e} = \frac{1}{2\mu}\dot{s}_{ij} + \frac{1}{3K}\dot{\sigma}_{ij} \qquad\qquad (2.57)$$

Where μ = Shear modulus,

K = Bulk modulus,

$\dot{s}_{ij}$ = Deviator stress rate tensor, and

$\dot{\sigma}_{ij}$ = volumetric stress rate tensor.

The viscoplastic constitutive equation based on Drucker-Prager is obtained in terms of effective stress and effective strain rate as:

$$\bar{\dot{\varepsilon}}^{vp} = \gamma * \left(\frac{\bar{\sigma}}{a\bar{\varepsilon}^{vp^{b}}} - 1\right)^{n} \qquad\qquad (2.58)$$

Where $\gamma*$ = viscosity constant = $\gamma\chi$

γ = viscosity coefficient; $\chi = \left(\sqrt{\frac{1}{3}} - \bar{\alpha}\right)^{n-1}$ and $\bar{\alpha} = \frac{\alpha}{3}$

$\bar{\sigma}$ = effective stress = $\dfrac{\sqrt{J_2} - \bar{\alpha}I_1}{\sqrt{\frac{1}{3}} - \bar{\alpha}}$ $\qquad\qquad (2.59)$

J_2 = second invariant of the deviator stress tensor = $\dfrac{2}{3}S_{ij}S_{ij}$

I_1 = first invariant of the stress tensor = $\dfrac{\sigma_{ij}}{3}$

The hardening parameter κ is given by:

$$\kappa = a\bar{\varepsilon}^{vp^{b}} \qquad\qquad (2.60)$$

Where a and b are material constants and $\bar{\varepsilon}^{vp}$ is the effective viscoplastic strain.

Material parameters for the elastic viscoplastic constitutive model were obtained using uniaxial compressive strength tests at seven different strain rates. The elastic modulus (E) and Poissons ratio (ν) were determined from the uniaxial compression strength test. The hardening parameter, κ, was obtained as a function of viscoplastic strain, by assuming that the lowest strain rate (0.0001 sec^{-1}) is 0 sec^{-1}. Therefore, κ is the same as the effective yield stress at the smallest strain rate. The viscoplastic material properties, viscosity constant $\gamma*$ and exponent n were determined from the relationship between static and dynamic loading. The effective viscoplastic

strain rate $\bar{\dot{\varepsilon}}^{vp}$ was plotted against $\left(\dfrac{\bar{\sigma}}{a\bar{\varepsilon}^{vp^b}} - 1 \right)$ for each strain rate. The values of γ* and n were estimated from the best fit equation which produced the minimum least squares error.

The triaxial compression test was conducted at 4 different confining stress and minimum strain rate (0.0001 sec^{-1}) to obtain the Drucker-Prager yield function constant α. For the elastic viscoplastic model the material properties required include, elastic modulus E, Poisson's ratio ν, Drucker-Prager friction angle α, and constants γ* and n.

To verify the elastic-viscoplastic constitutive model, Park (2004) used the Simple Shear Test and Constant Height (SST-CH) test at 68.9 and 137.8kPa. Recoverable strains were assumed to be elastic. The recoverable elastic strains were calculated by subtracting the non-recoverable strains from the peak total strains. Park used the upper and lower limits of γ* and n, to predict shear strains, the predicted values bracketed the measured values of total shear strain.

Park (2004) used the ABAQUS FE program to simulate permanent deformation of asphalt mixtures. The elastic viscoplastic model was used for the asphalt concrete layer. Viscoplastic material properties γ* and n which produced greater value of permanent strain were used. Linear elasticity was assumed for the material properties of the base and subgrade layers. Park, (2002) used results from WesTrack test sections as measured values of permanent deformation, which were compared to values obtained form the prediction model. The trend of permanent deformation profiles was similar and the elastic-viscoplastic model, could be used to characterize permanent deformation of asphalt mixtures [Park 2004].

2.2.5.1 Laboratory Testing

Laboratory tests carried out by Park to be used in the constitutive model include:
1. Repeated load triaxial (dynamic modulus) test at three temperature (30, 40, and 50°C), and four confining pressure (0, 68.9, 137.9, 206.7 kPa), with loading cycles 0.1sec loading 0.9sec unloading for 10,000 cycles or specimen failure. Measured parameters include angle (α), cohesion (κ) Elastic modulus (E) and Poisson's ratio (ν) at each test temperature.

2. Uniaxial compressive strength test at 60°C, and seven strain rates (0.0001, 0.0002, 0.0042, 0.063, 0.017, 0.033 and 0.0702 sec) to measure elastic modulus |E*|, dynamic Poison's ratio (v), and permanent strain.

3. Repetitive Shear Test at constant height (RSCH) was conducted at 60 ± 3°C with 0.1s loading and 0.6s unloading up to 5000 cycles or 5% strain. Strains at 1%, 2% and 5% were noted. The test was used to obtain elastic and viscoplastic characteristics of materials and also to estimate rut depth.

2.2.5.2 Advantages and limitations of the model

This model uses Drucker-Prager yield function, linear Drucker-Prager model, a viscoplastic model using Perzyna's (1966) theory, and a 3-D FE analysis using ABAQUS software to predict permanent deformation in asphalt mixtures. The model is reported to predict close to the measured values. The plots of transverse rutting profiles of measured permanent deformation had similar trends to those from the prediction but the measured values were not very close. When a value of K (ratio of yield stress in triaxial tension to the yield stress in triaxial compression) = 0.78 was used, the predicted rut depth was higher than measured value. When K = 1 was used, the predicted rut depth was lower than measured values. The model predicts rut depth close to measured values but it is not accurate because damage parameters are not included in the model. The limitation to this model is that it cannot be used to predict tertiary permanent deformation because damage parameters are not considered and are required for tertiary permanent deformation prediction [Park, 2004].

2.2.6 Multi-criteria Visco-plasticity Model by Nguyen et. al.

Nguyen D.T., Nedjar B., Tamagny P, and de La Roche C. (2006) developed a continuum 3-D elasto-viscoplastic model under cyclic loading. The model is based on a double-criteria visco-plasticity model and focuses on coupling of Drucker-Prager type criterion with customized quadratic criterion. The kinematic hardening law is introduced following the continuum thermodynamics framework together with Koiter's evolution law of plasticity followed by an extension to visco-plasticity by using a Duvaut-Lions type formulation. The model is validated using experiment results from dynamic creep tests.

This is a multi-mechanism multi-criteria model which makes it capable to simulate cyclic responses while accounting for different behavior at the same time. The model uses complementary laws, i.e. total strain is classically decomposed into an elastic part and plastic part; $\varepsilon = \varepsilon^e + \varepsilon^p$ and $\sigma = C:\varepsilon^e = C:(\varepsilon - \varepsilon^p)$, where σ is Cauchy stress tensor and C denotes the elastic tensor. Linear kinematic hardening is introduced via the hardening stress tensor X; $X = H\alpha$. Where H is the kinematic hardening modulus and α is the corresponding conjugate internal variable.

The elastic domain of the model is defined by a group of yield functions. Drucker-Prager is used to define the elastic domain with two yield surfaces given by:

$$f_1(\sigma, X) = \sqrt{(q_1^2 + \alpha_1^2 \cdot (p + \beta\sigma_y)^2)} - \gamma \cdot \sigma_y \tag{2.61}$$

$$f_2(\sigma, X) = q_2 + \alpha_2 \cdot p - \sigma_y \tag{2.62}$$

$$q_i = \sqrt{(^3/_2 \cdot \text{dev}(\sigma - \delta_i \cdot X):\text{dev}(\sigma - \delta_i \cdot X))} \quad \text{and} \quad p = {}^1/_3 \cdot \text{tr}(\sigma) \tag{2.63}$$

Where q_i = the shear stress of the yield function i,

p = isotropic (confining) stress,

σ_y = the elastic limit of material and

$\alpha_1, \alpha_2, \beta$ and γ are model parameters.

Non-associated rule was selected for the model.

The model was extended from elasto-plastic to elasto-viscoplastic. At relatively high temperature, permanent strain of asphalt mixture is mainly contributed by viscoplastic deformation (including plastic component) and the contribution of time-dependent reversible strain is insignificant. The total strain is therefore assumed to comprise of an elastic and viscoplastic components, $\varepsilon = \varepsilon^e + \varepsilon^{vp}$. Perzyna type viscoplastic formulation was used:

$$\dot{\varepsilon}^{vp} = \left(\frac{<\phi(f)>}{\eta}\right)\left(\frac{\partial g}{\partial \sigma}\right) \tag{2.64}$$

Where: η = fluidity parameter establishing the rate of relative viscoplastic strain;

$\left(\dfrac{\partial g}{\partial \sigma}\right)$ = direction of evolution of viscoplastic strain;

$\varphi(f)$ = viscoplastic yield function;

$< >$ = Macauley bracket.

It was shown by Simo (1988) that as η approaches zero the model would not reduce to the corresponding rate independent formulation. The Duvault-Lions type formulation was chosen to be used in order to deduce the problem from the inviscid solution of time independent corresponding. The Duvault-Lions formulation is:

$$\dot{\varepsilon}^{vp} = \left(\frac{1}{\eta}\right) C^{-1} : [\sigma - \bar{\sigma}] \dot{\alpha} = \left(\frac{1}{\eta}\right) D^{-1} : [X - \bar{X}] \qquad (2.65)$$

Where: η = fluidity parameter;

C = elastic moduli

D = hardening moduli

$\bar{\sigma}$, $\bar{X}$ = inviscid solution of time dependent problem

The model was validated using laboratory results of dynamic creep test with cyclic loading. The model was tested at two pressures 0.4MPa and 0.2MPa. The results of prediction model and laboratory test are close.

To validate the model, Nguyen, et. al. (2006) used the simulation of cyclic loading tests on asphalt concrete cylindrical specimens. The test was conducted at 25°C, 10 Hz and two stress levels 0.2 MPa and 0.4MPa. The measured permanent strains are close to predicted permanent strains.

2.2.6.1 Advantages and limitations of the model

This model uses Drucker-Prager criterion with customized quadratic criterion, kinematic hardening law, continuum thermodynamics framework, Koiter's evolution law for plasticity and Duvaut-Lions type formulations. Material characterization tests are neither mentioned nor explained in the paper.

2.3   Full Scale Accelerated Pavement Testing

Accelerated pavement testing (APT) is defined by Hugo as the "controlled application of wheel loading to a layered pavement structure to determine pavement response and performance under controlled, accelerated accumulation of damage in a compressed time period" [Hugo 2006]. Hugo's definition of APT is more general when compared to that given by Metcalf (1996), which defines APT as a "controlled application of a prototype wheel loading, at or above the appropriate legal load limit to a prototype or actual, layered, structural pavement system to determine pavement response and performance under a controlled, accelerated, accumulation of damage in compressed time period" [Metcalf, 1996].

The APT facilities, although expensive, have proved to be important tools for improvement of performance and economics of pavements. They play an important role as research tools, since they can be used to improve design procedures, validate new and existing procedures, calibrate models, evaluate pavement performance and develop innovative theories in road research. APT has been used widely due to its capacity to test a pavement section to failure in a shortest possible time. The damage acceleration is induced by increasing the number of load repetitions, simulating severe weather conditions in APT, modifying loading conditions, and testing on sections with reduced structural capacity. The induced damage is monitored throughout the testing period in relation to traffic loading. The results obtained are used for designing, evaluating, validating and improving new and existing procedures.

Full-scale and accelerated pavement testing (FS/APT) began as early as 1909 with a test track in Detroit. By 1996, there were 35 APT facilities reported worldwide, of which 19 facilities were active [Metcalf, 1996]. In the NCHRP Synthesis 325 Hugo, et. al., (2004) reported 48 APT facilities world wide, 35 being in USA, others from Europe, China, Australia, South Africa and New Zealand. Out of the 48 APT facilities, 28 were reported to be active, 15 being in USA [Hugo, et. al., 2004].

Full scale APT facilities have unique features and different configuration. They are divided in three categories based on traffic loading or simulation:

- Test roads with controlled accelerated traffic;

- Test tracks with linear, circular or free form layout; and

- Other configurations with static or pulsed loading assembly.

2.3.1 Test Roads

Test roads are full scale, full size experimental pavement sections, subjected to actual heavy vehicles or actual traffic loading [Coetzee et al, 2000]. Performance results obtained from test roads are more realistic than those from other APT facilities because of the application of actual traffic loading and environmental conditions.

The use of test road research in USA started as early as 1920. Some of the major test roads include: a test road constructed in Plata, Maryland in 1941 by the Highway Research Board [Huang, 2004]. A concrete pavement section of 1.76 km (1.1 mi) long was constructed on US 301. The test road was about of 14.4 km (9 mi) south of Plata, Maryland. It comprised of four separate test section having two 12 ft lanes each, constructed on A-1 to A-7-6 soils subgrade. Controlled traffic loading was conducted from June to December 1950. Major findings from this research project were: increase in pavement cracking and settlement with increase in axle loads. Pumping effect, which occurred predominantly in plastic clay soils, was not observed in granular subgrade. Findings from this research contributed in the improvements on concrete pavement design methods. This research project was funded by eleven Midwestern and Eastern states.

The Western Association of State Highway Officials (WASHO) conducted a similar research project on asphalt pavements from 1952 to 1954. The test road comprised of two test loops each having 580 m (1900 ft) tangents made up of five 92 m (300 ft) test sections separated by 30 m (100 ft) transition sections. Different HMA mixture types and subbase materials were tested. Traffic loading of 18,000 lb (80 kN) and 22,400 lb (100 kN) single axles loads and 32,000

lb (142 kN) and 40,000 lb (178 kN) tandem axles were applied on the test road. Major findings include [Huang 2004]:

- Asphalt sections with same thickness but coarser aggregates performed better.

- Permanent deformation was caused by lateral displacement, not compression.

- Subgrade moisture contributed highly to pavement distress.

- Thicker asphalt pavement with 4-in HMA performed better than a 2-in HMA pavement.

- The outer wheel path was more distressed that inner wheel path.

- Deflection of pavement section under traffic loading was influenced by vehicle speed, temperature of surfacing, load and moisture content of the top layers of subgrade soil.

The American Association of State Highway and Transportation Officials (AASHTO) road test (1956 to 1960) was constructed with an objective to determine significant relationship between the number of repetition of specific axle loads of different magnitudes and arrangement and performance of different thickness of flexible and rigid pavements [Huang 2004; HRB, 1962]. The test road was constructed along I-80 near Ottawa, Illinois. The test section consisted of four large loops and two smaller loops. Each loop had four lane divided highway, whose parallel roadways or tangents were connected by a turnaround at each end. In all loops, the north tangents were surfaced with HMA and the south tangents with Portland Cement Concrete. The construction began in 1956. Until 1962, a total of 1,114,000 axle loads were applied. This was a $27 million project [Huang, 2004]. Major findings from this road test were development of:

- Pavement serviceability concept of both flexible and rigid pavements.

- Equivalent single axle load concept for converting damage induced to pavement structures by axles with different loads.

- A set of robust statistical relationships between pavement parameters, axle load configuration and number of load repetitions.

- 1973, 1983 and 1996 AASHTO pavement design guides, developed based on regression equations, which resulted from the data collected at the AASHO road test.

The Strategic Highway Research Program (SHRP) established long term pavement performance (LTPP) monitoring sites all over USA. The sites are used as test roads to collect pavement data from different settings of traffic loading and environmental conditions. LTPP program established a national pavement performance database, which is available to scientists and researchers.

The Pennsylvania Transportation Institute research facility designed and built a test road in 1970's, which was intended as a satellite to the AASHO Road test. The test road is 1.6 km (1.0 mi) loop on which four cycles of experiments were conducted, the last ending in 1983. Other test roads include: WesTrack in Nevada, Ohio test road which is 4.8 km (3 mi), and the National Centre for Asphalt Technology Pavement Test Track (NCAT-PTT) [Metcalf, 1996].

The WesTrack test road is an experimental road test facility constructed in Nevada under a contract awarded by the Federal Highway Administration (FHWA). The facility was constructed with two primary objectives:

1. To continue the development of performance-related specifications (PRS) for hot-mix asphalt construction by evaluating the impact on performance of deviations in materials and construction properties (e.g., asphalt content, air void content and aggregate gradation) from design values in a large scale accelerated field test.

2. To provide early field verification of the SHRP SUPERPAVE$_{(TM)}$ Level III mix design procedures.

The test road is oval shaped, 2.9 km (1.8 mi.) in length and has been used to construct, load, monitor, and evaluate the performance of 26 experimental hot-mix asphalt pavement sections. One of the subtasks on the project involves the use of autonomous (driverless) vehicle technology to achieve the desired 10 million, 80 kN (18-kip) equivalent single axle load applications. Four triple trailer combinations are operating on the track up to 22 hours per day, 7 days per week during the 2-year loading period [Hodges, 1999].

Ohio Department of transportation constructed a 4.8 km (3 mi) test road on US. Rt. 23, near Delaware. The test road encompasses four Specific Pavement Studies (SPS) formulated be Strategic Highway Research Program (SHRP) [Shanklin et. al., 2000].

SPS 1: Strategic Study of Structural Factors for Flexible Pavements,

SPS 2: Strategic Study of Structural Factors for Rigid Pavements,

SPS 8: Study of Environmental Effects in the Absence of Heavy Traffic, and

SPS 9: Asphalt Program Field Verification Studies

The construction of the test road was initiated in 1994. One of the early priorities was to provide a uniform subgrade for the forty, 500-foot long test sections included in the project and, thereby, permit a more direct comparison of section performance [ORITE-3, 1999].

The National Centre for Asphalt Technology Pavement Test Track (NCAT-PTT), in Alabama, was constructed with the main objective to study the rutting performance of different HMA mixes. Secondary objectives include pavement smoothness and friction over time and monitoring the fuel consumption of trucks. The track consists of forty six (46) 61-m (200-ft) long test sections Figure 2.13 and Figure 2.14. Out of these, thirty six (36) sections have the same HMA surface and binder course thickness and 10 sections have different thicknesses for the binder and the surface courses. All test sections have the same support structure consisting of a 305-mm (12-in.) improved roadbed, a 152-mm (6-in.) crushed granite stone base, and a 127-mm (5-in.) asphalt-treated drainage layer. The binder and surface courses vary according to the experiment requirements. The facility also includes a 436.6-m^2 (4,700-ft^2) testing laboratory, a 241.5-m^2 (2,600-ft^2) truck maintenance facility, and an asphalt plant. [Metcalf, 1996, Saeed et. al. 2003].

Figure 2.14 Aerial photo of NCAT-PTT [http://www.pavetrack.com/]

Figure 2.14 Test Track showing test sections [http://www.pavetrack.com/]
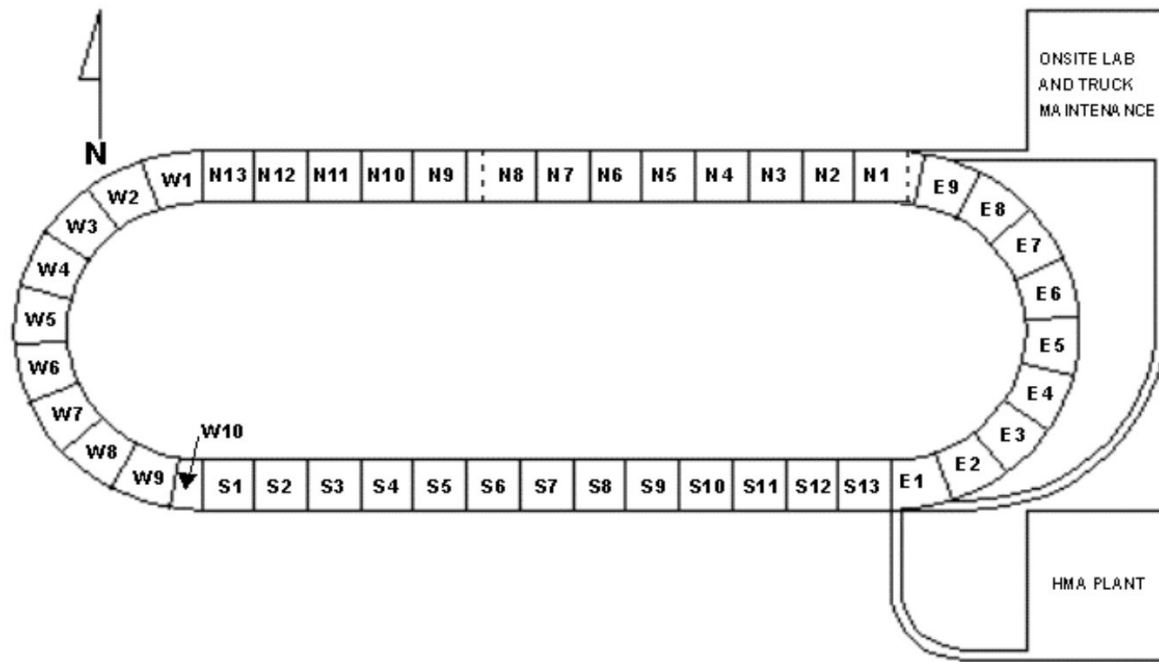
The most recent test roads in US is the Minnesota test road (Mn/Road), which started in 1993 [Metcalf, 1996]. This is an outdoor project consisting of two pavements; a 4,8 km (3 mi) 2-lane closed loop high volume traffic research and a 4 km (2.5 mi) 2-lane closed loop for low-volume traffic research. The loading of high traffic lanes is accomplished by diverting westbound traffic on Interstate route I-94 onto the test pavement. Approximately 14,000 vehicles, with 15% heavy trucks use the route daily. In the original configuration, the test road comprises of 14 asphalt concrete sections and 9 cement concrete sections with variety base course configurations. A weigh in motion scale is installed on I-94 to collect traffic data and configuration. The low volume loop comprise of 17 sections, which are trafficked by calibrated test trucks to form a controlled full scale accelerated loading experiment. Some sections were replaced with new pavement structures.

The sections are heavily instrumented with 17 different types of sensors totaling to 4572 sensors. The sensors include: soil pressure cells and strain gauges mounted horizontally and vertically at different levels in the pavement subgrade, moisture probes that measures moisture content, resistively probes for frozen zones and an open stand pipe that measures water tale and pore pressure cells that measures pore pressure [Metcalf, 1996].

2.3.2 Test Tracks

Test tracks are full-scale full size experimental pavement sections, subjected to specially designed mechanical traffic loading system [Coetzee et al, 2000]. Test tracks are either linear or circular with traffic loading applied as real wheels or simulated by plate loading. Circular tracks can be operated at high speed (60 mph) as compared to linear tracks [Metcalf, 1996]. Linear tracks have traffic limitations but have some advantages such as minimized lateral wheel loading. Each section is tested separately; therefore failure in one section cannot affect the loading of other sections [Metcalf, 1992].

The first test track in USA was constructed at the Public Works Department in Detroit, in 1909. The test track was simulated by horse and cart traffic. Other early test tracks include the "Road Machine" built in 1933 and rebuilt in 1963 at the British Road Research Laboratory. The University of Illinois original circular track that built in 1963. It had a mean radius of 0.8-m (2.6

54

ft) loaded by single axle wheel loads of 84 to 145 kN (11,000 to 17600 lb) at a speed of up to 24 kph (15mph). A study of permeable bases was conducted [Metcalf, 1996].

The Manège de Fatigue of the Laboratoire Central des Ponts et Chausées (LCPC), France (Figure 2.15 and Figure 2.16) is the largest circular track in operation [Metcalf, 1996]. The test track has four-arm rotating loading system, running two wheel assemblies, on an inner track and outer track. Axle loads ranging from 80 - 150 kN (17,600 - 33,000 lb) are simulated at test speed of 155 km/h (65 mph). It is possible to simulate tandem axle loads of up to 280 kN (61,522 lb). The first test was conducted in 1978 [Metcalf, 1996].

Figure 2.15 LPCP test track in France [www.gautrans-hvs.co.za]

Other circular test tracks are the university of Central Florida central track commissioned in 1988, Washington State University track; Shell laboratories in Amsterdam, Japan Highway Public Corporation (JHPC) test track, Centerbury facility in New Zealand and Dubendorf test track in Switzerland [Metcalf, 1996].

Figure 2.16 Circular LPCP test track in France [www.gautrans-hvs.co.za]
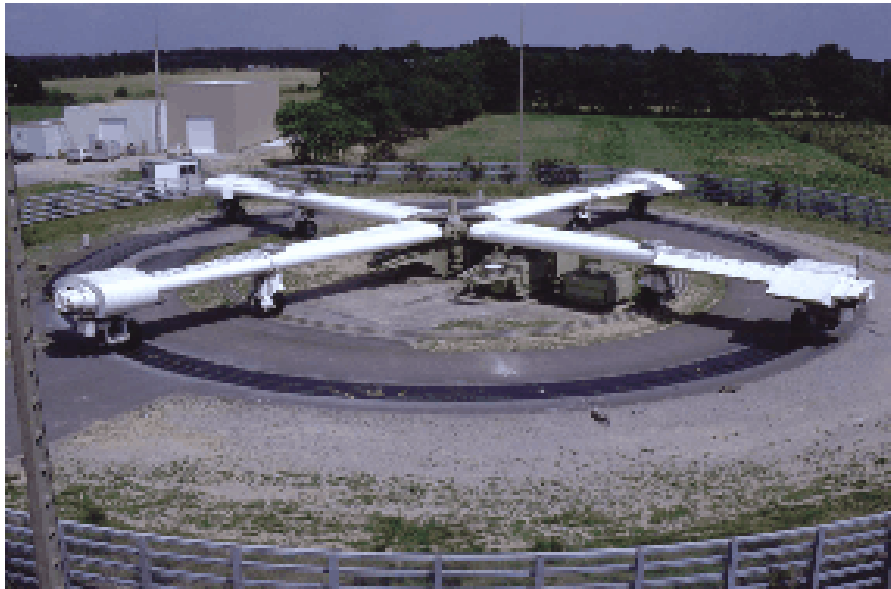
Linear tracks' main characteristic is that traffic travels in one direction only, that is, the load passes a point in a test road only in one direction. South Africa was the first to develop a mobile linear facility (the Heavy Vehicle Simulator (HVS)) in 1968 to 1972, which can operate on in-service highways [Metcalf, 1996]. The HVS has a hydraulically operated loading assembly carrying a single or dual tire test wheel, capable of loading from 20 to 200 kN (4,400 to 44,000 lb) at speed up to 14 km/h (8.6 mph).

California Department of Transportation, (CALTRANS), began its CAL-APT program using the HVS technology in 1994 [Metcalf, 1996]. California installed two South African HVS, one at CALTRANS and the other at the University of California Berkeley (UCB), which is constructed in a more environmental controlled laboratory. The University of Texas installed a mobile load simulator (TxMLS), which is a transportable linear device capable of applying six single- of dual- tire bogies with tandem axle loaded up to a nominal 190 kN (42,000 lb) at test speeds of up to 20 km/h 912.5 mph) (Figure 4.2). The test pavement length is 11 m (36 ft) with optional transverse lateral load application of 0.6 m (24 in). The facility has full axle load, regular truck suspensions to simulate short wave length dynamics, load frequency of up to 8800 per hour, and a fully enclosed environmental control chamber. The device can be dismantled and

reassembled in one day, and can be jacked up to allow in situ testing of in-service highways [Metcalf, 1996].

Other linear test track APT facilities [Metcalf, 1996] include:

- The Australian Accelerated Loading Facility (ALF). The facility travels at a speed on 12.5 mph (20 km/hr) and loads vary from 4500 lb (41kn) and 9000 lb (80kN)

- The Danish Road Testing Machine capable of testing full-scale pavements under wheel loads up to 656 kN (14,300 lb) at speed of up to 30 km/h (12.6 mph).

- The Pavement Test Facility at the UK Transportation Research Laboratory (TRL).

- The Indiana Department of Transportation in association with Purdue University APT (InDoT-Purdue APT).

- The Civil Infrastructure Systems Laboratory (CISL) at Kansas State University.

- The University of Minnesota, which is a single tire load assembly working on a 4.5m (15 ft) long by 6.2 m (12 ft) wide track. The testing length is 2.4m (8 ft) with maximum load of 24,000 lb and speed of up to 20 km/h (12.5 mph).

More APT facilities are described in details in the NCHRP Synthesis 235 by Metcalf, 1996 and NCHRP Synthesis 325 by Hugo et. al.

Figure 2.17 Texas Mobile Load Simulator [www.gautrans-hvs.co.za]

Other configuration

Other APT configurations include the BASt Pulse Loading Facility, in Germany, which as three hydraulic plate loading rigs testing base courses of various waste/recycled materials, mainly recycled pavement or building materials. The pulse load plates move along the test section to simulate traffic at approximately 20 km/h (12.5 mph) and applies loads up to 200 kN (44,000 ln). For data collection, the facility uses H-bar strain gauges and surface deformation measurements, with a traveling straight edge on two reference points [Metcalf 1996]. Michigan State commissioned a pulse loading assembly in 1990 to simulate wheel loads across cracked pavement slabs; the facility was decommissioned in 1993 [Metcalf, 1996]. In Japan several facilities have been in use since 1969. The first was a test tank at the Harbor Research Institute (PHRI), which could apply plate loads of up to 2200 kN (484,000 lb) and repeated loads of up to 5400 kN (110,000 lb) on a dual tandem aircraft wheel assembly at speeds up to 30 km/h (8.6 mph) [Metcalf, 1996].

2.3.3 Benefits of APT Facilities

The benefits of APT facilities as pavement research tools include: reduced testing cost, shorter data collection period and controlled environmental conditions in pavement layer. This ensures that pavement materials are subjected to identical load environmental conditions. The advantages of APT testing over observation of behavior of in-service pavements are:

- Provides a safe environment for researchers and traveling public (tests on in-service highway often involves safety hazards);
- Test can be conducted faster and in a more controlled manner;
- The number of wheel load applications and load magnitudes can be controlled accurately and loads can be positioned at desired locations;
- Several factors can be evaluated simultaneously.

CHAPTER 3 - CIVIL INFRASTRUCTURE SYSTEMS LABORATORY (CISL) - EXPERIMENT 14

3.1 The Civil Infrastructure Systems Laboratory

The Civil Infrastructure Systems Laboratory for Accelerated Pavement Testing (CISL-APT) at Kansas State University was established in 1997. It is financed through the Midwest States Accelerated Pavement Testing Pooled Fund from the Departments of Transportation (DOTs) of Kansas, Nebraska, Iowa and Missouri [Hugo, 2004]. It is owned by Kansas State University (KSU) and operated by KSU. The laboratory is an indoor facility, which allows full-scale accelerated pavement testing on pavement structures. It comprises of about 650 m^2 (7000 ft^2) floor space, out of which 537 m^2 (5775 ft^2) is a test space which includes about 418 m^2 (4500 ft^2) containing two pavement testing pits; about 93 m^2 (1000 ft^2) FWD calibration room and about 26 m^2 (275 ft^2) for the electrical and mechanical rooms where the pavement cooling and heating equipment is installed [Melhem 1999, Dumitru 2006].

The test pits are 6ft deep, the main (largest) pit is 32' x 20' x 6' and has been partitioned into two smaller pits of 20' x 20' x 6' and 12' x 20' x 6'. The smaller pit, 20' x 16' x 6', is equipped with metal (copper) pipes that circulates a heated or cooled glycol solution to control the temperature of the subgrade. This pit contains thermal insulation and can maintain a steady temperature in the subgrade between 5°F and 72°F.

The facility comprise of a steel frame that can be moved on rails between the testing pits. The frame, comprise of a bogie with conventional truck axle, which can accommodate single, dual and/or super single tires, and single or tandem axles (Figures 3.1 and 3.2). The bogie can move forward and backwards while the load is applied on the test pavement by means of two longitudinal girders with span of about 42' center to center. At the end of each travel way, the energy absorption and release system transforms the kinetic energy of the carriage into potential energy in the air cylinders. The air cylinders then launch the bogie in the opposite direction. The bogie can carry a maximum load of 178 kN (40,000 lbs). The wheel assembly consists of a tandem or single axle load with air suspension bags. The axle loading is achieved by varying

pressure in the suspension system, which is controlled in an open loop mode using load cells. The distance traveled by carriage is longer than the test pavement; this gives room for acceleration and deceleration of the bogie outside the test pavement so that the test speed is maintained constant while the bogie travels above the pavement. The maximum load application speed is 12 km/hr (7.6 mph).

Figure 3.1 Single Axle Wheel Assembly at CISL

Figure 3.2 Single Axle Wheel Assembly at CISL

The machine is equipped with a lateral wandering device that moves the entire frame in a lateral direction with a maximum lateral wander of ±610 mm (± 24 inch). The lateral movement is applied in steps of 12.5 mm (0.5 inch). The lateral position of the frame (Figure 3.4) is controlled by an electronic controller (Figure 3.3). Provided in Table 3.1 are the number of wheel load passes at each lateral step.

Figure 3.3 Lateral Wonder Device
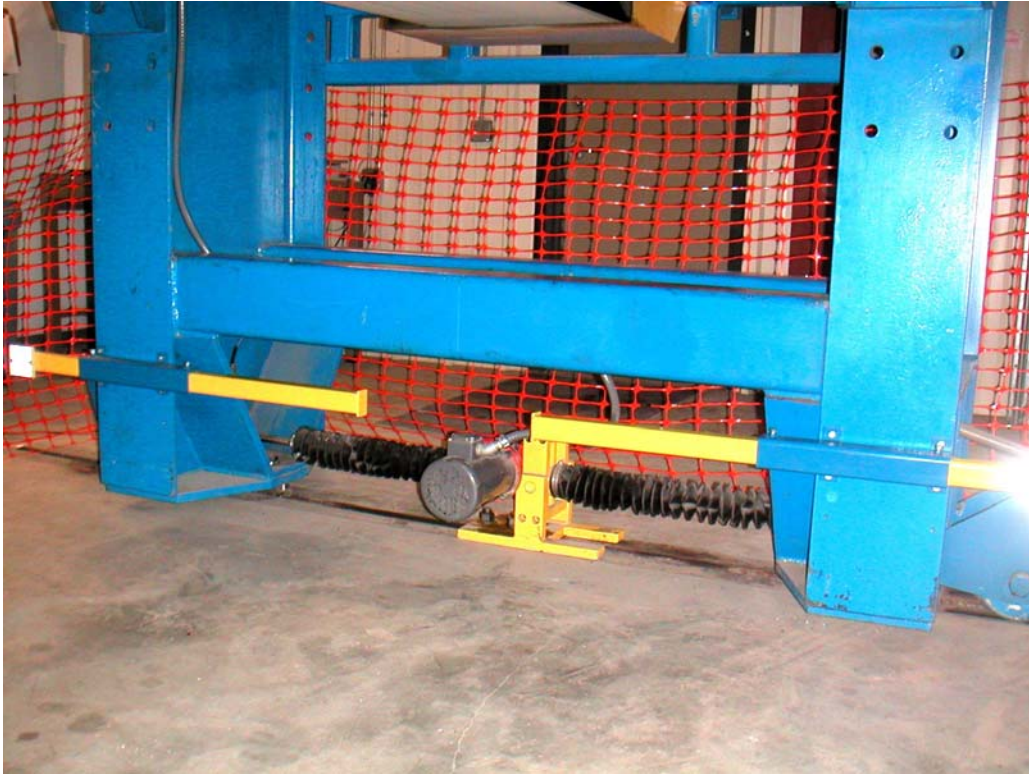
Figure 3.4 Lateral Wonder: Truncated Normal distribution

D_{max} = 6 in.

P = 90%

N=640

STD=3.65"
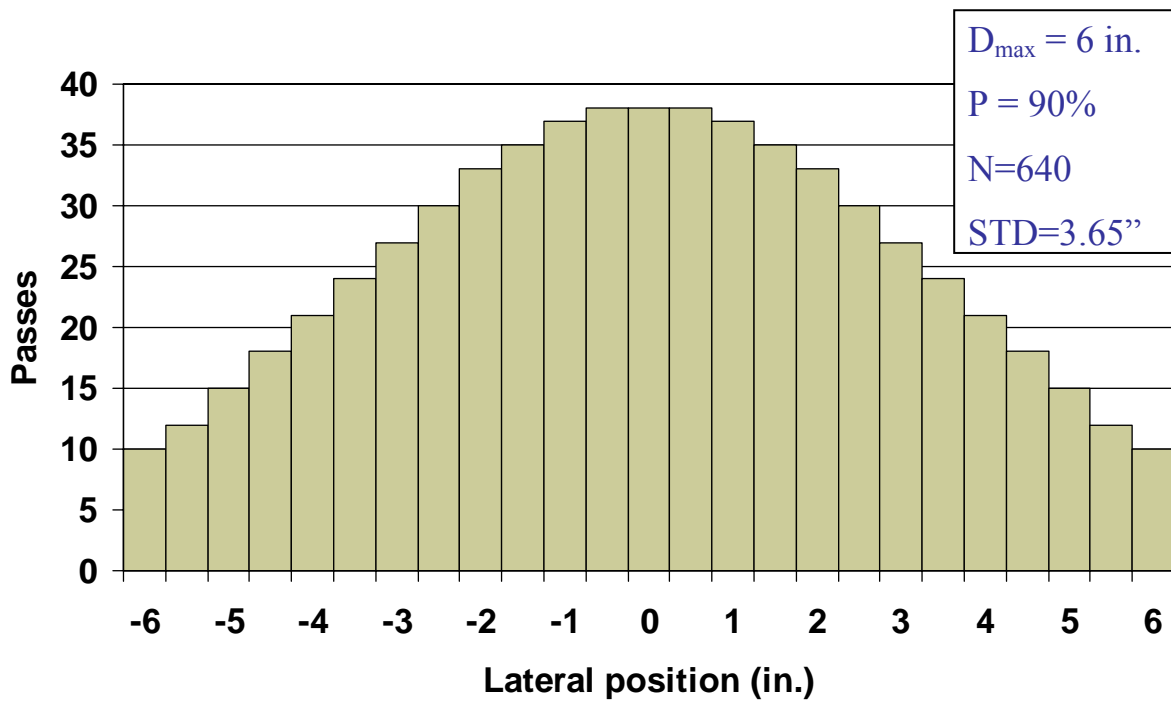
Table 3.1 Wheel lateral wonder positions and number of passes

Lateral Position	Number of wheel passes	Lateral Position	Number of wheel passes
-6	10	0	38
-5.5	12	0.5	38
-5	15	1	37
-4.5	18	1.5	35
-4	21	2	33
-3.5	24	2.5	30
-3	27	3	27
-2.5	30	3.5	24
-2	33	4	21
-1.5	35	4.5	18
-1	37	5	15
-0.5	38	4.5	12
0	38	6	10

The measurements or data collection is performed using different techniques suitable for a particular case (project). Strain gauges are used to measure horizontal and vertical strains below the hot mix asphalt layer. The Linear Variable Differential Transducers (LVDTs) are used to measure single layer deflection and pressure cells measure pressure below the base layer. For temperature measurements, thermocouples are used. Moisture in subgrade is measured using moisture probes (Figure 3.5). The most recently used method for moisture measurement is Time Domain Reflectometry (TDR).

Figure 3.5 Sensor Location
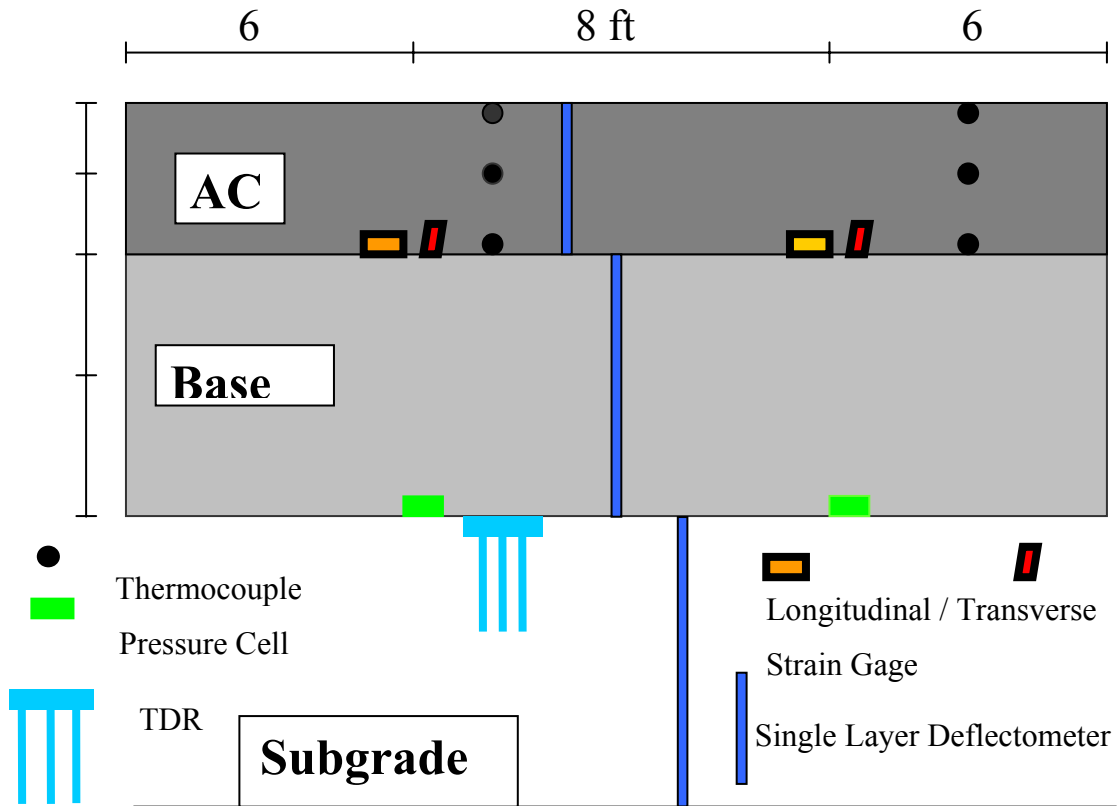
In 2005 a temperature control within ± 1°C (± 2°F) chamber was built to encase the entire steel frame. This made it possible to run tests in CISL-APT at controlled temperatures. For the current project, CISL 14, the test temperatures are 20°C (68°F) and 35°C (95°F). Figure 3.6 shows the temperature control chamber as constructed in 2005.

Figure 3.6 APT Machine with Temperature Control Chamber

3.2   The CISL 14 Experiment

Since its construction, the Kansas State University Civil Infrastructure Systems Laboratory, has been used to conduct a number of research projects. The current research project, CISL 14, is funded by Midwest Pooled Fund with the aim to Verify Mechanistic-Empirical Design Models for Flexible Pavements through Accelerated Pavement Testing. Models that are verified in this research project are those provided in the Mechanistic Empirical Pavement Design Guide (MEPDG). The objectives of CISL 14 research project [Romanoschi, 2004] include to:

- validate and calibrate the dynamic resilient modulus model for six mixes
- validate the relationship between the dynamic modulus and pavement response;
- validate the relationship between pavement response (strains) and performance;
- compare the performance of coarse and fine Superpave mixes; and
- validate and calibrate the Asphalt Pavement Analyzer (APA) as a screening tool for rutting.

Six HMA mixes from the States of Kansas, Missouri and Iowa were used for model verification. Twelve pavement sections were constructed for Accelerated Pavement Testing in CISL, six sections for cracking evaluation and six for rutting evaluation. Pavement sections for cracking evaluation had 100-mm (4-in) thick asphalt layer, while those used for rutting evaluation had a thickness of 175-mm (7-in) (Figure 3.7). The pavement sections had same base and subgrade materials.

The sections were loaded with up to 700,000 load repetitions of a 22,000 lb single axle load and the transverse profiles at the pavement surface were measured periodically. Results from APT testing were used as field measurements for the evaluation of mechanistic permanent deformation prediction models. Figure 3.8, Figure 3.9 and Figure 3.10 shows examples of transverse profiles measured from the APT for Kansas, Missouri and Iowa mixes respectively.

Figure 3.7 Experimental Setup for CISL 14 project
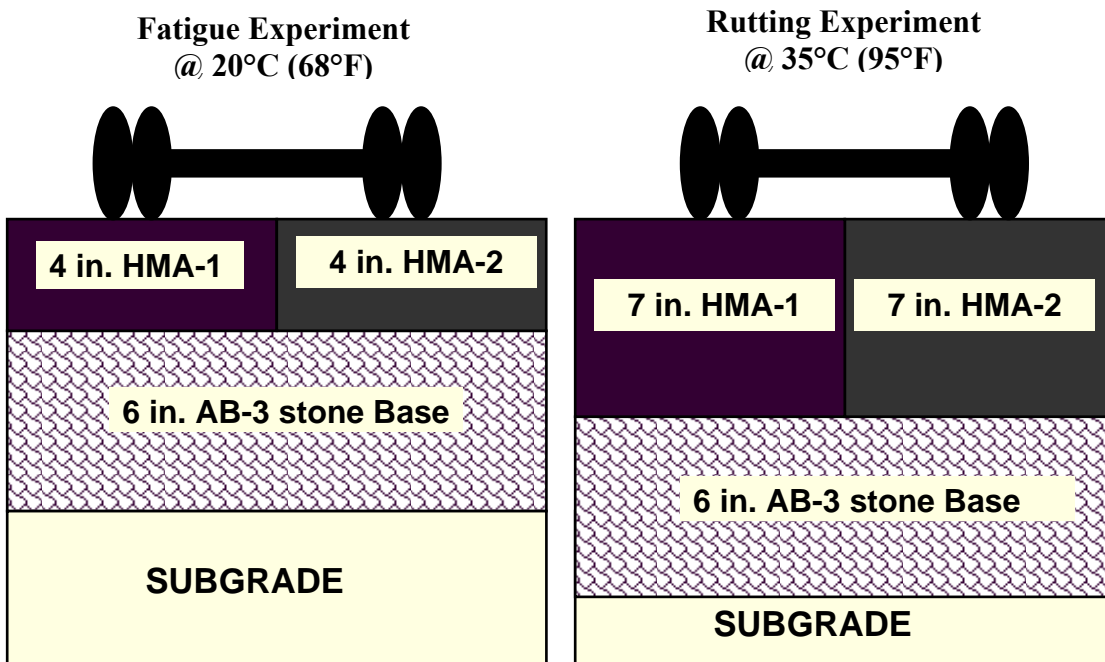
Figure 3.8 Transverse Profile - KS Mix (Middle East- 5 ft from the right end)
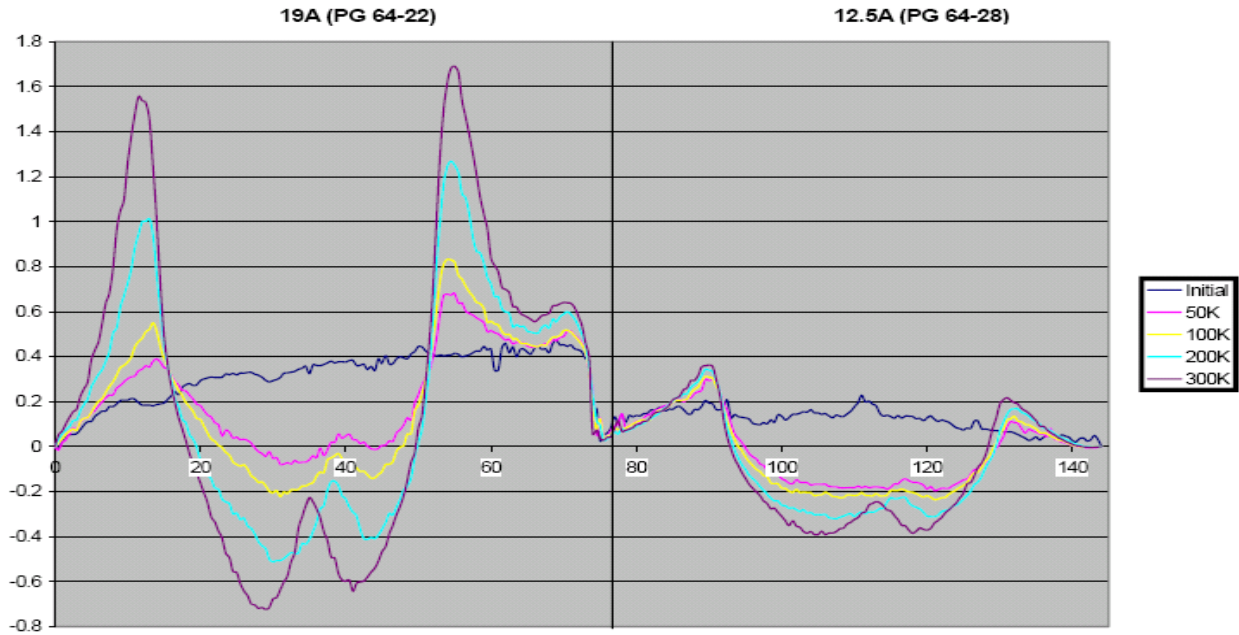
Note: Rut depth is in inches

Figure 3.9 Transverse Profile - MO Mix (Middle East- 5 ft from right end)
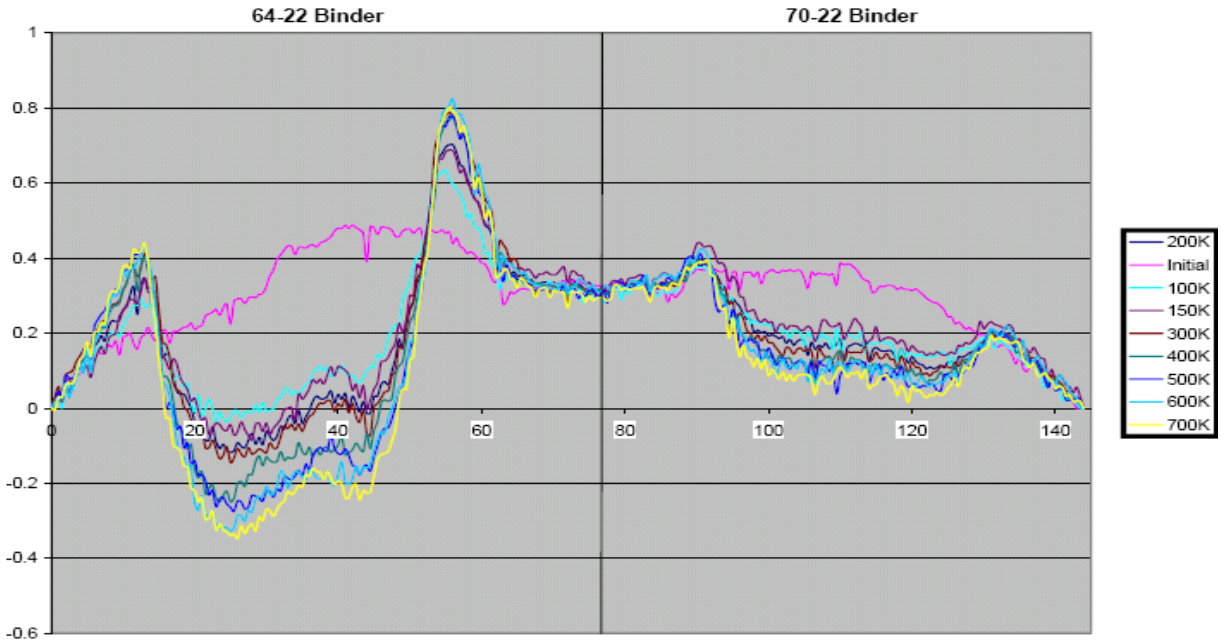
Note: Rut depth is in inches

Figure 3.10 Transverse Profile - IA Mix (Middle East- 5 ft from right end)
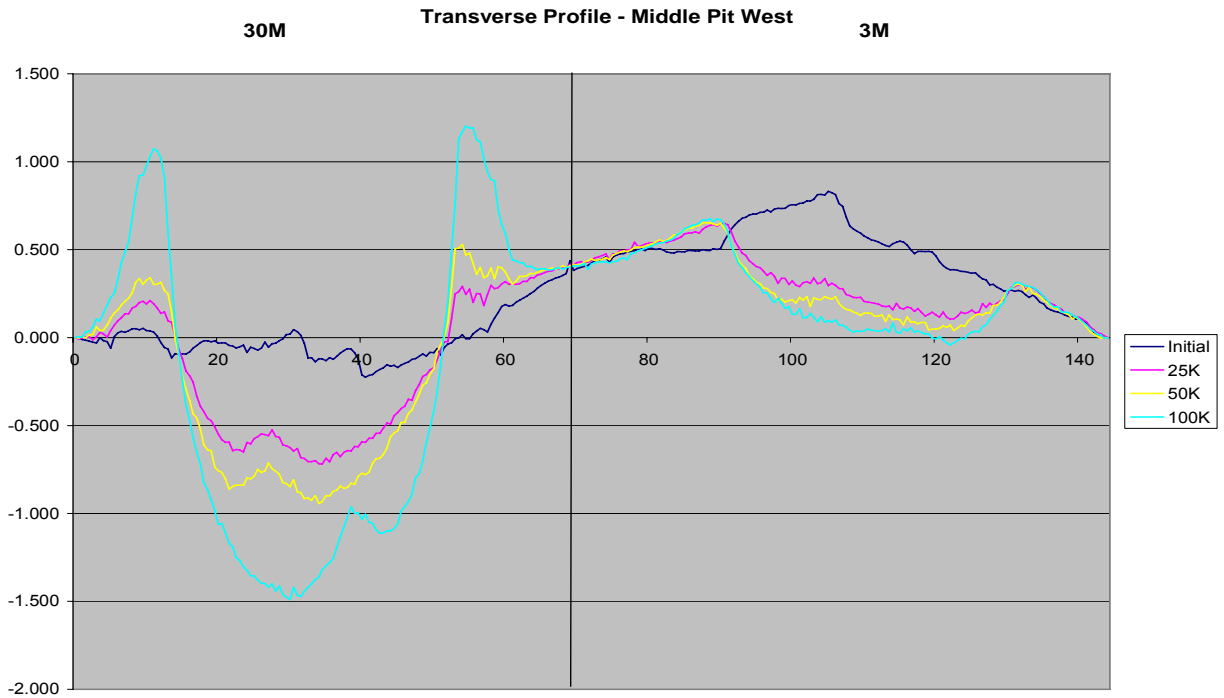
3.3   Asphalt Mix Design and Testing

Asphalt mix designs for the six asphalt mixes were provided by Kansas, Missouri and Iowa Departments of Transportation (DOTs). Two asphalt mix designs used for HMA design and road construction in each state were provided. The asphalt mix specifications and abbreviations are given in Table 3.2. The required mix design parameters for the asphalt mixes provided by the DOTs are given in Table 3.3. These mix designs were used by a local contractor to mix and construct pavement sections for APT in CISL. Table 3.4 summarizes as built volumetric properties and in place density. The constructed sections were somehow deviated from the asphalt mix design parameters provided. This affected the performance of some of the mixes. The tests performed to characterize asphalt mixes were used to evaluate mechanistic empirical material models and mechanistic permanent deformation prediction models. Laboratory tests for material characterization were performed on individual materials and on asphalt mixtures.

68

Material selection is a key aspect to better performing asphalt mixes. Asphalt mix comprises of fine and course aggregates and asphalt binder. For this project, the materials used were provided by respective DOT. These are materials used in typical asphalt mix designs in those state. Aggregates and binders were hauled from Missouri and Iowa States to the contractor's site in Manhattan Kansas, and were used to replicate accurately the actual mixes used in those states. Laboratory tests were performed on individual materials and on the asphalt mixes as detailed in section 3.3.1.

Table 3.2 Mixture specification and abbreviation

SN	State	Asphalt mix type	Binder grade	Abbreviation used
1	Kansas	SM 19A	PG 64-22	KS-1
2	Kansas	SM 12.5A	PG 64-28	KS-2
3	Missouri	SP125C	PG 70-22	MO-1
4	Missouri	SP125C	PG 64-22	MO-2
5	Iowa	HMA 30M L-4	PG 64-22	IA-1
6	Iowa	HMA 3M L-4	PG 64-22	IA-2

Table 3.3 Mix design parameters

Parameter	KS-1	KS-2	MO-1	MO-2	IA-1	IA-2
NMAS	19.0	12.5	12.5	12.5	12.5	12.5
Design ESALs (million)	6.4	2.6	3.3	3.3	30.0	3.0
Ndesign	100	75	100	100	109	86
Binder	PG 64-22	PG 64-28	PG 70-22	PG 64 - 22	PG 64-22	PG 64-22
Design AC (%)	5.3	4.9	5.3	5.4	5.69	6.12

Table 3.4 As-constructed volumetric properties and in-place air voids

Parameter	KS-1	KS-2	MO-1	MO-2	IA-1	IA-2
AC (%)	5.61	5.2	5.3	5.4	7.5	7.0
AV @ N_{design} (%)	4.08	3.33	4.4	4.4	4.0	4.0
VMA	18.4	15.8	18.862	17.4	22.0	19.1
VFA	55.2	59.1	51.8	57.1	59.5	61.7
%G_{mm}@N_{ini}	88.2	88.8	85.4	85.5	92.2	89.8
% G_{mm}@N_{des}	96.1	95.6				
%G_{mm}@N_{max}	97.2	99.9	97.2	97.3	99.6	99.4
Dust-binder ratio	1.0	0.9	1.1	1.1	0.5	0.5
In-place AV (%)	6.00±0.5	6.75±0.5	9.38±0.5	7.00±0.5	8.9±0.5	7.00±0.5

3.3.1 Laboratory Tests on Constituent Materials

To verify Mechanistic-Empirical design models, laboratory tests were performed on individual materials and on the asphalt mixtures from the three Midwest states, Kansas, Missouri and Iowa. From Kansas State, the mixes are Kansas course mix (KS-1) with NMAS 19 mm and asphalt binder grade PG 64-22 and Kansas fine mix (KS-2) having NMAS 12.5 mm and binder grade PG 64-28. Missouri mixes had NMAS 12.5 mm, MO-1 having binder grade PG 70-22 and MO-2 with binder grade PG 64-22. Both Iowa mixes had aggregate NMAS of 12.5 mm and PG 64-22 binder grade, the difference was on the fine aggregate content (Figure 3.14) and design ESALs. Mix IA-1 was designed for 30 million ESALs and IA-2 for 3 million ESALs (Table 3.1).

Quality of materials is critical to the performance of asphalt mixes. Aggregates makes up 80 to 85% of the mixture by volume. Therefore aggregates characteristics are important for the performance of asphalt mixture. The Superpave asphalt mix design recommended tests that should be performed on aggregates to ensure that they meet required specifications, and they will result into asphalt mixture with the desirable performance. Laboratory tests were performed on aggregates and asphalt binder to ensure that all materials used met specification requirements. The following tests were performed on aggregates:

- Gradation Analysis AASHTO T 27

- Fine Aggregate Angularity (FAA) KT 50

- Los Angeles Abrasion test (LAA) ASTM C131 method B

- Flat and elongated particles ASTM D4791

- Fractures particles ASTM D5821

Asphalt binder is a viscoelastic material. It is affected by loading time and temperature. Superpave uses performance grade (PG) asphalt to optimize its effect on the performance of asphalt pavement at a range of temperatures. The asphalt binders for this project were provided by the respective DOTs. The Dynamic Shear Rheometer test was performed on asphalt binder to obtain shear modulus (G^*) and phase angle (δ) of each binder used. These parameters were determined at seven different temperatures as required by AASHTO T 315 protocol. The test temperatures were 4, 13, 21, 29, 38, 46, and 54°C. The tests were conducted on original binder, on a residual binder after rolling thin film oven test (RTFO), and residue from a pressure aging vessel (PAV). The tests description and results from this test are given in section 3.3.1.6.

3.3.1.1 Gradation Analysis AASHTO T 27

This test was conducted in accordance to AASHTO T 27, to obtain particle size distribution of individual aggregate samples as well as aggregate blends that met mix design specifications (job mix formula). The individual aggregates blend percentages are given in Table 3.5 to Table 3.7 and the 0.45 power gradation charts of the job mix formulas for Kansas, Missouri and Iowa aggregates are given in Figures 3.11 to Figure 3.14. The aggregate blends (job mix formula) for the six mix designations met the Superpave gradation specification. Tables 3.8 to 3.10 give the job mix formula for each mix and the grading band limits. The aggregate blend percentages were adopted for the laboratory sample fabrication.

Table 3.5 Aggregate blends for Kansas mixes

Mix	Aggregate Designation	Source location	%	Mix	Aggregate Designation	Source location	%
Kansas KS-1	CS-1	$^3/_4$" Bayer Zeandale rock	31	Kansas KS-2	CS-1	$^1/_2$" Bayer Zeandale rock	19
	CS-1A	Bayer Zeandale Man. sand	22		CS-1A	Bayer Zeandale Man. sand	16
	CS-2	Bayer Zeandale screenings	12		MSD 1	Bayer Zeandale Man Sand	16
	SH-1A	Bingham drag sand - chat	25		CG-5	MCM Crushed gravel	21
	SSG-1	MSM concrete sand*	10		SSG	MCM concrete sand *	28

* Kansas river sand

Table 3.6 Aggregate blends for Iowa mixes

Mix	Aggregate Designation	Source location	%	Mix	Aggregate Designation	Source	%
Iowa 30M ESALS (IA-1)	A85006	$^1/_2$" minus - M.M. Ames	30	Iowa 3M ESALS (IA-2)	A85006	$^1/_2$" cr. Limestone -M.M. Ames	35
	A85006	$^3/_8$" chip - M.M. Ames	20		A85006	$^3/_8$" chip - M.M. Ames	20
	A85006	Man. sand - M.M. Ames	40		A85006	Man. sand - M.M. Ames	20
	6A77502	Sand - M.M. Johnson	10		6A77502	Sand - M.M. Johnson	25

Table 3.7 Aggregate blends for Missouri mixes

Mix	Aggregate Designation	Source location	%
Missouri Mix	64D1T037	$^3/_4$" APAC sugar creek rock	27
	64D1T038	$^3/_8$" APAC sugar creek rock	40
	64D1T040	Humble S & G flint chat	25
	64D1T039	APAC Sugar creek SG	8

Table 3.8 Job Mix formula for Kansas mixes

Sieve size (in)	Upper Limit	Gradation KS-1	Lower Limit	Upper Limit	Gradation KS-2	Lower Limit
1"	**100**	100	**100**	**100**	100	**100**
¾"	**90**	100	**100**	**100**	100	**100**
½"		90.3	**90**	**90**	93	**100**
$^3/_8$"		82.1			88	**90**
#4		59.0			72	
#8	**49**	39.3	**35**	**58**	50	**39**
#16		25.9			31	
#30		17			19	
#50		10.1			11	
#100		6.0			5	
#200	**8**	4.7	**2**	**10**	3.2	**2**

Figure 3:11 Aggregate gradation with grading band for Kansas KS-1 NMAS 19.0

0.45 Power Chart
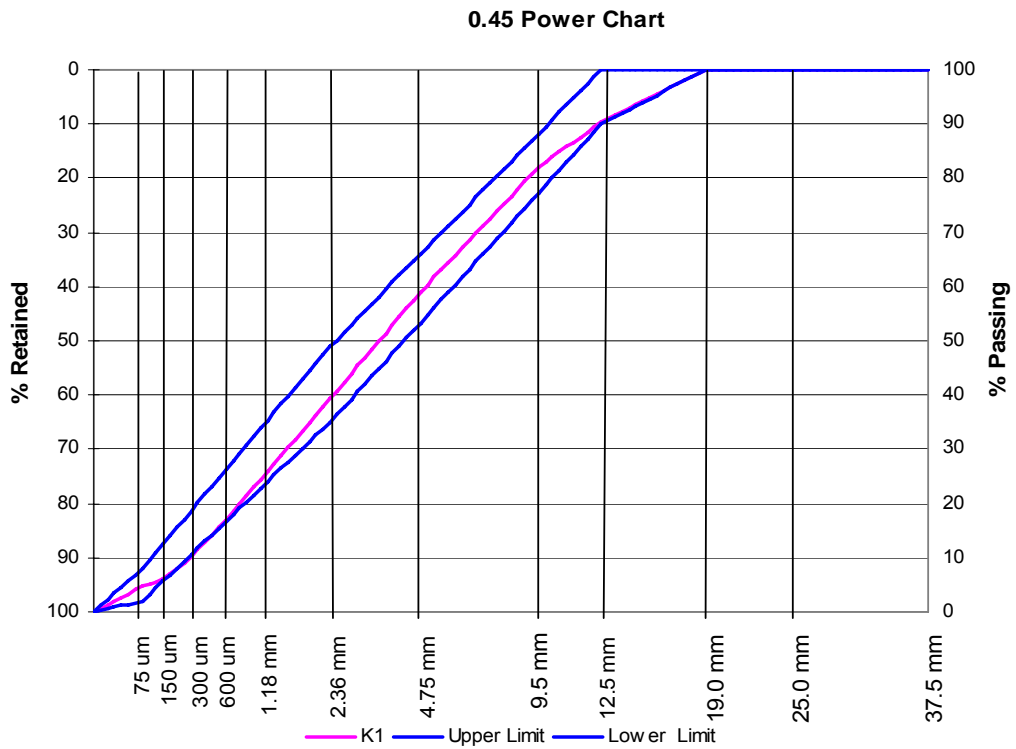
Figure 3:12 Aggregate gradation with grading band for Kansas KS-2 NMAS 12.5

0.45 Power Chart
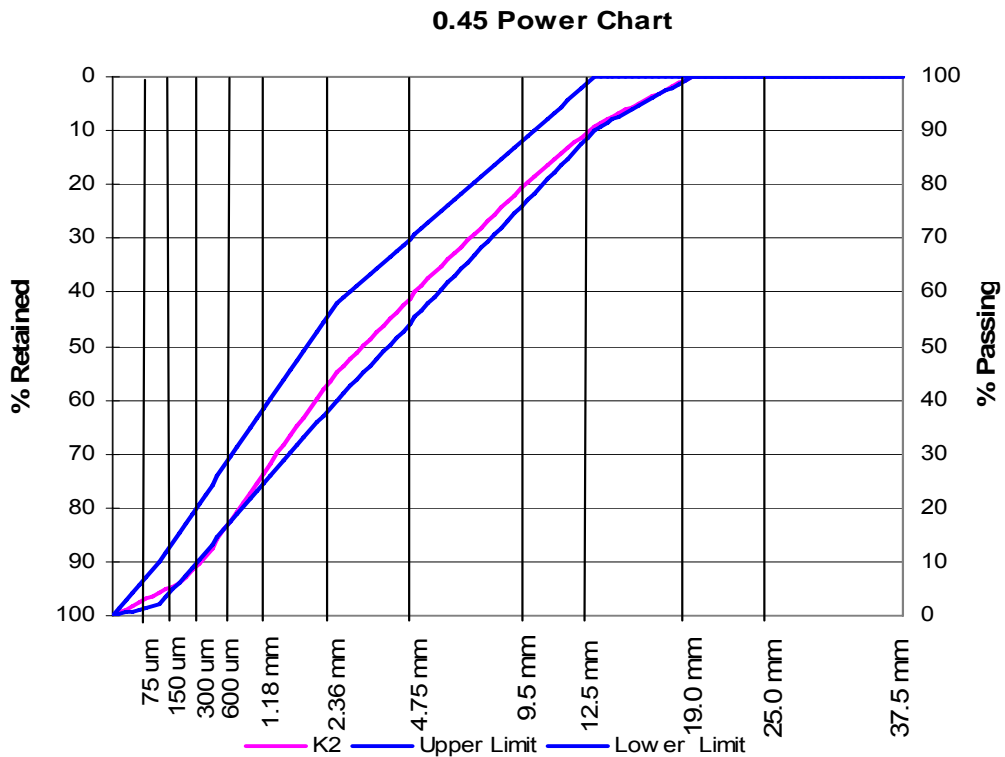
Table 3.9 Job Mix formula for Missouri mixes

Sieve size (in)	Upper Limit	Gradation MO	Lower Limit
1"	**100**	100	**100**
¾"	**100**	100	**100**
½"	**90**	90.6	**100**
³/₈"		79.8	**90**
#4		49.3	
#8	**58**	31.8	**28**
#16		21.1	
#30		13.6	
#50		7.7	
#100		5.0	
#200	**10**	4.1	**2**

Figure 3:13 Aggregate gradation with grading band for Missouri mixes NMAS = 12.5

0.45 Power Chart
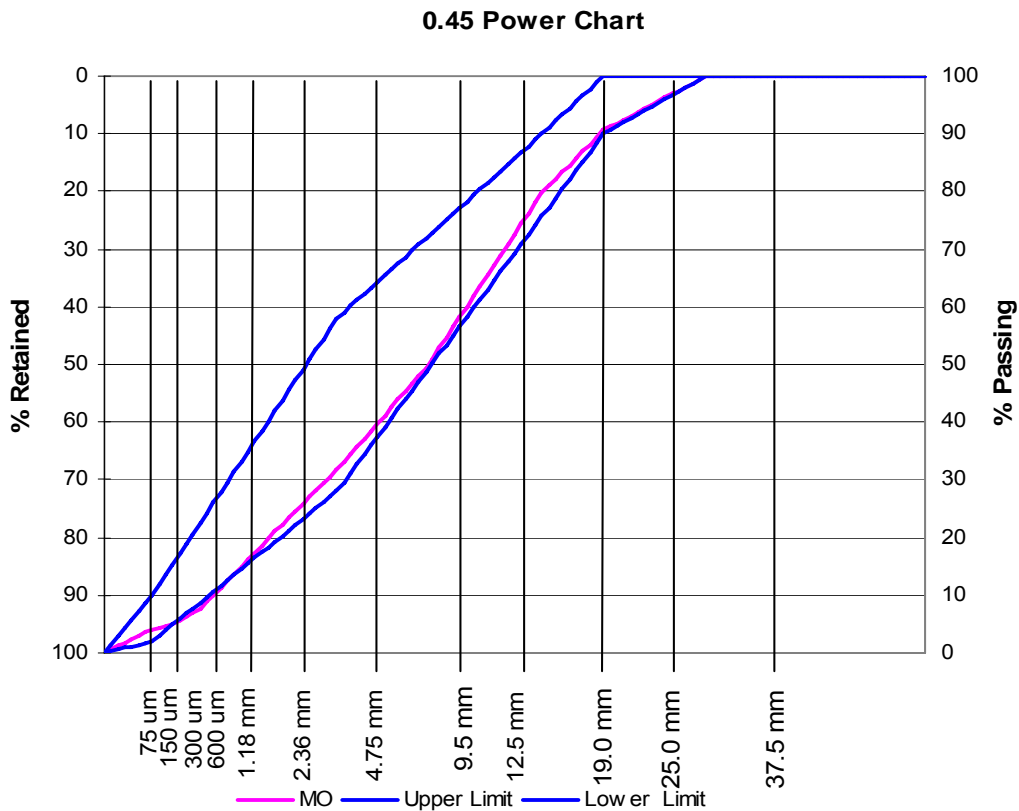
Table 3.10 Job Mix formula (combined gradation) for IA mixes

Sieve size (in)	Upper Limit	Gradation IA-1	Lower Limit	Upper Limit	Gradation IA-2	Lower Limit
1"	**100**	100	**100**	**100**	100	**100**
¾"	**100**	100	**100**	**100**	100	**100**
½"	**100**	98	**91**	**100**	98	**91**
³/₈"	**96**	89	**82**	**96**	89	**82**
#4	**69**	62	**55**	**69**	62	**55**
#8	**49**	44	**39**	**49**	44	**39**
#16		29			33	
#30	**22**	18	**14**	**24**	20	**16**
#50		9.2			9.5	
#100		4.5			4.4	
#200	**5.3**	3.3	**1.3**	**5.4**	3.4	**1.4**

Figure 3:14 Individual aggregate gradations for Iowa mixes NMAS 12.5

0.45 Power Chart

76
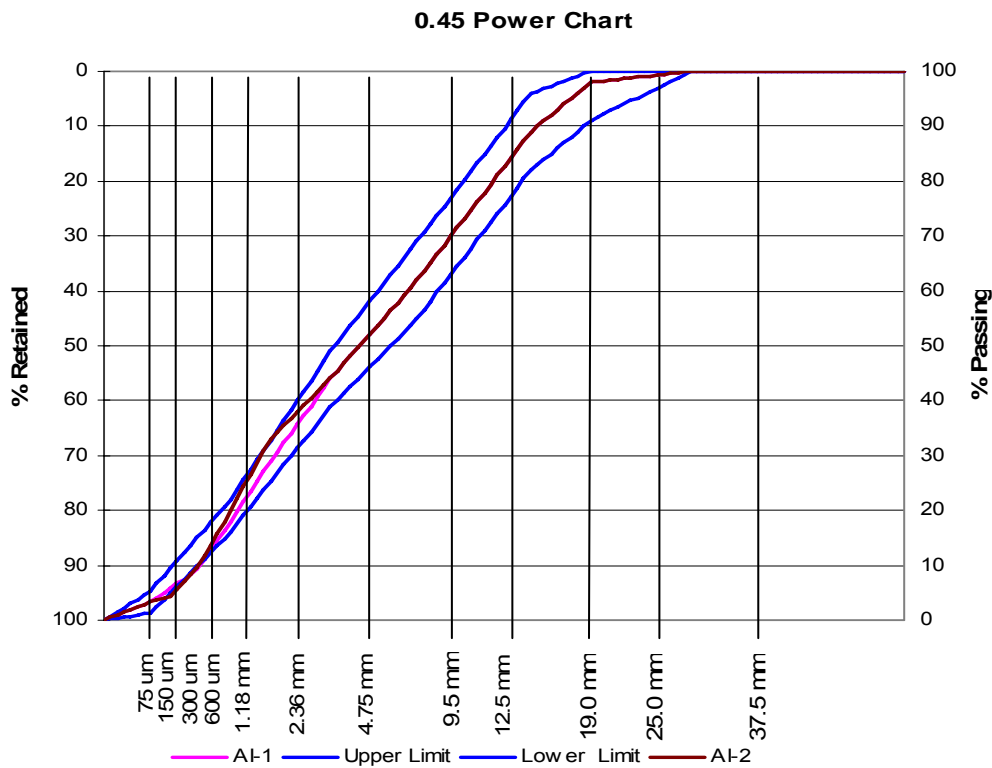
3.3.1.2 Fine Aggregate Angularity (FAA) KT 50

The fine aggregate angularity test was conducted to assess the texture of fine aggregates. Fine aggregate angularity is desired for formation of a strong aggregate skeleton that can resist permanent deformation. Angular aggregated have high friction between particles, therefore they are desired over smooth aggregates due to its ability to resist deformation. This test was performed on individual fine aggregates passing 2.36mm (No.8) sieve. Researchers suggest that natural sand should have FAA less than 44 while manufactured (crushed) sand should have FAA more than 44 [D'Angelo, 2004]. Results obtained for fine aggregates tested had FAA values greater that 44 for manufactured sand, and FAA less than 44 for natural sand (SSG). Table 3.7 provides results from this test. It is expected for natural sand to have lower values of FAA as compared with manufactures sand, because natural sand has fewer fractured faces and has smoother texture. Table 3.11 summarizes the results from this test.

Table 3.11 Fine Aggregates Angularity test results

Aggregate mix blend	Aggregate Designation	FAA	Specification (AASHTO)
KS-1	CS-1A	47.9	Min 40.00
	CS-2	47.25	
	SH-1A	48.55	
	SSG-1	38.00	
KS-2	CS-1C	47.55	Min 40.00
	CG-5	44.4	
	SSG	38.38	
MO	64D1T040	48.35	Min 40.00
	64D1T039	48.15	
IA-1	NMAS 12.5	44.2	Min 40.00
IA-2	NMAS 12.5	45.2	Min 40.00

3.3.1.3 Los Angeles Abrasion test (LAA) ASTM C131 methods B and C

Aggregates are required to be hard and tough to resist crushing, degradation, and disintegration that occur when stockpiled or in the mixing, laying and compaction process. They are also supposed to provide internal friction that will transmit wheel loads to underlying layers and at the same time be resistant to abrasion and polishing due to traffic load. The Los Angeles Abrasion test was carried out to obtain an indication of desired toughness and abrasion characteristic of aggregates. This test was carried out on course aggregates in accordance to ASTM C 131 method B for Kansas and Missouri aggregates and method C for Iowa aggregates. The test was performed to determine aggregate toughness and resistance to abrasion. AASHTO recommends a maximum LAA value of 40% for aggregates used for surface course of high type HMA roads. Table 3.12 summarizes the results.

Table 3.12 Results of Los Angeles Abrasion Test

Aggregate mix blend	Aggregate Designation	LAA (%)	Specification (AASHTO)
KS-1	CS-1	26.1	
KS-2	CS-1B	27.0	
MO	64D1T037	23.6	Max 40.0
IA-1	12.5 NMAS	24.3	
IA-2	12.5 NMAS	25.3	

3.3.1.4 Flat and elongated particles ASTM D4791

Aggregate particles suitable for use in hot mix asphalt should be cubical rather than round, flat, thin or elongated. Angular shaped aggregates are desired in HMA because they exhibit greater interlock and internal friction. Rounded aggregates provide better workability but are prone to continual densification under traffic, ultimately leading to rutting. Flat thin and elongated particles are not desired in the mix because they form slip planes and reduce aggregate interlock. This test was performed in accordance to ASTM D4791, on material courser than 9.5mm. Flat (thickness to width) and elongated (width to length) aggregates were manually tested using a proportional caliper. Superpave recommends the percent of flat and/or elongated

aggregates to be limited to 10% using a length to width or thickness ratio of 5 to 1. Table 3.13 summarizes results from this test. The percentage of flat and elongated particles is given below.

Table 3.13 Flat and Elongated Particles

Aggregate mix blend	Aggregate Designation	Flat (%)	Elongated (%)	Flat and Elongated (%)	Specification (AASHTO)
KS-1	CS-1	0.48	0.09	1.47	Max 10.00
KS-2	CS-1B	0.21	0.04	0.25	Max 10.00
	CS-1	0.16	0	0.16	
MO	64D1T040	0.07	0	0.07	Max 10.00
	64D1T039	0.38	0	0.38	
IA-1	NMAS 12.5	0.16	0.34	0.5	Max 10.00
IA-2	NMAS 12.5	0.11	0.18	0.29	Max 10.00

3.3.1.5 Fractures particles ASTM D5821

Fractured faces on aggregate particles increase aggregate interlock and hence improve mix stability and increase resistance of the mix to permanent deformation. This test was performed in accordance to ASTM D5821 to determine the percent of aggregate particles having at least one fractured face and at lease two fractured faces. The requirement is at least 95% should have at least one fractured face. Results are as tabulated in Table 3.14 below they show that all aggregate samples passed the fractured faces test. Superpave mix specifications requires for 9.5mm chips, particles with at least one fractured face to be 99%, and for particles with at least two fracture faces should be 95%.

Table 3.14 Flat and Elongated Particles

Aggregate mix blend	Aggregate Designation	Fractured Faces		Specification (AASHTO)
		At least one	At least two	
KS-1	CS-1	100	100	At least one
KS-2	CS-1B	99.98	99.98	Fractured face
	CS-1	99.95	99.95	Min 95%
MO	64D1T040	100	100	
	64D1T039	100	100	At least two
IA-1	NMAS 12.5	99.36	99.47	Fractured faces
IA-2	NMAS 12.5	100	99.28	Min 90%

3.3.1.6 Test on asphalt binder - Dynamic Shear Test

The Dynamic Shear Rheometer (DSR) test was performed on asphalt binder to characterize the viscous and elastic behavior of asphalt binders at high and intermediate (service) temperatures. The DSR test measures the complex shear modulus (G*) and phase angle (δ) of asphalt binder. The complex modulus, G*, is considered as the total resistance of binder to deformation when sheared repeatedly. It is comprised of two components: storage modulus G' which is elastic (recoverable) and loss modulus G", the viscous (non-recoverable). The phase angle, delta (δ) is the time lag between applied stress and the resulting strain [Roberts et. al., 1996]. For perfectly elastic materials, delta is zero, and for viscous materials like hot asphalt binder delta is close to 90°. At intermediate service temperature asphalt binder is viscoelastic, possessing both elastic and viscous characteristics. It is therefore important to use both G* and δ to characterize the asphalt binders. For resistance to permanent deformation, a high complex shear modulus (G*) and low phase angle (δ) are desired because the higher the G* value, the stiffer the binder and the lower the phase angle, the more elastic the asphalt binder [Roberts et. al., 1996]. The test was performed at seven temperatures; 4, 13, 21, 29, 38, 46, and 54°C on original binders and on the residual binders after rolling thin film oven test (RTFO) and pressure aging vessel (PAV). As expected, that binder stiffness increased with binder aging while binder stiffness decreased when the temperature increased. The DSR test results are given in Tables 3.15 to Table 19 and Figure 3.15 to Figure 3.18.

Table 3.15 Kansas binder PG 64-22 results (KS-1)

Temp °C	Original		RTFO		PAV	
	Shear Mod. (G*) Pa	phase angle δ (°)	Shear Mod. (G*) Pa	phase angle δ (°)	Shear Mod. (G*) Pa	phase angle δ (°)
4	1.40E+07	0	3.43E+07	41.31	NA	NA
13	1.02E+07	65.17	1.03E+07	45.2	NA	NA
21	1.76E+06	66.7	4.11E+06	54.3	7.15E+08	42
29	4.67E+05	72.04	1.13E+06	63.32	2.48E+08	48.52
38	89600	78.37	2.28E+05	70.64	5.97E+07	56.63
46	22120	82.31	57800	75.76	1.72E+07	62.85
54	5938	85.23	15420	80.03	5.12E+06	68.32

Table 3.16 Kansas binder PG 64-28 results (KS-2)

Temp °C	Original		RTFO		PAV	
	Shear Mod. (G*) Pa	phase angle δ (°)	Shear Mod. (G*) Pa	phase angle δ (°)	Shear Mod. (G*) Pa	phase angle δ (°)
4	1.49E+07	180	NA	NA	NA	NA
13	3.94E+06	62.27	NA	NA	NA	NA
21	8.28E+05	67.95	NA	NA	NA	NA
29	2.20E+05	69.9	1.60E+05	63.95	NA	NA
38	51310	72.66	2.20E+05	67.22	2.88E+07	58.63
46	16080	74.88	49960	69.48	9.24E+06	62.06
54	5464	76.96	16580	71.76	3.17E+06	64.63

Table 3.17 Missouri binder PG 70-22 results (MO-1)

Temp °C	Original		RTFO		PAV	
	Shear Mod. (G*) Pa	phase angle δ (°)	Shear Mod. (G*) Pa	phase angle δ (°)	Shear Mod. (G*) Pa	phase angle (°)
4	NA	NA	NA	NA	NA	NA
13	NA	NA	NA	NA	NA	NA
21	1.66E+06	65.75	3.97E+06	53	4.62E+08	41.95
29	3.82E+05	68.77	1.32E+06	59.97	1.61E+08	47.84
38	1.10E+05	71.19	3.04E+05	64.99	4.30E+07	54.29
46	31770	72.53	1.44E+05	66.69	1.44E+07	57.54
54	10280	73.23	52370	67.97	5.03E+06	60.48

Figure 3.15 DSR test results on original binder and after TFOT for Kansas mixes
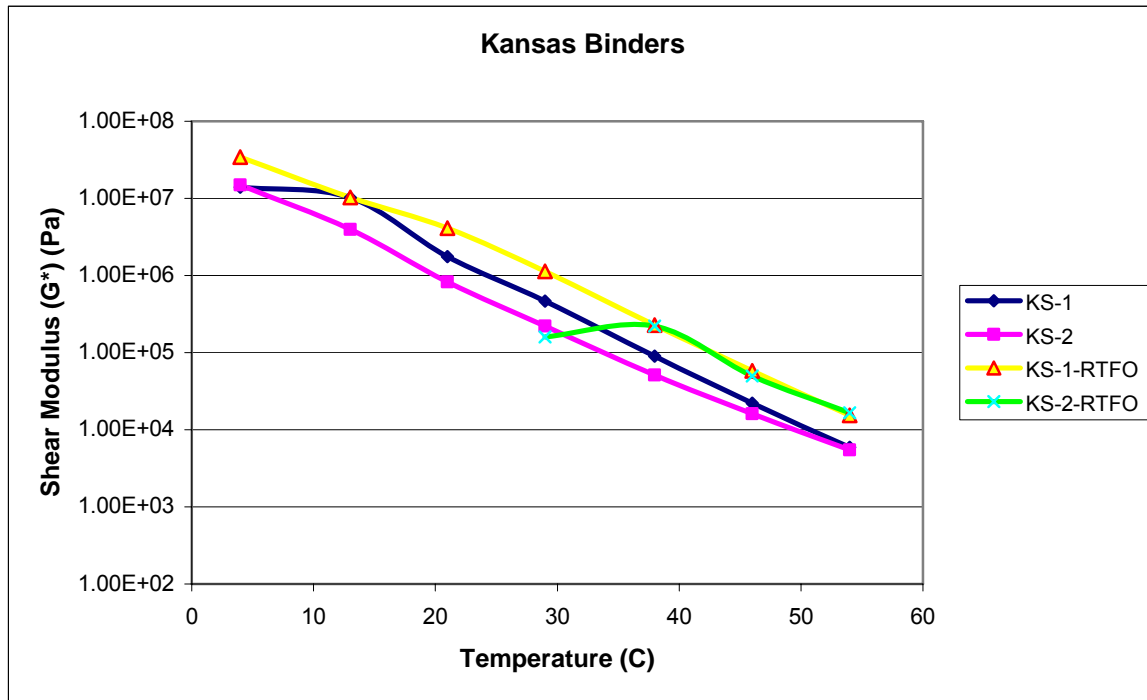
Table 3.18 Missouri binder PG 64-22 results (MO-2)

Temp °C	Original		RTFO		PAV	
	Shear Mod. (G*) Pa	phase angle δ (°)	Shear Mod. (G*) Pa	phase angle δ (°)	Shear Mod. (G*) Pa	phase angle δ (°)
4	NA	NA	NA	NA	NA	NA
13	NA	NA	NA	NA	NA	NA
21	2.02E+06	64.27	8.82E+06	56.1	4.85E+08	42.65
29	4.35E+05	71.44	1.00E+06	63.16	1.60E+08	48.48
38	78130	79.94	2.09E+05	70.07	4.06E+07	55.39
46	19270	81.61	55750	74.88	1.26E+07	59.83
54	5390	84.38	29760	77.14	4.00E+06	65.51

Figure 3.16 DSR test results on original binder and after TFOT for Missouri mixes
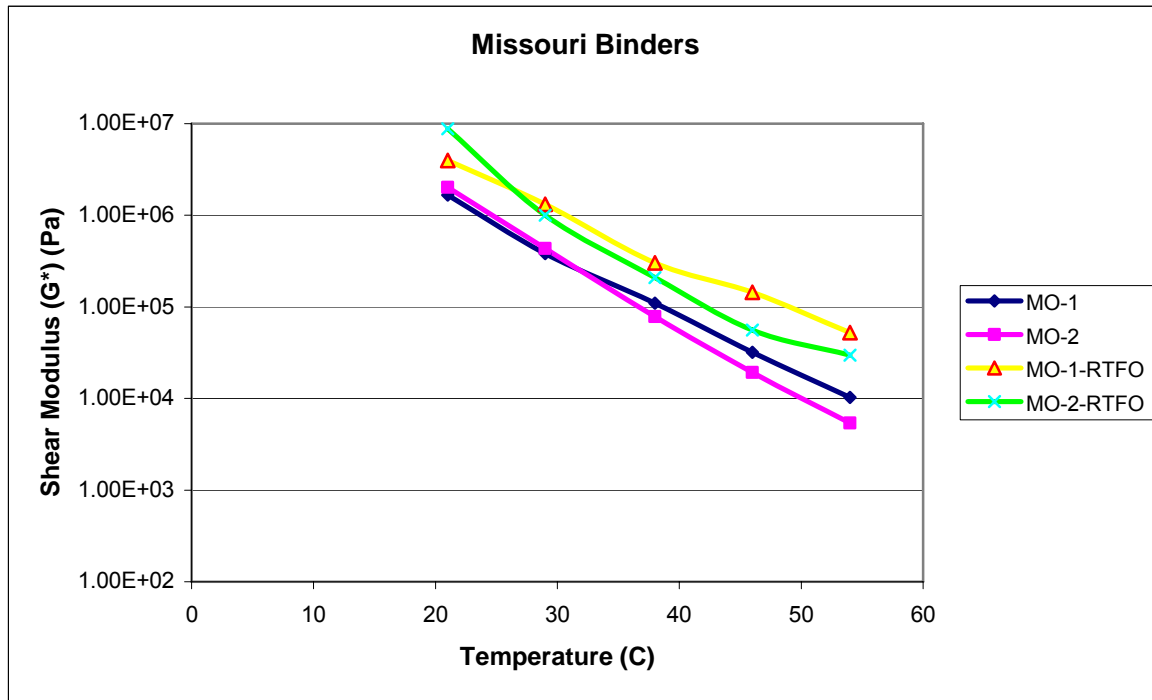
Table 3.19 Iowa binder PG 64-22 results (IA)

Temp ^{o}C	Original		RTFO		PAV	
	Shear Mod. (G*) Pa	phase angle δ (^{o})	Shear Mod. (G*) Pa	phase angle δ (^{o})	Shear Mod. (G*) Pa	phase angle δ (^{o})
4	NA	NA	NA	NA	1.05E+08	26.77
13	NA	NA	NA	NA	3.91E+07	34.3
21	2.06E+06	65.7	7.03E+06	56.79	1.41E+07	41.57
29	4.11E+05	72.68	9.60E+05	62.81	4.39E+06	49.3
38	76150	78.53	1.93E+05	69.97	1.11E+06	57.31
46	19420	82.26	50710	74.78	3.32E+05	63.49
54	5566	85.04	14310	79.33	1.00E+05	68.7

Figure 3.17 DSR test results on original binder and after TFOT for Iowa mixes
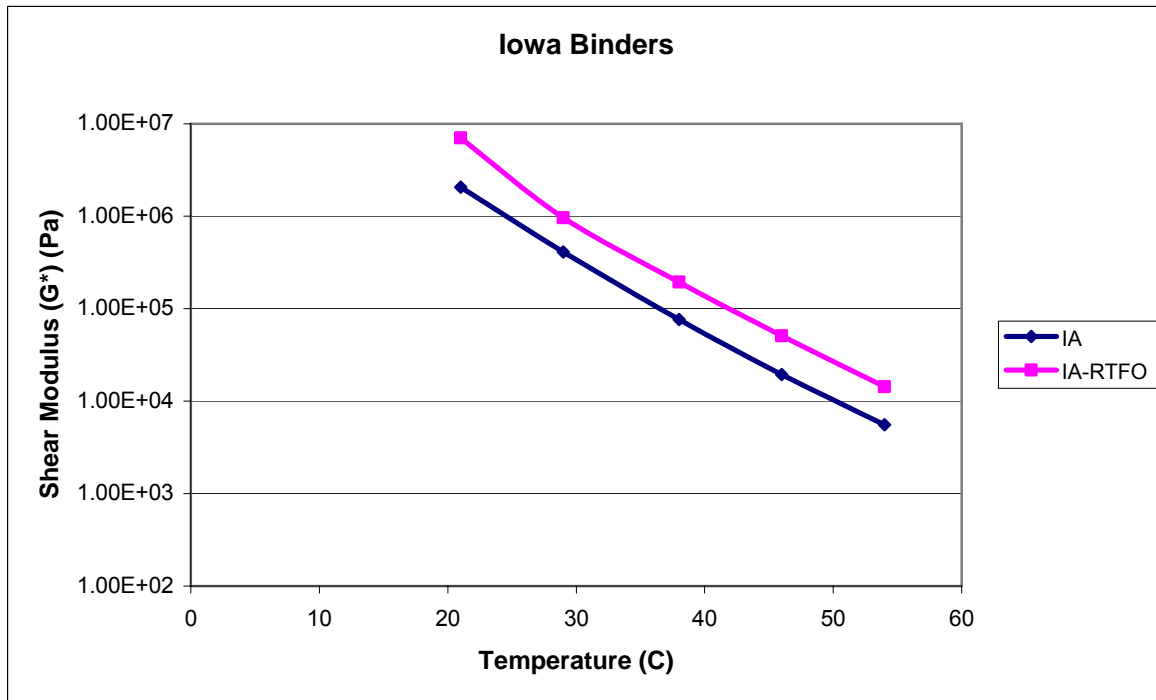
Figure 3.18 DSR test results after PAV for Kansas and Missouri mixes
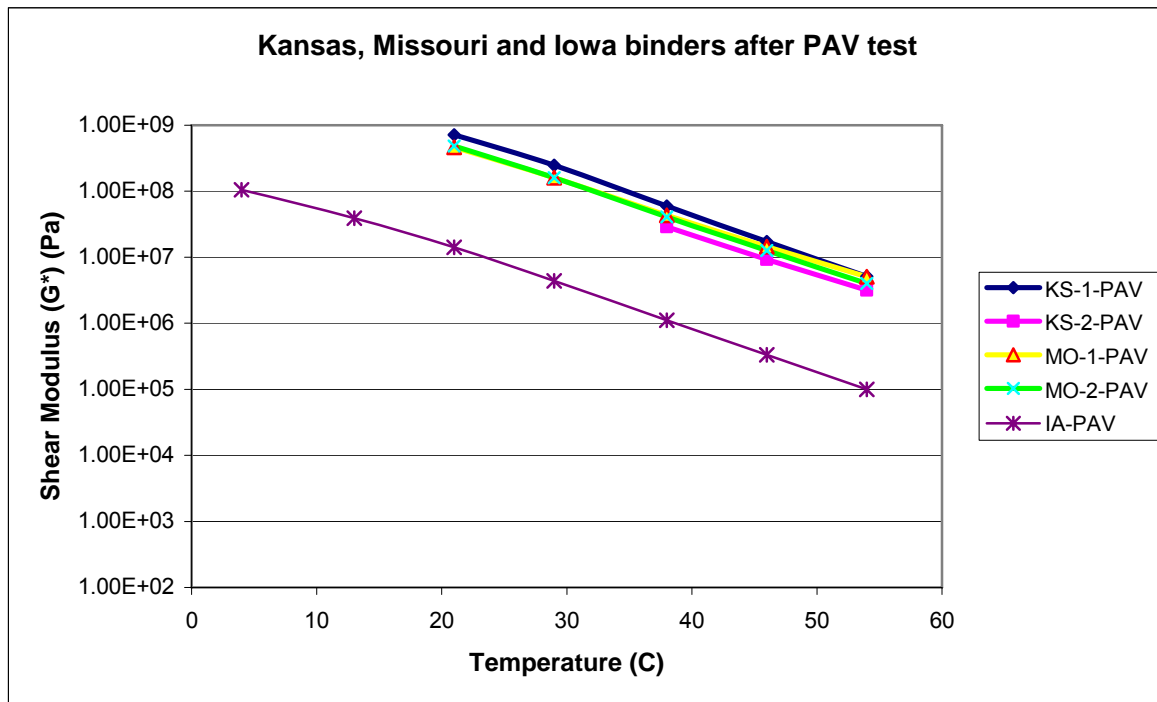
3.3.2 Laboratory Tests on Asphalt Mixes

A limited amount of materials was provided by Kansas, Missouri and Iowa Departments of Transportation (DOTs). These materials were used for construction of road sections in CISL, testing constituent materials and testing asphalt mixes to obtain fundamental properties of materials. The asphalt mix designs were also provided by the DOTs for their respective asphalt mixes. A local contractor was employed to construct the pavement sections in Civil Infrastructure Systems Laboratory (CISL) at Kansas State University. After the construction of pavement sections in CISL, cores were taken and field percent air voids were measured. The contractor provided information on the mix quality control and actual binder content used. This information was used to fabricate samples in the laboratory.

3.3.2.1 Mix Preparation

Samples for Kansas and Missouri mixes were fabricated in the laboratory using individual aggregate samples and asphalt binder that were provided for each mix. Aggregates were blended, heated and mixed with heated asphalt at prescribed mixing temperature (Figure 3.19). Due to shortage of constituent materials, specimens for Iowa mixes were prepared from field mixed, laboratory compacted (FMLC) asphalt mixes. Mixes were collected during the construction of the pavement sections at CISL.

The in-place (field) binder content, provided by the contractor (Table 3.3) was used for the laboratory mixes. Superpave mix design procedure was followed. Asphalt mixes were aged by heating in the oven at 136°C for 3 hrs. Cylinders having 150mm diameter and 170mm height were compacted using the Superpave gyratory compactor (Figure 3.20). The cylinders were compacted at the field percent air voids and were left to cool down before they were removed from the gyratory compactor to the table, for further cooling. Eighteen (18) specimens with 100mm ± 1mm diameter and 150mm ± 2.5mm height were then cored and cut from the cylinders (Figure 3.21). These specimens were used to perform the dynamic modulus test. Twelve (12) specimens for Hamburg Wheel Tester and 12 specimens for Asphalt Pavement Analyzer (APA) test were also fabricated for CISL 14 project.

The specific gravity test was performed on each mix to obtain the theoretical maximum specific gravity. This value is used to calculate sample percent air voids when used with sample bulk specific gravity (G_{mm}). For each fabricated sample, a bulk specific gravity (G_{mb}) was measured and percent air voids was calculated. Samples having air void within ± 0.5 percent of the target air void, were accepted for further testing. Given in Table 3.20 is the summary of sample Maximum specific gravity G_{mm}, binder content and target percent air voids that were used for each asphalt mixtures. The laboratory prepared / laboratory compacted (LPLC) specimens, were used for the tests listed below:

- Dynamic Modulus
- Hamburg Wheel Tester
- Asphalt Pavement Analyzer (APA)

Figure 3.19 mixing asphalt and aggregates

Table 3.20 Laboratory volumetric properties and density

Mix Desg.	KS-1	KS-2	MO-1	MO-2	IA-1	IA-2
% binder	5.61	5.2	5.3	5.4	7.5	7.0
% air voids	6.75±0.5	6.00±0.5	7.00±0.5	9.38±0.5	8.9±0.5	7.00±0.5
Gmm $_{Lab}$	2.4278	2.4586	2.473	2.4526	2.4370	2.439

Figure 3.20 Compaction of Specimens using the Superpave Gyratory Compactor

Figure 3.21 Cored and sawn specimen

3.3.2.2 The Dynamic Modulus Test

The dynamic modulus test was performed to characterize asphalt mixtures and obtain the dynamic (complex) modulus (E*) and phase angle (δ) at a given loading frequency and effective temperature. The dynamic modulus (E*) is among tests that are recommended as simple performance tests (SPT). NCHRP Report 465 (2002) defines the simple performance tests as test methods that "accurately and reliably measures mixture response characteristic or parameter that is highly correlated to the occurrence of pavement distress (i.e. rutting and cracking) over a diverse range of traffic and climatic conditions". For permanent deformation three tests are recommended as having a potential to correlate laboratory results to field performance. These tests are dynamic modulus (E*), Repeated load testing - flow number (F_n) and static creep - flow time (F_t). The repeated load and static creep tests results are reported in Chapter 4 of this dissertation. The dynamic modulus test can be performed on laboratory prepared samples or on cores from existing pavement with dimensions similar to laboratory prepared samples [NCHRP Report 465, 2002].

Dynamic modulus (|E*|) is the norm value of complex modulus obtained by dividing peak to peak stress by peak to peak strain for a material subjected to a sinusoidal (haversine) axial loading (Figure 3.17). The dynamic load ranges between 10 and 690 kPa (1.5 to 100psi), higher load is used for lower test temperatures. The effective temperature (T_{eff}) ranges between 25 - 60°C (77 - 140°F) and the design frequency ranges between 0.1 and 25 Hz. The dynamic load should be adjusted to obtain axial strains between 50 and 150 micro-strains. Specimen ends are treated to reduce friction. The specimen is then placed on the testing chamber at the derived test temperature, and it is left to stabilize before the sample is tested. The test specimen is first preconditioned with 200 cycles at 25 Hz using the target dynamic loads. Then the specimen is loaded using specified temp, frequency and number of cycles. The loading stress and recoverable axial strain are computed for each frequency. Dynamic modulus and the phase angle are then obtained.

Figure 3.22 Sinusoidal loading for Dynamic Modulus

$$\sigma = \sigma_0\, SIN(\omega t)$$

$$\varepsilon = \varepsilon_0\, SIN(\omega t - \phi)$$
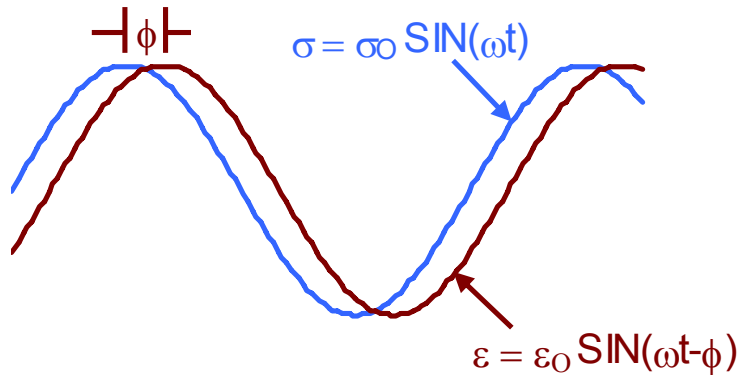
Measurement of the dynamic/complex modulus and phase angle represents one of the methods used to measure stress-strains relationship of visco-elastic materials. The modulus is a complex quantity, of which the real part represents the elastic stiffness and the imaginary part characterizes the internal damping of the material. The absolute value of complex modulus is commonly referred to dynamic modulus [Huang 2004]. Yoder and Witczak 1975 defined the sinusoidal stress $\sigma = \sigma_o$ Sin (wt)

σ_o = Stress amplitude (psi)

w = Angular frequency (rad/sec) and

t   = time in sec

The resultants sinusoidal strain is given by $\varepsilon = \varepsilon_o$ Sin (wt – φ)

ε_o = Recoverable strain amplitude (in/in)

φ = Phase lag (degrees) It is the angle at which ε_o lags σ_o. $\varphi = t_i/t_p(360^o))$

t_i = time lag between a cycle of sinusoidal stress and cycle of strain (sec)

t_p = time for stress cycle (sec)

By definition, the complex modulus E* = E' + iE"

E' = σ_o/ε_ocosφ and refers to the real portion of the complex modulus

E" = σ_o/ε_osinφ and refers to the imaginary portion of the complex modulus

i = an imaginary number.

E* can also be written as E* = | E*| $e^{j\varphi}$

When $\varphi = 0$ (elastic material) E* = | E*| = σ_o/ε_o.

The elastic or dynamic modulus of material (ignoring the viscous effect) may be determined by the ratio of peak stress to strain amplitudes from the complex modulus test.

For CISL 14 project, the dynamic modulus test was performed on the six asphalt mixes from Kansas Missouri and Iowa, on laboratory fabricated samples. The test was performed in accordance to AASHTO TP-62-03, at 20°C and 35°C. A sinusoidal vertical load was applied with no rest periods, on cylindrical samples, 100 mm diameter by 150 mm height, while measuring the corresponding vertical strain (deformation) and phase angle. The test was performed at six loading frequencies, 0.1, 0.5, 1, 5, 10 and 25 Hz. For this test, three Linear Variable Differential Transducers (LVDTs) were used for axial deformation data collection, providing an estimated limit of accuracy of 13.1%. Figure 3.23 shows a schematic diagram of a dynamic modulus test setup. Figure 3.24 presents the test set-up at Kansas State University, in the universal testing machine (UTM). Figure 3.25 shows specimen set-up and LVDT connection. Three specimen replicas were tested for each asphalt mix. Test results from dynamic modulus test at 6 frequencies and two test temperatures are given in Table 3.20 to Table 3.22 and Figures 3.26 and 3.27. More dynamic modulus plots at 6 frequencies are given in Appendix A as figures A-1 to A-6.

Figure 3.23 Schematic of Dynamic (Complex) Modulus Test Device [NCHRP 465]
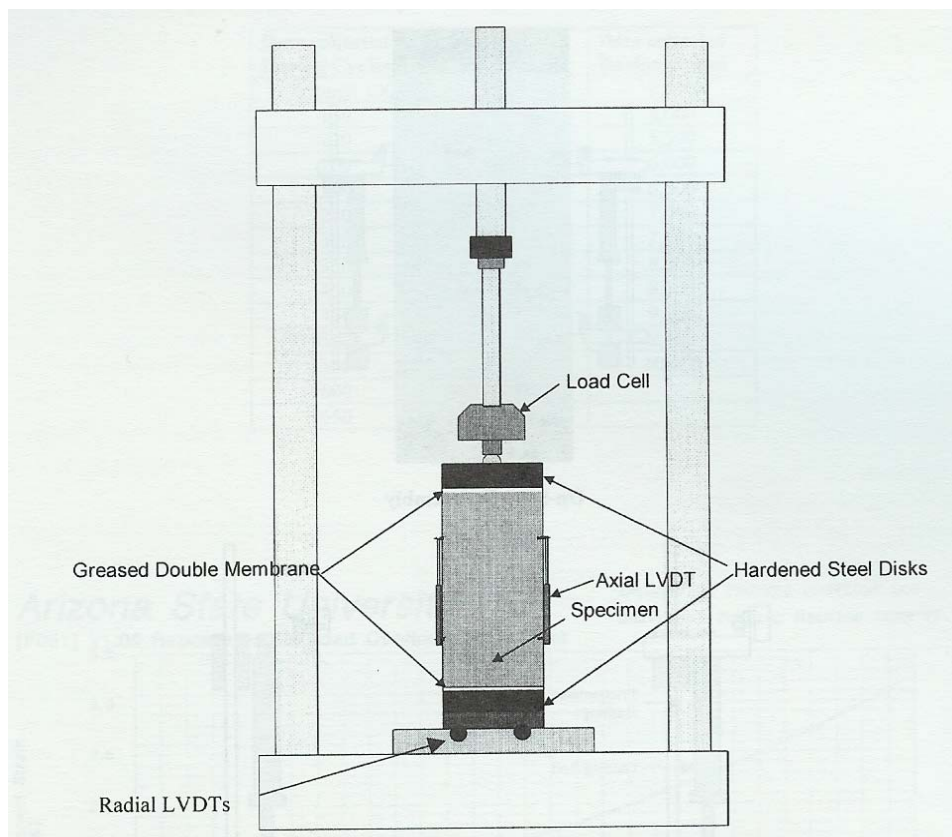
Figure 3.24 Universal Testing Machine (UTM) at KSU

Figure 3.25 Sample set-up and LVDT connections

Table 3.21 Dynamic Modulus test results for Kansas mixes (KS-1 and KS-2) (MPa)

	Sample ID	AV %	20º C						35º C					
			Frequency (Hz)						Frequency (Hz)					
			25	10	5	1	0.5	0.1	25	10	5	1	0.5	0.1
Dynamic Modulus (MPa)	KS-1-07	6.74	11831	10047	8922	6414	5775	3859	5138	3929	3246	2018	1646	1067
	KS-1-08	6.84	13201	11411	10459	8283	7403	5562	7323	5921	5053	3458	2857	1927
	KS-1-09	6.68	10433	8997	7819	5661	5067	3456	4751	3716	3033	1860	1504	999
	Average	6.75	11822	10152	9067	6786	6082	4292	5737	4522	3777	2445	2002	1331
	SD	0.08	1384	1210	1326	1350	1198	1118	1387	1216	1110	881	744	517
	C.V.%	1.20	11.71	11.92	14.62	19.89	19.70	26.04	24.17	26.90	29.38	36.01	37.13	38.86
	KS-2-05	6.93	8128	6374	5398	3581	3004	1903	5229	3192	2398	1426	1118	812
	KS-2-06	6.84	7151	5989	5007	3358	2747	1753	2839	2095	1674	1042	848	620
	KS-2-07	6.74	8433	6797	5863	4047	3415	2224	2702	2011	1633	1059	874	657
	Average	6.84	7904	6387	5423	3662	3055	1960	3590	2433	1902	1176	947	696
	SD	0.10	670	404	429	352	337	241	1421	659	430	217	149	102
	C.V.%	1.39	8.47	6.33	7.90	9.60	11.03	12.28	39.58	27.09	22.63	18.45	15.73	14.63
Phase Angle (Degrees)	KS-1-07	6.74	11.08	15.38	17.86	22	27.78	32.45	22.03	24.54	26.12	28.32	34.39	31.57
	KS-1-08	6.84	9.85	14.75	14.6	18.63	22.48	27.14	17.19	19.85	22.54	27.21	33.92	37.32
	KS-1-09	6.68	11.84	15.81	16.34	21.91	27.7	32.58	22.04	25.06	27.03	28.23	33.96	30.36
	Average	6.75	10.92	15.31	16.27	20.85	25.99	30.72	20.42	23.15	25.23	27.92	34.09	33.08
	SD	0.08	1.00	0.53	1.63	1.92	3.04	3.10	2.80	2.87	2.37	0.62	0.26	3.72
	C.V.%	1.20	9.19	3.48	10.03	9.21	11.69	10.10	13.70	12.40	9.41	2.21	0.76	11.24
	KS-2-05	6.93	17.53	20.92	23.14	27.17	34.78	36.97	24.04	25.84	26.99	26.67	31.2	27.86
	KS-2-06	6.84	20.09	22.04	24.51	29.59	36.45	40.38	23.23	24.65	25.63	25.15	28.73	25.29
	KS-2-07	6.74	12.6	18.38	21.37	26.26	33.08	36.67	23.51	24.49	25.21	24.22	27.56	23.87
	Average	6.84	16.74	20.45	23.01	27.67	34.77	38.01	23.59	24.99	25.94	25.35	29.16	25.67
	SD	0.10	3.81	1.88	1.57	1.72	1.69	2.06	0.41	0.74	0.93	1.24	1.86	2.02
	C.V.%	1.39	22.74	9.17	6.84	6.22	4.85	5.42	1.74	2.95	3.59	4.88	6.37	7.88

Table 3.22 Dynamic Modulus test results for Missouri mixes (MO-1 and MO-2) (MPa)

	Sample ID	AV %	20°C Frequency (Hz)						35°C Frequency (Hz)					
			25	10	5	1	0.5	0.1	25	10	5	1	0.5	0.1
Dynamic Modulus (MPa)	MO-1-09	9.45	9045	7757	6615	4617	4034	2707	4024	3014	2533	1602	1334	934
	MO-1-10	9.56	9315	7564	6434	4340	3767	2370	5036	3856	3146	1867	1534	1008
	MO-1-11	9.29	8854	7326	6432	4528	3940	2563	3399	2526	1991	1226	1012	697
	Average	9.43	9071	7549	6494	4495	3914	2547	4153	3132	2557	1565	1293	880
	SD	0.14	232	216	105	141	135	169	826	673	578	322	263	162
	C.V.%	1.44	2.55	2.86	1.62	3.15	3.46	6.64	19.89	21.48	22.60	20.58	20.36	18.47
	MO-2-02	6.99	6330	5248	4689	3457	3047	2083	3702	2690	2145	1295	1092	764
	MO-2-07	7.09	8490	7075	6003	4004	3375	2159	3942	2990	2397	1488	1233	850
	MO-2-10	7.19	7244	6023	5217	3568	3112	2043	3489	2562	2053	1246	1022	712
	Average	7.09	7355	6115	5303	3676	3178	2095	3711	2747	2198	1343	1116	775
	SD	0.10	1084	917	661	289	174	59	227	220	178	128	107	70
	C.V.%	1.41	14.74	14.99	12.47	7.87	5.46	2.81	6.11	8.00	8.10	9.53	9.63	8.99
Phase Angle (Degrees)	MO-1-09	9.45	14.5	18.31	20.25	26.42	33.84	40.54	22.34	25.11	27	29.31	35	35.4
	MO-1-10	9.56	15.9	18.9	22.69	28.68	36.51	42.94	21.95	25.29	27.76	29.95	36.14	36.61
	MO-1-11	9.29	14.36	17.53	20.33	24.3	31.23	33.59	21.75	24.37	25.77	26.81	32.01	31.6
	Average	9.43	14.9	18.2	21.1	26.5	33.9	39.0	22.0	24.9	26.8	28.7	34.4	34.5
	SD	0.14	0.9	0.7	1.4	2.2	2.6	4.9	0.3	0.5	1.0	1.7	2.1	2.6
	C.V.%	1.44	5.71	3.77	6.57	8.28	7.80	12.44	1.36	1.96	3.74	5.78	6.20	7.57
	MO-2-02	6.99	13.27	16.35	20.22	27.77	35.44	45.1	25.08	27.89	28.5	28.51	32.52	29.53
	MO-2-07	7.09	15.85	19.45	22.79	27.27	35.07	38.54	22.77	25.42	26.87	27.3	31.35	27.61
	MO-2-10	7.19	17.26	21.13	24.66	32.6	42.07	51.65	23.64	27.12	28.71	29.49	32.94	30.11
	Average	7.09	15.5	19.0	22.6	29.2	37.5	45.1	23.8	26.8	28.0	28.4	32.3	29.1
	SD	0.10	2.0	2.4	2.2	2.9	3.9	6.6	1.2	1.3	1.0	1.1	0.8	1.3
	C.V.%	1.41	13.09	12.78	9.88	10.08	10.50	14.54	4.90	4.71	3.59	3.86	2.55	4.50

Table 3.23 Dynamic Modulus test results for Iowa mixes IA-1 and IA-2 (MPa)

	Sample ID	AV %	20º C						35º C					
			Frequency (Hz)						Frequency (Hz)					
			25	10	5	1	0.5	0.1	25	10	5	1	0.5	0.1
Dynamic Modulus (MPa)	IA-1-01	8.71	5838	4790	4216	3035	2642	1719	1746	1203	970	570	480	336
	IA-1-05	8.88	7773	6356	5372	3498	3046	1824	2124	1492	1206	738	594	383
	IA-1-08	8.43	5479	4533	3882	2590	2252	1454	1885	1368	1088	642	528	354
	Average	8.67	6363	5226	4490	3041	2647	1666	1918	1354	1088	650	534	358
	SD	0.23	1234	987	782	454	397	191	191	145	118	84	57	24
	C.V.%	2.62	19.39	18.88	17.41	14.93	15.00	11.45	9.97	10.71	10.85	12.97	10.72	6.63
	IA-2-02	7.13	9312	8161	7320	5586	4992	3501	3312	2617	2218	1416	1177	803
	IA-2-04	7.49	8689	6934	5919	4080	3562	2242	2939	2314	1881	1260	1046	744
	IA-2-05	7.17	6064	5089	4493	3255	2890	2011	3270	2446	2051	1436	1210	830
	Average	7.26	8022	6728	5911	4307	3815	2585	3174	2459	2050	1371	1144	792
	SD	0.20	1724	1546	1414	1182	1074	802	204	152	169	96	87	44
	C.V.%	2.72	21.49	22.98	23.91	27.44	28.14	31.03	6.44	6.18	8.22	7.03	7.58	5.55
Phase Angle (Degrees)	IA-1-01	8.71	16.22	21.25	24.97	32.79	42.13	50.54	25.54	29.52	29.91	27.29	29.01	27.05
	IA-1-05	8.88	15.78	19.61	21.9	28.56	36.73	44.39	26.1	28.8	30.76	31.99	37.77	38.04
	IA-1-08	8.43	15.99	19.3	23.25	29.78	37.59	45.44	25.98	28.38	30.3	30.37	34.74	32.43
	Average	8.67	16.00	20.05	23.37	30.38	38.82	46.79	25.87	28.90	30.32	29.88	33.84	32.51
	SD	0.23	0.22	1.05	1.54	2.18	2.90	3.29	0.29	0.58	0.43	2.39	4.45	5.50
	C.V.%	2.62	1.38	5.23	6.58	7.17	7.47	7.03	1.14	1.99	1.40	7.99	13.15	16.91
	IA-2-02	7.13	10.28	13.77	16.85	22.05	29.07	35.44	20.06	22.8	25.44	27.43	33.42	33.53
	IA-2-04	7.49	15.89	18.16	21.56	27.33	34.5	40.35	23.01	25.51	27.52	28.59	33.31	31.75
	IA-2-05	7.17	13.51	17.41	20.11	24.81	31.65	37.72	21.24	24.4	26.66	29.1	34.98	35.18
	Average	7.26	13.23	16.45	19.51	24.73	31.74	37.84	21.44	24.24	26.54	28.37	33.90	33.49
	SD	0.20	2.82	2.35	2.41	2.64	2.72	2.46	1.48	1.36	1.05	0.86	0.93	1.72
	C.V.%	2.72	21.29	14.28	12.37	10.68	8.56	6.49	6.93	5.62	3.94	3.02	2.76	5.12

Figure 3.26 Dynamic modulus results at 20°C for Kansas, Missouri and Iowa mixes
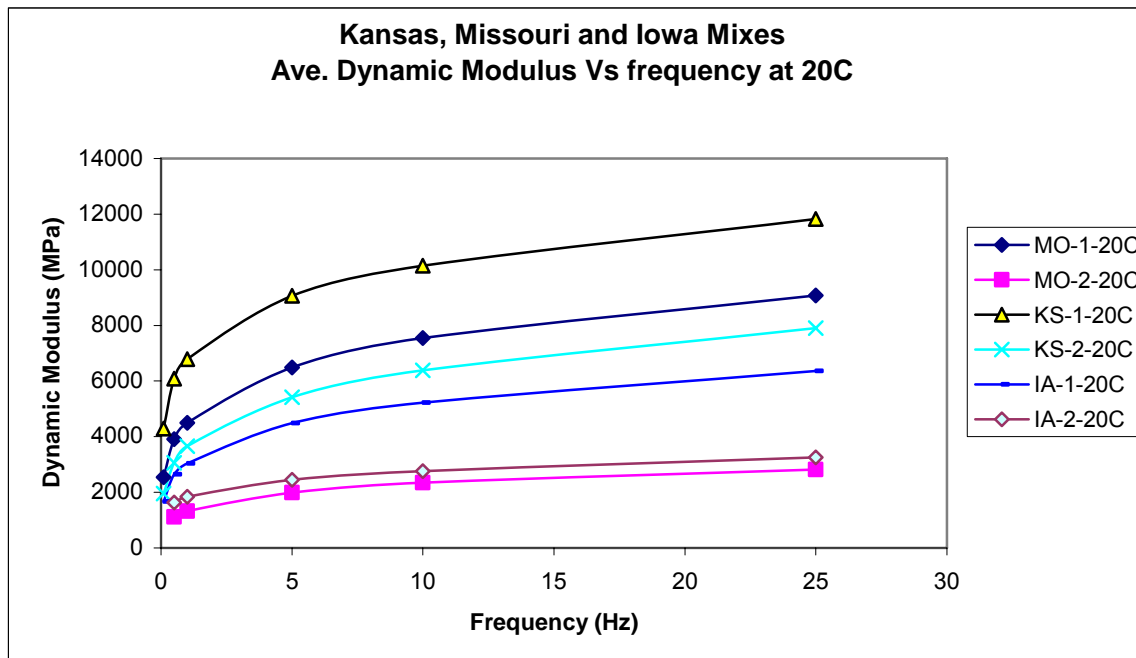
Figure 3.27 Dynamic modulus results at 35°C for Kansas, Missouri and Iowa mixes
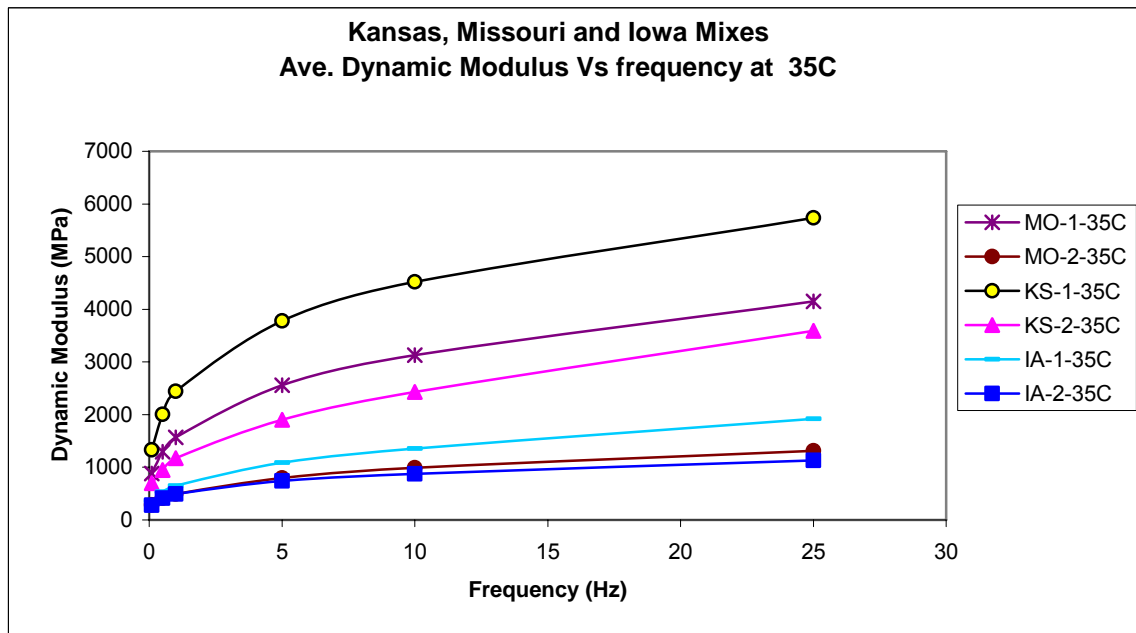
The dynamic modulus test results (Figure 3.26 and 3.27) indicate that dynamic modulus values are higher at lower temperature and lower at higher temperature. This is how asphalt mixes are expected to behave because asphalt is a temperature susceptible material. From the same figures, it is observed that, dynamic modulus is higher at higher loading frequencies. This is because asphalt is dependant on rate of loading, it is stiffer at faster loading rate than at slow loading rate.

Figure 3.26 and Figure 3.27 summarizes results from all the six mixes. Average values from each mix are used. Kansas mix KS-1 has the highest dynamic modulus followed by Missouri mix MO-1. Iowa mix IA-1 has the lowest dynamic modulus. This is because Iowa 30M mix was constructed with a higher binder content than the design requirement and also higher percent of air voids. Figure A-1 and A-2 (Appendix A) shows that, for Kansas mixes, KS-1 has high values of dynamic modulus than KS-2 mix. Missouri mix MO-1 has higher average values of dynamic modulus than MO-2 mix (Figure A-3, and Figure A-4). Iowa mix IA-2 has higher values of dynamic modulus than IA-1 mixes (Figure A-5 and Figure A-6).

Dynamic modulus master curves were plotted with 35°C as reference temperature. Results obtained at 20°C were shifted to form a master curve at 35°C. Master solver version 2 (see section 4.2.5) was used for plotting the master curves. Given below in Figures 3.28 to Figure 3.33 are master curve plots for the six asphalt mixes. The average of three replicas was used to plot the master curves. The phase angle plots are given in Appendix A Figure A-7 to A-12, and shift factor plots are given in Figures A-13 to A-14. The MEPGD input values are also provided in Tables A-1 to A-6 in Appendix A. Equation 3.1 provides the sigmoid function (master curve equation) and Table 3.24 provides the sigmoid function parameters used for each mix. "E_a" stands for activation energy and it is used as a fitting parameter.

$$\log|E*| = \delta + \frac{(Max - \delta)}{1 + e^{\beta + \gamma \log w_r}}$$

3.1

Where:

|E*|	= dynamic Modulus
ω_r	= reduced frequency, Hz
Max	= limiting maximum modulus
δ, β and γ	= fitting parameters

Table 3.24 Sigmoid function fitting parameters

Fit Parameter	KS-1	KS-2	MO-1	MO-2	IA-1	IA-2
Delta (δ)	1.2777	1.2895	0.5248	0.7363	0.8027	1.7462
Beta (β)	-0.2000	0.3000	-0.5000	0.7340	0.7340	0.7340
Gamma (γ)	-0.5684	-0.5000	-0.5000	-0.5000	-0.5684	-0.5684
E_a	200000	200000	200000	200000	200000	200000

Figure 3.28 Master curve plot for Kansas mix (KS-1) at 35°C
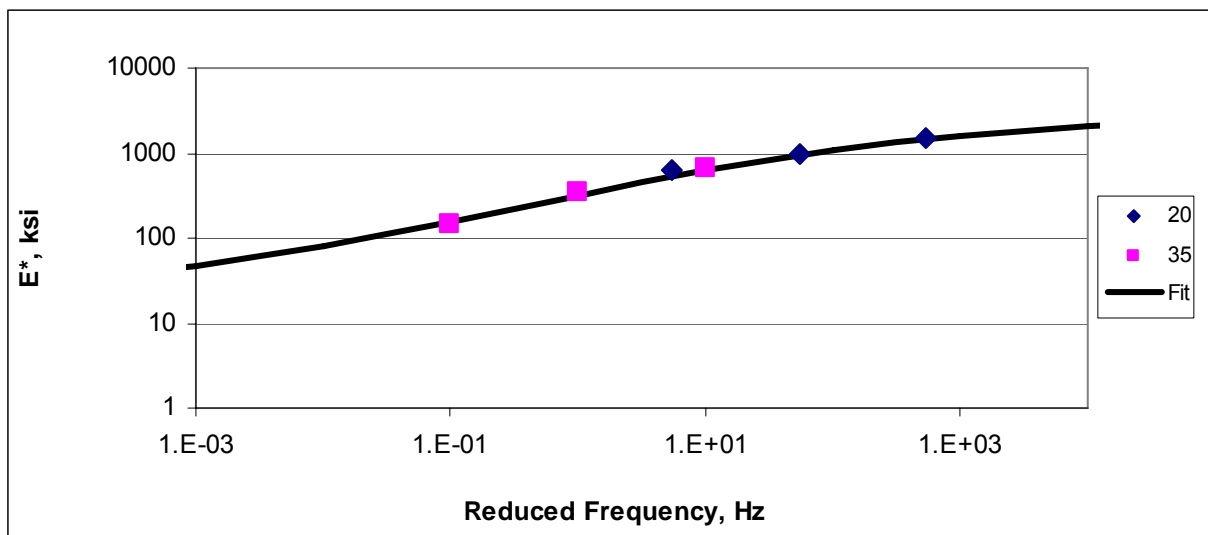
Figure 3.29 Master curve plot for Kansas mix (KS-2) at 35°C
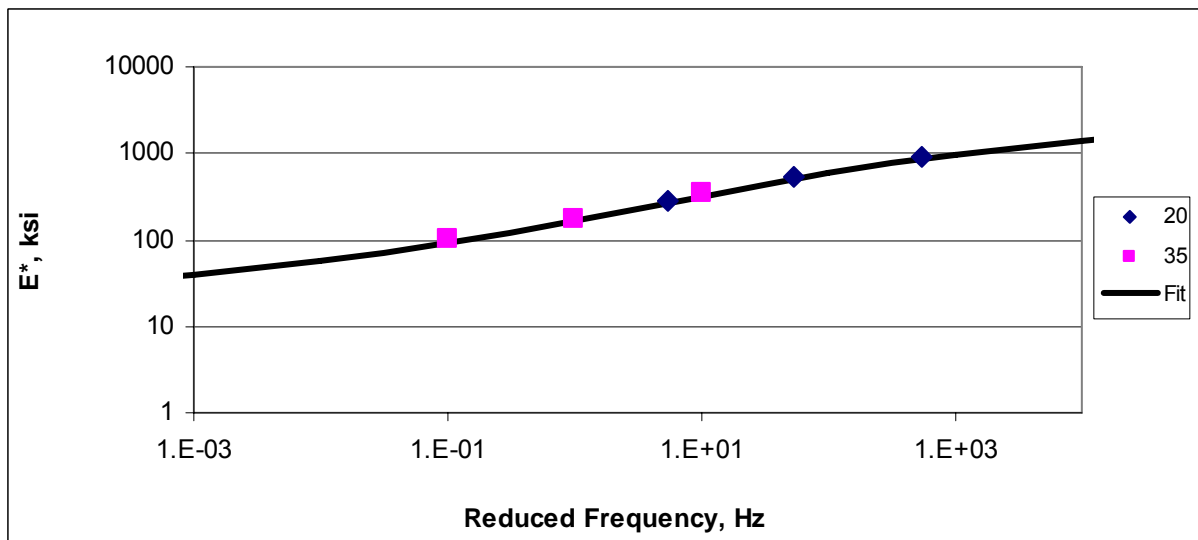
Figure 3.30 Master curve plot for Missouri mix (MO-1) at 35°C
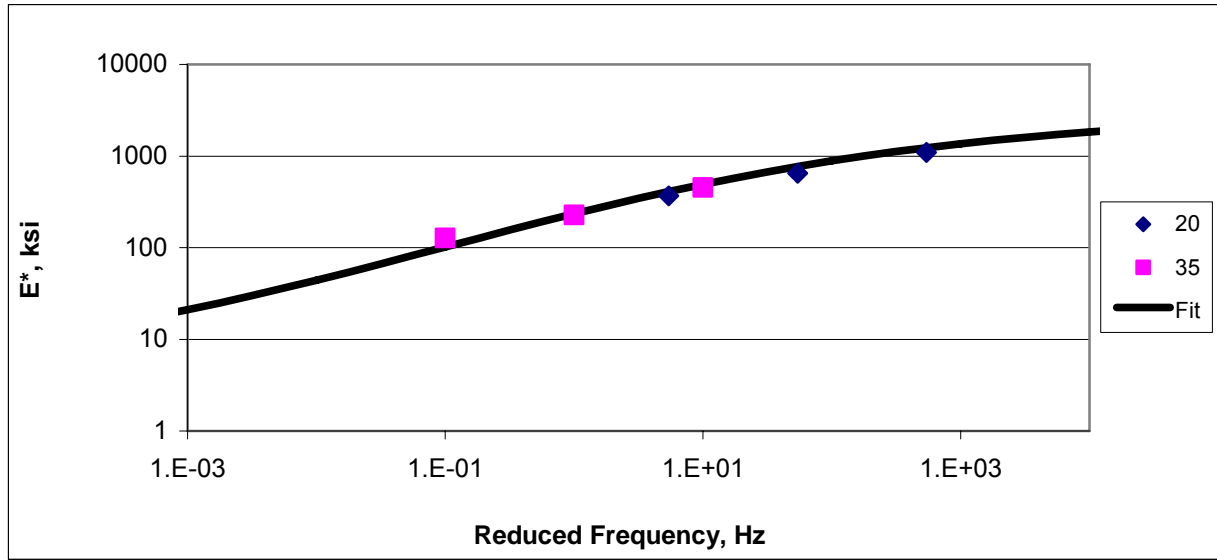
Figure 3.31 Master curve plot for Missouri mix (MO-2) at 35°C
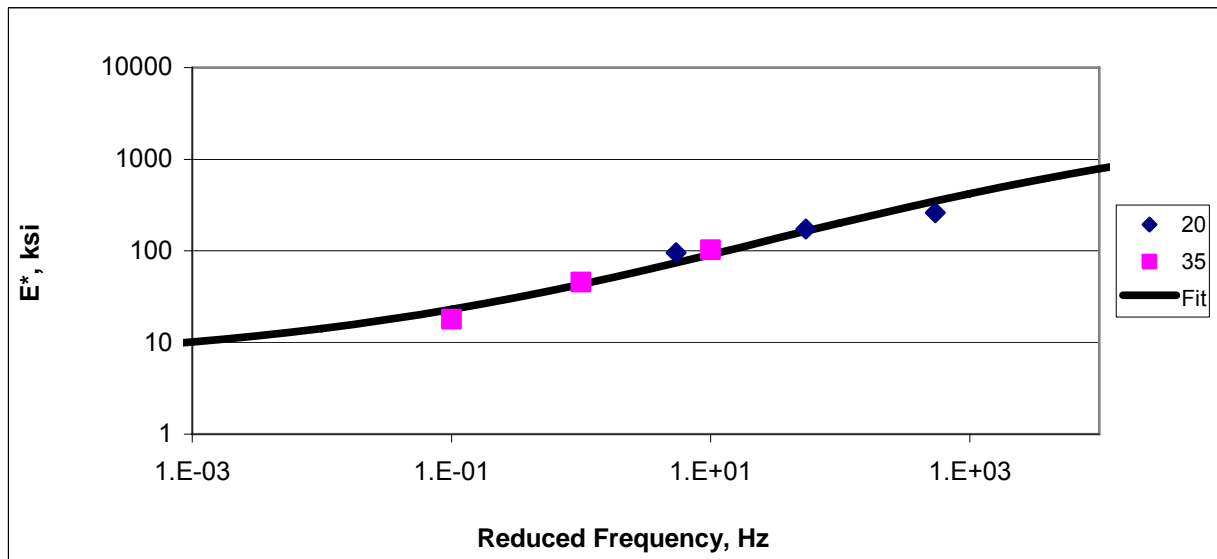
Figure 3.32 Master curve plot for Iowa mix (IA-1) at 35$^{\text{o}}$C
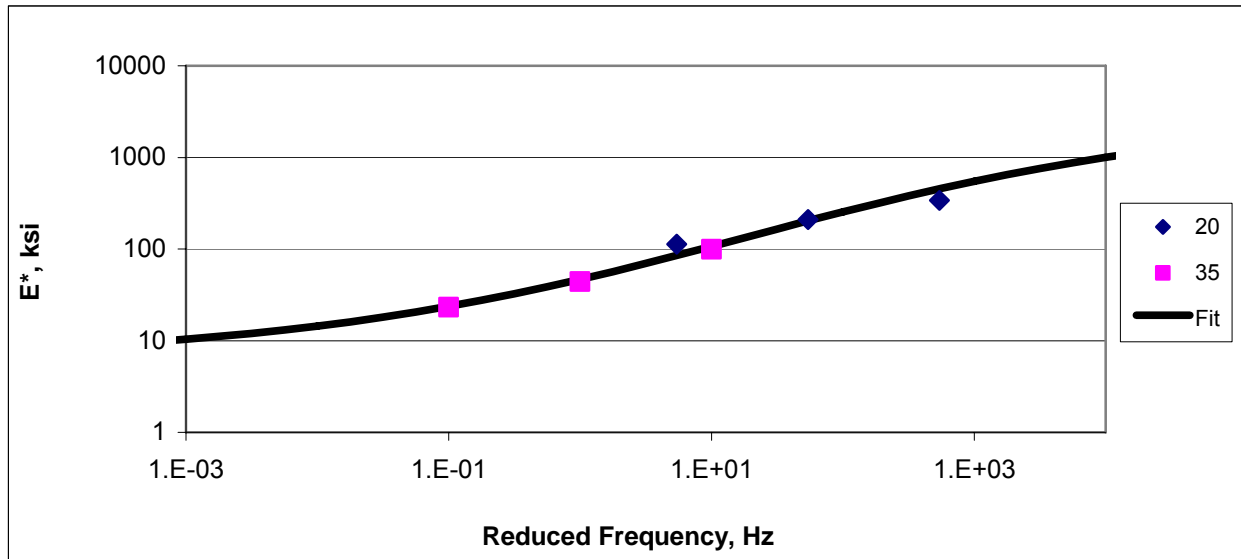
Figure 3.33 Master curve plot for Iowa mix (IA-2) at 35$^{\text{o}}$C
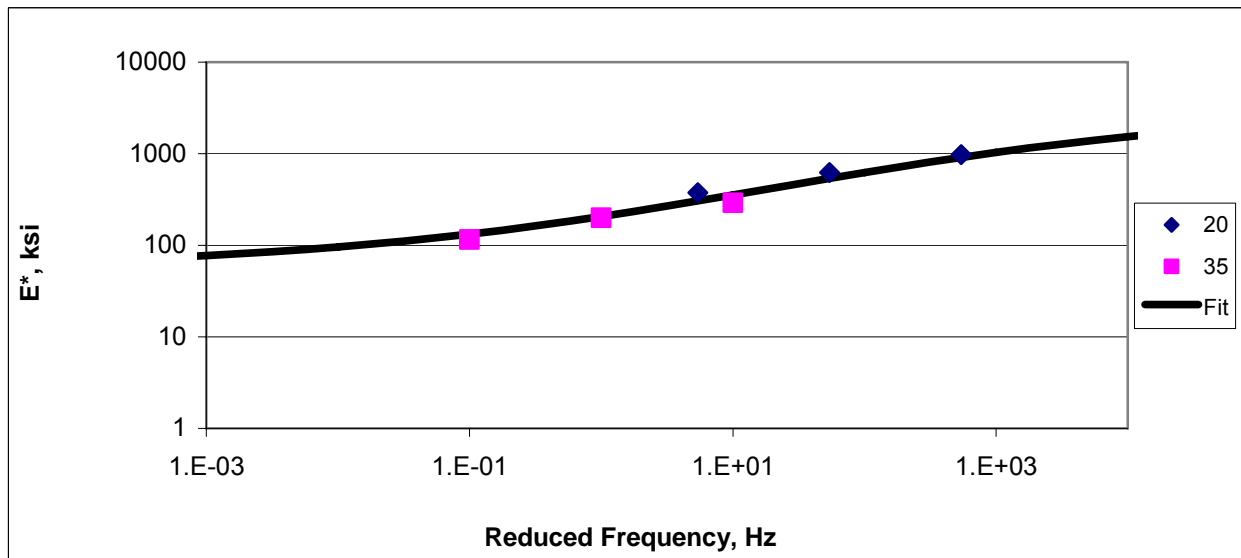
From the master curves the values of dynamic modulus at reference temperature, 35$^{\text{o}}$C were obtained for each frequency. Table 3.25 below provides the dynamic modulus values (E*) measured from the dynamic modulus test.

Table 3.25 Dynamic Modulus values measured at different frequencies

(a) values in ksi

Frequency (Hz)	E* (ksi)					
	KS-1	KS-2	MO-1	MO-2	IA-1	IA-2
25.0	788.0	407.0	633.7	124.8	150.9	444.6
10.0	620.5	317.9	491.4	91.0	106.6	354.1
5.0	510.7	262.8	398.8	72.0	82.3	298.9
1.0	314.0	169.1	234.2	43.1	46.7	206.0
0.5	252.6	140.6	183.2	35.1	37.3	178.0
0.1	152.9	94.1	101.5	22.9	23.6	131.9

(b) Values in MPa

Freq. (Hz)	E* (MPa)					
	KS-1	KS-2	MO-1	MO-2	IA-1	IA-2
25.0	5435.1	2806.8	4370.8	860.8	1040.7	3066.4
10.0	4279.3	2192.8	3388.9	628.0	735.4	2442.4
5.0	3522.0	1812.8	2750.3	496.9	567.7	2061.3
1.0	2166.0	1166.4	1615.2	297.0	321.8	1420.9
0.5	1742.4	970.0	1263.6	242.1	257.4	1227.4
0.1	1054.7	648.7	700.3	158.2	163.0	910.0

The CISL testing speed was 7.6 mph. This vehicle travel speed induces a loading with a corresponding frequency of approximately 3.8 Hz (7.6/2). The E* values were then obtained from the master curves at a frequencies of 3.8 Hz, between 1.0 Hz and 5Hz. The values E* values obtained, given in Table 3.26, were used for implementation of the models.

Table 3.26 Measured dynamic modulus (E*) values

Mix	KS-1	KS-2	MO-1	MO-2	IA-1	IA-2
E* (ksi)	452	235	349	63	72	271
E* (MPa)	3115	1619	2410	437	494	1869

3.3.2.3 The Hamburg Wheel-Tracking Machine

The Hamburg wheel tracking test was performed in accordance with AASHTO T324 to evaluate the rutting and moisture-susceptibility of hot-mix asphalt (HMA) samples using the Hamburg Wheel-Tracking Device. The test consists of two separate steel wheels moving back and forth on asphalt concrete specimens (Figure 3.34). The test was run simultaneously on two laboratory compacted asphalt concrete slabs, which are mounted and placed in a temperature controlled water bath. The slabs were compacted using the Linear Kneading Compactor. The kneading action of the compactor achieves the desired density without fracturing aggregates. The rut depth and number of passes were measured. The performance of the HMA was evaluated, to determine the failure susceptibility of the HMA due to weakness in the aggregate structure, inadequate binder stiffness, or moisture damage. The Hamburg test was performed at two temperatures $35^{o}C$ and $50^{o}C$ for each asphalt mix. Maximum number of 20,000 loads repetitions or maximum failure depth of 20mm were adopted as failure criteria. Results from this test are given in Table 3.27 and Figures 3.36 to 3.41.The test has been used to evaluate rutting in asphalt mixes.

Figure 3.34 The Hamburg Wheel-Tracking Machine

Figure 3.35 Typical Hamburg test Curve and major characteristics
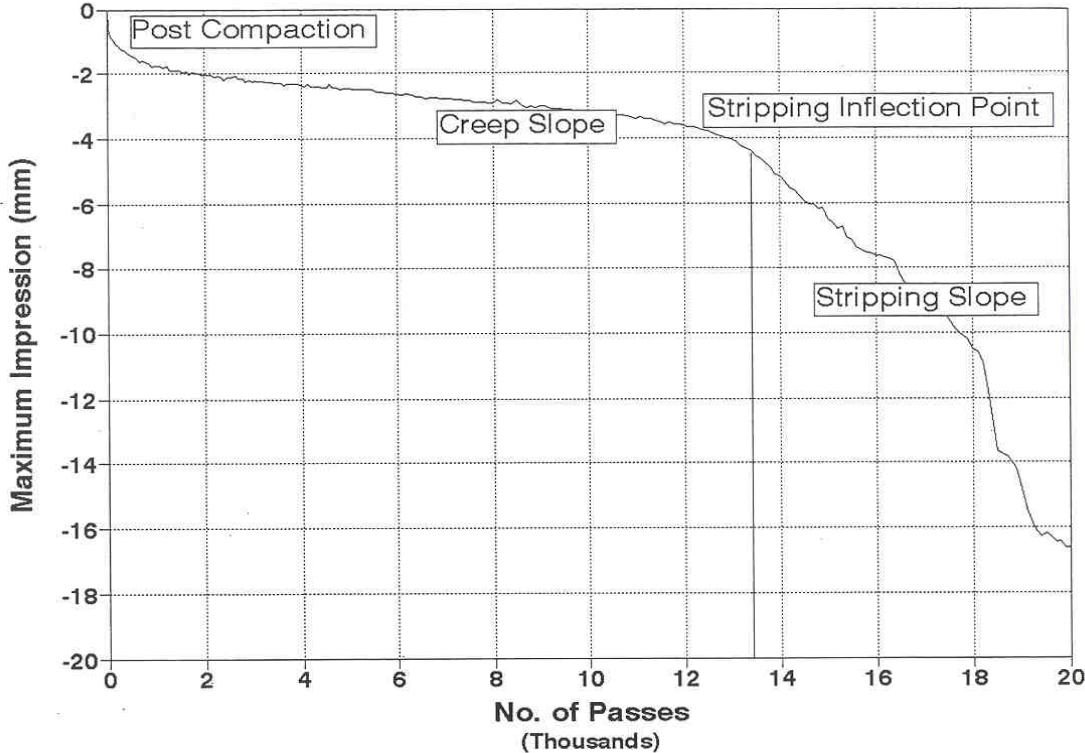
Table 3.27 Hamburg Wheel Test Results

Sample ID	Mix type	Binder Grade	Air Voids (%)	Max. No. of passes	Max. Depth (mm)	Tests Temp (oC)
MO-1-L	M 12.5	PG 70-22	9.02	20,000	6.24205	50
MO-2-L	M 12.5	PG 64-22	6.945	16,046	20.00*	50
KS-1-L	SM 19A	PG 64-22	6.02	20,000	2.38442	50
KS-2-L	SM 12.5A	PG 64-28	6.76	11,350	20.00*	50
MO-1-C	M 12.5	PG 70-22	7.47	20,000	4.54	50
MO-2-C	M 12.5	PG 64-22	7.87	16,702	20.00*	50
KS-1-C	SM 19A	PG 64-22	6.63	10,006	20.00*	50
KS-2-C	SM 12.5A	PG 64-28	6.30	12,270	20.00*	50
MO-1-L	M 12.5	PG 70-22	9.61	20,000	3.71951	35
MO-2-L	M 12.5	PG 64-22	7.33	20,000	3.74809	35
KS-1-L	SM 19A	PG 64-22	6.17	20,000	2.38442	35
KS-2-L	SM 12.5A	PG 64-28	6.85	20,000	3.39566	35
MO-1-C	M 12.5	PG 70-22	7.63	20,000	3.47	35
MO-2-C	M 12.5	PG 64-22	7.86	20,000	3.96	35
KS-1-C	SM 19A	PG 64-22	6.14	20,000	4.69	35
KS-2-C	SM 12.5A	PG 64-28	5.80	20,000	4.21	35
IA-1-C	12.5	PG 64-22	8.86	3,324	20.00*	50
IA-2-C	12.5	PG 64-22	7.24	6,500	20.00*	50
IA-1-C	12.5	PG 64-22	9.02	20,000	10.15	35
IA-2-C	12.5	PG 64-22	8.16	20,000	5.31	35

NOTE:

* = Sample failed

L = Laboratory prepared sample

C = Sample cored from the test road section.

Figure 3.36 Hamburg Wheel Test Results for Kansas mixes tested at 35°C
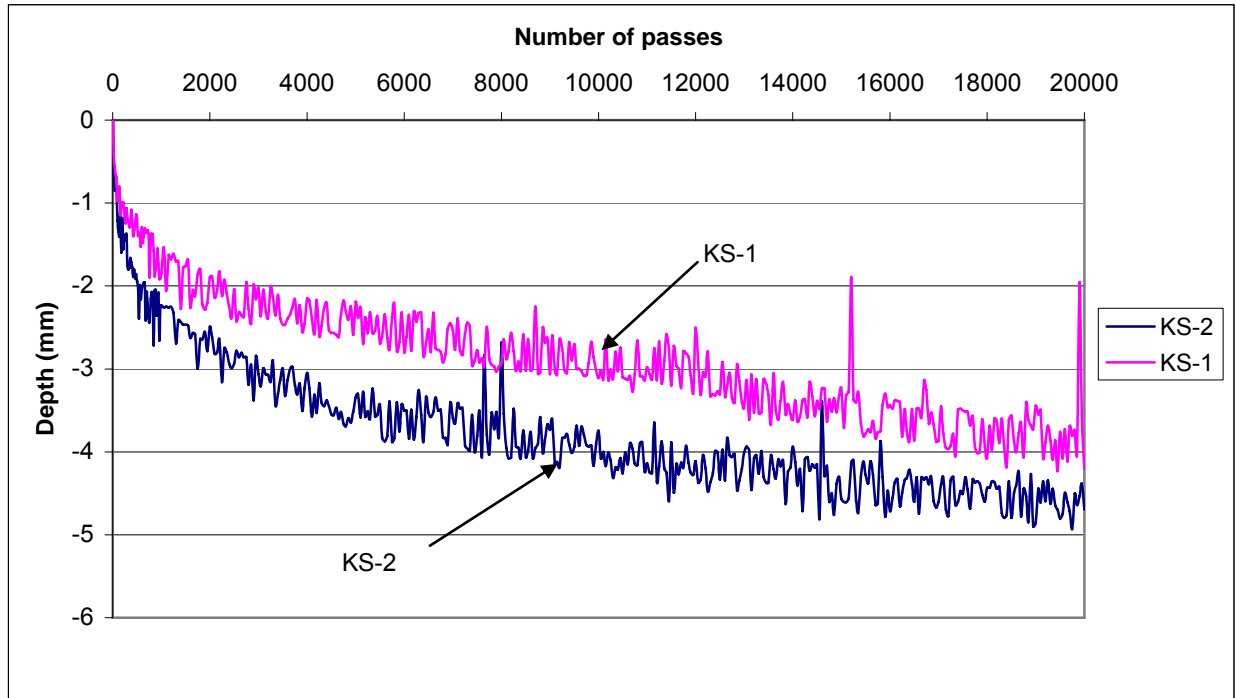
Figure 3.37 Hamburg Wheel Test Results for Kansas mixes tested at 50°C
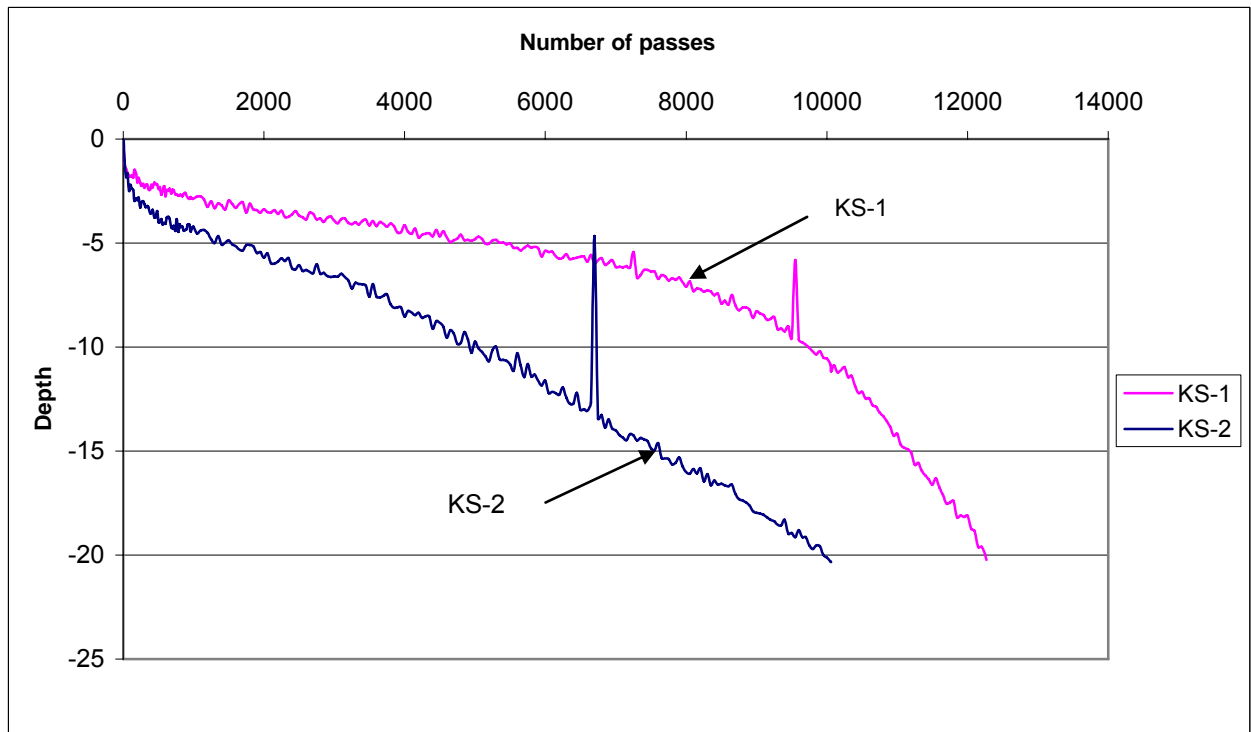
Figure 3.38 Hamburg Wheel Test Results for Missouri mixes tested at 35°C
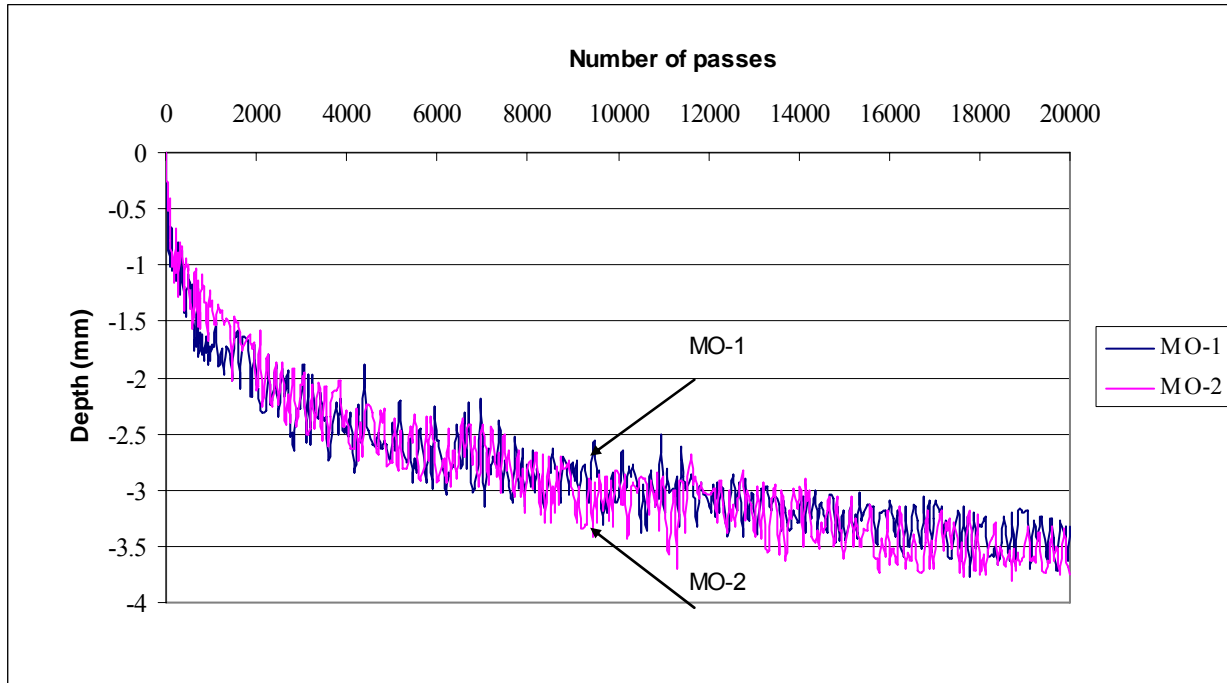
Figure 3.39 Hamburg Wheel Test Results for Missouri mixes tested at 50°C
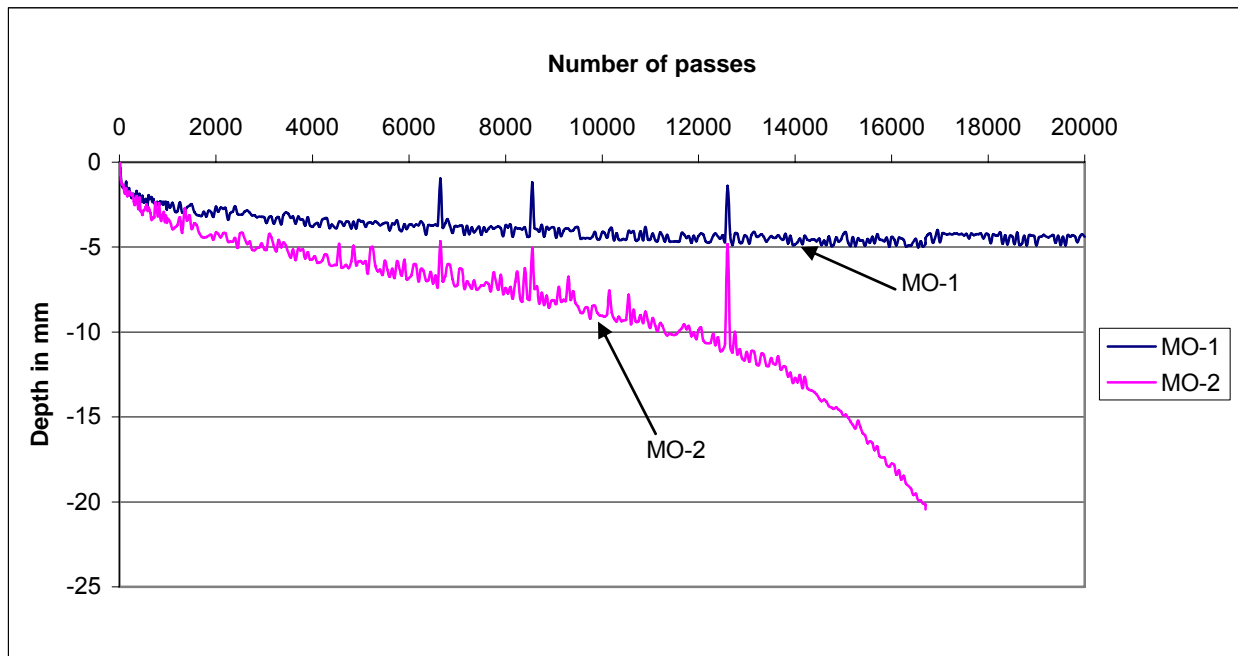
Figure 3.40 Hamburg Wheel Test Results for Iowa mixes tested at 35°C
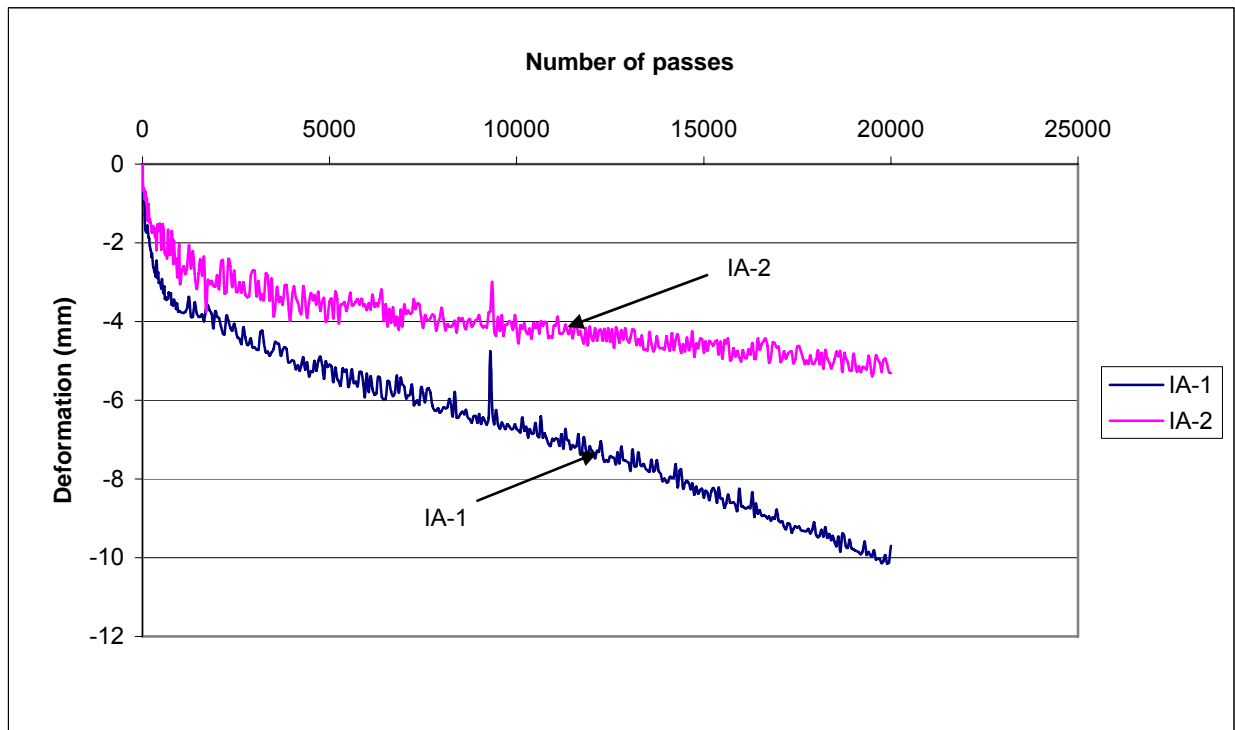
Figure 3.41 Hamburg Wheel Test Results for Iowa mixes tested at 50°C
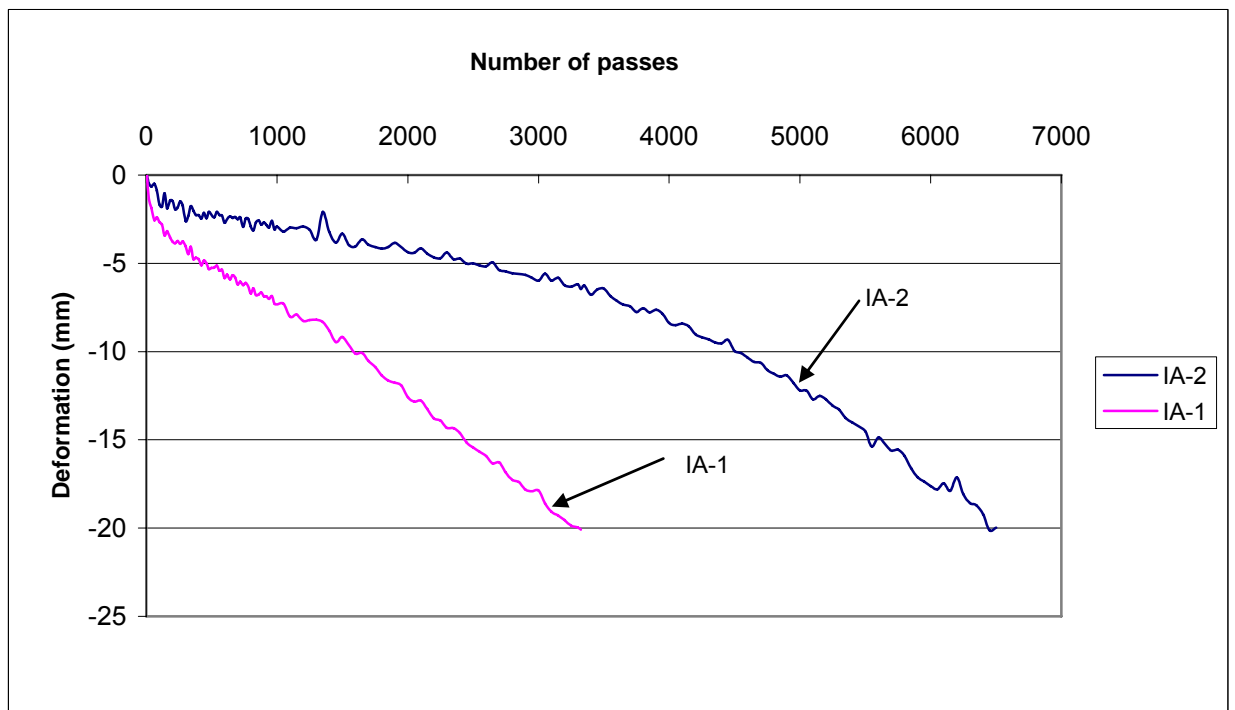
Kansas mix KS-2, Missouri mix MO-2 and both Iowa mixes IA-1 and IA-2 failed after 11,350, 16,046, 3,324 and 6,500 repetitions respectively when tested at 50°C. KS-1 and MO-1 mixes did not fail at neither 35°C nor 50°C, indicating that they are more resistant to permanent deformation than the other four mixes. At 35°C all six mixes did not fail.

3.3.2.4 Asphalt Pavement Analyzer

The use of Asphalt Pavement Analyzer (APA) started in the mid 1990's after the modification of the Georgia Wheel Load Tester. APA evaluates the fatigue cracking and rutting susceptibilities of asphalt concrete specimens or pavement samples. The APA is a multifunctional loaded wheel tester that uses pneumatic cylinders on a concave metal wheel to apply repetitive load applications through a pressurized rubber hose. Typically, 8,000 repetitions or strokes are applied to the HMA specimens. Contact pressure of up to 1,378 kPa (200 psi) can be generated, but typically a contact pressure of 690 kPa (100 psi) contact pressure is used to simulate actual field loading conditions. Calibration of the applied load, contact pressure and deformation measurement is built in to the APA system and it is computer controlled. The APA can accommodate triplicate beam specimens (100 mm x 300 mm x 75 mm thick) or three sets of two cylindrical specimens. Cylindrical specimens are 150 mm diameter with a standard thickness of 75 mm (Figure 3.42).

The APA test was performed on samples having 150mm diameter and 75 mm thickness fabricated in KSU Asphalt Laboratory. The APA test was performed at Missouri Department of Transportation because Kansas State University does not own an Asphalt Pavement Analyzer. The laboratory fabricated samples were tested at two temperatures, 35°C and 64°C, to a maximum number of passes of 8,000 while measuring the rut depth. Results from APA test are given in Table 3.28 and Figure 3.43 to Figure 3.46. Results provided are for Kansas and Missouri mixes. Iowa mixes were weaker than the other mixes and failed at a lower number of load repetitions. For instance, IA-1 samples at 64°C failed at sitting. Due to the difficult in testing Iowa mixes, results were manually obtained and no plots are available for these samples

Figure 3.42 Asphalt Pavement Analyzer (APA) test setting

Table 3.28 Asphalt Pavement Analyzer (APA) Test Results

Tests Temp (°C)	Sample ID	Mix type	Binder Grade	Air Voids (%)	Max. No. of passes	Max. Depth (mm)
35	KS-1	SM 19A	PG 64-22	6.16	8,000	1.08
	KS-2	SM 12.5 A	PG 64-28	6.58	8,000	1.59
	MO-1	M 12.5	PG 70-22	9.69	8,000	1.71
	MO-2	M 12.5	PG 64-22	7.27	8,000	2.15
	IA-1	12.5	PG 64-22	9.14	8,000	2.27
	IA-2	12.5	PG 64-22	7.71	8,000	3.18
64	KS-1	SM 19A	PG 64-22	6.32	8,000	4.17
	KS-2	SM 12.5A	PG 64-28	6.70	8,000	8.61
	MO-1	M 12.5	PG 70-22	9.28	8,000	3.90
	MO-2	M 12.5	PG 64-22	7.21	8,000	5.50
	IA-1	12.5	PG 64-22	8.7	8,000	Failed
	IA-2	12.5	PG 64-22	7.20	8,000	9.48

Figure 3.43 Asphalt Pavement Analyzer (APA) test results for Kansas mixes at 35ºC
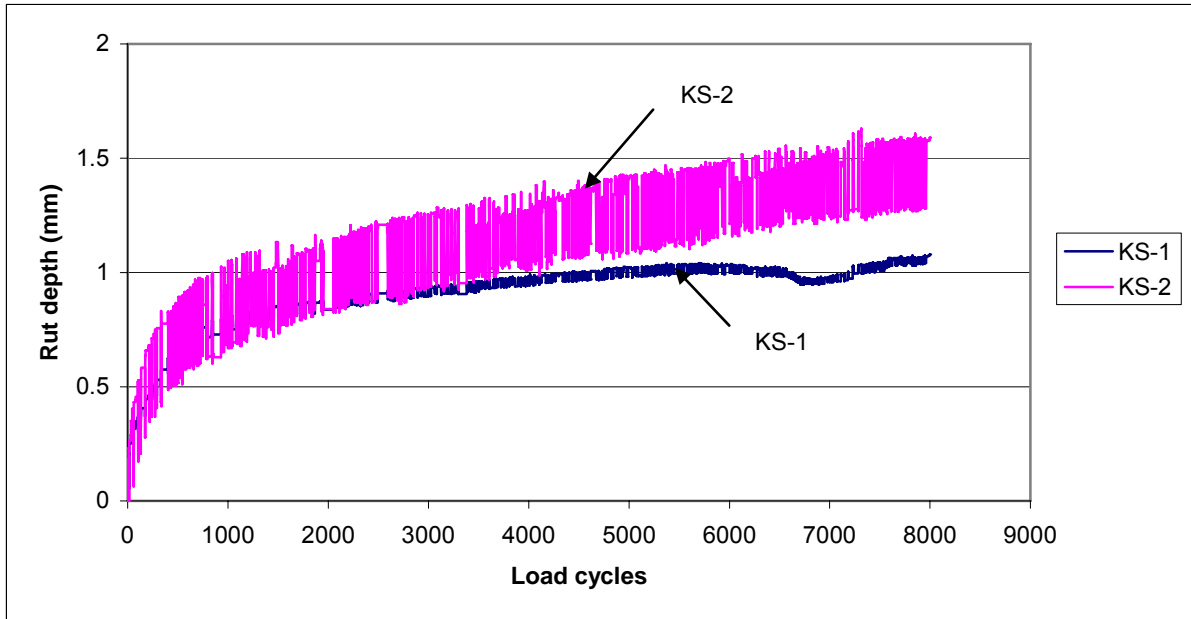
Figure 3.44 Asphalt Pavement Analyzer (APA) test results for Kansas mixes at 64ºC
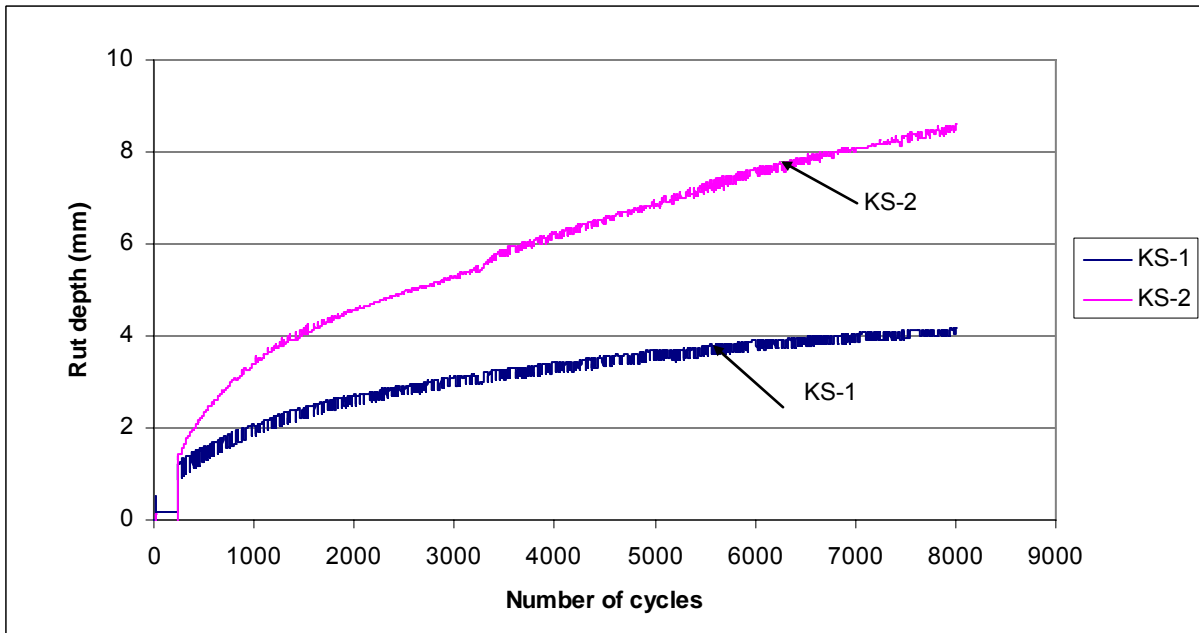
Figure 3.45 Asphalt Pavement Analyzer (APA) test results for Missouri mixes at 35°C
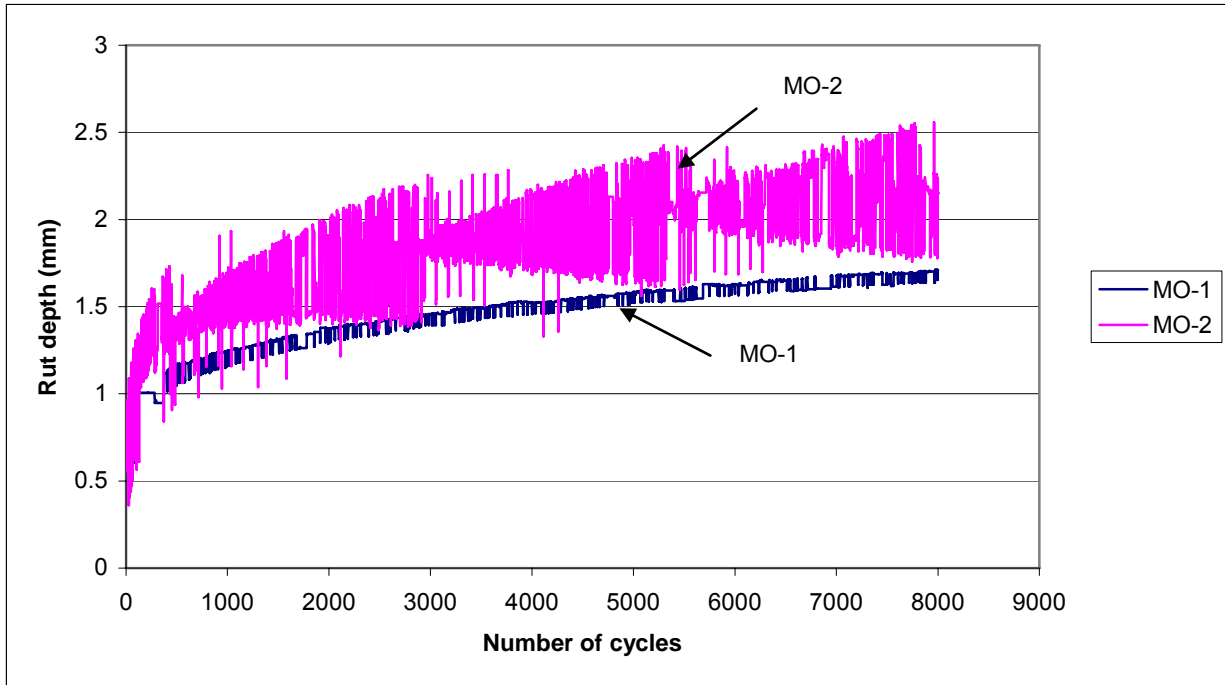
Figure 3.46 Asphalt Pavement Analyzer (APA) test results for Missouri mixes at 64°C
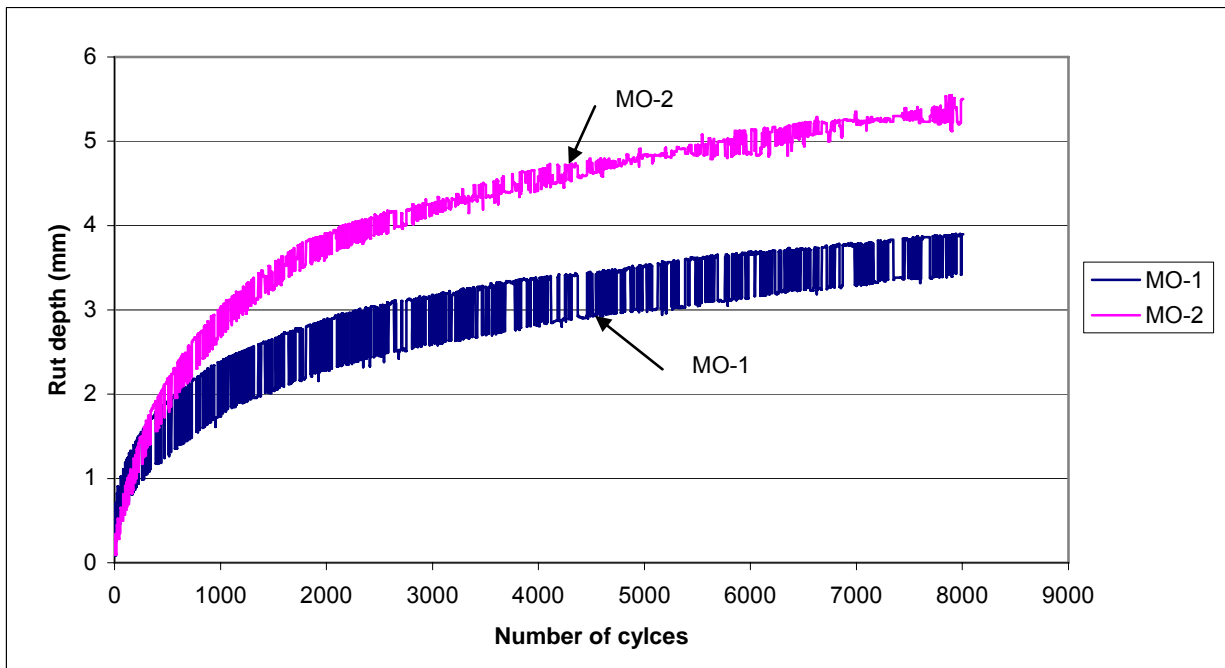
CHAPTER 4 - DETERMINATION OF MECHANICAL PROPERTIES OF HOT MIX ASPHALT

The aim of this research effort is to verify selected mechanistic prediction models for permanent deformation by comparing computed permanent deformations to those measured in a full-scale accelerated pavement test. Prediction models were selected for verification after literature review. Selection criteria for the models included material characterization method and the ability of the model to be integrated into the Abaqus finite element software. Models that required laboratory tests that could not be performed at Kansas State University or can not be implemented into Abaqus software, were avoided. Laboratory tests were performed on asphalt mixes to obtain parameters required by each model. Chapter two provides the details of the models reviewed for this research. Four models were selected for evaluation: creep model, elasto-plastic model (Drucker-Prager), viscoelastic and elasto-visco-plastic model. Six asphalt mixtures from Kansas, Missouri and Iowa were used to verify the models.

Six pavement sections were constructed in the Civil Infrastructure Systems Laboratory (CISL) at Kansas State University with asphalt mixes from Kansas, Missouri and Iowa. The percent air voids and binder contents measured from the road sections were used as inputs for sample fabrication in the laboratory. The sections were loaded with up to 700,000 load repetitions of a 22,000lb single axle. The transverse profiles at the pavement surface were measured periodically. Results obtained from this test were compared with results obtained using Abaqus simulations. Asphalt mix samples fabricated in the laboratory using a gyratory compactor were subjected to dynamic modulus, static and dynamic creep tests, and triaxial and uniaxial strength tests. Other tests performed to evaluate the mixes include Asphalt Pavement Analyzer (APA), Hamburg test, and Repetitive simple shear test at constant height (RSST-CH).

4.1 Development of Testing Factorial

For this research project, four permanent deformation prediction models, creep, Elasto-visco-plastic, Drucker-Prager and viscoelastic are evaluated using the Abaqus/CAE finite element software. Six asphalt mixes from Kansas, Missouri and Iowa (two mixes from each

state) were used for the evaluation. In order to obtain fundamental engineering properties, the test factorial is developed for the four prediction models, using six asphalt mixes tested at one test temperature (35°C). At least two replicas were tested for each laboratory test performed for each mix. Tests required for fundamental engineering properties are listed in Table 4.1. Engineering properties obtained from these tests were used in the permanent deformation prediction models. A total of 216 samples were tested, 36 samples per mixture. Table 4.1 shows the tests performed per mix and the number of specimens tested.

Table 4.1 Development of Test factorial

	Test	Test protocol	Measured Eng. Properties	Mixtures			
				KS	IA	MO	Model
1.	Dynamic modulus at 2 temp and six frequencies	AASHTO TP 62-03	Dynamic modulus |E*| and phase angle φ	2*3	2*3	2*3	All
2.	Static creep at 35°C	NCHRP-465	Creep compliance and flow time, power law parameters at time T, D(T)	1*2	1*2	1*2	Creep Model
3.	Dynamic creep test at 35°C	NCHRP-465	Creep compliance D and flow number	1*2	1*2	1*2	Creep model
4.	Triaxial repeated load test, at 35°C, 4 confining pressures loaded with 0.1 sec loading 0.9 sec unloading.	NCHRP-465	Elastic modulus |E*|, Drucker-Prager parameters angle of internal friction α, cohesion c, φ_p, and φ_{cv}.	2*4	2*4	2*4	Elasto-plastic model, D-P
6.	Uniaxial stain test (unconfined) at five strain rates and 35°C	ASTM D 4123	Viscoplastic parameters	2*5	2*5	2*5	Elasto-plastic model D-P
7.	Shear frequency sweep at constant height (FSCH) at 35°C	AASHTO T320-07	Linear viscoelastic parameters, mix stiffness G*, phase angle φ,	2*2	2*2	2*2	Visco-elastic model.
8.	Repetitive shear at constant height (RSCH) at 35°C.	AASHTO T320-07	Rutting susceptibility of mix, permanent shear stain	2*2	2*2	2*2	Viscoelastic model
	Total number of tests			**36 *2**	**36*2**	**36*2**	

*D-P = Drucker-Prager Model

The tests listed in Table 4.1 are explained below and results from the tests are provided in Chapter 5. The dynamic modulus test was covered in the description of CISL 14 experiment (Chapter 3), and will not be covered in this chapter.

4.2 Material characterization

Asphalt mixtures were characterized to obtain fundamental engineering properties required as model parameters for models implementation in Abaqus. Asphalt mixtures for specimen fabrication were prepared as described in section 3.3.2.1. Tests performed for model implementation include:

1. Dynamic Modulus
2. Static Creep
3. Dynamic Creep
4. Triaxial Strength at 4 confining pressures
5. Uniaxial strength at 5 strain rates
6. Frequency Sweep at Constant Height (FSCH)
7. Repetitive Shear at Constant Height (RSCH)

The first five tests were performed in the Universal Testing Machine (UTM-25) available at Kansas State University. The UTM-25, manufactured by Industrial Process Controls (IPS) of Melbourne Australia, is a closed loop, servo control material testing machine, designed as versatile, high performance and wide ranging testing facility. The UTM-25 consists of four main components namely: the Personal Computer (PC), the Computer Data Acquisition System (CDAS), hydraulic system and environmental chamber.

The CDAS is a compact, self contained unit that provides all critical control, timing and data acquisition functions for the testing frame and transducers, it controls the input and output data. It records the signals from transducers, digitizes the information and passes the information to the PC. It also controls the testing frame and transducers and it adjusts and applies the load through the actuator.

The Hydraulic system comprises of the hydraulic power packs, hydraulic service manifold and hydraulic servo valve, which are controlled using the pendant controls. The hydraulic system is connected to the actuator through an electrically controlled hydraulic servo valve. The hydraulic power pack is the energy source for the servo valve using high pressure oil. The power pack provides to the hydraulic service manifold, the low and high pressure operating modes which are used during testing. The hydraulic servo actuator maintains high frequency performance at significantly reduced pressures, supplies oil to the machine, eliminates hydraulic noise and it increases efficiency of servo valve. The force applied to the sample is determined using a load cell mounted inline with the loading shaft.

The environmental chamber is provided to controls test temperatures, it is comprised of a thermometer and thermostat that controls and maintains the set temperature. Figure 3.24 in Chapter 3, shows a photo of the UTM-25 at KSU. Figure 3.25 shows the mounting of LVDT to the sample and sample in the UTM-25 testing frame during creep test.

4.2.1   Static creep / Flow Time test

The static creep test is conducted to measure the resistance of asphalt concrete to flow. This is why this test is also known as the flow time test. The test may be conducted in a uniaxial or triaxial state of compressive loading. The test is conducted in one cycle of load unload that provides information concerning the asphalt mixture response characteristics (elastic/plastic viscoelastic/viscoplastic). A test may be conducted at different temperature stress and confining pressures levels. The effective temperature ranges between 25°C to 60°C (77°F to 141°F). The design stress levels ranges between 69 and 207 kPa (10-30 psi) for unconfined tests and 483 to 966 kPa for confined tests. Typical confinement levels ranges between 35 and 207 kPa (5-30 psi) [NCHRP-465, 2002]. The test is conducted on laboratory prepared samples, having diameter of 100 mm (4 in) and height of 150 mm (6 in), cored from Superpave gyratory compacted plugs.

The static creep test was conducted in accordance to NCHRP Report 465 Appendix C. The test was performed on laboratory prepared specimen having 100 mm (4in) diameter and 150 mm (6in) in height using the UTM-25 testing equipment. The axial load of 207 kPa (30 psi) was applied for 10,000 seconds or until failure. When this test is performed, creep is obtained in three

stages, primary, secondary and tertiary. The primary and tertiary stages have a nonlinear relationship between strain and time. In the secondary stage, the relationship between strain and time is linear (Figure 4.1). Model parameters are obtained by using the linear part of the relationship using plots of log strain vs log time. For this test, axial loads on some of the mixes were increased in order to obtain tertiary flow. This was because the specimens were tested at the APT test temperature of 35°C. Results are plotted as log strain vs log time or log compliance vs log time. From Figure 4.1, the three creep stages can be clearly seen the creep model parameter, slope (m), intercept (d$_o$), flow time F_t and creep compliance (D) can be obtained. The creep compliance is calculated using quasi-elastic method to approximate the linear viscoelastic convolution integral [NCHRP-465, 2002].

$$D(t) = \varepsilon(t)/\sigma(t),$$

Where:

D(t) is the creep compliance,

$\varepsilon(t)$ is strain response and

$\sigma(t)$ is the applied stress

Figure 4.1 Creep Compliance vs. Time from a Static Creep test
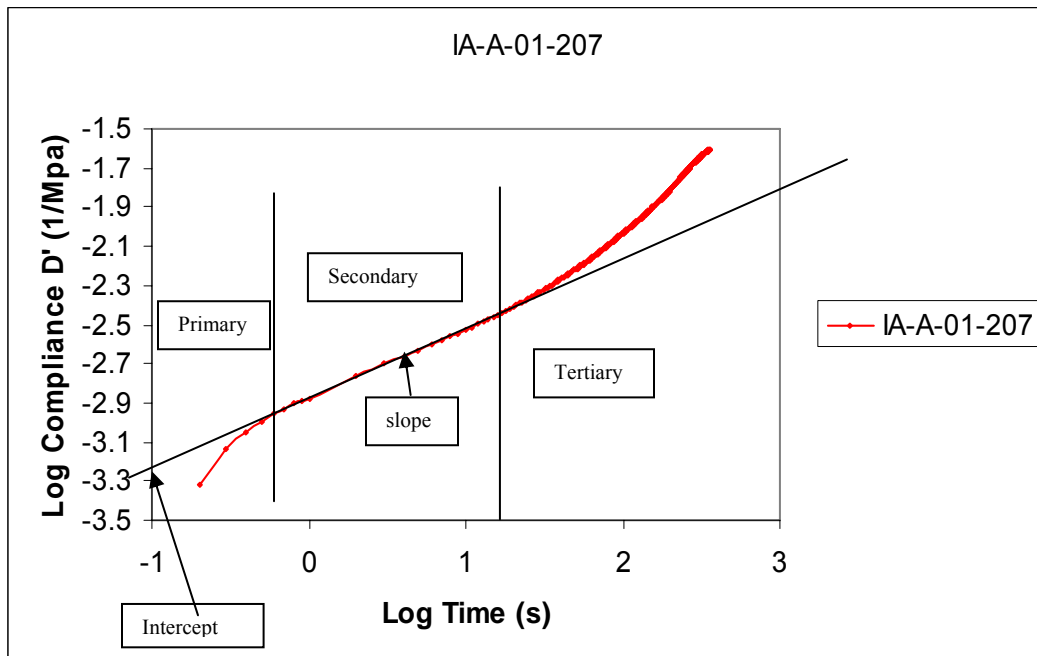
From the plot of log compliance versus log time above, (Figure 4.1), compliance parameters d_o, d_1 and m are obtained from a linear portion of the creep compliance plot where:

- *Creep compliance* (D) is the reciprocal of creep modulus and presented as a ratio of strain (ε) to stress (σ) for a viscoelastic material;

    D(t) = ε(t) / σ(t), (1/MPa).

- d_o is the instantaneous compliance, and can be assumed to be the value of the total compliance at a time equal to 100 ms (if the load is applied rapidly at 50ms),

- d_1 (or sometimes "a") is the intercept of the creep compliance-time relationship, which is the estimated value of the total compliance at a time of one second,

- m (or sometimes "b") is the slope of the creep compliance-time relationship and the *flow point* is the lowest point in the curve of rate of change in axial compliance versus loading time.

The Power law model is used to analyze creep test results and it is mathematically expressed as shown in equation 4.1

$$\varepsilon_p = at^b \qquad\qquad 4.1$$

where: ε is permanent strain,

t is time of loading cycle in seconds, and

a and b are the regression constants explained above.

The Static creep test was conducted at 35^oC with uniaxial constant loading (without confinement) varying from 207 kPa to 690kPa. Asphalt mixes from Kansas KS-1, Missouri MO-1 and MO-2 and Iowa IA-2 did not fail after 10,000 seconds when tested at 207kPa (30psi), therefore, the tertiary flow was not reached and hence flow time was not obtained. For these mixtures either a higher load or longer loading time was required for tertiary flow time to be observed. Since the APT test was performed at 35^oC it was logical to increase the load in order to obtain the tertiary flow and flow times. From this test, the flow time, creep modulus, creep compliance and compliance parameters, d_1, d_o and m were obtained. Flow time is the time at which shear deformation under constant volume begins. The higher the flow time is, the higher the asphalt resistance to permanent deformation is. d_1 and m are material regression coefficients, generally known as compliance parameters, where d_1 is the intercept and m is the slope (Figure

4.1), d_o is instantaneous compliance. Power models are used to model the secondary (linear) phase of the creep compliance curve using this relationship:

$$D'=D(t) - d_o = d_1t^m \qquad\qquad 4.2$$

Tables 4.2 provides results of static creep test for samples tested at 207, 345 and 609 kPa.

Table 4.2 Static creep parameters tested with axial load of 207, 345 and 690 kPa

Sample ID	Axial load (kPa)	D1 (1/Mpa)	m	Do (1/Mpa)	Flow time (sec.)	Creep Modulus (MPa)	Creep Compliance (1/Mpa)	Permanent deformation (mm)
IA-1	207	0.000795	0.52665	0.00117	512.5	29.30	0.036275	0.76100
IA-2	207	0.000578	0.20995	0.00073	1131.0	105.70	0.015105	0.07169
KS-1	207	0.00058	0.2843	0.0004	7944.0	157.70	0.059400	0.12970
KS-2	207	0.000252	0.3854	0.001045	3162.0	42.95	0.022310	0.47520
MO-1	207	0.00075	0.3405	0.000675	7944.0	81.80	0.011515	0.25085
MO-2	207	0.00099	0.2342	0.00084	5012.0	224.65	0.004375	0.10705
KS-2	345	0.00102	0.2792	0.000775	1807.5	71.80	0.013580	0.49155
MO-2	345	0.000209	0.2727	0.00079	5012.0	83.80	0.011144	0.44110
KS-1	690	0.001325	0.13165	0.00045	7944.0	194.30	0.004725	0.35615
MO-1	690	0.001495	0.32545	0.00051	1585.0	69.55	0.013890	0.97845
MO-2	690	0.001333	0.348344	0.000725	566.0	77.80	0.012640	0.99944

The static creep test was performed on two replicas for each mix. The histograms below provide the average results from the individual mix tested. From Figure 4.2, it can be seen that KS-1 and MO-1 samples had high flow time values when tested at 207 kPa axial load, indicating that these mixes have more rutting resistance as compared to the rest of the mixes. Mixes MO-2 and KS-2 were tested at 345 kPa, MO-2 had flow time of 5012 seconds, indicating that it has a better rutting resistance than KS-2 mix (Figure 4.2). KS-1, MO-1 and MO-2 mixes were tested again at 690 kPa. KS-1 had flow time of 7944 sec, MO-1 1585 sec and MO-2 an average of 566 sec (Figure 4.3). Iowa mixes were tested at 207 kPa axial load and failed with flow times of 512 and 1131 seconds for IA-1 and IA-2 respectively. From this test it can be observed that Kansas mix KS-1 and Missouri mix MO-1 have the highest rutting resistance while IA-1 mix is the most prone to permanent deformation (rutting).

Figure 4.2 Flow time (Ft) at axial load of 207 kPa

Flow times at 207 kPa
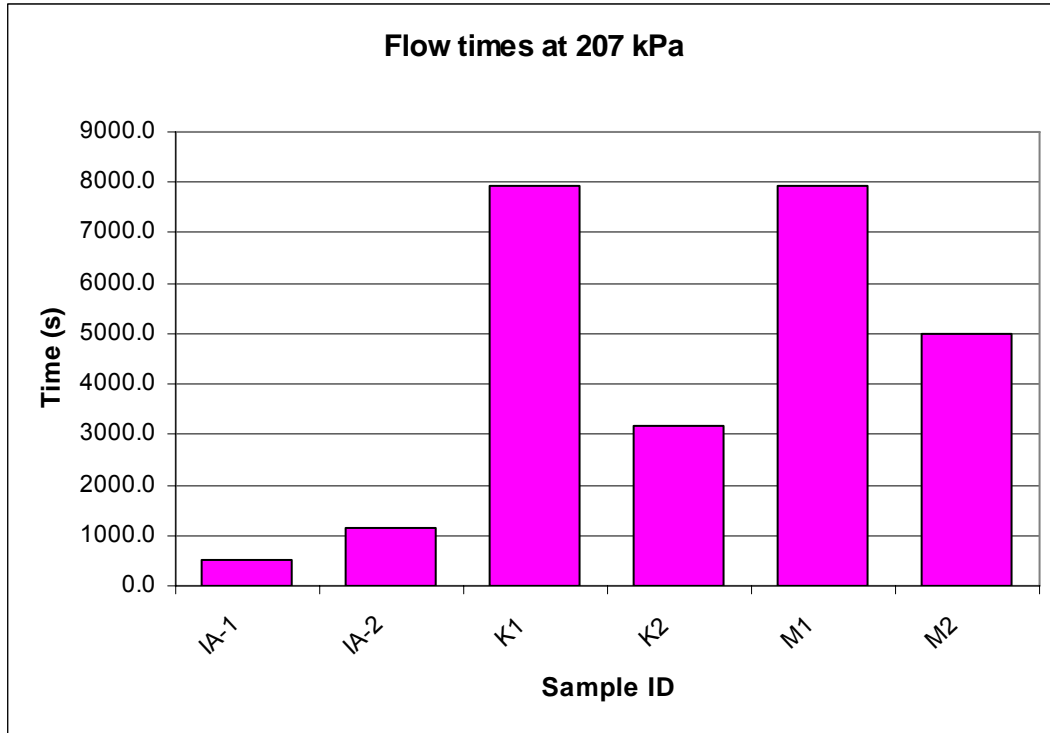
Figure 4.3 Flow time (Ft) axial load of 345 and 690 kPa

Flow times at 345 and 690 kPa
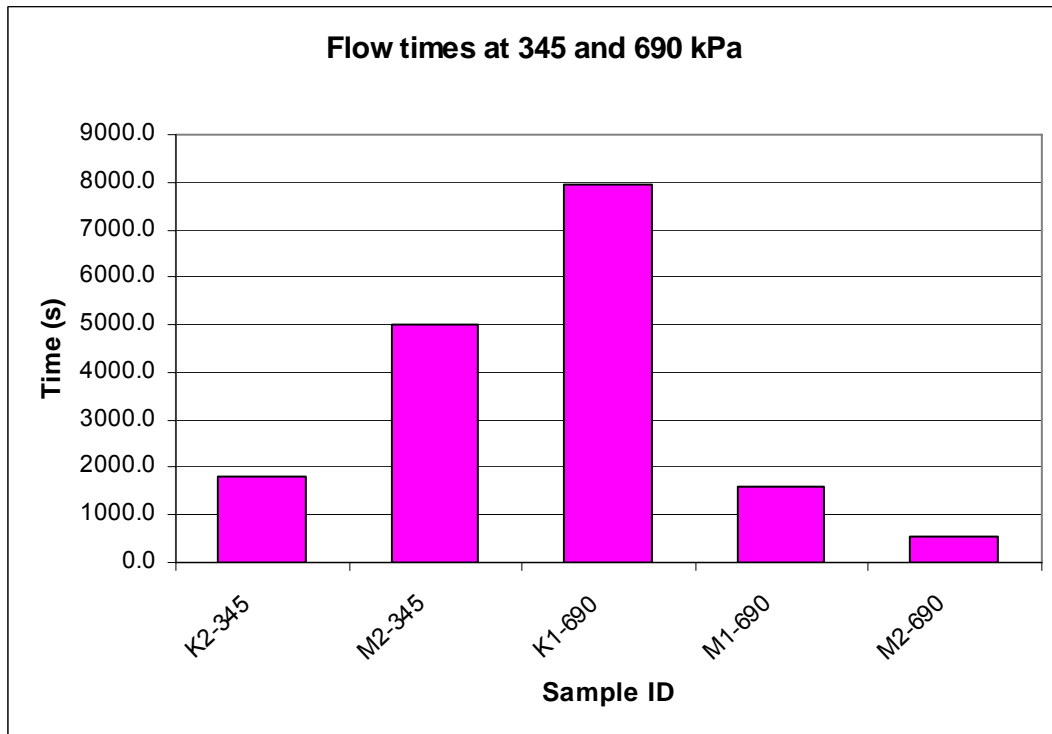
4.2.2   Dynamic creep / Flow Number test

This test is conducted to measure the resistance of asphalt concrete to tertiary deformation (asphalt flow). The test can be conducted in a uniaxial or triaxial state of compressive loading. The test applies a repeated pulsed axial stress/load (cyclic), haversine loading with 0.1 sec loading and 0.9 sec unloading, up to 10,000 cycles or until a specimen failure, which ever comes first. The mixture's response characteristics (elastic/plastic viscoelastic/viscoplastic) are obtained. Like in the static creep test, the recommended test temperatures range from 25°C to 60°C (77°F to 141°F). The design stress levels ranges between 69 and 207 kPa (10-30 psi) for unconfined tests and 483 to 966 kPa for confined tests. Typical confinement levels ranges between 35 and 207 kPa (5-30 psi) [NCHRP-465, 2002].

The test was conducted in accordance with NCHRP Report 465 Appendix B, on laboratory prepared samples with diameter of 100 mm (4 in) and height of 150 mm (6 in), cored from Superpave gyratory compacted plugs. The dynamic creep test setup is similar to static creep test, but the loading is different. Dynamic creep is performed by applying a repetitive (dynamic) haversine loading while static creep test is loaded with a static load. The loading is applied for 0.1 sec. and 0.9 sec. unloading (rest period) for up to 10,000 repetitions or until failure, whichever comes first. The dynamic creep parameters, intercept (a), slope (b) and flow number F_n are obtained from the plots (Figure 4.4). Also the dynamic creep test data is managed using a different software in the UTM-25 system.

The dynamic creep test results are presented in cumulative permanent strain (ε_p) against number of loading repetition. The permanent strain curve comprises of three zones: primary, secondary and tertiary flow (Figure 4.4). The number of pulses (cycles) at which tertiary flow begins is known as the flow number F_n. Power law model is used to model the secondary strain as follows:

$$\varepsilon_p = aN^b$$

4.3

The regression constants a, intercept and b, slope are obtained from the plots of permanent strain against number of cycles. Figure 4.5 shows permanent strain against number of cycles and Figure 4.6 shows strain slope against number of cycles. These are some of the typical dynamic creep test results obtained at Kansas State University laboratory.

Figure 4.4 permanent strain against number of cycles on log-log scale
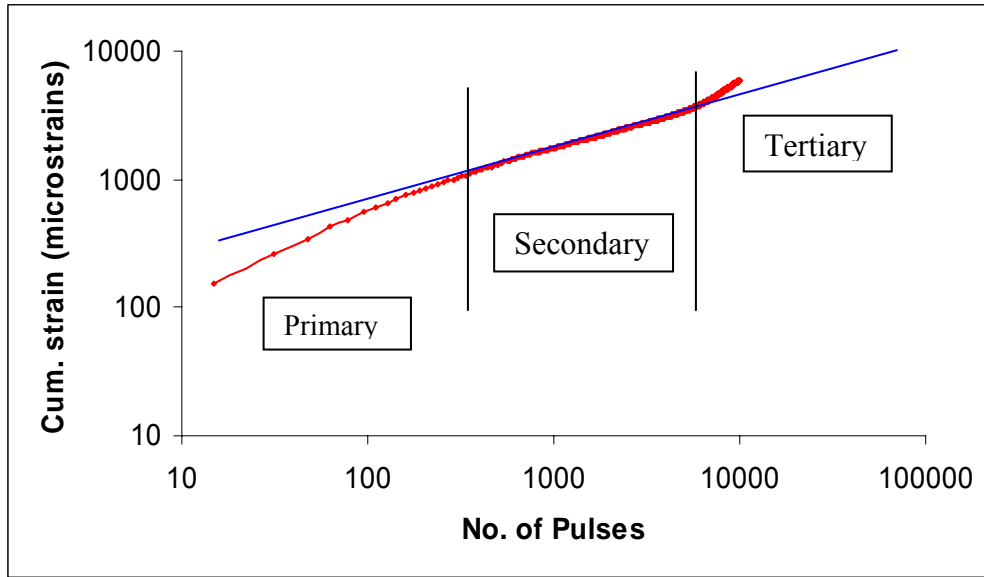
Figure 4.5 permanent strain against number of cycles
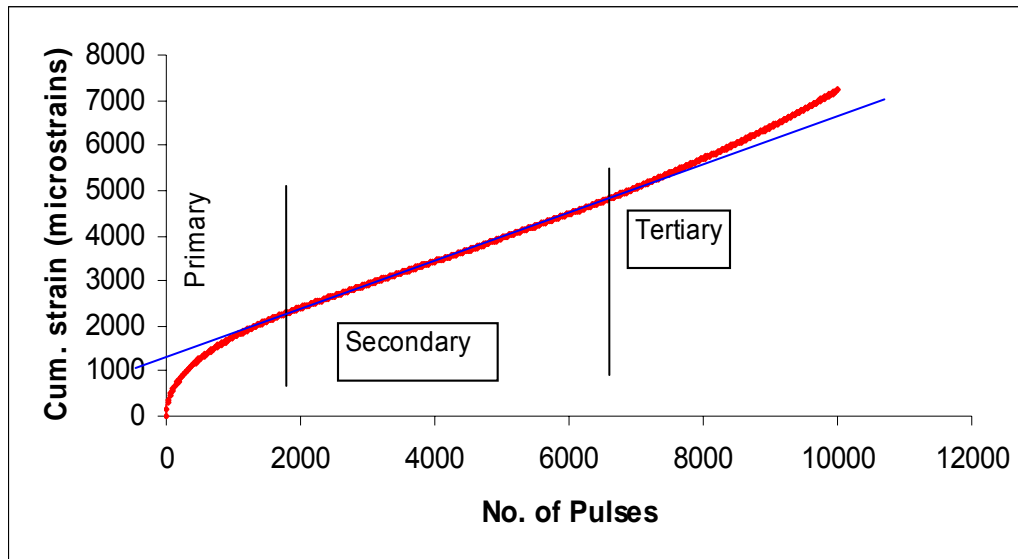
Figure 4.6 strain slope against number of cycles
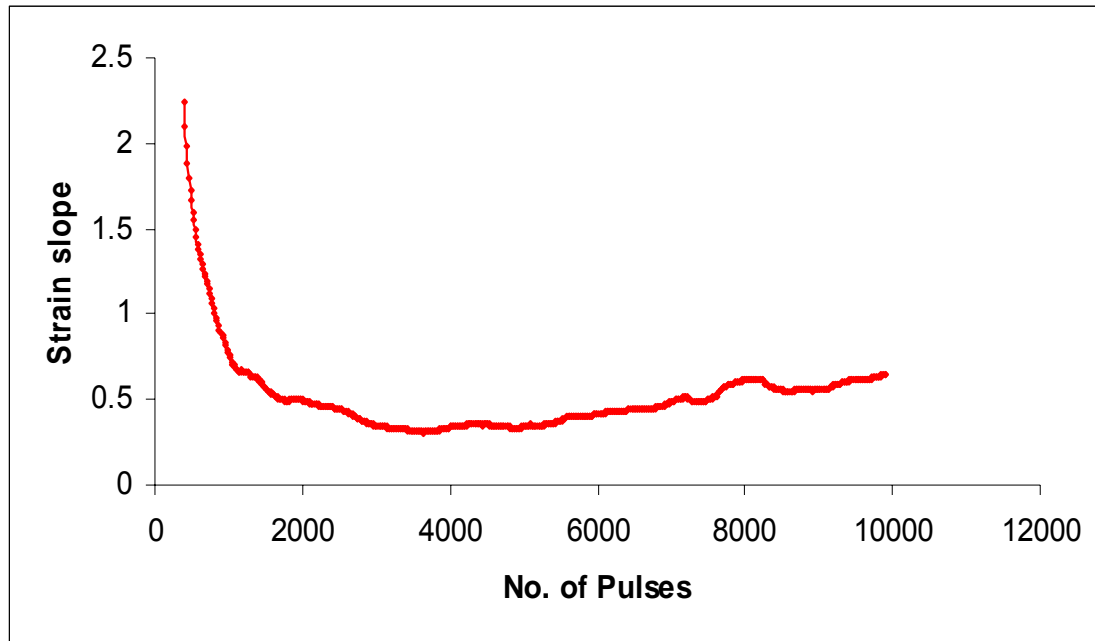
Table 4.3 Summary of dynamic creep test results

Sample ID	Test load	Dynamic creep parameters		
	(kPa)	a (x10^{-6})	b	FN
IA-1	207	25.5	0.81465	2500
IA-2	207	25	0.01665	4000
KS-1	207	21.75	0.1506	10000
KS-2	207	105	0.60165	7239.5
MO-1	207	28.7	0.1642	10000
MO-2	207	53.1	0.4352	10000
KS-2	345	185	0.6128	3000
MO-2	345	275	0.5918	10000
KS-1	690	465	0.11665	10000
MO-1	690	595	0.6831	10000
MO-2	690	750	0.776867	7639

The dynamic creep test was conducted at 207kPa, 345kPa and 690kPa as shown in Table 4.3 and summarized on plots given in Figures 4.7 and Figure 4.8. At 207 kPa KS-1, MO-1 and MO-2 mixes did not fail (Figure 4.7). When tested at 345 kPa KS-2 failed at 3,000 flow number and MO-2 did not fail. At 690 kPa MO-1 and KS-1 mixes did not fail and MO-2 obtained a flow number of 7,639. From these results, KS-1 and MO-1 mixes are the most resistant to flow, indicating that they have less potential to permanent deformation. Asphalt mixes MO-2, follows in the list then KS-2, IA-2 and IA-1 (Figure 4.7 and Figure 4.8).

Figure 4.7 Flow number (Fn) at 207 kPa
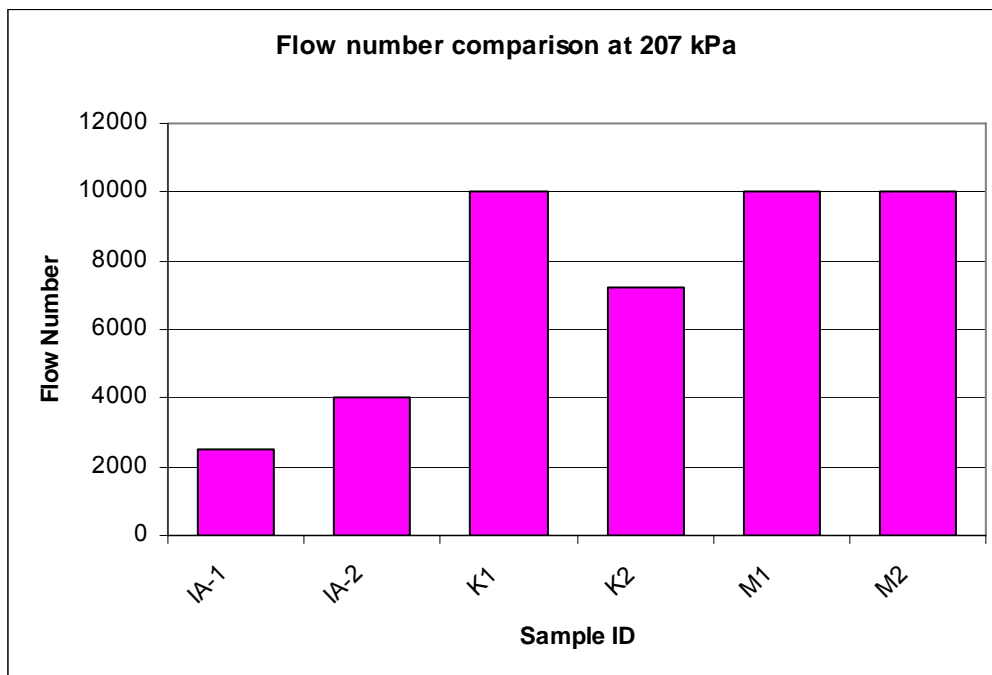
Figure 4.8 Flow number (Fn) at 345 and 690 kPa
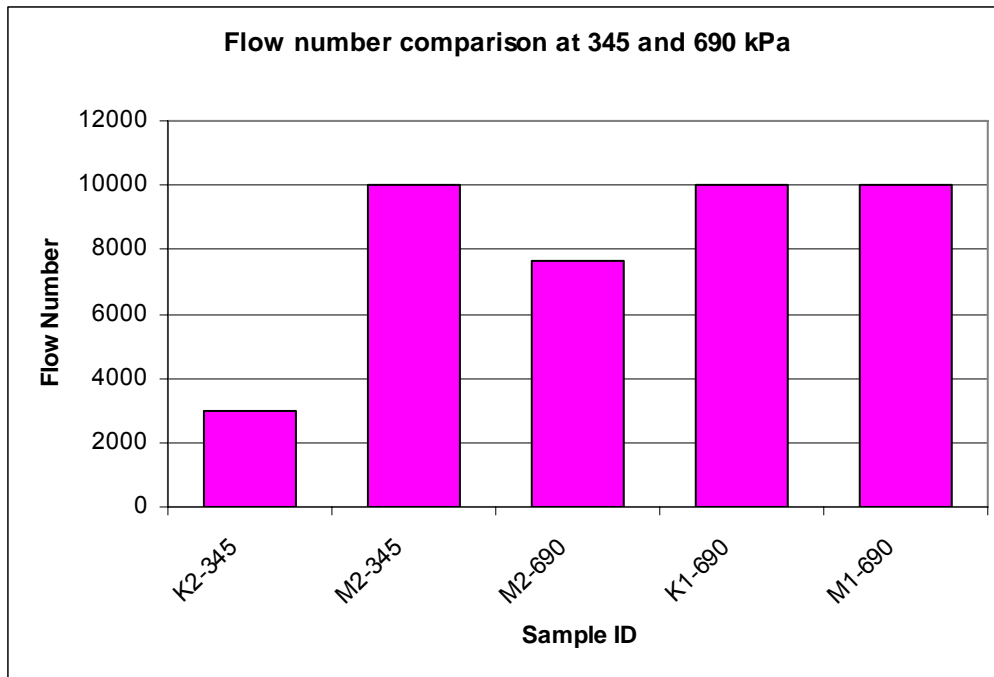
4.2.3 *Repeated load triaxial compressive strength test*

The repeated load triaxial strength tests were conducted on specimens having 100 mm (4in) diameter by 150 mm (6in) height, cored and sawed from the centre of the gyratory compacted cylindrical plugs. The specimens were tested at four confining pressures, 0, 68.9, 137.9 and 206.7 kPa (0, 10, 15 and 30 psi respectively). A haversine load was applied for 0.1 seconds loading and 0.9 seconds unloading at a strain rate of 0.0001 ε/s. Two replicate specimens were tested for each mix at every confining pressure, a total of 48 specimens were tested. The test was conducted at 35°C to obtain viscoplastic (Drunker-Prager) model parameters, cohesion (κ), internal angle of friction (α) and elastic modulus (E).

The results obtained from the triaxial strength test are summarized in Table 4.4 and Figures 4.6 to 4.14. From the Figures it can be seen that maximum strain increases with the increase in confining pressure, indicating that at intermediate temperatures the compressive strength of asphalt concrete is depended on the confining pressure. These results were then used to obtain the Ducker-Prager model parameters as presented in Chapter 5.

Table 4.4 Triaxial compressive strength test results

Sample ID	% AV	Confining pressure (kPa)	Initial yield stress (kPa)	Failure strength (kPa)	Elastic Modulus MPa
KS-1	6.51	0	1094.50	1870.0	66.48
KS-1	6.64	69	1486.66	1990.0	68.29
KS-1	6.73	138	1567.62	2245.0	79.98
KS-1	6.46	207	1650.02	2361.1	83.38
KS-2	6.71	0	919.84	1145.5	57.14
KS-2	6.49	69	975.01	1256.6	66.67
KS-2	6.99	138	1120.44	1366.3	54.54
KS-2	6.66	207	1200.77	1433.6	57.14
MO-1	9.42	0	384.39	1211.4	90.45
MO-1	9.57	69	617.43	1357.8	52.18
MO-1	9.68	138	604.22	1459.4	66.50
MO-1	9.61	207	864.76	1525.1	60.91
MO-2	7.19	0	520.58	851.4	31.07
MO-2	7.43	69	558.86	966.0	27.63
MO-2	6.53	138	619.86	1123.5	34.68
MO-2	6.93	207	792.47	1268.3	37.00
IA-1	7.00	0	74.12	240.9	6.35
IA-1	7.56	69	86.55	250.8	8.30
IA-1	7.62	138	116.96	276.7	9.21
IA-1	7.66	207	122.88	319.0	9.08
IA-2	7.90	0	397.12	802.5	38.5
IA-2	7.91	69	561.79	875.8	34.50
IA-2	7.93	138	625.4	968.8	36.12
IA-2	8.00	207	749.74	1095.6	41.54

Figure 4.9 Triaxial strength plots for Kansas course mix (KS-1)
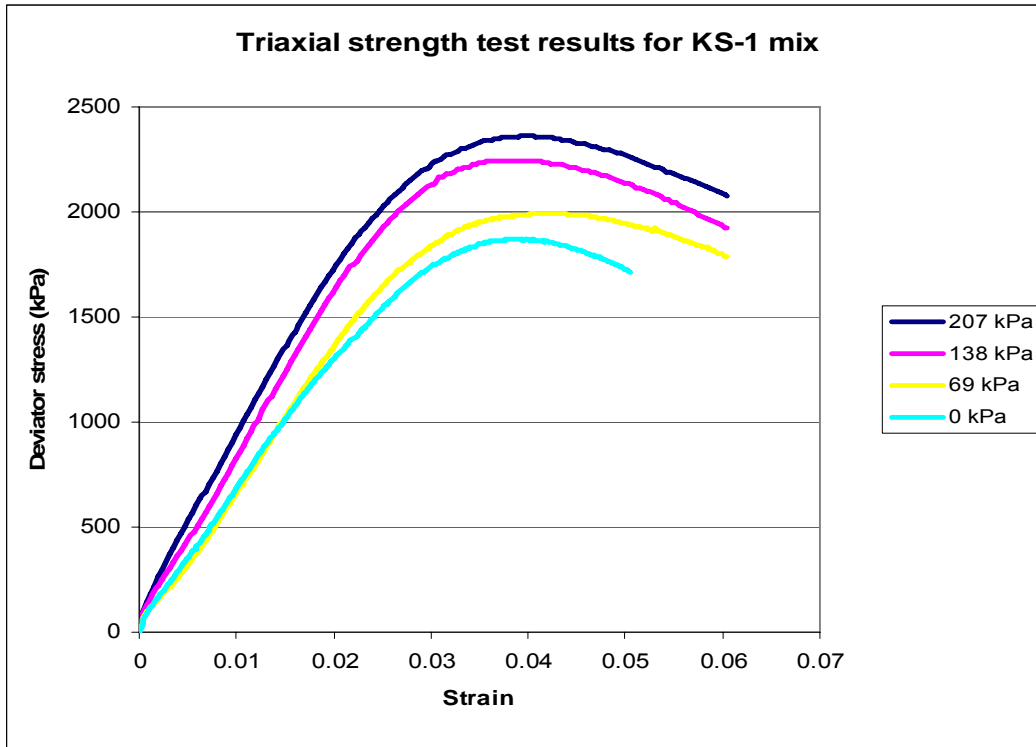
Figure 4.10 Triaxial strength plots for Kansas course mix (KS-2)
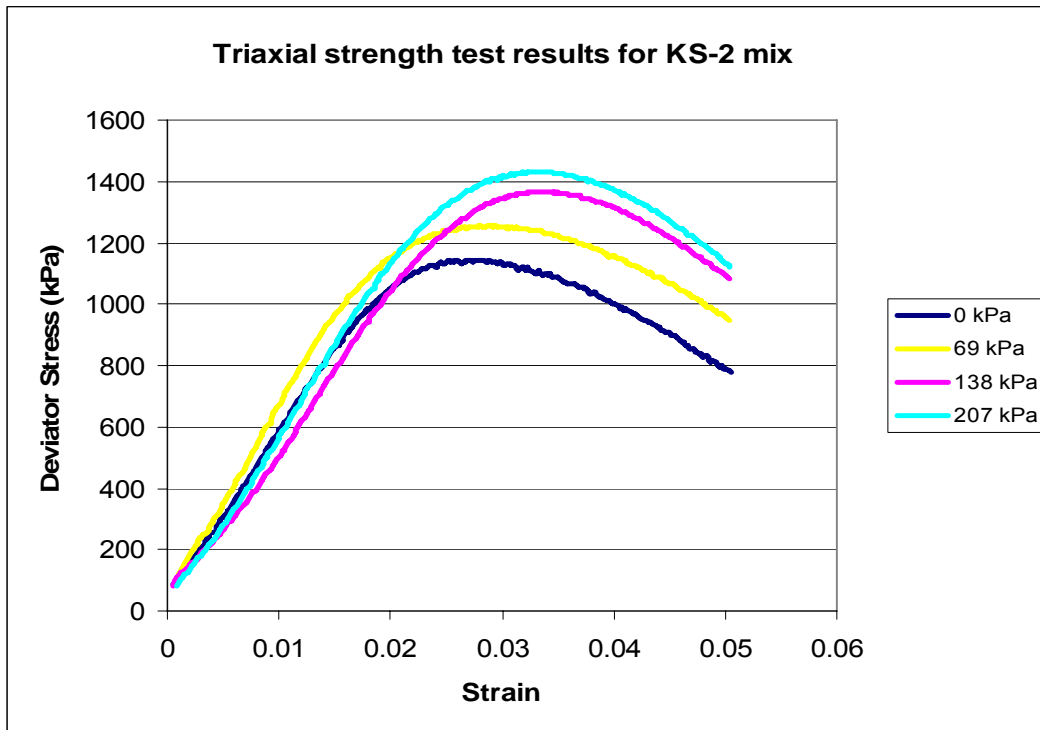
Figure 4.11 Triaxial strength plots for Missouri mix (MO-1)

Triaxial strength test results for MO-1 mix

Legend: 207 kPa, 138 kPa, 69k, 0 kPa

X-axis: Strain

Y-axis: Deviator stress (kPa)
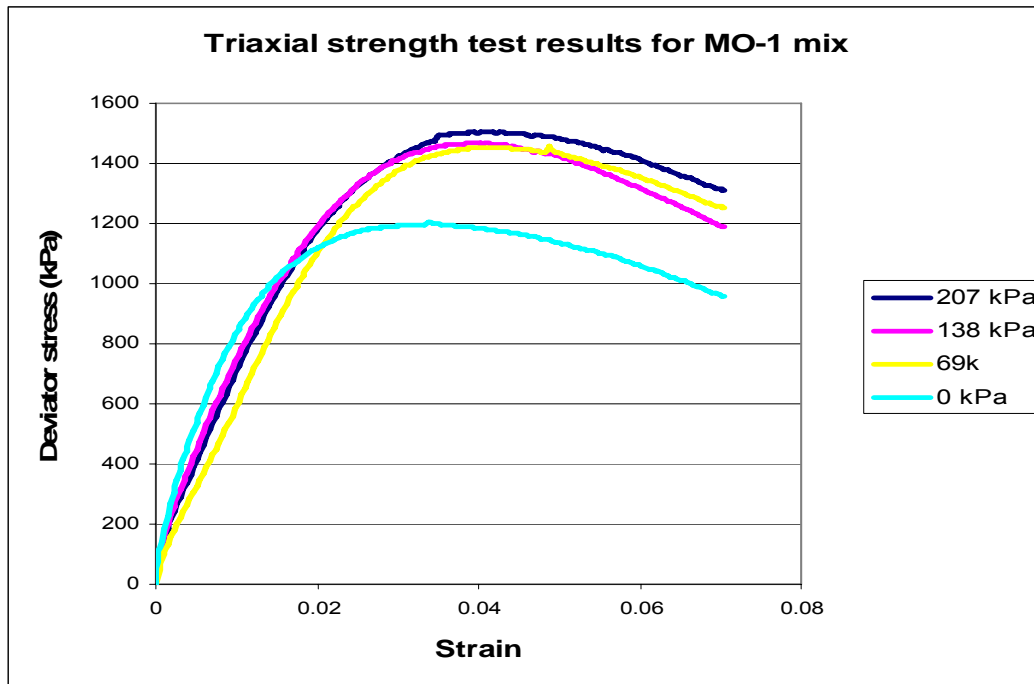
Figure 4.12 Triaxial strength plots for Missouri mix (MO-2)

Triaxial strength test results for MO-2 mix

Legend: 207 kPa, 138 kPa, 69 kPa, 0 kPa

X-axis: Strain

Y-axis: Deviator Stress (kPa)
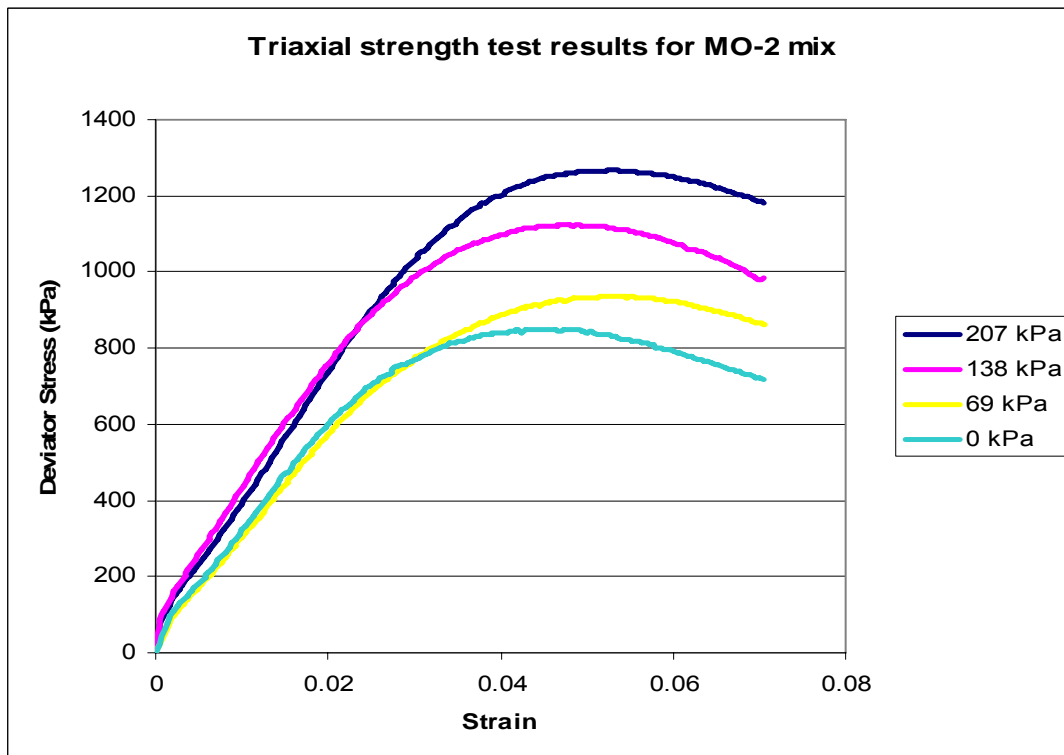
Figure 4.13 Triaxial strength plots for Iowa mix (IA-1)
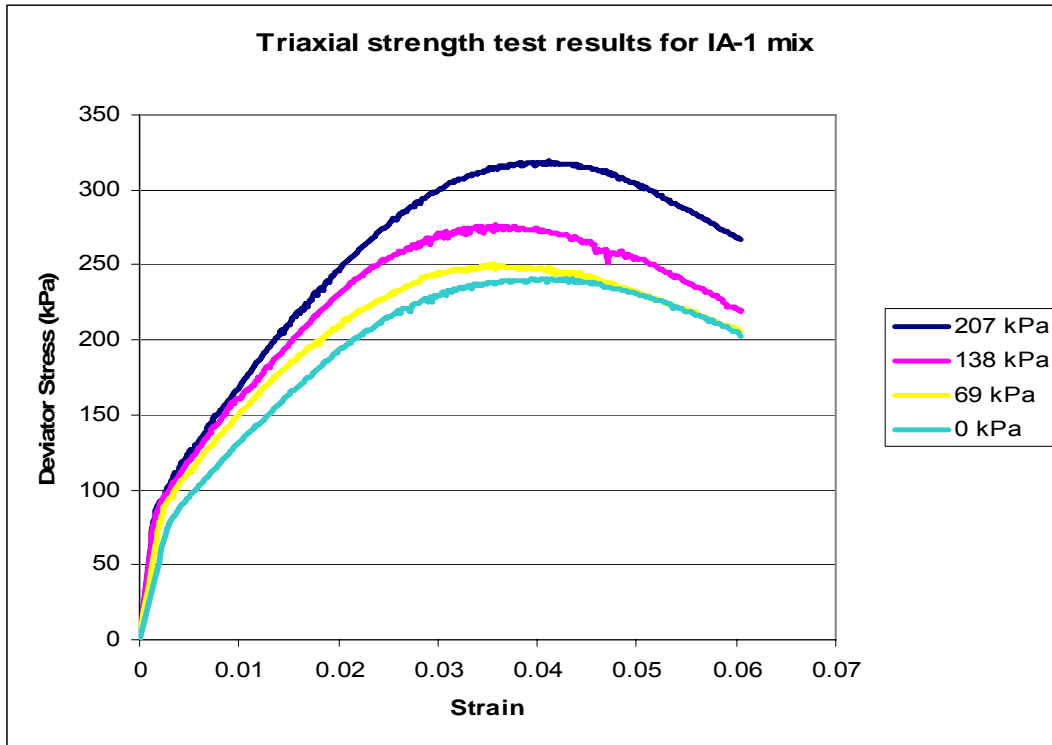
Figure 4.14 Triaxial strength plots for Iowa mix (IA-2)
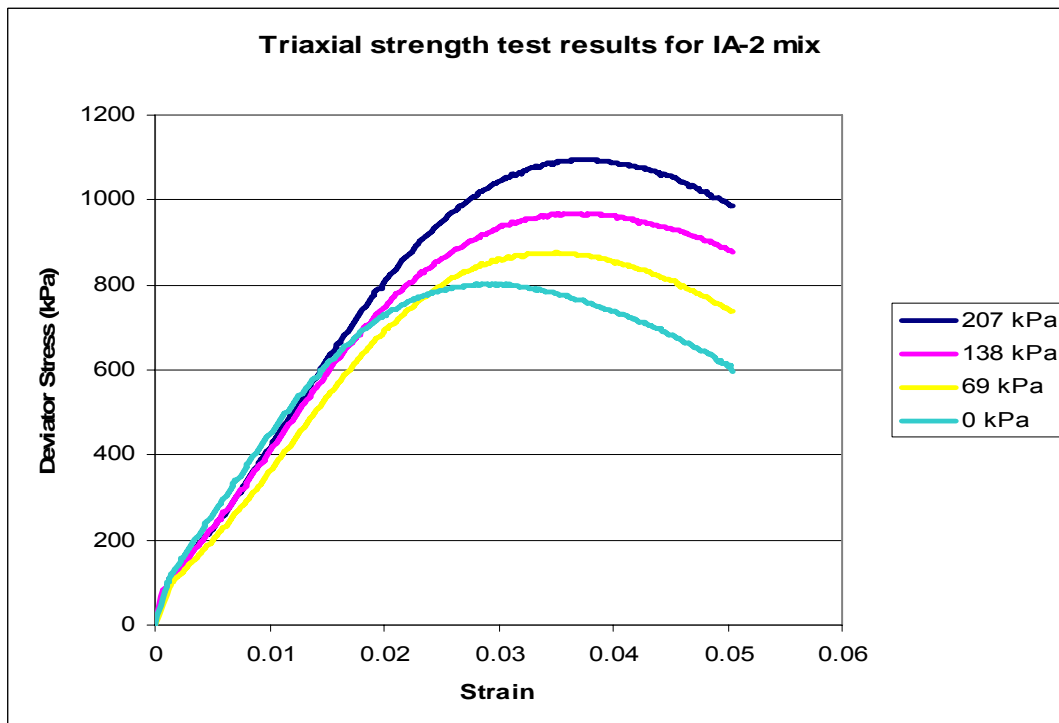
4.2.4 Uniaxial (Unconfined) strength test at five strain rates

The uniaxial strength test was conducted at five strain rates to obtain the elastic viscoplastic material parameters for the constitutive model and the initial elastic modulus. Two replicates specimens having 100 mm (4 in) in diameter and 150 mm (6 in) in height, cored out of compacted Superpave gyratory plugs were prepared and tested at each strain rate. The test was conducted using the UTM-25, which has a load cell capacity of 25kN. Two (2) LVDTs with 100 mm gauge length were used to measure axial deformation. Radial deformation data was not collected due to lack of a radial displacement transducer. The test was conducted at $35 \pm 0.5^{\circ}C$ with series of uniaxial compressive strength tests at five different strain rates 0.00001, 0.0001, 0.002, 0.0042, 0.072, ε/sec.

4.2.4.1 Determination of test conditions

The uniaxial strength test was conducted at five strain rates to obtain the initial and yield strain for the viscoplastic model. The test was conducted at a range of strain rates to characterize the viscoplastic model at representative field vehicle speed. The maximum vertical strain was obtained using Kenlayer program [Huang, 2004]. The material properties, layer thickness and loading conditions used for the strain analysis are given in Table 4.5.

Table 4.5 Kenlayer program loading conditions

Property	Asphalt	Base	Subgrade
Layer thickness (mm)	175	150	1475
Modulus (MPa)	250	80	8
Poisson's ratio (Assumed)	0.35	0.4	0.45
Loading	Single axle – dual wheel		
Tire radius	106.7 mm		
Tire pressure	690 kPa		
Tire spacing	360.68 mm		
Point of interest	50 mm below asphalt surface		

Kenlayer program was used to obtain strain magnitude under the wheel after one load repetition. The Kenlayer input values given in Table 4.5, were used to obtain the maximum

vertical strain of 0.001315 under the center of each tire. A triangular pulse loading time was used to obtain the loading time with respect to speed travelled and depth below pavement surface [Huang 2004]. At a depth of 50 mm below pavement surface and a speed of 11.6 kph (7.2 mph), (the axle speed at CISL 14 experiment), an equivalent triangular loading time of 0.48 seconds was obtained [Huang, 2004]. With these parameters, 0.24 sec is required to reach the maximum vertical strain. The strain rate was then determined as a ratio of maximum vertical strain to the time required to reach the maximum vertical strain. Slow moving vehicle speeds between 1.6 to 48 km/h (1 - 30 mph) were considered to obtain the strain rates used for testing. For each vehicle speed, the equivalent triangular loading time was obtained and the strain rate was determined. Table 4.6 gives the vehicle speed, loading time and the corresponding strain rate.

Table 4.6 Vehicle speed and corresponding strain rate

Vehicle speed km/h (mph)	1.6 (1)	8.08 (5)	11.6 (7.2)	16.1 (10)	32.2 (20)	48.3 (30)
Time (sec)	1.7	0.6	0.48	0.3	0.09	0.06
Strain rate (sec^{-1})	1.55 e-3	4.38 e-3	5.48e-3	8.77 e-3	2.92 e-2	4.38 e-2

The method explained above was used for estimation of strain rates that can be used in the lab to obtain the initial and yield stress for Drucker-Prager model. For laboratory tests, strain rates of 0.0001, 0.002, 0.0042 and 0.0071 strains per second were adopted representing vehicle speeds ranging from almost stationary to 15 km/h. These are strain rates for slow moving vehicles.

Table 4.7 and Figures 4.15 to 4.20 present results from the uniaxial strength test for the six mixes tested. From the Figures it can be seen that asphalt mix at intermediate temperatures is strain rate dependent, because maximum strain increased with increase in strain rate. Kansas mix, KS-1 was not tested to failure at higher strain rates because its material strength exceeded the capacity of the UTM-25 machine used for testing (Figure 4.15). The maximum load in UTM-25 is 25kN, and KS-1 at strain rates of 0.0071/sec and 0.0042/sec needed more than 25 kN load to be tested to failure and obtain the maximum yield strength.

Table 4.7 Triaxial compressive strength test results

Sample ID	% AV	Strain rate (sec⁻¹)	Initial yield stress (kPa)	Failure stress (kPa)	Elastic Modulus (MPa)
KS-1	6.12	0.00001	526.02	992.70	53.40
KS-1	6.51	0.0001	1094.50	1870.00	74.03
KS-1	6.26	0.0020	1504.73	2843.40	109.21
KS-1	6.51	0.0042	1991.77	3058.50	102.65
KS-1	6.46	0.0071	2027.94	3058.50	142.86
KS-2	7.25	0.00001	484.76	664.10	36.2
KS-2	6.71	0.0001	981.62	1145.50	57.14
KS-2	6.56	0.0020	1493.95	2256.20	66.67
KS-2	6.95	0.0042	1686.77	2672.50	54.54
KS-2	6.50	0.0071	2152.66	2846.00	100
MO-1	8.97	0.00001	416.16	721.50	27.40
MO-1	9.42	0.0001	587.42	1211.40	106.81
MO-1	9.08	0.0020	1063.93	2110.50	130.45
MO-1	9.46	0.0042	1128.78	2365.00	110.00
MO-1	9.16	0.0071	1932.00	2902.40	123.43
MO-2	7.41	0.00001	343.49	784.00	31.44
MO-2	7.19	0.0001	520.58	851.4	31.07
MO-2	7.29	0.0020	688.83	1439.00	81.93
MO-2	6.96	0.0042	994.65	1953.40	100.75
MO-2	7.50	0.0071	1913.99	2577.50	131.97
IA-1	7.00	0.0001	74.12	240.90	6.35
IA-1	6.94	0.0020	230.23	665.70	40.94
IA-1	6.72	0.0042	367.39	864.40	32.06
IA-1	6.72	0.0071	544.29	986.70	32.97

Table 4.7 Triaxial compressive strength test results -continued-

Sample ID	% AV	Strain rate (sec^{-1})	Initial yield stress (kPa)	Failure stress (kPa)	Elastic Modulus (MPa)
IA-2	7.38	0.00001	378.15	605.3	27.48
IA-2	7.90	0.0001	397.12	802.50	38.5
IA-2	7.63	0.0020	630.55	1561.60	71.8
IA-2	7.38	0.0042	1145.11	2095.70	85.81
IA-2	7.86	0.0071	1508.74	2368.00	88.66

Figure 4.15 Uniaxial strength plots for Kansas mix (KS-1)
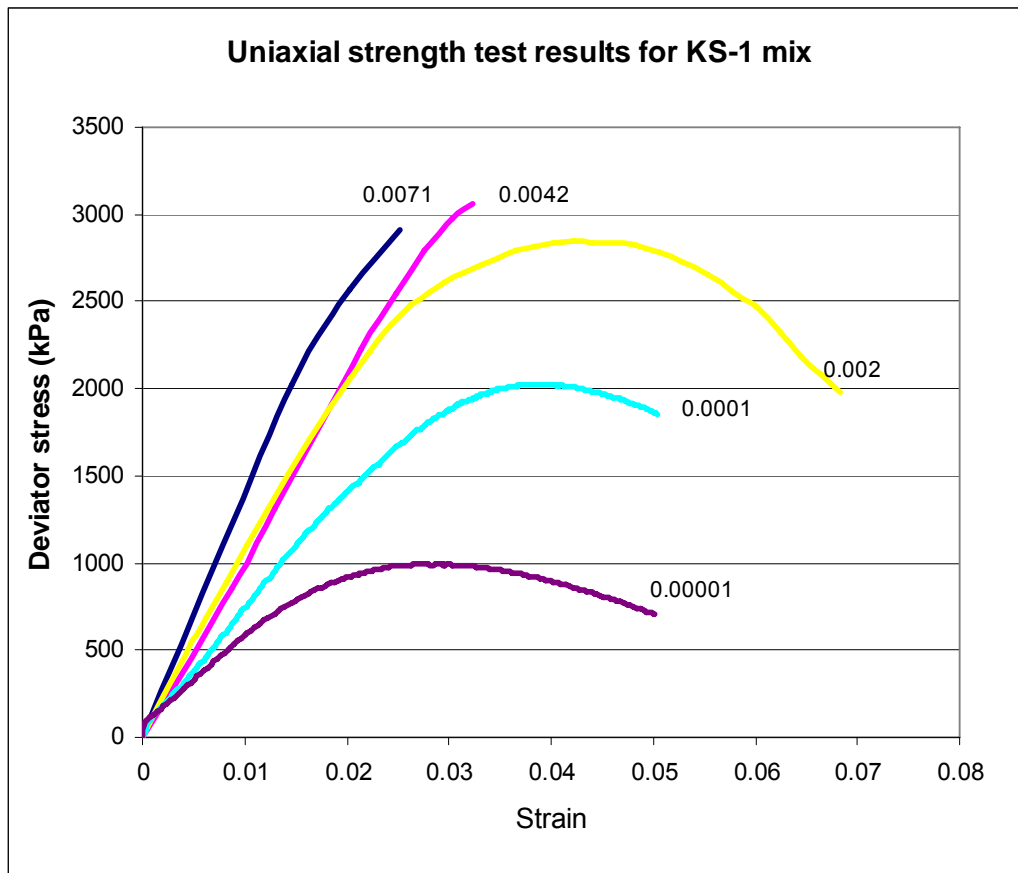
Figure 4.16 Uniaxial strength plots for Kansas mix (KS-2)

Uniaxial strength test results for KS- 2 mix

0.0071
0.0042
0.002
0.0001
0.00001
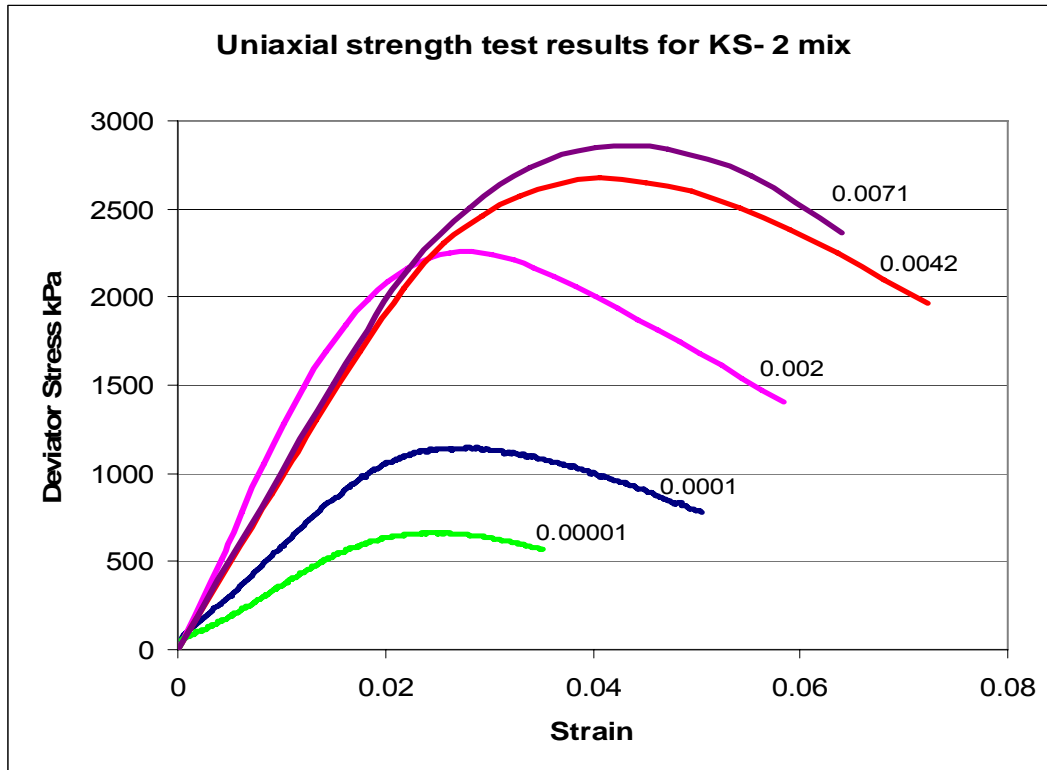
Figure 4.17 Uniaxial strength plots for Missouri mix (MO-1)

Uniaxial strength test results for MO-1 mix

0.0071
0.0042
0.002
0.0001
0.00001
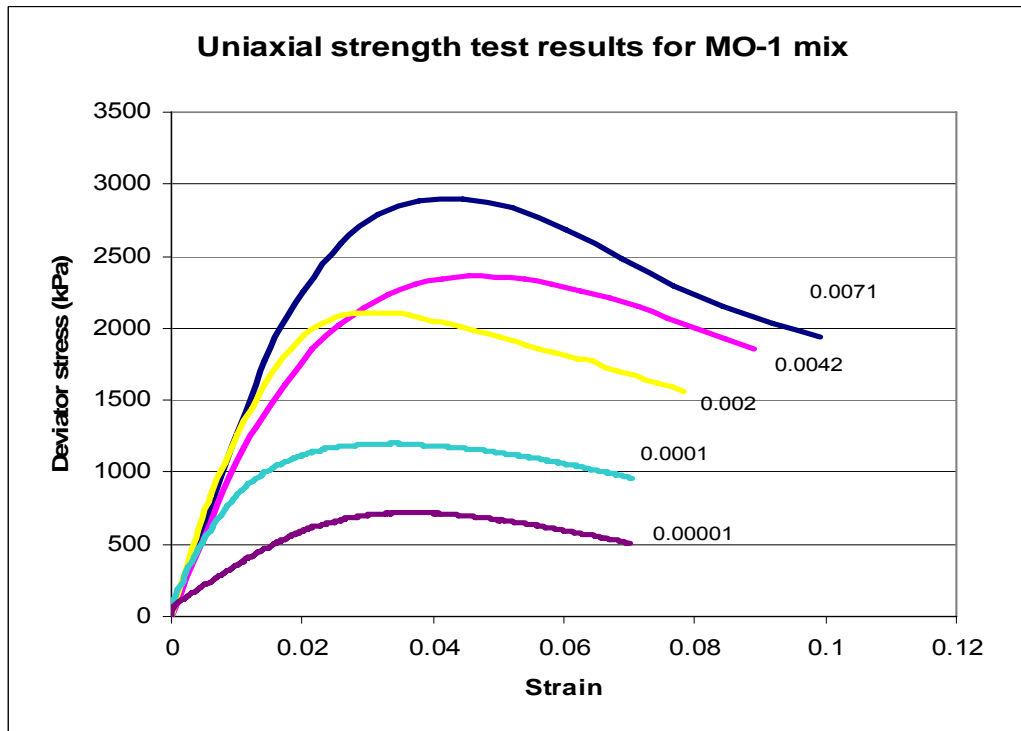
Figure 4.18 Uniaxial strength plots for Missouri mix (MO-2)
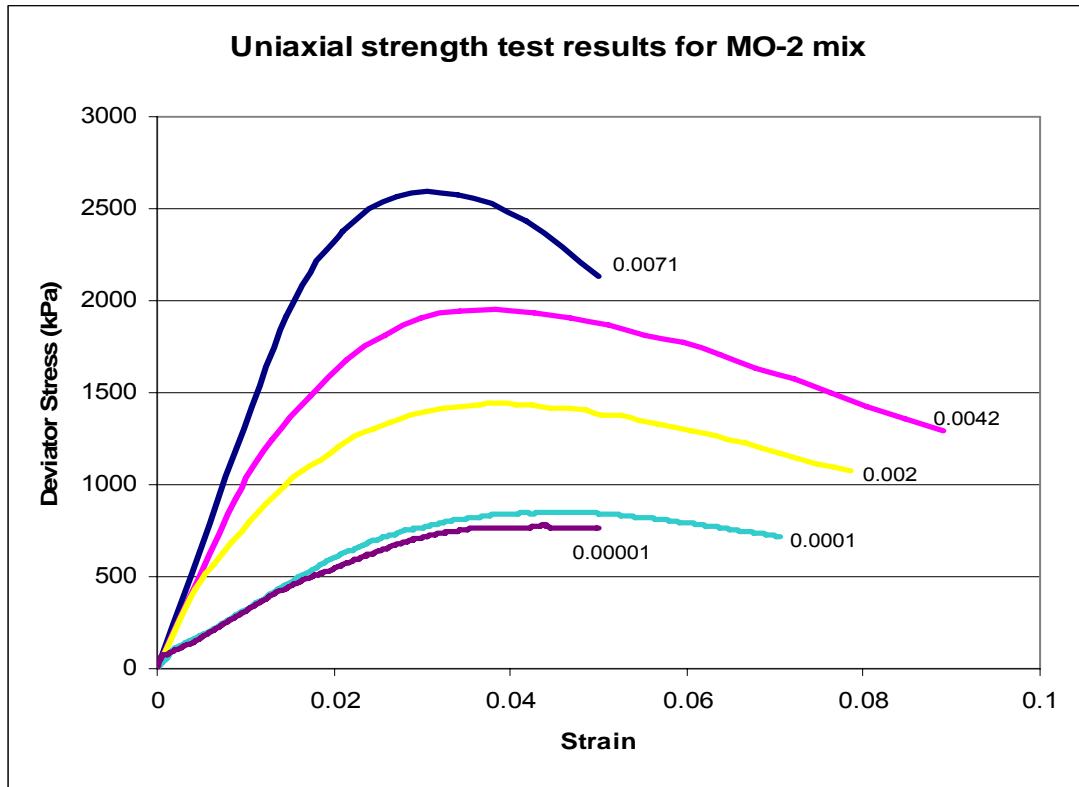
Figure 4.19 Uniaxial strength plots for Iowa mix (IA-1)
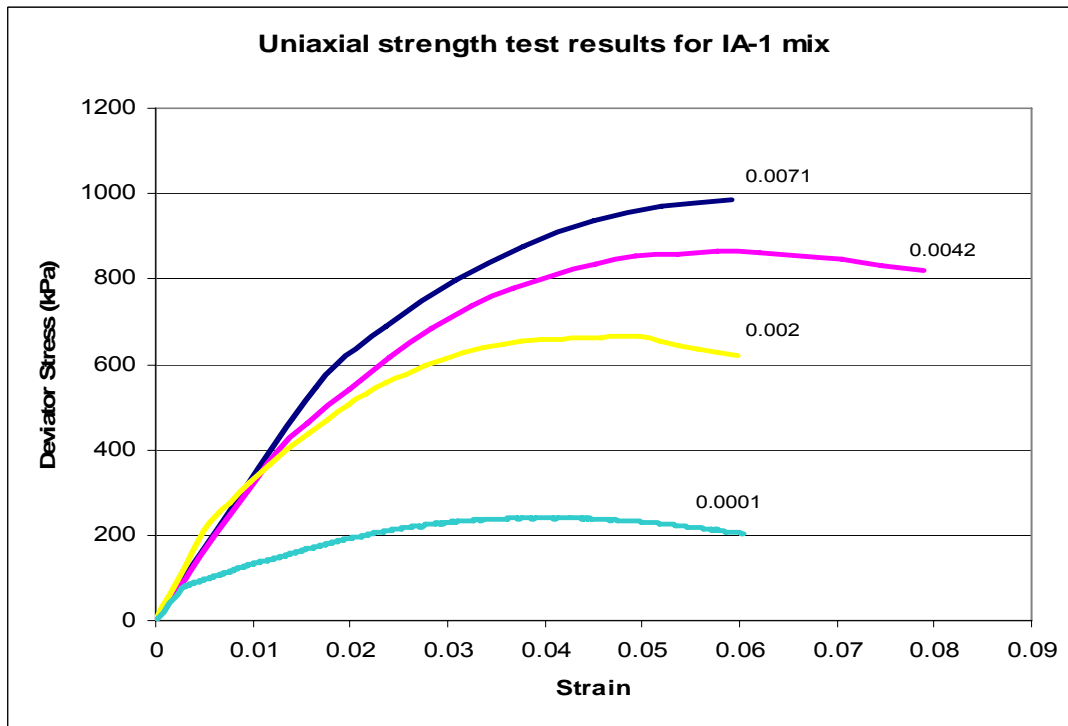
Figure 4.20 Uniaxial strength plots for Iowa mix (IA-2)

Uniaxial strength test results for IA-2 mix

(Y-axis: Deviator Stress (kPa); X-axis: Strain)

Curve labels: 0.0071, 0.0042, 0.002, 0.0001, 0.00001
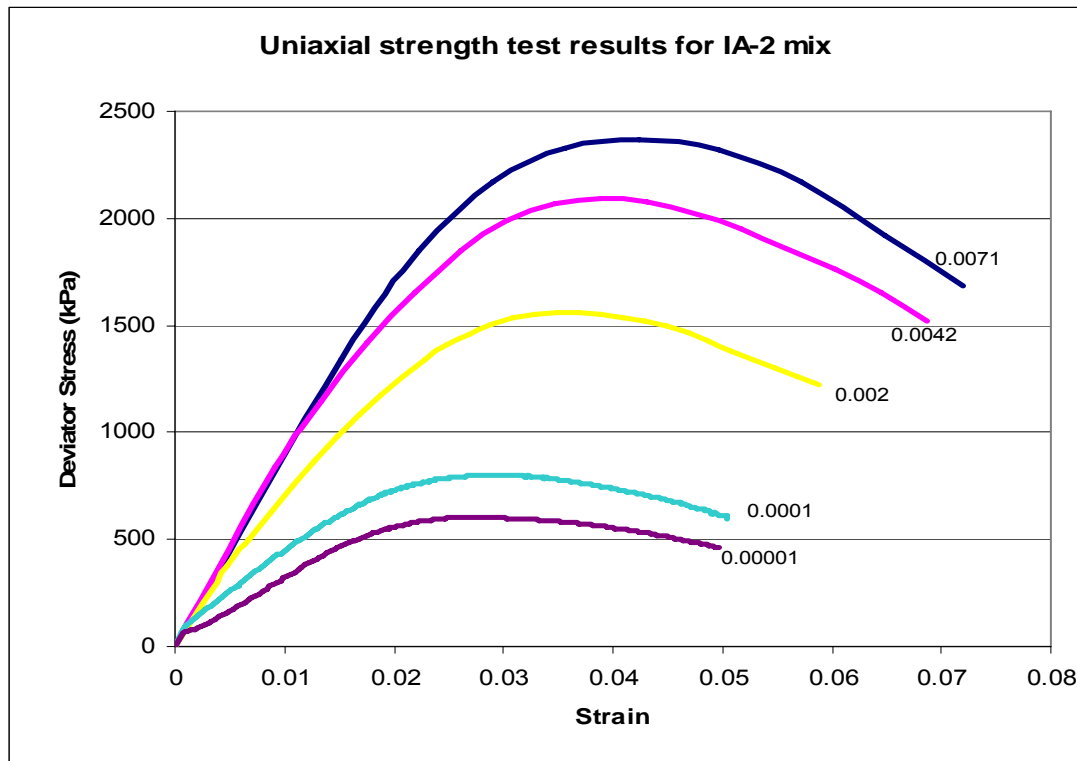
4.2.5 Simple Shear Tests (SST)

The Superpave Shear Tests were developed as a way to measure the shear characteristics of HMA [Brown et al 2001]. The test consists of a loading device, specimen deformation measurement, an environmental chamber, and a control and data acquisition system. The loading device is capable of applying both vertical and horizontal loads to the specimen. It is also capable of applying static, ramped (increasing or decreasing), and vertical and horizontal loads. It is controlled by closed-loop feedback using either stress control or strain control throughout the entire range of frequencies, temperatures and confining pressures. The SST also simulates the high shear stresses (which lead to the lateral and vertical deformation associated with permanent deformation in surface layers) that exist near the pavement surface at the edge of vehicle tires. [Brown et al 2001].

Six SST tests can be performed using the Simple Shear Tester: simple shear, frequency sweep, uniaxial strain, volumetric shear, repeated shear at constant stress ratio and repeated shear at constant height. These properties measure the resistance to permanent deformation and fatigue

135

cracking in asphalt mixtures [Brown et. al., Huang B. 2001]. Two SST tests were performed for this research; the simple shear test at constant height (SSCH) and repetitive shear at constant height (RSCH). The tests were performed at the Asphalt Institute Laboratory in Lexington, Kentucky.

The tests were conducted on 150 mm in diameter and 50.0 ±2.5 mm high specimens. Specimens with a diameter of 150 mm and a height of 75 mm were fabricated using the Superpave gyratory compactor at KSU asphalt lab. The specimens were then sawn and accurately measured to make sure that the top and bottom faces of the specimen are smooth and parallel. The specific gravity of the specimens was determined using AASHTO T166, *Bulk Specific Gravity of Compacted Bituminous Mixtures* procedure. Specimens were then packed and shipped to the Asphalt Institute Laboratory in Kentucky.

The repetitive shear at constant height test is performed by placing a pair of platens into a gluing jig provided with the shear test device (Figure 4.21). The platens are aligned and clamped into place. A thin coating of epoxy cement (~1.5 mm) is applied to each end of the dust free test specimen. The epoxy coating should completely cover the specimen ends and it should be of uniform thickness. Mounting screws are then attached with epoxy cement to the sides of the test specimen for the horizontal LVDT(s). LVDTs are mounted on the sample in such a way that both vertical and horizontal strains can be measured. The specimen is placed and secured tightly in the testing machine. The control chamber is adjusted to testing temperature. The specimen is preconditioned for 100 cycles with a shear stress of 69 ± 5 kPa. Each cycle is 0.7 second in duration, and consists of the application of a 0.1 second haversine load followed by a 0.6 second rest period. The test is conducted until 5000 cycles or a shear failure occurs, usually at 2.5mm or 5 percent shear strain. Axial deformation, shear deformation, axial load, and shear load at a rate of about 50 data points per second are recorded. The permanent shear strain is then computed. The Repetitive Simple Shear Test at Constant Height (RSST-CH) test can also be used to obtain Creep compliances D(t) and parameters to be used in the power law of the creep compliance equation, d_o, d_i and m. For these samples the shear load of 69 kPa was low because the samples were tested at 35^oC. Therefore the shear load was increased to 137.5 kPa (20 psi); the measured shear strains are provided in the results section (Chapter 5).

Figure 4.21 The Superpave Shear Test (SST)
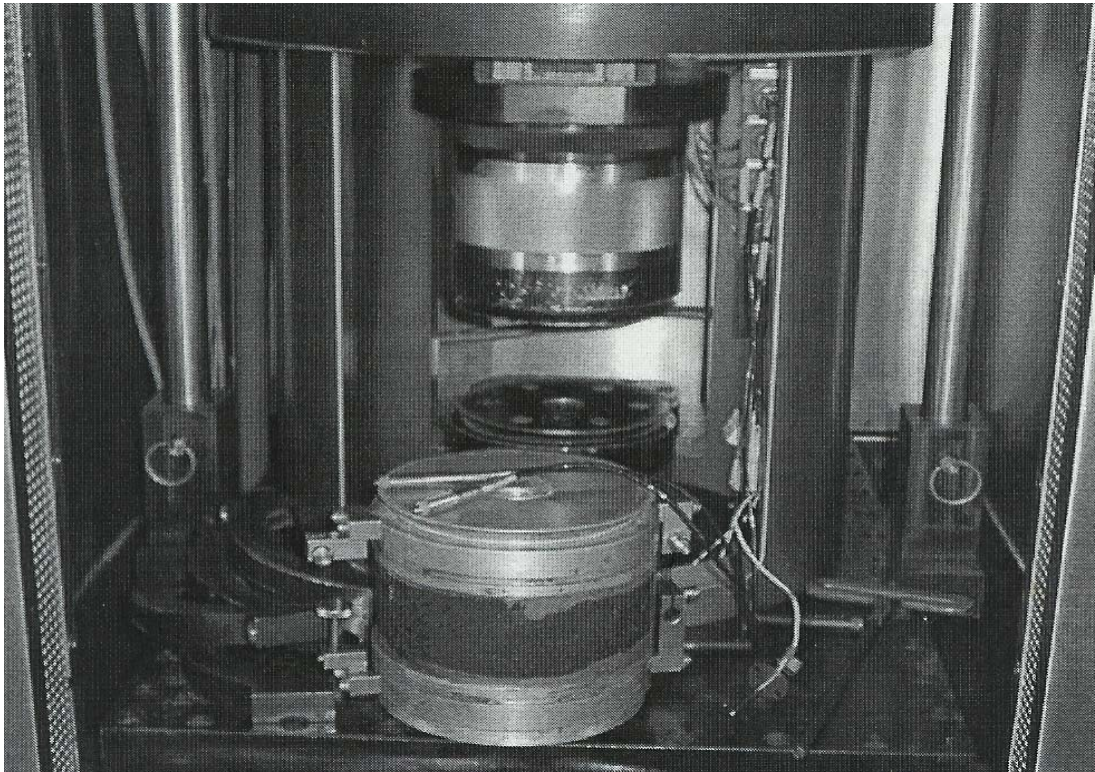
Figure 4.22 Cox SST testing machine
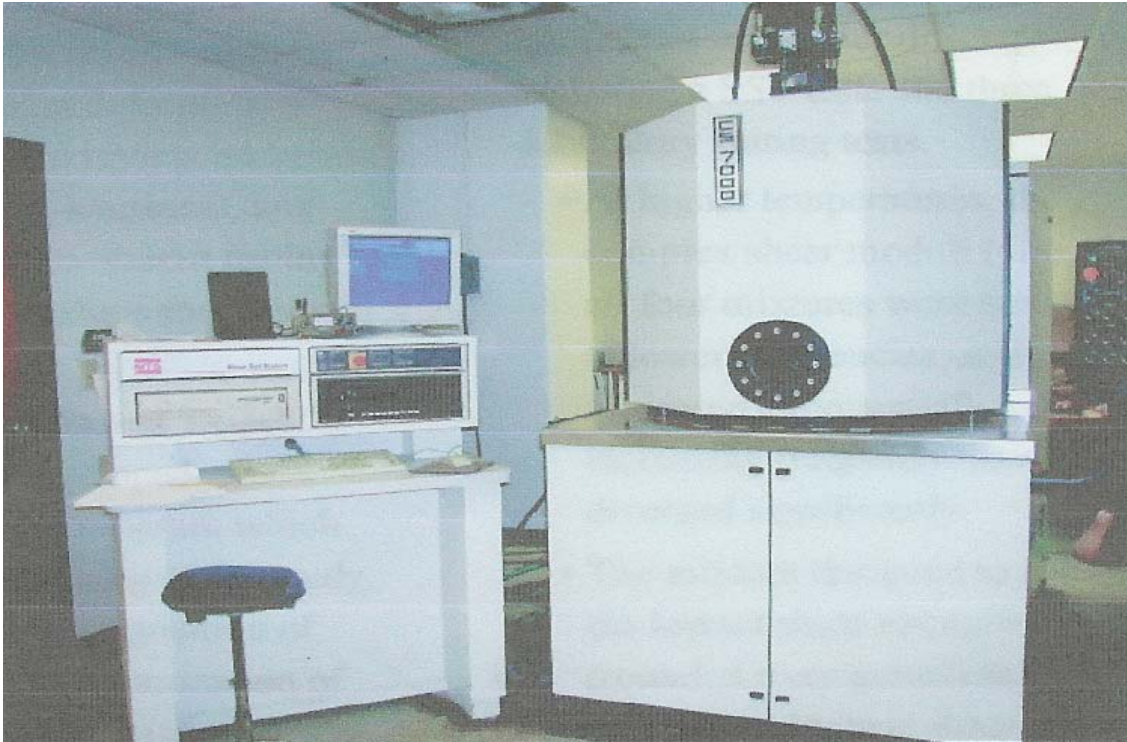
For this project, the SST Repeated Shear Test at Constant Height (RSCH), AASHTO T320, Procedure C, was conducted at 35°C with a shear load of 137.5 kPa (20 psi) and tested up to 50,000 number offload repetitions. From Table 4.8 above, it can be observed that, Iowa mix IA-1 attained maximum permanent strain of 11.28% after 40,000 cycles. The rest of the samples had better resistance to permanent deformation. At 5000 cycles all samples pass specification, having permanent strain less than 5% or 2.5mm deformation. After 10000 cycles, Iowa mix IA-1, the fails faster to 11.28% at 40,000 cycles (Figure 4.23).

Table 4.8 The results of the SST repetitive shear at constant height.

Specimen	Mix ID	KS-1	KS-2	MO-1	MO-2	IA-1	IA-2
% Air Voids		6.49	6.59	8.63	6.82	9.18	7.75
g_{perm} (strain) @ cycles	10	0.01%	0.08%	0.03%	0.04%	0.08%	0.05%
	50	0.04%	0.24%	0.08%	0.11%	0.23%	0.13%
	100	0.06%	0.35%	0.12%	0.17%	0.34%	0.19%
	500	0.15%	0.72%	0.26%	0.40%	0.70%	0.44%
	1,000	0.20%	0.94%	0.37%	0.55%	0.89%	0.59%
	5,000	0.39%	1.63%	0.75%	0.97%	1.61%	1.05%
	10,000	0.51%	1.92%	0.99%	1.17%	2.41%	1.30%
	20,000	0.63%	2.17%	1.27%	1.38%	4.76%	1.59%
	30,000	0.70%	2.29%	1.45%	1.50%	8.38%	1.78%
	40,000	0.75%	2.37%	1.58%	1.58%	11.28%	1.91%
	50,000	0.78%	2.43%	1.69%	1.65%	na	2.00%

Figure 4.23 RSCH, permanent strain against number of cycles
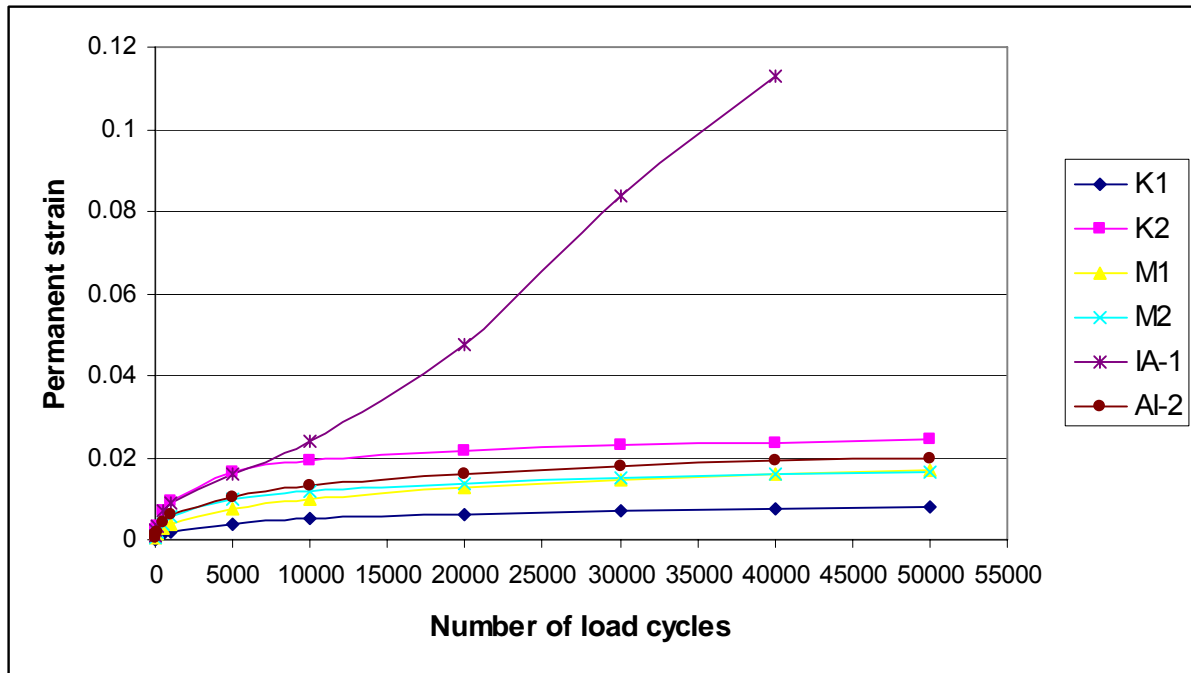
Frequency sweep at constant height (FSCH) Master Curves and Shift Factors

The FSCH test was performed to obtain the dynamic shear modulus G*, storage modulus G' and loss modulus G" of asphalt mixtures. The test was performed as Asphalt Institute laboratories, in Kentucky. The storage and loss moduli represents the behavior of asphalt at intermediate temperatures, where G* = G' + iG". The storage modulus is the elastic (recoverable) and the loss modulus is viscous and non recoverable. The dynamic modulus and phase angle are affected by both temperature and loading frequency. At low temperature and high loading frequency, the asphalt concrete is elastic and has a high dynamic modulus. At high temperature and low loading frequency, asphalt concrete is more viscous has a low elastic modulus. The results from the FSCH test were used to construct master curves and obtain modulus values at a representative temperature of 35°C.

The Dynamic Shear modulus master curves were calculated using Mastersolver Version 2.0, developed by Ramon Bonaquist of Advanced Asphalt Technologies, LLC. Mastersolver has a capability to solve a modified version of Mechanistic-Empirical Design Guide master curve equation, Equation 4.1.

$$\log|E*| = \delta + \frac{(Max - \delta)}{1 + e^{\beta + \gamma \log w_r}}$$
<div align="right">4.1</div>

Where:

$|E*|$ = dynamic Modulus

ω_r = reduced frequency, Hz

Max = limiting maximum modulus

δ, β and γ = fitting parameters

The reduced frequency is computed using the Arrhenius equation, Equation 4.2.

$$\log \omega_r = \log \omega + \frac{\Delta E_a}{19.14714}\left(\frac{1}{T} - \frac{1}{T_r}\right)$$
<div align="right">4.2</div>

Where:

ω_r = reduced frequency at the reference temperature

ω = loading frequency at the test temperature

T_r = reference temperature in ^{o}K

T = test temperature in ^{o}K

ΔE_a = activation energy (treated as a fitting parameter)

Substituting equation 4.2 into equation 4.1 yields the master curve that is used for dynamic modulus computation.

$$\log|E*| = \delta + \frac{(Max - \delta)}{1 + e^{\beta + \gamma\left\{\log \omega + \frac{\Delta E_a}{19.14714}\left(\frac{1}{T} - \frac{1}{T_r}\right)\right\}}}$$
<div align="right">4.3</div>

The temperature shift factors are given by Equation 4.4

$$\log a(T) = \frac{\Delta E_a}{19.14714}\left(\frac{1}{T} - \frac{1}{T_r}\right)$$
<div align="right">4.4</div>

Where:

a(T) = shift factor at temperature T

T_r = reference temperature in ^{o}K

$$T \quad = \text{ test temperature in } {}^{\circ}K$$

$$\Delta E_a \quad = \text{ activation energy (treated as a fitting parameter)}$$

Bonaquist uses the Hirsch model and a limiting binder modulus of 1 GPa (145,000 psi) to estimate the maximum modulus from mixture volumetric properties, Equations 4.5 and 4.6.

$$|E*|_{max} = P_c \left[4,200,000 \left(1 - \frac{VMA}{100} \right) + 435,000 \left(\frac{VFAxVMA}{10,000} \right) \right] + \frac{1 - P_c}{\left[\dfrac{1 - \dfrac{VMA}{100}}{4,200,000} + \dfrac{VMA}{453,000(VFA)} \right]} \qquad 4.5$$

Where:

$$P_c = \frac{\left(20 + \dfrac{435,000(VFA)}{VMA} \right)^{0.58}}{650 + \left(\dfrac{4355,000(VFA)}{VMA} \right)^{0.58}} \qquad 4.6$$

$$|E*| \quad = \text{ limiting maximum mixture dynamic modulus}$$

$$VMA \quad = \text{ voids in mineral aggregates, \%}$$

$$VFA \quad = \text{ voids filled with asphalt, \%}$$

These equations are used in the Mastersolve Version 2.0. The solver and results from the FSCH test were used to compute the dynamic shear modulus, storage modulus and loss modulus. Figure 4.24 to Figure 4.29 contains the dynamic shear modulus master curves plots. Figure 4:30 to Figure 4:35 shows the master curve plots of storage modulus for the six asphalt mixes and Figures 4.36 to Figure 4.41 are the master curve plots for loss modulus. Tables 4.9 to 4.11 provide the values used as fit parameter in the MEPDG master curve equation (the sigmoidal equation). Plots for shift factors, phase angle and MEPGD input values are provided in Appendix B.

Figure 4.24 Dynamic Shear Modulus (G*) Master Curve for Kansas KS-1 Mix fitted at 35ºC
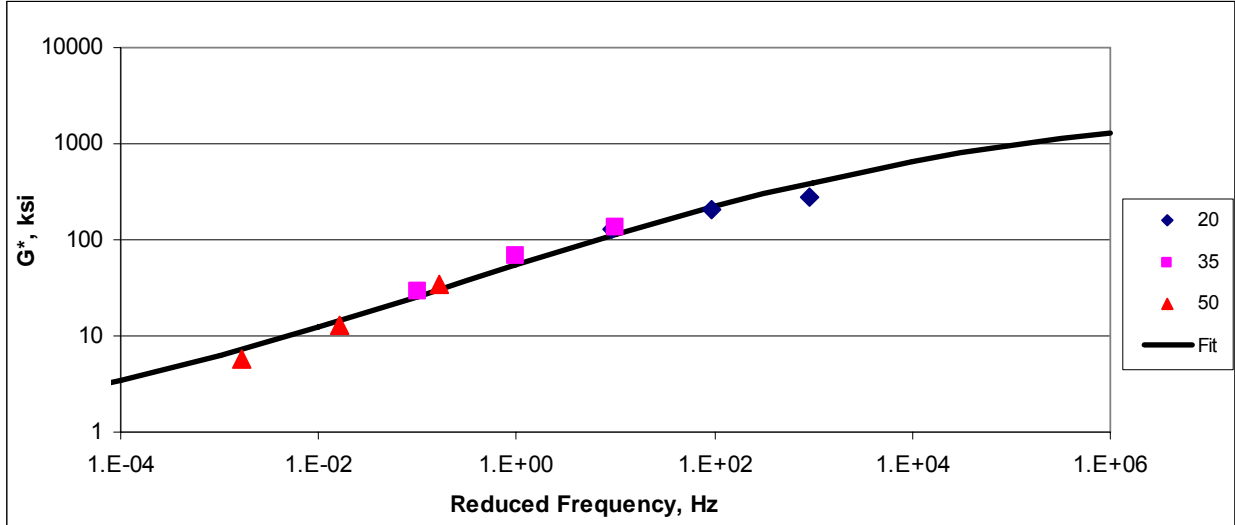
Figure 4.25 Dynamic Shear Modulus (G*) Master Curve for Kansas KS-2 Mix fitted at 35ºC
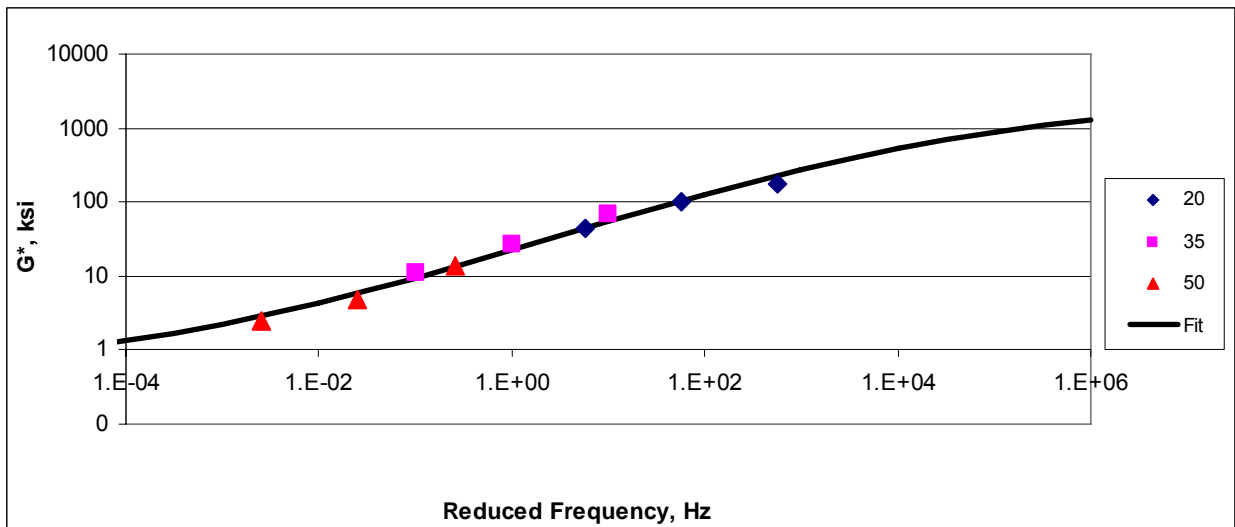
Figure 4.26 Dynamic Shear Modulus (G*) Master Curve for Missouri MO-1 Mix fitted at 35°C
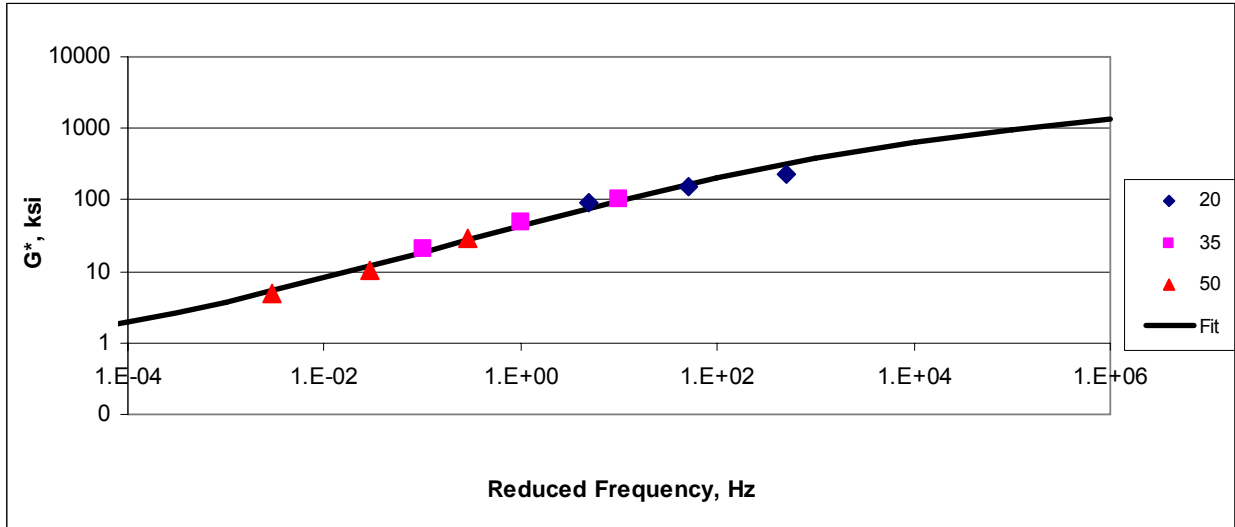
Figure 4.27 Dynamic Shear Modulus (G*) Master Curve for Missouri MO-2 Mix fitted at 35°C
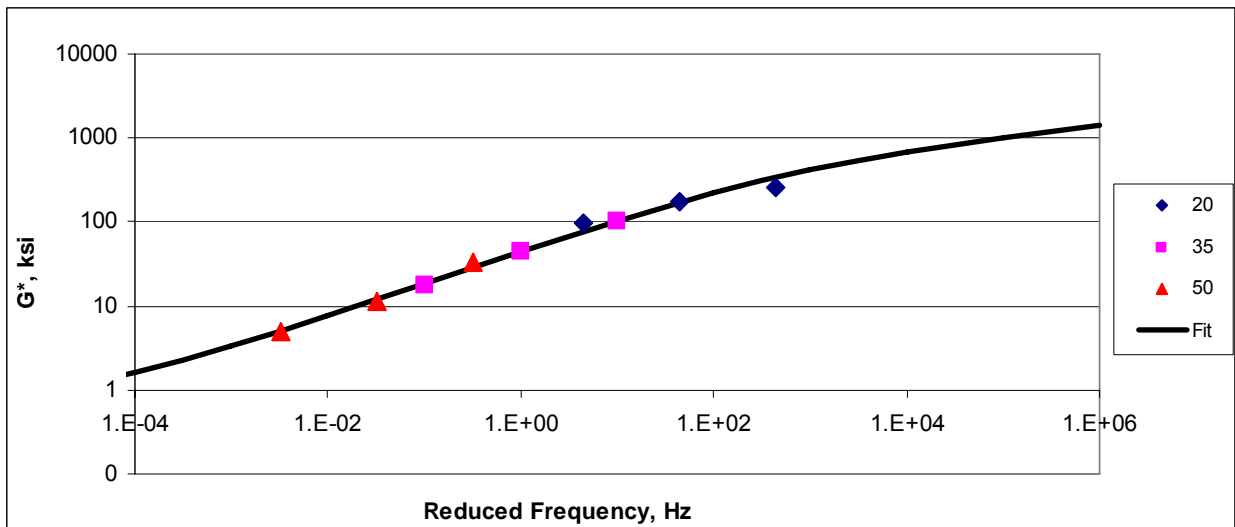
Figure 4.28 Dynamic Shear Modulus (G*) Master Curve for Iowa IA-1 Mix fitted at 35°C
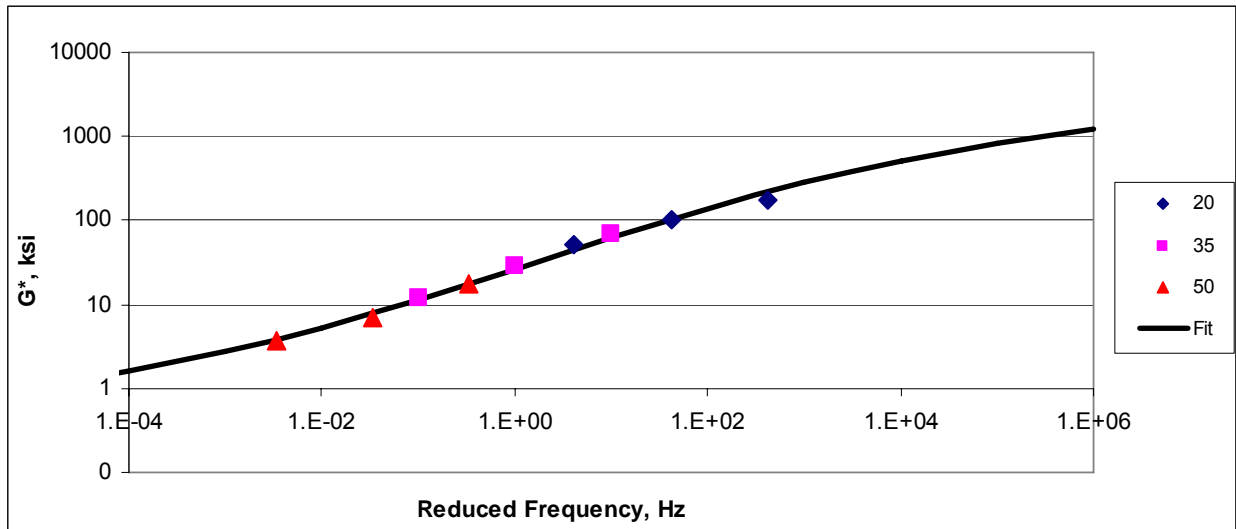
Figure 4.32 Dynamic Shear Modulus (G*) Master Curve for Iowa IA-2 Mix fitted at 35°C
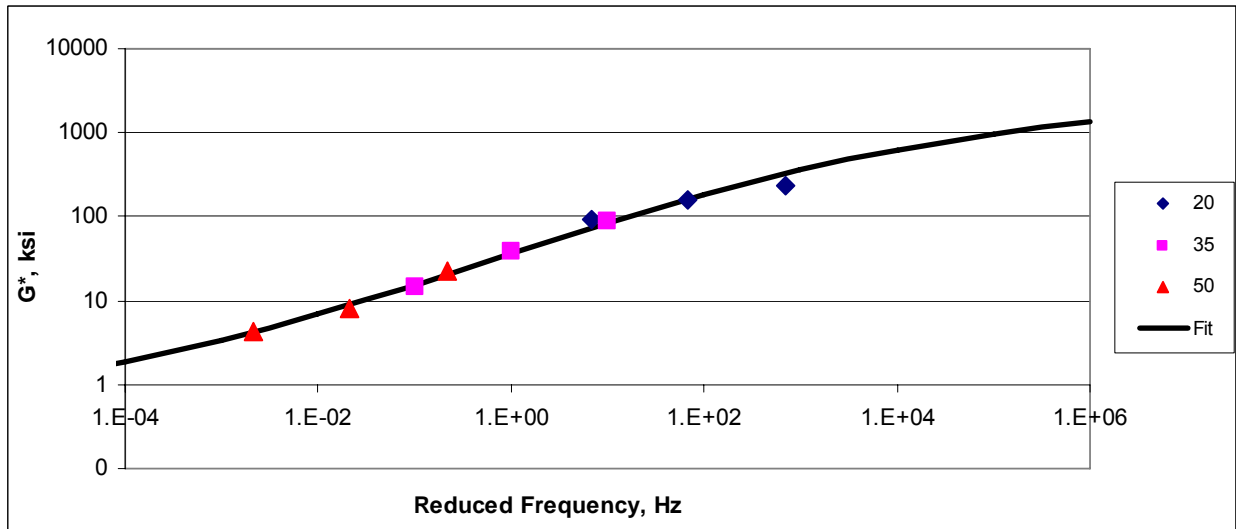
The dynamic shear modulus (G*) values at 35°C were obtained using Equation 4.1 and fitting parameters in Table 4.9. The dynamic shear modulus (G*) values at 35°C (test temperature) and six loading frequencies are given in Table 4.10, and in Table 4.11 are the shift factors used to shift dynamic shear modulus values with respect to temperature to obtain the master curve.

Table 4.9 Dynamic shear modulus fitting parameters

Fit Parameters	Fit Parameters for shear modulus G*					
	KS-1	KS-2	MO-1	MO-2	IA-1	IA-2
Delta (δ)	-0.4023	-0.5000	-0.7351	-0.9120	-0.4512	-0.5232
Beta (β)	-0.2000	0.1546	-0.2512	-0.3273	0.0892	-0.0720
Gamma (γ)	-0.3365	-0.3864	-0.3500	-0.3500	-0.3800	-0.3700
Ea	226928	202655	195866	189921	186672	211911
Max (MPa)	21584.62	21584.62	21584.62	21584.62	21584.62	21584.62

Table 4.9 Dynamic shear modulus values at 35°C and six frequencies

Freq. (Hz)	G* (MPa)					
	KS-1	**KS-2**	**MO-1**	**MO-2**	**IA-1**	**IA-2**
25	1035.1	537.7	918.9	976.3	597.8	796.1
10	786.5	380.0	678.6	716.9	429.7	578.7
5	634.8	290.9	535.0	562.0	333.0	451.5
1	379.7	155.9	301.4	311.3	183.0	249.9
0.5	302.9	119.5	233.9	239.3	141.5	193.1
0.1	178.8	65.7	129.1	128.8	79.0	106.7

Table 4.11 Shift factors for dynamic shear modulus G*

Temp	**KS-1**	**KS-2**	**MO-1**	**MO-2**	**IA-1**	**IA-2**
-10	6.575	5.871	5.675	5.503	5.408	6.140
4.4	4.232	3.779	3.653	3.542	3.481	3.952
20	1.967	1.757	1.698	1.647	1.618	1.837
35	0.000	0.000	0.000	0.000	0.000	0.000
50	-1.785	-1.594	-1.540	-1.494	-1.468	-1.667

Figure 4:33 to Figure 4:38 presents the master curve plots of storage modulus (G') for the six asphalt mixes.

Figure 4.33 Storage Modulus (G') Master Curve for Kansas KS-1 Mix fitted at 35°C
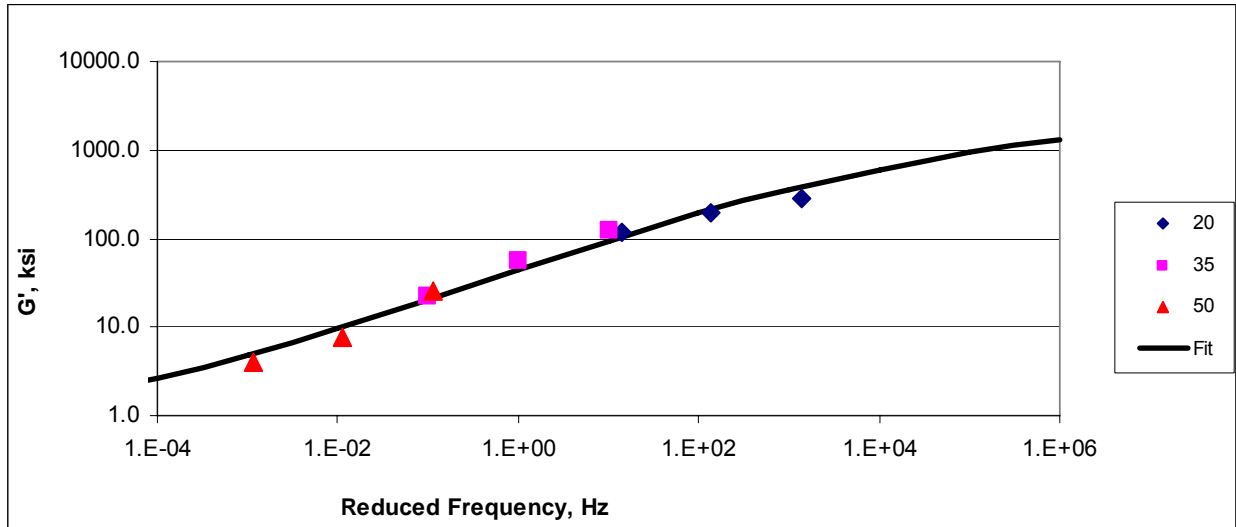
Figure 4.34 Storage Modulus (G') Master Curve for Kansas KS-2 Mix fitted at 35°C
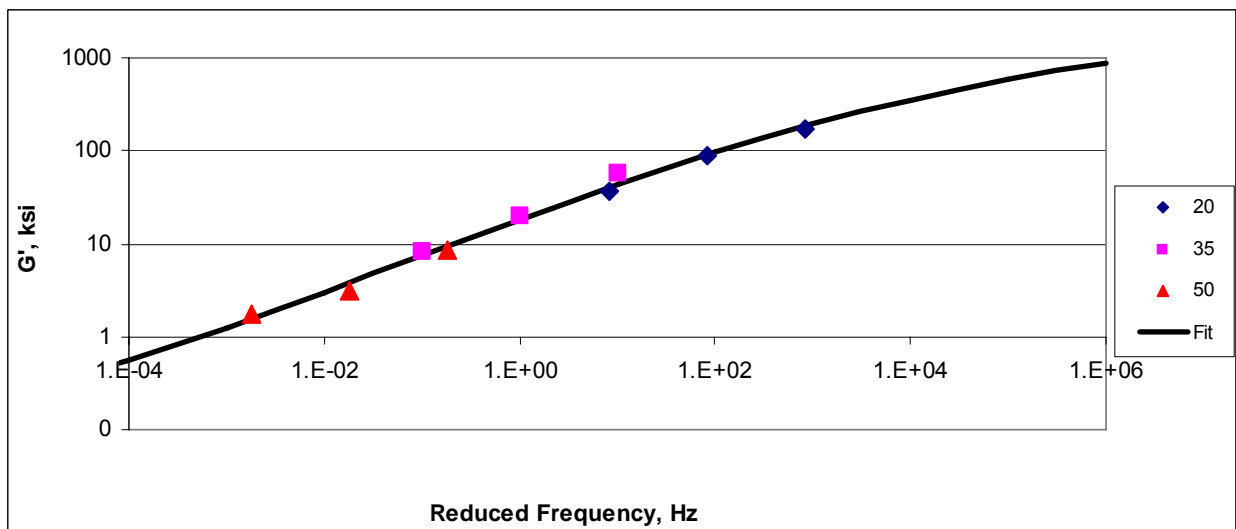
Figure 4.35 Storage Modulus (G') Master Curve for Missouri MO-1 Mix fitted at 35°C
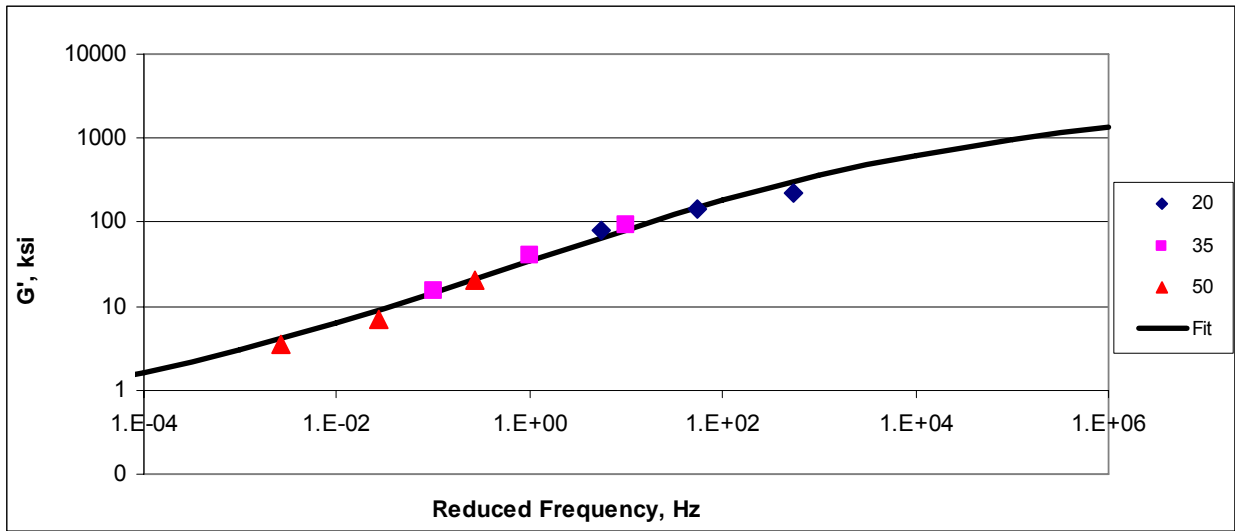
Figure 4.36 Storage Modulus (G') Master Curve for Missouri MO-2 Mix fitted at 35°C
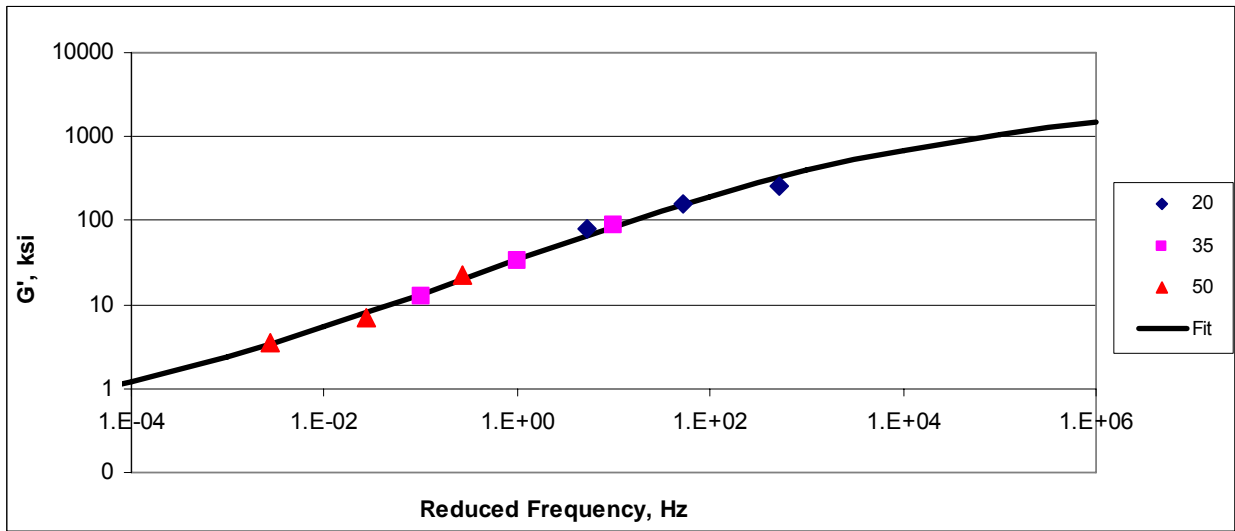
Figure 4.37 Storage (G') Modulus Master Curve for Iowa IA-1 Mix fitted at 35°C
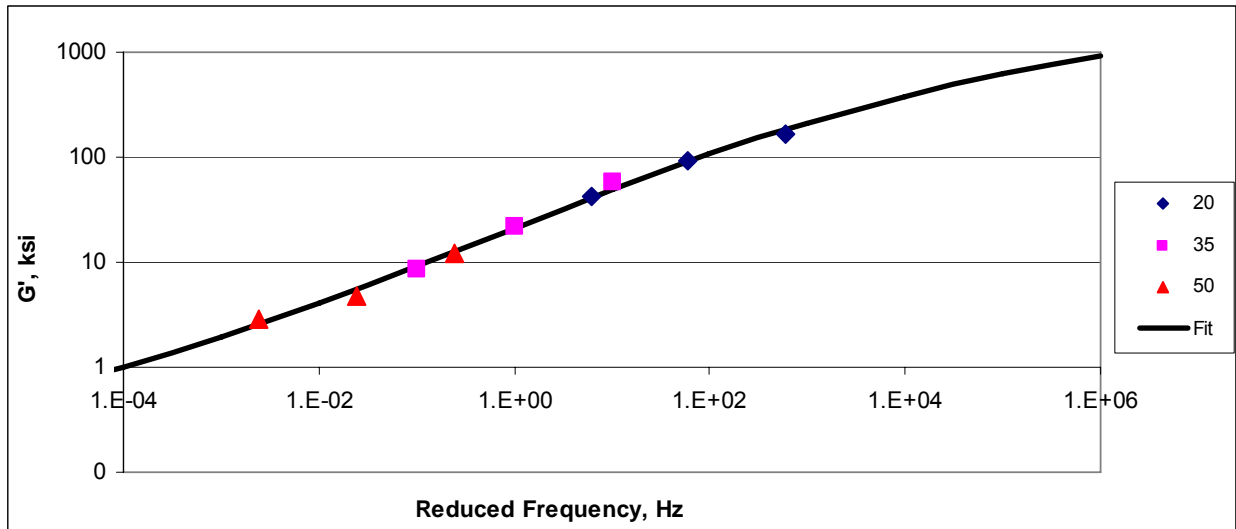
Figure 4.38 Storage (G') Modulus Master Curve for Iowa IA-2 Mix fitted at 35°C
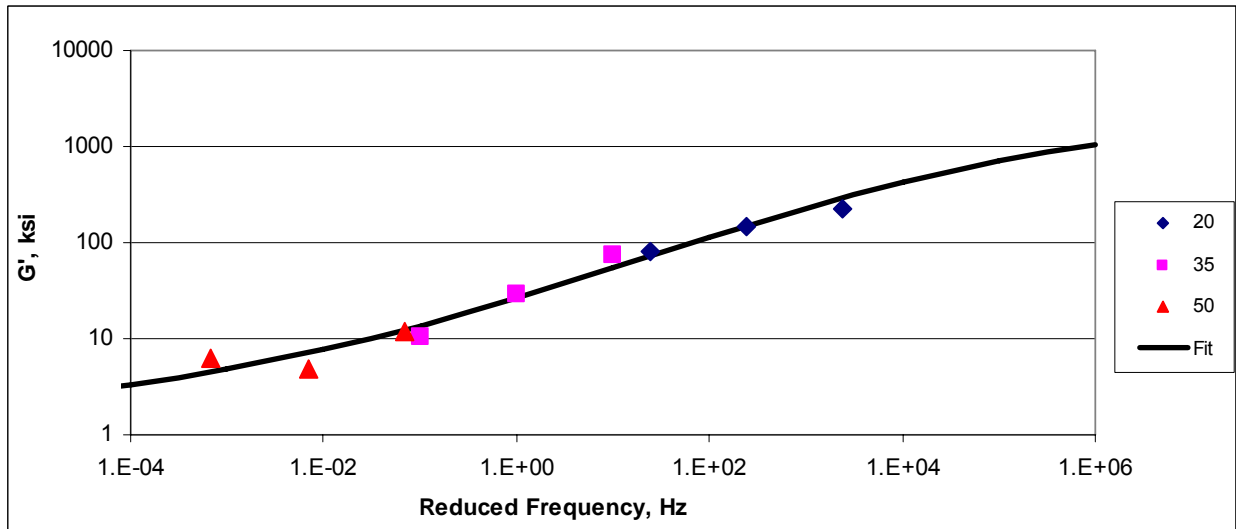
The storage modulus (G') values at 35°C were obtained using Equation 4.1 and fitting parameters in Table 4.12. The storage modulus (G') values at 35°C (test temperature) and six loading frequencies are given in Table 4.13, and in Table 4.14 are the shift factors used to shift storage modulus values with respect to temperature to obtain the master curves.

Table 4.12 Storage modulus fitting parameters

Fit Parameters	Fit Parameters for storage modulus G'					
	KS-1	KS-2	MO-1	MO-2	IA-1	IA-2
Delta (δ)	-0.4064	-1.7980	-0.5588	-0.8128	-1.0203	0.1100
Beta (β)	-0.1000	-0.3065	-0.0686	-0.1775	-0.0899	0.4604
Gamma (γ)	-0.3500	-0.2984	-0.3800	-0.3800	-0.3274	-0.3787
Ea	246659	220776	199847	198340	205520	275157
Max (MPa)	21584.62	22775.03	21246.77	22051.59	20530.34	21651.54

Table 4.13 Storage modulus values at 35°C and six frequencies

	G' (MPa)					
Freq. (Hz)	KS-1	KS-2	MO-1	MO-2	IA-1	IA-2
25	874.6	537.7	781.4	829.8	463.0	501.6
10	652.8	380.0	562.3	590.4	336.9	373.9
5	520.0	290.9	435.1	452.0	263.3	299.8
1	302.4	155.9	236.0	237.5	146.6	181.5
0.5	238.7	119.5	180.8	178.9	113.7	147.4
0.1	138.2	65.7	97.9	92.6	63.1	93.4

Table 4.14 Shift factors for storage modulus G'

Temp	KS-1	KS-2	MO-1	MO-2	IA-1	IA-2
-10	7.146	6.396	5.790	5.746	5.954	7.972
4.4	4.600	4.117	3.727	3.699	3.833	5.132
20	2.138	1.914	1.733	1.719	1.782	2.385
35	0.000	0.000	0.000	0.000	0.000	0.000
50	-1.940	-1.736	-1.572	-1.560	-1.616	-2.164

Figures 4.39 to Figure 4.44 are master curve plots of loss modulus after FSCH test for the six asphalt mixes. From the plots it can be observed that the loss modulus at low temperatures is over estimated using the master curve equations. This is the best fitting that could be achieved.

Figure 4.39 Loss Modulus (G") Master Curve for Kansas KS-1 Mix fitted at 35°C
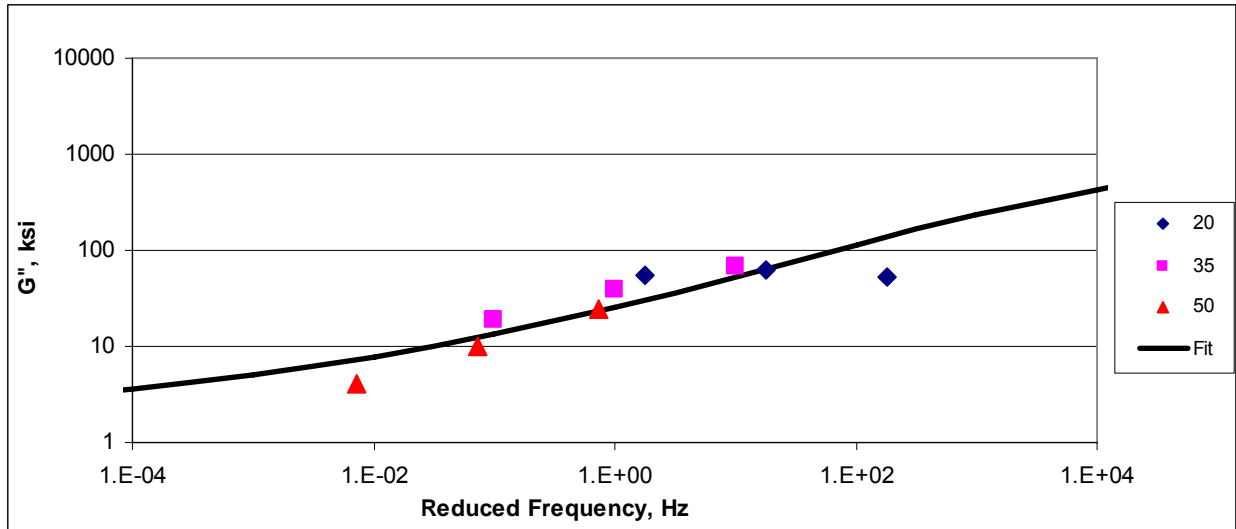
Figure 4.40 Loss Modulus (G") Master Curve for Kansas KS-2 Mix fitted at 35°C
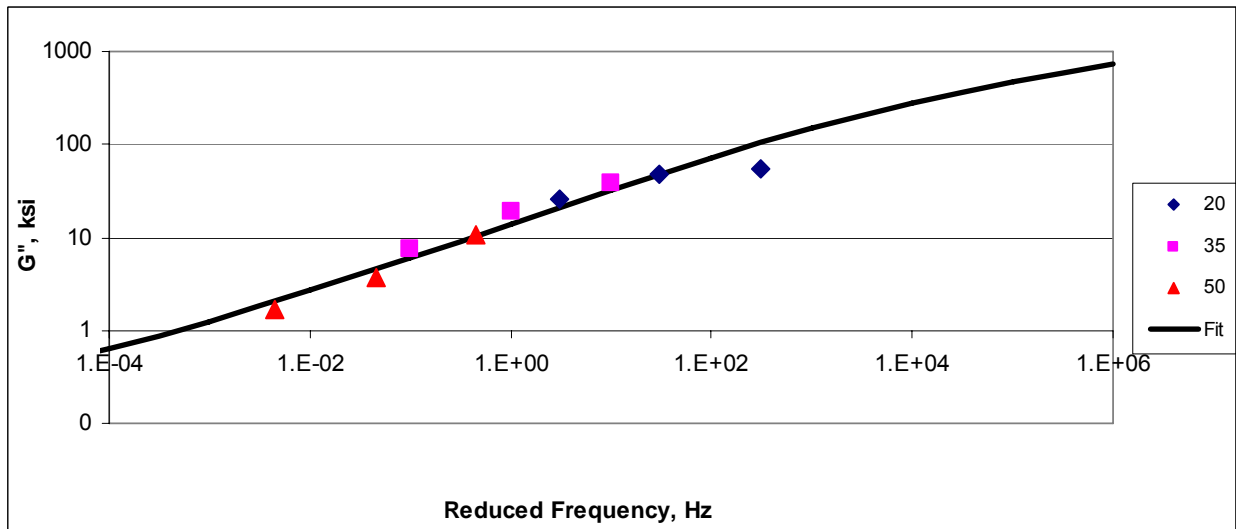
Figure 4.41 Loss Modulus (G") Master Curve for Missouri MO-1 Mix fitted at 35°C
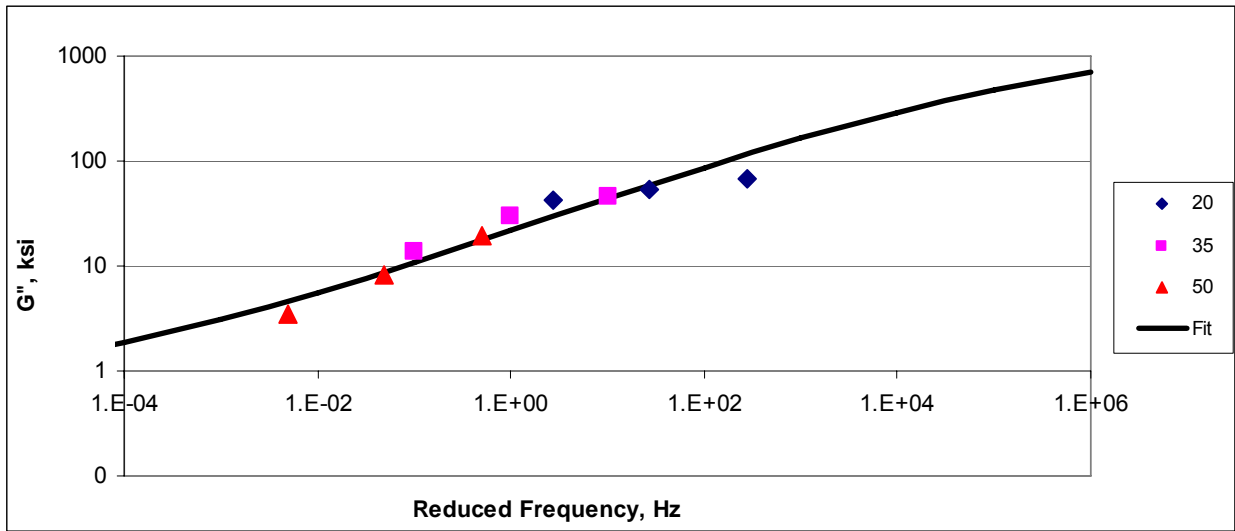
Figure 4.42 Loss Modulus (G") Master Curve for Missouri MO-2 Mix fitted at 35°C
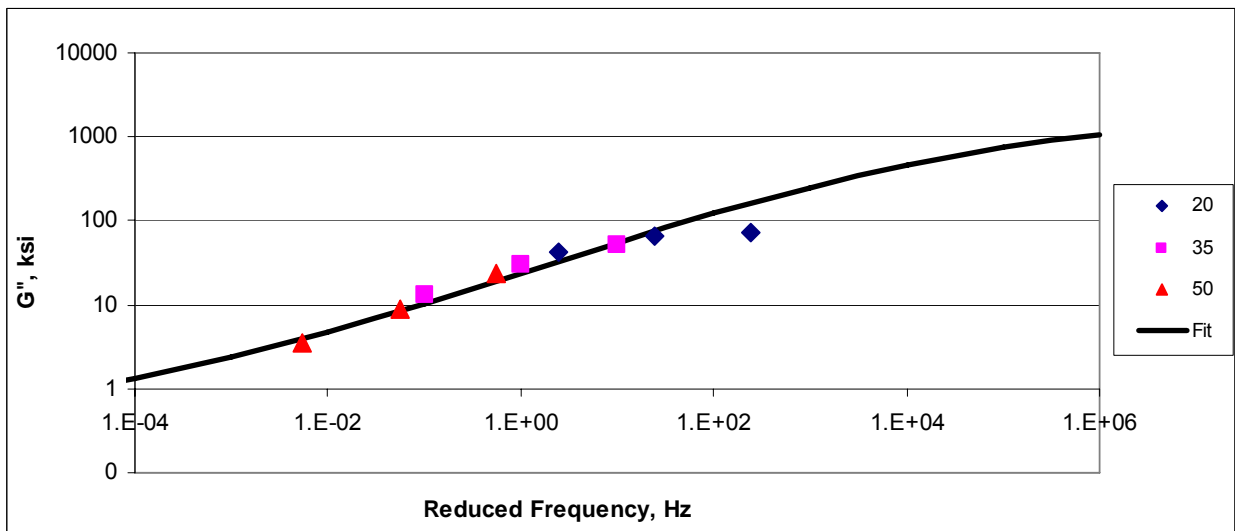
Figure 4.43 Loss Modulus (G") Master Curve for Iowa IA-1 Mix fitted at 35°C
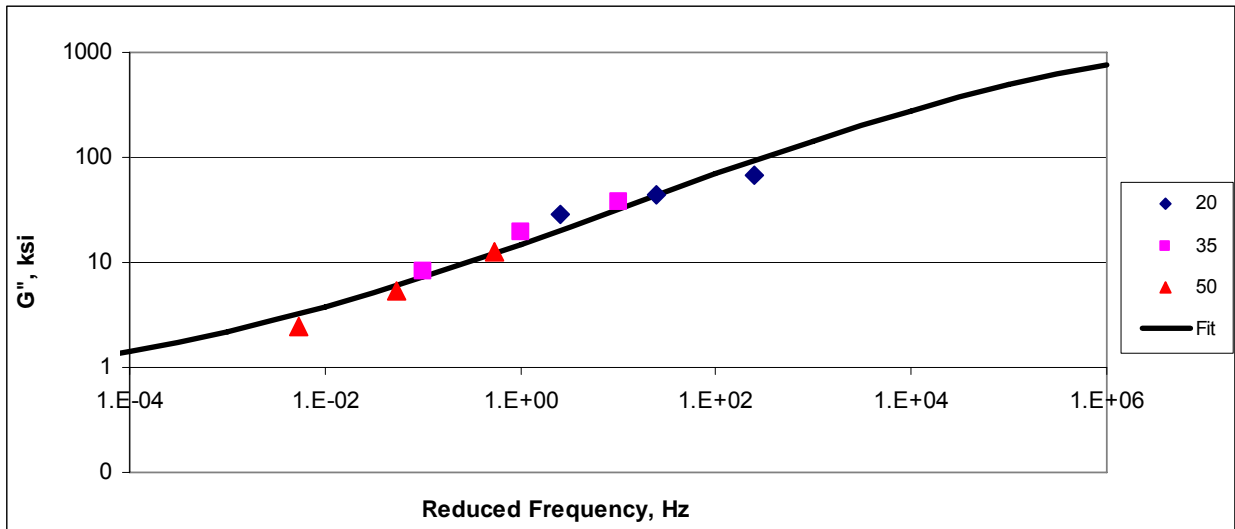
Figure 4.44 Loss Modulus (G") Master Curve for Iowa IA-2 Mix fitted at 35°C
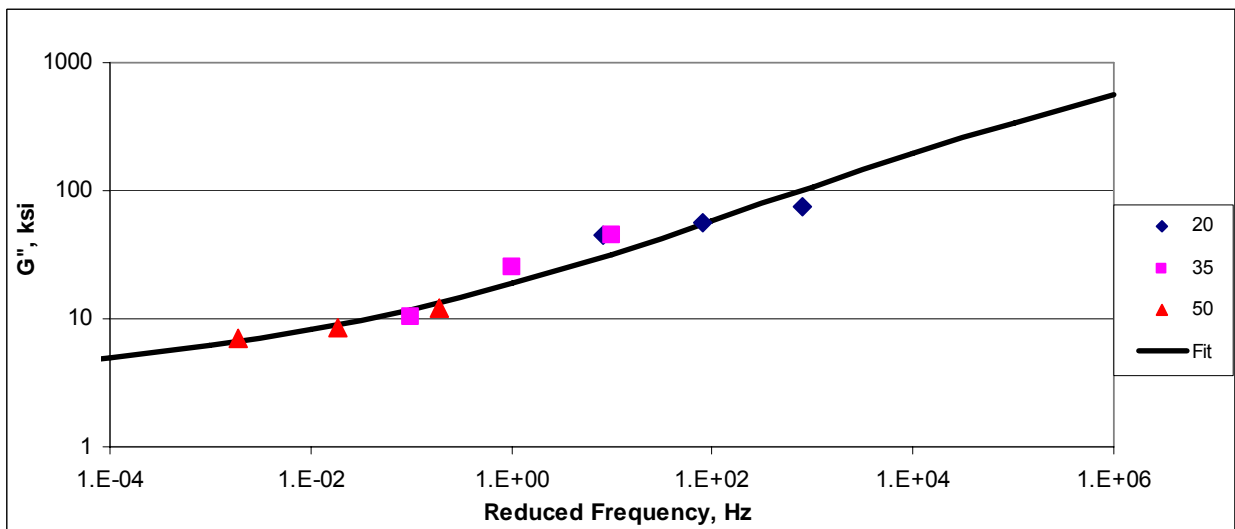
The fitting parameters used in Equation 4.1 to obtain the loss modulus (G") are given in Table 4.15. The loss modulus (G") values at 35°C (test temperature) and six loading frequencies are given in Table 4.16, and in Table 4.17 are the shift factors used to shift loss modulus values with respect to temperature to obtain the master curves.

Table 4.15 Loss modulus fitting parameters

Fit Parameters	Fit Parameters for storage modulus G"					
	KS-1	KS-2	MO-1	MO-2	IA-1	IA-2
Delta (δ)	0.2253	-1.3920	-0.6030	-0.7013	-0.4052	0.4262
Beta (β)	0.5642	-0.0688	0.1087	0.0259	0.3796	0.9661
Gamma (γ)	-0.4000	-0.3000	-0.3000	-0.3500	-0.3500	-0.3500
Ea	144847	170924	165705	159777	161506	219532
Max (MPa)	21584.62	22775.03	21246.77	22051.59	20530.34	21651.54

Table 4.16 Loss modulus values at 35°C and six frequencies

	G" (MPa)					
Freq. (Hz)	KS-1	KS-2	MO-1	MO-2	IA-1	IA-2
25	4.197	4.952	4.801	4.629	4.679	6.360
10	2.701	3.188	3.090	2.980	3.012	4.094
5	1.256	1.482	1.437	1.385	1.400	1.903
1	0.000	0.000	0.000	0.000	0.000	0.000
0.5	-1.139	-1.344	-1.303	-1.257	-1.270	-1.727
0.1	4.197	4.952	4.801	4.629	4.679	6.360

Table 4.17 Shift factors for loss modulus G"

Temp	KS-1	KS-2	MO-1	MO-2	IA-1	IA-2
-10	4.197	4.952	4.801	4.629	4.679	6.360
4.4	2.701	3.188	3.090	2.980	3.012	4.094
20	1.256	1.482	1.437	1.385	1.400	1.903
35	0.000	0.000	0.000	0.000	0.000	0.000
50	-1.139	-1.344	-1.303	-1.257	-1.270	-1.727

CHAPTER 5 - FINITE ELEMENT MODELING AND RESULTS

Four permanent deformation prediction models were selected for evaluation of the model's capacity to predict permanent deformation in asphalt concrete mixtures. The models selection criteria were the ability to conduct material characterization the tests and the possibility of characterizing permanent deformation in asphalt mixtures using the commercial finite element software, Abaqus. The four models selected are the creep, Drucker-Prager, elasto-visco-plastic and viscoelastic. These models can be implemented using Abaqus/CAE software. Material characterization for the first three models was performed at KSU laboratories, while the tests for the fourth model were conducted at the Asphalt Institute. Using Abaqus/CAE software, the CISL 14 asphalt pavement sections were modeled to simulate permanent deformation characteristics of asphalt mixes. The simulations were then compared with results obtained from the accelerated pavement testing of the pavement sections. Six sections were constructed and tested in CISL 14 project. Material characterization was conducted for the six asphalt mixes, and four prediction models were developed using Abaqus/CAE software for the six asphalt mixes.

The asphalt pavement sections in CISL were constructed in a pit that is 16 feet wide, 20 feet long and six feet deep. The pavement was constructed in three layers having 7.0 inch hot mix asphalt surface layer, 6.0 inch AB3 unbound base course and 59 inches A-7-6 soil subgrade. Each layer was constructed and compacted with convention asphalt pavement construction equipment. Two asphalt concrete mixtures, one for each half of the pit, were constructed with the same base and subgrade layers. This means, when Kansas mix was constructed, one side had KS-1 asphalt mix and the other had KS-2 asphalt mix. Same construction setup was applied for Missouri and Iowa mixes. The Abaqus/CAE model simulated only one part of the pavement structure (half of the pit), in a longitudinal direction. Figure 5.1 below shows the pavement cross section, and Figure 5.2 shows the pavement section (half of the pit) as built in the Abaqus software.

Figure 5.1 Pavement cross section
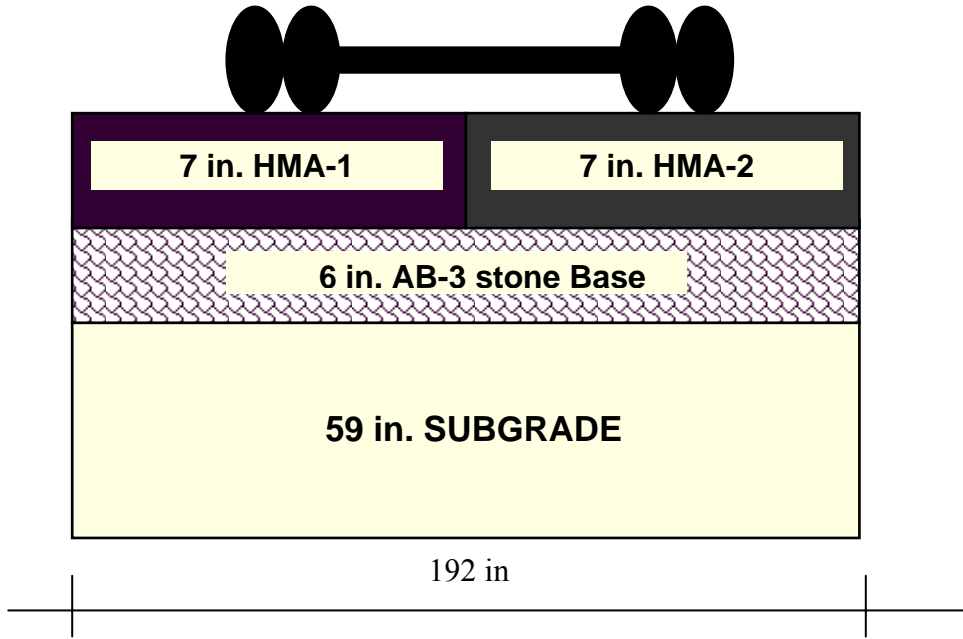
Figure 5.2 Pavement section built in Abaqus
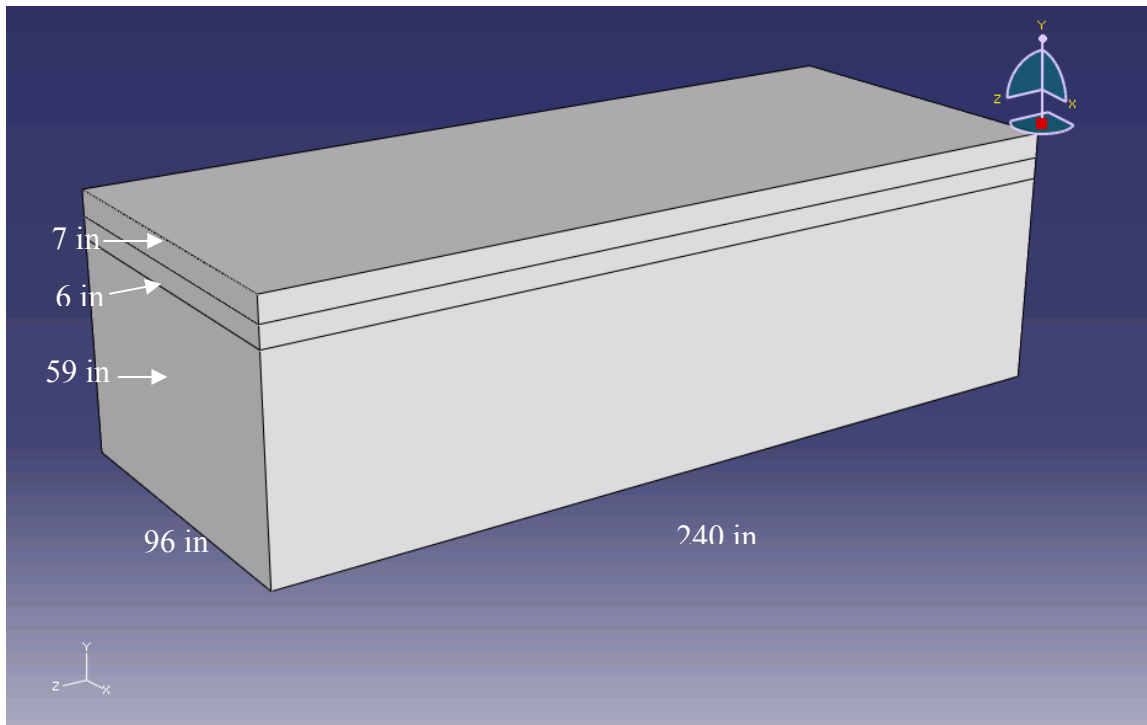
5.1   ABAQUS/CAE

Abaqus/CAE is a complete environment that provides a simple and consistent interface for creating, submitting, monitoring, and evaluating results from Abaqus/Standard and Abaqus/Explicit simulations. Abaqus/CAE is divided into modules, where each module defines a logical aspect of the modeling process; for example, defining the geometry, defining material properties, and generating a mesh. By moving from module to module, a model is built from which Abaqus/CAE generates an input file that is submitted to the Abaqus/Standard or Abaqus/Explicit analysis product. The analysis module performs the analysis, sends information to Abaqus/CAE to allow the job progress to be monitored, and generates an output database. Finally, the Visualization module of Abaqus/CAE (also licensed separately as Abaqus/Viewer) is used to read the output database and view the analysis results [Abaqus, 2004].

Permanent deformation models in this research were simulated using Abaqus/CAE. Abaqus/CAE comprise of modules which are used for the model inputs, implementation and visualization. These modules include: part module, property module, assembly module, steps module, interaction module, load module, mesh module, job module, sketch module and visualization module.

Part Module

Parts are the building blocks of an Abaqus/CAE model. Part module is used to create each part, and the assembly module assembles instances of the parts. The part can be created using Abacus/CAE tools (this is known as a native part) or imported from various CAD software packaged. The pavement sections for analysis in this project were created using the part module of Abaqus/CAE (Figure 5.3), it is a native part. The pavement section has three layers: 175 mm (7.0 in) asphalt mix layer (surface layer), 150 mm (6.0 in) granular subbase (AB 3) and 1,475 mm (59.0 in) subgrade soil with A-7-6 AASHTO classification.

Figure 5.2 Pavement Section Part created using Abaqus CAE software
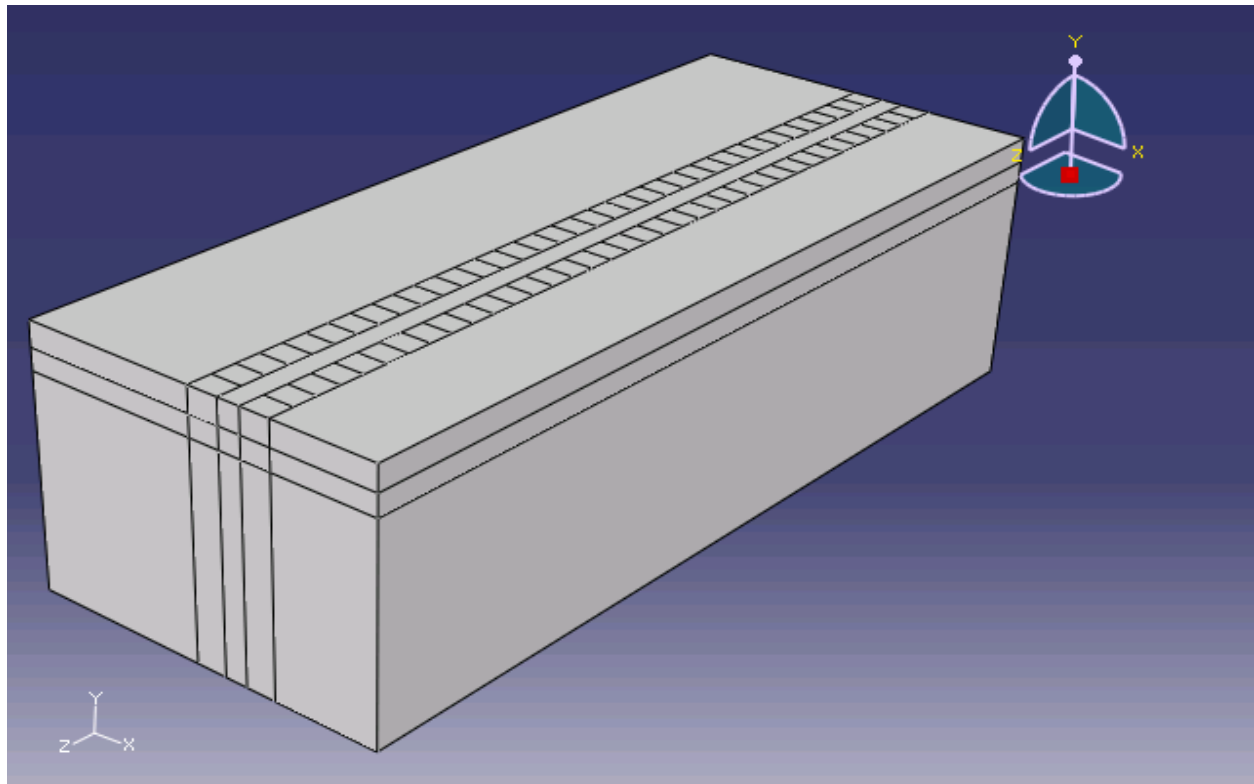
The property module

The Property module is used to define materials, beam section profiles, sections, composite lay-ups, skin reinforcements, inertia (point mass, rotary inertia, and heat capacitance) on a part, and springs and dashpots between two points or between a point and ground. It also assigns sections, orientations, normals, and tangents to parts. [Abaqus, 2004].

The Assembly Module

The assembly module is used to create and modify the assembly. When a part is created in Abaqus/CAE, it exists in its own coordinate system, independent of other parts in the model. The Assembly module is used to create instances the parts and to position the instances relative to each other in a global coordinate system, thus creating the assembly. Part instances are positioned by sequentially applying position constraints that align selected faces, edges, or vertices or by applying simple translations and rotations. A model can contain many parts, and a part can be instanced many times in the assembly; however, a model contains only one assembly.

Loads, boundary conditions, predefined fields, and meshes are all applied to the assembly. An assembly has to be created even if the model consists of only a single part [Abaqus 2004].

Steps Module

The Step module is used to create analysis steps, specify output requests, adaptive meshing, and analysis controls. The analysis step is created by defining a sequence of one or more analysis steps within the model. The step sequence provides a convenient way to capture changes in the loading and boundary conditions of the model, changes in the way parts of the model interact with each other, the removal or addition of parts, and any other changes that may occur in the model during the course of the analysis. In addition, steps allow the user to change the analysis procedure, the data output, and various controls. Abaqus writes output from the analysis to the output database; the user specifies the output by creating output requests that are propagated to subsequent analysis steps. An output request defines which variables will be output during an analysis step, from which region of the model, and at what rate will be the output [Abaqus, 2004].

The step module was used to create steps that simulate a moving load on a pavement section. A rectangular shaped tire imprint was used, with a tire pressure of 690 kPa (100psi), single axle load of 97.68 kN (22,000lbs) applied on dual tires, and tire width of 208.28 mm (8.2 in). The axle speed of 7.6 mph was used. This is the speed used in CISL 14 for testing pavement sections. This information was used to obtain a tire print length of 170.18 mm (6.7 in) and loading time of 0.05 seconds.

Interaction Module

The Interaction module is used to define and manage the following objects:

- Mechanical and thermal interactions between regions of a model or between a region of a model and its surroundings.
- Analysis constraints between regions of a model.
- Assembly-level wire features, connector sections, and connector section assignments to model connectors.
- Inertia (point mass, rotary inertia, and heat capacitance) on regions of the model.

- Cracks on regions of the model.

- Springs and dashpots between two points of a model or between a point of a model and ground

Interactions are step-dependent objects, which mean that when you define them, you must indicate in which steps of the analysis they are active. Abaqus/CAE does not recognize mechanical contact between part instances or regions of an assembly unless that contact is specified in the Interaction module; the mere physical proximity of two surfaces in an assembly is not enough to indicate any type of interaction between the surfaces.

Load Module

Load module is used to define and manage loads, boundary conditions, predefined fields and load cases. Prescribed conditions in Abaqus/CAE are step-dependent objects, which mean that the analysis steps in which they are active must be specified. The stepwise history of prescribed conditions is viewed and manipulated using the load, boundary condition, and predefined field managers. The Step list located in the context bar, can also be used to specify the steps in which new loads, boundary conditions, and predefined fields become active by default. The Amplitude toolset in the Load module is used to specify complicated time or frequency dependencies that can be applied to prescribed conditions. Load cases are sets of loads and boundary conditions used to define a particular loading condition. A load case can be created in static perturbation and steady-state dynamic, direct steps [Abaqus, 2004].

In this Load module, a load of 690 kPa (100 psi) was applied on each tire print for 0.05 seconds and moved to the next step. A total of 36 steps were created to simulate a moving load. Figure 5.4 shows boundary conditions and a moving wheel load on load step 5. The boundary conditions were fixed (encastre: U1=U2=U3=UR1=UR2=UR3=0) on the bottom; X-Symm (U1=UR2=UR3=0) on the sides parallel to z-axis; and Z-Symm (U3=UR1=UR2=0) on the sides parallel to x-axis.

Figure 5.4 Pavement Section Assembly boundary conditions and step loading
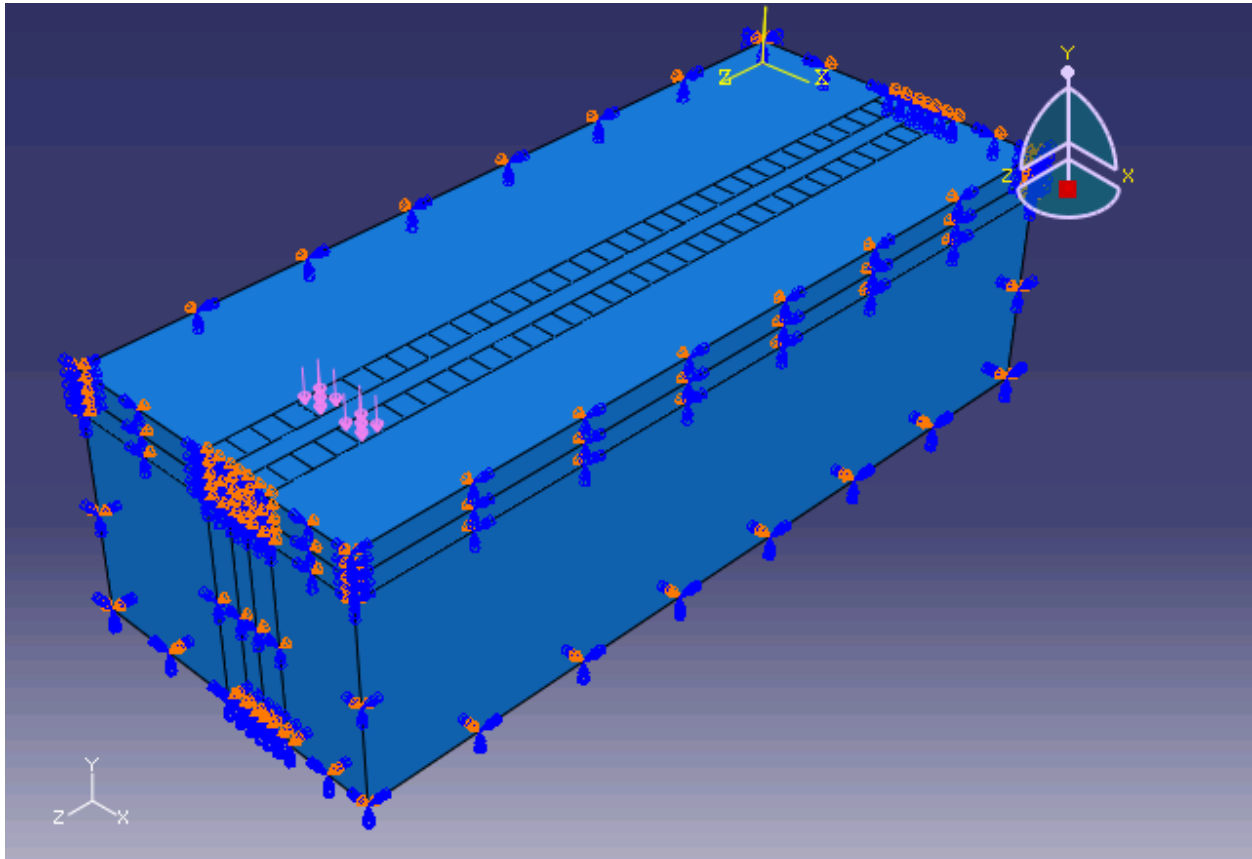
Mesh Module

The Mesh module contains tools that allow the user to generate meshes on parts and assemblies created within Abaqus/CAE. It also contains functions that verify an existing mesh. Various levels of automation and control are available so that a mesh that meets the analysis needs is created. As with creating parts and assemblies, the process of assigning mesh attributes to the model - such as seeds, mesh techniques, and element types, is feature based. As a result the parameters that define a part or an assembly can be modified, and the mesh attributes specified within the Mesh module are regenerated automatically. Figure 5.5 shows a typical mesh used for Kansas mix KS-1 simulation using creep model. This mesh using Abaqus meshing tools to contain a total of 12,168 elements. This mesh was used for all the models. The only change was on the material input parameters for hot mix asphalt.

Figure 5.5 The Mesh of KS-1 Pavement Section
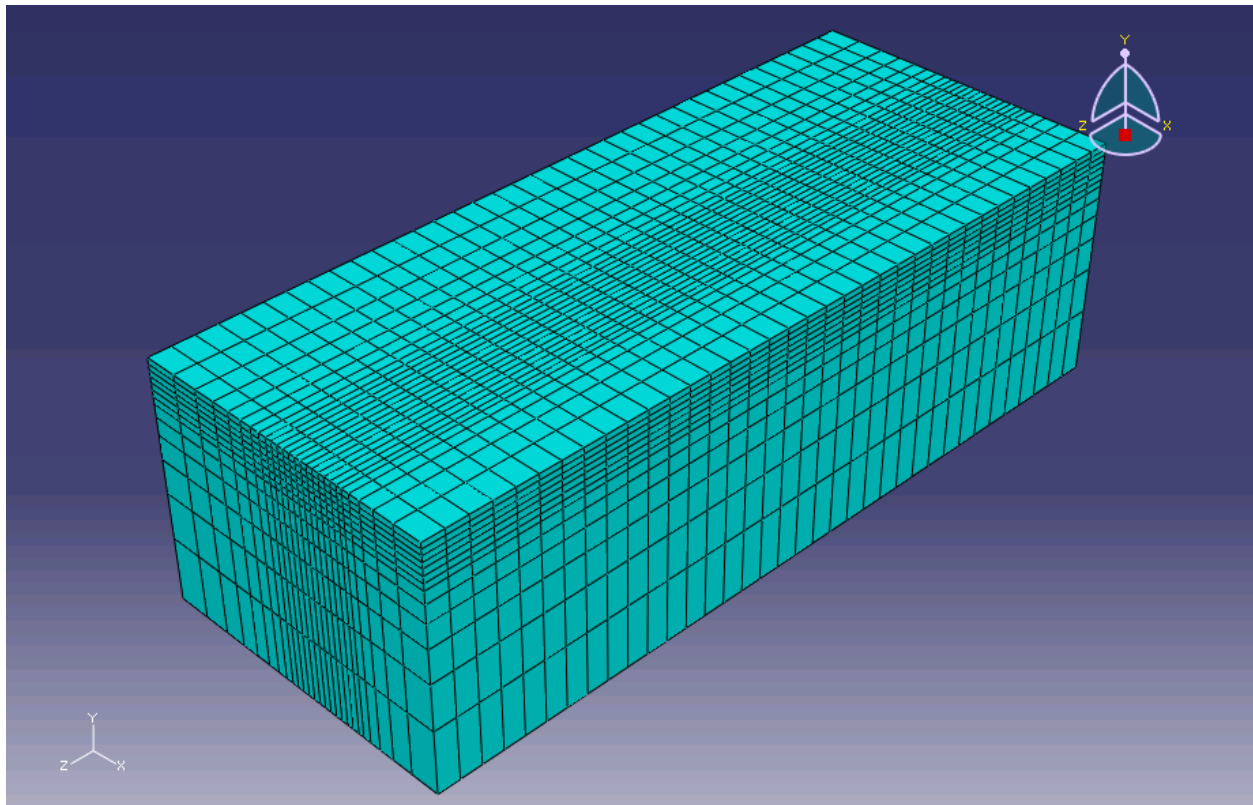
Job Module

  The Job module is used to analyze a model once all tasks involved in defining a model (such as defining the geometry of the model, assigning section properties, and defining contact etc.) are finished. In the Job module a job is created and submitted to Abaqus/Standard or Abaqus/Explicit for analysis, and for monitoring its progress. Analysis file input is created and run, this makes it possible to view and edit the input file before submitting it for full analysis [Abaqus, 2004].

Sketch Module

  Sketches are two-dimensional profiles that are used to help form the geometry defining an Abaqus/CAE native part. The Sketch module is used to create a sketch that defines a planar part, a beam, or a partition or to create a sketch that might be extruded, swept, or revolved to form a three-dimensional part [Abaqus, 2004].

Visualization

The Visualization module provides graphical display of finite element models and results. It obtains model and result information from the output database; the information placed in the output database is controlled by modifying output requests in the Step module. The model and results are viewed by producing plots such as undeformed shape , deformed shape contours symbols , X–Y data , time history animation scale factor animation and harmonic animation. Figure 5.6 shows a contoured deformed shape plot of KS-1 pavement section modeled using creep model after a single passage of a 690 kPa (100 psi) wheel load. The deformation is factored 13470 times. The Un-factored deformed plot is given in Figure 5.7 [Abaqus, 2004].

Figure 5.6 Deformed plot of KS-1 section using the Visualization module scale factor = 13470
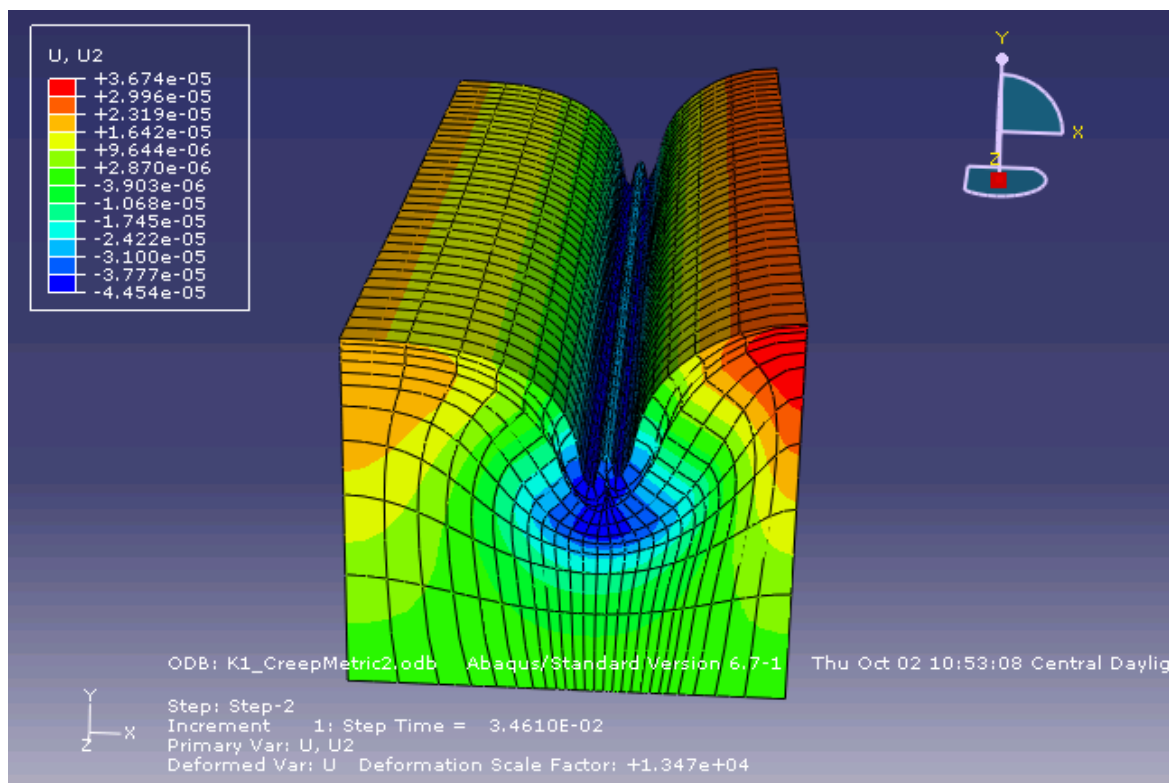
Figure 5.7 Deformed plot of KS-1 section using the visualization module – scale factor = 0
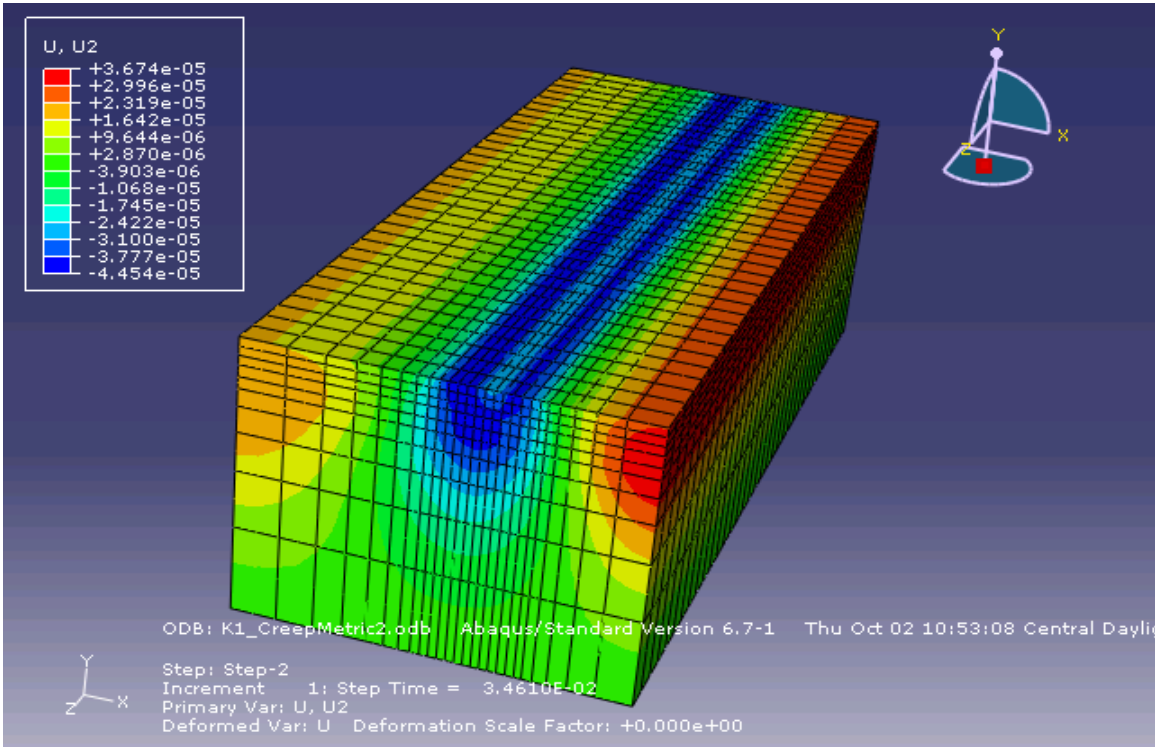
5.2 Creep Model

Creep is a time dependant material property. For asphalt mixtures, creep phenomenon is accelerated by an increase in stress or temperature. A typical creep behavior is categorized using static or dynamic creep test, into three creep stages, primary, secondary and tertiary (Figure 5.8). In a primary stage, creep rate usually decays with application of instantaneous strain. The secondary stage comprises of constant creep rate, where increase in strain is proportion to increase in time. In the third stage, creep rate increases and it is normally associated with fracture or failure.

Figure 5.8 A plot of axial strain vs. time showing the creep stages
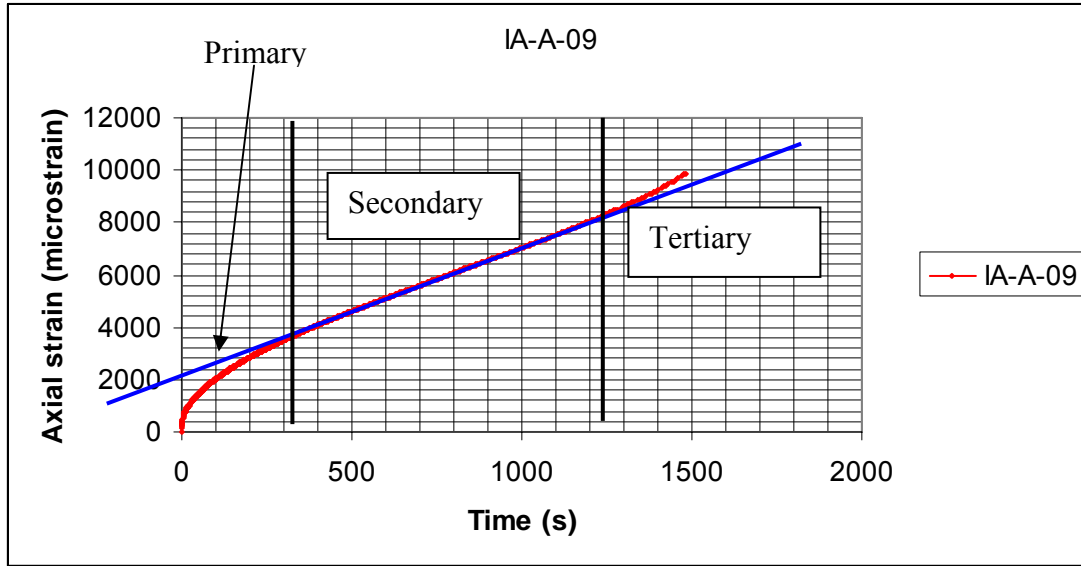
Creep strain (ε^c), is a function of stress (σ), time (t) and temperature (T).

$$\varepsilon^c = F(\sigma, T, t) \qquad\qquad 5.1$$

Equation 5.1 is only valid for constant stress and temperature. Kraus, 1980 explains the Bailey-Norton law which is capable of modeling primary and secondary creep. The formulation is based on a basic assumption that material depends on the present stress state explicitly. In this approach, strain is represented by:

$$\varepsilon^c = \frac{A}{m+1}\sigma^n t^{m+1} \qquad\qquad 5.2$$

A, m and n are constants that are a function of temperature. Strain rate can be obtained by differentiating equation 5.2 to obtain:

$$\dot{\varepsilon}^c = \frac{\partial \varepsilon^c}{\partial t} = A\sigma^n t^m \qquad\qquad 5.3$$

Where:

ε = Uniaxial equivalent creep strain rate, $\sqrt{(\varepsilon^{cr} : \varepsilon^{cr})}$

σ = Uniaxial equivalent deviatoric stress (Misses equivalent stress),

t = Total time, and

A, n, m = user defined functions of temperature.

A and n must be positive, and $-1 < m \leq 0$.

This is the time hardening formulation which is used for time hardening creep model in Abaqus software. Equation 5.3 is used for the evaluation of permanent deformation in this study. Creep can also be modeled using strain hardening, in which the creep strain rate depends on stress, strain and temperature. For this research project, time hardening creep was adopted. In Abaqus software, the time hardening version is used when stress state remains constant and strain hardening is used when the stress varies during the analysis.

5.2.1 Modeling Asphalt Mixes Using Creep Model Available in Abaqus/CAE

Six mixes from Kansas, Missouri and Iowa were modeled using time hardening creep model in Abaqus/CAE. Parameters used for the creep model are given in Table 5.1. The dynamic modulus values were obtained from the dynamic modulus test (Section 3.3.2.2). The values of Poisson's ratios were estimated from typical values since they could not be measured in the lab. Subgrade and subbase resilient modulus were also estimated using typical values. The creep model was implemented on the asphalt surface only. Linear elastic material model was used for base course and subgrade.

The creep model is defined by five material parameters, creep parameters, A, m, and n, and elastic parameters, elastic modulus (E), and Poisson's ratio (v). However, creep behavior is not sensitive to elastic parameters (E and v). This leaves creep parameters A, m and n to define creep behavior in asphalt mixes. These creep parameters uniquely define the time-dependent behavior of asphalt mixtures. It is expected to have different sets of creep parameters defining different asphalt materials. The creep parameters used in this research project (Table 5.1) varies according to asphalt material characteristics. The m value was set at –0.5 while n value varied from 0.5 to 0.8 and A values was from 1e-9 to 9.9e-9. Huang, 2001 , used values of A = 1.8e-3, n = 0.8 and m = -0.5 to model creep behavior of course asphalt mixes. The elastic modulus used was from FWD back calculation [Huang, 2001]. Sivasubramaniam [2005] used A values that ranged from 7e-5 to35e-5, n value of 0.8 and m ranged from -0.79 to -0.87. Sivasubramaniam performed a sensitivity analysis for parameters A and m while n was held constant at a value of 0.8. He reported that the predicted rut depth increases with increasing m and/or A.

Table 5.1 Creep model parameters

Parameter	KS-1	KS-2	MO-1	MO-2	IA-1	IA-2
Asphalt Elastic Modulus (MPa)	3115	1619	2410	437	494	1869
Asphalt Poisson's Ratio	0.35	0.35	0.35	0.35	0.35	0.35
Creep model parameter A	$1*10^{-9}$	$5*10^{-9}$	$4.5*10^{-9}$	$5*10^{-9}$	$6*10^{-9}$	$4*10^{-8}$
n	0.67	0.56	0.50	0.6	0.8	0.8
m	-0.5	-0.5	-0.5	-0.5	-0.5	-0.5
Base Resilient Modulus (MPa)	650	650	650	350	350	650
Base Poisson's ratio	0.4	0.4	0.4	0.4	0.4	0.4
Subgrade resilient modulus (MPa)	350	350	350	200	200	350
Subgrade Poisson's ratio	0.45	0.45	0.45	0.45	0.45	0.45

Lateral wheel wonder is the distribution of wheel loading in the transverse direction across a pavement. On actual roads, traffic do not follow the same wheel path, each vehicle follows a slightly different path. Sivasubramaniam (2005) and Hua (2000) incorporated lateral wonder into Abaqus FEM using a normal distribution of total loading time. Assuming the standard deviation is equal to one third of maximum wheel wonder (99.74%), the standard deviation, was obtained as

$$S = D/3 \hspace{6cm} 5.1$$

Where,

       S = standard deviation,

       D = Maximum wheel wonder

The total loading time included in the area of the normal distribution curve is given by:

$$2 s [\Phi((D-0)/D-3)-0.5]=0.9974 \hspace{4cm} 5.2$$

$\Phi(x)$ = value of the normal distribution at x.

They also used the principal of super positioning to obtain permanent deformation resulting form both wheels.

For this research, actual lateral wheel wonder percentages in CISL 14 project were available (Table 3.1). One pass of the wheel load was modeled using the Abaqus/CAE software. Permanent deformation values were then obtained at the pavement mid section. Three paths were

created on the pavement surface, on top of base course and on top of subgrade layer to obtain pavement transverse profiles at mid section on each of these layers (Figure 5.11). The permanent deformation was obtained by using the nodal displacement along the paths. Abaqus visualization tool was used to obtain x-y values along the paths. The transverse distance x and permanent deformation y were then transferred in Excel spread sheet. These values were truncated in a normal distribution manner. The maximum permanent deformation is given by equation 5.3 and transverse profiles were plotted in the Excel spread sheet.

$$P_{d\,(max)} = \sum_{i=-n}^{N} \left(W(x) * d(x) \right)$$ 5.3

Where,

$P_{d(max)}$ = Permanent deformation after N load repetitions

W(x) = Permanent deformation at point x on a transverse profile

d(x) = Percent of load repetition that is applicable at a transverse point (x)

N = Total number of load repetitions

i = transverse point on x axis ranging from -n to n

To account for lateral wheel wonder equation 5.4 could be used in the Excel spread sheet taking into account superposition of permanent deformation.

$$P_{d\,(max)} = \sum_{i=-n}^{n} \left(w_i * d(x - i) \right)$$ 5.4

The typical values of lateral wheel wonder percentages (d(x-i)) from CISL 14 project (Table 3.1) were used in Excel spread sheet to predict permanent deformation at repeated wheel load, and transverse sections were plotted. Figures 5.9 and 5.10 provide transverse profiles of Kansas (KS-1) and Iowa (IA-2) mixes respectively, taking into consideration wheel lateral wonder (Eq. 5.4). Figures 5.18 and 5.22 provide transverse profiles of Kansas (KS-1) and Iowa (IA-2) mixes respectively, considering maximum permanent deformation (Eq. 5.3). The values of permanent deformation obtained by taking into consideration the lateral wonder are 7.7% lower for KS-1 mix and 16% lower for IA-2 as compared to maximum permanent deformation. The values of maximum permanent deformation were therefore used for the analysis.

Figure 5.9 Permanent deformation predicted for KS-1 mix by simulating wheel wonder
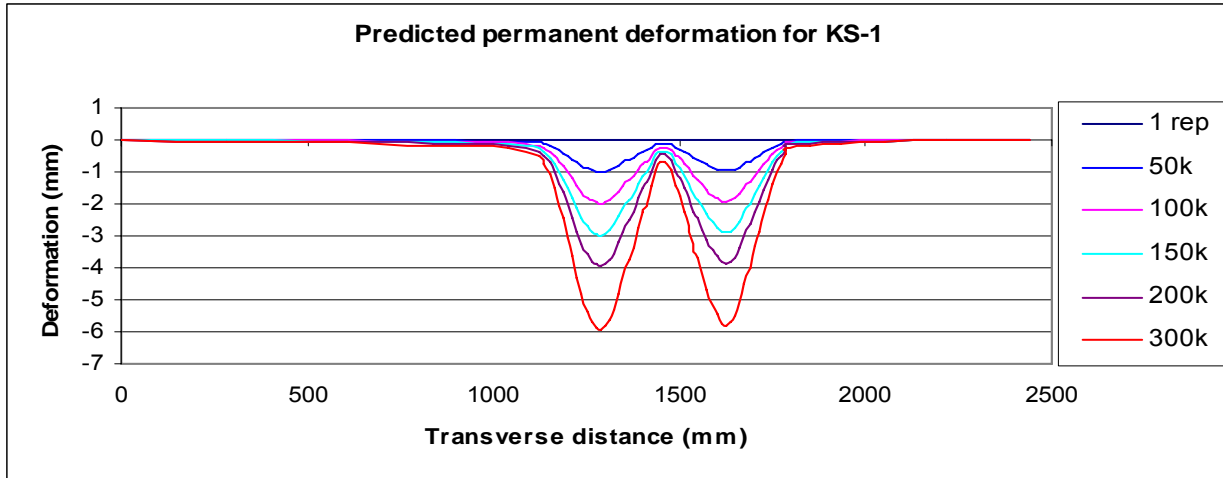
Figure 5.9 Permanent deformation predicted for IA-2 mix by simulating wheel wonder
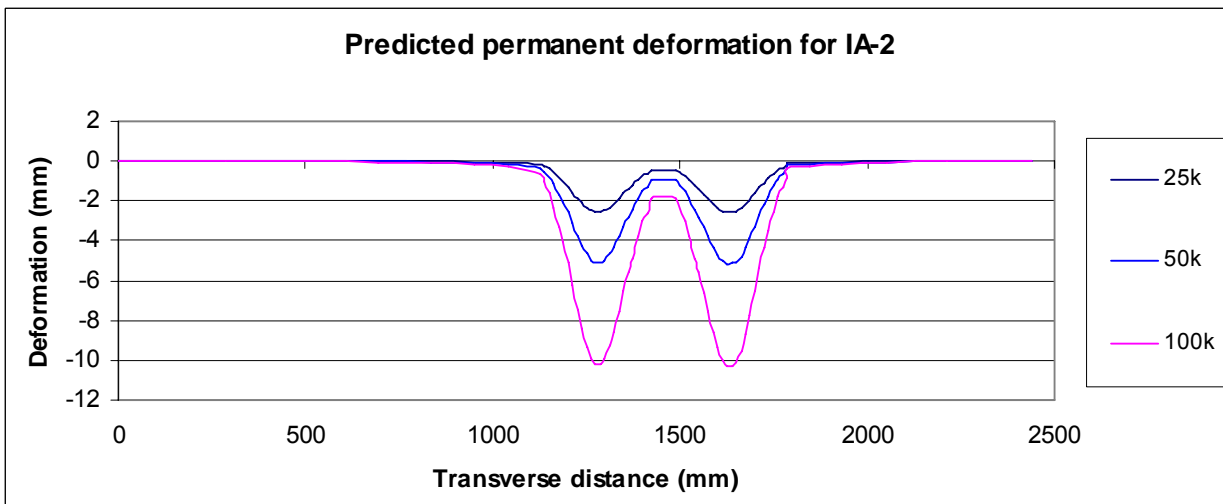
A moving load (modeled as step load) was used with creep model to evaluate permanent deformation of asphalt materials. A total of 36 steps were created in Abaqus/CAE. Each step was loaded with a 690 kPa (100 psi) load for 0.05 seconds and de-activated when the next load step is activated. Abaqus visco analysis procedure was used for creep model. The model takes more that 3 hours to run because of the step loading and the element type used: twenty node brick elements, CD20R, with reduced integration. After running the model, unequal permanent deformation was observed (Figure 5.12). The location where the wheel load is applied first had more permanent deformation than at the end of the wheel loading application. According to

Abaqus Analysis Users' Manual volume 5, "If the load amplitude was given in terms of step time, the load remains constant at the magnitude associated with the end of the previous step". Having this in mind, a trapezoidal load amplitude shown in Figure 5.13 was applied, but in this case no deformation was observed (Figure 5.14). This is because creep is a time dependent material behavior.

Figure 5.11 Nodal path at pavement mid section
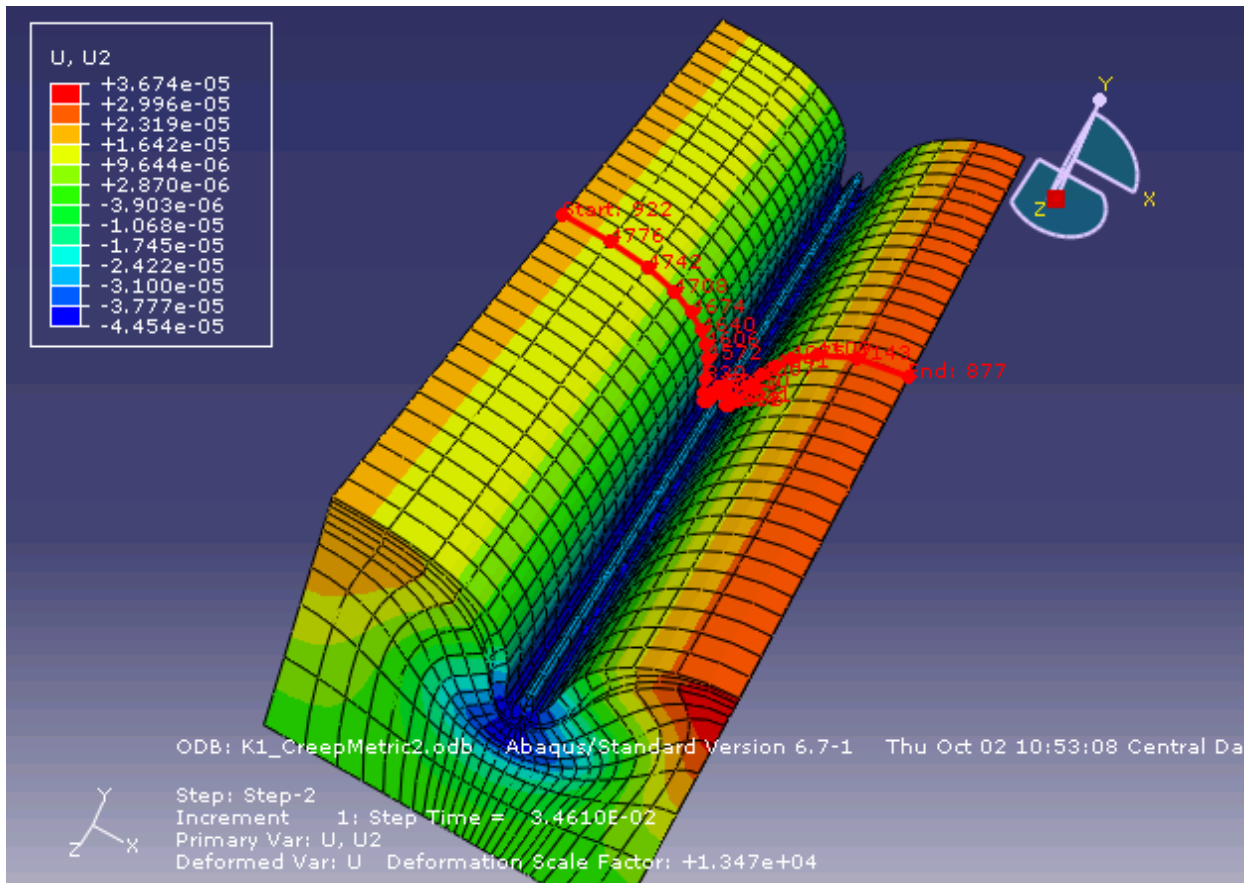
Figure 5.12 Deformed pavement section implemented using creep model and a moving load
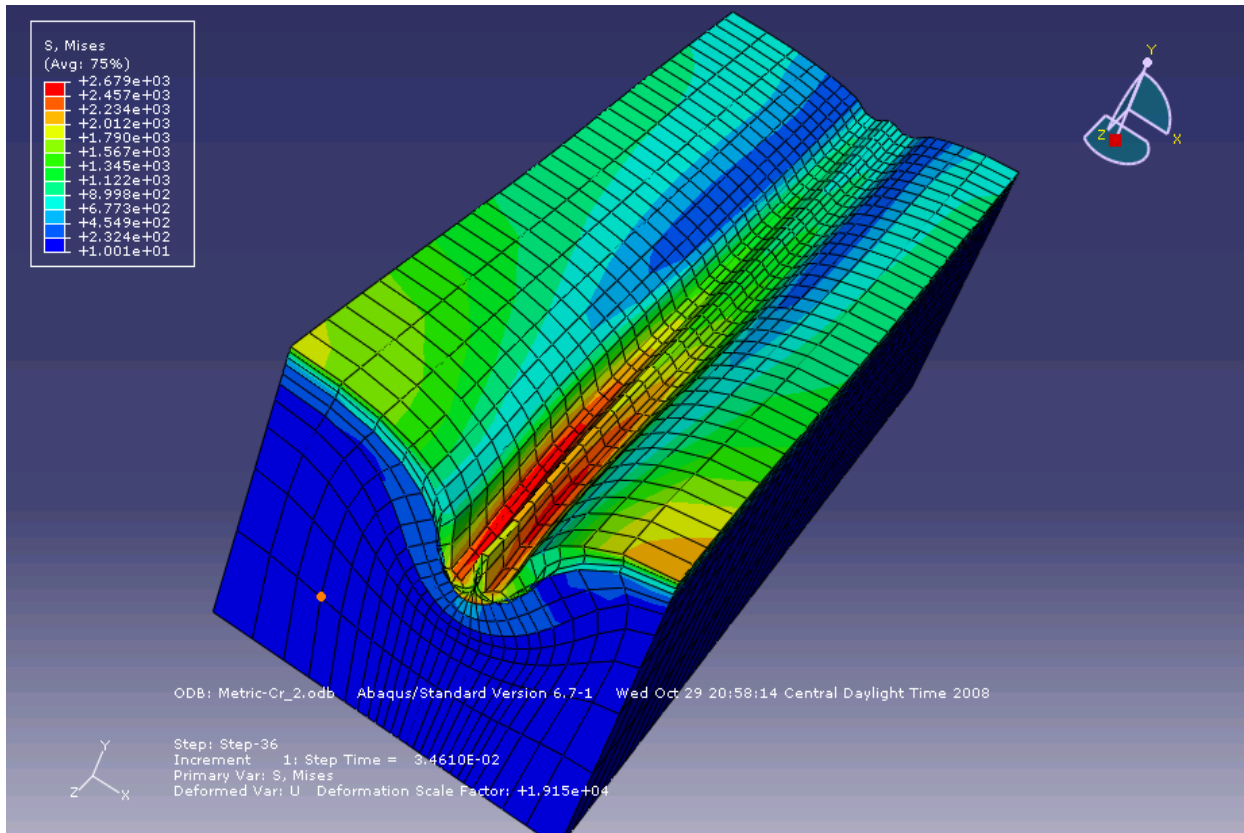
Figure 5.13 Trapezoidal load amplitude
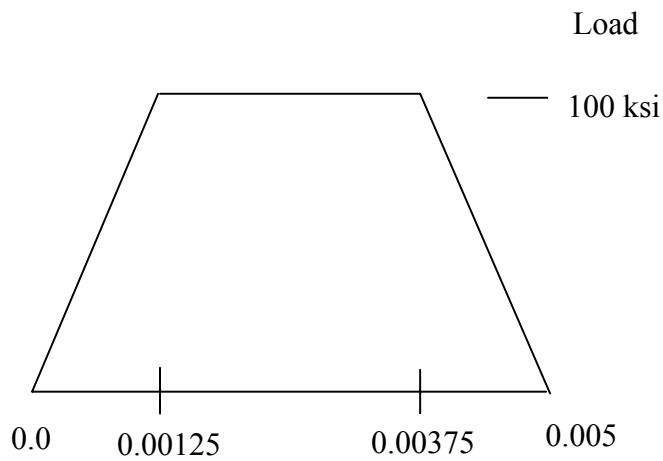
Figure 2.14 Abaqus results after using trapezoidal wheel load amplitude
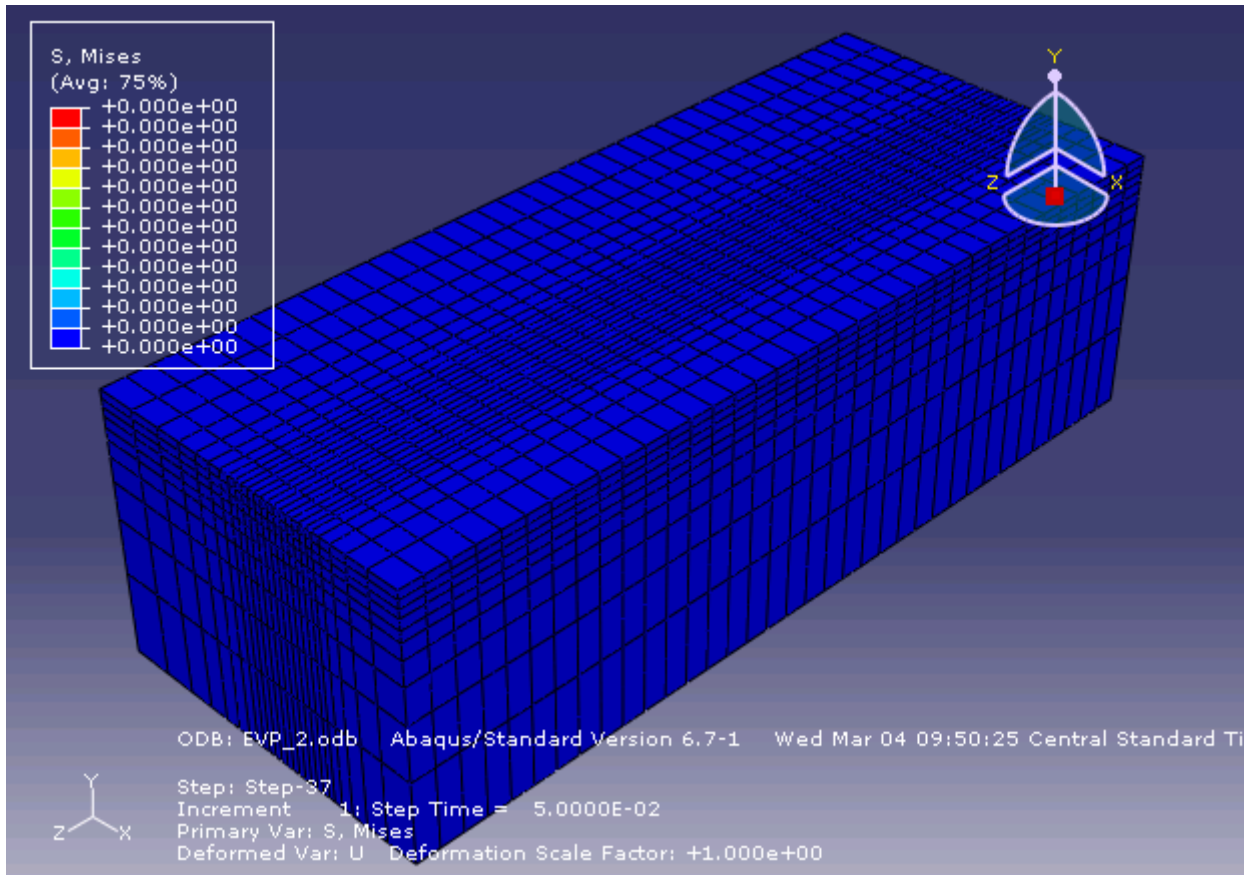
Sivasubramaniam (2005) Huang (2000), Hua (2000) and Fang (2000) used creep model with alternative simplified loading method which was introduced by Huang (1995). With this approach, the load is applied over the entire length of the wheel path. The total cumulative loading time is estimated using the number of wheel passes and time required for traversing the tire print of the wheel during a single pass. To obtain the cumulative loading time, the length of the tire print was divided by the wheel speed to determine the load time corresponding to a single wheel pass. The computed single wheel load time was then multiplied by the number of wheel passes to obtain the cumulative loading time. This method was applied to reduce computational time. The deformation behavior of a step loading is not mentioned [Sivasubramaniam, 2005].

The simplified load alternative (Figure 5.15) was then adopted for analysis with creep model parameters given in Table 5.1. With this approach, a uniformly deformed pavement section was obtained (Figure 5.16).

Figure 5.15 Simplified load approach
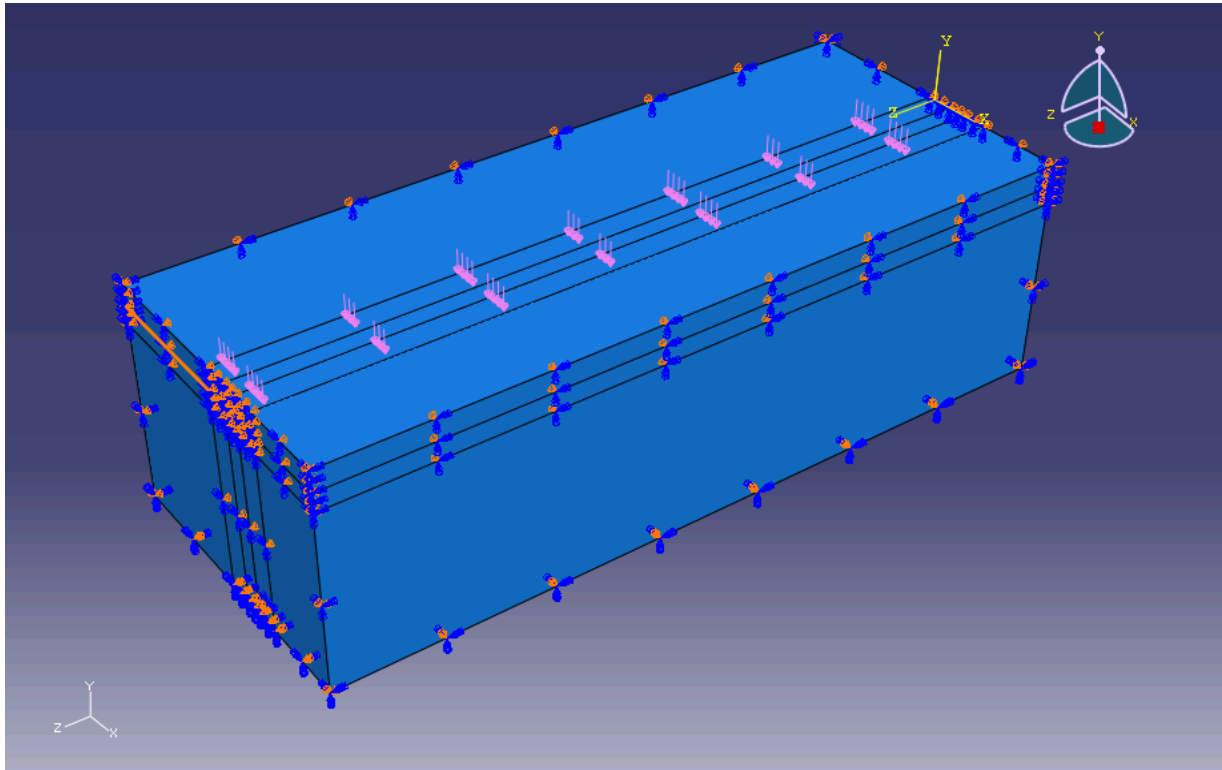
Figure 5.16 Permanent deformation after simplified load approach
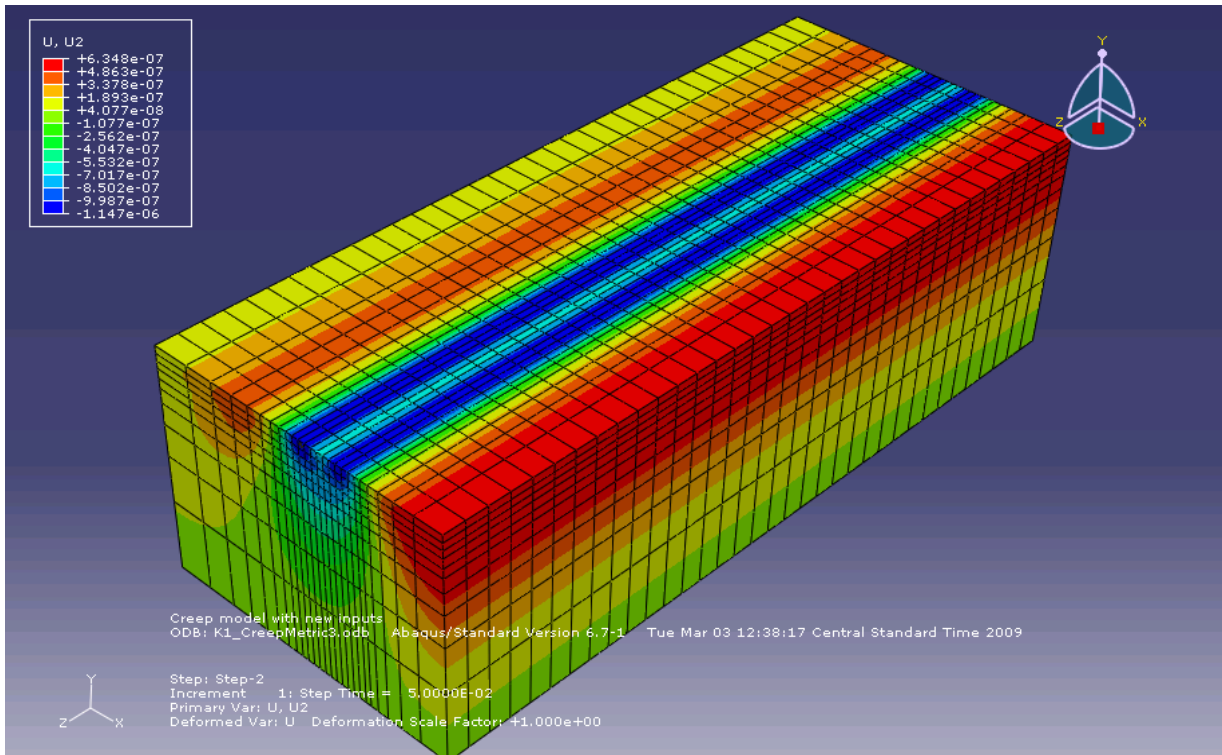
5.2.2 Results from Creep Model in Abaqus/CAE

Pavement transverse profiles were obtained by creating a nodal path at pavement mid section. Deformation values were obtained as x-y values using the visualization tool in Abaqus/CAE. These values were obtained after one load repetition using creep model. It was not feasible to run Abaqus with repeated wheel loads due to time constrain. The deformation values obtained after one load repetition were truncated in a normal distribution to take care of wheel load lateral wonder (Equation 5.4). Percentages provided in Table 3.1 were used to simulate the traffic wonder. These values were then multiplied with the number of load repetitions to obtain transverse profiles at different load repetitions. Figure 5.17 shows the transverse profiles as plotted in Abaqus CAE. Figure 5.18 to Figure 5.23 presents transverse sections of maximum permanent deformation for the six asphalt mixes at different numbers of wheel load repetitions. The transverse sections of base and subgrade layers are given in Appendix C. The values of permanent deformation in asphalt mix were obtained by subtracting deformation in the base course from that of the surface layer. Figures 5.22 to 5.29 show plots of permanent deformation in asphalt mixes only.

Figure 5.17 Abaqus predicted permanent deformation for KS-1 mix

173
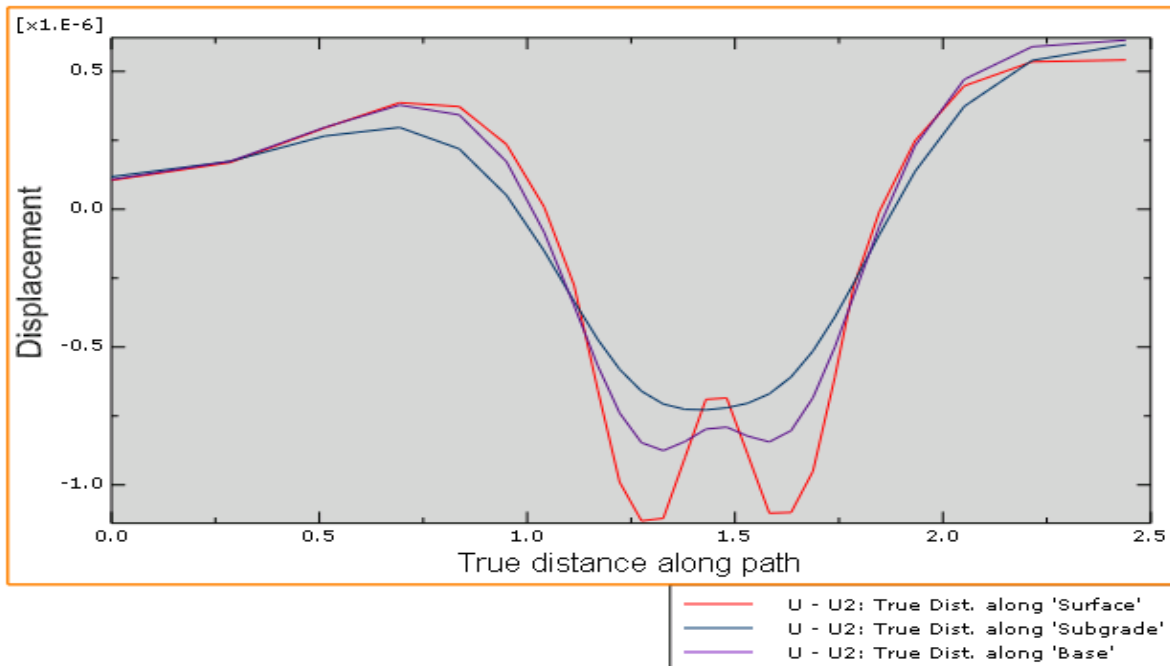
Table 5.2 Abaqus displacement values from nodes at mid section of KS-1 section

Distance	Displacement on nodes (m)			Distance	Displacement on nodes (m)		
	Surface	Base	Subgrade		Surface	Base	Subgrade
0.0000	3.6E-08	3.7E-08	4.1E-08	1.4300	-2.3E-07	-2.7E-07	-2.5E-07
0.2857	5.8E-08	6.0E-08	6.0E-08	1.4800	-2.3E-07	-2.7E-07	-2.4E-07
0.5128	1.0E-07	1.0E-07	9.2E-08	1.5300	-3.0E-07	-2.8E-07	-2.4E-07
0.6932	1.3E-07	1.3E-07	1.0E-07	1.5825	-3.7E-07	-2.9E-07	-2.3E-07
0.8365	1.3E-07	1.2E-07	7.5E-08	1.6350	-3.7E-07	-2.7E-07	-2.1E-07
0.9504	7.9E-08	5.7E-08	1.6E-08	1.6875	-3.2E-07	-2.3E-07	-1.8E-07
1.0409	1.1E-10	-3.1E-08	-5.3E-08	1.7400	-2.1E-07	-1.7E-07	-1.3E-07
1.1129	-9.6E-08	-1.2E-07	-1.2E-07	1.7851	-9.8E-08	-1.1E-07	-9.3E-08
1.1700	-2.2E-07	-2.0E-07	-1.6E-07	1.8472	-5.1E-09	-2.3E-08	-3.3E-08
1.2225	-3.4E-07	-2.5E-07	-2.0E-07	1.9330	8.3E-08	7.7E-08	4.5E-08
1.2750	-3.8E-07	-2.9E-07	-2.3E-07	2.0514	1.5E-07	1.6E-07	1.3E-07
1.3275	-3.8E-07	-3.0E-07	-2.4E-07	2.2147	1.8E-07	2.0E-07	1.8E-07
1.3800	-3.1E-07	-2.9E-07	-2.5E-07	2.4400	1.9E-07	2.1E-07	2.0E-07

Figure 5.18 Predicted permanent deformation for KS-1 mix
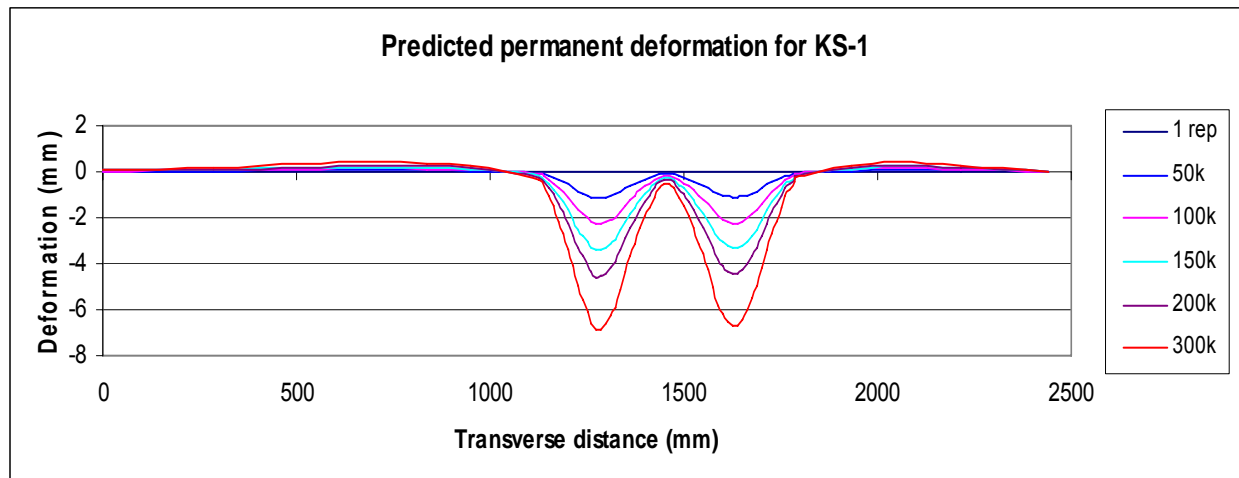
Figure 5.19 Predicted permanent deformation for KS-2 mix
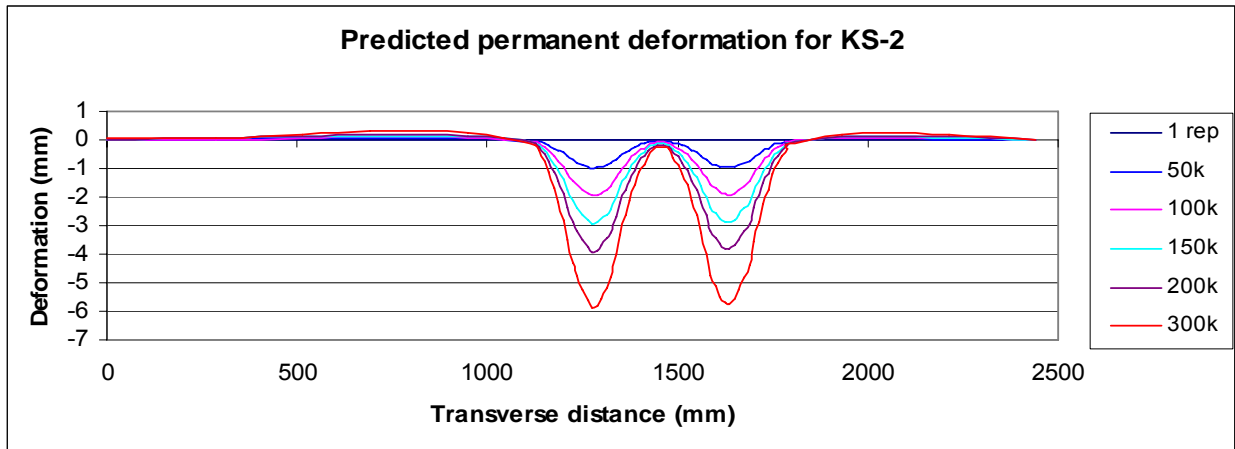
Figure 5.20 Predicted permanent deformation for MO-1 mix
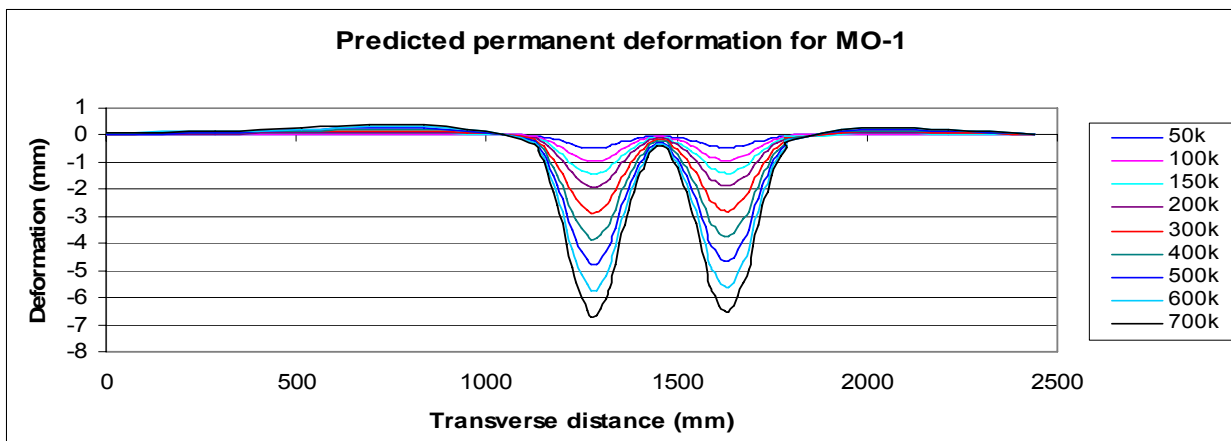
Figure 5.21 Predicted permanent deformation for MO-2 mix
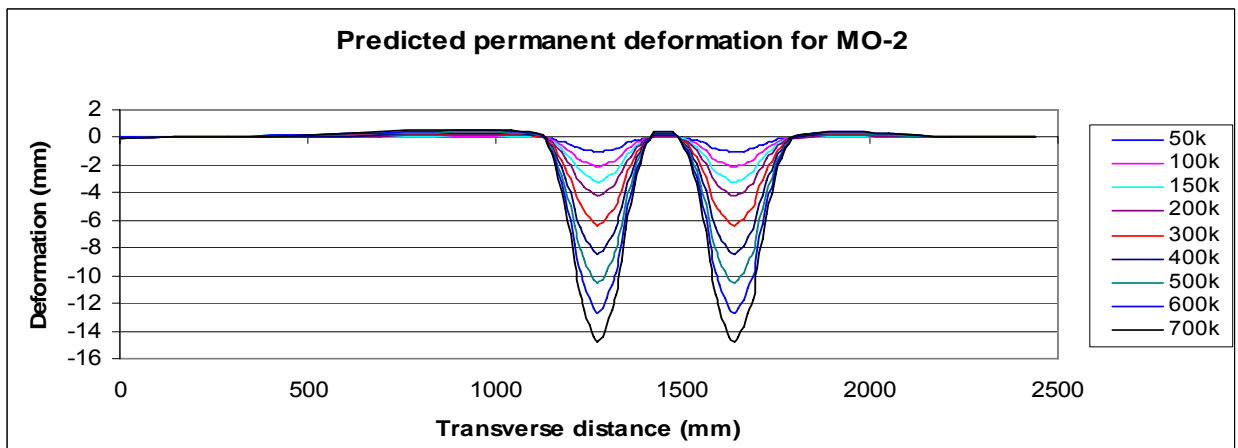
Figure 5.22 Predicted permanent deformation for IA-1 mix
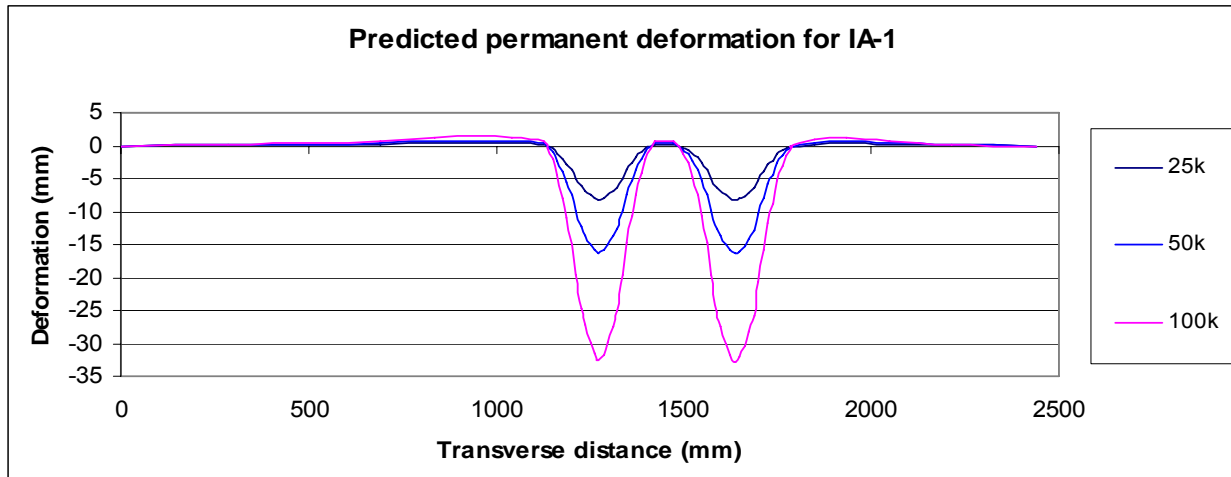
Figure 5.23 Predicted permanent deformation for IA-2 mix
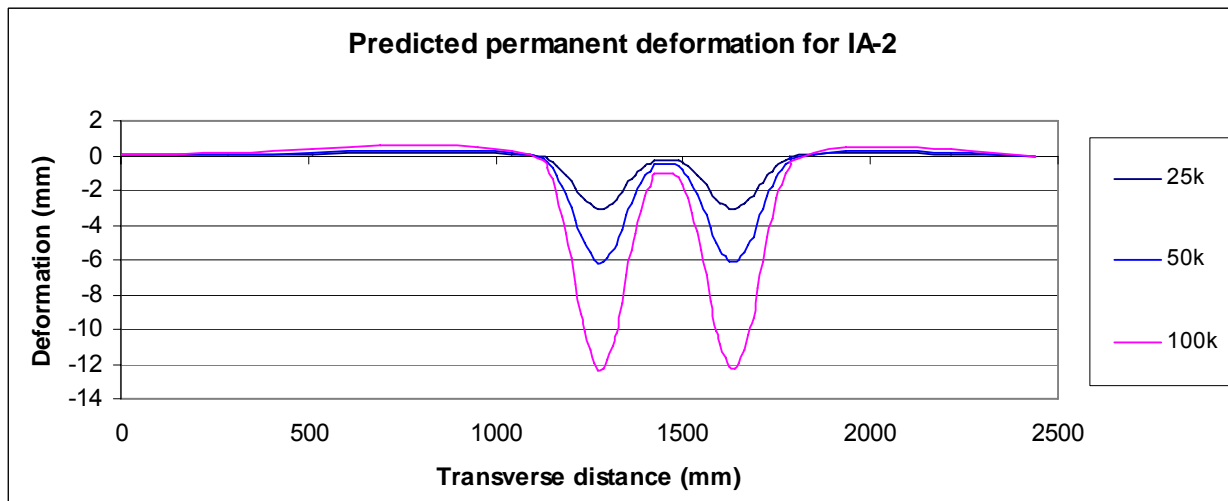
Figures 5.24 to 5.29 below present plots of permanent deformation in asphalt layer only. This was obtained by subtracting the permanent deformation on top of base layer from permanent deformation on asphalt surface. This assists in evaluating the amount of permanent deformation that was predicted in asphalt mix only.

176

Figure 5.24 Predicted permanent deformation in KS-1 asphalt mix
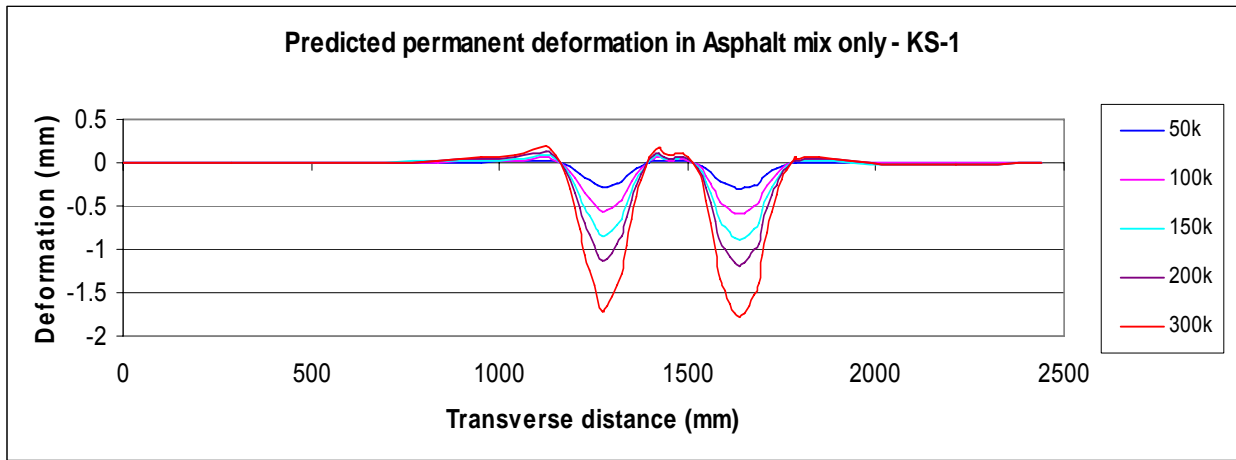
Figure 5.25 Predicted permanent deformation in KS-2 asphalt mix
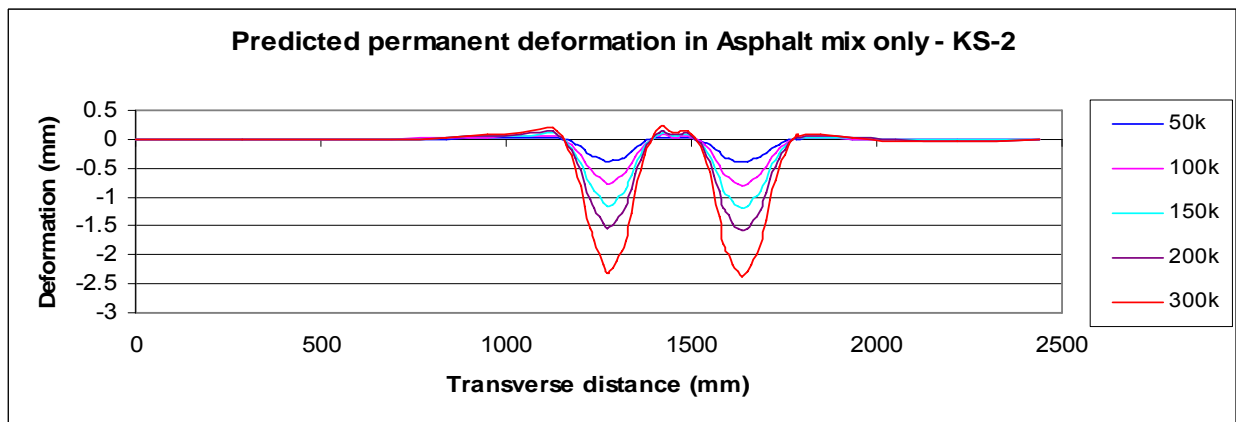
Figure 5.26 Predicted permanent deformation in MO-1 asphalt mix
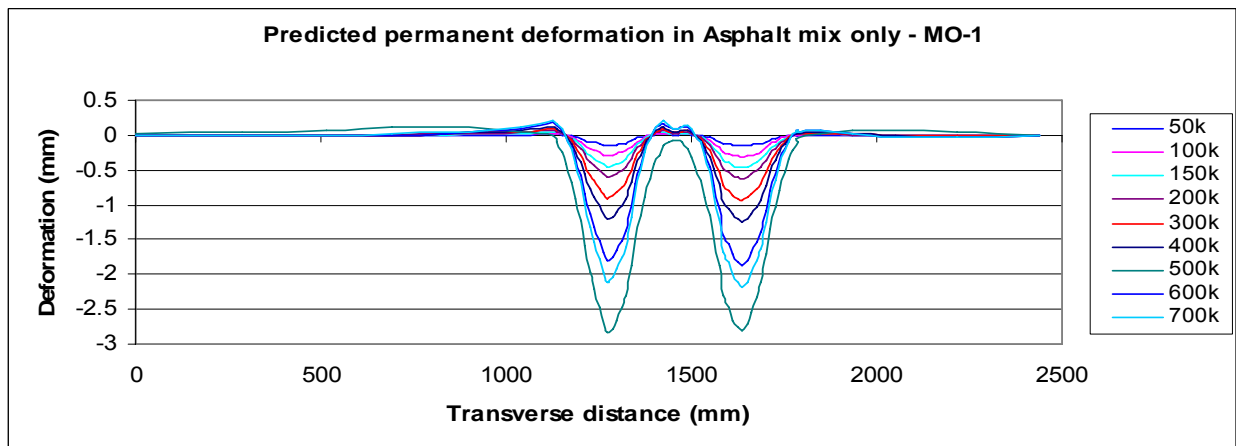
Figure 5.26 Predicted permanent deformation in MO-2 asphalt mix
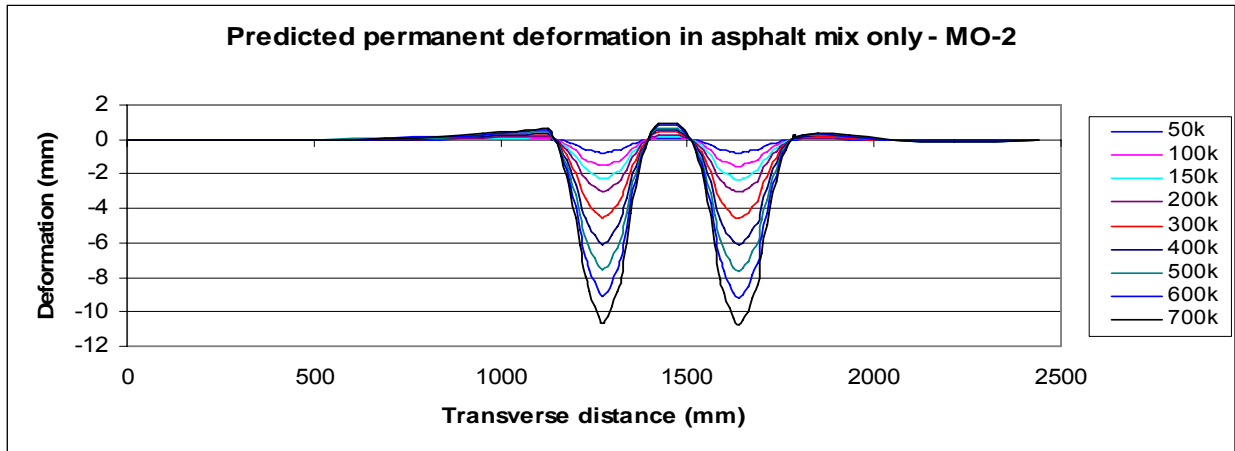
Figure 5.28 Predicted permanent deformation in IA-1 asphalt mix
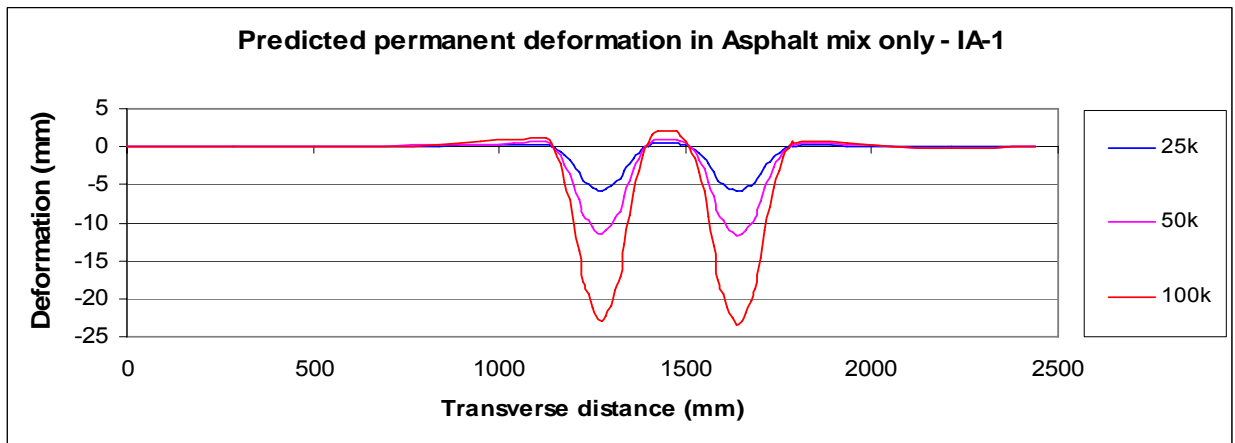
Figure 5.29 Predicted permanent deformation in IA-2 asphalt mix
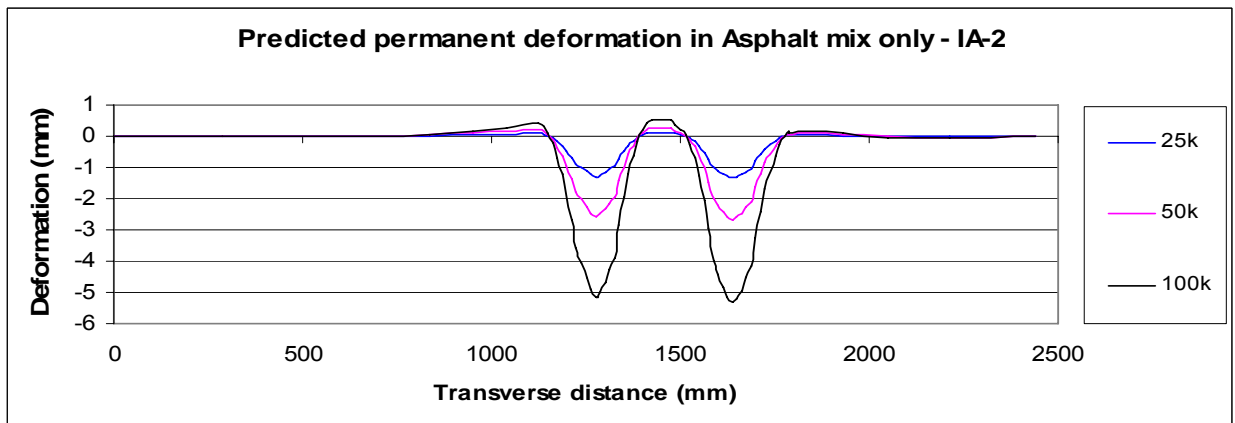
The evolution of predicted permanent deformation was compared to the evolution of measured permanent deformation. Figures 5.30 for 5.35 compared the evolution of permanent deformation for the whole pavement section and in asphalt mix only. Tables 5.3 to 5.8 shows values of permanent deformation measured and predicted at each number of load repetition.

Table 5.3 Evolution of permanent deformation in KS-1 section

Load Repetition x1000	Predicted deformation			Measured deformation		Deformation in Asphalt mix		
	mm	in	%	mm	in	mm	in	%
0	0	0	0	0	0	0	0	0
50	1.11	0.0444	52.9	2.4	0.096	0.29	0.00035	12.1
100	2.28	0.0912	48.3	4.725	0.189	0.85	0.00103	18.0
150	3.32	0.1328	-	-	-	0.87	0.00105	-
200	4.56	0.1824	79.0	5.775	0.231	1.16	0.00141	20.0
300	6.84	0.2736	111.2	6.15	0.246	1.74	0.00211	28.3

Figure 5.30 Evolution of permanent deformation in KS-1 section

179
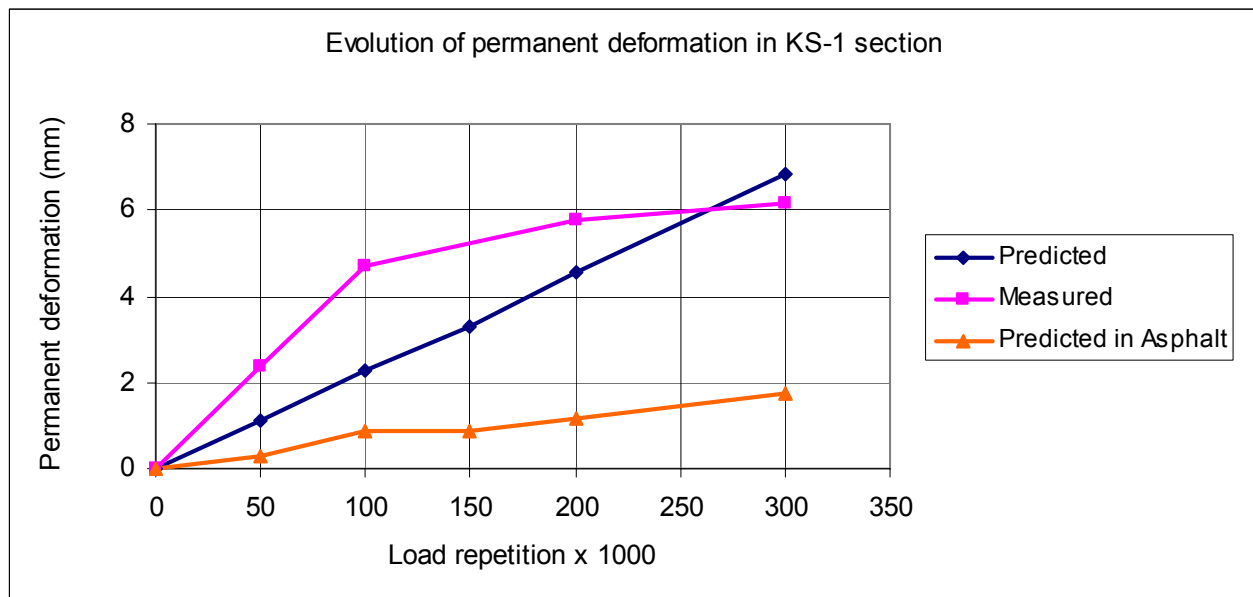
Table 5.4 Evolution of permanent deformation in KS-2 section

Load Repetition x1000	Predicted deformation			Measured deformation		Deformation in Asphalt mix		
	mm	in	%	mm	in	mm	in	%
0	0	0	0	0	0	0	0	0
50	0.97	0.0388	52.0	1.85	0.074	0.37	0.0148	20
100	1.93	0.0772	35.0	5.4	0.216	0.75	0.03	13
150	2.78	0.1112	-	-	-	1.12	0.0448	-
200	3.86	0.1544	71.8	5.375	0.215	1.49	0.0596	27.7
300	5.79	0.2316	101.3	5.175	0.207	2.31	0.0924	44.6

Figure 5.31 Evolution of permanent deformation in KS-2 section

180
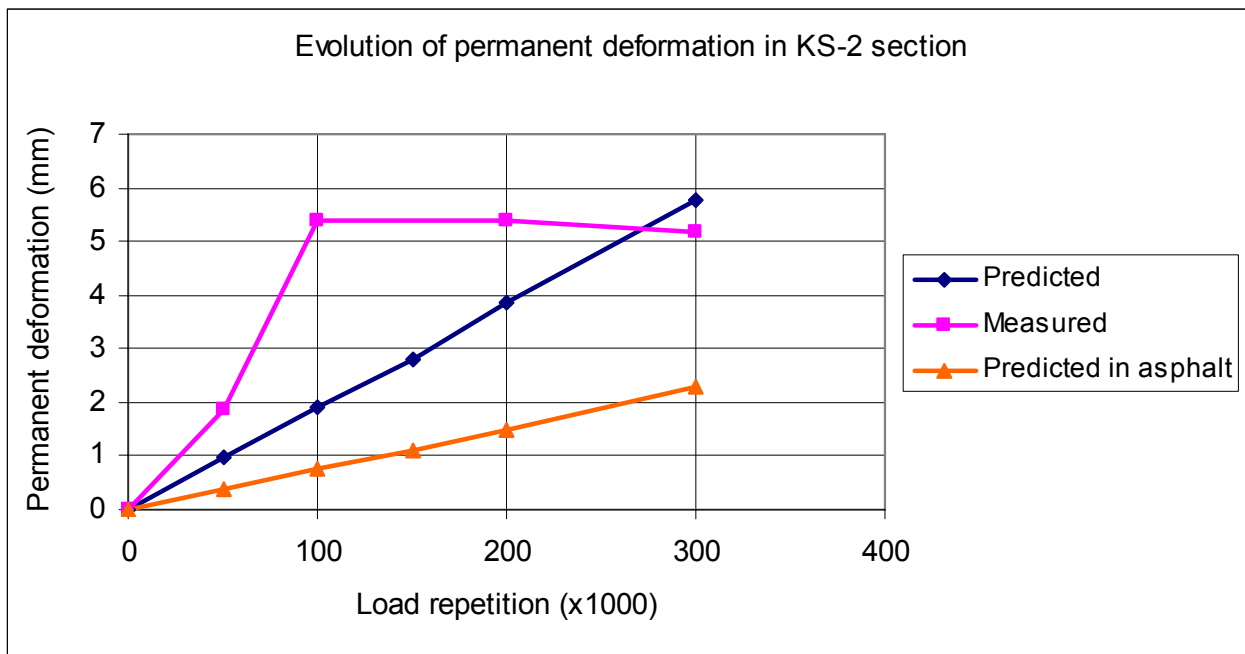
Table 5.5 Evolution of permanent deformation in MO-1 section

Load Repetition x1000	Predicted deformation			Measured deformation		Deformation in Asphalt mix		
	mm	in	%	mm	in	mm	in	%
0	0	0	0	0	0	0	0	0
50	0.48	0.019	14.9	3.23	0.129	0.15	0.000182	4.6
100	0.95	0.038	26.0	3.65	0.146	0.29	0.000352	7.9
150	1.43	0.057	37.3	3.83	0.153	0.44	0.000533	11.5
200	1.91	0.076	49.6	3.85	0.154	0.59	0.000715	25.0
300	2.86	0.114	53.7	5.33	0.213	0.88	0.001067	16.5
400	3.81	0.152	70.6	5.40	0.216	1.17	0.001418	21.7
500	4.77	0.191	82.2	5.80	0.232	1.75	0.002121	30
600	5.72	0.229	96.5	5.93	0.237	2.11	0.002558	35.6
700	6.73	0.269	105.5	6.38	0.255	2.78	0.00337	43.6

Figure 5.32 Evolution of permanent deformation in MO-1 section
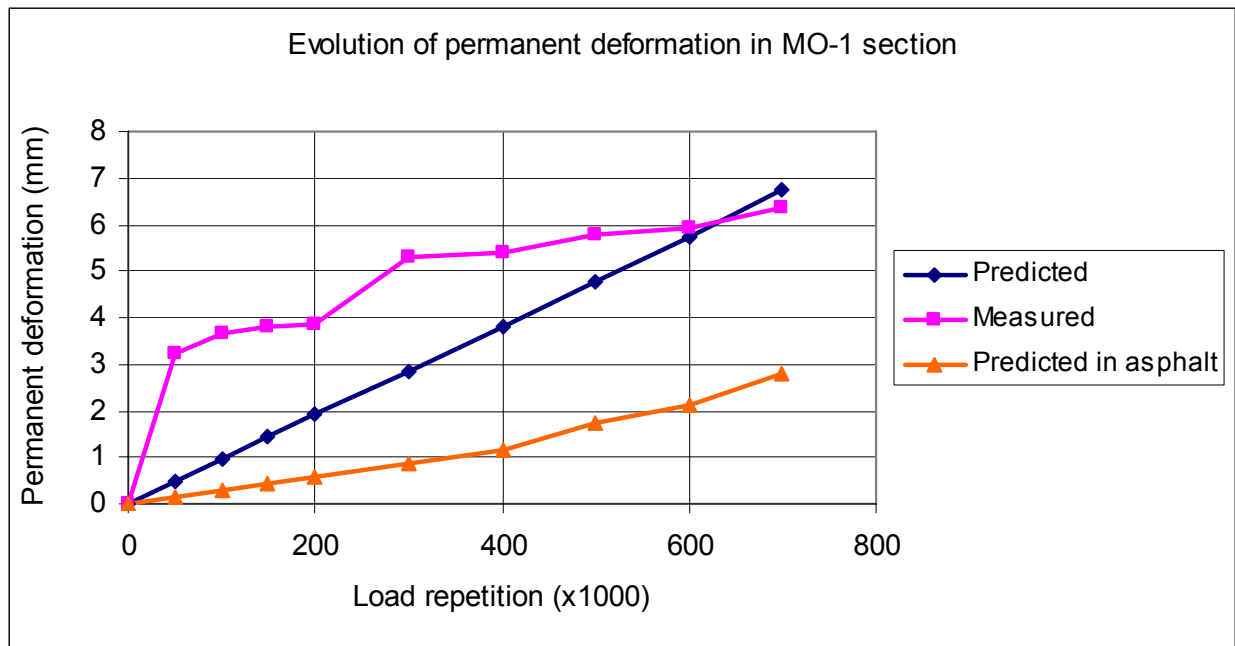
Table 5.6 Evolution of permanent deformation in MO-2 section

Load Repetition x1000	Predicted deformation			Measured deformation		Deformation in Asphalt mix		
	mm	in	%	mm	in	mm	in	%
0	0	0	0	0	0	0	0	0
50	1.03	0.0412	20.6	5	0.2	0.47	0.0188	9.4
100	2.12	0.0848	35.3	8	0.32	1.49	0.0596	24.8
150	3.08	0.1232	44.3	8.95	0.358	2.24	0.0896	32.2
200	4.23	0.1692	43.5	9.725	0.389	2.99	0.1196	30.7
300	6.17	0.2468	53.1	11.625	0.465	4.48	0.1792	38.5
400	8.47	0.3388	68.7	12.325	0.493	5.98	0.2392	48.5
500	10.3	0.412	74.1	13.9	0.556	7.47	0.2988	53.7
600	12.3	0.492	87.1	14.125	0.565	8.97	0.3588	63.5
700	14.4	0.576	98.5	14.625	0.585	10.7	0.428	73.2

Figure 5.33 Evolution of permanent deformation in MO-2 section
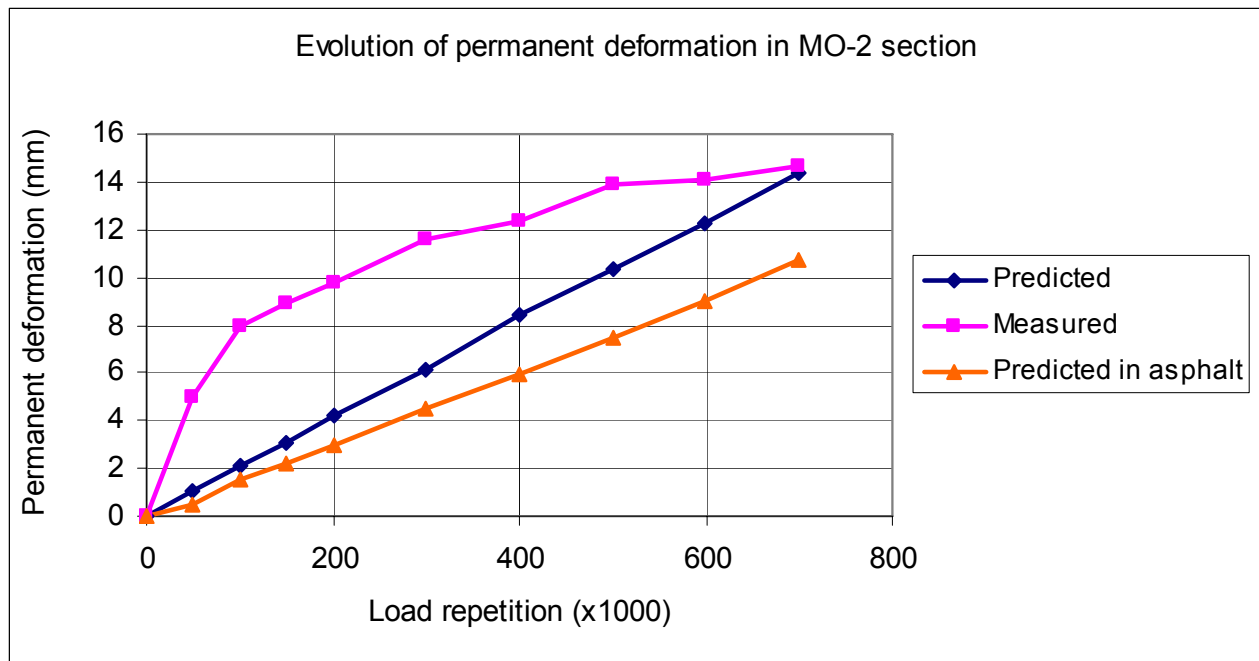
Table 5.7 Evolution of permanent deformation in IA-1 section

Load Repetition x1000	Predicted deformation			Measured deformation		Deformation in Asphalt mix		
	mm	in	%	mm	in	mm	in	%
0	0	0	0	0	0	0	0	0
25	8.15	0.326	55.6	14.65	0.586	5.56	0.2224	38.0
50	15.8	0.632	82.4	19.175	0.767	11.1	0.444	57.9
100	32.26	1.2904	103.8	31.075	1.243	22.2	0.888	71.4

Figure 5.34 Evolution of permanent deformation in IA-1 section
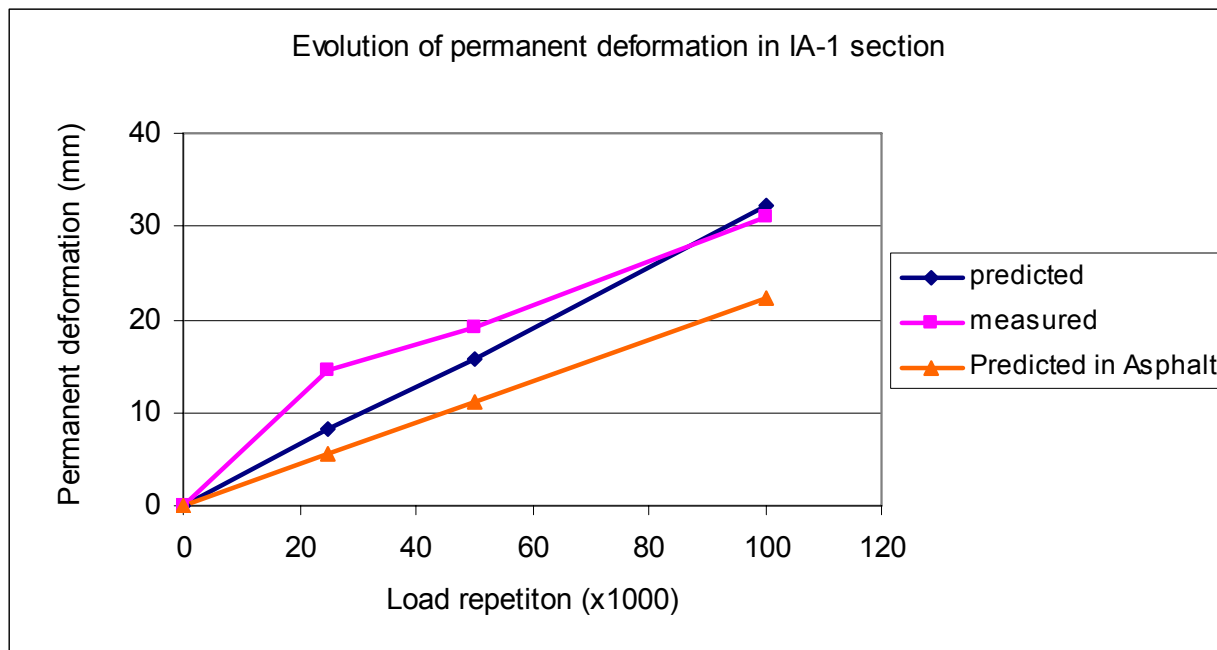
Table 5.8 Evolution of permanent deformation in IA-2 section

Load Repetition x1000	Predicted deformation			Measured deformation		Deformation in Asphalt mix		
	mm	in	%	mm	in	mm	in	%
0	0	0	0	0	0	0	0	0
25	2.94	0.1176	34.5	8.525	0.341	1.29	0.0516	15.1
50	5.88	0.2352	65.0	9.05	0.362	2.49	0.0996	27.5
100	12.3	0.492	103.8	11.85	0.474	5.16	0.2064	43.5

183

Figure 5.35 Evolution of permanent deformation in IA-2 section
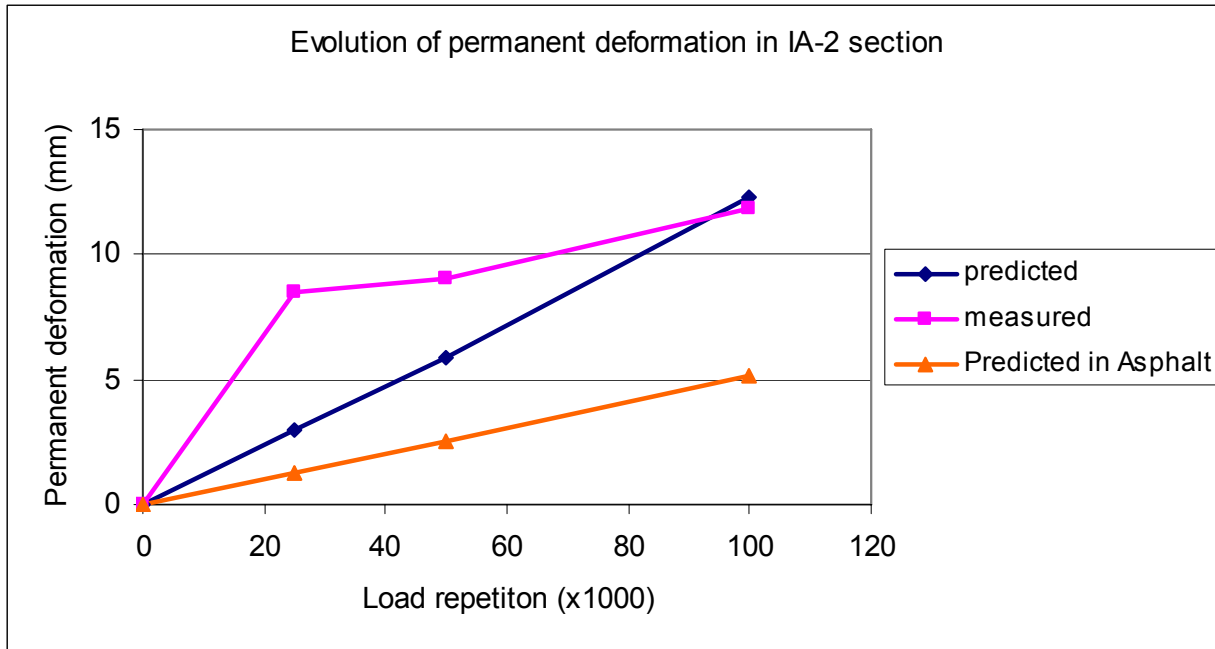
From the tables and figures above, it can be seen that, the creep model has a potential of predicting permanent deformation in asphalt mixtures. A linear model was used to predict the propagation of permanent deformation, but a different model is required to be able to capture the non linear behavior of asphalt mixture. It can also be seen that, the permanent deformation that was captured in asphalt mixes at the final number of repetitions was 28.3% of total permanent deformation for KS-1, 44.6% for KS-2, 43.6 for MO-1, 73.2% for MO-2, 71.4 for IA-1, and 43.5 for IA-2. The APT measured permanent deformation was mostly in the asphalt layer only.

5.3 Elasto-plastic (Drucker-Prager) Model

The Elasto-plastic model was implemented in Abaqus/CAE software using the extended Drucker-Prager model. The Drucker-Prager models are used to model frictional materials, which are typically granular, like soil, rock and sometimes asphalt concrete. They can also be used to model materials in which the compressive yield strength is greater that tensile yield strength. They allow materials to harden or soften isotropically and allow for volume change with inelastic behavior [Abaqus, 2004]

The yield criteria for Drucker-Prager models are based on the shape of the yield surface in the meridional plane. The yield surface can have a linear form, a hyperbolic form, or a general exponent form. These surfaces are illustrated in Figure 5.36 a, b and c.

Figure 5.36 Yield surfaces in the meridional plane [Abaqus, 2004]

a) Linear Drucker-Prager: $F = t - p \tan \beta - d = 0$

b) Hyperbolic: $F = \sqrt{(d'|_0 - p_t|_0 \tan \beta)^2 + q^2} - p \tan \beta - d' = 0$

c) Exponent form: $F = aq^b - p - p_t = 0$
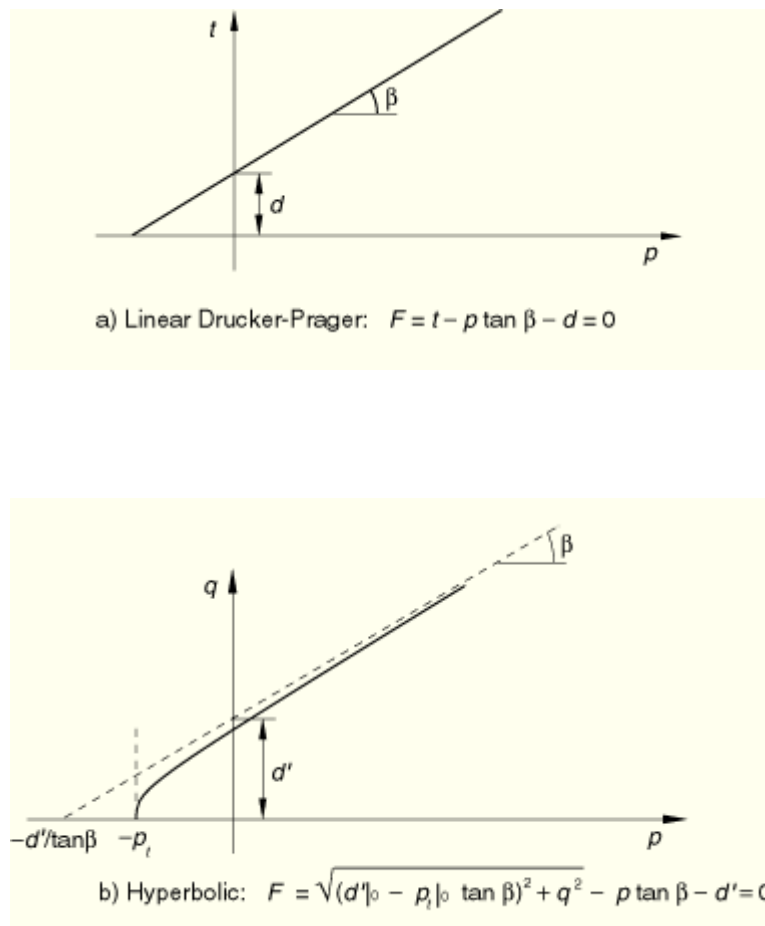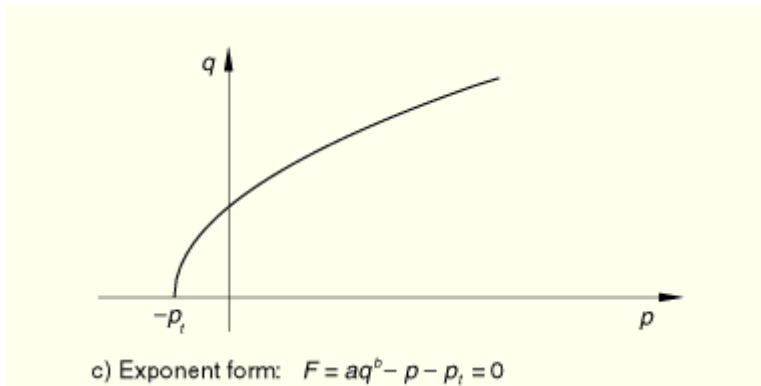
The linear model (Figure 5.36 a) provides for a linear yield surface in the deviatoric plane to match different yield values in triaxial tension and compression; associated inelastic flow in the deviatoric plane; and separate dilation and friction angles. The original Drucker-Prager model is available within this model. However, this model cannot provide a close match to Mohr-Coulomb behavior.

The hyperbolic and general exponent models (Figure 5.36 b and c) use a von Misses (circular) section in the deviatoric stress plane. In the meridional plane a hyperbolic flow potential is used for both models, which, in general, means non associated flow. The required yield criteria is activated in Abaqus CAE by setting the shear criterion equal to linear, hyperbolic or exponent form to define linear, hyperbolic or exponent yield criterion, respectively [Abaqus, 2004].

The linear yield Drucker-Prager model was adopted for this analysis because laboratory tests could be performed at KSU to obtain model parameters. Compressive triaxial test and uniaxial strength test at different strain rates were performed. The yield linear function is given by : $F = t - p\tan\beta - d = 0$ 5.5

where

$$t = \frac{1}{2}q\left[1 + \frac{1}{K} - \left(1 - \frac{1}{K}\right)\left(\frac{r}{q}\right)^3\right].$$ 5.6

186

β = the slope of the linear yield surface in the p–t stress plane and is commonly referred to as the friction angle of the material

d = the cohesion of the material; and

K = is the ratio of the yield stress in triaxial tension to the yield stress in triaxial compression.

Figure 5.37 Typical yield/flow surfaces of the linear model in the deviatoric plane [Abaqus, 2004]

$$t = \frac{1}{2}q\left[1+\frac{1}{K}-\left(1-\frac{1}{K}\right)\left(\frac{r}{q}\right)^3\right]$$

Curve	K
a	1.0
b	0.8
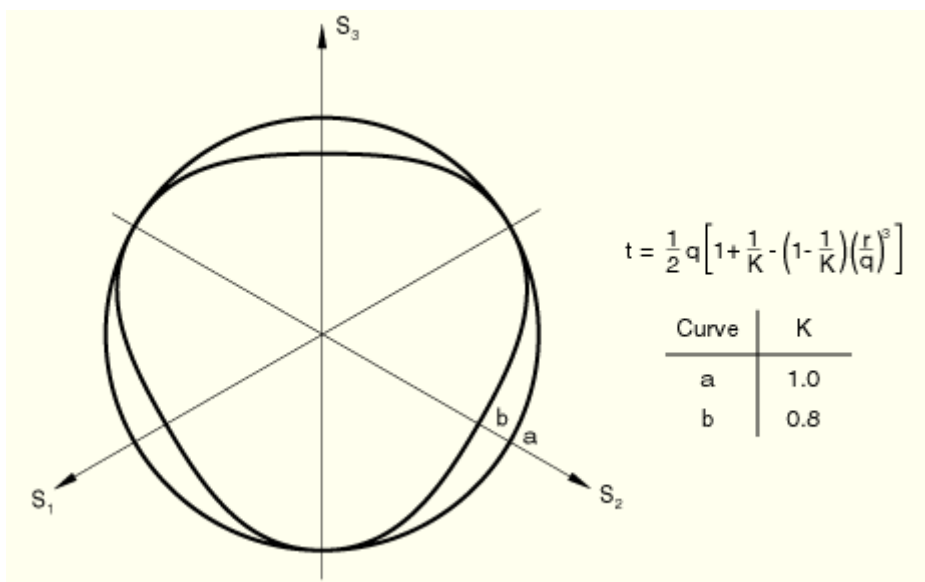
The value of K lies between $0.778 \leq K \leq 1$ to ensure that the yield surface remains convex. When $K = 1$, $t = q$, which implies that the yield surface is the von Misses circle in the deviatoric principal stress plane (the Π-plane), in which case the yield stresses in triaxial tension and compression are the same [Abaqus, 2004]. The cohesion, d, of the material is related to the input data as $d = (1 + 1/3 \tan \beta)\sigma_c$, where σ_c is yield stress.

The plastic flow potential chosen in this model is given as

$G = t = p \tan \psi$, 5.7

where ψ is the dilation angle in p-t plane.

The linear model is normally used with non associated flow in the p–t plane, where usually $\psi < \beta$, as illustrated in Figure 5.33. Associated flow is obtained by setting $\psi = \beta$ and the original Drucker-Prager model is available by setting $\psi = \beta$ and K = 1. Non associated flow is also generally assumed when the model is used for polymeric materials. If $\psi = 0$, the inelastic deformation is incompressible; if $\psi \geq 0$, the material dilates. Hence, ψ is referred to as the dilation angle

Figure 5.38 Linear Drucker-Prager model: yield surface and flow direction in the p–t plane [Abaqus, 2004]
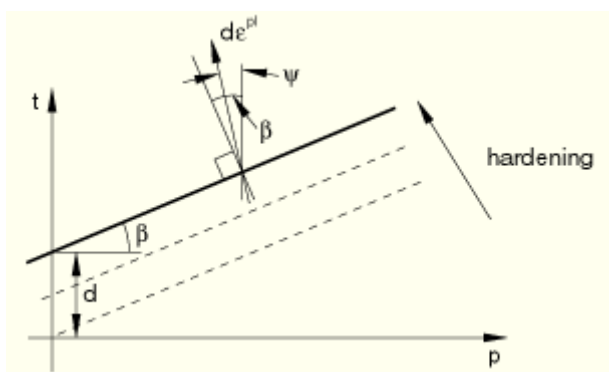
Material parameters for Druker-Pruger model were obtained from two laboratory tests. Uniaxial compressive strength tests at five different strain rates, which was used to obtain the initial elastic modulus (E), initial yield stress and failure strength. The triaxial compression test was conducted at 4 different confining stresses, 0, 69, 138, and 207 kPa and a strain rate of 0.0001 sec^{-1} to obtain the Drucker-Prager yield function constants β, ψ and d, which are input values for the Drucker-Prager model. Table 5.8 presents the model parameters required for the D-P model. Values for initial yield stress and failure strength are given in Tables 4.4 and 4.7 in sections 4.2.3 and 4.2.4 respectively. In Figures 5.39 to 5.41 are the t-p plots at values of K = 0.78, 9, and 1 and presented.

Table 5.9 Drucker-Prager model parameters

Parameter	KS-1			KS-2			MO-1		
Stress Ratio (K)	1	0.9	0.78	1	0.9	0.78	1	0.9	0.78
Internal angle of friction (β)	45.5	48.5	52.5	20.1	22.27	25.2	24.0	26.3	29.7
Dilation angle (ψ)	30.3	32.3	35.0	13.4	14.8	16.8	16.0	17.5	19.8
Cohesion (d)	1225	1361	1570	1012	1125	1298	1044	1160	3387
Creep Parameters A	1e-11			6e-18			1e-10		
n	0.8			0.8			0.8		
m	-0.5			-0.7			-0.5		
Elastic Modulus (MPa)	3115			1619			2410		
Poisson's ratio	0.35			0.35			0.35		
Base M_r (MPa)	350			350			450		
Base Poisson's ratio	0.4			0.4			0.4		
Subgrade M_r (MPa)	200			200			250		
Subgrade Poisson's ratio	0.45			0.45			0.45		

Table 5.9 (Continues): Drucker-Prager model parameters

Parameter	MO-2			IA-1			IA-2		
Stress Ratio (K)	1	0.9	0.78	1	0.9	0.78	1	0.9	0.78
Internal angle of friction (β)	37.8	40.7	44.8	37.77	40.73	44.8-	20.44	22.5	25.53
Dilation angle (ψ)	25.2	27.1	29.9	25.18	27.15	29.87	13.62	15	17.02
Cohesion (d)	623.5	692.8	799.4	623.5	692.8	799.4	696.8	774.2	893.4
Creep Parameters A	1e-14			-			1e-9		
n	0.8			-			0.6		
m	-0.8			-			-0.6		
Elastic Modulus (MPa)	437			494			1869		
Poisson's ratio	0.35			0.35			0.35		
Base M_r (MPa)	180			350			650		
Base Poisson's ratio	0.4			0.4			0.4		
Subgrade M_r (MPa)	80			200			350		
Subgrade Poisson's ratio	0.45			0.45			0.45		

Figure 5.39 t-p plot for Kansas mix (KS-1) with K = 1, 0.9, and 0.78

t-p plot for Kansas KS-1 mix
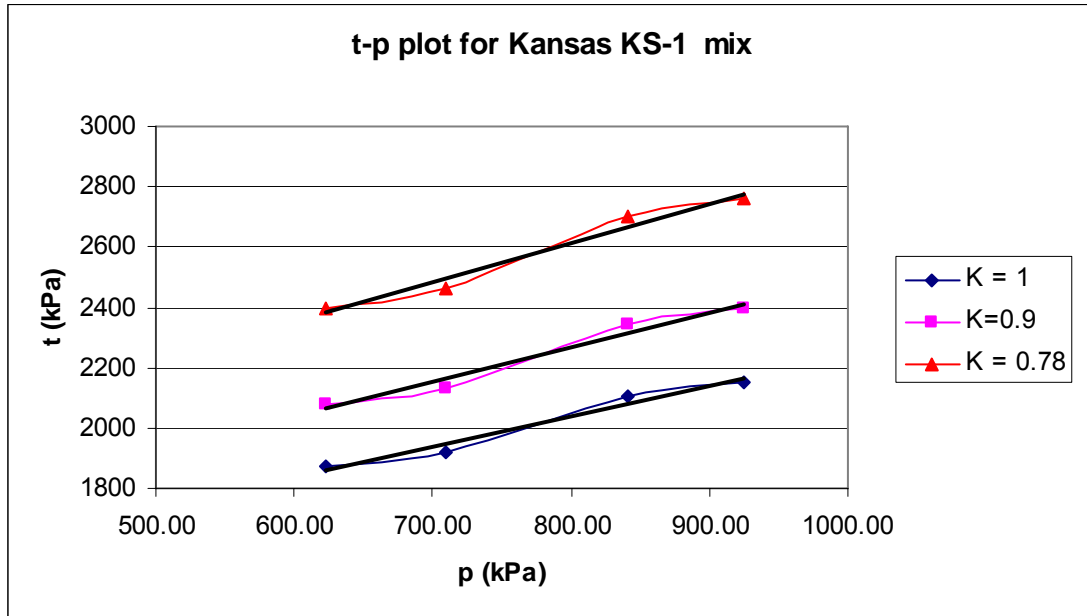
Figure 5.40 t-p plot for Kansas mix (KS-2) with K = 1, 0.9, and 0.78

t-p plot for Kansas KS-2 mix
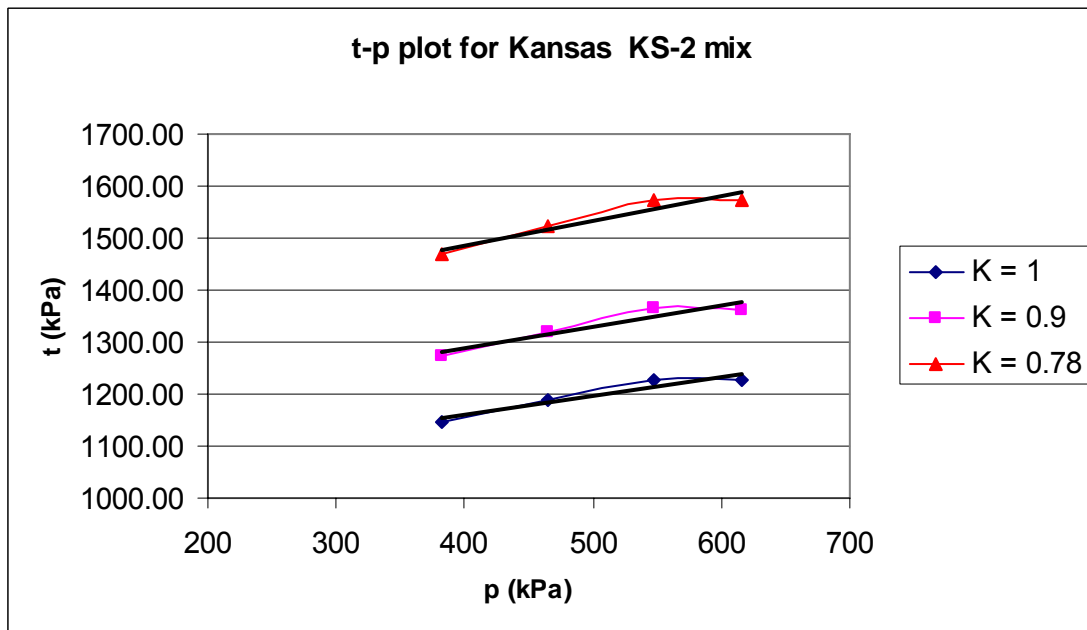
Figure 6.41 t-p plot for Missouri mix (MO-1) with K = 1, 0.9, and 0.78
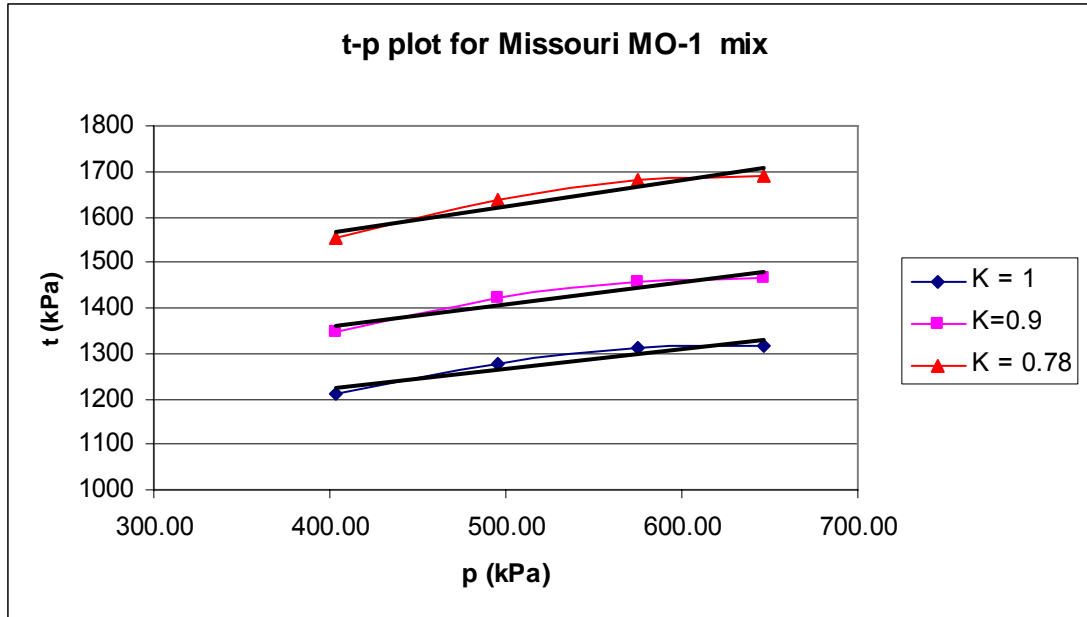
Figure 5.42 t-p plot for Missouri mix (MO-2) with K = 1, 0.9, and 0.78
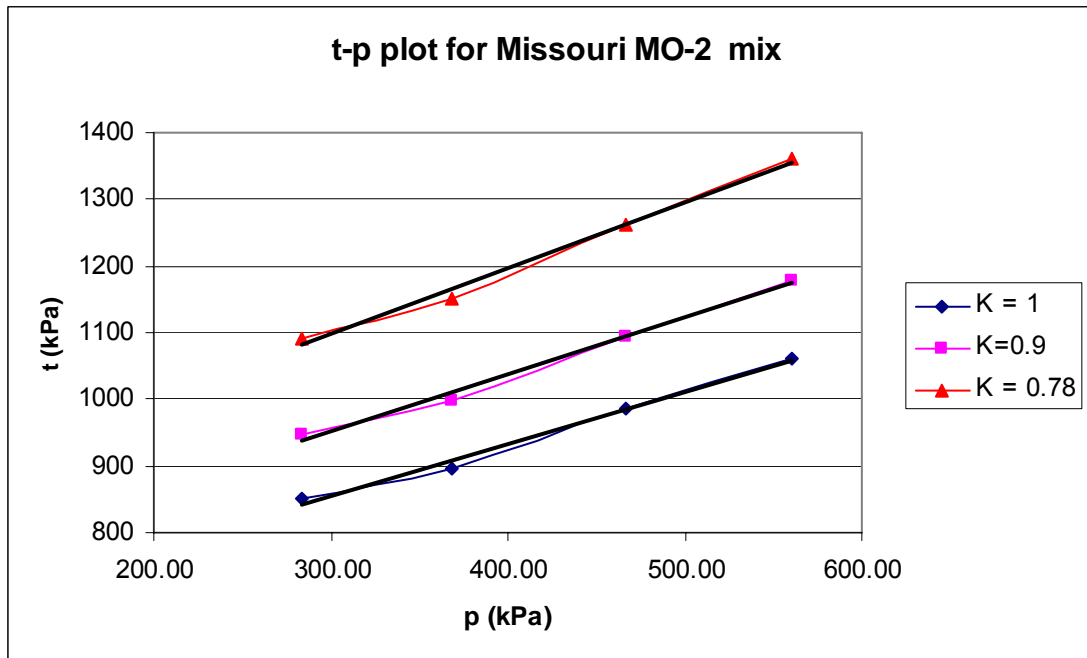
Figure 5.43 t-p plot for Iowa mix (IA-2) with K = 1, 0.9, and 0.78
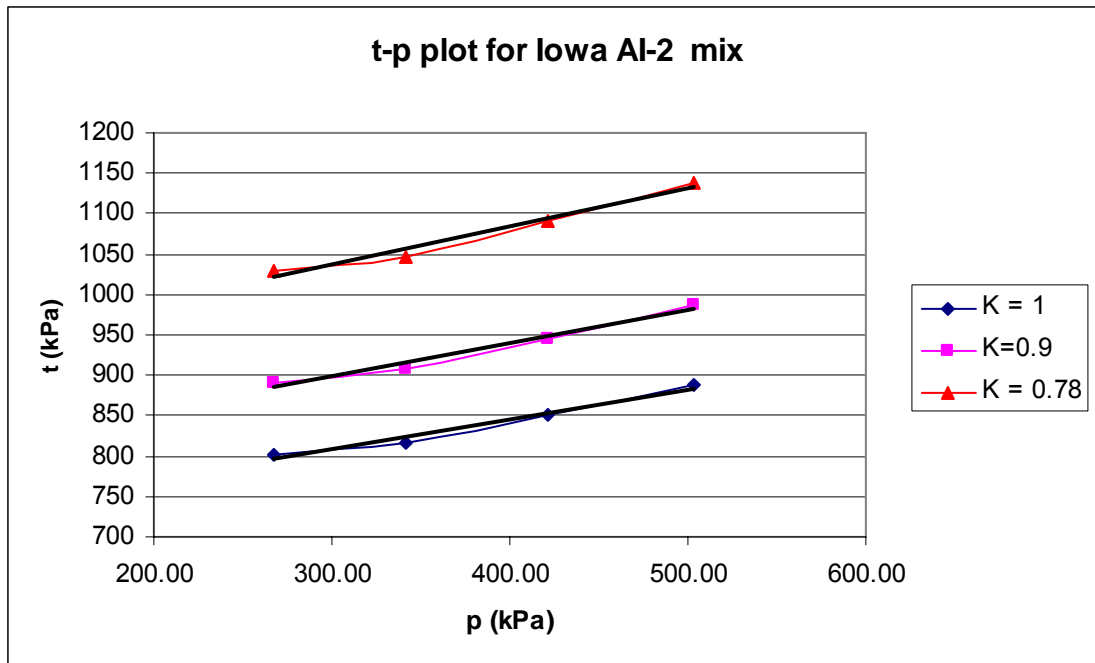
Iowa IA-1 mixture was very weak and failed at low values of yield strength during both laboratory tests, this made it difficult to correctly obtain model parameters and plot the t-p plots. For this reason, Iowa (IA-1) mix could not be evaluated using the Drucker-Prager model.

5.3.1 Modeling Asphalt Mixes Using Drucker-Prager Model Available in Abaqus/CAE

After obtaining model parameters the Drucker-Prager model available in Abaqus/CAE was used to model permanent deformation in asphalt mixes. Hardening in Drucker-Prager model is modeled using:

1. Drucker-Prager hardening, which uses yield stress, corresponding plastic strain, and strain rate as inputs.
2. Drucker-Prager creep, which is uses creep parameters A, m and n, in conjunction with Drucker-Prager hardening.
3. Rate dependent, which is uses power law in conjunction with Drucker-Prager hardening.
4. Triaxial test data, which uses triaxial confining stress, loading stress and material constants a, b, and pt obtained from the exponent yield function. This is used in conjunction with Drucker-Prager hardening.

The model was run using the Drucker-Prager hardening criterion, which uses yield stress and plastic strain obtained from the uniaxial strength test at different strain rates, internal angle of friction β, dilation angle ψ and K value obtained from triaxial strength test at different confining stresses. This hardening criterion did not yield good results (Figure 5.44). Very small values of vertical displacements were observed. This could be due to a single wheel load application, which could not load the asphalt section to its yield stress values and hence plastic deformation is not captured.

Figure 5.44 Vertical displacements after single wheel load pass on a pavement section
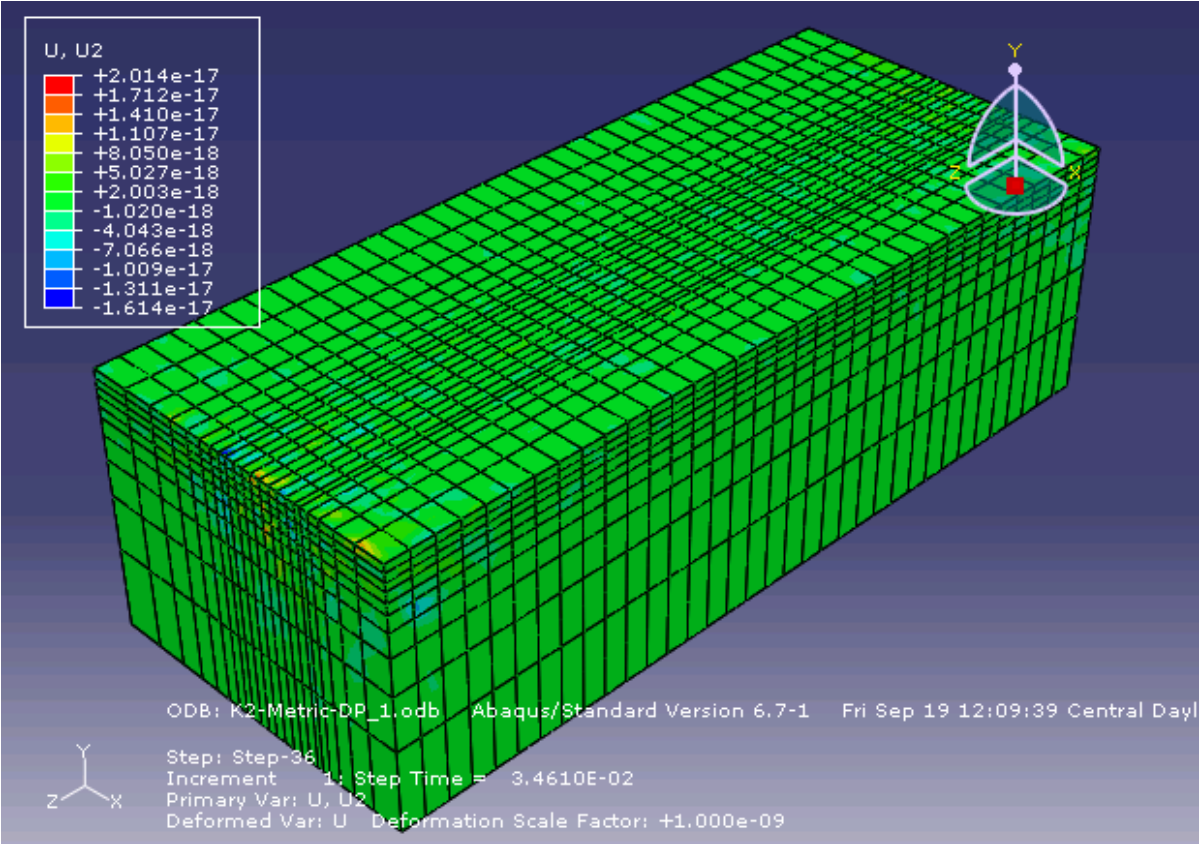
A creep criterion was then added to the Drucker-Prager hardening criterion explained above, with a moving wheel load applied as a step load. Using creep parameter and time hardening, a failure pattern similar to that explained in section 5.2.1 was obtained. More displacement was observed at the beginning of the wheel load than at the end of it due to time loading effect in the creep model (Figure 5.45). A simplified load, explained in section 5.2.1 and shown in Figure 5.15 was then used.

Figure 5.45 Vertical displacements contours after single adding creep hardening criterion
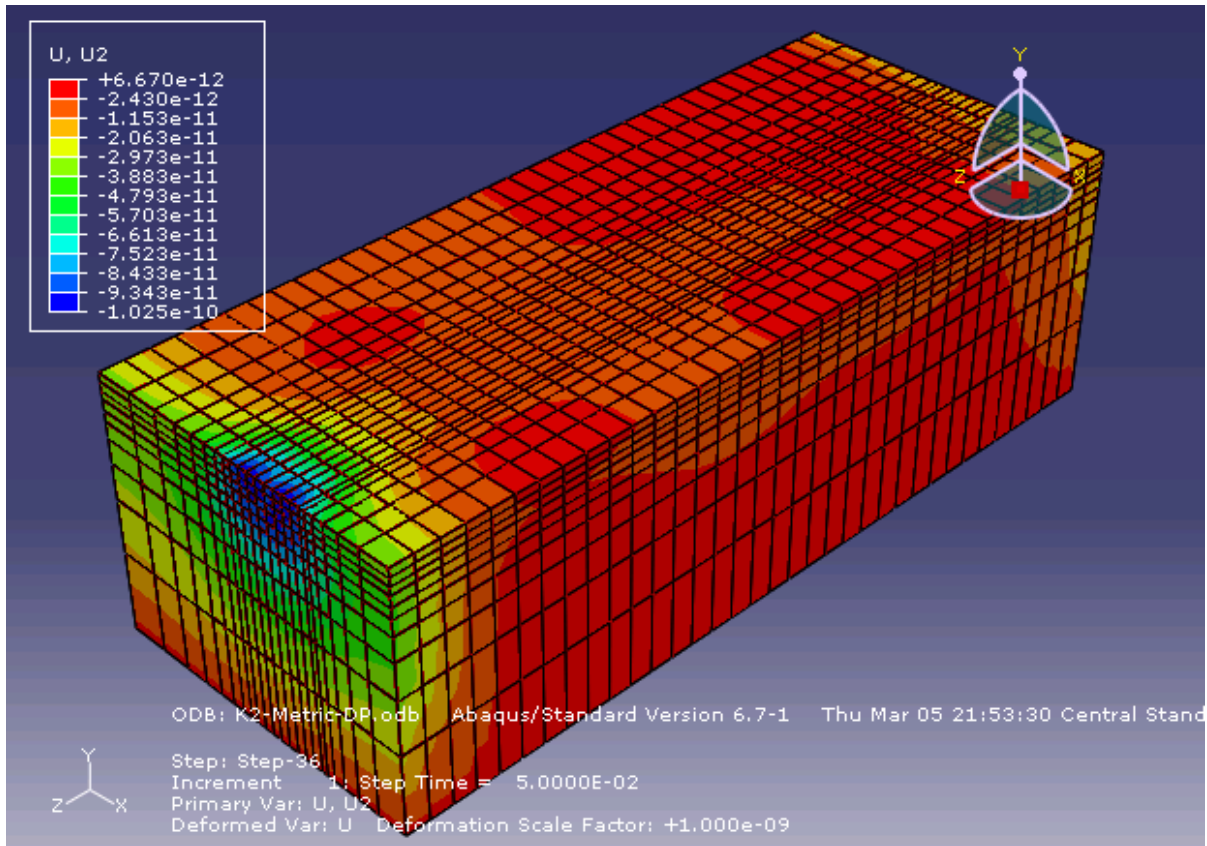
5.3.2 Results from Finite Element Viscoplastic model

The values obtained from the triaxial and uniaxial tests were used to obtain model parameters, which are the inputs in the simulation of the viscoplastic model. According to Huang, 2001, the stress ratio value, K, of 0.78 underestimates predictions and K of 1 overestimates predictions of permanent deformation. For this analysis values of K = 0.78, 0.9 and 1 were used and all of them underestimated permanent deformation predictions. A value of K = 1.0 was then used in conjunction with creep hardening parameters because, when Drucker-Prager model is used with creep hardening a value of K = 1 is required. A linear shear criterion and shear hardening behavior were used for Drucker-Prager hardening. A simplified wheel load was adopted with Abaqus visco analysis. Kansas mix KS-1 was modeled first and using Drucker-Prager model with creep hardening. It was hard to model the creep behavior, at last, with A value of 1e-11, n = 0.8 and m = -0.5, nodal displacement were observed (Figure 5.44)

194

Figure 5.46 Vertical displacement contours after modeling with creep hardening
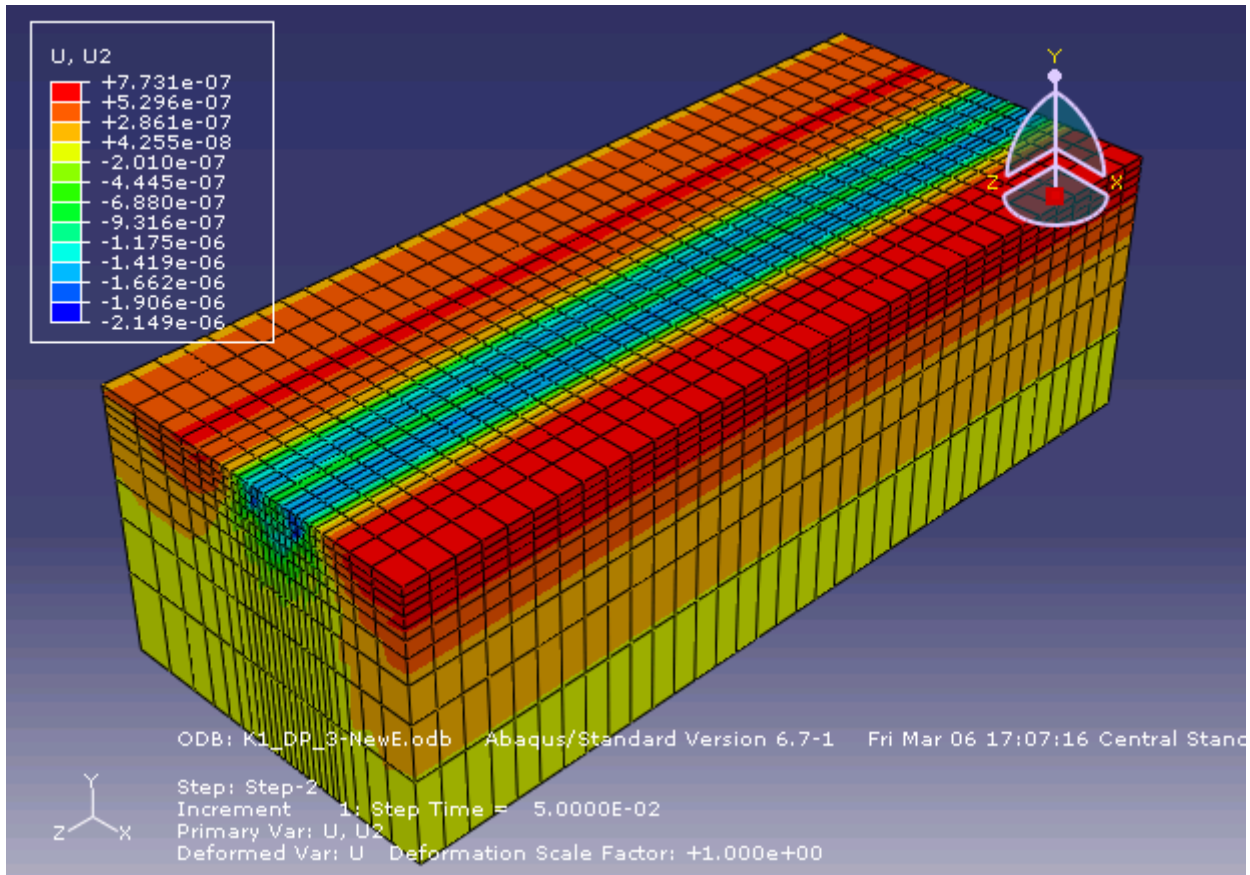
A path was created at the mid section and nodal displacement values were obtained. When these values were plotted for Kansas KS-1 mix, the failure pattern indicated very high deformation in the base and subgrade layers than it was in the asphalt layer. This is because the model could not run with elastic modulus higher than 450MPa and 250MPa for base and subgrade layers respectively, while the elastic modulus in the asphalt layer is 3,115 MPa. Uneven displacement along the transverse sections was observed. Figure 5.47 shows the path plotted in Abaqus for MO-1 mix where more displacement is observed on one wheel than the other. Figure 5.48 to Figure 4.57 provide the transverse profiles of the maximum permanent deformation plotted in excel sheet and the development of permanent deformation with increase in load repetitions for each pavement section modeled, the values are provided in Tables 5.11 to 5.15.

Figure 5.47 Abaqus predicted permanent deformation for MO-1 mix
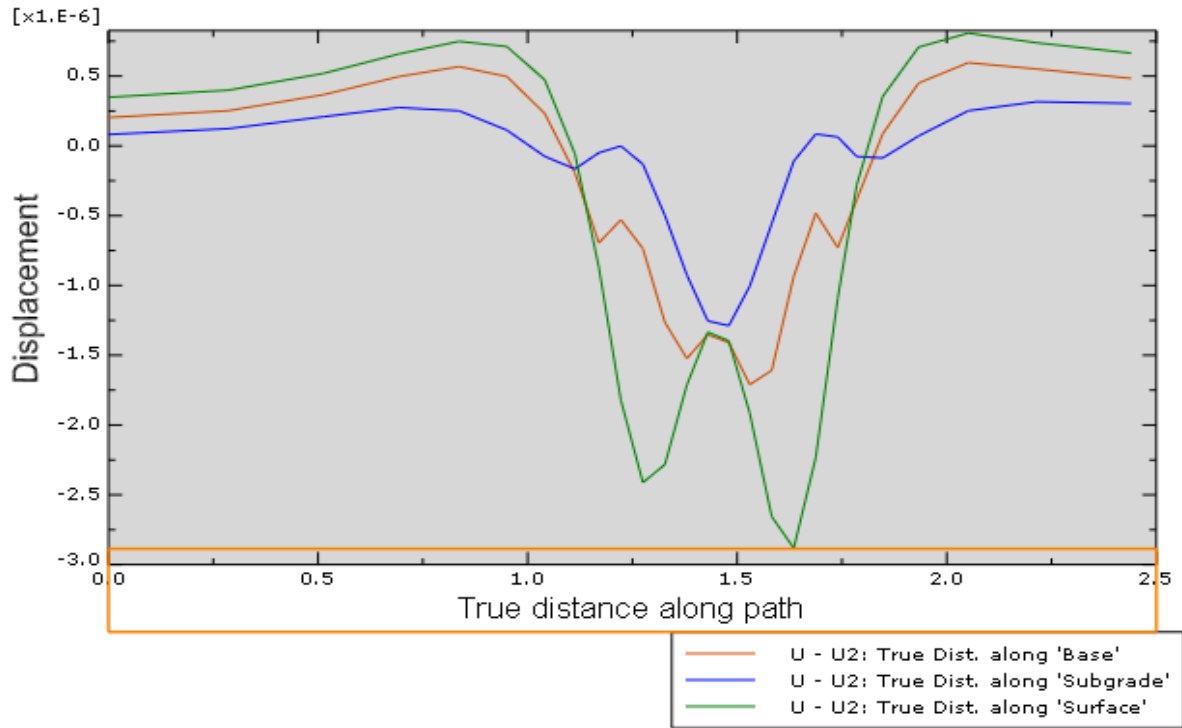
Table 5.10 Abaqus displacement values from nodes at mid section of KS-1 section

Distance (m)	Displacement on nodes (m)			Distance (m)	Displacement on nodes (m)		
	Surface	Base	Subgrade		Surface	Base	Subgrade
0.0000	3.5E-07	2.1E-07	8.5E-08	1.4300	-1.4E-06	-1.4E-06	-1.3E-06
0.2857	4.1E-07	2.6E-07	1.3E-07	1.4800	-1.4E-06	-1.5E-06	-1.3E-06
0.5128	5.4E-07	3.8E-07	2.2E-07	1.5300	-2.0E-06	-1.8E-06	-1.0E-06
0.6932	6.9E-07	5.2E-07	2.9E-07	1.5825	-2.7E-06	-1.7E-06	-5.9E-07
0.8365	7.8E-07	5.9E-07	2.6E-07	1.6350	-2.9E-06	-9.8E-07	-1.4E-07
0.9504	7.8E-07	5.1E-07	1.2E-07	1.6875	-2.3E-06	-5.2E-07	5.7E-08
1.0409	7.3E-07	2.3E-07	-8.3E-08	1.7400	-1.1E-06	-7.6E-07	4.1E-08
1.1129	4.8E-07	-2.1E-07	-1.8E-07	1.7851	-2.9E-07	-4.1E-07	-9.1E-08
1.1700	-6.5E-08	-7.3E-07	-7.4E-08	1.8472	3.6E-07	8.2E-08	-9.2E-08
1.2225	-9.0E-07	-5.7E-07	-3.1E-08	1.9330	7.3E-07	4.6E-07	7.9E-08
1.2750	-1.9E-06	-7.8E-07	-1.7E-07	2.0514	8.4E-07	6.2E-07	2.7E-07
1.3275	-2.3E-06	-1.3E-06	-5.3E-07	2.2147	7.7E-07	5.8E-07	3.5E-07
1.3800	-1.8E-06	-1.6E-06	-9.6E-07	2.4400	7.0E-07	5.2E-07	3.4E-07

Figure 5.48 Transverse profile of KS-1 section after Drucker-Prager model with creep hardening.
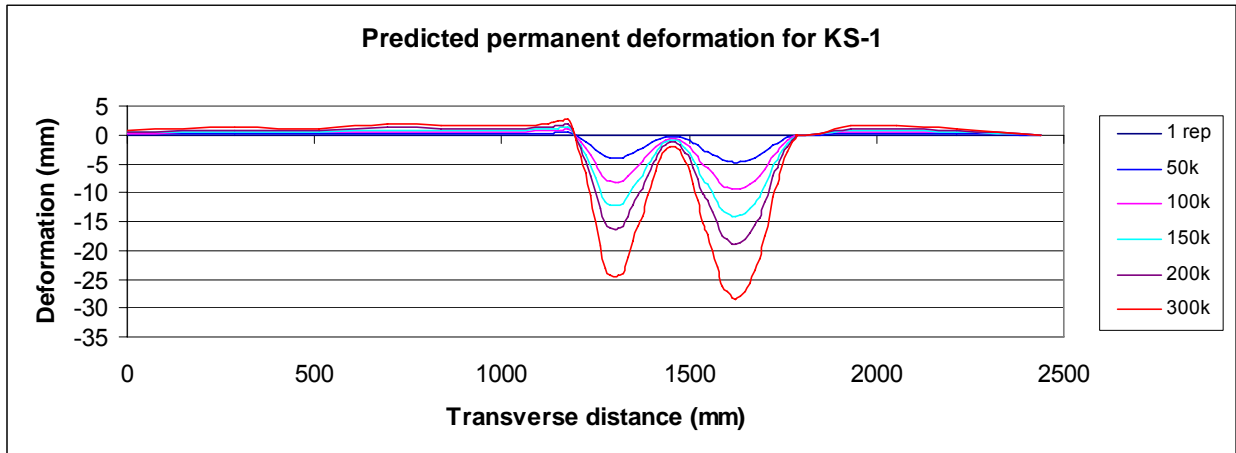
Given in Figure 5.48 is the prediction of the evolution of permanent deformation that was computed using this model, Table 5.11 gives the values at different numbers of load repetition. At 300,000 load repetitions the predicted permanent deformation is 27.9 mm while the measured deformation is 6.15mm. The model over predicts permanent deformation. The prediction is 308% of the measured value, which is very high.

Table 5.11 Evolution of permanent deformation in KS-1 mix

Load Repetition x1000	Predicted deformation			Measured deformation		Deformation in Asphalt mix		
	mm	in	%	mm	in	mm	in	%
0	0	0	0	0	0	0	0	0
50	4.65	0.186	193.8	2.4	0.096	2.31	0.00280	96.3
100	9.3	0.372	196.8	4.725	0.189	4.62	0.00560	97.8
150	14.2	0.568	-	-	-	6.93	0.00840	-
200	19	0.76	245.9	5.775	0.231	9.2	0.01115	120.0
300	27.9	1.116	308.9	6.15	0.246	14.9	0.01806	149.6

197

Figure 5.49 Evolution of permanent deformation in KS-1 mix

Evolution of permanent deformation in KS-1 section
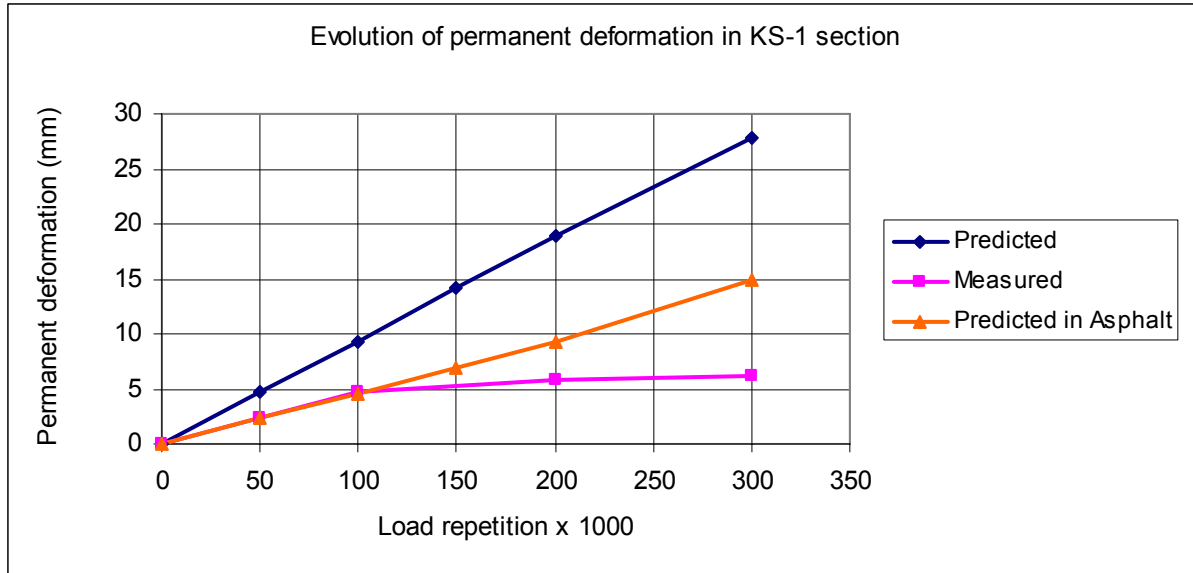
Figure 5.50 Transverse profile of KS-2 section after Drucker-Prager model with creep hardening.

Predicted permanent deformation for KS-2
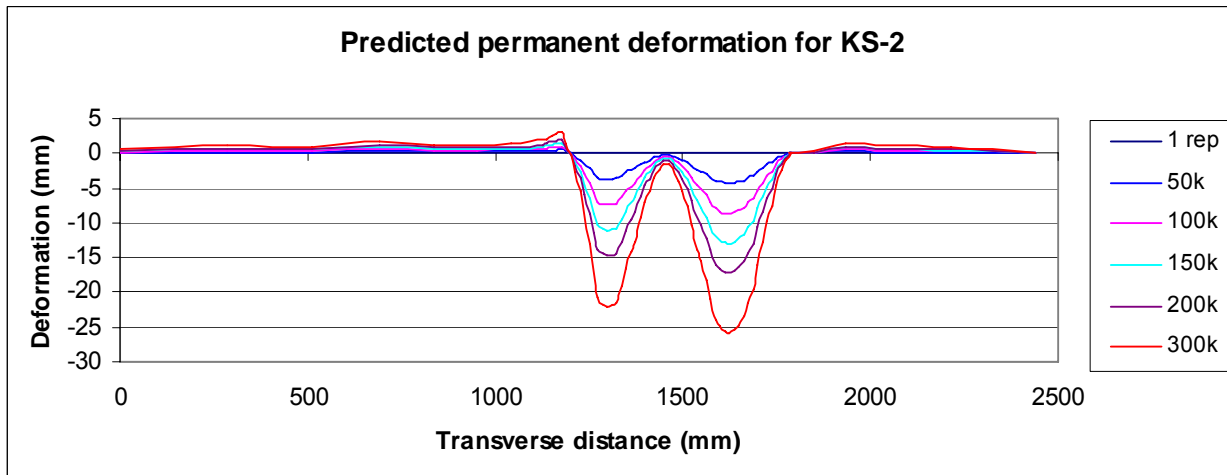
Table 5.12 Evolution of permanent deformation in KS-2 mix

Load Repetition x1000	Predicted deformation			Measured deformation		Deformation in Asphalt mix		
	mm	in	%	mm	in	mm	in	%
0	0	0	0	0	0	0	0	0
50	4.32	0.1728	233.5	1.85	0.074	2.28	0.0912	123.2
100	8.64	0.3456	160.0	5.4	0.216	4.56	0.1824	84.4
150	13	0.52		-	-	6.84	0.2736	-
200	17.3	0.692	241.9	5.375	0.215	9.12	0.3648	127.3
300	25.4	1.016	334.3	5.175	0.207	14.7	0.588	176.2

Figure 5.51 Evolution of permanent deformation in KS-2 mix
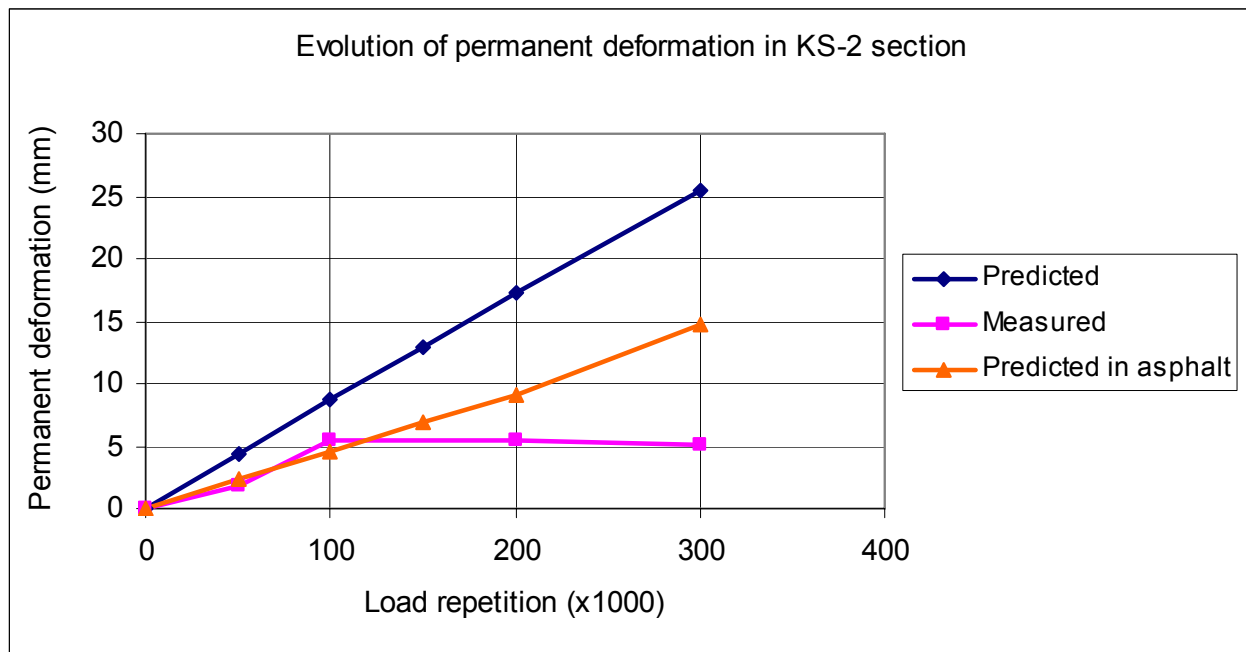
Figure 5.52 Transverse profile of MO-1 section after Drucker-Prager model with creep hardening
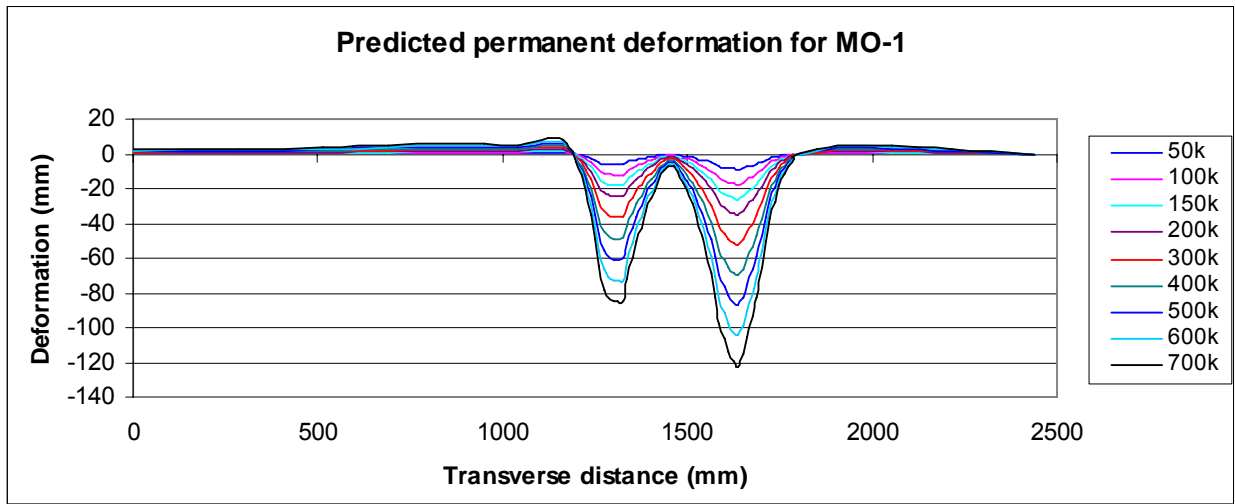
Table 5.13 Evolution of permanent deformation in MO-1 mix

Load Repetition x1000	Predicted deformation			Measured deformation		Deformation in Asphalt mix		
	mm	in	%	mm	in	mm	in	%
0	0	0	0	0	0	0	0	0
50	8.73	0.349	270.7	3.23	0.129	5.38	0.006521	166.8
100	17.5	0.700	479.5	3.65	0.146	15.5	0.018788	424.7
150	26.2	1.048	685.0	3.83	0.153	20.6	0.02497	538.6
200	34.9	1.396	906.5	3.85	0.154	22.7	0.027515	589.6
300	49.5	1.980	929.6	5.33	0.213	34.1	0.041333	640.4
400	69.9	2.796	1294.4	5.40	0.216	43.1	0.052242	798.1
500	82.5	3.300	1422.4	5.80	0.232	68.1	0.082545	1174.1
600	105	4.200	1772.2	5.93	0.237	69.5	0.084242	1173.0
700	122	4.880	1913.7	6.38	0.255	79.5	0.096364	1247.1

Figure 5.53 Evolution of permanent deformation in MO-1 mix
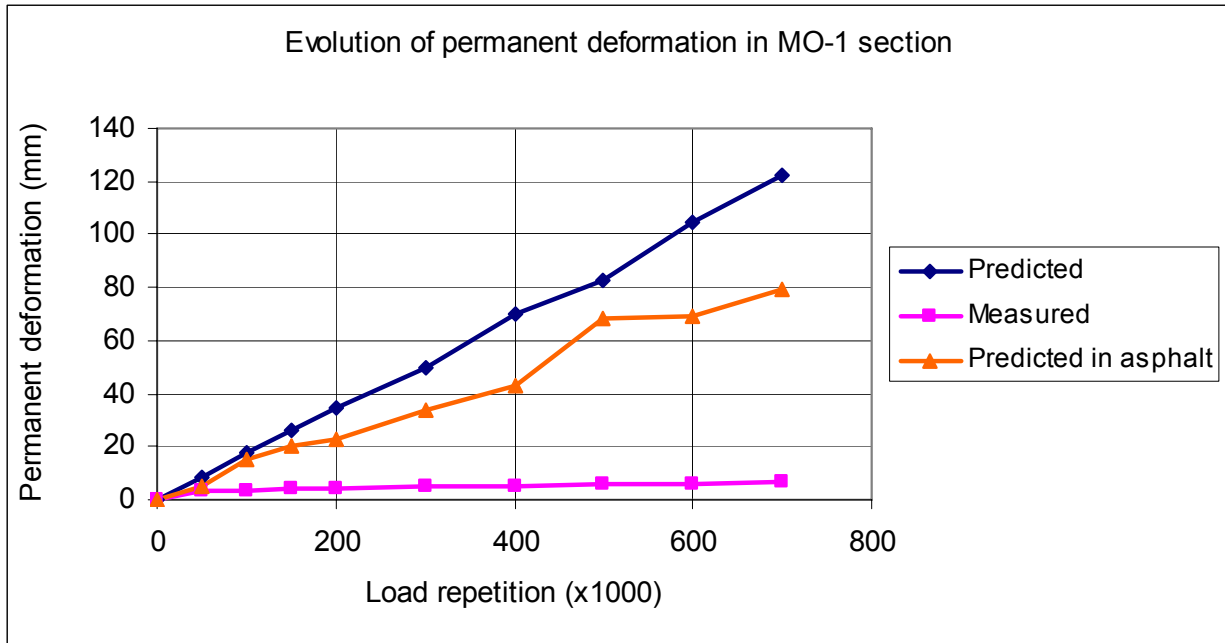
Figure 5.54 Transverse profile of MO-2 section after Drucker-Prager model with creep hardening
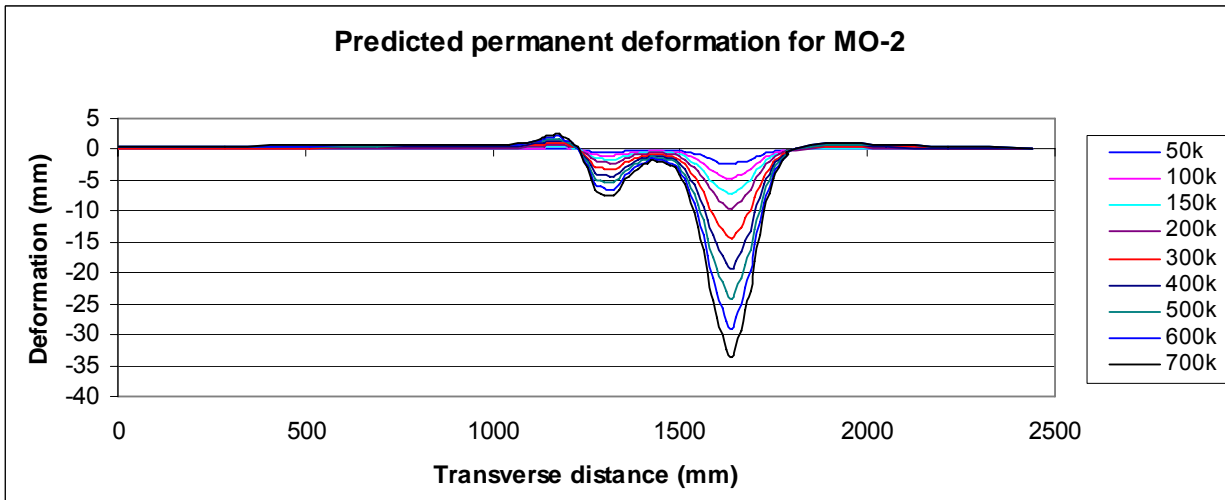
Table 5.14 Evolution of permanent deformation in MO-2 mix

Load Repetition x1000	Predicted deformation			Measured deformation		Deformation in Asphalt mix		
	mm	in	%	mm	in	mm	in	%
0	0	0	0	0	0	0	0	0
50	2.41	0.0964	48.2	5	0.2	1.5	0.06	30.0
100	4.56	0.1824	57.0	8	0.32	4.26	0.1704	53.3
150	7.23	0.2892	80.8	8.95	0.358	6.02	0.2408	67.3
200	9.64	0.3856	99.1	9.725	0.389	8.53	0.3412	87.7
300	13.7	0.548	117.8	11.625	0.465	12	0.48	103.2
400	19.3	0.772	156.6	12.325	0.493	17.1	0.684	138.7
500	24.1	0.964	173.4	13.9	0.556	21.1	0.844	151.8
600	28.9	1.156	204.6	14.125	0.565	25.6	1.024	181.2
700	33.7	1.348	230.4	14.625	0.585	29.8	1.192	203.8

Figure 5.55 Evolution of permanent deformation in MO-2 mix
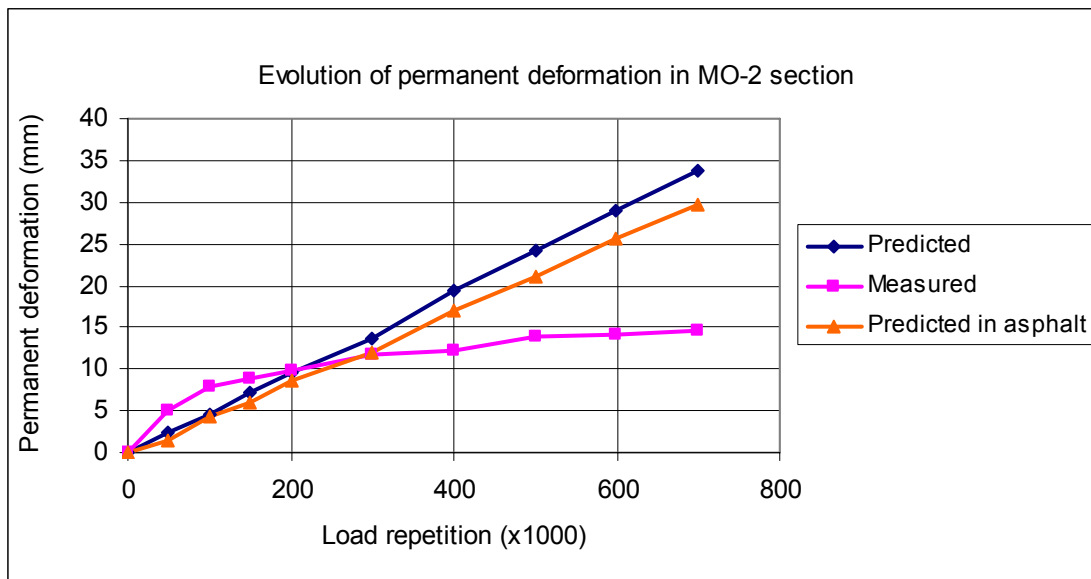
Figure 5.58 Transverse profile of IA-2 section after Drucker-Prager model with creep hardening
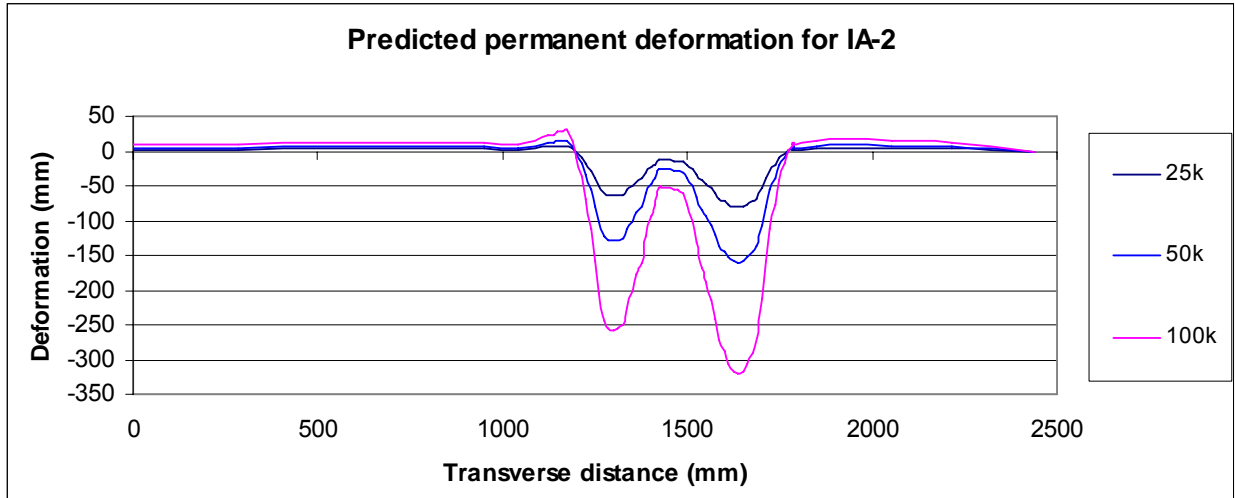
Table 5.15 Evolution of permanent deformation in IA-2 mix

Load Repetition x1000	Predicted deformation			Measured deformation		Deformation in Asphalt mix		
	mm	in	%	mm	in	mm	in	%
0	0	0	0	0	0	0	0	0
25	79	3.16	926.7	8.525	0.341	16.4	0.656	15.1
50	160	6.4	1768.0	9.05	0.362	41.3	1.652	27.5
100	307	12.28	2590.7	11.85	0.474	82.5	3.3	43.5

Figure 5.57 Evolution of permanent deformation in IA-2 mix
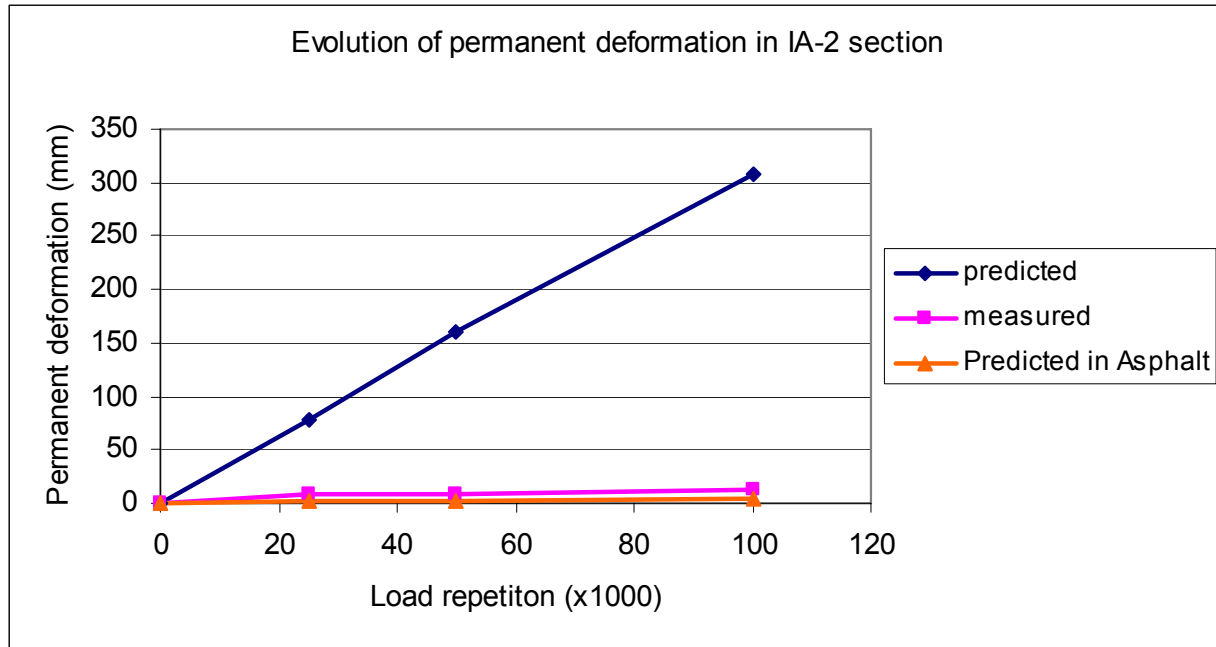
Figures 5.48 to 5.57 shows the results of permanent deformation, implemented in Abaqus/CAE using Drucker-Prager model with creep hardening. It can be clearly seen from the figures that the model over predicts permanent deformation up to 2590% in some cases. Also the transverse profiles have uneven or unsymmetrical deformation; one wheel causes more deformation than the other which should not be the case. This could be due to the fact that Drucker-Pruger model is suitable for granular materials or asphalt concrete tested at higher temperatures (such as 60°C). Asphalt at intermediate temperature is more of a solid structure and the model cannot capture well the properties of asphalt concrete. According to Park, (2004), the elasto-visco plastic model cannot predict tertiary deformation due to the lack of damage parameters.

5.4 Viscoelastic Model

The viscoelastic model was evaluated using Abaqus/CAE software. The model parameters were obtained from the frequency sweep at constant height (FSCH) tests that were performed at the Asphalt Institute laboratories. Results from these tests are given in section 4.2.5. The values of dynamic shear modulus G* with its loss modulus G" and storage modulus G' were obtained from the FSCH test. These values are used to assess the shear properties of asphalt mixtures. The volumetric properties of asphalt mixes used the bulk modulus K*. This value could not be obtained using laboratory tests, therefore it was calculated from the dynamic shear modulus (G*), obtained form the FSCH test and Poisson's ratio (v), which could not be measured from lab tests due to lack of radial LVDT. A value of $v = 0.35$ was assumed for all asphalt mixes. The expression from classical mechanics was used to obtain bulk modulus K

$$K* = \frac{2G*(1+v)}{3(1-2v)}$$

5.8

Table 5.16 provides the computed values of K*, K' and K" at 35°C and six frequencies for each mix. Since the values required for the model are G', G", K' and K", equation 5.8 was used to obtain the values of bulk modulus, K' and K".

Table 5.16 Computed values of bulk modulus K

Asphalt Mix	Frequency	Dynamic shear modulus (MPa)			Bulk Modulus (MPa)		
		G*	G'	G"	K*2	K'	K"
KS-1	25	991.0	869.0	690.7	2973.11	2606.93	2071.99
	10	692.3	597.8	462.6	2076.98	1793.51	1387.87
	5	529.9	452.4	343.1	1589.62	1357.09	1029.43
	1	294.8	245.4	178.2	884.29	736.28	534.61
	0.5	234.0	192.9	137.7	702.06	578.83	413.12
	0.1	146.0	118.0	81.3	438.02	353.94	243.88
KS-2	25	547.6	456.2	412.7	1642.71	1368.67	1238.00
	10	354.8	289.4	258.7	1064.31	868.11	776.11
	5	256.7	206.1	182.6	770.08	618.25	547.94
	1	126.2	97.9	85.1	378.75	293.69	255.36
	0.5	95.5	73.0	63.0	286.47	219.12	189.10
	0.1	54.0	40.1	34.1	161.87	120.40	102.32
MO-1	25	906.6	729.0	583.9	2719.77	2186.88	1751.61
	10	628.0	492.3	384.2	1883.86	1476.77	1152.67
	5	477.6	367.3	281.2	1432.67	1102.02	843.75
	1	262.0	193.3	141.9	785.94	579.96	425.67
	0.5	206.9	150.2	108.4	620.56	450.51	325.20
	0.1	127.6	89.6	62.5	382.85	268.81	187.56
MO-2	25	924.1	711.3	675.4	2772.37	2134.01	2026.23
	10	638.8	476.9	450.1	1916.26	1430.76	1350.33
	5	485.0	354.0	332.6	1455.03	1061.98	997.78
	1	265.2	184.1	171.3	795.47	552.37	513.88
	0.5	209.1	142.4	131.9	627.24	427.10	395.80
	0.1	128.6	84.1	77.4	385.90	252.45	232.10
IA-1	25	624.6	518.2	439.7	1873.70	1554.70	1319.22
	10	415.9	337.7	281.1	1247.69	1013.02	843.29
	5	307.1	245.4	201.4	921.40	736.08	604.08
	1	158.0	121.8	96.9	473.93	365.39	290.64
	0.5	121.6	92.5	72.6	364.84	277.38	217.93
	0.1	71.2	52.6	40.3	213.72	157.91	120.98
IA-2	25	804.83	664.5	804.8	2414.50	1993.58	2414.50
	10	548.59	443.0	548.6	1645.77	1328.89	1645.77
	5	412.23	327.4	412.2	1236.70	982.12	1236.70
	1	220.28	168.7	220.3	660.85	506.01	660.85
	0.5	172.14	129.9	172.1	516.43	389.80	516.43
	0.1	103.98	76.2	104.0	311.95	228.65	311.95

The viscoelastic model was implemented using a moving load simulated as a step load. The general expression for total strains in this model are given by equation 5.9.

$$\varepsilon^{ve} = \varepsilon^e + \varepsilon^v \qquad\qquad 5.9$$

Where: ε^{ve} = total viscoelastic strains

ε^e = elastic strains (instantaneous recoverable strains)

ε^v = visco strains (recoverable strains with time)

The formulation of the viscoelastic strains is comprised of recoverable strains only. Plastic strains are not computed using this model. This is the reason why the displacement measured on nodes is very small (2 E-11mm) no plastic strains is recorded after one passage of the wheel load. This model, if used to predict permanent deformation, it may predict longer pavement performance than what it actually is due to lack of plastic and viscoplastic strains. Figure 5.58 shows the nodal displacement along the transverse path at pavement midsection. Figure 5.59 shows a contoured vertical displacement computed for a pavement section modeled using Abaqus/CAE. Very small nodal displacements are obtained using the viscoelastic model. The transverse profile is very different from what is expected for pavements. Since this model did not predict deformations at all, other sections deformation are not reported. Long (2001) used a nonlinear viscoelastic model to predict permanent deformation in asphalt mixtures at 60°C. The modified asphalt rubber hot mix, predicted permanent deformation less than field measured values, but in general the nonlinear viscoelastic model captured the permanent deformation of asphalt mixture reasonably well, although the model was unable to capture densification in the mix. Long (2001) used nonlinear viscoelastic model and for this simulation a linear viscoelastic model was used and it was not able to capture permanent deformation in asphalt mixtures.

Figure 5.58 Results for KS-2 mix using viscoelastic prediction model
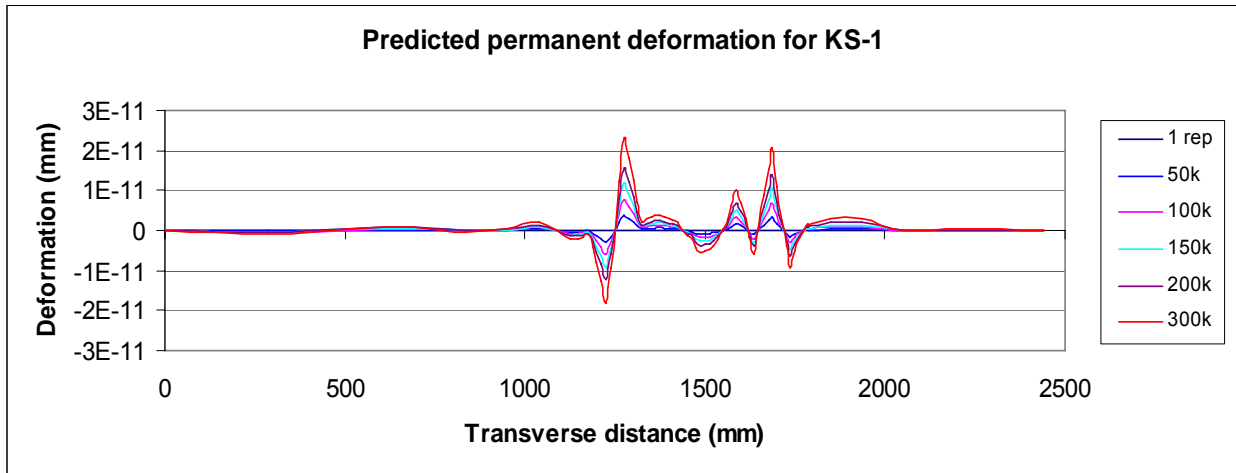
Figure 5.59 Abaqus results for KS-2 mix using viscoelastic prediction model
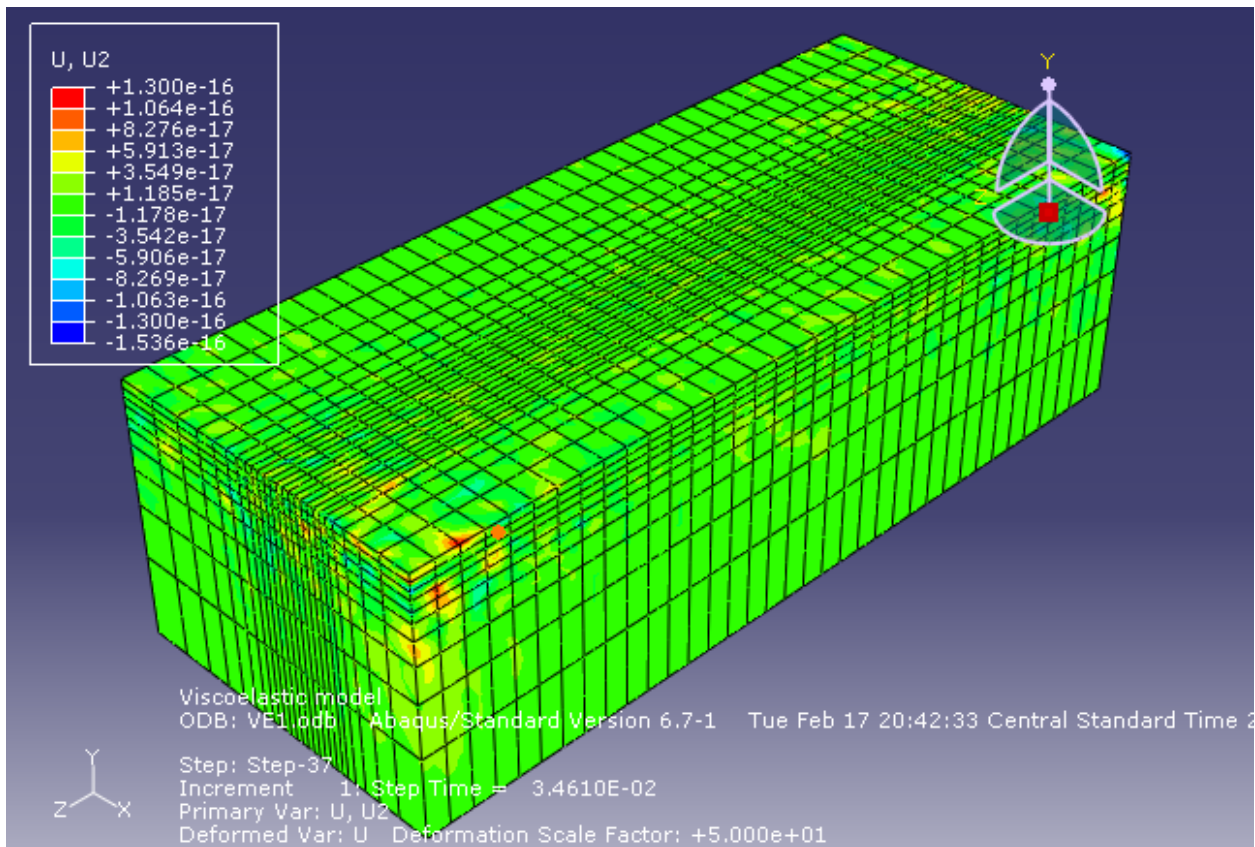
5.5 Elasto-visco-plastic model

The elasto-visco-plastic model comprise of elastic, plastic and viscous properties of materials. It is an ideal model which could capture the properties of asphalt material which are elasto-visco-plastic. The model is intended for modeling materials in which significant time-dependent behavior as well as plasticity is observed. It consists of an elastic-plastic network that is in parallel with an elastic-viscous network (in contrast to the coupled creep and plasticity capabilities in which the plastic and the viscous networks are in series). It is based on a Misses or Hill yield condition in the elastic-plastic network and any of the available creep models in Abaqus/Standard in the elastic-viscous network. Assumes a deviatoric inelastic response (hence, the pressure-dependent plasticity or creep models cannot be used to define the behavior of the two networks). It can model material response under fluctuating loads over a wide range of temperatures.

The material behavior is broken down into three parts: elastic, plastic, and viscous. Figure 5.60 shows a one-dimensional idealization of this material model, with the elastic-plastic and the elastic-viscous networks in parallel. The following subsections describe the elastic and the inelastic (plastic and viscous) behavior in detail [Abaqus 2004].

Figure 5.60 One-dimensional idealization of the elasto-visco-plastic model.
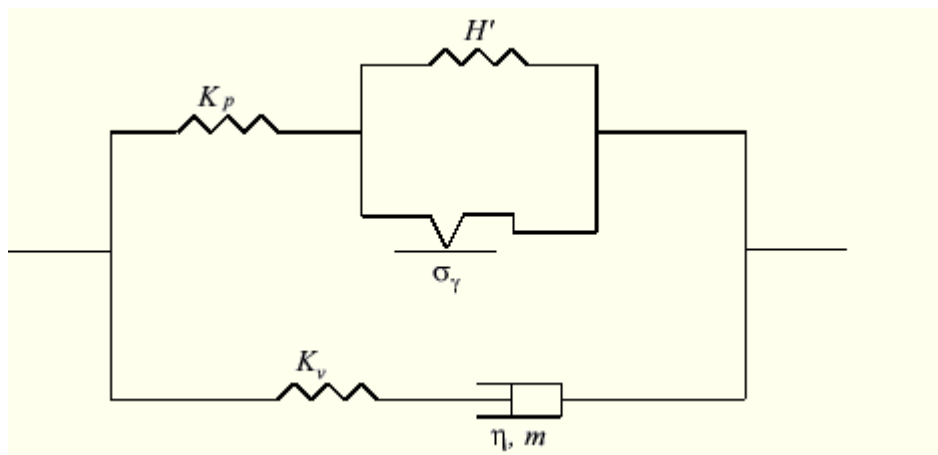
The elastic model defines the linear elastic behavior of the material and requires the elastic modulus E and Poisson's ratio v as inputs. The total stress is defined from the total elastic strain as

$$\sigma = \mathbf{D}^{el}\varepsilon^{el},$$ 5.10

Where: σ = the total stress ("true," or Cauchy stress in finite-strain problems)

$\mathbf{D}^{el}$ = is the fourth-order elasticity tensor, and

ε^{el} = is the total elastic strain (log strain in finite-strain problems).

The viscous behavior of the material can be governed by any of the available creep laws in Abaqus/Standard (rate dependent plasticity, creep and swelling). When viscous behavior is defined, the viscosity parameters are specified and a specific type of viscous behavior is chosen. For instance, the creep law is chosen, through user subroutine CREEP, only deviatoric creep should be defined, more specifically; volumetric swelling behavior should not be defined within user subroutine CREEP. In addition, you also specify the fraction, f, which defines the ratio of the elastic modulus of the elastic-viscous network (K_v) to the total (instantaneous) modulus ($K_p + K_v$); f should be a number between 0 and 1

$$f = \frac{K_v}{K_p + K_v}$$ 5.11

A plasticity definition can be used to provide the static hardening data for the material model. All available metal plasticity models in Abaqus, including Hill's plasticity model to define anisotropic yield, can be used.

5.5.1 Elasto-visco-plastic model results

Figure 5.61 shows a contour picture of vertical displacement after modeling with a moving load. The beginning of the loading has more displacement that the end of the wheel load. This is because the Abaqus visco analysis uses creep law and so it has behavior that is similar to creep. A simplified loading was then used and results from this analysis are given in Figures 5.62 to 5.72 and Tables 5.17 to 5.22 below. Table 5.17 summarizes input parameters used in this model for the six asphalt mixes.

Figure 5.61 Elasto visco plastic displacement contours modeled with a moving load
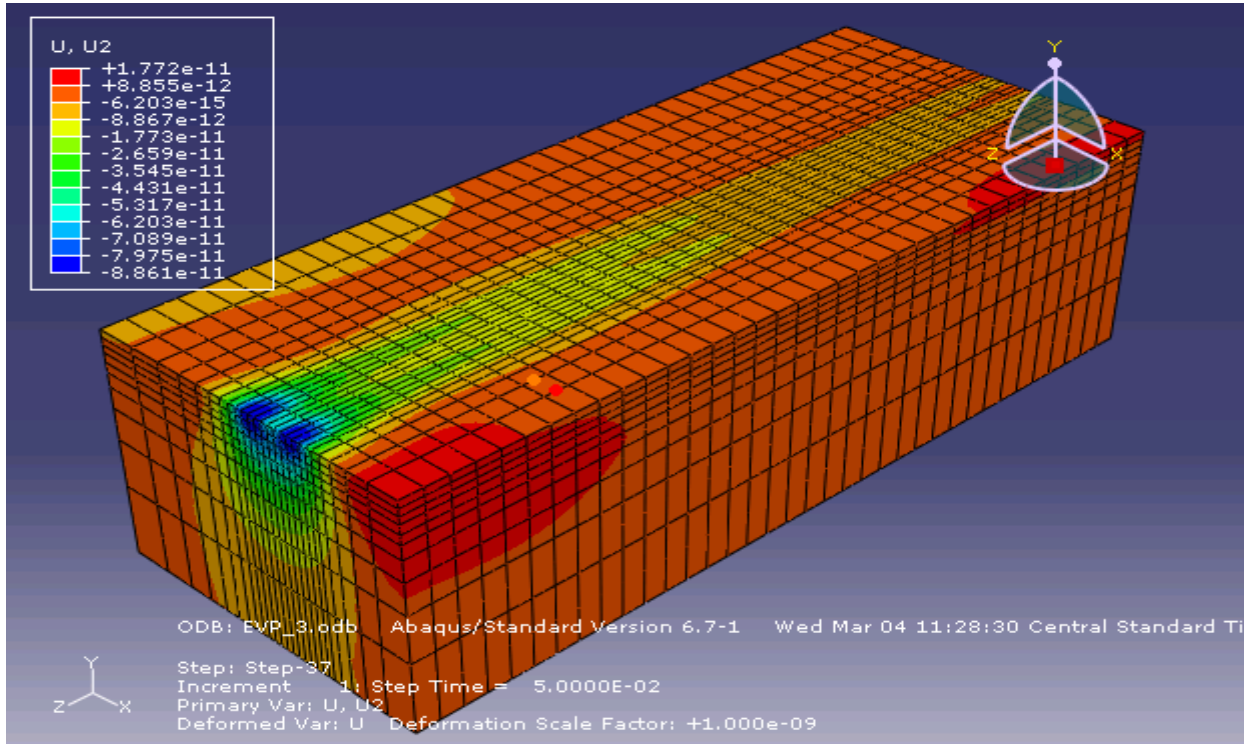
Table 5.17 Elasto-visco-plastic model parameters

Parameter	KS-1	KS-2	MO-1	MO-2	IA-1	IA-2
Asphalt Elastic Modulus (MPa)	3115	1619	2410	437	494	1869
Asphalt Poisson's Ratio	0.35	0.35	0.35	0.35	0.35	0.35
Visco analysis A	$3*10^{-6}$	$6*10^{-6}$	$6.2*10^{-6}$	$1*10^{-5}$	-	$4.5*10^{-6}$
n	0.7	0.7	0.7	1.0	-	0.6
m	-0.5	-0.5	-0.5	-0.5	-	-0.5
f	0.5	0.5	0.5	0.5	-	0.5
Plastic analysis (kPa) σ_y	1434	1145.5	2110	1439	665.7	902.45
Plastic strains γ	0.03013	0.0252	0.0254	0.0313	0.0381	0.0178
Base Resilient Modulus (MPa)	650	650	650	350	350	650
Base Poisson's ratio	0.4	0.4	0.4	0.4	0.4	0.4
Subgrade resilient modulus (MPa)	350	350	350	200	200	350
Subgrade Poisson's ratio	0.45	0.45	0.45	0.45	0.45	0.45

Six pavement sections were created and analyzed in Abaqus/CAE using elasto-visco-plastic model. This formulation was able to capture permanent deformation in a form of magnitude of vertical displacement. Figure 5.62 and Table 5.17 shows the Abaqus plot of the transverse profile for MO-1 section and values for nodal displacement obtained from Abaqus, respectively. Figures 5.63 to 5.72 and Tables 5.19 to 5.23 presents results from model implementation for the six mixes, using elasto-visco-plastic formulation.

Figure 5.62 Transverse profile of MO-1 section as plotted in Abaqus
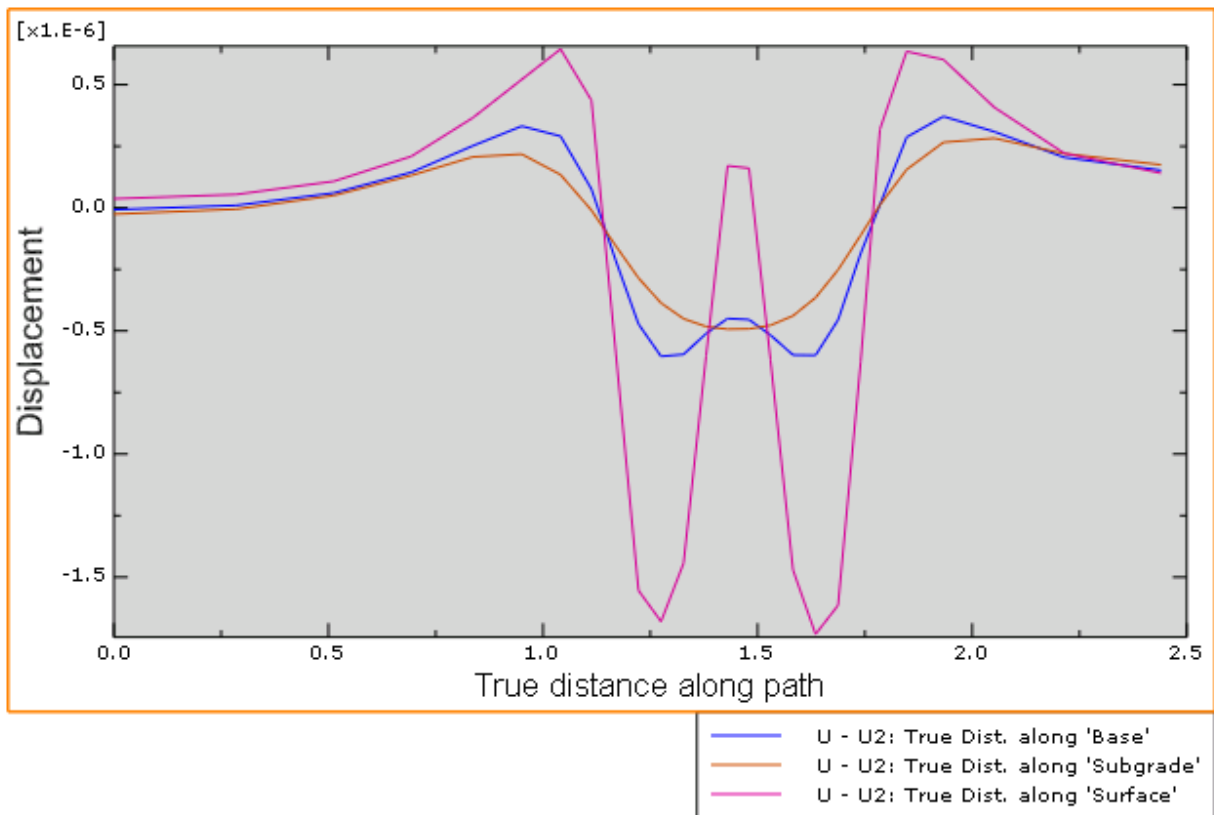
Table 5.17 Node displacement values at mid section of MO-1 Pavement section

Distance	Displacement on nodes (m)			Distance	Displacement on nodes (m)		
	Surface	Base	Subgrade		Surface	Base	Subgrade
0	3.68E-08	-7.27E-09	-2.58E-08	1.43	1.71E-07	-4.50E-07	-4.93E-07
0.285729	5.44E-08	1.01E-08	-5.29E-09	1.48	1.61E-07	-4.54E-07	-4.92E-07
0.512805	1.08E-07	6.03E-08	5.03E-08	1.53	-6.17E-07	-5.17E-07	-4.77E-07
0.693173	2.09E-07	1.44E-07	1.32E-07	1.5825	-1.47E-06	-5.98E-07	-4.38E-07
0.836523	3.66E-07	2.52E-07	2.07E-07	1.635	-1.73E-06	-5.99E-07	-3.65E-07
0.950428	5.05E-07	3.32E-07	2.18E-07	1.6875	-1.61E-06	-4.55E-07	-2.52E-07
1.04094	6.45E-07	2.91E-07	1.34E-07	1.74	-6.27E-07	-1.86E-07	-1.12E-07
1.11285	4.36E-07	7.61E-08	-9.89E-09	1.78506	3.19E-07	5.06E-08	1.20E-08
1.17	-5.97E-07	-2.17E-07	-1.56E-07	1.84724	6.35E-07	2.87E-07	1.55E-07
1.2225	-1.55E-06	-4.72E-07	-2.85E-07	1.93302	6.02E-07	3.71E-07	2.66E-07
1.275	-1.68E-06	-6.03E-07	-3.87E-07	2.05138	4.08E-07	3.09E-07	2.83E-07
1.3275	-1.44E-06	-5.95E-07	-4.50E-07	2.21468	2.21E-07	2.05E-07	2.20E-07
1.38	-6.01E-07	-5.10E-07	-4.82E-07	2.44	1.41E-07	1.53E-07	1.75E-07

Figure 5.63 Transverse profile of KS-1 section after elasto-visco-plastic model
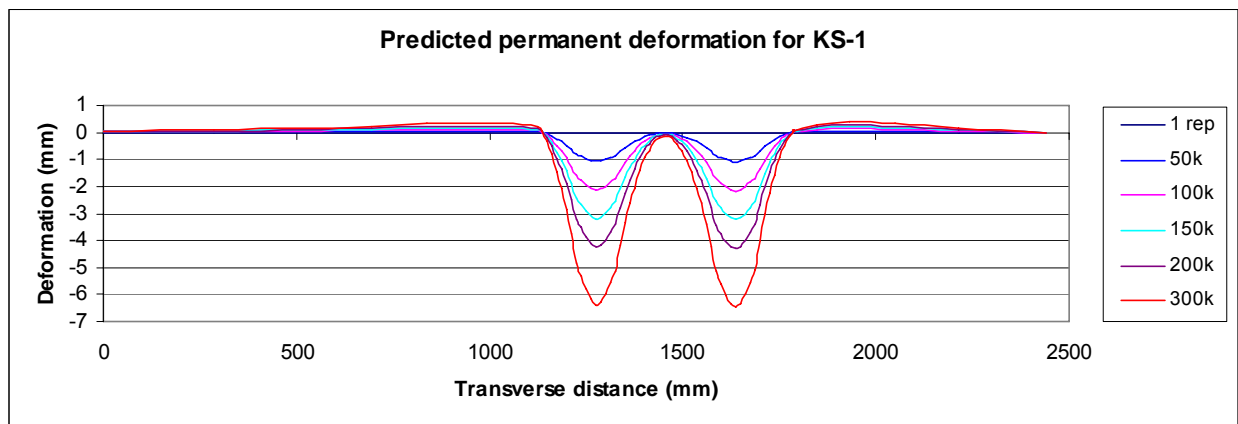
Table 5.19 Evolution of permanent deformation in KS-1 mix

Load Repetition x1000	Predicted deformation			Measured deformation		Deformation in Asphalt mix		
	mm	in	%	mm	in	mm	in	%
0	0	0	0	0	0	0	0	0
50	1.05	0.042	43.8	2.4	0.096	0.51	0.00062	21.3
100	2.11	0.0844	44.7	4.725	0.189	1	0.00121	21.2
150	3.24	0.1296	-	-	-	1.49	0.00181	-
200	4.32	0.1728	74.8	5.775	0.231	2	0.00242	34.6
300	6.23	0.2492	101.3	6.15	0.246	3	0.00364	48.8

Figure 5.64 Evolution of Transverse permanent deformation in KS-1 mix
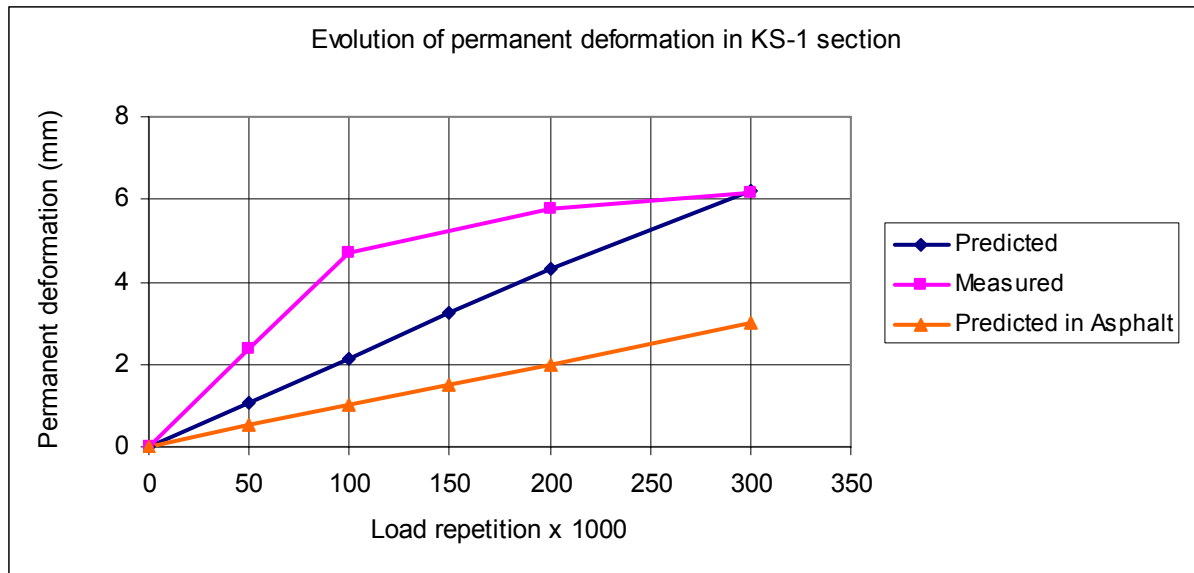
Figure 5.65 Transverse profile of KS-2 section after elasto-visco-plastic model

Predicted permanent deformation for KS-2

Legend:
- 1 rep
- 50k
- 100k
- 150k
- 200k
- 300k

X-axis: Transverse distance (mm)
Y-axis: Deformation (mm)
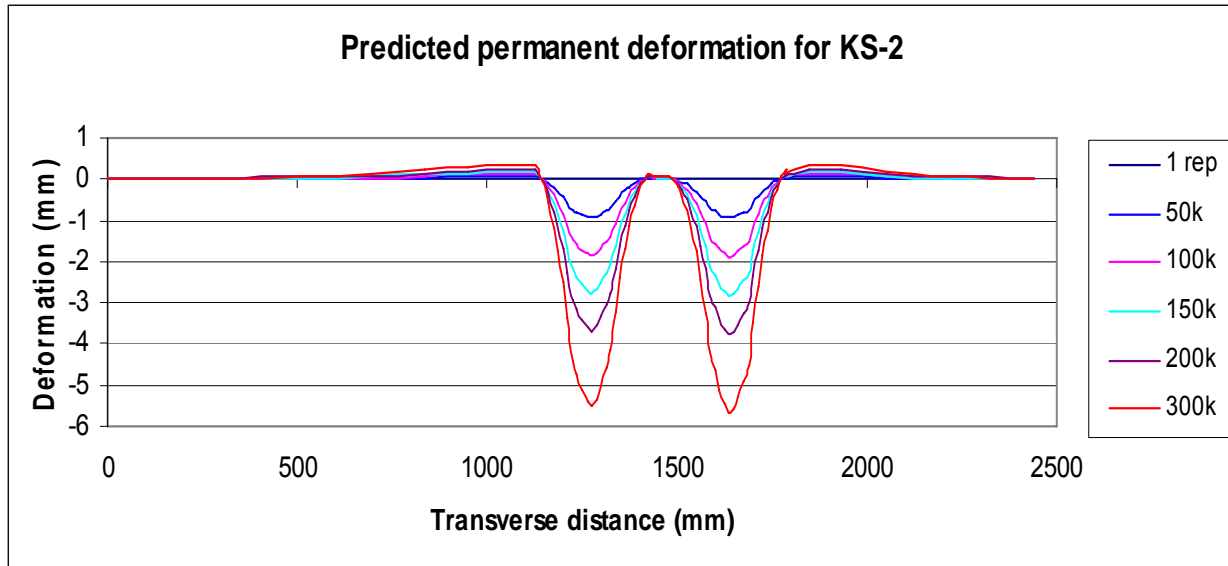
Table 5.20 Evolution of permanent deformation in KS-2 mix

Load Repetition x1000	Predicted deformation			Measured deformation		Deformation in Asphalt mix		
	mm	in	%	mm	in	mm	in	%
0	0	0	0	0	0	0	0	0
50	0.92	0.0368	49.7	1.85	0.074	0.61	0.0244	33.0
100	1.76	0.0704	32.6	5.4	0.216	1.18	0.0472	21.9
150	2.77	0.1108	-	-	-	1.77	0.0708	-
200	3.76	0.1504	70.0	5.375	0.215	2.36	0.0944	43.9
300	5.54	0.2216	107.1	5.175	0.207	3.54	0.1416	68.4

Figure 5.66 Evolution of Transverse permanent deformation in KS-2 mix

Evolution of permanent deformation in KS-2 section

Legend:
- Predicted
- Measured
- Predicted in asphalt

X-axis: Load repetition (x1000)
Y-axis: Permanent deformation (mm)
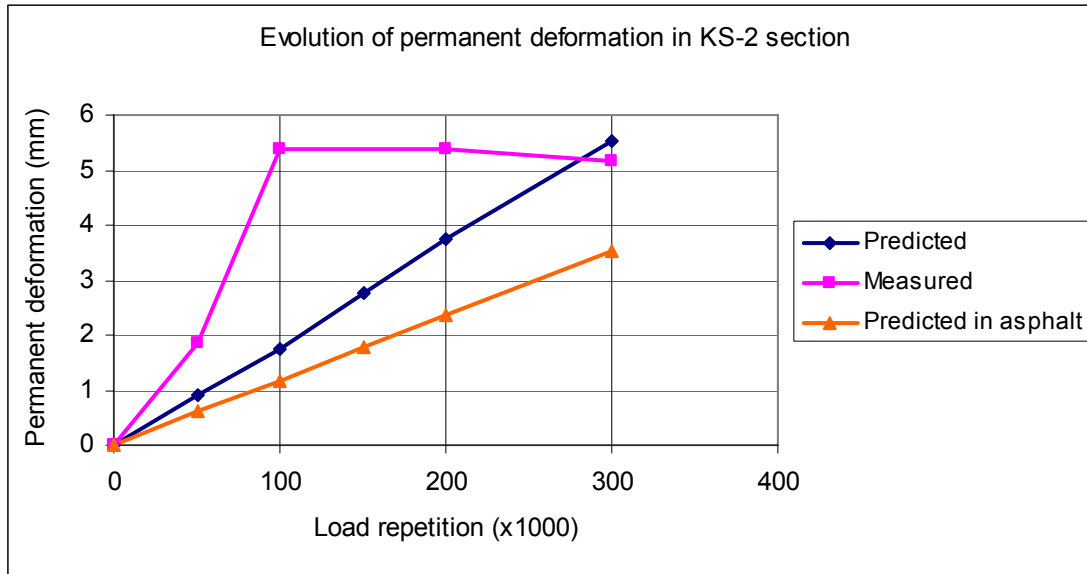
Figure 5.67 Transverse profile of MO-1 section after elasto-visco-plastic model

Predicted permanent deformation for MO-1

Legend:
- 50k
- 100k
- 150k
- 200k
- 300k
- 400k
- 500k
- 600k
- 700k

X-axis: Transverse distance (mm)
Y-axis: Deformation (mm)
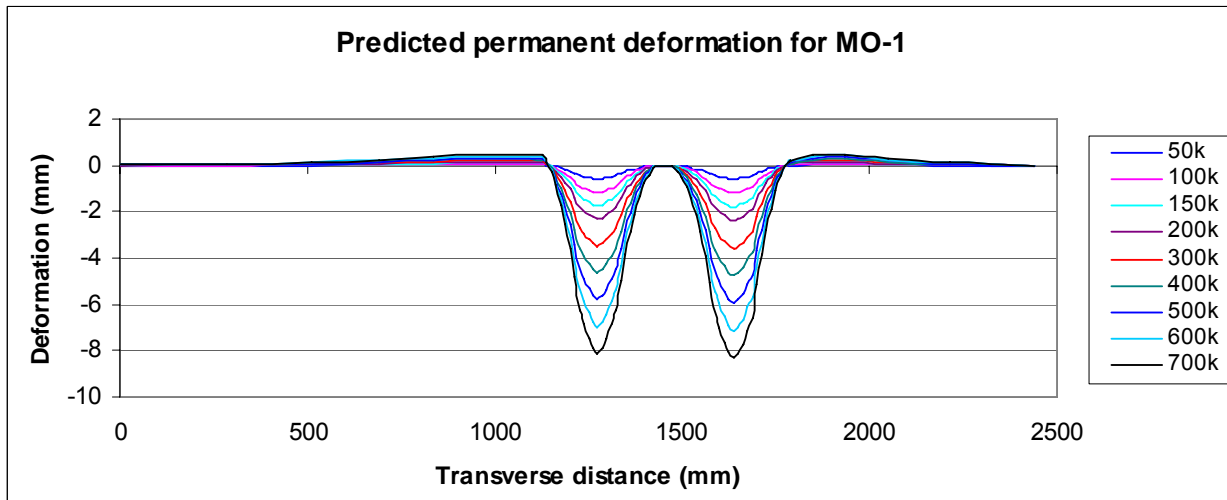
Table 5.21 Evolution of permanent deformation in MO-1 mix

Load Repetition x1000	Predicted deformation			Measured deformation		Deformation in Asphalt mix		
	mm	in	%	mm	in	mm	in	%
0	0	0	0	0	0	0	0	0
50	0.81	0.032	25.1	3.23	0.129	0.33	0.0004	10.2
100	1.16	0.046	31.8	3.65	0.146	0.65	0.0008	17.8
150	1.74	0.070	45.5	3.83	0.153	1.01	0.0012	26.4
200	2.32	0.093	60.3	3.85	0.154	1.34	0.0016	34.8
300	3.49	0.140	65.5	5.33	0.213	1.96	0.0024	36.8
400	4.65	0.186	86.1	5.40	0.216	2.62	0.0032	48.5
500	5.81	0.232	100.2	5.80	0.232	3.42	0.0041	59.0
600	6.97	0.279	117.6	5.93	0.237	4.12	0.0050	69.5
700	8.31	0.332	130.4	6.38	0.255	4.69	0.0057	73.6

Figure 5.68 Evolution of Transverse permanent deformation in MO-1 mix
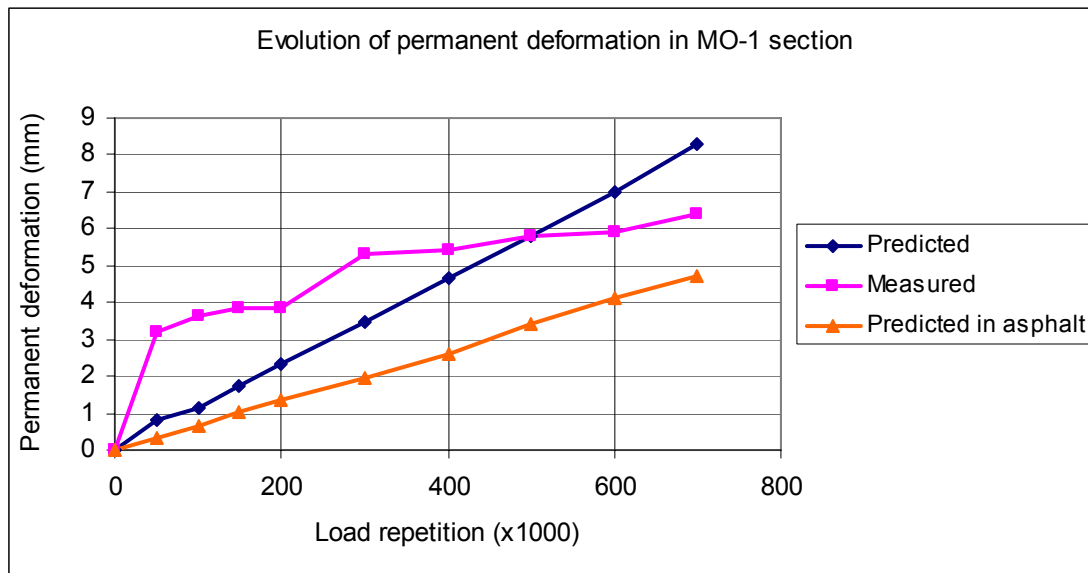
Figure 5.69 Transverse profile of MO-2 section after elasto-visco-plastic model
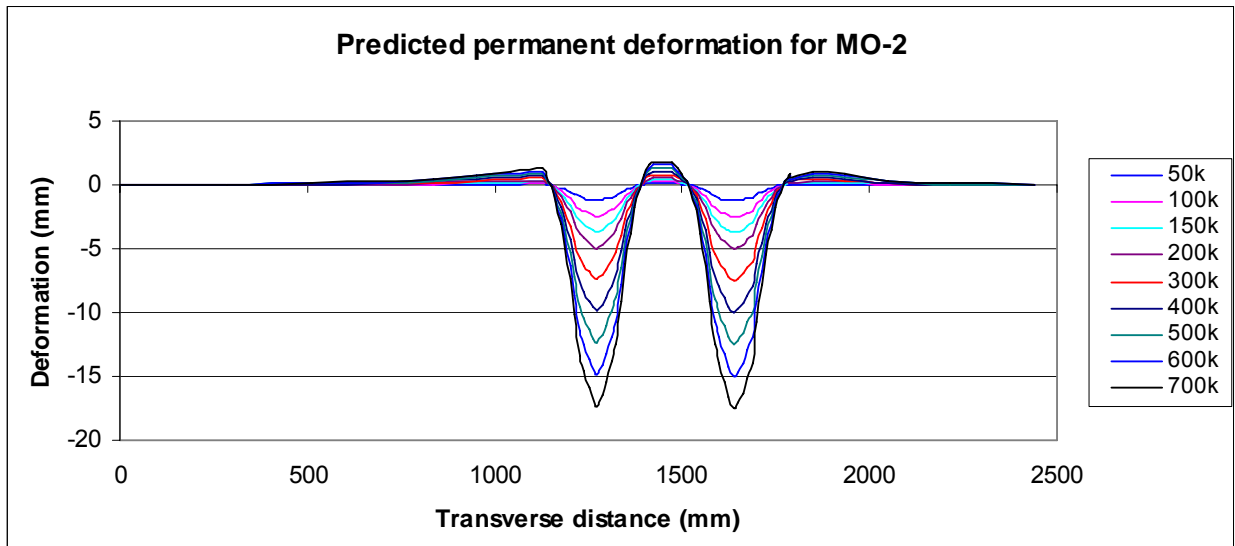
Table 5.22 Evolution of permanent deformation in MO-2 mix

Load Repetition x1000	Predicted deformation			Measured deformation		Deformation in Asphalt mix		
	mm	in	%	mm	in	mm	in	%
0	0	0	0	0	0	0	0	0
50	1.22	0.0488	24.4	5	0.2	1.08	0.0432	21.6
100	2.44	0.0976	30.5	8	0.32	2.16	0.0864	27.0
150	3.66	0.1464	40.9	8.95	0.358	3.25	0.13	36.3
200	4.88	0.1952	50.2	9.725	0.389	4.41	0.1764	45.3
300	7.32	0.2928	63.0	11.625	0.465	6.49	0.2596	55.8
400	9.76	0.3904	79.2	12.325	0.493	8.66	0.3464	70.3
500	12.2	0.488	87.8	13.9	0.556	10.8	0.432	77.7
600	14.6	0.584	103.4	14.125	0.565	13.0	0.548	92.0
700	17.4	0.696	119.0	14.625	0.585	15.4	0.616	105.3

Figure 5.70 Evolution of Transverse permanent deformation in MO-2 mix

Evolution of permanent deformation in MO-2 section
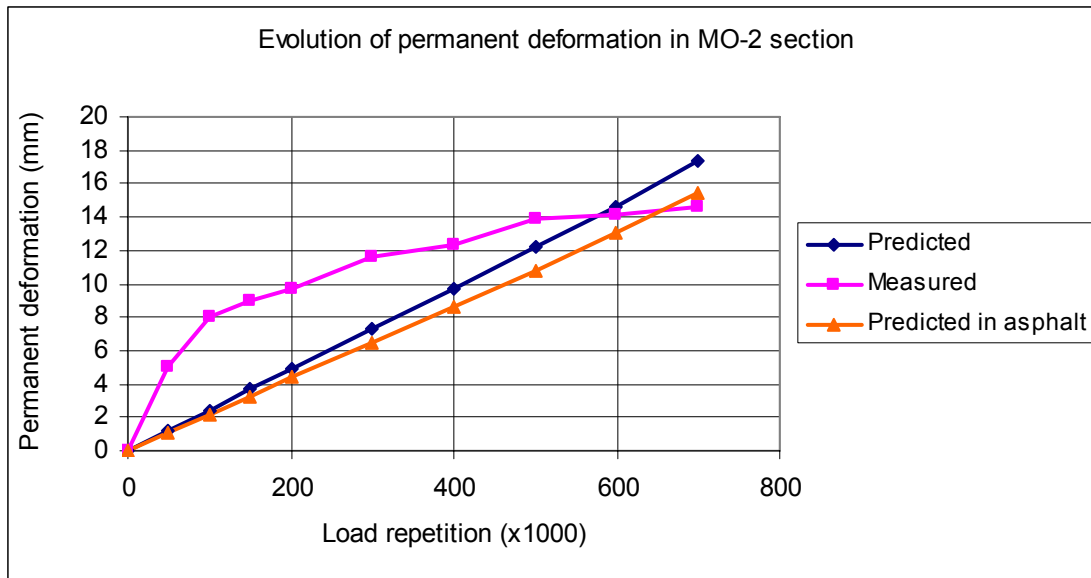
Permanent deformation for IA-1 mix could not be easily obtained using this model. The values obtained for permanent deformation are too high, this could be due to low yield strength and high values of plastic strain as compared to other mixes. This mix was constructed with higher binder content than the optimum binder content required, that is the reason why it is weaker when compared to the other mixes.

Figure 5.71 Transverse profile of IA-2 section after elasto-visco-plastic model

Predicted permanent deformation for IA-2
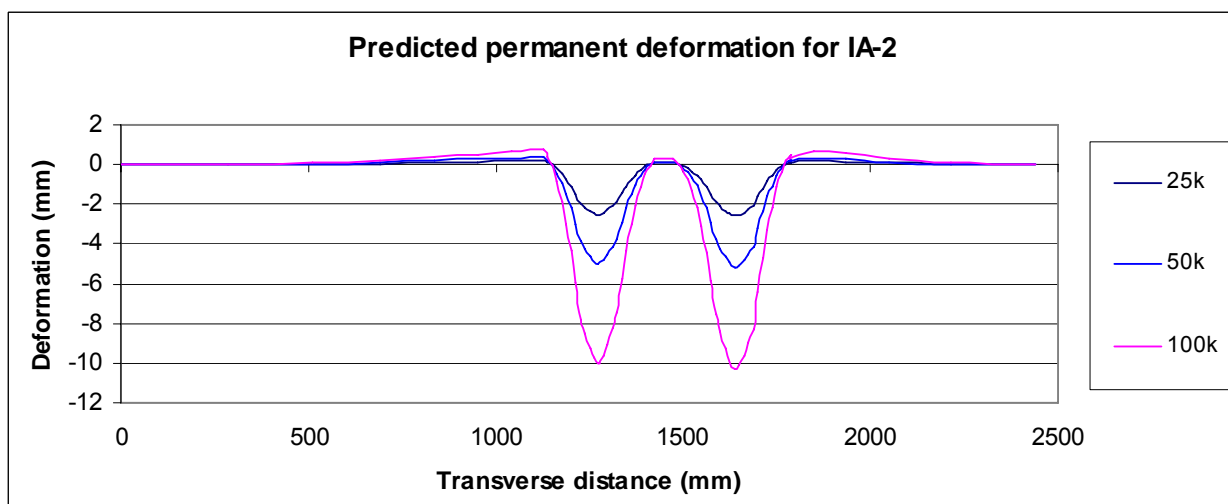
Table 5.23 Evolution of permanent deformation in IA-2 mix

Load Repetition x1000	Predicted deformation			Measured deformation		Deformation in Asphalt mix		
	mm	in	%	mm	in	mm	in	%
0	0	0	0	0	0	0	0	0
25	2.42	0.0968	28.4	8.525	0.341	1.66	0.0664	19.5
50	5.06	0.2024	55.9	9.05	0.362	3.31	0.1324	36.6
100	10.1	0.404	85.2	11.85	0.474	6.62	0.2648	55.9

Table 5.72 Evolution of permanent deformation in IA-2 mix
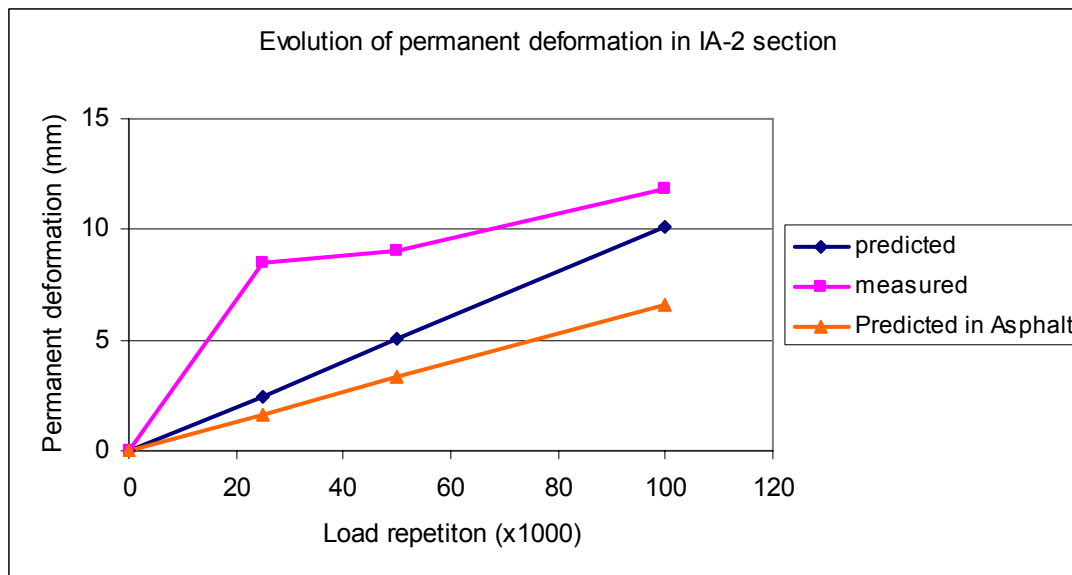
From the results, the elasto-visco-plastic model predicts maximum permanent deformation values that are close to measured values. The percent of predicted values at failure load ranges from 82% to 130% having some values as close as 101.3% of the measured values. The permanent deformation predicted in asphalt mixes is 48.8 % of the measured value for KS-1 mix, 68.4% for KS-2, 73.6% for MO-1, 105.3 for MO-2, and 55.9% for IA-2 mix. IA-1 mix was not modeled using this model due to difficult in obtaining model parameters.

CHAPTER 6 - EVALUATION OF PERMANENT DEFORMATION MODELS

This research project was conducted to evaluate mechanistic prediction models using Abaqus/CAE commercial software. Four models; creep, Drucker-Prager, viscoelastic and elasto-visco-plastic were evaluated as detailed in Chapter 5. Material input parameters for each model were obtained from laboratory tests explained in Chapters 3 and 4. To evaluate the models measured permanent deformation from accelerated pavement testing in CISL 14 project were used as field data. Using Abaqus/CAE, vertical displacements on pavement transverse sections were obtained after a single wheel load pass. The displacements obtained were then projected by multiplying with number of repeated wheel loads. The lateral wheel wonder was implemented by using the percentage of lateral wheel load distribution as it is applied in CISL at Kansas State University. A linear model was used to project the evolution of permanent deformation.

In the Civil and Infrastructure Systems Laboratory (CISL) at Kansas State University, six pavement sections were constructed and tested from December of 2005 to December 2008. The pavement sections were loaded with a full scale single axle of 22,000 lb with up to 700,000 load repetitions. Transverse profiles were measured periodically while testing each of the pavement section. Figures 6.1 to 6.3 shows the transverse profile measured at different numbers of load repetitions, while testing Kansas, Missouri and Iowa mixes. Table 6.1 to Table 6.3 shows the evolution of permanent deformation as measured in CISL for each asphalt mix, at different numbers of load repetition. Figure 6.4 is a plot that shows the evolution of permanent deformation obtained using accelerated testing for the six mixes. In this chapter the four models will be evaluated with respect to their ability to predict permanent deformation in asphalt mixes.

Figure 6.1 Transverse Profile - KS Mix (Middle East- 5 ft from the right end)
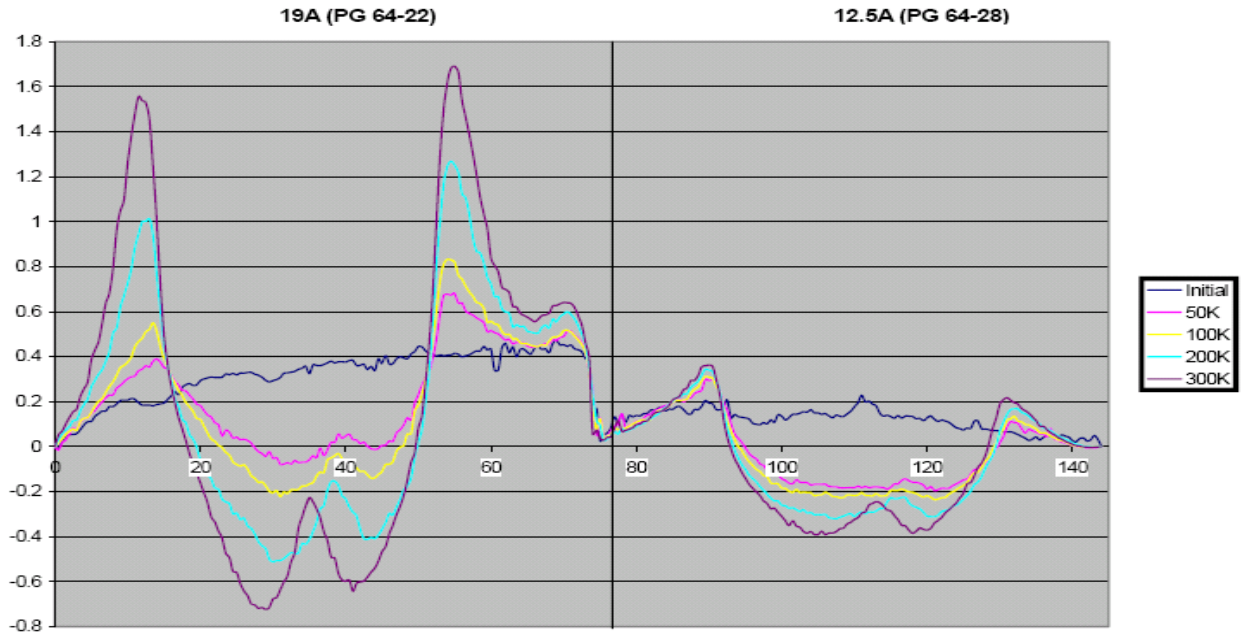
Note: Rut depth is in inches

Figure 6.2 Transverse Profile - MO Mix (Middle East- 5 ft from right end)
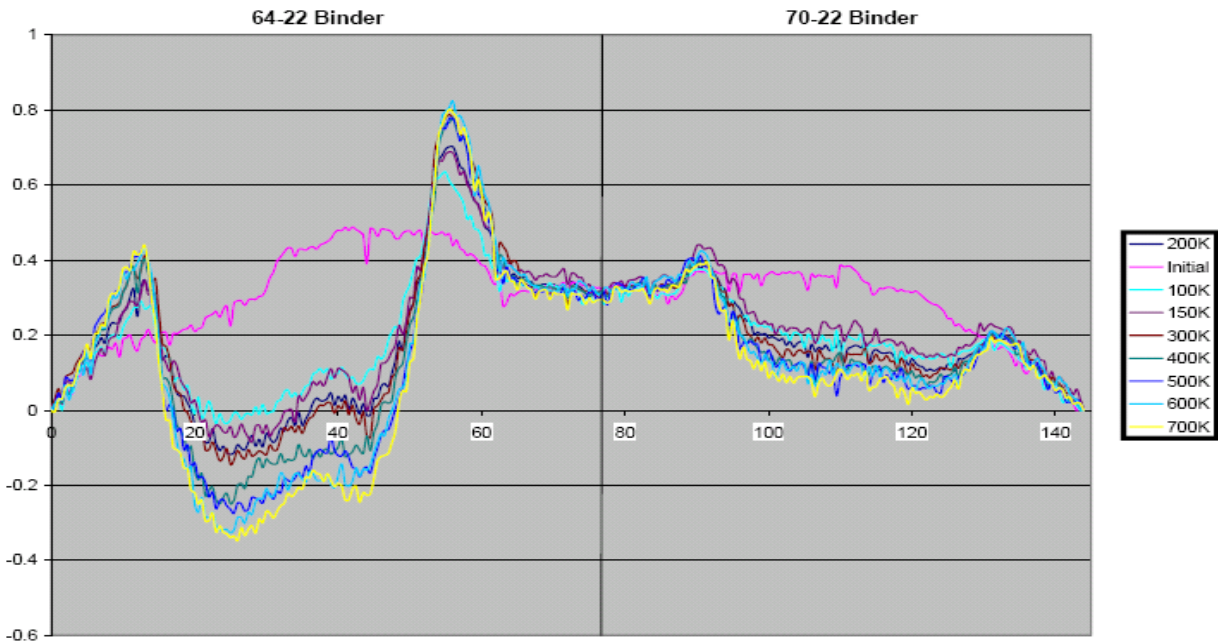
Note: Rut depth is in inches

Figure 6.3 Transverse Profile - IA Mix (Middle East- 5 ft from right end)

Transverse Profile - Middle Pit West
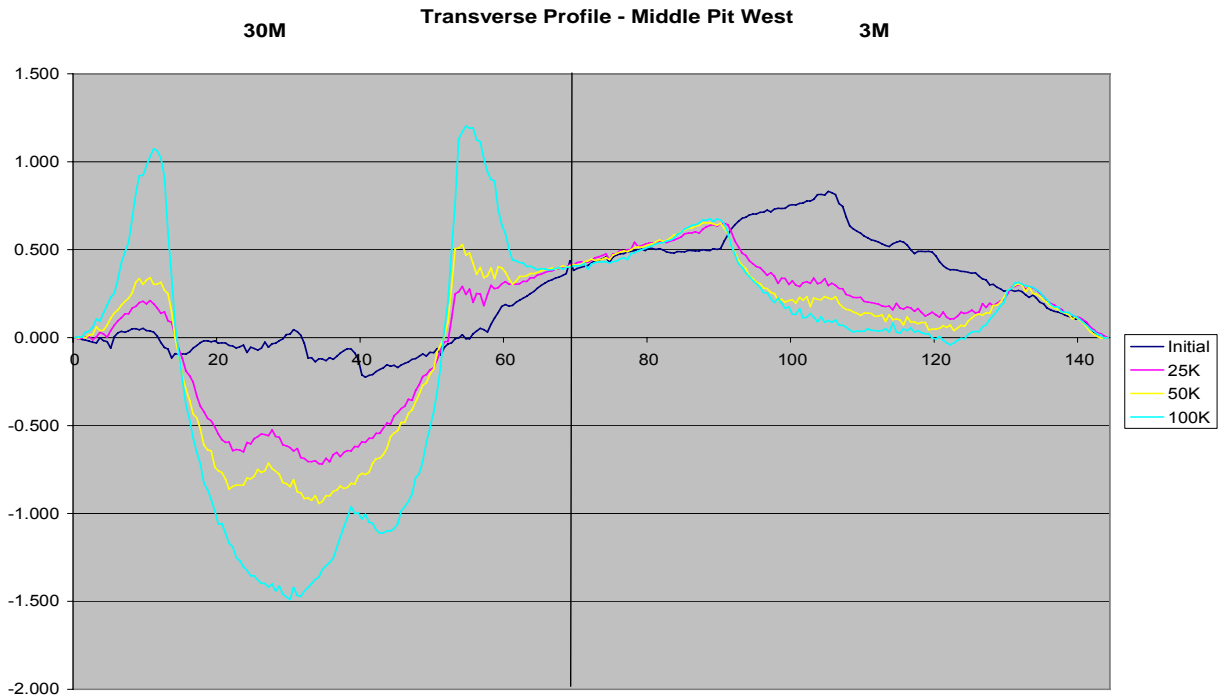
Table 6.1 Evolution of permanent deformation in Kansas mixes (in)

Date	Passes (x1,000)	KS-1				KS-2			
		East	Middle	West	Average	East	Middle	West	Average
1/26/2006	0	0	0	0	0	0	0	0	0
5/23/2006	50	0.095	0.116	0.077	0.096	0.045	0.104	0.072	0.074
5/30/2006	100	0.215	0.188	0.165	0.189	0.221	0.219	0.208	0.216
6/7/2006	200	0.09	0.414	0.191	0.231	0.125	0.339	0.18	0.215
6/19/2006	300	0.285	0.259	0.195	0.246	0.232	0.221	0.168	0.207

Table 6.2 Evolution of permanent deformation in Missouri mixes (in)

Date	Passes (x1,000)	MO-1				MO-2			
		East	Middle	West	Average	East	Middle	West	Average
1/23/2007	0	0	0	0	0	0	0	0	0
6/27/2007	50	0.142	0.119	0.14	0.137	0.268	0.216	0.297	0.260
7/16/2007	100	0.172	0.129	0.136	0.146	0.362	0.269	0.328	0.32
7/20/2007	150	0.153	0.152	0.155	0.153	0.38	0.296	0.399	0.358
7/24/2007	200	0.176	0.16	0.126	0.154	0.411	0.324	0.431	0.389
7/31/2007	300	0.246	0.189	0.206	0.213	0.465	0.418	0.512	0.465
8/10/2007	400	0.218	0.207	0.223	0.216	0.51	0.437	0.533	0.493
8/21/2007	500	0.231	0.22	0.246	0.232	0.57	0.498	0.602	0.556
8/31/2007	600	0.241	0.228	0.242	0.237	0.557	0.541	0.596	0.565
9/13/2007	700	0.264	0.245	0.255	0.255	0.618	0.517	0.618	0.585

Table 6.3 Evolution of permanent deformation in Iowa mixes (in)

Date	Passes (x1,000)	IA-1				IA-2			
		East	Middle	West	Average	East	Middle	West	Average
6/3/2008	0	0	0	0	0	0	0	0	0
6/12/2008	25	0.599	0.589	0.571	0.586	0.338	0.353	0.332	0.341
6/20/2008	50	0.792	0.771	0.737	0.767	0.402	0.385	0.298	0.362
7/1/2008	100	1.384	1.182	1.163	1.243	0.489	0.472	0.461	0.474

Table 6.4 Comparizon of permanent defomation at 100,000 and 300,000 load repetitions

Sample ID	No of passes x1000	Permanent Deformation (in)	Rank	No of passes x1000	Permanent Deformation (in)	Rank
KS-1	100	0.189	2	300	0.246	3
KS-2	100	0.216	3	300	0.207	1
MO-1	100	0.146	1	300	0.213	2
MO-2	100	0.32	4	300	0.465	4
IA-1	100	1.243	6	300	-	
AI-2	100	0.474	5	300	-	

Figure 6.4 Evolution permanent deformation in CISL 14 sections
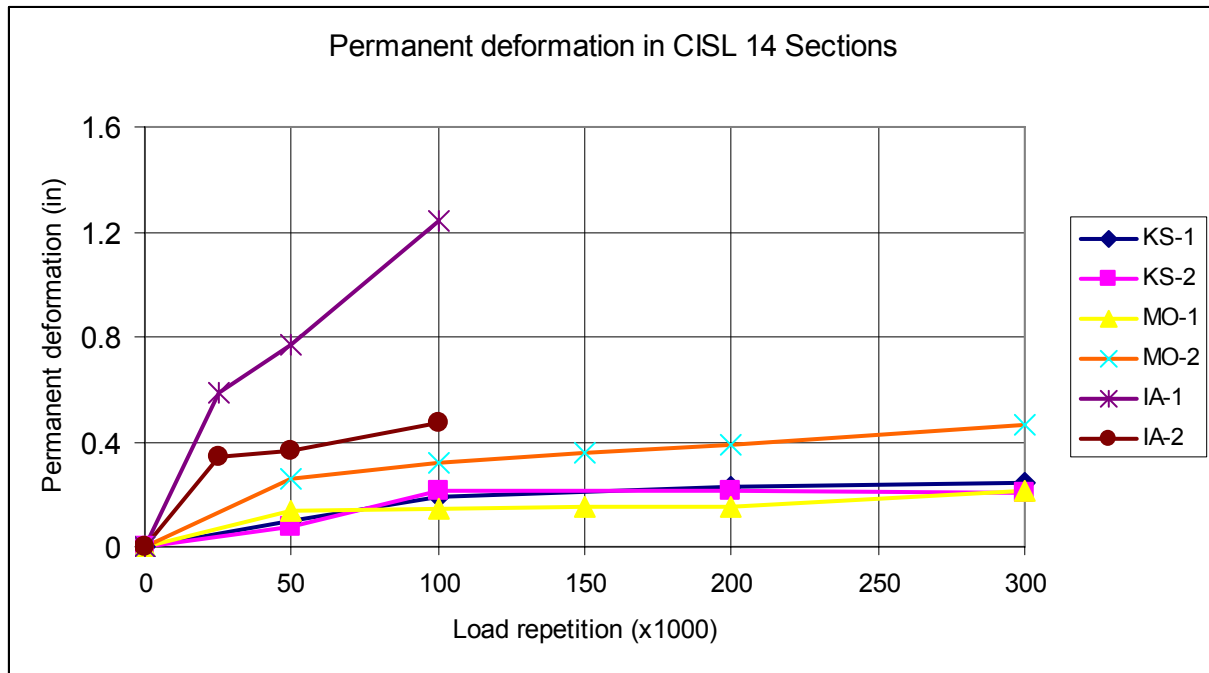
Table 6.4 and Figure 6.4 shows that the values of measured permanent deformation in CISL 14 project. KS-1, KS-2 and MO-1 had very close measured values. At 100,000 load repetitions, MO-1 had the least permanent deformation followed by KS-1, KS-2, MO-1, IA-1 and IA-1. MO-2 and KS-2 show a steady and small increase in permanent deformation with increase in load repetition.

6.1 Repeated Load Tests

For evaluation of the models CISL 14 results were used. Other repeated load test results were also used to compare the performance of asphalt mixes in this research project. These tests are Hamburg Wheel Tester, Asphalt Pavement Analyzer and Repetitive Shear at Constant Height (RSCH). Table 6.5 and Figure 6.5 presents the results of Hamburg Wheel Tester, tested at 35°C, up to 20,000 wheel passes. From this test, MO-1 had a better performance followed by MO-2, KS-2, KS-1, IA-2 and IA-1. The value of permanent deformation ranges from 3.47 mm to 5.31mm for five mixes, and IA-1 had a deformation of 10.15mm.

Table 6.5 Results summary from the Hamburg Wheel Tester

Sample ID	Mix type	Binder Grade	Air Voids (%)	Max. No. of passes	Max. Depth (mm)	Rank
KS-1	SM 19A	PG 64-22	6.14	20,000	4.69	4
KS-2	SM 12.5A	PG 64-28	5.8	20,000	4.21	3
MO-1	M 12.5	PG 70-22	7.63	20,000	3.47	1
MO-2	M 12.5	PG 64-22	7.86	20,000	3.96	2
IA-1	12.5	PG 64-22	9.02	20,000	10.15	6
IA-2	12.5	PG 64-22	8.16	20,000	5.31	5

Figure 6.5 Comparizon of rutting of the six mixes using the Hamburg Wheel Tester

226
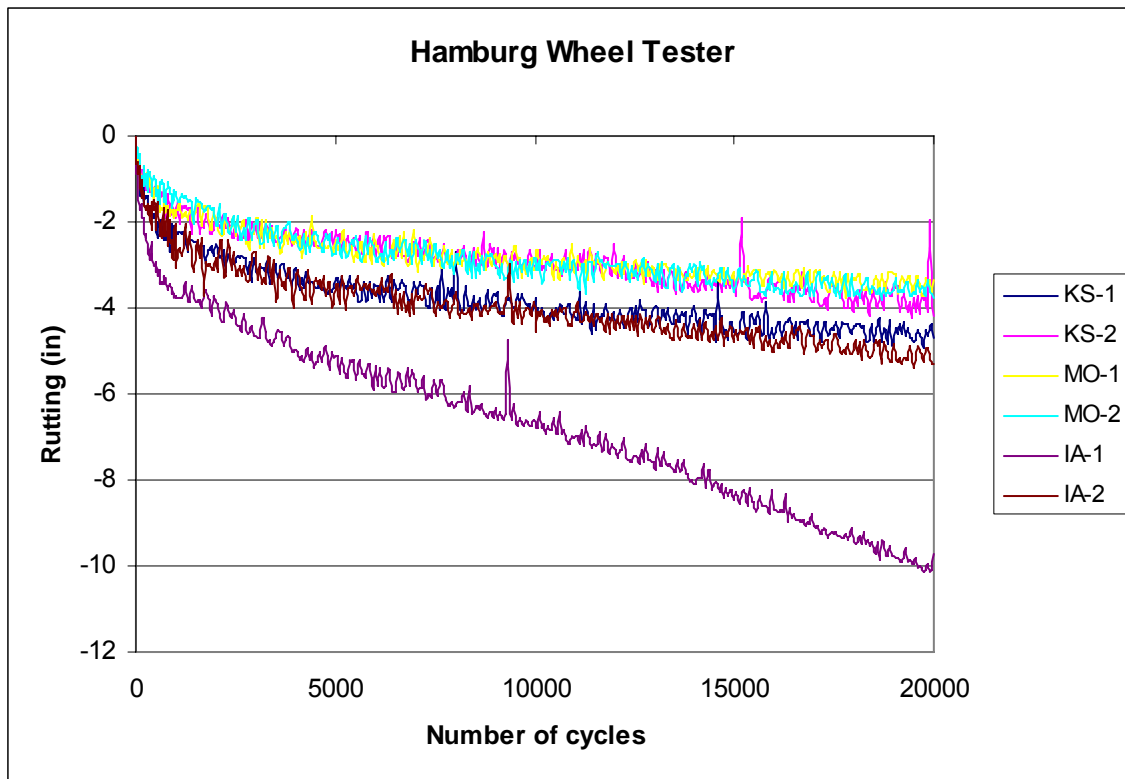
The Asphalt Pavement Analyzer (APA) was conducted to evaluate the performance of asphalt mixes against rutting. The specimens were loaded with up to 8,000 load repetitions and the maximum rut depth was recorded and presented in Table 6.6.

Table 6.6 Results summary from the APA test

Tests Temp (°C)	Sample ID	Mix type	Binder Grade	Air Voids (%)	Max. No. of passes	Max. Depth (mm)	Rank
	KS-1	SM 19A	PG 64-22	6.16	8,000	1.08	1
	KS-2	SM 12.5 A	PG 64-28	6.58	8,000	1.59	2
35	MO-1	M 12.5	PG 70-22	9.69	8,000	1.71	3
	MO-2	M 12.5	PG 64-22	7.27	8,000	2.15	4
	IA-1	12.5	PG 64-22	9.14	8,000	2.27	5
	IA-2	12.5	PG 64-22	7.71	8,000	3.18	6

From Table 6.6, the rut depth measured for the mixes ranged from 1.08 mm to 3.18 mm. In this test all the mixes performed well at 35°C. KS-1 was the best mix followed by KS-2, MO-1, MO-3, IA-1 and IA-2, in that order.

The repetitive shear at constant height (RSCH) test was performed to obtain permanent strains after 5,000 cycles. This test was conducted with up to 50,000 load cycles and results summary is presented in Table 6.7 and Figure 6.6 shows increase of permanent strains with increase in load repetitions. At 5,000 cycles all the mixes performed well with permanent deformation ranging from 0.0156 in to 0.0652 in. At 50.000 cycles, five mixes performed well except for IA-1 which had a permanent deformation value of 11% permanent strains.

Table 6.7 Results summary from the FSCH test

Mix ID		KS-1	KS-2	MO-1	MO-2	IA-1	IA-2
	5,000	0.0156	0.0652	0.03	0.0388	0.0644	0.042
g_{perm} **(in)**	Rank	1	6	2	3	5	4
@ cycles	50,000	0.0312	0.0972	0.0676	0.066	-	0.08
	Rank	1	5	3	2	6	4

Figure 6.6 A plot of permanent deformation against load cycles during the FSCH test
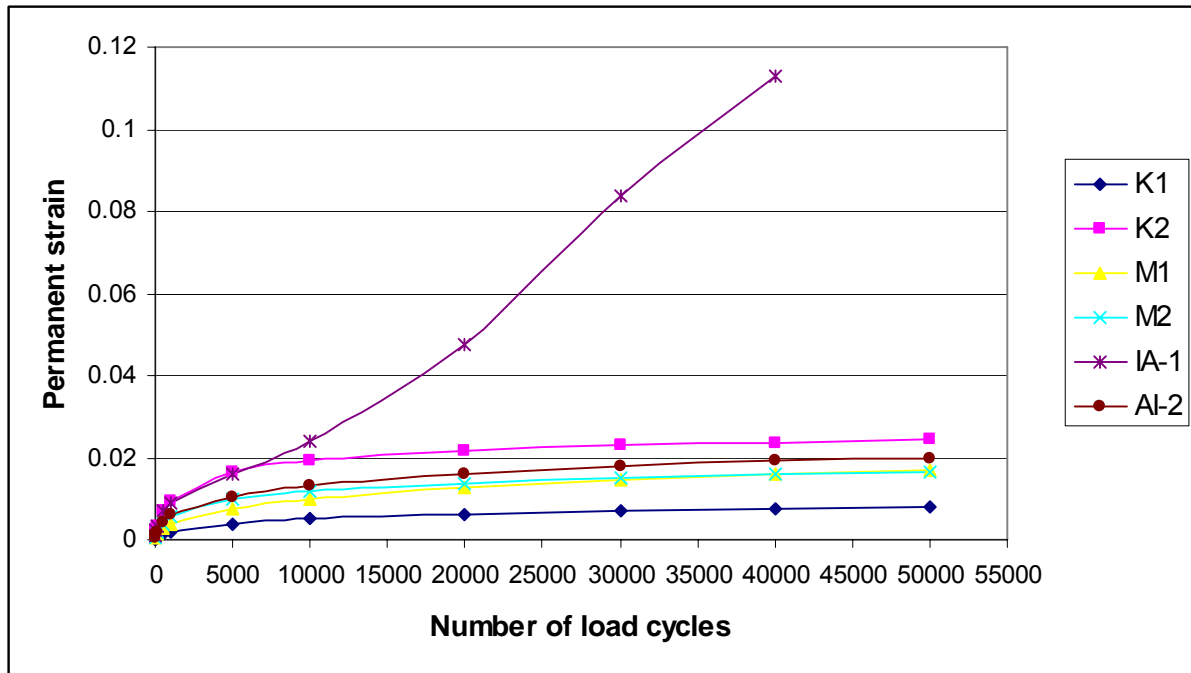
A summary of performance ranking of each test is presented in Table 6.8. For CISL 14, a comparison of permanent deformation at 100,000 load repetitions was used because AI mixes were tested with up to 100,000 load repetitions. For the FSCH test 50,000 repetitions were used for comparisons and ranking. The performance of asphalt mixes varies with a test procedure. For these mixes MO-1 performed better on CSIL 14 and Hamburg Wheel Tester and KS-1 performed better on the APA and FSCH tests.

Table 6.8 Performance ranking of each of the mix for four tests.

Mix ID	Repeated load tests performed			
	CISL 14	Hamburg	APA	FSCH
KS-1	2	4	1	1
KS-2	3	3	2	5
MO-1	1	1	3	3
MO-2	4	2	4	2
IA-1	6	6	5	6
IA-2	5	5	6	4

6.2 Models Evaluation

Permanent deformation prediction models implementation in chapter 5 show that the viscoelastic model could not capture permanent deformation, the displacements measured were too small (2*E-11 mm), which can be considered negligible. This model was run on one mix only KS-1. Due to small displacement obtained the model was not run on other asphalt mixtures. The Drucker-Prager model over-predicted permanent deformation and could not develop transverse profiles that are consistent and similar to measured transverse profile. This could be resulted from the model's disability to capture damage in asphalt mix, since asphalt mix was tested at $35^{o}C$. Two models, the creep and elasto-visco-plastic, were able to capture permanent deformation in asphalt mixes. A linear formulation was used to predict the evolution of permanent deformation in asphalt mixtures. This makes the models predict more permanent deformation with increase in number of wheel load repetition. A different model, which is nonlinear, could be used to predict permanent deformation. The prediction needs to have more permanent deformation measured at the beginning of load repetitions and deformation decreases with increase in load repetitions. With these modifications, two models, creep and elasto-visco-plastic could be used to predict permanent deformation in asphalt mixtures. Figures 6.7 to Figure 6.12 show the comparisons of total permanent deformation obtained for each mix for Drucker-Prager, creep and elasto-visco-plastic models, and measured values (CISL 14).

Figure 6.7 Models comparison on Kansas KS-1 mix
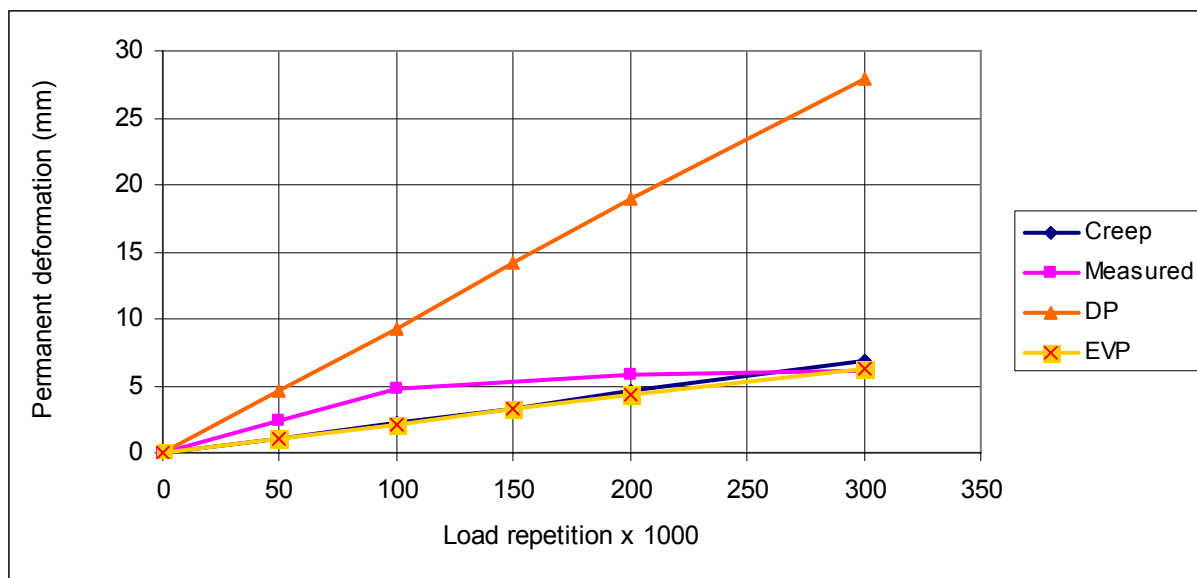
Figure 6.8 Models comparison on Kansas KS-2 mix
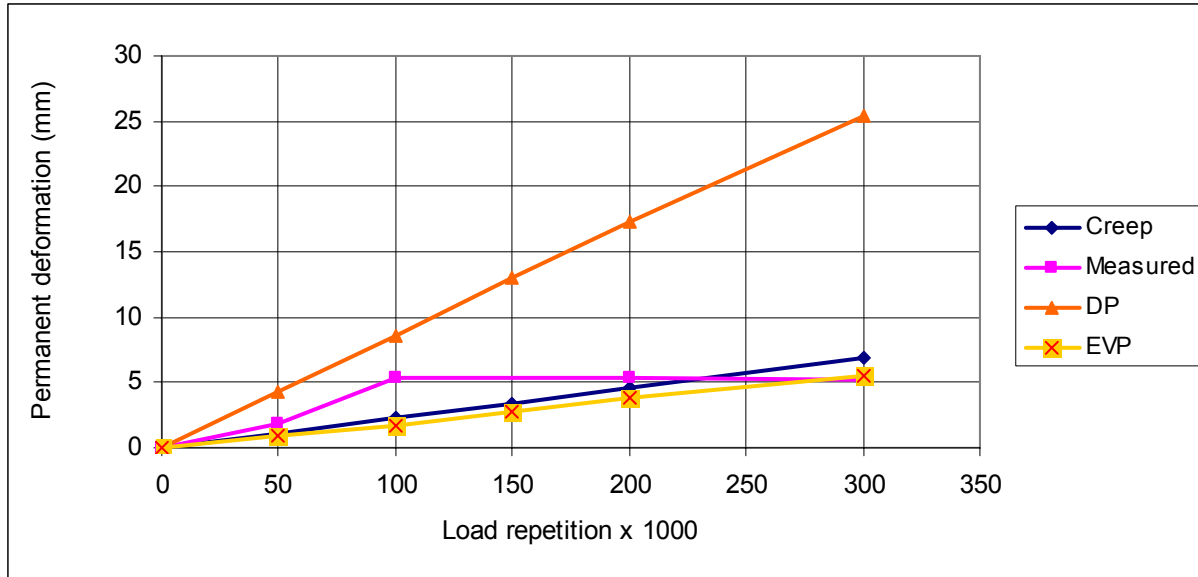
Figure 6.9 Models comparison on Missouri MO-1 mix
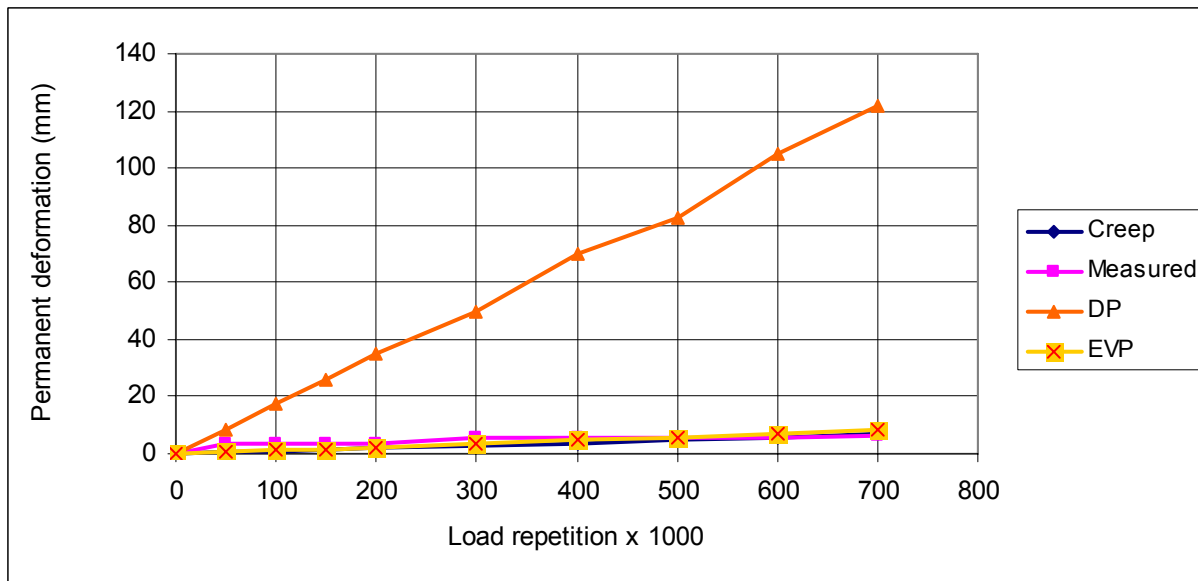
Figure 6.10 Models comparison on Missouri MO-2 mix
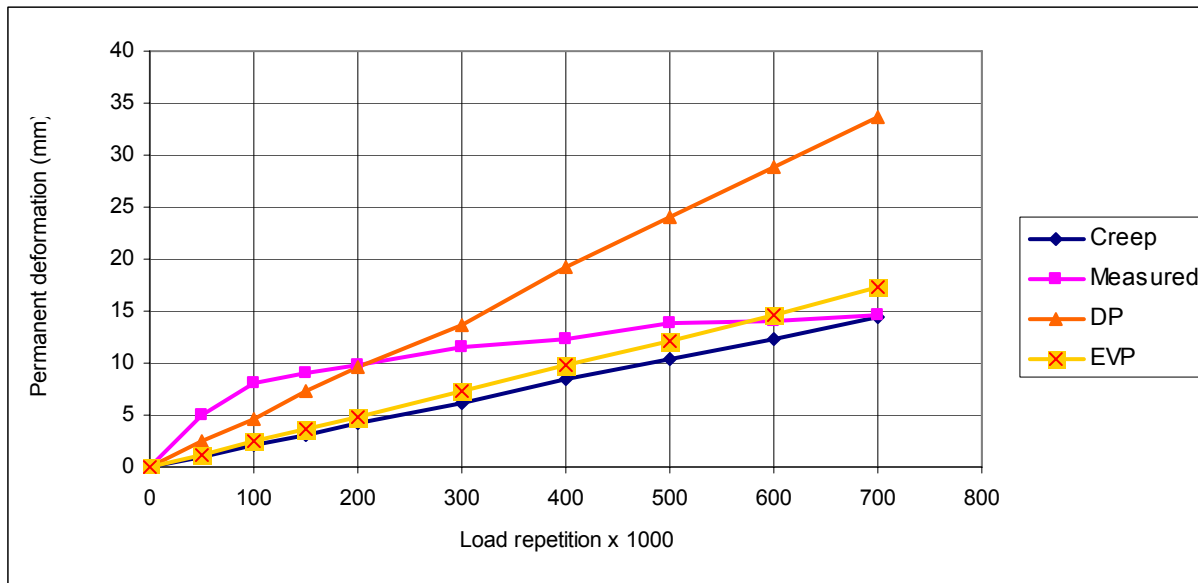
Figure 6.11 Models comparison For Iowa IA-2 mix
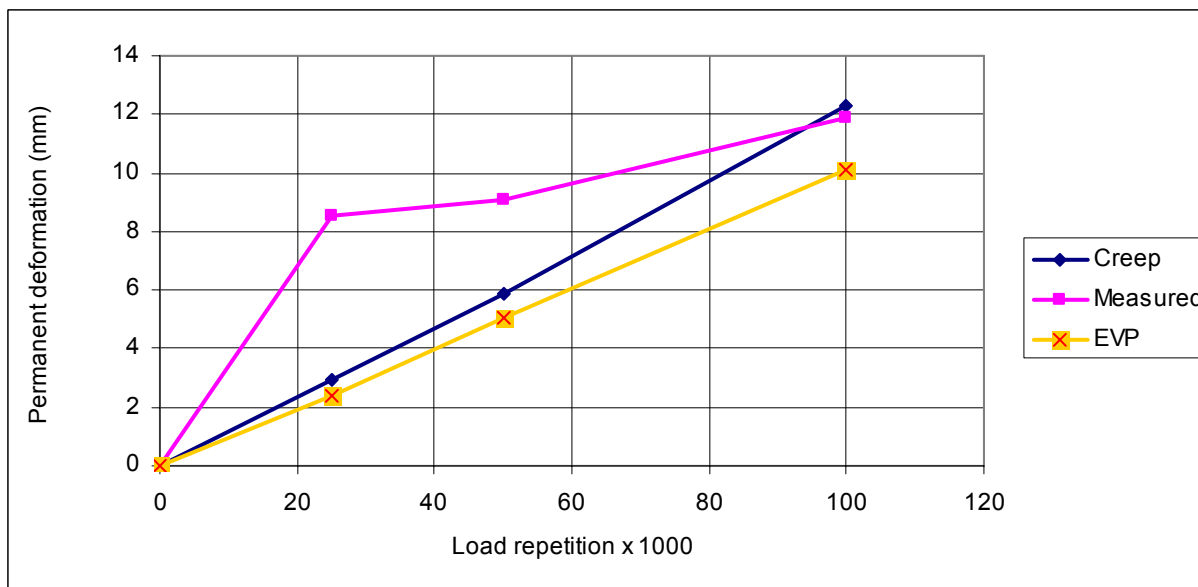
Modeling IA mixes using DP model was very challenging. IA-2 had a permanent deformation of 307mm using Drucker-Prager model and IA-1 could not be modeled, it had unrealistically high permanent deformation values, this is why Figure 6.10 does not include the permanent deformation predicted using Drucker-Prager model.

Two models were found to possess a potential to predict permanent deformation, these are creep and elasto-visco-plastic. Using these models, the predicted permanent deformation of the six mixes were compared for each model. Table 6.9 shows the ranking of the models using total predicted permanent deformation in the six mixes after modeling with creep and elasto-visco-plastic models in Abaqus. Table 6.10 provides the percentage of permanent deformation that occurred in asphalt mix only for each mix. Figure 6.12 and Figure 6.13 shows plots of total permanent deformation predicted using creep and elasto-visco-plastic models respectively, and Figures 6.14 and 6.15 present permanent deformations in asphalt mix only.

Table 6.9 Performance ranking of each of the mix for the two prediction models

	Elasto-visco-plastic model				Creep model		
Mix ID	No of rep. (x1,000)	Permanent deformation (mm)	Rank	Mix ID	No of rep. (x1,000)	Permanent deformation (mm)	Rank
KS-1	300	6.23	3	KS-1	300	6.84	4
KS-2	300	5.54	2	KS-2	300	5.79	2
MO-1	300	3.49	1	MO-1	300	2.81	1
MO-2	300	7.32	4	MO-2	300	6.17	3
IA-1	100	-		IA-1	100	32.26	6
IA-2	100	10.1	5	IA-2	100	12.3	5

Both prediction models indicated that Missouri mix MO-1 had the best performance followed by Kansas KS-2. Kansas KS-1 and Missouri MO-2 are third and fourth and Iowa IA-1 is the poorest mix of the six. This can be seen from all the tests as well as the prediction models. Compared to measured values in CISL, MO-1 is the best mix followed by KS-1, KS-2, MO-1, IA-2, and lastly IA-1. Also, the difference in deformation values is small.

Figure 6.12 Models comparison for all mixes after the creep model
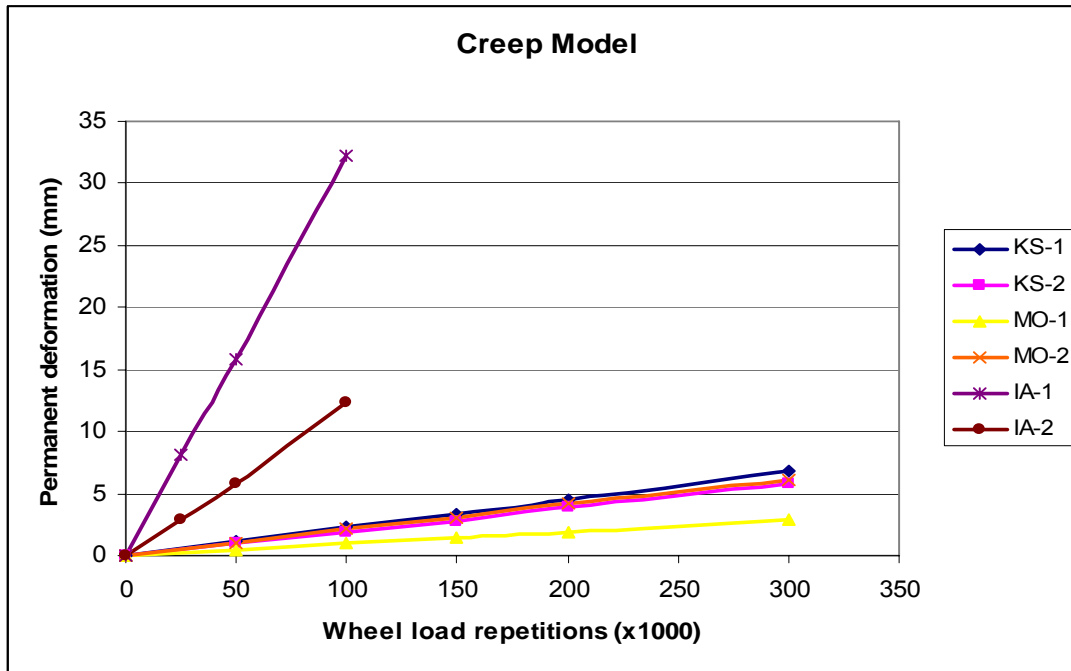
Figure 6.13 Models comparison for all mixes after the elasto-visco-plastic model
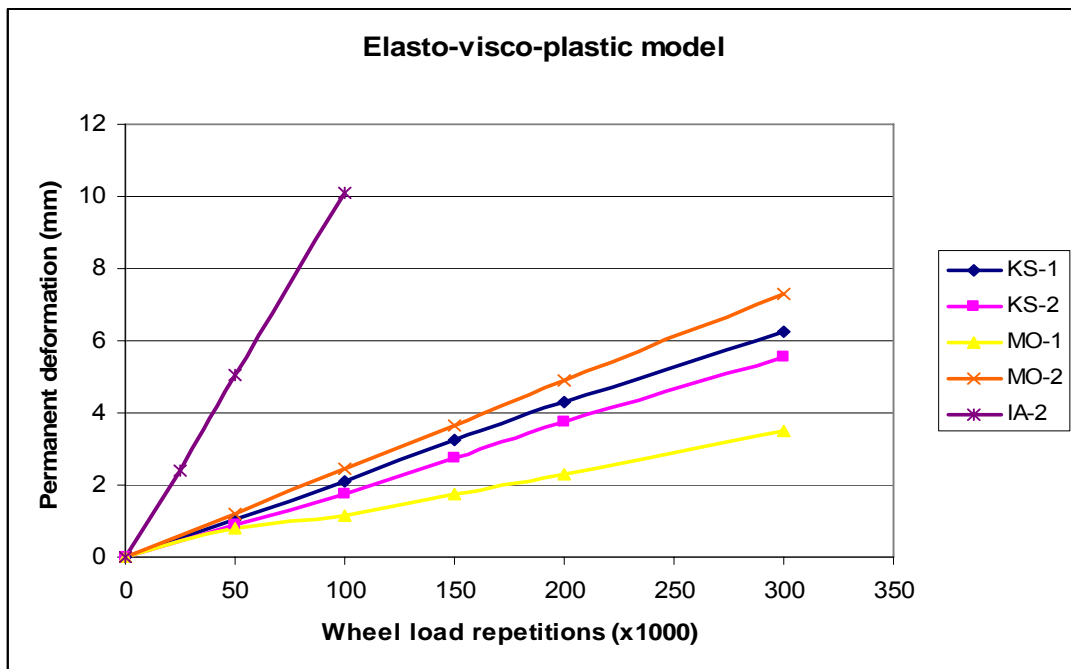
Table 6.10 Ranking of the asphalt mixes using permernent deformation in asphalt mix only

	Elasto-visco-plastic model				Creep model		
Mix ID	No of rep. (x1,000)	Percent of deformation in asphalt mix (%)	Rank	Mix ID	No of rep. (x1,000)	Percent of deformation in asphalt mix (%)	Rank
KS-1	300	48.8	5	KS-1	300	28.3	6
KS-2	300	68.4	3	KS-2	300	44.6	3
MO-1	300	73.6	2	MO-1	300	43.6	4
MO-2	300	105.3	1	MO-2	300	73.2	1
IA-1	100	-		IA-1	100	71.4	2
IA-2	100	55.9	4	IA-2	100	43.5	5

Figure 6.14 presents permanent deformation predicted in asphalt mix only by using the creep model. Figure 6.15 shows the same plot without IA-1 mix. Figure 6.16 presents permanent deformation predicted in asphalt mix only by using the Elasto-visco-plastic model. Tables 6.11 and 6.12 shows the values predicted for each mix.

Table 6.11 Permanent deformation predicted in asphalt mix only for the creep model

Rep. x 1000	Deform. (mm) KS-1	Deform. (mm) KS-2	Rep. x 1000	Deform. (mm) MO-1	Deform. (mm) MO-2	Rep. x 1000	Deform. (mm) IA-1	Deform. (mm) IA-2
0	0	0	0	0	0	0	0	0
50	0.29	0.37	50	0.15	0.67	25	5.56	1.29
100	0.55	0.75	100	0.29	1.49	50	11.1	2.49
150	0.87	1.12	150	0.44	2.24	100	22.2	5.16
200	1.16	1.49	200	0.59	2.99			
300	1.74	2.31	300	0.88	4.48			
			400	1.17	5.98			
			500	1.75	7.47			
			600	2.11	8.97			
			700	2.78	10.7			

Figure 6.14 Permanent deformation in asphalt mix only using the creep model
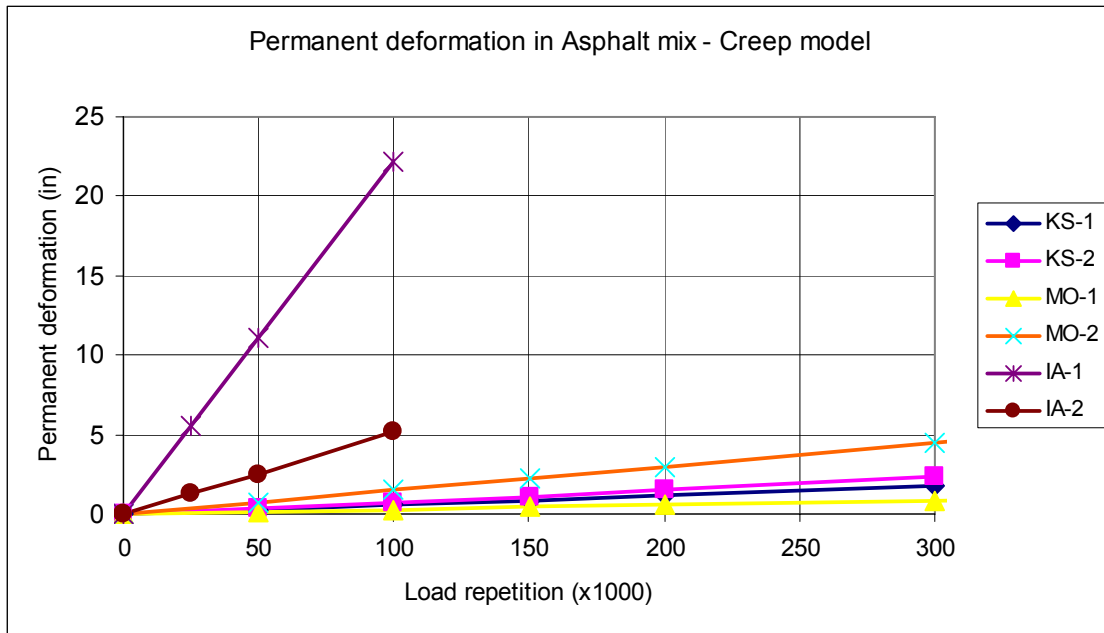
Figure 6.15 Permanent deformation in asphalt mix only using the creep model
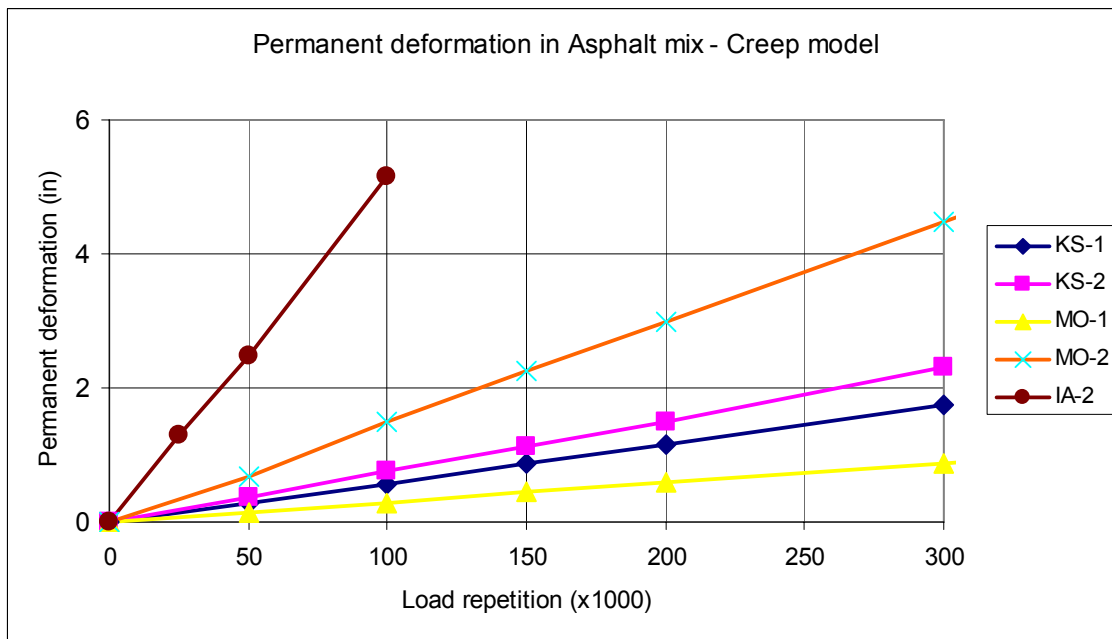
Table 6.12 Permanent deformation predicted in asphalt mix only - elasto-visco-plastic model

Rep. x 1000	Deform. (mm)		Rep. x 1000	Deform. (mm)		Rep. x 1000	Deform. (mm)	
	KS-1	KS-2		MO-1	MO-2		IA-1	IA-2
0	0	0	0	0	0	0	-	0
50	0.51	0.61	50	0.33	1.08	25	-	1.66
100	1	1.18	100	0.65	2.16	50	-	3.31
150	1.49	1.77	150	1.01	3.25	100	-	6.62
200	2	2.36	200	1.34	4.41			
300	3	3.54	300	1.96	6.49			
			400	2.62	8.66			
			500	4.02	10.8			
			600	4.42	13.7			
			700	4.69	15.4			

Figure 6.16 Permanent deformation in asphalt mix only using the elasto-visco-plastic model
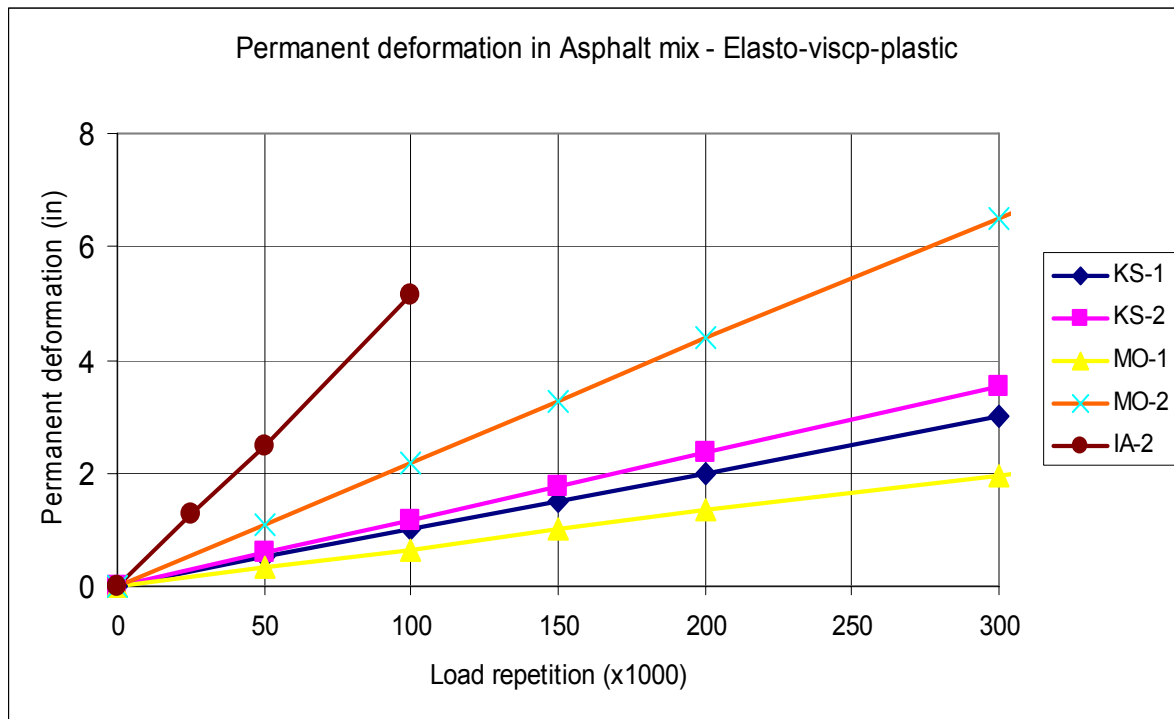
The permanent deformation measured in CISL 14 project was from asphalt layer. For model evaluation, both total predicted permanent deformation and the deformation predicted in asphalt mix only were compared with measured values. For prediction in asphalt mix, a good model is that which will capture most of the measured permanent deformation in asphalt mixes (Table 6.10).

CHAPTER 7 - CONCLUSIONS AND RECCOMMENDATIONS

The objective of this research project was to evaluate the existing permanent deformation prediction models that could be implemented using Abaqus/CAE commercial finite element software. Four prediction models were selected after literature review. These models are:

1. Creep Model
2. Viscoelastic Model
3. Drucker-Prager Model and
4. Elasto-visco-plastic Model

Laboratory tests were performed to obtain model parameters needed for each of the models listed above. Dynamic modulus test was performed to obtain the elastic modulus that was used in the analysis for all models. For creep model, dynamic and static creep tests were performed to obtain flow number and flow time respectively. The Frequency sweep at constant height test was performed to obtain the dynamic shear moduli (G*, G' and G") and bulk moduli (K*, K', K") as input parameters for the viscoelastic model. The dynamic uniaxial and triaxial strength tests were performed to obtain initial and final yield strength, plastic strain and cohesion and dilation angle as input parameters for Drucker-Prager model. For the Elasto-visco-plastic model, results from uniaxial strength test, yield strength and plastic strain and creep parameters were used. Other tests like Hamburg wheel tester, Asphalt Pavement Analyzer (APA) and repetitive shear at constant height (RSCH) were performed to further assess the performance of the six asphalt mixes. The laboratory tests performed and results obtained are detailed in chapters 3 and 4. Chapter 5 presents the model implementation in Abaqus using six asphalt mixes from Kansas, Missouri and Iowa. Chapter 6 comprise of model evaluation. Conclusions and recommendations are given Chapter 7.

To evaluate the models, six asphalt pavement sections were constructed and tested in the Accelerated Pavement Testing (APT) facility at the Civil and Infrastructures Systems Laboratory (CISL) of Kansas State University. The sections comprised of six asphalt mixes from Kansas, Missouri and Iowa. The sections were loaded with up to 700,000 load repetitions of a 22,000lb single axle. Transverse profiles at the pavement surface were measured periodically. The APT results were used as field measurements for evaluating the models.

From the Evaluation, two models were found to be suitable for predicting permanent deformation of asphalt mixes; these are creep model and elasto-visco-plastic model. The viscoelastic model greatly under predicts permanent deformation since the nodal displacements obtained indicated deformation of 2 x E-18m. This is a very small displacement, it could be considered negligible. This model was dropped from further evaluation. The Drucker-Prager model can predict some permanent deformation, after adding creep hardening to it, but uneven displacement on nodes is observed, which is different from expected transverse profiles. This could be due to the fact that this model is mostly used for modeling soils. It could be used to model asphalt at higher temperature (such as 60°C). For this case, asphalt was tested and modeled at 35°C which makes it hard for the model to capture damage in asphalt mixes and hence not predict so well.

Two models creep and elasto-visco-plastic, predicted a total permanent deformation that was somehow close to APT measured values, except that a linear relationship was used to predict the evolution of permanent deformation. Permanent deformation predicted using creep model ranks MO-1 mix as the best mix that resist permanent deformation, followed by KS-2, MO-2, KS-1, IA-2 and IA-1 in that order. The creep model predicts total permanent deformation measurements that are very close for KS-2, MO-2 and KS-1 (Figure 6.12). APT measured values rank MO-1 as the best performing mix followed by KS-1, KS-2, MO-2, IA-2 and IA-1. The predicted and measured values both rank MO-1 as the best mix and IA-1 as the worst mix. The elasto-visco-plastic model ranks MO-1 as the best mix followed by KS-2, KS-1, MO-2, IA-2 and IA-1 in that order. The ranking by the elasto-visco-plastic model is much closer to the APT performance ranking, having same ranking except for KS-1 and KS-2, which are interchanged. This indicates that these models could be used to predict permanent deformation that is close to measured values.

The total permanent deformation predicted by the two models, creep and elasto-visco-plastic, were somehow close to measured values. The predicted values thou, provided the permanent deformation predicted in the three layers, surface, base and subgrade. The evaluation was further carried out to assess the ability of the model to capture most of permanent deformation measured in the asphalt mix only. It is also clear that the permanent deformation

predicted in asphalt mix only is a function of dynamic (elastic) moduli used in each layer. From the values given in Table 6.10, the elasto-visco-plastic model predicted more permanent deformation in asphalt mix only than the creep model for each mix. Using the creep model, the mix that predicted more deformation in asphalt mix was MO-2 followed by IA-1, KS-2, MO-1, IA-2, and KS-1. Using the Elasto-visco-plastic model, MO-2 predicted more permanent deformation in asphalt mix only followed by MO-1, KS-2, IA-2, and KS-1. Both models have MO-2 as the mix that can capture more permanent deformation in asphalt mix and KS-1 as the model that capture the least permanent deformation.

The Hamburg wheel tester and Asphalt Pavement Analyzer (APA) are simulative tests which are used to simulate traffic wheel loads and evaluate performance of asphalt mixes due to loading. These tests were conducted to assess the performance of the six asphalt mixes. The Hamburg wheel tester ranks MO-1 as the best mix followed by MO-2, KS-2, KS-1, IA-2 and IA-1 in that order. While the APA ranks KS-1 as the best mix followed by KS-2, MO-1, MO-2, IA-1 and IA-2. The measurements were performed at 35°C, values obtained were so close ranging from 1.08 mm to 3.18 mm for APA test and 3.47 mm to 5.31 mm for five mixes tested using Hamburg wheel tester and one mix IA-1 had 10.15 mm. None of the mixes failed (Table 6.6). The Hamburg Wheel Tester's ranking is much closer to APT ranking as well as predicted values ranking.

The repetitive shear at constant height (RSCH) test is used to predict rutting potential in asphalt mixes. This test ranks KS-1 as the best mix followed by MO-2, MO-1, IA-2, KS-2 and IA-1. The APT measured values, Hamburg wheel tester and the two permanent deformation prediction models rank MO-1 as the best mix and IA-1 as the worst. APA and FSCH test ranks KS-1 as the best mix. The permanent deformation values measured using these tests at 35°C are somehow close and samples did not fail during testing. This could be a reason why the ranking is not very consistent. Perhaps if all the samples were tested to failure using each of the tests, a more consistent ranking could have been obtained.

Other laboratory tests like Dynamic Modulus test had high E* value for KS-1, followed by MO-1, IA-2, KS-2, MO-2 and IA-2 suggesting that KS-1 is a better mix. The static creep test indicates that KS-1 had more resistance to tertiary failure followed by MO-1, MO-2, KS-2, IA_2 and IA-1. The triaxial compressive strength test ranks KS-1 as having more failure strength followed by MO-1, KS-2, MO-2, IA-2 and IA-1. Most of laboratory tests indicated that KS-1 was a best mix followed by MO-1. But measured and predicted values indicate that MO-1 is a better mix. Laboratory test samples were fabricated in the laboratory. Percent of air void, binder content percent compaction may affect laboratory results.

Recommendations

The following are recommendations for future work

1. A non-linear permanent deformation prediction of the number of wheel load repetitions should be used instead of a linear model. Permanent deformation is normally high at the beginning of loading cycles and decreases with increase in load repetition. A model other than linear model could predict permanent deformation values that are much closer to measured values.

2. Sensitivity analysis is required for creep and elasto-visco-plastic model parameters A, m and n in order to improve the modeling of asphalt mixes. Values of A, m and n are not the same for the two models and they don't change in the same manner. Sensitivity analysis will be help to distinguish how each of these values changes and how the change affects the prediction of permanent deformation using the two models.

3. Creep and visco parameters, A, m and n will need to be verified with a bigger sample of asphalt mixes in order to have an idea of how A, m, and n values would vary with variation in asphalt mixtures and how these values could be used for different types of asphalt mixes.

References

Ali, H. S. Tayabji, and La Torre, F. *Calibration of Mechanistic Empirical Rutting Model for In-Service Pavements.* Presented for Publication at the 77th Annual TRB Meeting, Washington DC, 1998.

Asphalt Institute. Superpave Mix Design, Series No.2 (SP-2), Third edition, Asphalt Institute, Kentucky USA, 2001.

Brown, E. Ray, Kandhal S. P., Zhang J. *Performance Testing for Hot Mix Asphalt*. National Center for Asphalt Technology (NCAT) report No. 01-05, Auburn University, Auburn Alabama, 2001.

Carvalho R. L. and Schwartz, C. W. Comparison of Flexible Pavement Designs: AASHTO empirical VS NCHRP 1-37A Mechanistic empirical. TRB Annual Meeting CD-ROM. Washington DC, 2006.

Center for Transportation Research and Education (CTRE), *implementing the Mechanistic-Empirical pavement Design Guide: Implementation Plan,* Department of Civil, Construction and Environmental Engineering, Iowa State University, 2005.

Daniel J. S. A Fatigue Cracking Constitutive Model of Asphalt Concrete Using Viscoelastic and Continuum Damage Theory. A PhD dissertation, University of North Carolina, North Carolina, 2001.

Dater, M, I., Becker J.M. Snyder, M.B and Smith R. E., *Portland Cement Concrete Pavement Evaluation System (COPES),* NCHRP Report 277, Transportation Research Board, 1985.

Deacon, J. A, Monismith, C. L, et al, *An Analytical-Based Approach to Rutting Prediction*. A paper presented to TRB Annual Meeting, (200ITS Papers at TRB), Washington DC, 2002.

Dumitru, C. A Comparison of Measured and Computed Strains in Experimental Thin PCC Overlays, Masters Thesis, Kansas State University Library, Kansas, 2006.

FHWA, *Highway Statistics*, Federal Highway Administration, 2006.

Hall K. T., Connor, J. M., Darter, M. I., and Carpenter, S. H., *Rehabilitation of Concrete Pavements,* Vol.3, *Concrete Pavement Evaluation and Rehabilitation System,* Report No. FHWA-RD-88-073, Federal Highway Administration, 1989.

Hodges, H. C. Jr., Nevada Automotive Test Center, Nevada, 1999,
http://www.westrack.com/wt_02.htm

HRB, 1962, The AASHTO Road Test, Report 5, Pavement Research; Report 6, Special Studies; and Report 7, Summary Report; Special Report 7, Summary Report. Highway Research Board.

Huang B. *Fundamental Characterization and Numerical Simulation of Large Stone Asphalt Mixtures*. PhD dissertation, Louisiana State University Library, Louisiana, 2000.

Huang Y. H., *Pavement Analysis and Design*, Prentice Hall Inc., New Jersey, 2004.

Hugo, F, and Martin A. L., NCHRP Synthesis of Highway Practice 325, Transportation Research Board, Washington D.C., 2004.

Hugo, F. Accelerated pavement testing overview – Comfort; concerns; constraints and, challenges.,http://mnroad.dot.state.mn.us/research/mnroad_project/index_files/pdfs/Hugo_F_ Overview.pdf. Minnesota DOT USA, 2006.

Kim, Y. R., Lee, H.-J., and Little, D. "Fatigue characterization of asphalt concrete using viscoelasticity and continuum damage theory." Association of Asphalt Paving Technologists, 66, 520-569, 1997.

Kim, Y. R., Lee, H.-J., and Little, D. "Fatigue characterization of asphalt concrete using viscoelasticity and continuum damage theory." Association of Asphalt Paving Technologists, 66, 520-569, 1997.

Kraus, H. (1980) Creep Analysis. John Wiley & Sons, Inc., New York, N.Y.

Long, M. F. *Permanent Deformation of Asphalt Concrete Pavements: A non-linear Viscoelastic Approach to Mix Analyses and Design*. Ph.D. Dissertation, University of California Library, Berkeley, 2001.

Melhem, H and Sheffield F. Accelerated Testing for Studying Pavement Design and Performance (Fy 99), Final Report No. FHWA-KS-99-7, Kansas Department of Transportation, Kansas 2000

Metcalf, J. B. NCHRP Synthesis of Highway Practice 235, Transportation Research Board, Washington D.C., 1996.

NCHRP report-465, *Simple Performance tests for Superpave Mix Designs*, Transportation Research Board, National Research Council, Washington DC, 2002.

NCHRP-37A, *Guide for Mechanistic-Empirical Design, Part 1 Chapter 1*, Final Report, Transportation Research Board, National Research Council, Washington DC, 2004a.

NCHRP-37A. *Guide for Mechanistic Empirical Design*, *Part 2: Design Inputs, Final Report*, University of Maryland, Maryland 2004b.

Nguyen D.T., Nedjar B., Tamagny P, and de La Roche C. *Rutting prediction of Asphalt concrete materials using a multi-criteria visco-plasticity model*, 2006.

Ohio Research Institute for Transportation and Environment, ORITE-3, Ohio Department of Transportation, Subgrade Variability on the Ohio SHRP Road Project, Ohio University Printing Resources, 1999 (http://isddc.dot.gov/OLPFiles/FHWA/013562.pdf).

Park D. *Microstructural viscoplastic continuum model for asphalt concrete.* PhD Dissertation Texas A & M University Library, Texas 2004.

Rand D. A, Hamburg Wheel Test, Texas DOT Technical Advisory Bulletin, Published by Construction and Bridge Design Divisions, Texas, 2006. ftp://ftp.dot.state.tx.us/pub/txdot-info/cmd/tech/hamburg.pdf.

Roberts, R. L., Kandhal, P. S. Brown, R. E., Hot Mix Asphalt Materails, Mixture, Design and Construction, Second Edition, NAPA Education Foundation, Lanham, Maryland, 1996.

Romanoschi, S. A., Hossain, M., *Verification of Mechanistic-Empirical Design Models for Flexible Pavements Through APT Testing*, A proposal submitted to Midwest States Accelerated Pavement Pooled Funds Program, Department of Civil Engineering, Kansas State University, Kansas, 2004.

Rosenberger Carlos, *Intersection Strategy 2,* Asphalt Magazine, Summer 1999, Asphalt Institute, Lexington KY 1999. www.asphaltinstitute.org.

Saeed Athar and Hall, Jim, W. Jr., Accelerated Pavement Testing: Data Guidelines, NCHRP Report 512, Transportation Research Board, Washington DC, 2003.

Shanklin D. W., Rademacher K. R., and Talbot J. R., Constructing and Controlling Compaction of Earth Fills, Published by ASTM International, 2000.

Sharp K, G. "Full Scale Accelerated Pavement Testing: A Southern Hemisphere and Asian Perspective" http://mnroad.dot.state.mn.us/research/mnroad_project/index_files/pdfs/Hugo_F_ Overview.pdf. Minnesota DOT USA, 2006.

SHRP. *Development and Validation of Performance Prediction Models and Specifications for Asphalt Binders and Paving Mixes.* SHRP-A-357, National Research Council, Washington D.C., 1993

SHRP. *Performance Prediction Models in the Superpave Mix design System.* SHRP-A-699, National Research Council, Washington D.C., 1994a.

SHRP. *The SUPERPAVE Mix Design System Manual of Specifications, Test Methods, and Practices.* SHRP-A-379, National Research Council, Washington D.C., 1994b.

SHRP-A-415, Permanent Deformation Response of Asphalt Aggregate Mixes, Asphalt Research Program, Institute of Transportation Studies University of California, Berkeley SHRP, National Research Council Washington, DC 1994.

Sivasubramaniam, S. "Validation of Superpave Mixture Design and Analysis Procedure using the NCAT Test Track", Ph.D. Dissertation, Purdue University, Publication Number AAT 3191562, 2005.

Tashman, L. "Microstructural viscoplastic continuum model for asphalt concrete" Ph.D dissertation, Texas A & M University Library, Texas 2003.

Ullidtz, P. *Pavement Analysis.* Elsevier Science Publishers B.V Amsterdam, 1987.

Wu, Zhong "Finite element simulation of rutting on Superpave pavements" PhD dissertation, KSU, Kansas State University, Kansas 2001.

Zhao Y. *Permanent Deformation Characterization of Asphalt Concrete Using a Viscoplastic Model.* PhD dissertation, North Carolina State University Library, North Carolina, 2002.

Appendix A - Dynamic Modulus results

Figures A-1 to A-6 shows the dynamic modulus (E*) for asphalt mixes tested at two temperatures, 35°C and 20°C.

Figure A-1 Kansas mixes dynamic modulus at 20°C
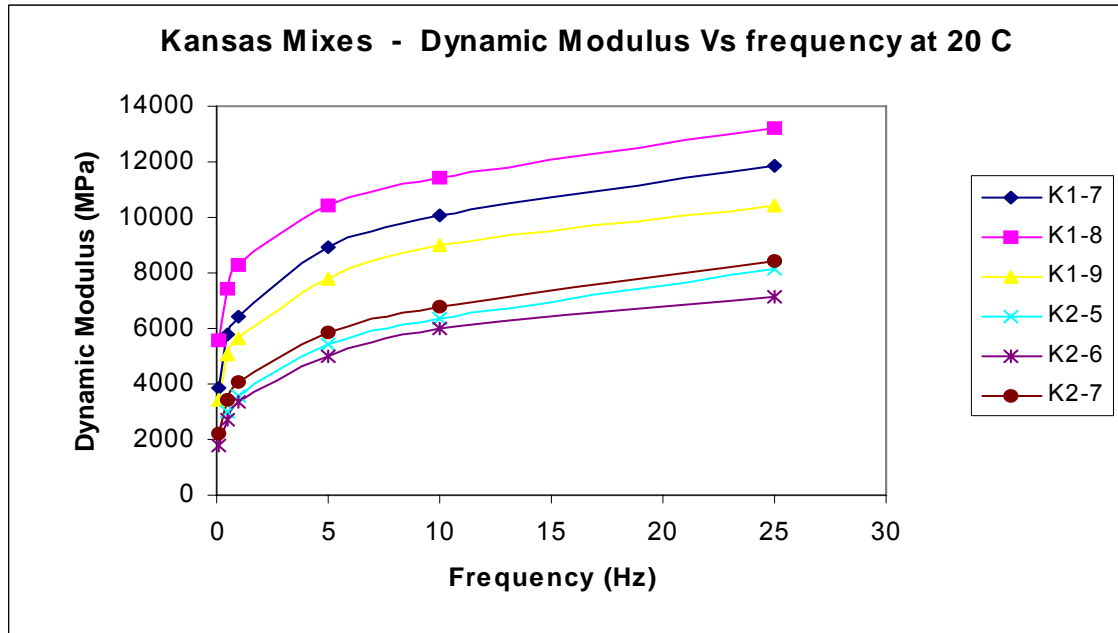
Figure A-2 Kansas mixes dynamic modulus at 35°C

Figure A-3 Missouri mixes dynamic modulus at 20°C
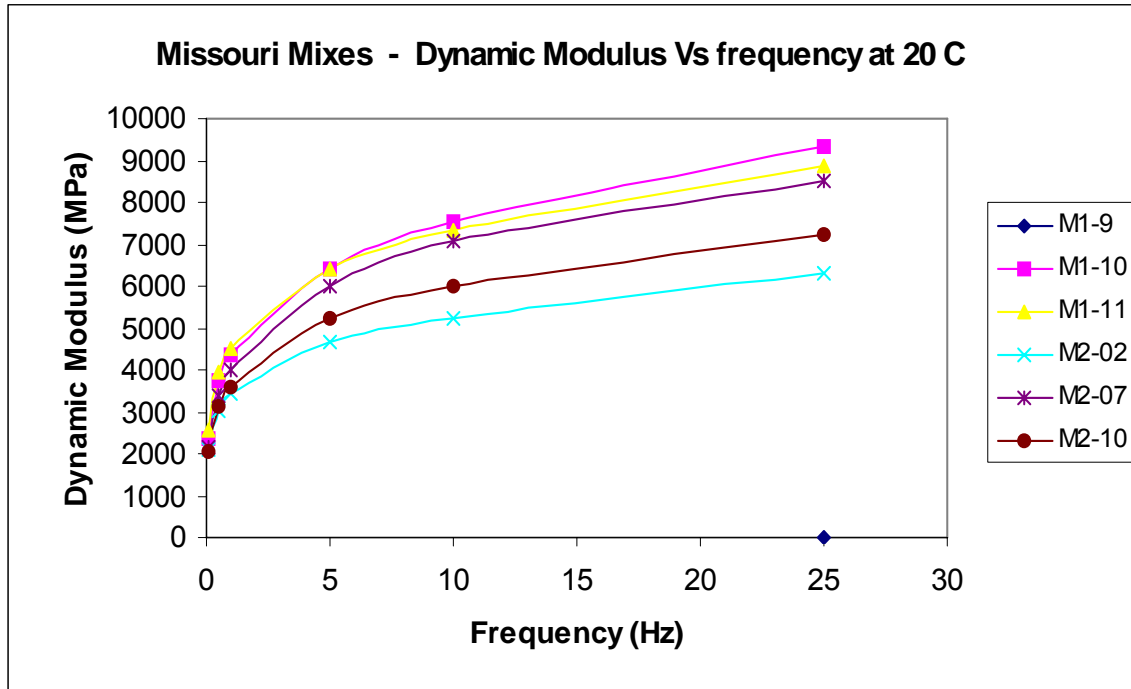
Figure A-4 Missouri mixes dynamic modulus at 35°C
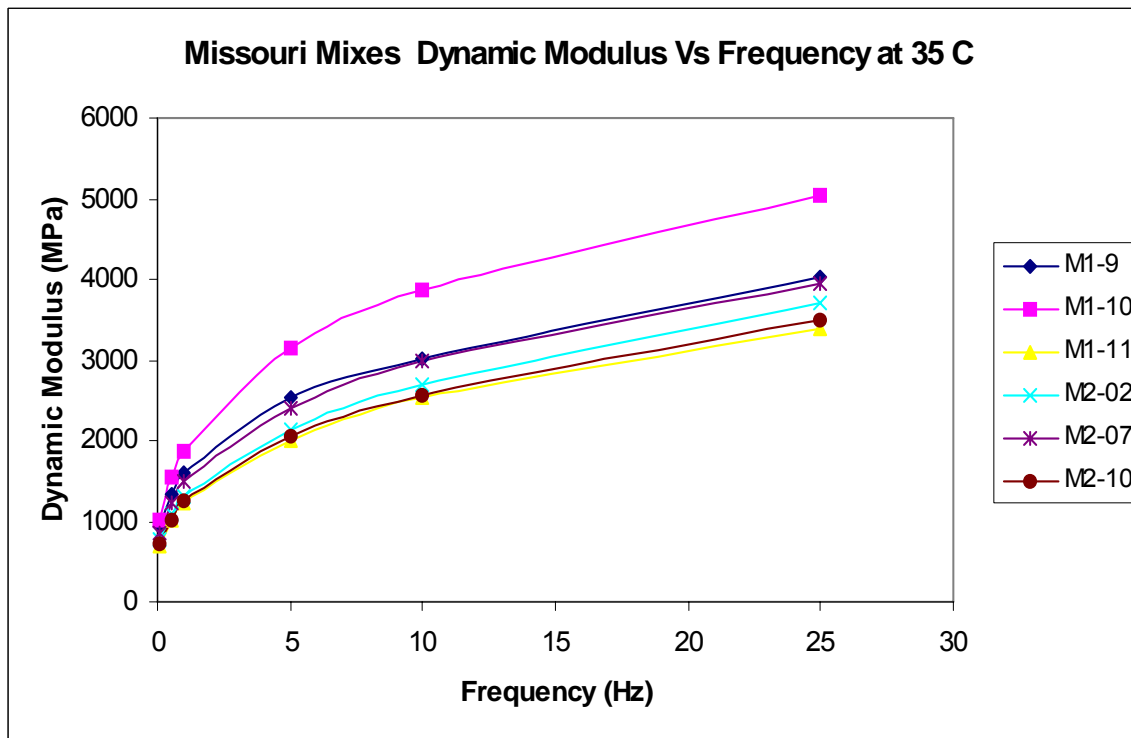
Figure A-5 Iowa mixes dynamic modulus at 20°C
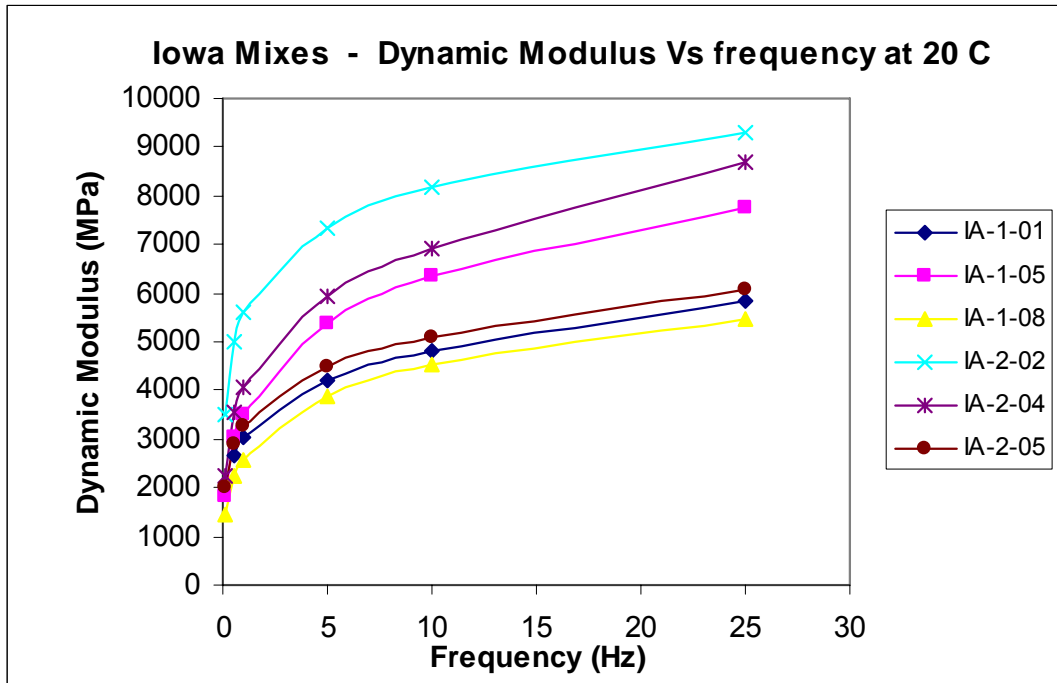
Figure A-6 Iowa mixes dynamic modulus at 35°C
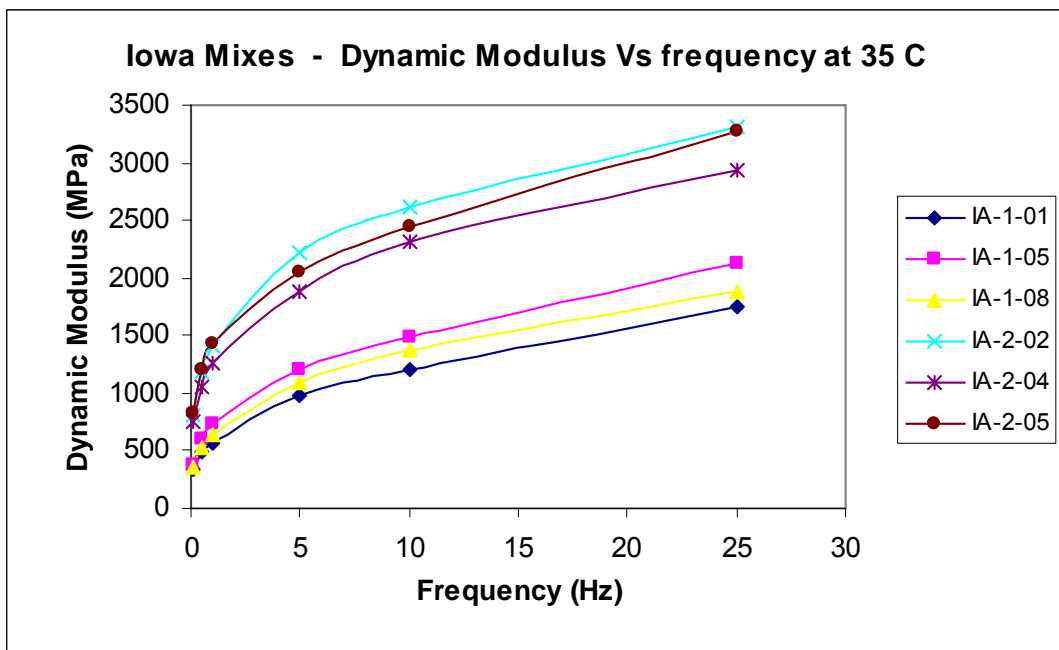
Figures A-7 to A-12 shows plots of the shift factors used to shift temperatures to 35°C for the dynamic modulus (E*) computation .

Figure A-7 Kansas mix KS-1 shift factors plot

Shift Factors for K1
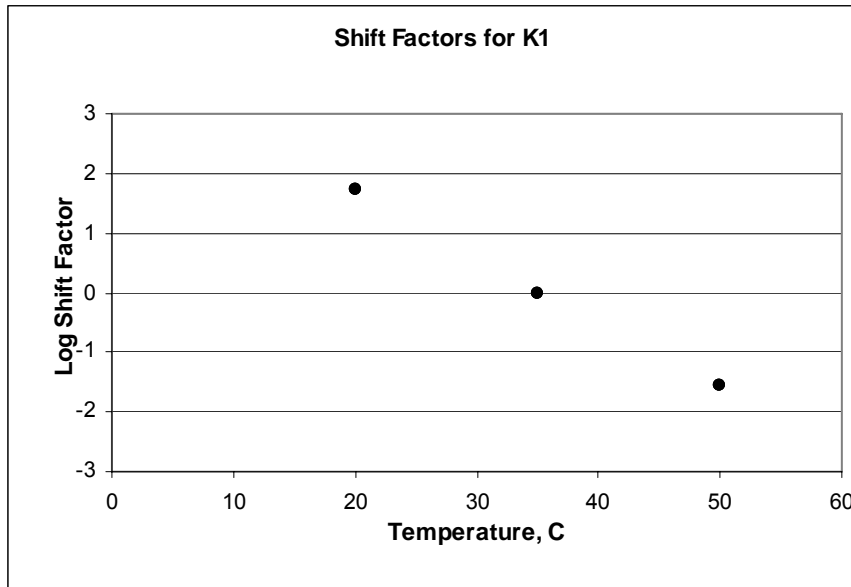
Figure A-8 Kansas mix KS-2 shift factors plot

Shift Factors for K2
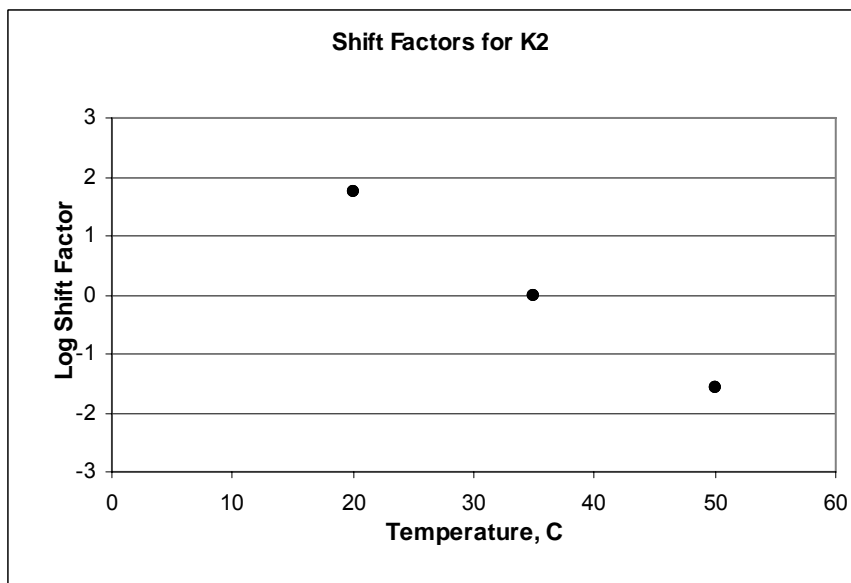
Figure A-9 Missouri mix MO-1 shift factors plot

Shift Factors for M1
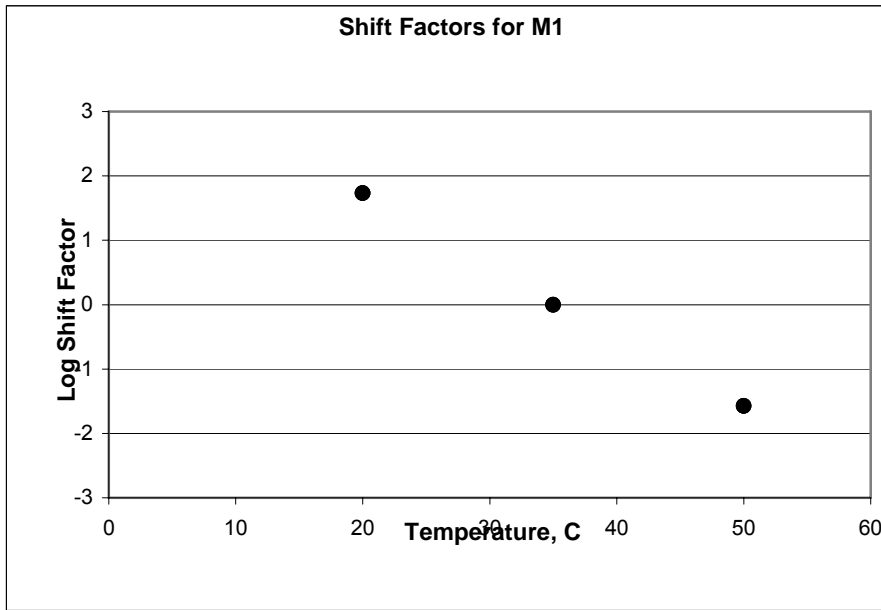
Figure A-10 Missouri mix MO2-1 shift factors plot

Shift Facotrs for M2
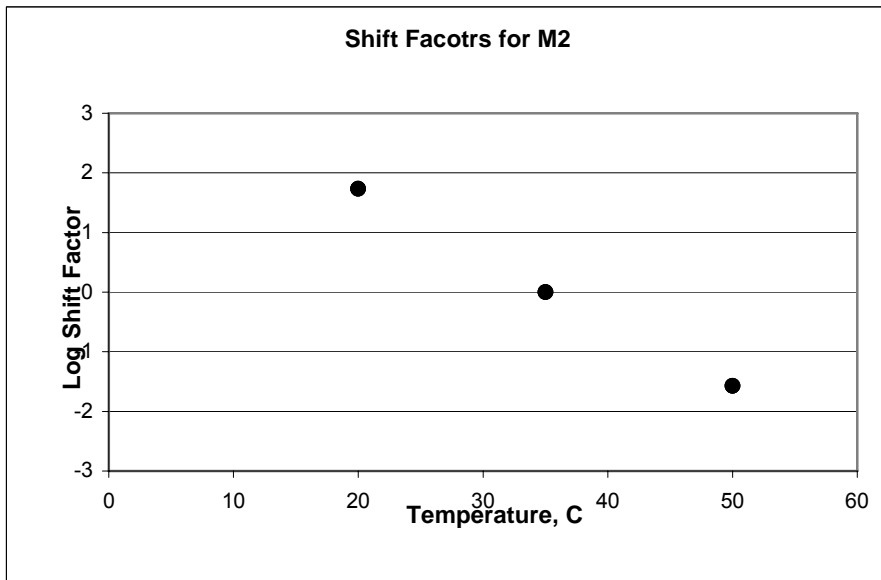
Figure A-11 Iowa mix IA-1 shift factors plot

Shift Factors for IA-1
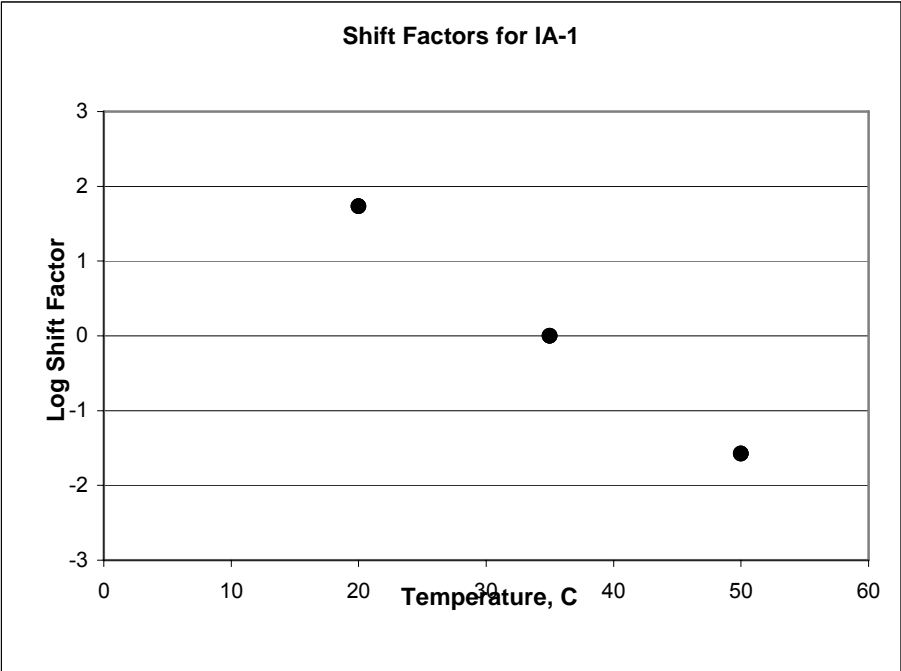
Figure A-12 Iowa mix IA-2 shift factors plot

Shift Factors for IA-2
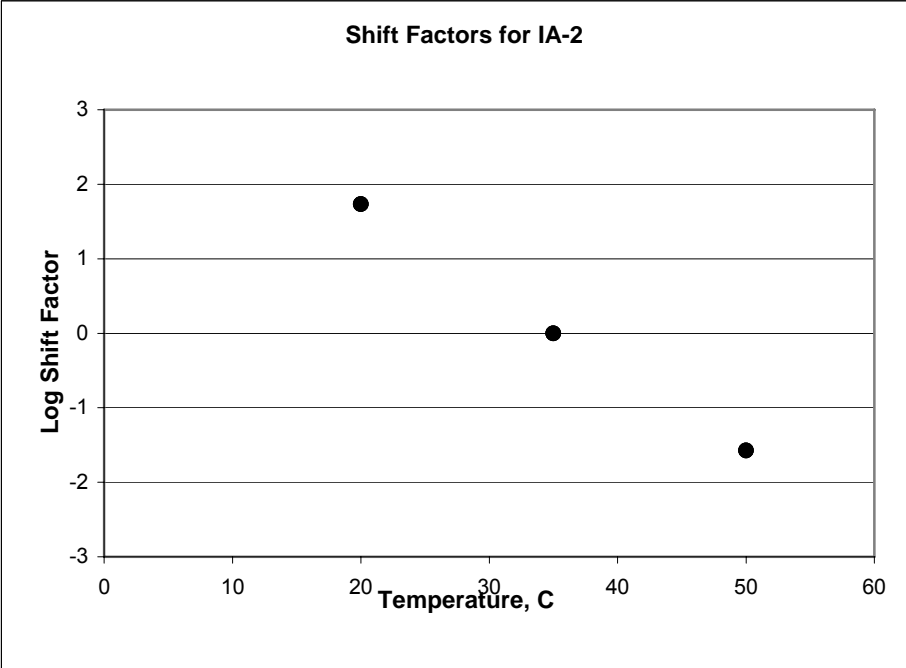
Figures A-13 to A-18 shows the plots of phase angles at 20ºC and 35ºC

Figure A-13 Phase angle plots for Kansas mix KS-1
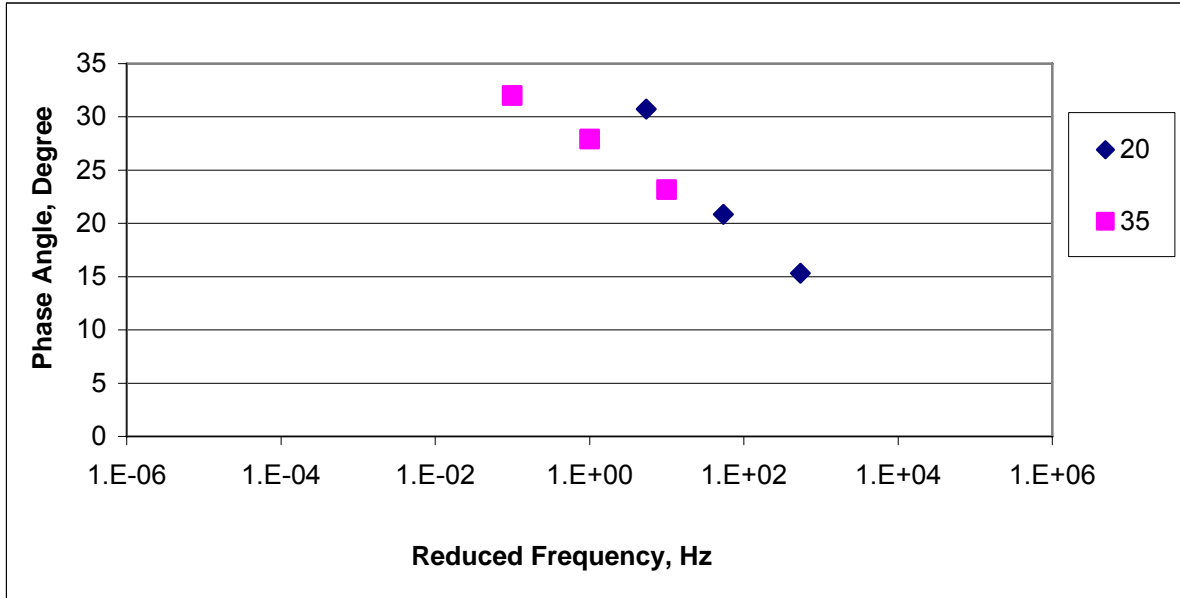
Figure A-14 Phase angle plots for Kansas mix KS-2
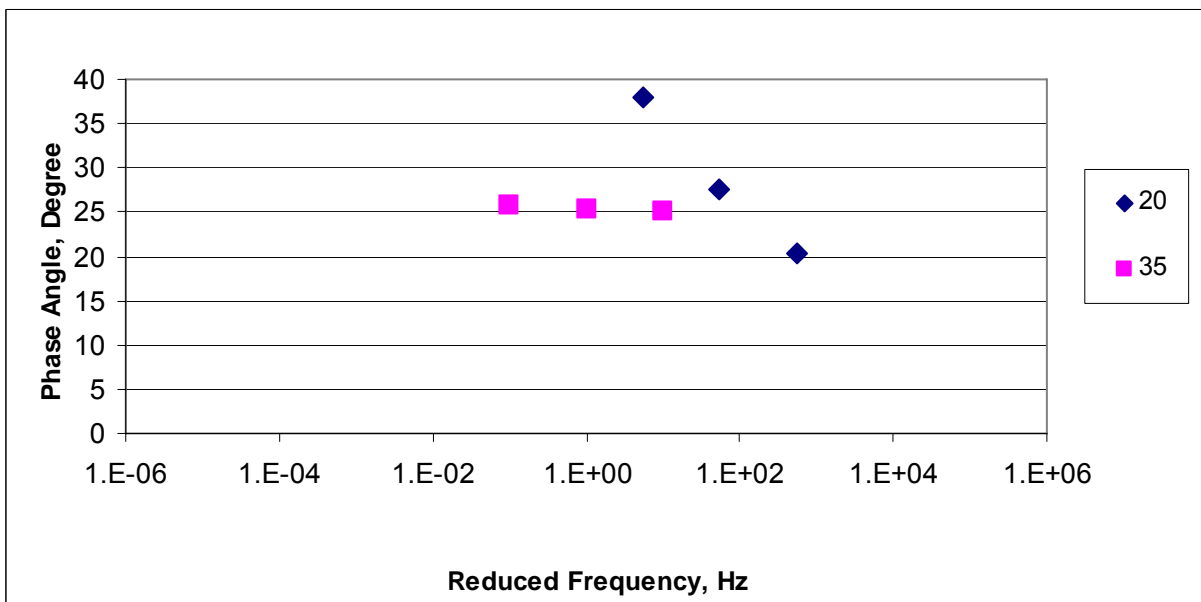
Figure A-15 Phase angle plots for Missouri mix MO-1
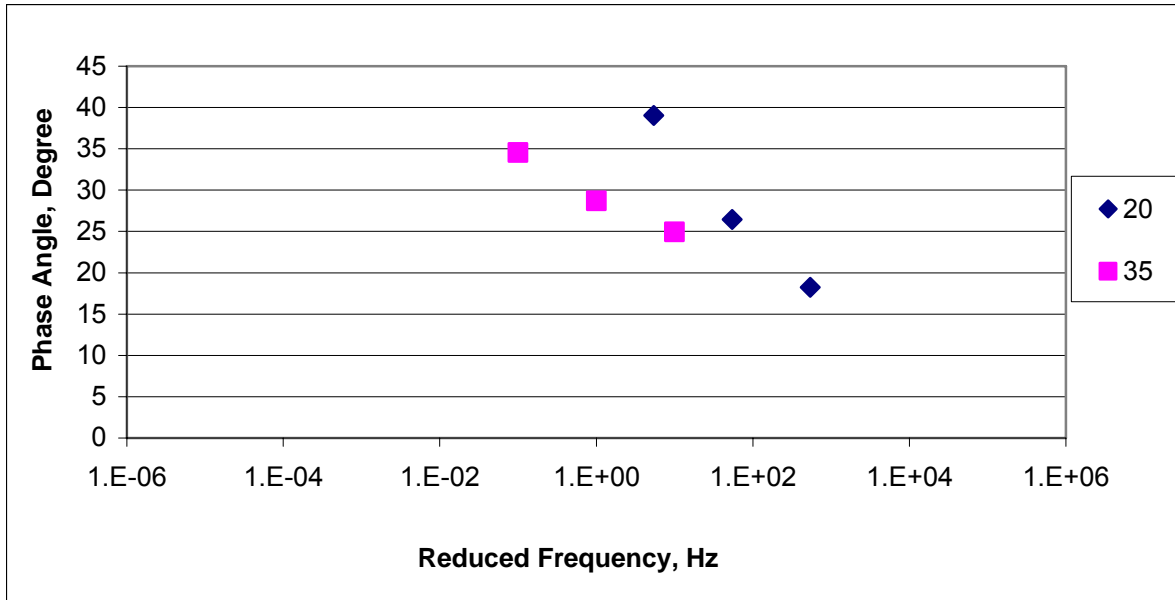
Figure A-16 Phase angle plots for Missouri mix MO-2
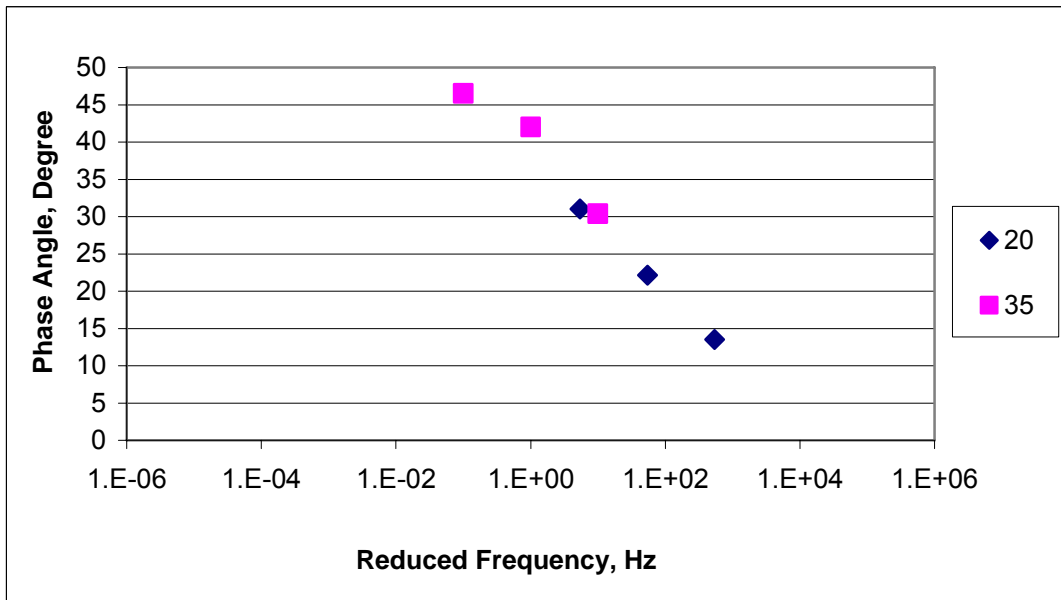
Figure A-17 Phase angle plots for Iowa mix IA-1
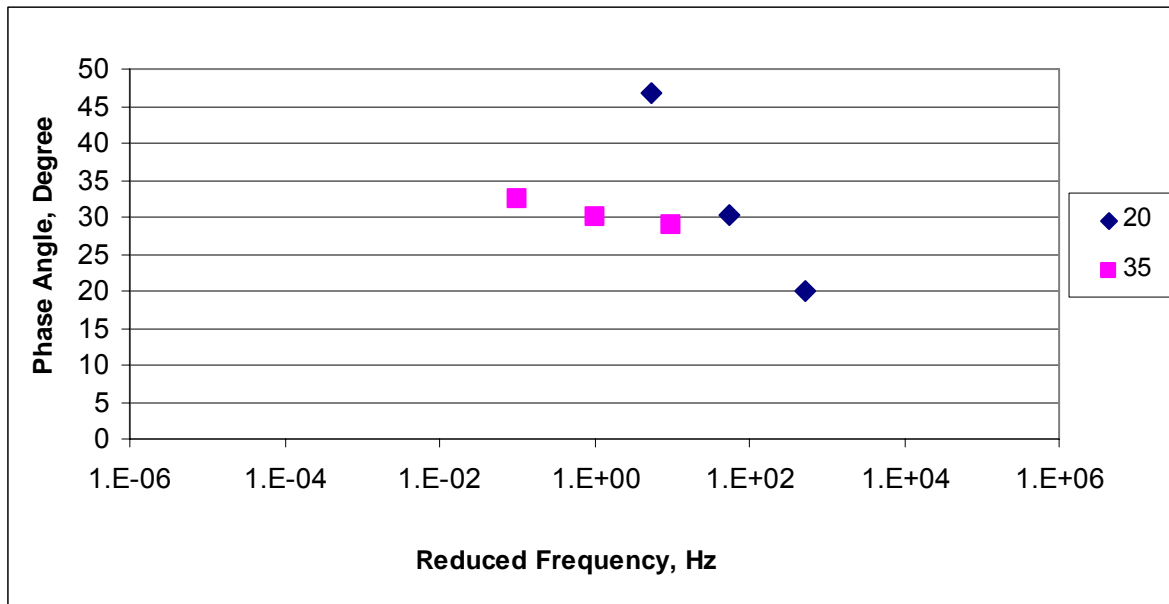
Figure A-18 Phase angle plots for Iowa mix IA-2
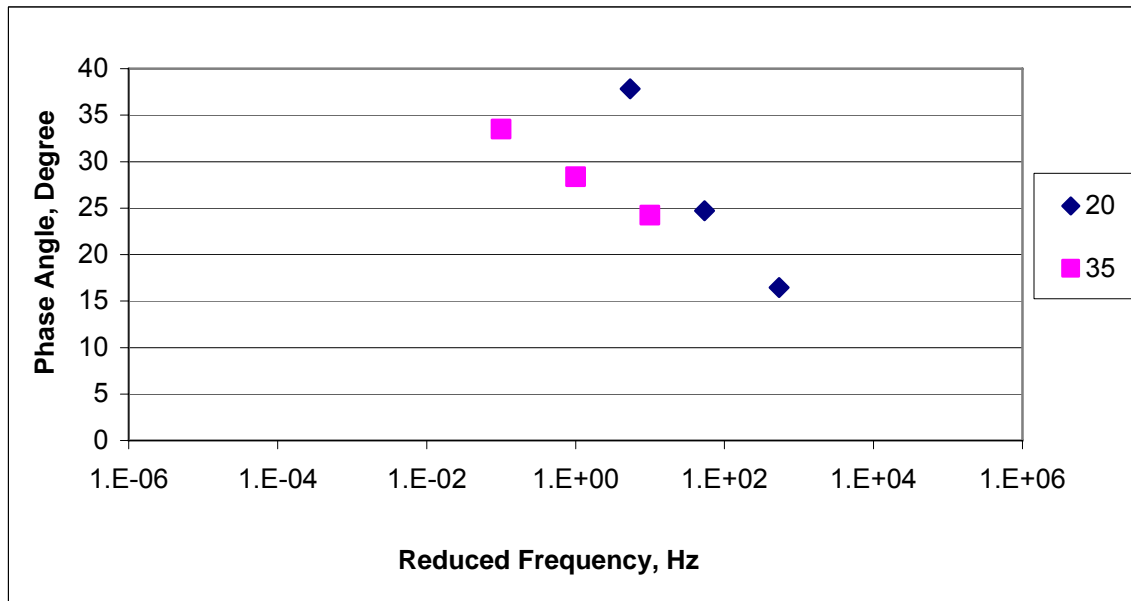
Tables A-1 to A-6 provide the Mechanistic-Empirical Pavement Design Guide (MEPDG) inputs computed from the dynamic modulus test.

Table A-1 MEPGD Inputs for Kansas Mix KS-1

Temp C	Temp F	Frequency Hz	Shift Factor	Reduced Frequency	E* ksi	E* MPa
-10.0	14	25	5.794554	15577363	2919.2	20134.0
-10.0	14	10	5.794554	6230945	2869.3	19789.6
-10.0	14	5	5.794554	3115473	2824.3	19479.4
-10.0	14	1	5.794554	623094.5	2690.9	18559.4
-10.0	14	0.5	5.794554	311547.3	2618.9	18062.8
-10.0	14	0.1	5.794554	62309.45	2412.1	16636.2
4.4	40	25	3.729878	134220.1	2518.0	17366.4
4.4	40	10	3.729878	53688.04	2390.0	16483.5
4.4	40	5	3.729878	26844.02	2279.9	15724.7
4.4	40	1	3.729878	5368.804	1981.1	13663.5
4.4	40	0.5	3.729878	2684.402	1835.4	12659.1
4.4	40	0.1	3.729878	536.8804	1470.5	10142.4
20.0	68	25	1.733887	1354.648	1683.9	11613.9
20.0	68	10	1.733887	541.8593	1472.7	10157.2
20.0	68	5	1.733887	270.9297	1310.6	9038.9
20.0	68	1	1.733887	54.18593	946.8	6530.3
20.0	68	0.5	1.733887	27.09297	803.9	5544.2
20.0	68	0.1	1.733887	5.418593	522.6	3604.5
35.0	95	25	0	25	788.0	5435.1
35.0	95	10	0	10	620.5	4279.3
35.0	95	5	0	5	510.7	3522.0
35.0	95	1	0	1	314.0	2166.0
35.0	95	0.5	0	0.5	252.6	1742.4
35.0	95	0.1	0	0.1	152.9	1054.7
50.0	122	25	-1.57294	0.668338	276.8	1909.1
50.0	122	10	-1.57294	0.267335	207.4	1430.7
50.0	122	5	-1.57294	0.133668	167.2	1152.9
50.0	122	1	-1.57294	0.026734	103.8	716.2
50.0	122	0.5	-1.57294	0.013367	86.0	593.3
50.0	122	0.1	-1.57294	0.002673	58.4	403.1

Table A-2 MEPGD Inputs for Kansas Mix KS-2

Temp C	Temp	Frequency Hz	Shift Factor	Reduced Frequency	E* ksi	E* MPa
-10.0	14	25	5.794554	15577363	2609.4	17997.4
-10.0	14	10	5.794554	6230945	2511.7	17323.0
-10.0	14	5	5.794554	3115473	2428.0	16746.0
-10.0	14	1	5.794554	623094.5	2199.9	15172.8
-10.0	14	0.5	5.794554	311547.3	2087.1	14394.9
-10.0	14	0.1	5.794554	62309.45	1795.0	12380.2
4.4	40	25	3.729878	134220.1	1939.1	13374.2
4.4	40	10	3.729878	53688.04	1766.2	12181.3
4.4	40	5	3.729878	26844.02	1628.9	11234.3
4.4	40	1	3.729878	5368.804	1299.7	8963.8
4.4	40	0.5	3.729878	2684.402	1158.7	7991.8
4.4	40	0.1	3.729878	536.8804	850.8	5867.7
20.0	68	25	1.733887	1354.648	1023.6	7059.6
20.0	68	10	1.733887	541.8593	852.4	5879.1
20.0	68	5	1.733887	270.9297	733.1	5055.9
20.0	68	1	1.733887	54.18593	497.7	3432.4
20.0	68	0.5	1.733887	27.09297	415.7	2867.1
20.0	68	0.1	1.733887	5.418593	268.7	1853.4
35.0	95	25	0	25	407.0	2806.8
35.0	95	10	0	10	317.9	2192.8
35.0	95	5	0	5	262.8	1812.8
35.0	95	1	0	1	169.1	1166.4
35.0	95	0.5	0	0.5	140.6	970.0
35.0	95	0.1	0	0.1	94.1	648.7
50.0	122	25	-1.57294	0.668338	151.8	1047.2
50.0	122	10	-1.57294	0.267335	119.7	825.3
50.0	122	5	-1.57294	0.133668	100.8	695.2
50.0	122	1	-1.57294	0.026734	70.1	483.8
50.0	122	0.5	-1.57294	0.013367	61.1	421.1
50.0	122	0.1	-1.57294	0.002673	46.2	318.3

Table A-3 MEPGD Inputs for Missouri Mix MO-1

Temp C	Temp F	Frequency Hz	Shift Factor	Reduced Frequency	E* ksi	E* MPa
-10.0	14	25	5.794554	15577363	2753.9	18993.8
-10.0	14	10	5.794554	6230945	2688.4	18541.6
-10.0	14	5	5.794554	3115473	2631.1	18146.5
-10.0	14	1	5.794554	623094.5	2468.8	17027.1
-10.0	14	0.5	5.794554	311547.3	2384.9	16448.9
-10.0	14	0.1	5.794554	62309.45	2155.2	14864.2
4.4	40	25	3.729878	134220.1	2270.9	15662.6
4.4	40	10	3.729878	53688.04	2131.4	14700.2
4.4	40	5	3.729878	26844.02	2015.2	13898.9
4.4	40	1	3.729878	5368.804	1713.6	11818.8
4.4	40	0.5	3.729878	2684.402	1572.7	10846.7
4.4	40	0.1	3.729878	536.8804	1232.9	8503.5
20.0	68	25	1.733887	1354.648	1429.5	9859.0
20.0	68	10	1.733887	541.8593	1234.9	8517.0
20.0	68	5	1.733887	270.9297	1088.9	7510.2
20.0	68	1	1.733887	54.18593	770.0	5310.7
20.0	68	0.5	1.733887	27.09297	647.2	4464.0
20.0	68	0.1	1.733887	5.418593	408.8	2819.7
35.0	95	25	0	25	633.7	4370.8
35.0	95	10	0	10	491.4	3388.9
35.0	95	5	0	5	398.8	2750.3
35.0	95	1	0	1	234.2	1615.2
35.0	95	0.5	0	0.5	183.2	1263.6
35.0	95	0.1	0	0.1	101.5	700.3
50.0	122	25	-1.57294	0.668338	203.2	1401.7
50.0	122	10	-1.57294	0.267335	146.0	1006.7
50.0	122	5	-1.57294	0.133668	113.1	779.8
50.0	122	1	-1.57294	0.026734	62.5	431.0
50.0	122	0.5	-1.57294	0.013367	48.7	336.2
50.0	122	0.1	-1.57294	0.002673	28.3	195.4

Table A-4 MEPGD Inputs for Missouri Mix MO-2

Temp C	Temp F	Frequency Hz	Shift Factor	Reduced Frequency	G* ksi	G* MPa
-10.0	14	25	5.794554	15577363	2264.5	15618.1
-10.0	14	10	5.794554	6230945	2109.5	14549.1
-10.0	14	5	5.794554	3115473	1981.8	13668.7
-10.0	14	1	5.794554	623094.5	1656.5	11425.1
-10.0	14	0.5	5.794554	311547.3	1507.7	10398.5
-10.0	14	0.1	5.794554	62309.45	1157.6	7984.0
4.4	40	25	3.729878	134220.1	1324.0	9131.8
4.4	40	10	3.729878	53688.04	1125.7	7764.2
4.4	40	5	3.729878	26844.02	980.6	6762.9
4.4	40	1	3.729878	5368.804	674.8	4654.2
4.4	40	0.5	3.729878	2684.402	561.6	3873.2
4.4	40	0.1	3.729878	536.8804	349.3	2409.2
20.0	68	25	1.733887	1354.648	462.6	3190.2
20.0	68	10	1.733887	541.8593	350.3	2416.1
20.0	68	5	1.733887	270.9297	280.6	1935.0
20.0	68	1	1.733887	54.18593	163.1	1124.6
20.0	68	0.5	1.733887	27.09297	128.3	885.1
20.0	68	0.1	1.733887	5.418593	74.0	510.4
35.0	95	25	0	25	124.8	860.8
35.0	95	10	0	10	91.0	628.0
35.0	95	5	0	5	72.0	496.9
35.0	95	1	0	1	43.1	297.0
35.0	95	0.5	0	0.5	35.1	242.1
35.0	95	0.1	0	0.1	22.9	158.2
50.0	122	25	-1.57294	0.668338	38.2	263.4
50.0	122	10	-1.57294	0.267335	29.5	203.4
50.0	122	5	-1.57294	0.133668	24.6	169.9
50.0	122	1	-1.57294	0.026734	17.1	117.9
50.0	122	0.5	-1.57294	0.013367	14.9	103.1
50.0	122	0.1	-1.57294	0.002673	11.5	79.3

Table A-5 MEPGD Inputs for Iowa Mix IA-1

Temp C	Temp F	Frequency Hz	Shift Factor	Reduced Frequency	E* ksi	E* MPa
-10.0	14	25	5.794554	15577363	2417.8	16675.5
-10.0	14	10	5.794554	6230945	2298.8	15854.8
-10.0	14	5	5.794554	3115473	2196.0	15145.5
-10.0	14	1	5.794554	623094.5	1913.7	13199.1
-10.0	14	0.5	5.794554	311547.3	1774.7	12239.9
-10.0	14	0.1	5.794554	62309.45	1421.6	9804.9
4.4	40	25	3.729878	134220.1	1594.1	10994.7
4.4	40	10	3.729878	53688.04	1387.6	9570.2
4.4	40	5	3.729878	26844.02	1228.4	8472.0
4.4	40	1	3.729878	5368.804	869.7	5998.4
4.4	40	0.5	3.729878	2684.402	728.6	5025.2
4.4	40	0.1	3.729878	536.8804	452.6	3121.3
20.0	68	25	1.733887	1354.648	601.6	4149.3
20.0	68	10	1.733887	541.8593	453.9	3130.6
20.0	68	5	1.733887	270.9297	360.5	2486.2
20.0	68	1	1.733887	54.18593	202.0	1393.0
20.0	68	0.5	1.733887	27.09297	155.6	1072.9
20.0	68	0.1	1.733887	5.418593	84.8	584.8
35.0	95	25	0	25	150.9	1040.7
35.0	95	10	0	10	106.6	735.4
35.0	95	5	0	5	82.3	567.7
35.0	95	1	0	1	46.7	321.8
35.0	95	0.5	0	0.5	37.3	257.4
35.0	95	0.1	0	0.1	23.6	163.0
50.0	122	25	-1.57294	0.668338	40.9	282.1
50.0	122	10	-1.57294	0.267335	30.9	213.2
50.0	122	5	-1.57294	0.133668	25.5	175.8
50.0	122	1	-1.57294	0.026734	17.4	120.1
50.0	122	0.5	-1.57294	0.013367	15.2	104.8
50.0	122	0.1	-1.57294	0.002673	11.7	81.0

Table A-6 MEPGD Inputs for Iowa Mix IA-2

Temp C	Temp F	Frequency Hz	Shift Factor	Reduced Frequency	E* ksi	E* MPa
-10.0	14	25	5.794554	15577363	2738.9	18889.9
-10.0	14	10	5.794554	6230945	2649.7	18275.3
-10.0	14	5	5.794554	3115473	2571.4	17735.2
-10.0	14	1	5.794554	623094.5	2349.8	16206.3
-10.0	14	0.5	5.794554	311547.3	2236.4	15424.4
-10.0	14	0.1	5.794554	62309.45	1933.8	13337.4
4.4	40	25	3.729878	134220.1	2084.5	14377.1
4.4	40	10	3.729878	53688.04	1903.3	13127.3
4.4	40	5	3.729878	26844.02	1757.2	12119.4
4.4	40	1	3.729878	5368.804	1401.3	9665.1
4.4	40	0.5	3.729878	2684.402	1247.8	8606.3
4.4	40	0.1	3.729878	536.8804	913.3	6299.0
20.0	68	25	1.733887	1354.648	1100.6	7591.0
20.0	68	10	1.733887	541.8593	915.1	6311.3
20.0	68	5	1.733887	270.9297	786.8	5426.5
20.0	68	1	1.733887	54.18593	538.2	3712.2
20.0	68	0.5	1.733887	27.09297	453.6	3128.3
20.0	68	0.1	1.733887	5.418593	304.7	2101.8
35.0	95	25	0	25	444.6	3066.4
35.0	95	10	0	10	354.1	2442.4
35.0	95	5	0	5	298.9	2061.3
35.0	95	1	0	1	206.0	1420.9
35.0	95	0.5	0	0.5	178.0	1227.4
35.0	95	0.1	0	0.1	131.9	910.0
50.0	122	25	-1.57294	0.668338	189.0	1303.5
50.0	122	10	-1.57294	0.267335	157.3	1084.9
50.0	122	5	-1.57294	0.133668	138.6	956.2
50.0	122	1	-1.57294	0.026734	108.0	744.9
50.0	122	0.5	-1.57294	0.013367	98.8	681.3
50.0	122	0.1	-1.57294	0.002673	83.4	575.5

Appendix B - Dynamic Shear Modulus results

Appendix B comprises of results obtained after the frequency shear at constant height (FSCH) test. The test is used to obtain values of dynamic shear modulus with storage and loss modulus. To obtain the G values, fitting parameters are used and shift factors were used to shift values from test temperature to reference temperature. The shift values and fitting values are given in Tables 4.12 to 4.17. Given below are the plots of shift factors, phase angles and tables of MEPGD inputs obtained. The plots and tables are given for dynamic shear modulus (G*), storage modulus (G') and loss modulus (G") for the six asphalt mixes tested. The make the presentation easy, Appendix B-1 will comprise of dynamic shear modulus (G*), Appendix B-2 comprise of storage modulus (G') and the loss modulus (G") is provide in Appendix B-3.

Appendix B-1 - Dynamic Shear Modulus (G*) Results

Appendix B-1 comprise of shift factor plots for six asphalt mixes (Figures B-1-1 to B-1-6) Phase angle plots (Figures B-1-7 to B-1-12) and Mechanistic Empirical Pavement Design Guide (MEPGD) input values Tables B-1-1 to B-1-6.

Figure B-1-1 Kansas mix KS-1 shift factor plots for G*
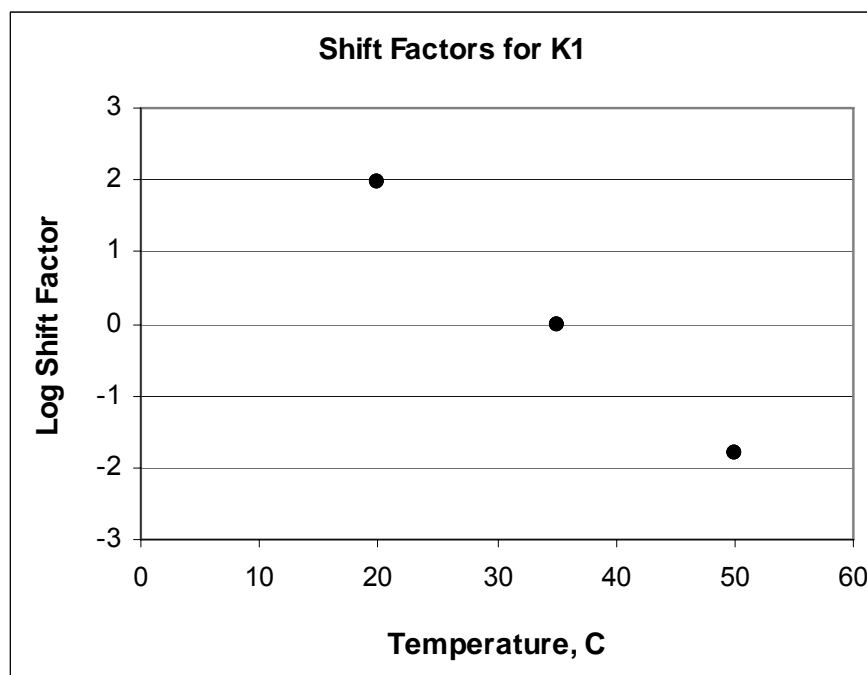
Figure B-1-2 Kansas mix KS-2 shift factors plots for G*

Shift Factors for K2
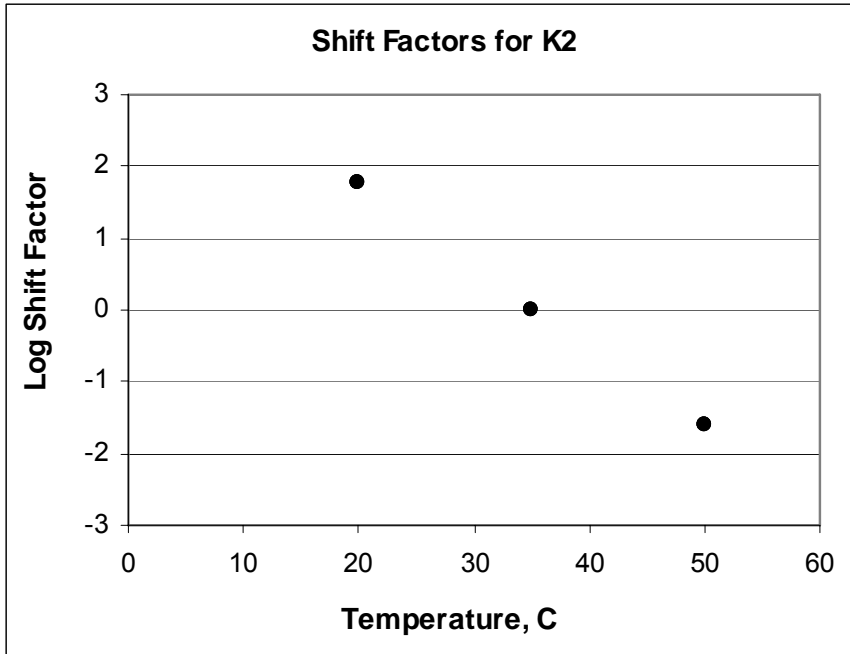
Figure B-1-3 Missouri mix MO-1 shift factors plots for G*

Shift Factors for MO-1
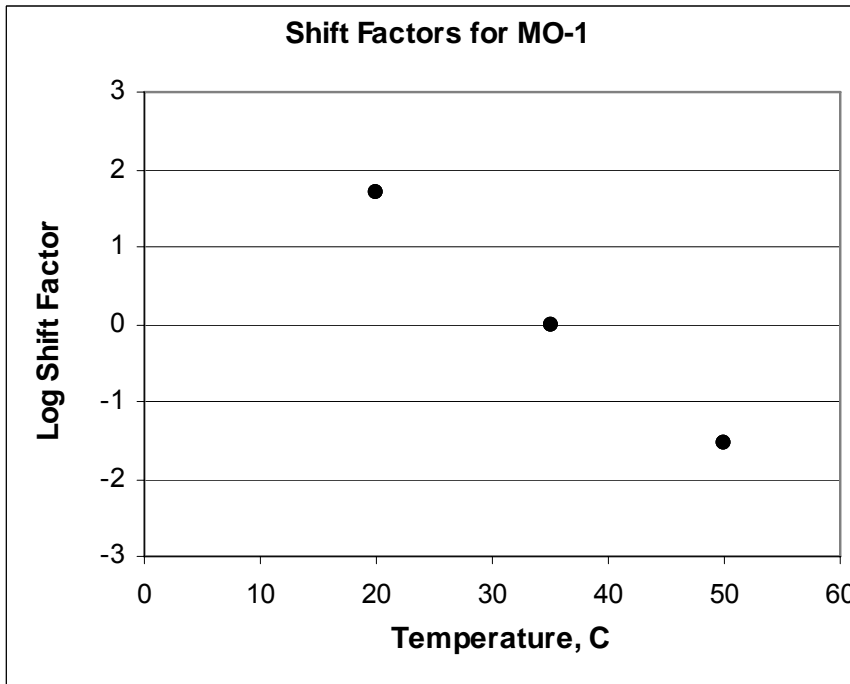
Figure B-1-4 Missouri mix MO-2 shift factors plots for G*

Shift Facotrs for MO-2
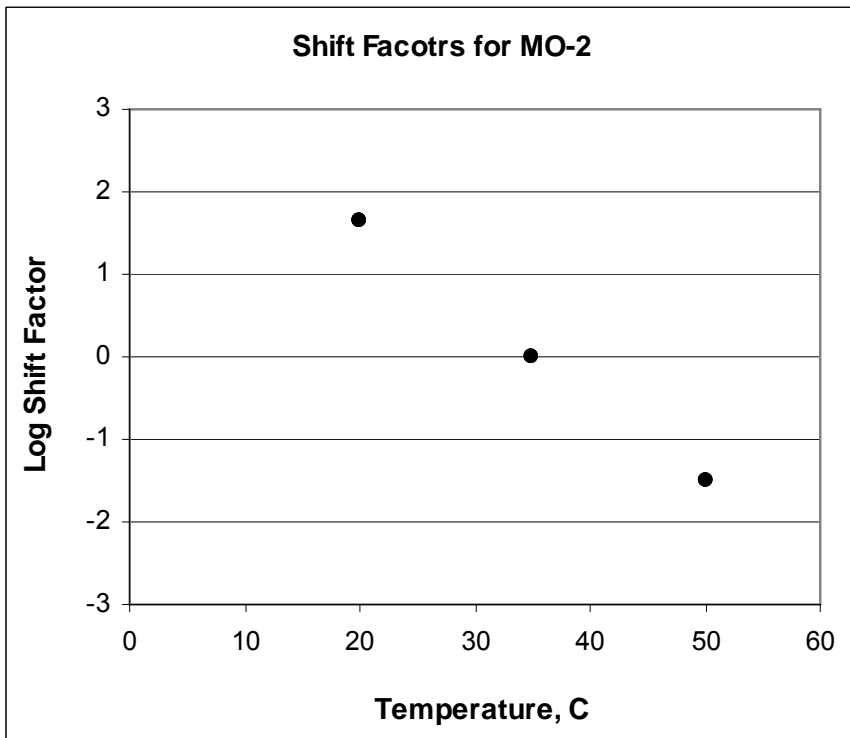
Figure B-1-5 Iowa mix IA-1 shift factors for plots G*

Shift Factors for IA-1
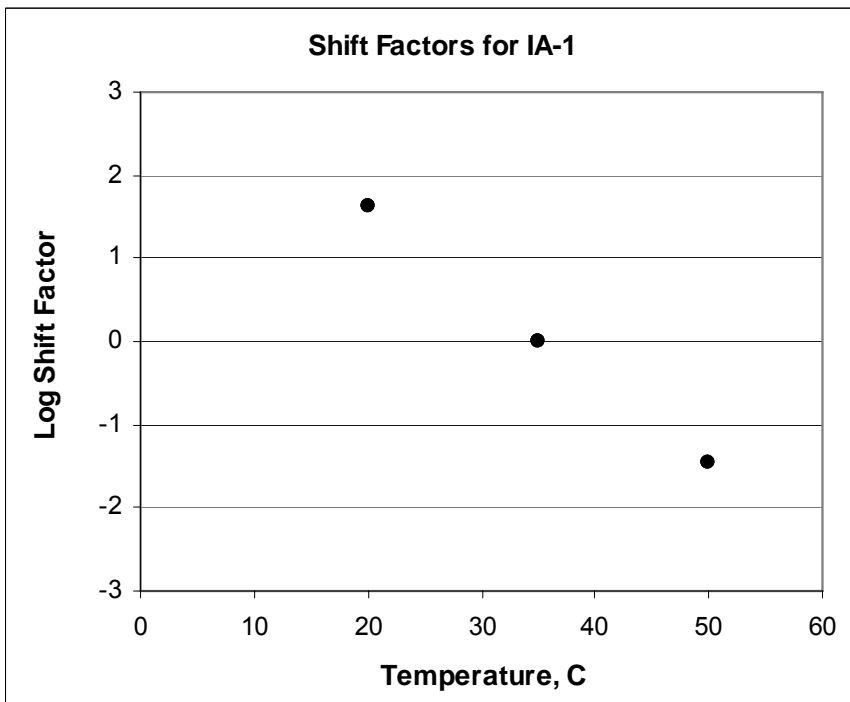
Figure B-1-6 Iowa mix IA-2 shift factors for plots G*
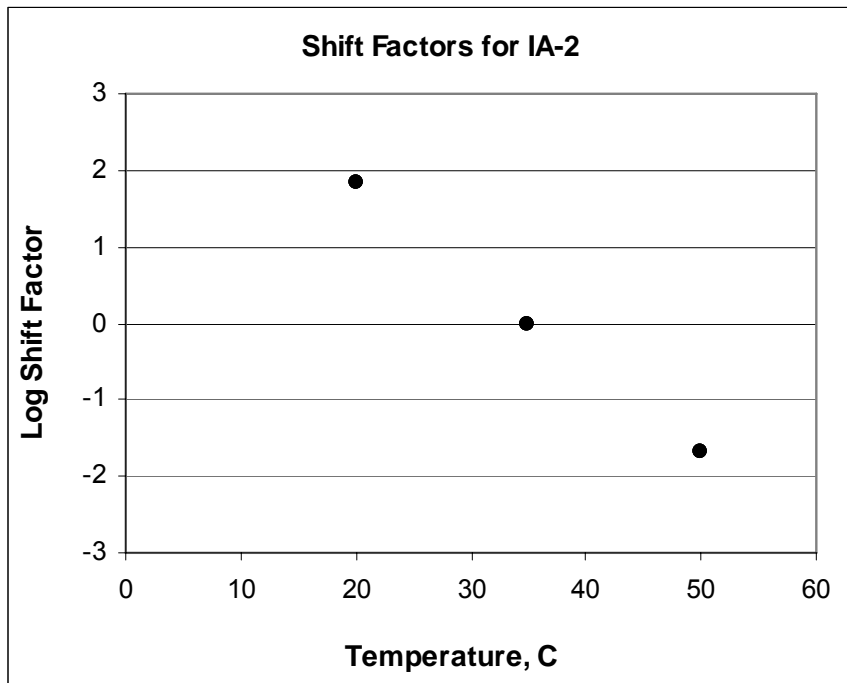
Given in Figures B-1-7 to B-1-12 are the phase angle plots for dynamic shear modulus G*.

Figure B-1-7 Kansas KS-1 Phase angle plots for G*
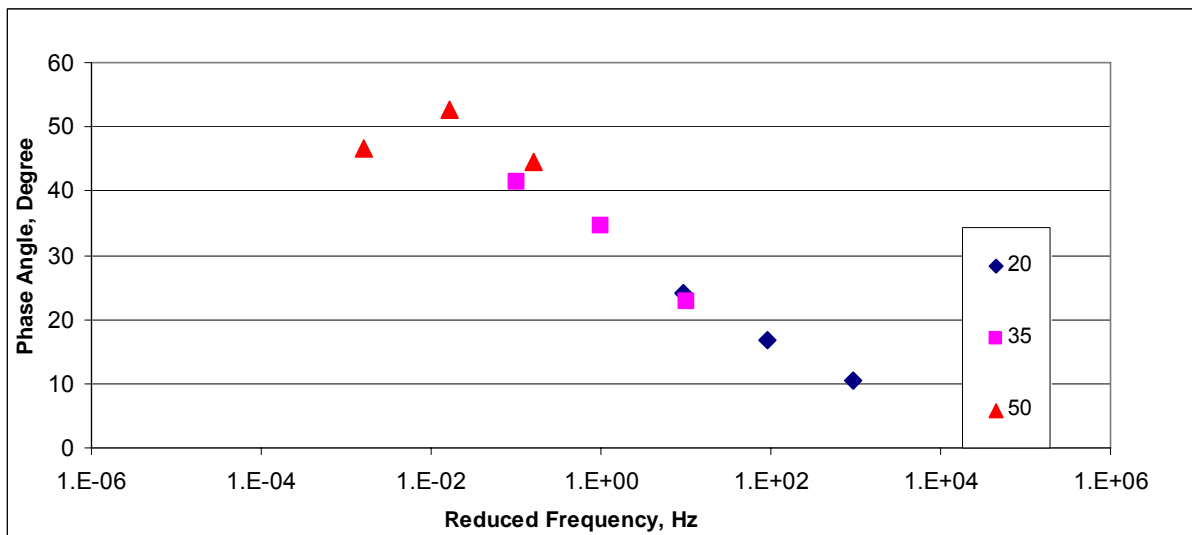
Figure B-1-8 Kansas KS-2 Phase angle plots for G*
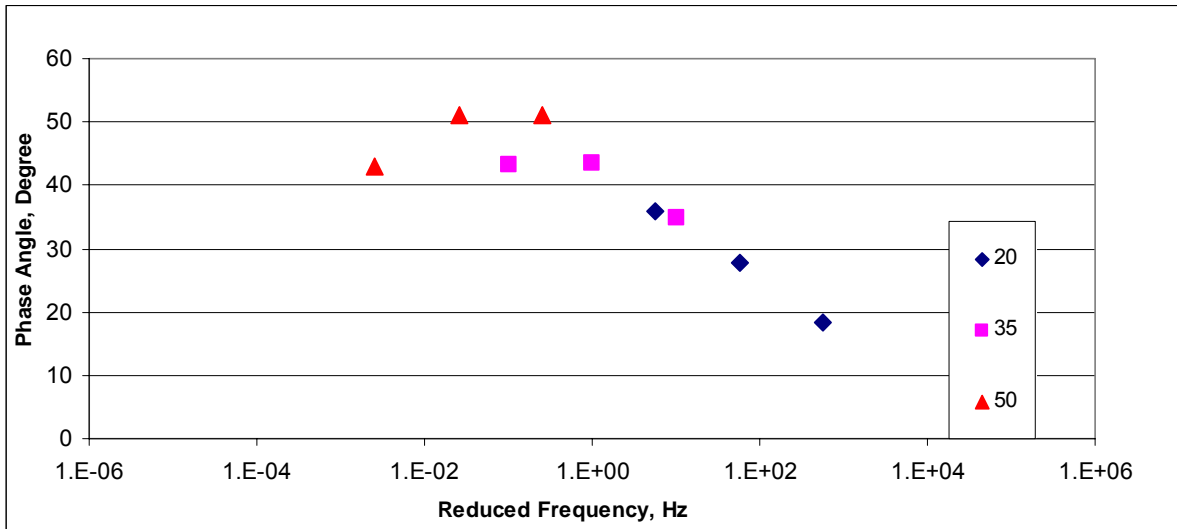
Figure B-1-9 Missouri MO-1 Phase angle plots for G*
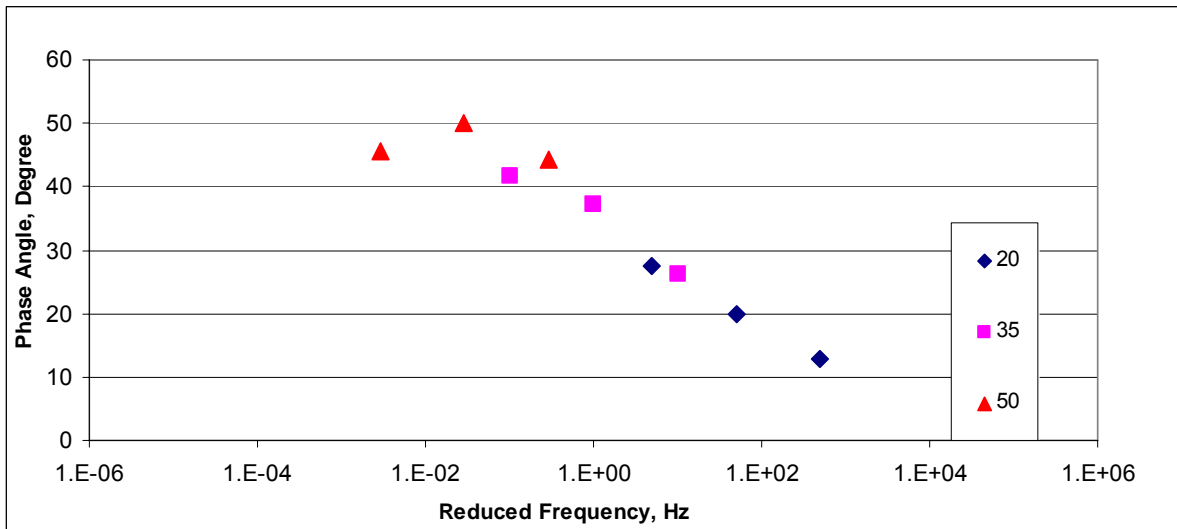
Figure B-1-10 Missouri MO-2 Phase angle plots for G*
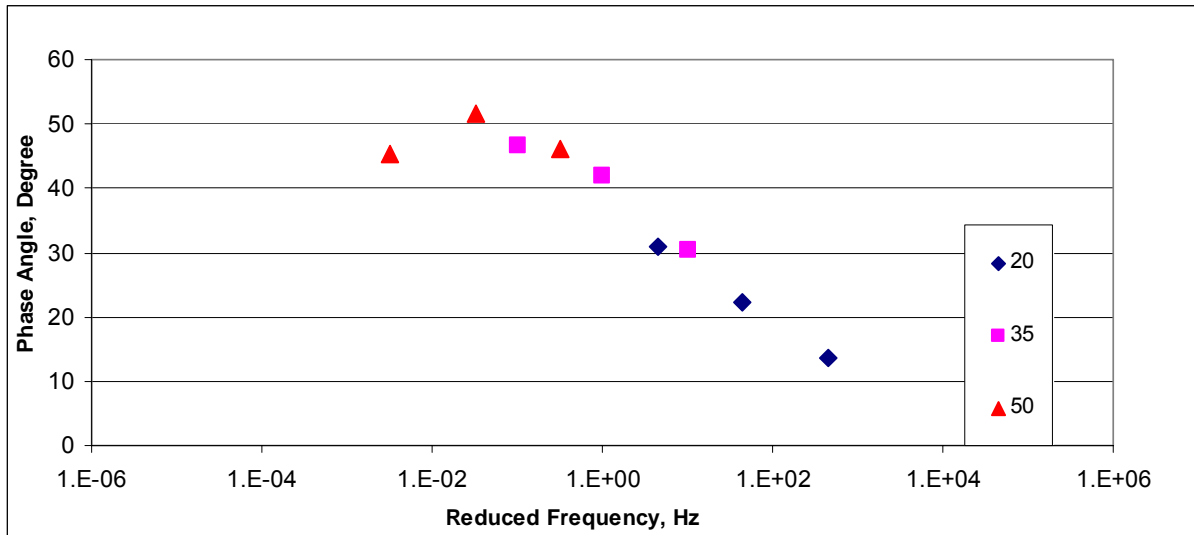
Figure B-1-11 Iowa IA-1 Phase angle plots for G*
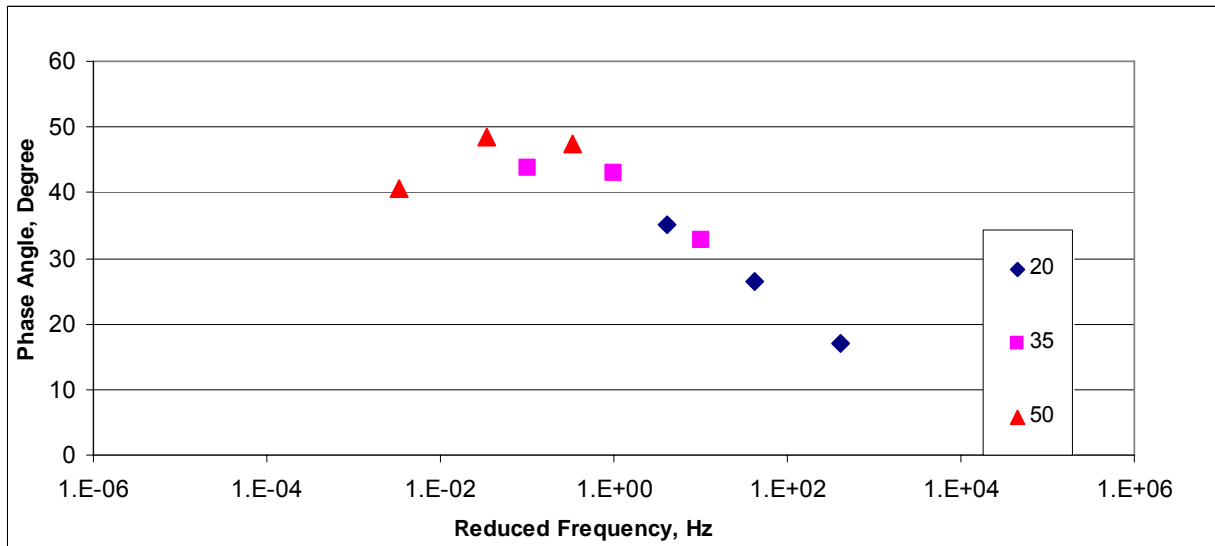
Figure B-1-12 Iowa IA-2 Phase angle plots for G*
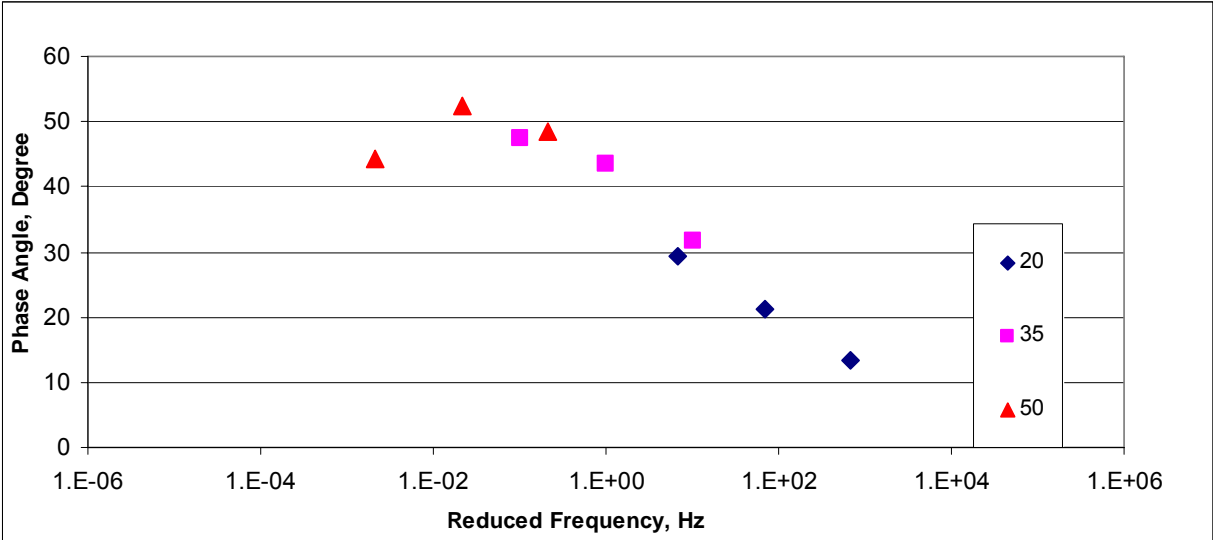
Tables B-1-1 to B-1-6 shows the MEPGD input values at 35ºC.

Table B-1-1 MEPGD Inputs values for Kansas Mix KS-1 for G*

Temp C	Temp F	Frequency Hz	Shift Factor	Reduced Frequency	G* ksi	G* MPa
-10.0	14	25	6.574731	93901259	1943.8	13406.5
-10.0	14	10	6.574731	37560504	1823.2	12574.5
-10.0	14	5	6.574731	18780252	1727.8	11916.5
-10.0	14	1	6.574731	3756050	1495.4	10313.7
-10.0	14	0.5	6.574731	1878025	1392.1	9601.2
-10.0	14	0.1	6.574731	375605	1150.3	7933.9
4.4	40	25	4.232067	426586.9	1169.4	8065.2
4.4	40	10	4.232067	170634.7	1033.4	7127.6
4.4	40	5	4.232067	85317.37	933.1	6435.4
4.4	40	1	4.232067	17063.47	713.8	4922.8
4.4	40	0.5	4.232067	8531.737	627.2	4325.6
4.4	40	0.1	4.232067	1706.347	449.1	3097.6
20.0	68	25	1.967337	2318.871	480.4	3313.2
20.0	68	10	1.967337	927.5485	390.9	2695.8
20.0	68	5	1.967337	463.7743	331.0	2283.0
20.0	68	1	1.967337	92.75485	217.8	1501.9
20.0	68	0.5	1.967337	46.37743	179.4	1237.6
20.0	68	0.1	1.967337	9.275485	111.4	768.6
35.0	95	25	0	25	150.1	1035.1
35.0	95	10	0	10	114.0	786.5
35.0	95	5	0	5	92.0	634.8
35.0	95	1	0	1	55.0	379.7
35.0	95	0.5	0	0.5	43.9	302.9
35.0	95	0.1	0	0.1	25.9	178.8
50.0	122	25	-1.78472	0.410407	41.2	283.9
50.0	122	10	-1.78472	0.164163	30.5	210.3
50.0	122	5	-1.78472	0.082081	24.3	167.7
50.0	122	1	-1.78472	0.016416	14.5	100.0
50.0	122	0.5	-1.78472	0.008208	11.7	80.6
50.0	122	0.1	-1.78472	0.001642	7.2	49.9

Table B-1-2 MEPGD Inputs values for Kansas Mix KS-2 for G*

Temp C	Temp F	Frequency Hz	Shift Factor	Reduced Frequency	E* ksi	E* MPa
-10.0	14	25	5.871486	18596276	1796.6	12390.9
-10.0	14	10	5.871486	7438510	1636.3	11285.6
-10.0	14	5	5.871486	3719255	1511.6	10425.8
-10.0	14	1	5.871486	743851	1217.9	8400.1
-10.0	14	0.5	5.871486	371925.5	1092.9	7538.0
-10.0	14	0.1	5.871486	74385.1	817.0	5634.8
4.4	40	25	3.779398	150431.1	934.5	6445.4
4.4	40	10	3.779398	60172.45	782.8	5399.2
4.4	40	5	3.779398	30086.23	675.8	4660.8
4.4	40	1	3.779398	6017.245	459.0	3165.4
4.4	40	0.5	3.779398	3008.623	380.8	2626.7
4.4	40	0.1	3.779398	601.7245	236.0	1627.5
20.0	68	25	1.756907	1428.39	307.5	2121.1
20.0	68	10	1.756907	571.3558	232.1	1601.0
20.0	68	5	1.756907	285.6779	185.3	1277.8
20.0	68	1	1.756907	57.13558	105.7	729.2
20.0	68	0.5	1.756907	28.56779	81.9	565.1
20.0	68	0.1	1.756907	5.713558	44.4	306.3
35.0	95	25	0	25	78.0	537.7
35.0	95	10	0	10	55.1	380.0
35.0	95	5	0	5	42.2	290.9
35.0	95	1	0	1	22.6	155.9
35.0	95	0.5	0	0.5	17.3	119.5
35.0	95	0.1	0	0.1	9.5	65.7
50.0	122	25	-1.59383	0.636961	19.0	131.1
50.0	122	10	-1.59383	0.254784	13.4	92.6
50.0	122	5	-1.59383	0.127392	10.4	71.7
50.0	122	1	-1.59383	0.025478	5.9	40.7
50.0	122	0.5	-1.59383	0.012739	4.7	32.4
50.0	122	0.1	-1.59383	0.002548	2.9	20.0

Table B-1-3 MEPGD Inputs values for Missouri Mix MO-1 for G*

Temp C	Temp F	Frequency Hz	Shift Factor	Reduced Frequency	G* ksi	G* MPa
-10.0	14	25	5.67477	11822522	1694.4	11686.5
-10.0	14	10	5.67477	4729009	1559.4	10755.5
-10.0	14	5	5.67477	2364504	1454.4	10030.7
-10.0	14	1	5.67477	472900.9	1205.3	8312.8
-10.0	14	0.5	5.67477	236450.4	1098.1	7573.3
-10.0	14	0.1	5.67477	47290.09	856.7	5908.7
4.4	40	25	3.652774	112386.5	984.7	6791.5
4.4	40	10	3.652774	44954.62	849.4	5858.3
4.4	40	5	3.652774	22477.31	751.6	5183.6
4.4	40	1	3.652774	4495.462	545.1	3759.3
4.4	40	0.5	3.652774	2247.731	466.8	3219.3
4.4	40	0.1	3.652774	449.5462	312.9	2158.1
20.0	68	25	1.698044	1247.338	405.8	2799.1
20.0	68	10	1.698044	498.935	321.7	2218.4
20.0	68	5	1.698044	249.4675	266.6	1838.5
20.0	68	1	1.698044	49.8935	165.9	1144.0
20.0	68	0.5	1.698044	24.94675	133.1	918.3
20.0	68	0.1	1.698044	4.98935	77.5	534.6
35.0	95	25	0	25	133.2	918.9
35.0	95	10	0	10	98.4	678.6
35.0	95	5	0	5	77.6	535.0
35.0	95	1	0	1	43.7	301.4
35.0	95	0.5	0	0.5	33.9	233.9
35.0	95	0.1	0	0.1	18.7	129.1
50.0	122	25	-1.54043	0.720297	38.8	267.4
50.0	122	10	-1.54043	0.288119	27.7	190.9
50.0	122	5	-1.54043	0.144059	21.4	147.8
50.0	122	1	-1.54043	0.028812	11.9	81.9
50.0	122	0.5	-1.54043	0.014406	9.3	63.9
50.0	122	0.1	-1.54043	0.002881	5.3	36.6

Table B-1-4 MEPGD Inputs values for Missouri Mix MO-2 for G*

Temp C	Temp F	Frequency Hz	Shift Factor	Reduced Frequency	G* ksi	G* MPa
-10.0	14	25	5.502526	7951814	1727.1	11911.9
-10.0	14	10	5.502526	3180726	1585.4	10934.3
-10.0	14	5	5.502526	1590363	1475.3	10175.0
-10.0	14	1	5.502526	318072.6	1215.3	8381.7
-10.0	14	0.5	5.502526	159036.3	1103.8	7613.0
-10.0	14	0.1	5.502526	31807.26	854.1	5891.0
4.4	40	25	3.541903	87064.92	1008.4	6955.0
4.4	40	10	3.541903	34825.97	867.7	5984.5
4.4	40	5	3.541903	17412.98	766.1	5283.9
4.4	40	1	3.541903	3482.597	552.1	3808.1
4.4	40	0.5	3.541903	1741.298	471.3	3250.4
4.4	40	0.1	3.541903	348.2597	313.0	2158.6
20.0	68	25	1.646504	1107.756	422.6	2914.3
20.0	68	10	1.646504	443.1023	334.0	2303.5
20.0	68	5	1.646504	221.5511	276.0	1903.9
20.0	68	1	1.646504	44.31023	170.3	1174.5
20.0	68	0.5	1.646504	22.15511	136.0	938.2
20.0	68	0.1	1.646504	4.431023	78.0	538.3
35.0	95	25	0	25	141.6	976.3
35.0	95	10	0	10	103.9	716.9
35.0	95	5	0	5	81.5	562.0
35.0	95	1	0	1	45.1	311.3
35.0	95	0.5	0	0.5	34.7	239.3
35.0	95	0.1	0	0.1	18.7	128.8
50.0	122	25	-1.49367	0.802172	41.5	286.4
50.0	122	10	-1.49367	0.320869	29.3	201.9
50.0	122	5	-1.49367	0.160434	22.4	154.6
50.0	122	1	-1.49367	0.032087	12.1	83.1
50.0	122	0.5	-1.49367	0.016043	9.3	63.9
50.0	122	0.1	-1.49367	0.003209	5.1	35.2

Table B-1-5 MEPGD Inputs for values for Iowa Mix IA-1 for G*

Temp C	Temp F	Frequency Hz	Shift Factor	Reduced Frequency	G* ksi	G* MPa
-10.0	14	25	5.408408	6402474	1496.4	10320.7
-10.0	14	10	5.408408	2560990	1350.8	9316.2
-10.0	14	5	5.408408	1280495	1238.9	8544.8
-10.0	14	1	5.408408	256099	980.6	6763.4
-10.0	14	0.5	5.408408	128049.5	873.0	6021.0
-10.0	14	0.1	5.408408	25609.9	640.5	4417.7
4.4	40	25	3.48132	75728.69	794.0	5476.4
4.4	40	10	3.48132	30291.48	663.3	4575.0
4.4	40	5	3.48132	15145.74	571.7	3942.9
4.4	40	1	3.48132	3029.148	387.6	2673.2
4.4	40	0.5	3.48132	1514.574	321.7	2219.0
4.4	40	0.1	3.48132	302.9148	200.2	1380.5
20.0	68	25	1.618341	1038.2	289.3	1995.5
20.0	68	10	1.618341	415.2802	220.7	1521.9
20.0	68	5	1.618341	207.6401	177.6	1225.1
20.0	68	1	1.618341	41.52802	103.6	714.7
20.0	68	0.5	1.618341	20.76401	81.1	559.6
20.0	68	0.1	1.618341	4.152802	45.1	310.9
35.0	95	25	0	25	86.7	597.8
35.0	95	10	0	10	62.3	429.7
35.0	95	5	0	5	48.3	333.0
35.0	95	1	0	1	26.5	183.0
35.0	95	0.5	0	0.5	20.5	141.5
35.0	95	0.1	0	0.1	11.5	79.0
50.0	122	25	-1.46812	0.850778	25.0	172.3
50.0	122	10	-1.46812	0.340311	17.8	122.8
50.0	122	5	-1.46812	0.170156	13.8	95.5
50.0	122	1	-1.46812	0.034031	7.9	54.5
50.0	122	0.5	-1.46812	0.017016	6.3	43.3
50.0	122	0.1	-1.46812	0.003403	3.8	26.4

Table B-1-6 MEPGD Inputs for values for Iowa Mix IA-2 for G*

Temp C	Temp F	Frequency Hz	Shift Factor	Reduced Frequency	G* ksi	G* MPa
-10.0	14	25	6.139637	34480769	1901.4	13114.3
-10.0	14	10	6.139637	13792307	1764.9	12172.5
-10.0	14	5	6.139637	6896154	1656.9	11427.8
-10.0	14	1	6.139637	1379231	1395.1	9622.3
-10.0	14	0.5	6.139637	689615.4	1279.9	8827.2
-10.0	14	0.1	6.139637	137923.1	1014.5	6996.7
4.4	40	25	3.952003	223842.7	1093.4	7541.0
4.4	40	10	3.952003	89537.08	945.3	6519.4
4.4	40	5	3.952003	44768.54	837.4	5775.3
4.4	40	1	3.952003	8953.708	607.6	4190.7
4.4	40	0.5	3.952003	4476.854	519.9	3585.8
4.4	40	0.1	3.952003	895.3708	347.0	2393.2
20.0	68	25	1.837145	1718.243	411.7	2839.3
20.0	68	10	1.837145	687.2973	322.9	2226.7
20.0	68	5	1.837145	343.6487	265.3	1829.6
20.0	68	1	1.837145	68.72973	161.6	1114.7
20.0	68	0.5	1.837145	34.36487	128.6	886.7
20.0	68	0.1	1.837145	6.872973	73.4	506.3
35.0	95	25	0	25	115.4	796.1
35.0	95	10	0	10	83.9	578.7
35.0	95	5	0	5	65.5	451.5
35.0	95	1	0	1	36.2	249.9
35.0	95	0.5	0	0.5	28.0	193.1
35.0	95	0.1	0	0.1	15.5	106.7
50.0	122	25	-1.66662	0.53867	28.8	198.5
50.0	122	10	-1.66662	0.215468	20.5	141.4
50.0	122	5	-1.66662	0.107734	15.9	109.6
50.0	122	1	-1.66662	0.021547	9.0	61.8
50.0	122	0.5	-1.66662	0.010773	7.1	48.8
50.0	122	0.1	-1.66662	0.002155	4.2	29.2

Appendix B-2 – Storage Modulus (G') Results

Appendix B-2 comprise of storage modulus (G') shift factor plots for six asphalt mixes (Figures B-2-1 to B-2-6) Phase angle plots (Figures B-2-7 to B-2-12) and Mechanistic Empirical Pavement Design Guide (MEPGD) input values Tables B-2-1 to B-2-6.

Figure B-2-1 Kansas mix KS-1 shift factor plots for G'
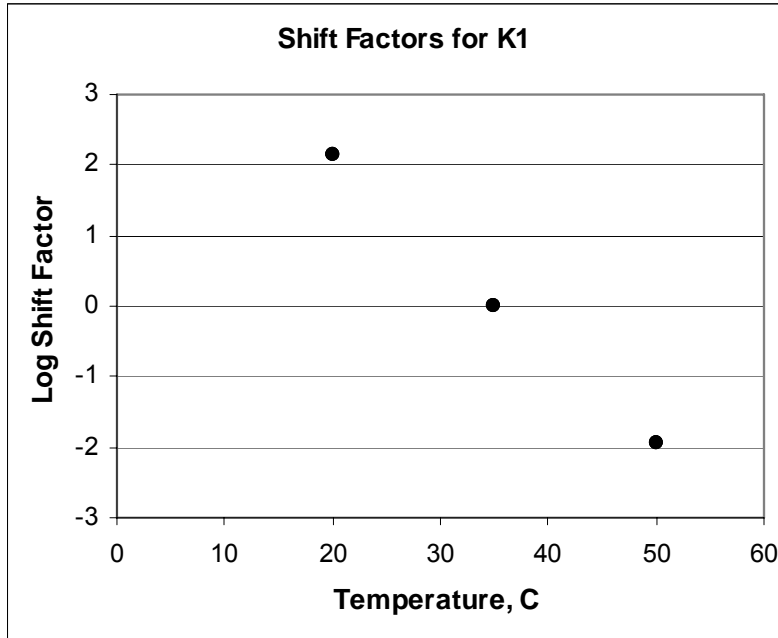
Figure B-2-2 Kansas mix KS-2 shift factors plots for G'
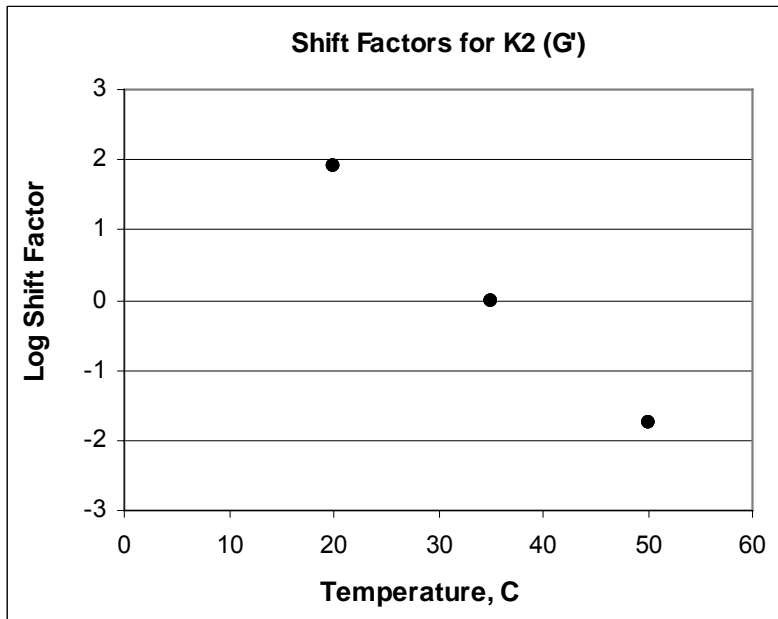
Figure B-2-3 Missouri mix MO-1 shift factors plots for G'
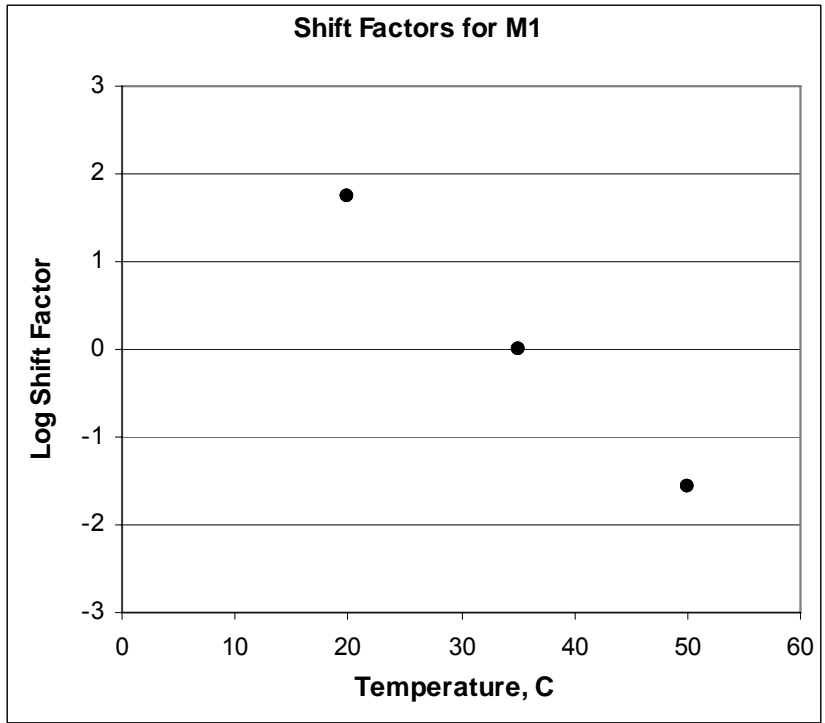
Figure B-2-4 Missouri mix MO-2 shift factors plots for G'
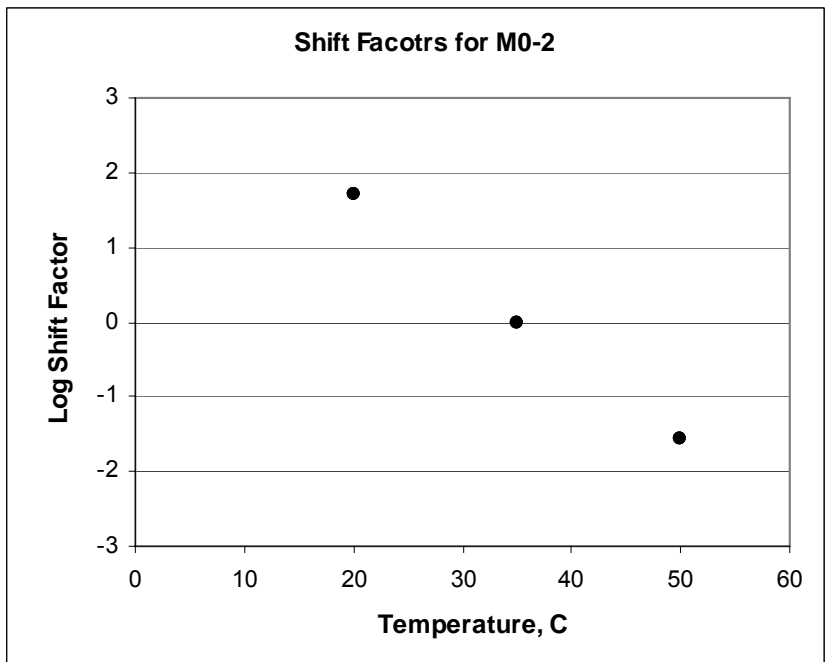
Figure B-2-5 Iowa mix IA-1 shift factors for plots G'

Shift Factors for IA-1

(Plot: Log Shift Factor vs Temperature, C. Data points at approximately (20, 1.8), (35, 0), (50, -1.6))
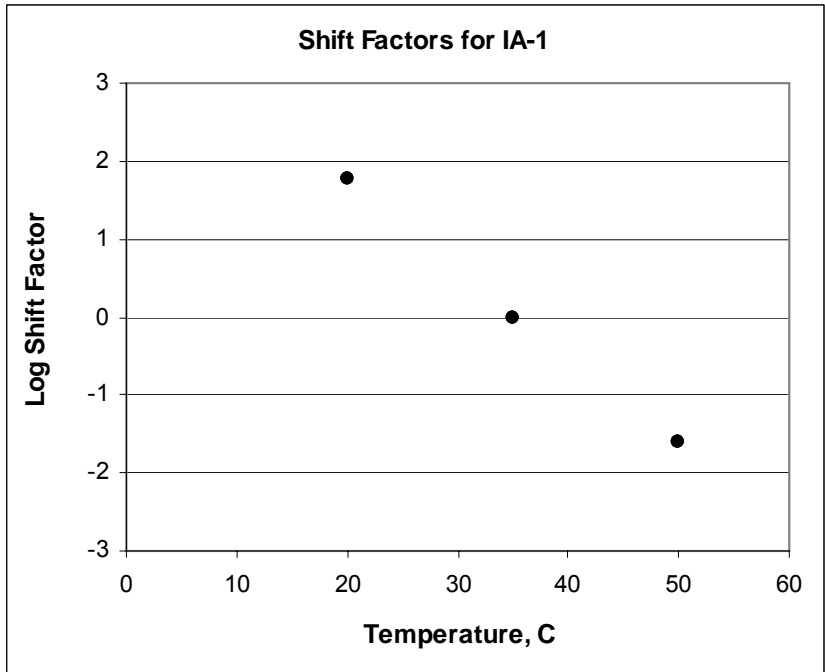
Figure B-2-6 Iowa mix IA-2 shift factors for plots G'

Shift Factors for IA-2

(Plot: Log Shift Factor vs Temperature, C. Data points at approximately (20, 2.4), (35, 0), (50, -2.15))
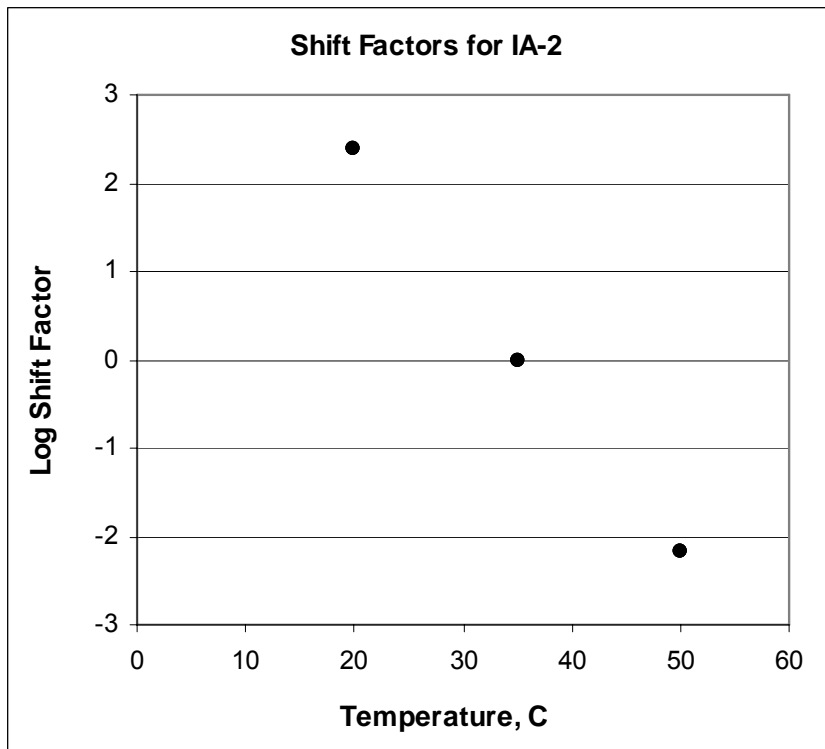
Figure B-2-7 Kansas KS-1 Phase angle plots for G'
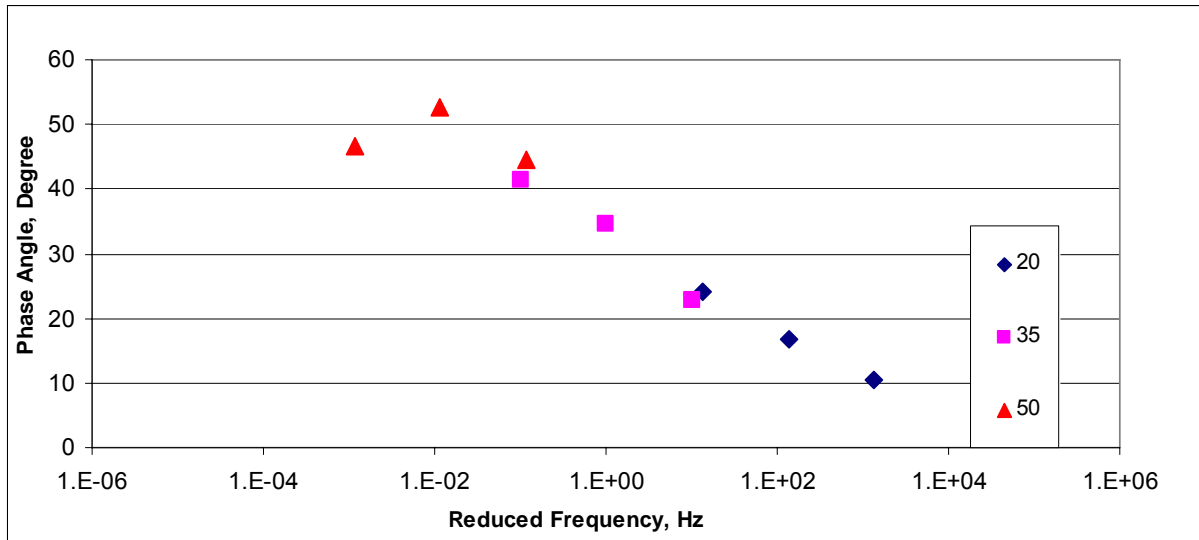
Figure B-2-8 Kansas KS-2 Phase angle plots for G'
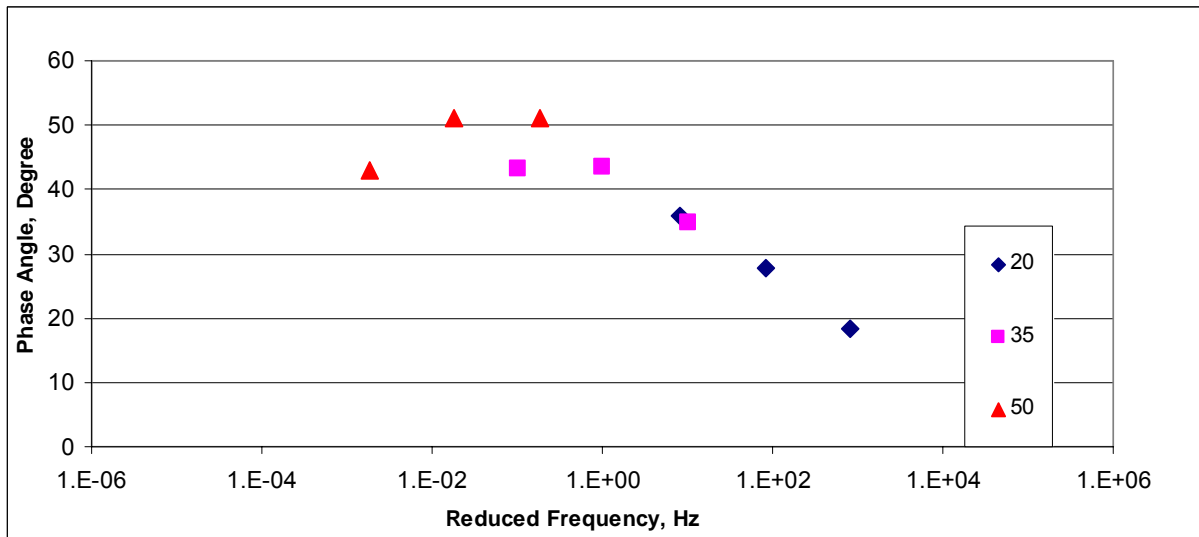
Figure B-2-9 Missouri MO-1 Phase angle plots for G'
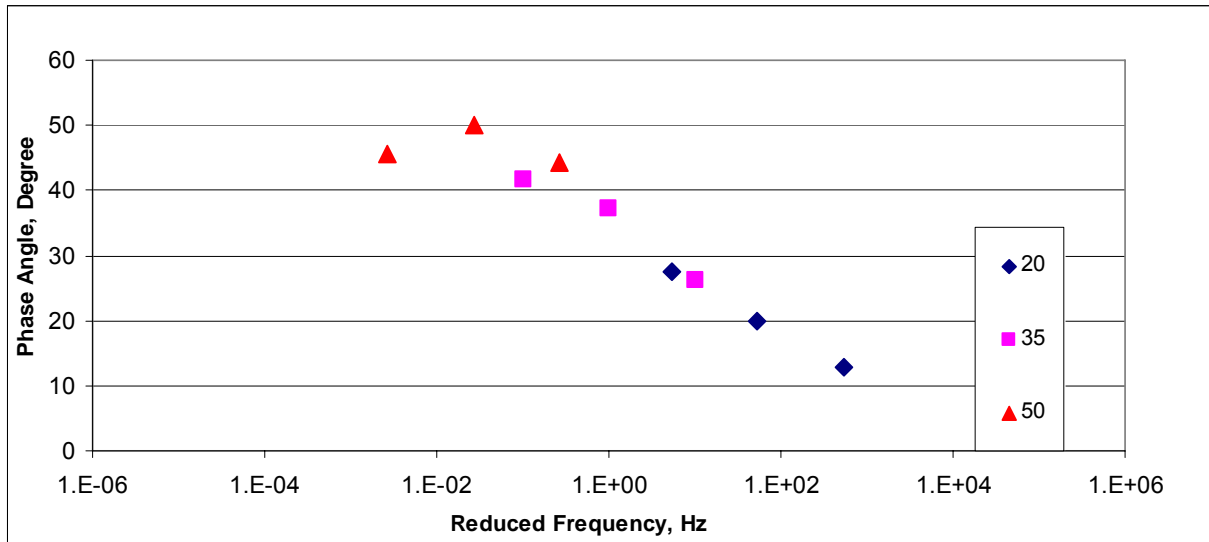
Figure B-2-10 Missouri MO-2 Phase angle plots for G'
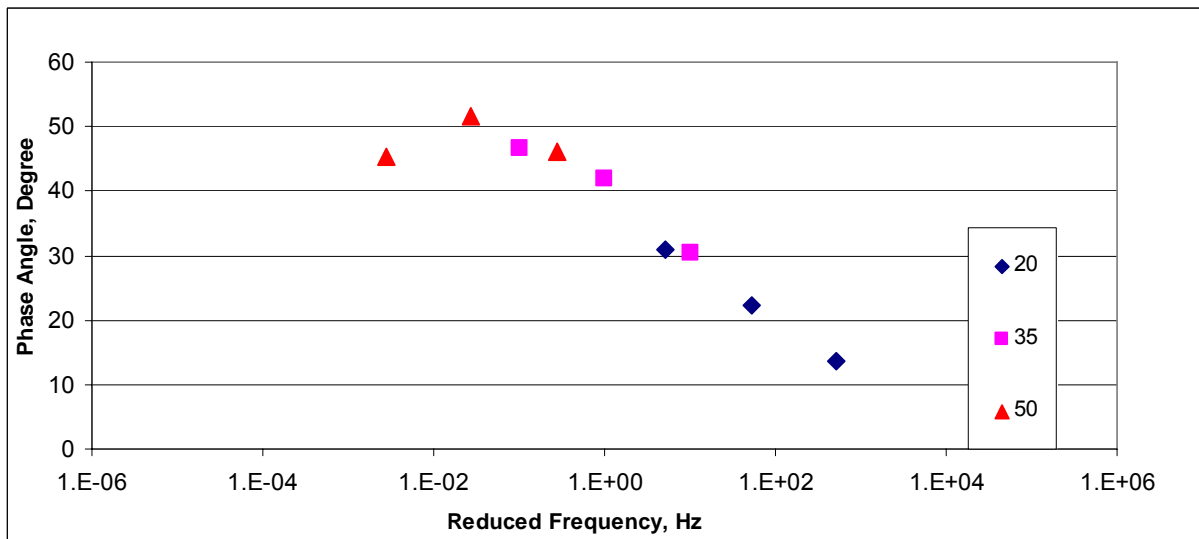
Figure B-2-11 Iowa IA-1 Phase angle plots for G'
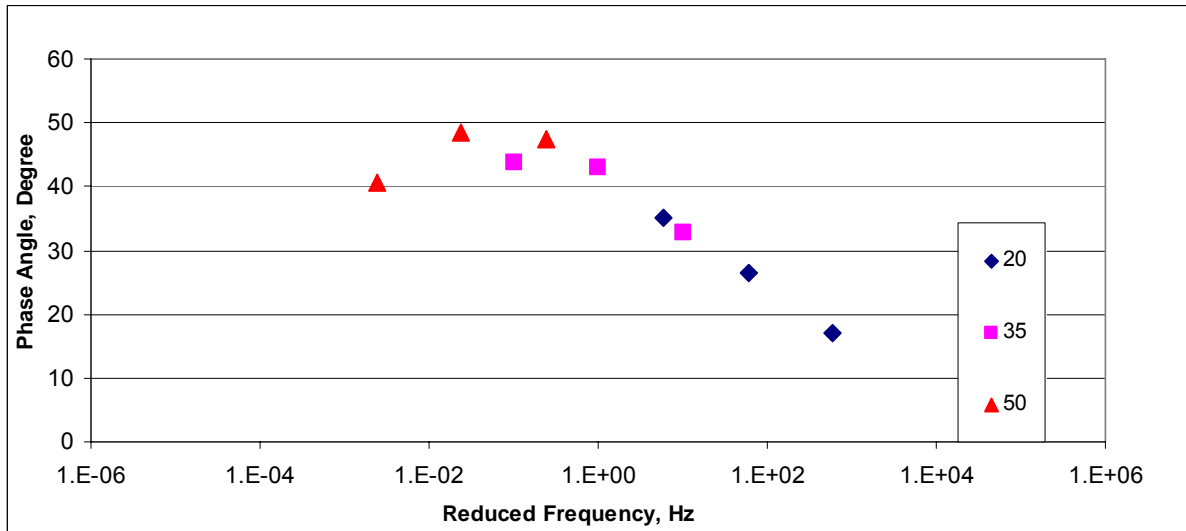
Figure B-2-12 Iowa IA-2 Phase angle plots for G'
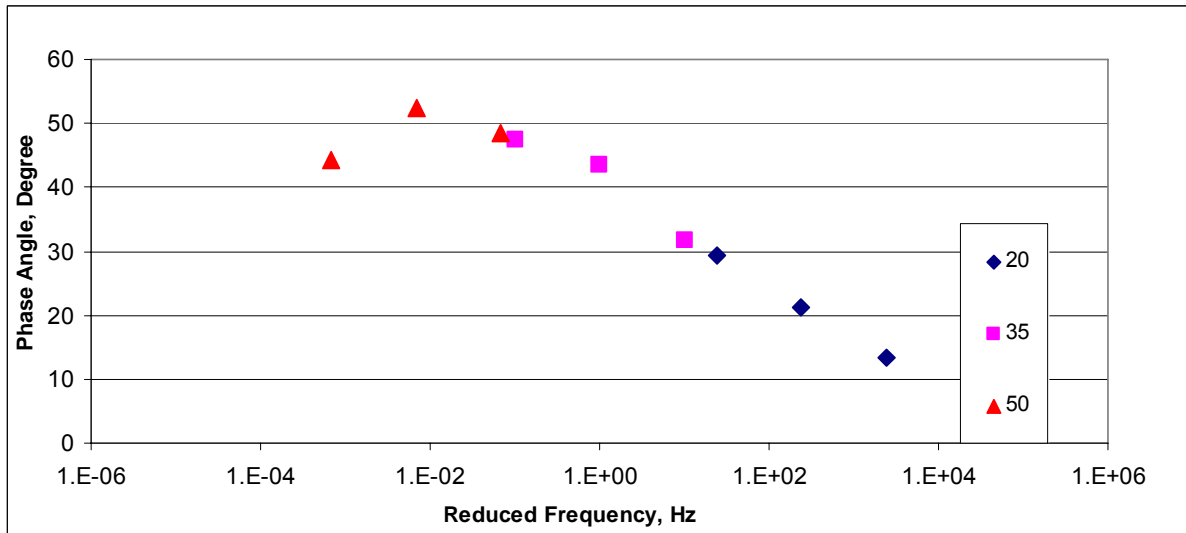
Table B-2-1 MEPGD Inputs values for Kansas Mix KS-1 for G'

Temp C	Temp F	Frequency Hz	Shift Factor	Reduced Frequency	G' ksi	G' MPa
-10.0	14	25	7.146406	3.5E+08	2116.3	14595.9
-10.0	14	10	7.146406	1.4E+08	2002.0	13807.8
-10.0	14	5	7.146406	70044856	1910.3	13175.6
-10.0	14	1	7.146406	14008971	1682.1	11601.3
-10.0	14	0.5	7.146406	7004486	1578.3	10885.5
-10.0	14	0.1	7.146406	1400897	1329.5	9169.5
4.4	40	25	4.600047	995375.6	1276.0	8800.5
4.4	40	10	4.600047	398150.2	1133.0	7814.3
4.4	40	5	4.600047	199075.1	1026.4	7078.8
4.4	40	1	4.600047	39815.02	790.1	5449.5
4.4	40	0.5	4.600047	19907.51	695.7	4798.1
4.4	40	0.1	4.600047	3981.502	499.4	3444.1
20.0	68	25	2.138397	3438.248	483.3	3333.1
20.0	68	10	2.138397	1375.299	390.0	2689.8
20.0	68	5	2.138397	687.6495	328.0	2261.9
20.0	68	1	2.138397	137.5299	211.7	1460.1
20.0	68	0.5	2.138397	68.76495	172.8	1192.1
20.0	68	0.1	2.138397	13.75299	104.9	723.5
35.0	95	25	0	25	126.8	874.6
35.0	95	10	0	10	94.6	652.8
35.0	95	5	0	5	75.4	520.0
35.0	95	1	0	1	43.8	302.4
35.0	95	0.5	0	0.5	34.6	238.7
35.0	95	0.1	0	0.1	20.0	138.2
50.0	122	25	-1.93991	0.2871	28.6	197.5
50.0	122	10	-1.93991	0.11484	21.0	144.8
50.0	122	5	-1.93991	0.05742	16.6	114.8
50.0	122	1	-1.93991	0.011484	9.9	68.2
50.0	122	0.5	-1.93991	0.005742	8.0	55.0
50.0	122	0.1	-1.93991	0.001148	5.0	34.4

Table B-2-2 MEPGD Inputs values for Kansas Mix KS-2 for G'

Temp C	Temp F	Frequency Hz	Shift Factor	Reduced Frequency	G' ksi	G' MPa
-10.0	14	25	6.396493	62292139	1451.5	10011.1
-10.0	14	10	6.396493	24916856	1318.9	9096.5
-10.0	14	5	6.396493	12458428	1218.5	8404.0
-10.0	14	1	6.396493	2491686	989.3	6823.5
-10.0	14	0.5	6.396493	1245843	894.2	6167.1
-10.0	14	0.1	6.396493	249168.6	686.7	4736.2
4.4	40	25	4.117338	327550.2	720.4	4968.4
4.4	40	10	4.117338	131020.1	610.5	4210.8
4.4	40	5	4.117338	65510.05	533.4	3679.2
4.4	40	1	4.117338	13102.01	376.8	2598.7
4.4	40	0.5	4.117338	6551.005	319.5	2203.3
4.4	40	0.1	4.117338	1310.201	210.0	1448.2
20.0	68	25	1.914003	2050.893	237.2	1636.1
20.0	68	10	1.914003	820.3572	184.1	1269.5
20.0	68	5	1.914003	410.1786	150.3	1036.5
20.0	68	1	1.914003	82.03572	90.6	624.9
20.0	68	0.5	1.914003	41.01786	71.8	495.4
20.0	68	0.1	1.914003	8.203572	40.7	280.5
35.0	95	25	0	25	60.6	417.6
35.0	95	10	0	10	43.7	301.4
35.0	95	5	0	5	33.9	233.7
35.0	95	1	0	1	18.4	126.8
35.0	95	0.5	0	0.5	14.0	96.8
35.0	95	0.1	0	0.1	7.4	51.3
50.0	122	25	-1.73634	0.458773	13.6	93.6
50.0	122	10	-1.73634	0.183509	9.5	65.2
50.0	122	5	-1.73634	0.091755	7.2	49.5
50.0	122	1	-1.73634	0.018351	3.8	26.2
50.0	122	0.5	-1.73634	0.009175	2.9	20.0
50.0	122	0.1	-1.73634	0.001835	1.6	10.9

Table B-2-3 MEPGD Inputs values for Missouri Mix MO-1 for G'

Temp C	Temp F	Frequency Hz	Shift Factor	Reduced Frequency	G' ksi	G' MPa
-10.0	14	25	5.790117	15419032	1804.9	12448.6
-10.0	14	10	5.790117	6167613	1663.8	11475.0
-10.0	14	5	5.790117	3083806	1552.6	10708.6
-10.0	14	1	5.790117	616761.3	1285.5	8866.3
-10.0	14	0.5	5.790117	308380.6	1169.2	8063.9
-10.0	14	0.1	5.790117	61676.13	905.2	6243.2
4.4	40	25	3.727022	133340.4	1029.9	7103.5
4.4	40	10	3.727022	53336.15	882.2	6084.7
4.4	40	5	3.727022	26668.07	775.4	5347.9
4.4	40	1	3.727022	5333.615	550.8	3798.6
4.4	40	0.5	3.727022	2666.807	466.4	3216.5
4.4	40	0.1	3.727022	533.3615	303.0	2089.6
20.0	68	25	1.732559	1350.513	391.6	2701.1
20.0	68	10	1.732559	540.2054	304.1	2097.3
20.0	68	5	1.732559	270.1027	247.8	1709.0
20.0	68	1	1.732559	54.02054	147.8	1019.3
20.0	68	0.5	1.732559	27.01027	116.4	802.9
20.0	68	0.1	1.732559	5.402054	64.9	447.8
35.0	95	25	0	25	113.3	781.4
35.0	95	10	0	10	81.5	562.3
35.0	95	5	0	5	63.1	435.1
35.0	95	1	0	1	34.2	236.0
35.0	95	0.5	0	0.5	26.2	180.8
35.0	95	0.1	0	0.1	14.2	97.9
50.0	122	25	-1.57174	0.670194	29.3	202.4
50.0	122	10	-1.57174	0.268077	20.6	142.4
50.0	122	5	-1.57174	0.134039	15.9	109.4
50.0	122	1	-1.57174	0.026808	8.8	60.4
50.0	122	0.5	-1.57174	0.013404	6.9	47.2
50.0	122	0.1	-1.57174	0.002681	4.0	27.7

Table B-2-4 MEPGD Inputs values for Missouri Mix MO-2 for G'

Temp C	Temp F	Frequency Hz	Shift Factor	Reduced Frequency	G' ksi	G' MPa
-10.0	14	25	5.746454	13944210	1895.7	13074.9
-10.0	14	10	5.746454	5577684	1749.8	12068.6
-10.0	14	5	5.746454	2788842	1634.7	11274.3
-10.0	14	1	5.746454	557768.4	1356.7	9357.2
-10.0	14	0.5	5.746454	278884.2	1235.1	8518.5
-10.0	14	0.1	5.746454	55776.84	957.9	6606.6
4.4	40	25	3.698916	124984.5	1095.3	7554.2
4.4	40	10	3.698916	49993.81	939.6	6480.6
4.4	40	5	3.698916	24996.9	826.6	5701.0
4.4	40	1	3.698916	4999.381	587.6	4052.5
4.4	40	0.5	3.698916	2499.69	497.3	3429.7
4.4	40	0.1	3.698916	499.9381	321.8	2219.3
20.0	68	25	1.719494	1310.49	421.0	2903.5
20.0	68	10	1.719494	524.196	326.2	2250.1
20.0	68	5	1.719494	262.098	265.2	1828.8
20.0	68	1	1.719494	52.4196	156.5	1079.2
20.0	68	0.5	1.719494	26.2098	122.4	844.1
20.0	68	0.1	1.719494	5.24196	66.8	460.4
35.0	95	25	0	25	120.3	829.8
35.0	95	10	0	10	85.6	590.4
35.0	95	5	0	5	65.5	452.0
35.0	95	1	0	1	34.4	237.5
35.0	95	0.5	0	0.5	25.9	178.9
35.0	95	0.1	0	0.1	13.4	92.6
50.0	122	25	-1.55989	0.688736	29.6	204.0
50.0	122	10	-1.55989	0.275494	20.3	140.1
50.0	122	5	-1.55989	0.137747	15.3	105.5
50.0	122	1	-1.55989	0.027549	8.0	55.3
50.0	122	0.5	-1.55989	0.013775	6.1	42.3
50.0	122	0.1	-1.55989	0.002755	3.4	23.4

Table B-2-5 MEPGD Inputs for values for Iowa Mix IA-1 for G'

Temp C	Temp F	Frequency Hz	Shift Factor	Reduced Frequency	G' ksi	G' MPa
-10.0	14	25	5.954474	22511999	1354.4	9341.4
-10.0	14	10	5.954474	9004800	1225.4	8451.4
-10.0	14	5	5.954474	4502400	1127.5	7776.1
-10.0	14	1	5.954474	900480	904.1	6235.4
-10.0	14	0.5	5.954474	450240	811.6	5597.7
-10.0	14	0.1	5.954474	90048	611.6	4218.0
4.4	40	25	3.832816	170120.3	687.8	4743.7
4.4	40	10	3.832816	68048.11	579.4	3995.8
4.4	40	5	3.832816	34024.05	503.5	3472.5
4.4	40	1	3.832816	6804.811	350.4	2416.8
4.4	40	0.5	3.832816	3402.405	295.0	2034.8
4.4	40	0.1	3.832816	680.4811	190.7	1315.1
20.0	68	25	1.781739	1512.443	238.3	1643.6
20.0	68	10	1.781739	604.9771	184.3	1271.3
20.0	68	5	1.781739	302.4886	150.2	1035.7
20.0	68	1	1.781739	60.49771	90.3	622.8
20.0	68	0.5	1.781739	30.24886	71.6	494.0
20.0	68	0.1	1.781739	6.049771	40.9	281.9
35.0	95	25	0	25	67.1	463.0
35.0	95	10	0	10	48.8	336.9
35.0	95	5	0	5	38.2	263.3
35.0	95	1	0	1	21.3	146.6
35.0	95	0.5	0	0.5	16.5	113.7
35.0	95	0.1	0	0.1	9.1	63.1
50.0	122	25	-1.61635	0.604763	17.7	121.9
50.0	122	10	-1.61635	0.241905	12.6	87.0
50.0	122	5	-1.61635	0.120953	9.8	67.6
50.0	122	1	-1.61635	0.024191	5.5	38.0
50.0	122	0.5	-1.61635	0.012095	4.3	29.9
50.0	122	0.1	-1.61635	0.002419	2.5	17.5

Table B-2-6 MEPGD Inputs for values for Iowa Mix IA-2 for G'

Temp C	Temp F	Frequency Hz	Shift Factor	Reduced Frequency	G' ksi	G' MPa
-10.0	14	25	7.97206	2.34E+09	2233.4	15403.8
-10.0	14	10	7.97206	9.38E+08	2119.1	14615.7
-10.0	14	5	7.97206	4.69E+08	2026.4	13976.2
-10.0	14	1	7.97206	93769189	1791.9	12358.7
-10.0	14	0.5	7.97206	46884594	1683.7	11612.7
-10.0	14	0.1	7.97206	9376919	1421.2	9802.2
4.4	40	25	5.131509	3384149	1251.1	8628.9
4.4	40	10	5.131509	1353660	1099.2	7581.2
4.4	40	5	5.131509	676829.8	986.8	6805.9
4.4	40	1	5.131509	135366	741.5	5114.5
4.4	40	0.5	5.131509	67682.98	645.4	4451.3
4.4	40	0.1	5.131509	13536.6	450.3	3105.8
20.0	68	25	2.385455	6072.885	369.2	2546.6
20.0	68	10	2.385455	2429.154	289.9	1999.7
20.0	68	5	2.385455	1214.577	239.1	1649.3
20.0	68	1	2.385455	242.9154	148.7	1025.6
20.0	68	0.5	2.385455	121.4577	120.0	827.9
20.0	68	0.1	2.385455	24.29154	72.1	497.0
35.0	95	25	0	25	72.7	501.6
35.0	95	10	0	10	54.2	373.9
35.0	95	5	0	5	43.5	299.8
35.0	95	1	0	1	26.3	181.5
35.0	95	0.5	0	0.5	21.4	147.4
35.0	95	0.1	0	0.1	13.5	93.4
50.0	122	25	-2.16403	0.171359	15.7	108.3
50.0	122	10	-2.16403	0.068544	12.2	84.5
50.0	122	5	-2.16403	0.034272	10.2	70.7
50.0	122	1	-2.16403	0.006854	7.0	48.5
50.0	122	0.5	-2.16403	0.003427	6.1	41.9
50.0	122	0.1	-2.16403	0.000685	4.5	30.9

Appendix B-3 - Loss Modulus (G") Results

Appendix B-3 comprise of loss modulus shift factor plots for six asphalt mixes (Figures B-3-1 to B-3-6) Phase angle plots (Figures B-3-7 to B-3-12) and Mechanistic Empirical Pavement Design Guide (MEPGD) input values (Tables B-3-1 to B-3-6).

Figure B-3-1 Kansas mix KS-1 shift factor plots for G"
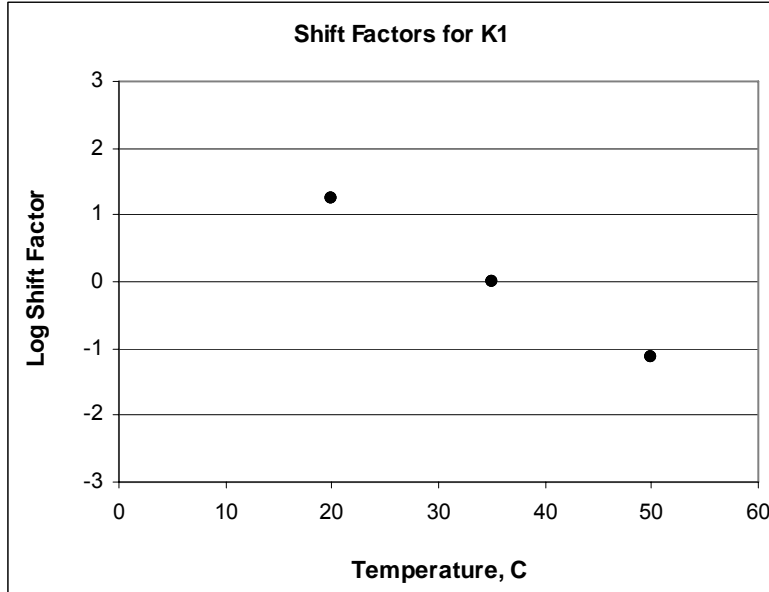
Figure B-3-2 Kansas mix KS-2 shift factors plots for G"
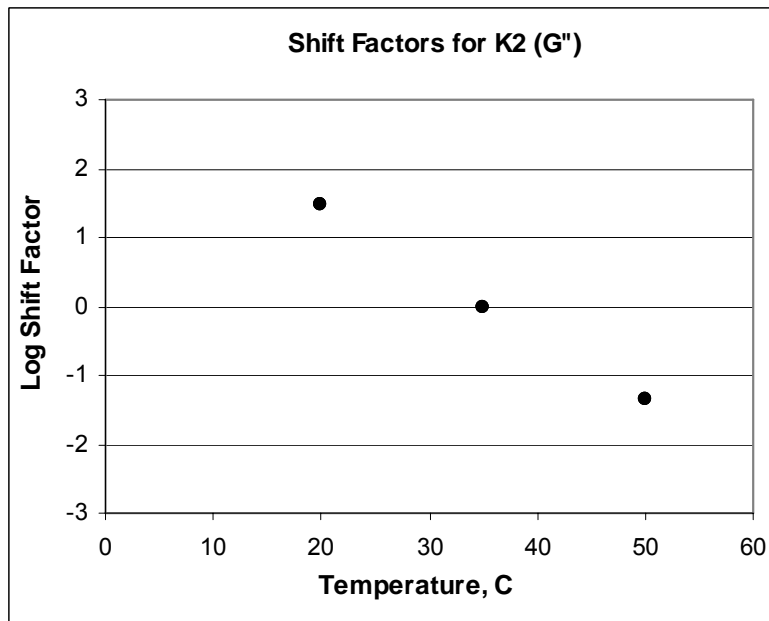
Figure B-3-3 Missouri mix MO-1 shift factors plots for G"
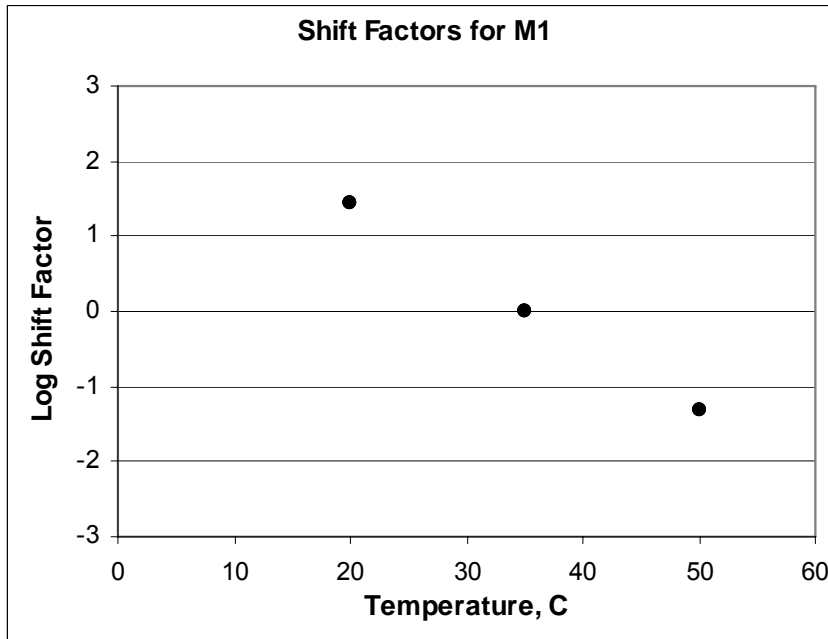
Figure B-3-4 Missouri mix MO-2 shift factors plots for G"
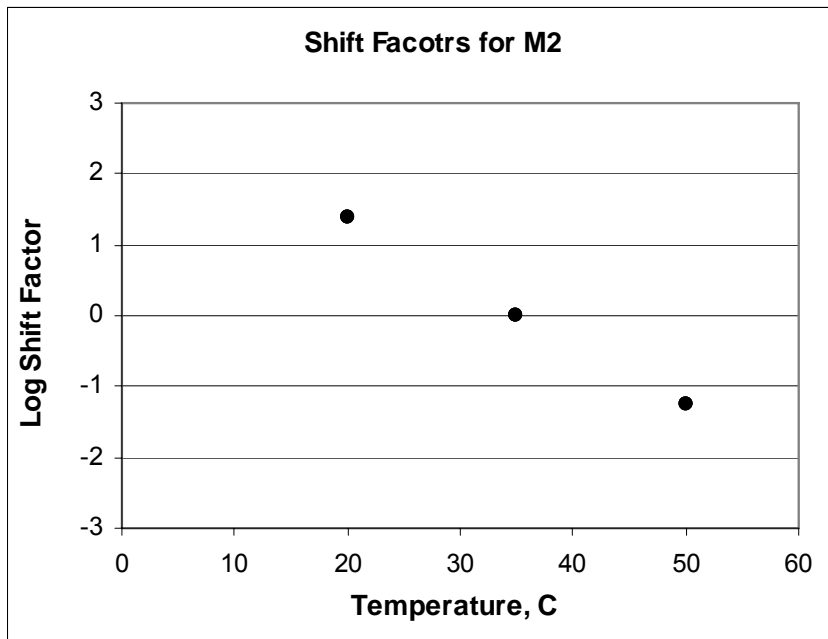
Figure B-3-5 Iowa mix IA-1 shift factors for plots G"

Shift Factors for IA-1
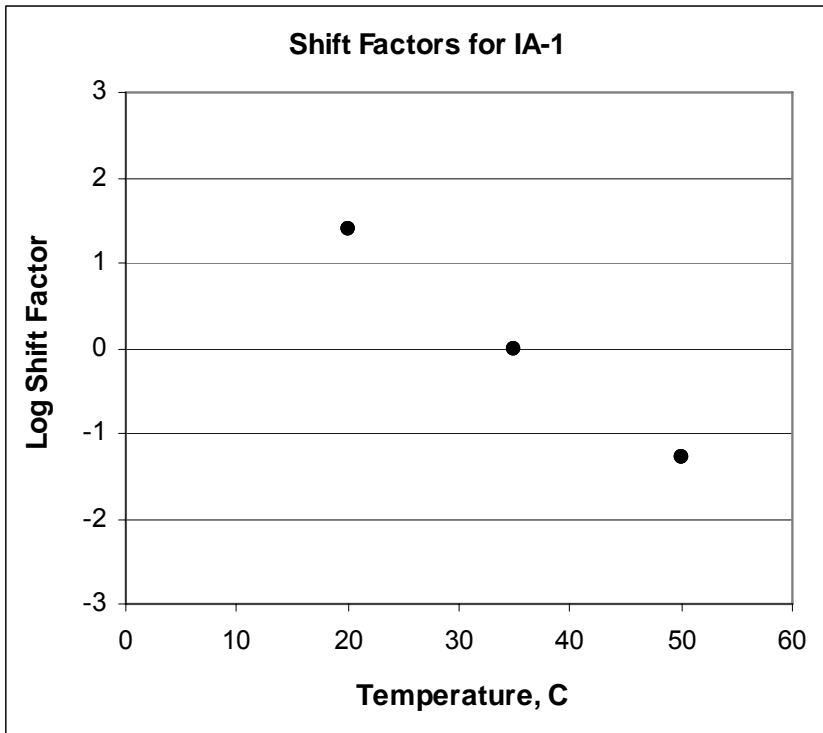
Figure B-3-6 Iowa mix IA-2 shift factors for plots G"

Shift Factors for IA-2
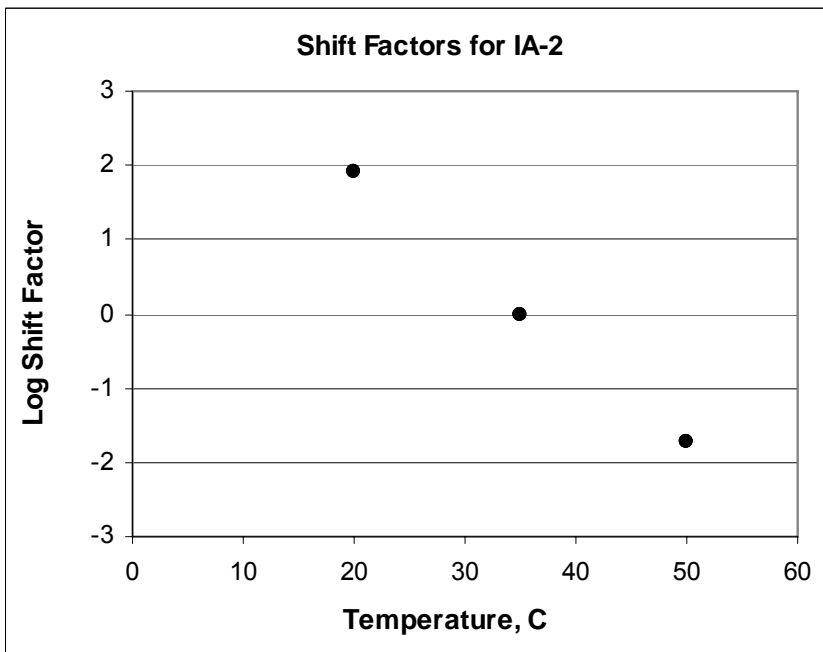
Figure B-3-7 Kansas KS-1 Phase angle plot for G"
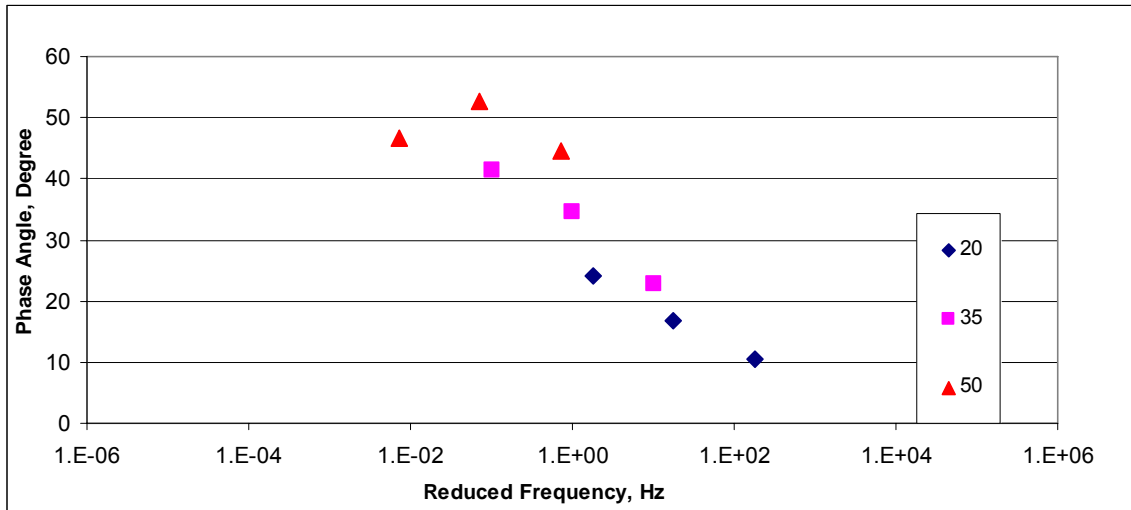
Figure B-3-8 Kansas KS-2 Phase angle plot for G"
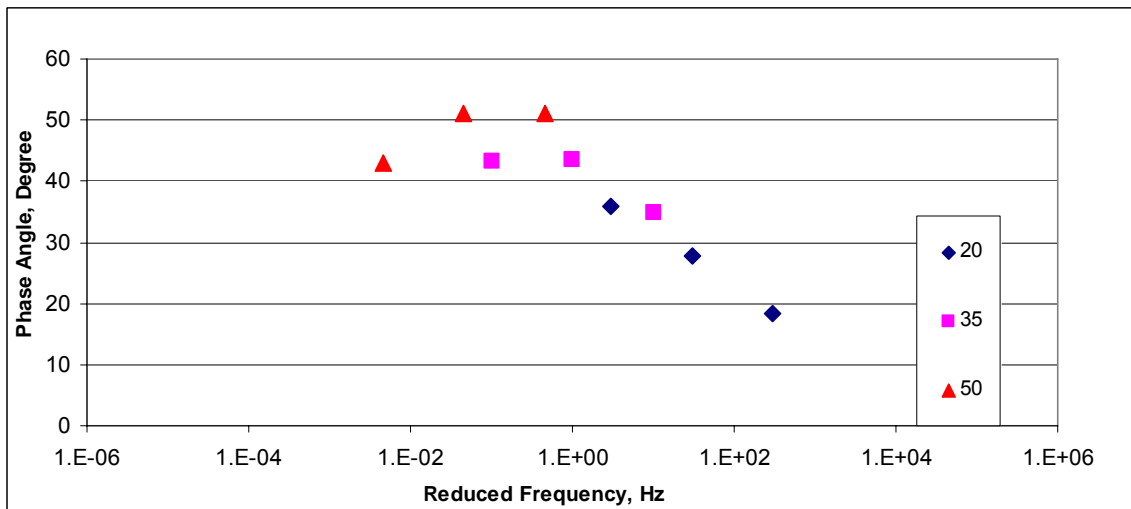
Figure B-3-9 Missouri MO-1 Phase angle plots for G"
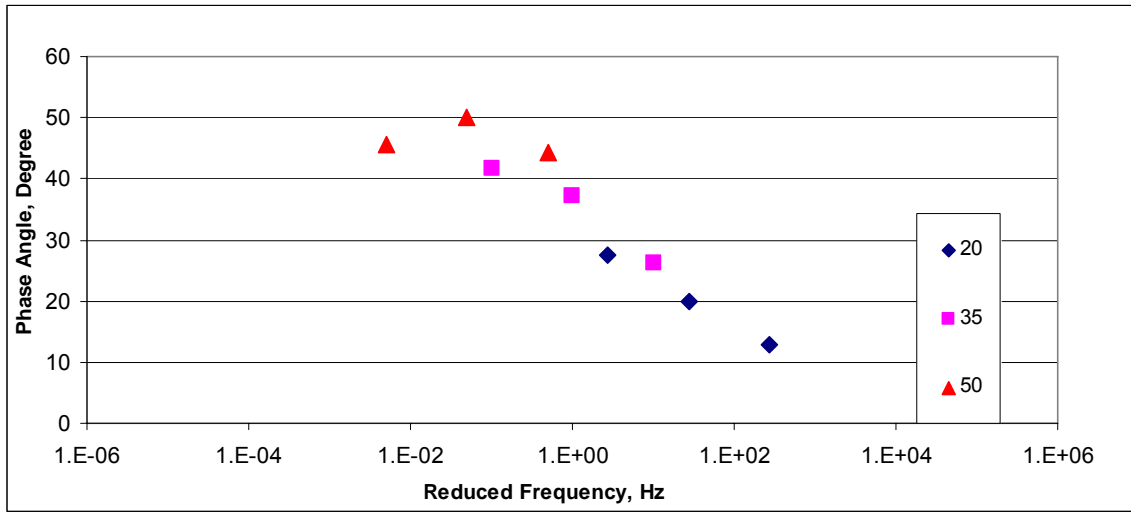
Figure B-3-10 Missouri MO-2 Phase angle plots for G"
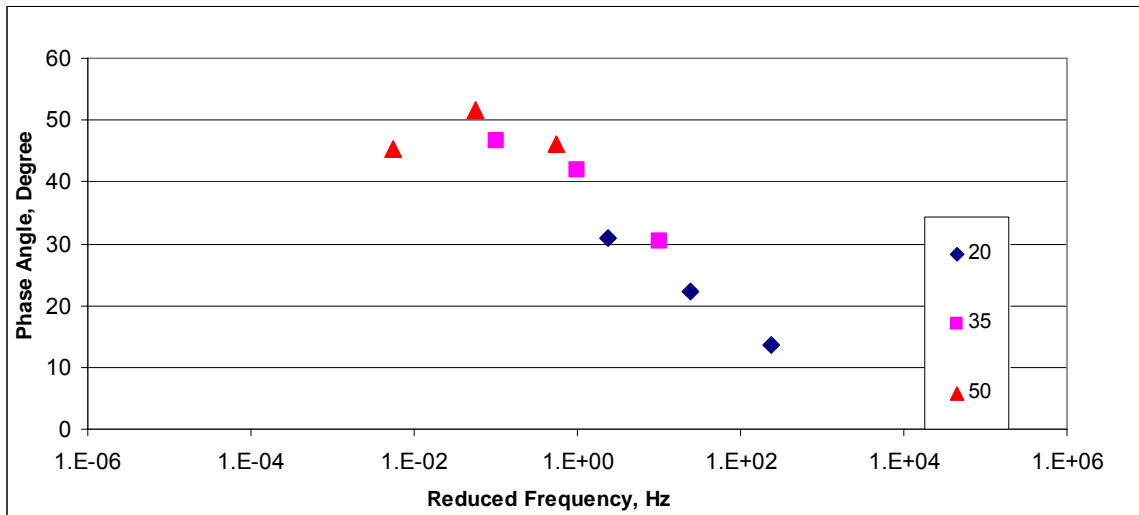
Figure B-3-11 Iowa IA-1 Phase angle plots for G"
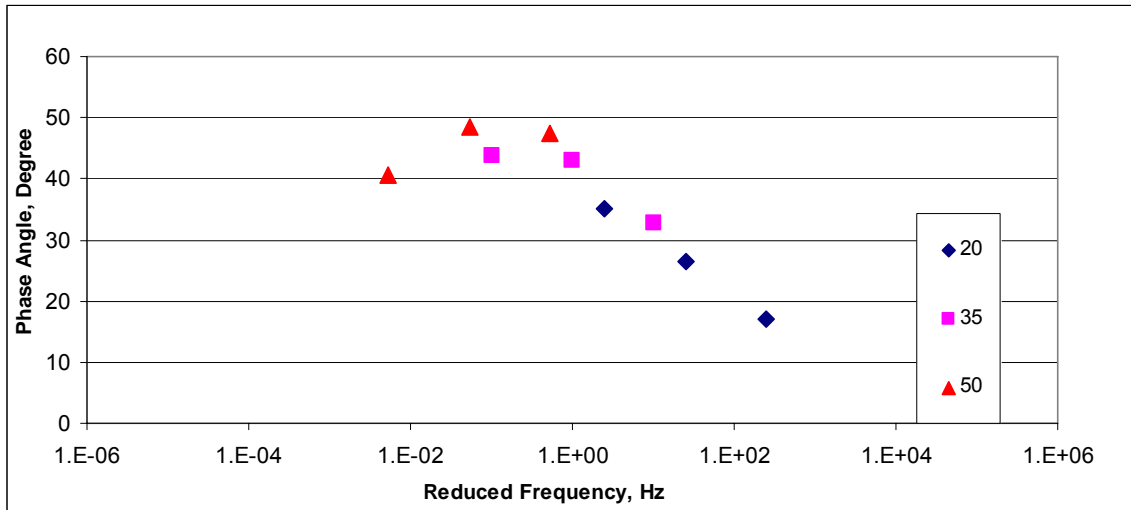
Figure B-3-12 Iowa IA-2 Phase angle plots for G"
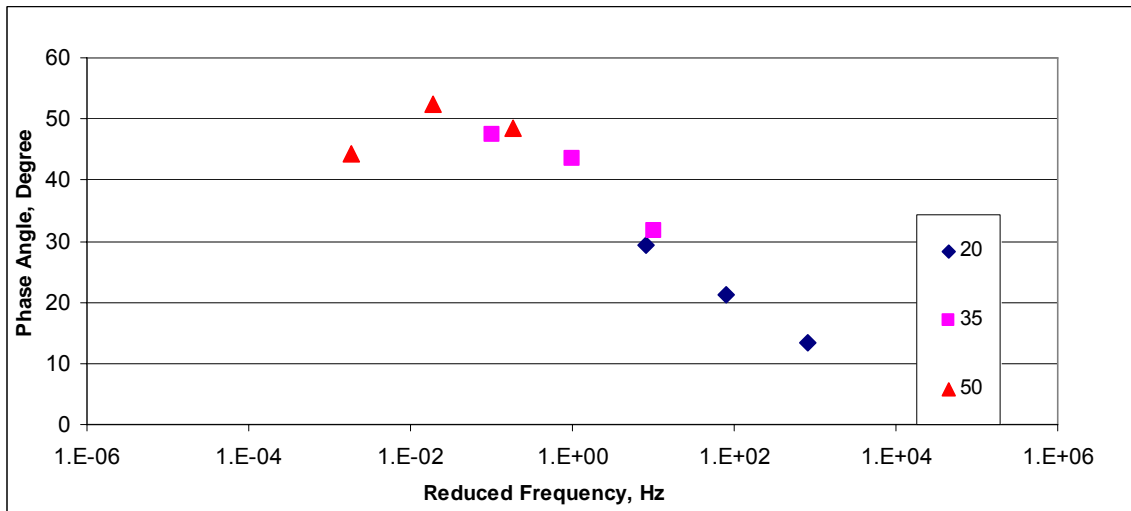
Table B-3-1 MEPGD Inputs values for Kansas Mix KS-1 for G"

Temp C	Temp F	Frequency Hz	Shift Factor	Reduced Frequency	G" ksi	G" MPa
-10.0	14	25	4.196612	393144.7	952.4	6568.9
-10.0	14	10	4.196612	157257.9	805.0	5552.0
-10.0	14	5	4.196612	78628.94	700.4	4830.6
-10.0	14	1	4.196612	15725.79	486.9	3358.4
-10.0	14	0.5	4.196612	7862.894	409.3	2822.9
-10.0	14	0.1	4.196612	1572.579	263.5	1817.2
4.4	40	25	2.701304	12567.35	460.8	3178.4
4.4	40	10	2.701304	5026.941	364.0	2510.2
4.4	40	5	2.701304	2513.471	301.1	2076.5
4.4	40	1	2.701304	502.6941	187.6	1294.0
4.4	40	0.5	2.701304	251.3471	151.3	1043.4
4.4	40	0.1	2.701304	50.26941	90.2	622.2
20.0	68	25	1.255739	450.4841	181.4	1251.2
20.0	68	10	1.255739	180.1936	136.2	939.2
20.0	68	5	1.255739	90.09681	109.0	752.0
20.0	68	1	1.255739	18.01936	64.5	445.0
20.0	68	0.5	1.255739	9.009681	51.5	355.1
20.0	68	0.1	1.255739	1.801936	30.9	212.8
35.0	95	25	0	25	71.8	495.3
35.0	95	10	0	10	53.3	367.3
35.0	95	5	0	5	42.6	293.7
35.0	95	1	0	1	25.8	177.7
35.0	95	0.5	0	0.5	21.0	144.6
35.0	95	0.1	0	0.1	13.4	92.6
50.0	122	25	-1.13918	1.814515	30.9	213.2
50.0	122	10	-1.13918	0.725806	23.4	161.4
50.0	122	5	-1.13918	0.362903	19.1	131.8
50.0	122	1	-1.13918	0.072581	12.4	85.3
50.0	122	0.5	-1.13918	0.03629	10.4	71.8
50.0	122	0.1	-1.13918	0.007258	7.3	50.2

Table B-3-2 MEPGD Inputs values for Kansas Mix KS-2 for G"

Temp C	Temp F	Frequency Hz	Shift Factor	Reduced Frequency	G" ksi	G" MPa
-10.0	14	25	4.952142	2239143	831.1	5731.9
-10.0	14	10	4.952142	895657.1	714.4	4927.5
-10.0	14	5	4.952142	447828.6	631.5	4355.1
-10.0	14	1	4.952142	89565.71	459.2	3167.1
-10.0	14	0.5	4.952142	44782.86	394.7	2722.1
-10.0	14	0.1	4.952142	8956.571	268.4	1851.3
4.4	40	25	3.187628	38509.51	381.4	2630.8
4.4	40	10	3.187628	15403.81	307.3	2119.4
4.4	40	5	3.187628	7701.903	258.3	1781.2
4.4	40	1	3.187628	1540.381	166.7	1150.1
4.4	40	0.5	3.187628	770.1903	136.2	939.1
4.4	40	0.1	3.187628	154.0381	82.5	569.0
20.0	68	25	1.481814	758.1483	135.5	934.7
20.0	68	10	1.481814	303.2593	102.4	706.1
20.0	68	5	1.481814	151.6297	82.1	566.1
20.0	68	1	1.481814	30.32593	47.9	330.2
20.0	68	0.5	1.481814	15.16297	37.6	259.3
20.0	68	0.1	1.481814	3.032593	21.1	145.5
35.0	95	25	0	25	44.8	308.8
35.0	95	10	0	10	32.4	223.7
35.0	95	5	0	5	25.3	174.5
35.0	95	1	0	1	14.1	96.9
35.0	95	0.5	0	0.5	10.9	75.1
35.0	95	0.1	0	0.1	6.0	41.6
50.0	122	25	-1.34427	1.131542	14.7	101.4
50.0	122	10	-1.34427	0.452617	10.5	72.4
50.0	122	5	-1.34427	0.226308	8.1	56.1
50.0	122	1	-1.34427	0.045262	4.5	31.3
50.0	122	0.5	-1.34427	0.022631	3.5	24.4
50.0	122	0.1	-1.34427	0.004526	2.0	14.1

Table B-3-3 MEPGD Inputs values for Missouri Mix MO-1 for G"

Temp C	Temp F	Frequency Hz	Shift Factor	Reduced Frequency	G" ksi	G" MPa
-10.0	14	25	4.800939	1580808	764.2	5270.9
-10.0	14	10	4.800939	632323.2	659.2	4546.8
-10.0	14	5	4.800939	316161.6	584.7	4032.7
-10.0	14	1	4.800939	63232.32	430.3	2967.8
-10.0	14	0.5	4.800939	31616.16	372.5	2569.0
-10.0	14	0.1	4.800939	6323.232	259.0	1786.4
4.4	40	25	3.090301	30778.04	370.3	2554.3
4.4	40	10	3.090301	12311.21	302.5	2086.2
4.4	40	5	3.090301	6155.607	257.4	1775.0
4.4	40	1	3.090301	1231.121	172.2	1187.7
4.4	40	0.5	3.090301	615.5607	143.3	988.3
4.4	40	0.1	3.090301	123.1121	91.5	631.1
20.0	68	25	1.43657	683.1408	147.4	1016.4
20.0	68	10	1.43657	273.2563	114.7	790.9
20.0	68	5	1.43657	136.6282	94.3	650.2
20.0	68	1	1.43657	27.32563	58.8	405.7
20.0	68	0.5	1.43657	13.66282	47.7	329.3
20.0	68	0.1	1.43657	2.732563	29.2	201.5
35.0	95	25	0	25	57.3	395.1
35.0	95	10	0	10	43.4	299.6
35.0	95	5	0	5	35.2	242.4
35.0	95	1	0	1	21.5	148.0
35.0	95	0.5	0	0.5	17.4	119.8
35.0	95	0.1	0	0.1	10.7	74.0
50.0	122	25	-1.30323	1.243698	22.9	158.2
50.0	122	10	-1.30323	0.497479	17.3	119.6
50.0	122	5	-1.30323	0.24874	14.1	97.0
50.0	122	1	-1.30323	0.049748	8.8	60.4
50.0	122	0.5	-1.30323	0.024874	7.2	49.5
50.0	122	0.1	-1.30323	0.004975	4.6	31.9

Table B-3-4 MEPGD Inputs values for Missouri Mix MO-2 for G"

Temp C	Temp F	Frequency Hz	Shift Factor	Reduced Frequency	G" ksi	G" MPa
-10.0	14	25	4.629185	1064450	1094.0	7545.1
-10.0	14	10	4.629185	425779.9	950.9	6558.3
-10.0	14	5	4.629185	212889.9	846.6	5838.8
-10.0	14	1	4.629185	42577.99	623.4	4299.4
-10.0	14	0.5	4.629185	21288.99	537.5	3707.3
-10.0	14	0.1	4.629185	4257.799	366.3	2526.2
4.4	40	25	2.979745	23860.81	551.2	3801.4
4.4	40	10	2.979745	9544.323	447.1	3083.5
4.4	40	5	2.979745	4772.162	377.1	2600.6
4.4	40	1	2.979745	954.4323	244.1	1683.2
4.4	40	0.5	2.979745	477.2162	199.0	1372.8
4.4	40	0.1	2.979745	95.44323	119.7	825.6
20.0	68	25	1.385177	606.8996	213.9	1475.0
20.0	68	10	1.385177	242.7598	161.7	1115.2
20.0	68	5	1.385177	121.3799	129.5	893.3
20.0	68	1	1.385177	24.27598	75.1	518.3
20.0	68	0.5	1.385177	12.13799	58.8	405.7
20.0	68	0.1	1.385177	2.427598	32.8	226.3
35.0	95	25	0	25	75.9	523.6
35.0	95	10	0	10	54.9	378.6
35.0	95	5	0	5	42.7	294.7
35.0	95	1	0	1	23.7	163.3
35.0	95	0.5	0	0.5	18.4	126.6
35.0	95	0.1	0	0.1	10.3	70.7
50.0	122	25	-1.2566	1.384643	26.7	184.1
50.0	122	10	-1.2566	0.553857	19.1	131.5
50.0	122	5	-1.2566	0.276929	14.8	102.1
50.0	122	1	-1.2566	0.055386	8.3	57.5
50.0	122	0.5	-1.2566	0.027693	6.6	45.3
50.0	122	0.1	-1.2566	0.005539	3.9	26.7

Table B-3-5 MEPGD Inputs for values for Iowa Mix IA-1 for G"

Temp C	Temp F	Frequency Hz	Shift Factor	Reduced Frequency	G" ksi	G" MPa
-10.0	14	25	4.67928	1194593	790.7	5453.7
-10.0	14	10	4.67928	477837.2	670.5	4624.2
-10.0	14	5	4.67928	238918.6	585.5	4038.5
-10.0	14	1	4.67928	47783.72	412.3	2843.5
-10.0	14	0.5	4.67928	23891.86	348.9	2406.4
-10.0	14	0.1	4.67928	4778.372	228.5	1575.8
4.4	40	25	3.011991	25699.85	355.2	2450.1
4.4	40	10	3.011991	10279.94	281.2	1939.4
4.4	40	5	3.011991	5139.969	233.2	1608.0
4.4	40	1	3.011991	1027.994	146.1	1007.5
4.4	40	0.5	3.011991	513.9969	117.9	813.5
4.4	40	0.1	3.011991	102.7994	70.2	484.0
20.0	68	25	1.400167	628.2125	125.6	866.0
20.0	68	10	1.400167	251.285	94.0	648.0
20.0	68	5	1.400167	125.6425	75.0	517.1
20.0	68	1	1.400167	25.1285	43.8	301.9
20.0	68	0.5	1.400167	12.56425	34.6	238.6
20.0	68	0.1	1.400167	2.51285	20.1	138.6
35.0	95	25	0	25	43.7	301.3
35.0	95	10	0	10	32.0	220.9
35.0	95	5	0	5	25.3	174.6
35.0	95	1	0	1	14.8	102.1
35.0	95	0.5	0	0.5	11.8	81.6
35.0	95	0.1	0	0.1	7.2	49.6
50.0	122	25	-1.2702	1.34196	16.3	112.5
50.0	122	10	-1.2702	0.536784	12.1	83.5
50.0	122	5	-1.2702	0.268392	9.7	67.0
50.0	122	1	-1.2702	0.053678	6.0	41.3
50.0	122	0.5	-1.2702	0.026839	4.9	34.0
50.0	122	0.1	-1.2702	0.005368	3.2	22.3

Table B-3-6 MEPGD Inputs for values for Iowa Mix IA-2 for G"

Temp C	Temp F	Frequency Hz	Shift Factor	Reduced Frequency	G" ksi	G" MPa
-10.0	14	25	6.360436	57329214	1101.0	7593.8
-10.0	14	10	6.360436	22931686	966.4	6665.2
-10.0	14	5	6.360436	11465843	868.3	5988.4
-10.0	14	1	6.360436	2293169	657.9	4537.6
-10.0	14	0.5	6.360436	1146584	576.6	3976.6
-10.0	14	0.1	6.360436	229316.9	412.5	2845.1
4.4	40	25	4.094128	310504.8	440.7	3039.2
4.4	40	10	4.094128	124201.9	359.5	2479.7
4.4	40	5	4.094128	62100.97	305.9	2110.0
4.4	40	1	4.094128	12420.19	205.8	1419.2
4.4	40	0.5	4.094128	6210.097	172.1	1187.3
4.4	40	0.1	4.094128	1242.019	112.5	775.6
20.0	68	25	1.903214	2000.57	127.7	880.9
20.0	68	10	1.903214	800.2279	100.0	689.4
20.0	68	5	1.903214	400.1139	83.0	572.3
20.0	68	1	1.903214	80.02279	54.1	372.8
20.0	68	0.5	1.903214	40.01139	45.1	311.3
20.0	68	0.1	1.903214	8.002279	30.2	208.0
35.0	95	25	0	25	40.0	276.0
35.0	95	10	0	10	31.8	219.6
35.0	95	5	0	5	26.9	185.8
35.0	95	1	0	1	18.7	129.2
35.0	95	0.5	0	0.5	16.2	111.7
35.0	95	0.1	0	0.1	11.9	82.1
50.0	122	25	-1.72655	0.46923	16.0	110.3
50.0	122	10	-1.72655	0.187692	13.4	92.2
50.0	122	5	-1.72655	0.093846	11.8	81.1
50.0	122	1	-1.72655	0.018769	9.0	62.2
50.0	122	0.5	-1.72655	0.009385	8.1	56.1
50.0	122	0.1	-1.72655	0.001877	6.6	45.4

Appendix C - Results from Creep Model Analysis

In this appendix are plots of permanent deformation observed in the base and subgrade layer as modeled using Abaqus/CAE. It can be seen that the most deformation in Kansas and Missouri mixes originated form the subgrade layer. For KS-a mix, about 50% of permanent deformation is from the subgrade.

Figure C-1 Predicted permanent deformation for KS-1 base plus subgrade layers
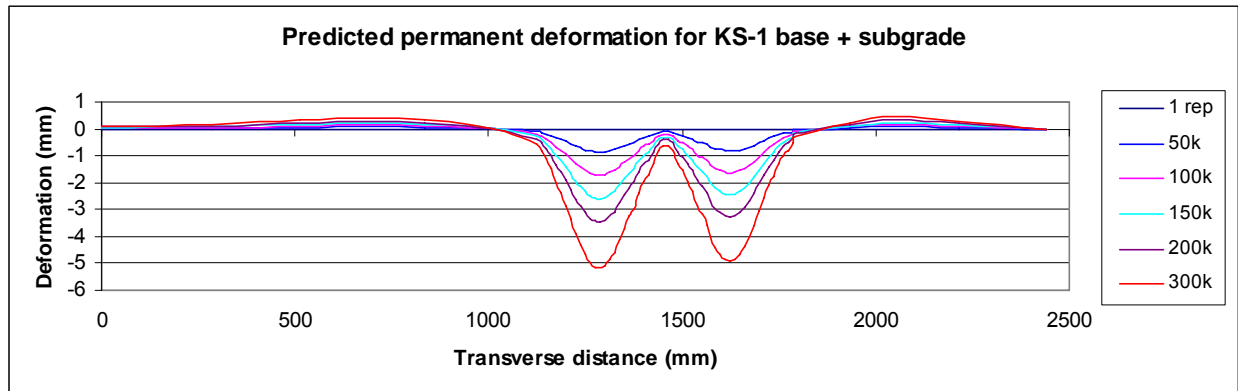
Figure C-2 Predicted permanent deformation for KS-1 subgrade
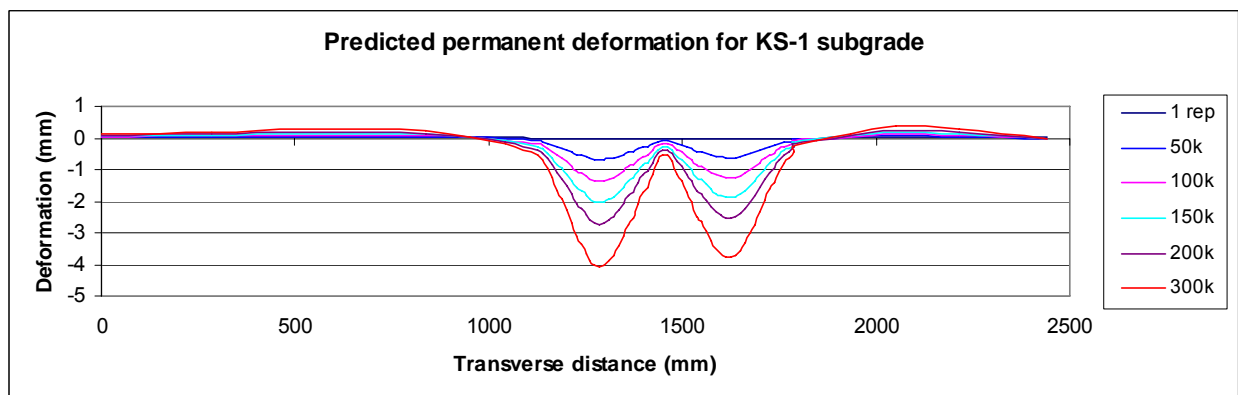
Figure C-3 Predicted permanent deformation for KS-2 base plus subgrade layers
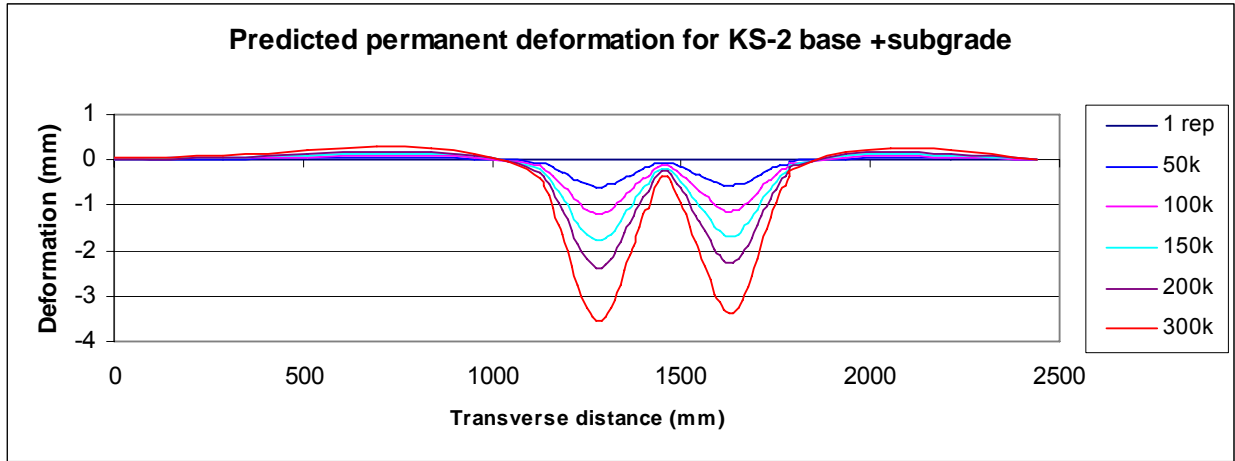
Figure C-4 Predicted permanent deformation for KS-2 subgrade
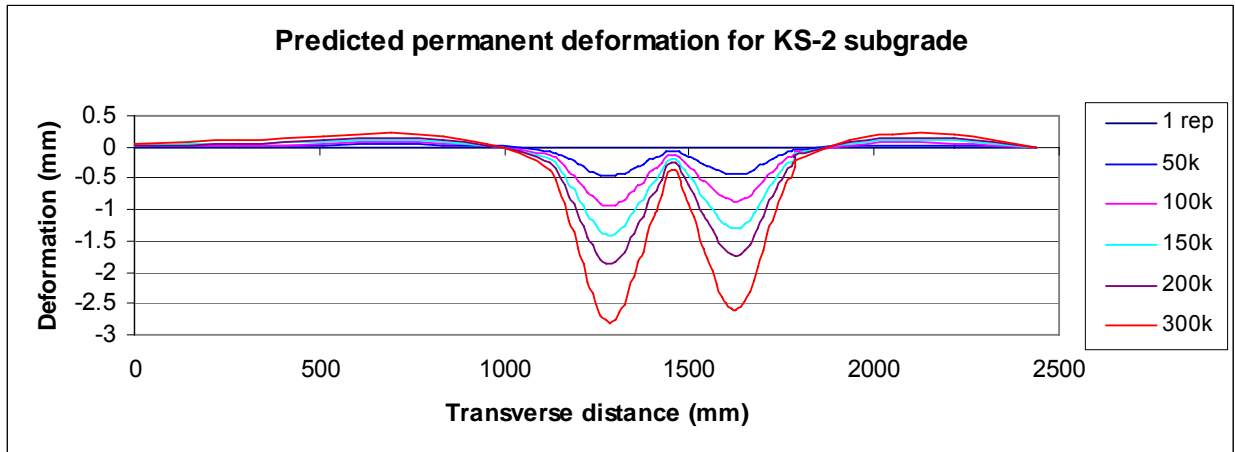
Figure C-5 Predicted permanent deformation for MO-1 base plus subgrade layers
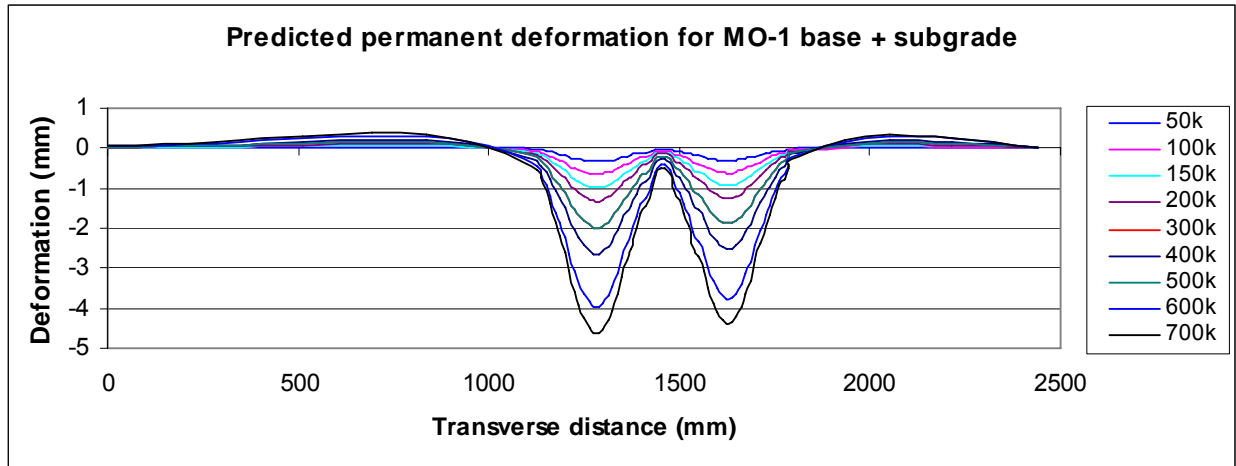
Figure C-6 Predicted permanent deformation for MO-1 subgrade
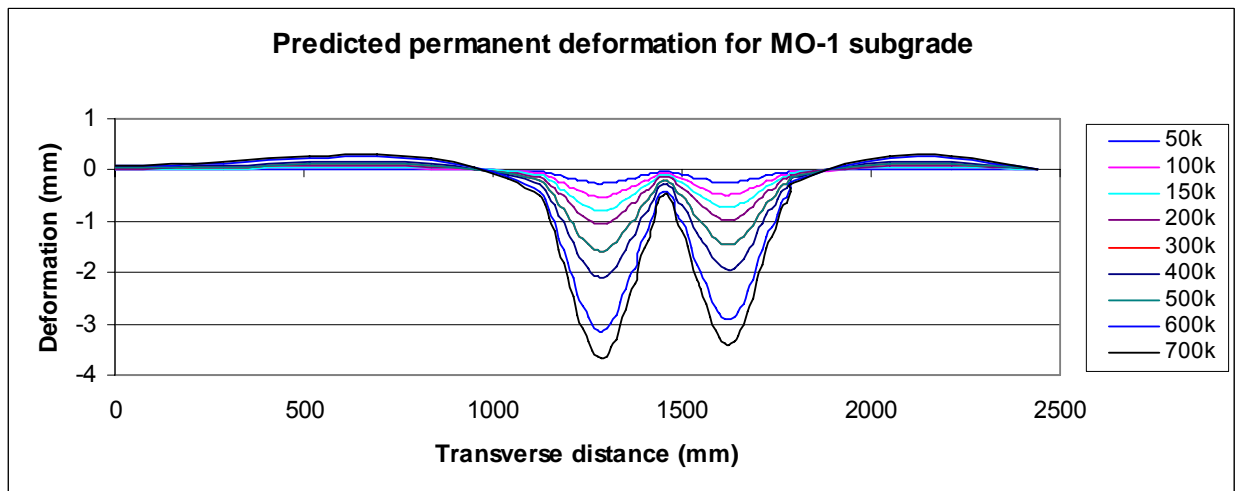
Figure C-1 Predicted permanent deformation for MO-2 base plus subgrade layers

Predicted permanent deformation for MO-2 base + subgrade

Figure C-1 Predicted permanent deformation for MO-2 subgrade
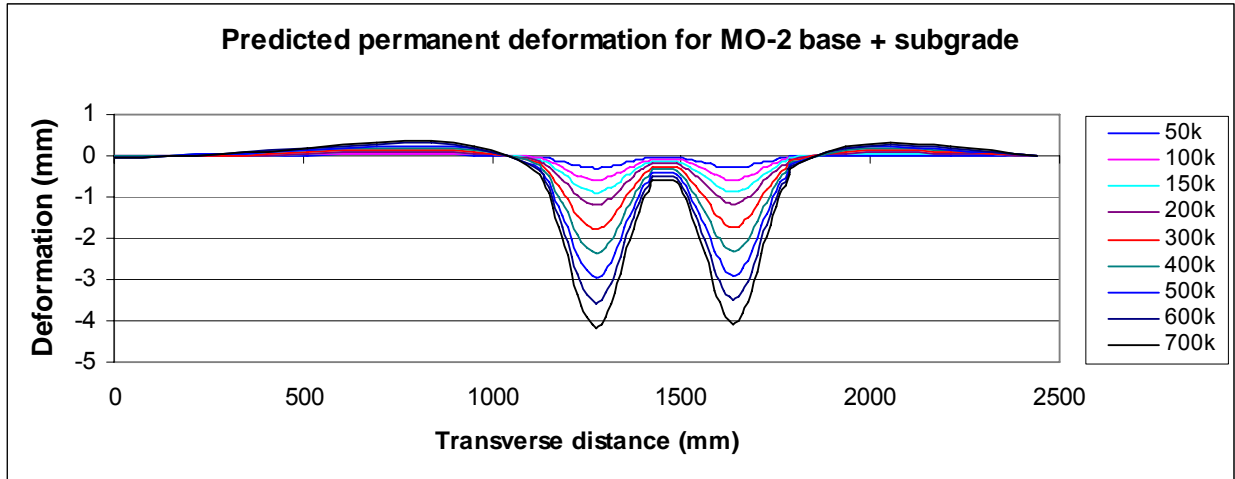
Predicted permanent deformation for MO-2 subgrade

Figure C-1 Predicted permanent deformation for IA-1 base plus subgrade layers

Predicted permanent deformation for IA-1 base course

Figure C-1 Predicted permanent deformation for IA-1 subgrade
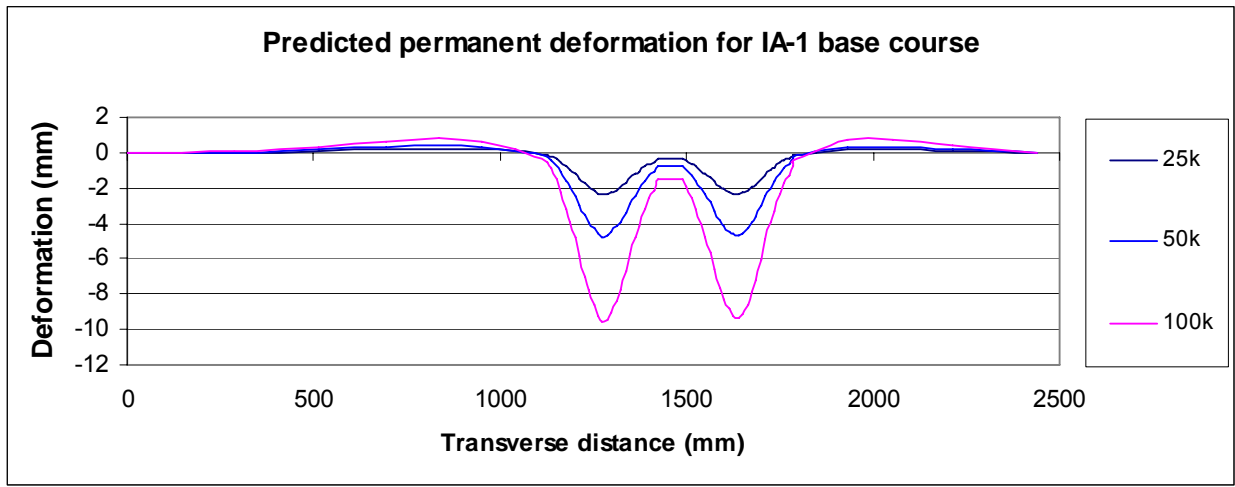
Predicted permanent deformation for IA-1 subgrade

Figure C-1 Predicted permanent deformation for IA-2 base plus subgrade layers
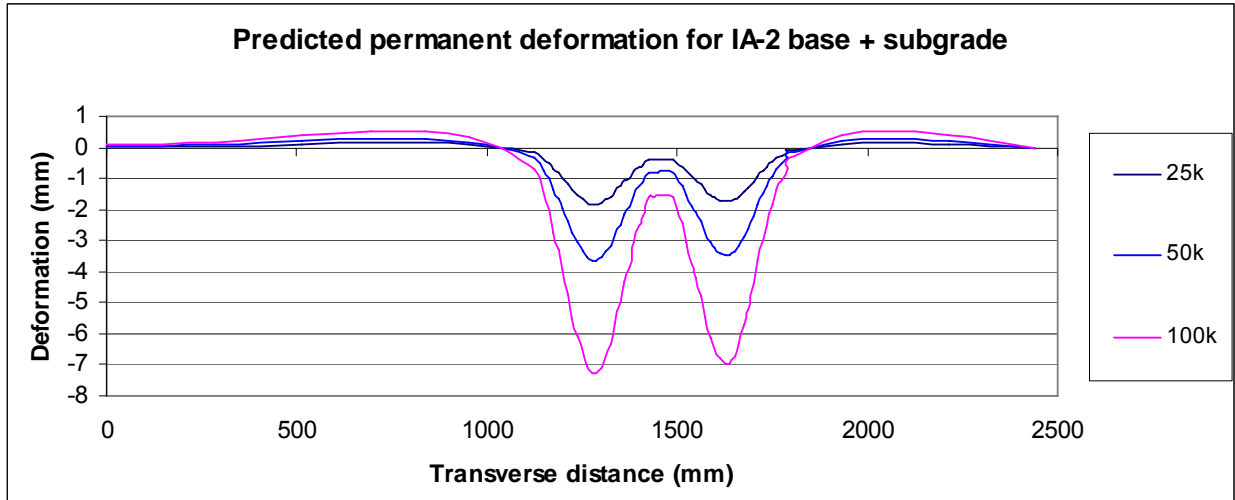
Figure C-1 Predicted permanent deformation for IA-2 subgrade